

AD \_\_\_\_\_

Award Number: DAMD17-98-1-8614

TITLE: Mechanisms of Virus-Induced Neural Cell Death

PRINCIPAL INVESTIGATOR: Kenneth L. Tyler, M.D.

CONTRACTING ORGANIZATION: University of Colorado Health  
Sciences Center  
Denver, Colorado 80262

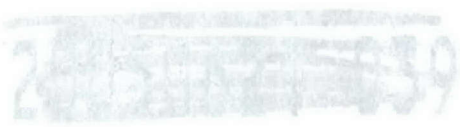
REPORT DATE: March 2005

TYPE OF REPORT: Final

PREPARED FOR: U.S. Army Medical Research and Materiel Command  
Fort Detrick, Maryland 21702-5012

DISTRIBUTION STATEMENT: Approved for Public Release;  
Distribution Unlimited

The views, opinions and/or findings contained in this report are  
those of the author(s) and should not be construed as an official  
Department of the Army position, policy or decision unless so  
designated by other documentation.



# REPORT DOCUMENTATION PAGE

*Form Approved  
OMB No. 074-0188*

Public reporting burden for this collection of information is estimated to average 1 hour per response, including the time for reviewing instructions, searching existing data sources, gathering and maintaining the data needed, and completing and reviewing this collection of information. Send comments regarding this burden estimate or any other aspect of this collection of information, including suggestions for reducing this burden to Washington Headquarters Services, Directorate for Information Operations and Reports, 1215 Jefferson Davis Highway, Suite 1204, Arlington, VA 22202-4302, and to the Office of Management and Budget, Paperwork Reduction Project (0704-0188), Washington, DC 20503

<b>1. AGENCY USE ONLY (Leave blank)</b>			<b>2. REPORT DATE</b> March 2005		<b>3. REPORT TYPE AND DATES COVERED</b> Final (15 Aug 98 - 14 Feb 05)		
<b>4. TITLE AND SUBTITLE</b> Mechanisms of Virus-Induced Neural Cell Death					<b>5. FUNDING NUMBERS</b> DAMD17-98-1-8614		
<b>6. AUTHOR(S)</b> Kenneth L. Tyler, M.D.							
<b>7. PERFORMING ORGANIZATION NAME(S) AND ADDRESS(ES)</b> University of Colorado Health Sciences Center Denver, Colorado 80262					<b>8. PERFORMING ORGANIZATION REPORT NUMBER</b>		
<b>E-Mail:</b> Ken.Tyler@uchsc.edu							
<b>9. SPONSORING / MONITORING AGENCY NAME(S) AND ADDRESS(ES)</b> U.S. Army Medical Research and Materiel Command Fort Detrick, Maryland 21702-5012					<b>10. SPONSORING / MONITORING AGENCY REPORT NUMBER</b>		
<b>11. SUPPLEMENTARY NOTES</b> Original contains color plates. All DTIC reproductions will be in black and white.							
<b>12a. DISTRIBUTION / AVAILABILITY STATEMENT</b> Approved for Public Release; Distribution Unlimited					<b>12b. DISTRIBUTION CODE</b>		
<b>13. ABSTRACT (Maximum 200 Words)</b> We have used experimental infection with reoviruses to study how viruses induce cell death (apoptosis), and the significance of apoptosis in the pathogenesis of viral infection. We have developed one of the best characterized experimental models for investigating and manipulating viral cell death pathways. We have shown that apoptosis is a major mechanism of reovirus-induced cell death in murine models of key human viral infections including myocarditis and encephalitis. We have shown that inhibiting apoptosis can reduce the degree of virus-induced injury in target organs and prolong the survival of infected animals. In virus infected cells apoptosis is initiated by the activation of death receptors, and its full expression requires augmentation by mitochondrial pro-apoptotic factors including Smac/DIABLO. We have identified the pro-apoptotic Bcl-2 family protein Bid as a key intermediary between the death receptor and mitochondrial apoptotic pathways. We have shown that reovirus infection induces the selective activation and up-regulation of both mitogen activated protein kinase (MAPK) cascades and transcription factor pathways including those involving JNK, c-Jun and NF-kappaB. We have used oligonucleotide microarrays to study reovirus-induced changes in gene expression in infected host cells.							
<b>14. SUBJECT TERMS</b> Apoptosis, caspases, reovirus, encephalitis, neurons, JNK, NF-kB					<b>15. NUMBER OF PAGES</b> 227		
					<b>16. PRICE CODE</b>		
<b>17. SECURITY CLASSIFICATION OF REPORT</b> Unclassified		<b>18. SECURITY CLASSIFICATION OF THIS PAGE</b> Unclassified		<b>19. SECURITY CLASSIFICATION OF ABSTRACT</b> Unclassified		<b>20. LIMITATION OF ABSTRACT</b> Unlimited	

## **Table of Contents**

Cover.....	1
SF 298.....	2
<b>Table of Contents.....</b>	<b>3</b>
Introduction.....	4
Body.....	5
Key Research Accomplishments.....	10
Reportable Outcomes.....	17
Conclusions.....	21
References.....	
Appendices.....	22

## **INTRODUCTION (Subject, Purpose, Scope of the Research)**

The clinical manifestations of viral infection result from the capacity of viruses to damage or kill cells in different organs. Two distinct patterns of cell death, necrosis and apoptosis can be distinguished based on a variety of biochemical and morphological criteria. Apoptotic cell death is characterized by diminution in cell size, membrane blebbing, and compaction, margination and fragmentation of nuclear DNA. DNA fragmentation occurs predominantly at internucleosomal regions resulting in the generation of pathognomonic DNA 'ladders' when DNA from apoptotic cells is subjected to agarose gel electrophoresis.

Most apoptotic processes are triggered by the activation of caspases, a family of cellular cysteinyl proteases. Caspases can be hierarchically ordered into initiator enzymes which trigger the proteolytic activation of downstream effector enzymes. Effector caspases in turn act on a variety of cellular substrates to induce the morphological changes characteristic of apoptosis. Individual initiator caspases are associated with different cellular organelles involved in extrinsic or intrinsic pathways of cell death. In the extrinsic pathway, death is mediated by the binding of apoptosis inducing ligands such as TRAIL, TNF, or FasL to their cognate cell surface "death receptors". This binding triggers the activation of death-receptor associated initiator caspases including caspase 8 and 10 through a death-inducing signal complex (DISC). Intrinsic death signals appear to act predominantly through their effect on either the mitochondrion, or the Golgi/ER system. Mitochondrial death signals result in the release of a variety of pro-apoptotic factors including cytochrome c, AIF, and Smac/DIABLO. Although the actions of mitochondrial pro-apoptotic factors are diverse, two important pathways include apoptosome-mediated activation of the initiator caspase 9 triggered by cytosolic release of cytochrome c, and potentiation of caspase activity by the inhibition of

cellular inhibitor of apoptosis proteins (IAPs) mediated by their binding to Smac/DIABLO.

The subject and purpose of this research project is to study the cellular mechanisms by which viruses induce apoptotic cell death.

## **PROGRESS REPORT**

This is the final report on this research project. Thirty-six (36) papers have been published or accepted for publication as part of the work funded by this grant (see Reportable Outcomes). Reprints of all published papers not previously supplied have been included as an appendix. The technical reporting requirements for this grant specify that journal publications can be substituted for detailed descriptions of specific aspects of the research. References to publications listed in reportable outcomes are keyed to the specific aims/statement of work (SOW) as outlined in the original research application and subsequent expansions. In addition to the papers cited below the work covered in this grant have been described in a number of reviews (2, 3, 14, 25).

### **Original SOW 1: Is apoptosis a general feature of human viral encephalitis?**

References 17 and 18 established that apoptosis is an important feature of human viral encephalitides including those caused by: (1) herpes simplex virus (HSV), the most common cause of acute sporadic encephalitis in immunocompetent adults, (2) cytomegalovirus (CMV), the most important cause of opportunistic viral encephalitis, and (3) progressive multifocal leukoencephalopathy, the most important opportunistic viral CNS infection in HIV infected individuals. References 19, 6, 19, 23, 28, and 34 include discussions of diagnosis and pathogenesis of human CNS infections caused by reovirus, human herpesvirus 6 (HHV6), Epstein- Barr virus (EBV), and HSV that were part of our initial review of pathological material to establish a pool of cases of defined etiology for the subsequent pathological studies of apoptosis (refs.17, 18). Reference 36 describes

apoptosis in a murine model of HSV encephalitis, and reference 9 describes apoptosis occurring in a mouse model utilizing a reovirus isolated from an infant with meningitis.

**Expanded SOW Aim 1.1: Cellular apoptotic pathways activated in human viral apoptosis.**

References 17 and 18 provide evidence for activation of specific caspases in encephalitis caused by HSV, CMV, and JCV including caspases 3 and 8.

**Expanded SOW Aim 1.2: Examine apoptotic pathways and the effects of inhibiting apoptosis in a murine model.**

References 1, 5, 10, 11, 20 all characterize aspects of the murine model of apoptosis induced by reoviruses. Reference 9 describes apoptosis with a novel human reovirus isolates and reference 36 describes apoptosis in a murine model of HSV encephalitis. The murine model of encephalitis was subsequently utilized to demonstrate a protective effect of minocycline (1).

Apoptosis pathways have also been characterized in a murine model of myocarditis (7, 30). Myocardial injury induced by reoviruses is associated with apoptosis and with the activation of both calpain (30) and caspases including caspase 3 and 8 (7).

Pharmacologic inhibitors of caspase activation inhibit the extent of reovirus-induced myocardial injury and injury and injury is reduced and survival of infected animals is enhanced in caspase 3 deficient mice (7).

**Expanded SOW Aim 1.3: Examine changes in gene expression in a murine model of CNS encephalitis in which apoptotic injury is critical to pathogenesis.**

Oligonucleotide microarrays were utilized to study changes in the expression of genes

induced by reovirus infection including those involved in apoptosis, DNA damage and repair, and cell cycle regulation (12, 24).

**Original SOW 2.0: Is the ceramide/sphingomyelin pathway involved in reovirus-induced apoptosis?**

Initial studies suggested that this aim should be broadened in scope as reflected in the expanded SOW items listed below. Progress is listed under these expanded SOW items.

**Expanded SOW 2.1 & 2.2: Identify cellular pathways leading to the activation of NF- $\kappa$ B and JNK/c-JUN in reovirus-infected cells.**

We demonstrated that reovirus infection is associated with the activation of the nuclear transcription factor NF- $\kappa$ B (33). We subsequently provided a more detailed characterization indicating that apoptosis-inducing reovirus strains were associated with an initial phase of NF- $\kappa$ B activation followed by a subsequent phase in which Nf-KB was inhibited (15). Reovirus infection was shown to induce a refractory state during which infected cells failed to respond to canonical NF- $\kappa$ B inducing stimuli such as etoposide and tumor necrosis factor (TNF)(15). Finally, we established that it was the late inhibition of NF- $\kappa$ B activation that was essential for reovirus-induced apoptosis, and that this was likely due to the prevention of the up-regulation of NF- $\kappa$ B dependent anti-apoptotic genes including the gene encoding c-FLIP (4).

Reovirus infection also results in activation of the c-Jun N-terminal kinase (JNK) pathway of mitogen activated protein kinases (MAPK) (6, 26). The MAP3K MEKK1 appears to play a critical role as an upstream regulator of the JNK pathway during reovirus infection (13).

**Expanded SOW 2.3: NF-κB and c-Jun regulated genes involved in apoptosis**

As described above the cellular inhibitor of apoptosis protein c-FLIP (cellular FLICE/caspase 8 inhibitory protein) was identified as a critical NF-κB regulated protein during reovirus infection (4).

**Expanded SOW 2.4: Identify the role of the mitochondrion in reovirus-induced apoptosis.**

Mitochondrial apoptotic pathways activated during reovirus infection have been extensively characterized (21, 22). Reovirus infection is initiated by death receptor signaling which results in the activation of caspase 8. Caspase 8 in turn leads to the proteolytic cleavage of the Bcl-2 family protein Bid to form truncated Bid (tBid). tBid translocates to the mitochondria where it triggers the release of a variety of mitochondrial pro-apoptotic factors including cytochrome c and Smac/DIABLO. Smac/DIABLO in turn binds to cellular inhibitor of apoptosis (IAP) proteins thereby preventing their capacity to inhibit caspases. There are cell specific differences in the capacity of reoviruses to induce mitochondrial release of cytochrome c. For example, cytochrome c release occurs late and at low levels in reovirus infected primary neuronal cultures and neuroblastoma cell lines as compared to epithelial cells and human cancer cell lines. Regardless of cell type it appears that Smac/DIABLO rather than cytochrome c is the critical mitochondrial apoptotic factor following reovirus infection, as inhibition of caspase 9 activity has only modest effects on reovirus-induced apoptosis.

**Expanded SOW 2.5: Identify the mechanism by which reovirus infection sensitizes cells to killing by TRAIL.**

Reovirus induced apoptosis in epithelial cells and a wide variety of human cancer cell lines is mediated by the apoptosis inducing ligand TRAIL (TNF-related apoptosis inducing ligand)(32). Reovirus infection sensitizes epithelial and a variety of human cancer cell lines to killing by TRAIL through a process that is dependent on caspase 8 (27).

**Original SOW 3.0: Is reovirus apoptosis associated with aberrant regulation of cell cycle progression?**

Reovirus infection is associated with inhibition of proliferation resulting from a G2/M cell cycle arrest in infected cells (24, 29, 31). The process is determined by the viral sigma 1s protein and involves dysregulation of the key G2/M checkpoint kinase p34 cdc2. Although apoptosis and cell cycle dysregulation appear to be at least partially independent events (31), the sigma 1s protein plays a key role in both processes (5, 8, 29,

**Expanded SOW 3.1: Evaluate apoptotic pathways in both primary and continuous neuronal cell lines.**

Reovirus induced apoptosis occurs in both neuroblastoma cell lines and primary neuronal cultures (10, 20). Apoptosis in both neurons and non-neuronal cells is initiated by death receptor activation. In epithelial cells and human cancer cell lines death receptor activation involves TRAIL and death receptors 4 and 5. By contrast, in neurons death receptor activation involves predominantly Fas and Fas ligand (FasL). Both neuronal and non-neuronal apoptosis pathways require augmentation of death receptor initiated signaling by mitochondrial apoptotic pathways. As indicated above, neurons differ from epithelial cells in having delayed and only low level release of cytochrome c from mitochondria. In both neuronal and non-neuronal cells Smac/DIABLO appears to

act as the central mitochondrial pro-apoptotic factor released following reovirus infection.

**Expanded SOW 3.2: Identify the role of reovirus σ1s protein in reovirus-induced cell cycle dysregulation.**

As discussed above it was shown that reovirus-induced G2/M cell cycle arrest was dependent on the viral sigma 1s protein (29). It was subsequently shown that this protein contained a nuclear localization signal (8). Once sigma 1s enters the host cell nucleus, subsequent to either infection or transfection, it induces striking changes in nuclear morphology ("herniations") associated with disruption of nuclear laminin and nuclear pore complexes (8).

**KEY RESEARCH ACCOMPLISHMENTS**

**SOW 1**

\*Apoptosis is an important feature of CNS injury in human CNS viral infections including herpes simplex virus and cytomegalovirus encephalitis and progressive multifocal leukoencephalopathy (PML).

\*Apoptosis in human CNS viral infections is associated with activation of caspase 3

\*Bystander apoptosis occurs with greater frequency in HSV compared to CMV encephalitis.

\*Apoptosis is a major feature of reovirus-induced encephalitis in mice, and is

associated with activation of caspase 3. Apoptosis occurs predominantly in neurons, both those that are virus-infected (direct apoptosis) and in cells in proximity to infected cells (bystander apoptosis).

\*Apoptosis is a major mechanism of myocardial injury in an in vivo model of viral myocarditis, is associated with calpain activation, and can be inhibited by treatment of mice with calpain inhibitor.

\*Reovirus-induced myocardial injury is also associated with activation of caspases and can be inhibited by pan-caspase inhibitors or in mice with a selective knockout of the caspase 3 gene

\* Inhibition of caspase activation by pancaspase inhibitors can inhibit apoptosis, reduce the extent and severity of CNS histopathological injury and prolong survival in a murine model of reovirus encephalitis.

\*Minocycline, an antibiotic which has been shown to both reduce glial activation and inhibit mitochondrial pathways of apoptosis, can reduce the extent and severity of CNS apoptosis and injury in a murine model of viral encephalitis.

\*Reovirus infection is associated with altered expression of genes involved in apoptosis and DNA repair. Down-regulation of DNA repair genes may contribute to reovirus-induced apoptosis.

## **SOW 2**

\*Reovirus infection is associated with activation of the nuclear transcriptional activation factor, NF $\kappa$ B. NF- $\kappa$ B is translocated to the nucleus in infected cells, and is capable of inducing expression of genes containing NF- $\kappa$ B responsive promoter elements.

\*Reovirus-induced apoptosis is inhibited in cells in which reovirus-induced NF $\kappa$ B activation is inhibited or prevented: (1) by over-expression of dominant negative forms of its cytoplasmic inhibitor I $\kappa$ B, (2) by treatment of cells with proteosome inhibitors or, (3) in cells lacking the p50 or p65 NF- $\kappa$ B subunits as a result of gene knockouts.

\*Reovirus-induced NF $\kappa$ B activation results in selective up-regulation of mRNA levels of the TNF superfamily death receptor DR4 and enhanced expression of mature DR5 protein.

\*Reovirus infection results in selective activation of mitogen associated protein kinase (MAPK) pathways including the extracellular related kinase (ERK) and c-Jun-N-terminal kinase (JNK) pathways.

\* Reovirus activation of JNK is associated with downstream activation of the JNK-dependent transcription factor c-Jun, and this activation correlates with the capacity of viral strains to induce apoptosis.

\*Differences in the capacity of reovirus strains to activate JNK are determined by the viral S1 gene.

\*Reovirus-induced apoptosis in non-neuronal cells is initiated by death-receptor activation, but requires augmentation by mitochondrial apoptotic pathways for its full expression.

\*Reovirus-induced activation of caspase 8 results in the cleavage of the Bcl-2 family protein Bid, and cleaved Bid translocates to the mitochondrion and activates mitochondrial apoptotic pathways.

\*Mitochondrial pro-apoptotic factors released following reovirus infection include both cytochrome c and Smac/DIABLO but not apoptosis inducing factor (AIF).

\*Activation of mitochondrial apoptotic pathways is associated with the subsequent down-regulation of cellular IAPs including XIAP, cIAP1, and survivin and this down-regulation is blocked by stable over-expression of Bcl-2 or DN-FADD.

\*Reovirus-induced oncolysis of human cervical, breast, and lung cancer cell lines results from apoptosis induction and is mediated by the apoptosis-inducing ligand TRAIL.

\* Reovirus infection can sensitize cancer kills to killing by TRAIL, and this process involves up-regulation of the death-receptor associated initiator caspase, caspase 8.

\*TRAIL induced killing of cancer cell lines involves down-regulation of cellular inhibitor of apoptosis proteins (IAPs).

\*Reovirus infection is associated with two distinct phases of NF- $\kappa$ B regulation including an early activation phase followed by later inhibition of both virus-induced and stimulus induced (TNF, etoposide) NF- $\kappa$ B activation.

\*MEKK1 is required for calpain-dependent proteolysis.

\*\*Reovirus-induced apoptosis in non-neuronal cells is initiated by death-receptor activation, but requires augmentation by mitochondrial apoptotic pathways for its full expression.

\*Mitochondrial pro-apoptotic factors released following reovirus infection in epithelial and human cancer cell lines include both cytochrome c and

Smac/DIABLO but not apoptosis inducing factor (AIF).

\*Activation of mitochondrial apoptotic pathways is associated with the subsequent down-regulation of cellular IAPs including XIAP, cIAP1.

\*Reovirus-induced apoptosis is specifically inhibited by antibodies directed against TRAIL, the ligand for death receptors DR4 and DR5, but not by antibodies against TNF or FasL. Apoptosis is also specifically inhibited by soluble DR4 or DR5 receptor, but not by soluble TNF-receptor.

\*Reovirus infection is associated with activation of caspase cascades in infected cells. This activation involves both cell death receptor associated and mitochondrial pathways of cell death. Both caspase-8, the initiator caspase for death-receptor mediated caspase cascades, and caspase-9, the initiator caspase for mitochondrially initiated caspase cascades, are activated in reovirus-infected cells. Inhibition of activation of either caspase-8 or caspase-9 inhibits reovirus-induced apoptosis. Caspase-3 is also activated in reovirus-infected cells, and appears to act as a key effector caspase for both the death-receptor and mitochondrial pathways.

### SOW 3

\*Reovirus-induced inhibition of cellular proliferation is associated with arrest of cells in the G2M phase of the cell cycle.

\*The reovirus S1 gene is the primary determinant of differences in the capacity of reovirus strains to induce G2M arrest.

\* The reovirus  $\sigma$ 1s protein, which is encoded by the S1 gene, is necessary for reovirus-induced G2M arrest, and over-expression of this protein in susceptible cells results in increased accumulation of cells in the G2M phase of the cell cycle.

\*Although the capacity of reovirus strains to induce apoptosis and G2M are closely associated, apoptosis can be inhibited without preventing the capacity of reoviruses to induce G2M arrest, indicating that G2M arrest is not simply the result of apoptosis-associated cellular DNA damage.

\*Reovirus-induced inhibition of cell cycle regulation and induction of G2/M arrest is mediated by the  $\sigma$ 1s protein and is associated with inhibition of the key G2/M regulatory kinase p34<sup>cdc2</sup>.

\*Reovirus infection results in the selective up-regulation of specific sets of genes involved in the control and regulation of cell cycle progression.

\*Reovirus  $\sigma$ 1s protein contains functional nuclear localization and nuclear export sequences.

## REPORTABLE OUTCOMES

- 1: Richardson-Burns, SM, Tyler KL. Minocycline delays disease onset and mortality in a murine model of viral encephalitis.  
*Exp. Neurol.* 2005;192:331-339.
- 2: Clarke P, Richardson-Burns SM, DeBiasi RL, Tyler KL. Mechanisms of apoptosis during reovirus infection.  
*Curr. Topics Microbiol. Immunol.* 2005; 289: 1-24.
- 3: Clarke P, DeBiasi RL, Goody R, Hoyt CC, Richardson-Burns S, Tyler KL. Mechanisms of reovirus-induced cell death and tissue injury: Role of apoptosis and virus-induced perturbation of host-cell signaling and transcription factor activation.  
*Viral Immunol* 2005; 8:89-116.
- 4: Clarke P, DeBiasi RL, Meintzer SM, Robinson BA, Tyler KL. Inhibition of NF- $\kappa$ B activity and cFLIP expression contribute to viral-induced apoptosis.  
*Apoptosis* 2005; (APPT2339R1, in press).
- 5: Hoyt CC, Richardson-Burns SM, Goody RJ, Robinson BA, DeBiasi RL, Tyler KL. Nonstructural protein sigma1s is a determinant of reovirus virulence and influences the kinetics and severity of apoptosis induction in the heart and central nervous system.  
*J Virol.* 2005 Mar;79(5):2743-53.  
PMID: 15708993 [PubMed - in process]
- 6: Clarke P, Meintzer SM, Wang Y, Moffitt LA, Richardson-Burns SM, Johnson GL, Tyler KL. JNK regulates the release of proapoptotic mitochondrial factors in reovirus-infected cells.  
*J Virol.* 2004 Dec;78(23):13132-8.  
PMID: 15542665 [PubMed - indexed for MEDLINE]
- 7: DeBiasi RL, Robinson BA, Sherry B, Bouchard R, Brown RD, Rizeq M, Long C, Tyler KL. Caspase inhibition protects against reovirus-induced myocardial injury in vitro and in vivo.  
*J Virol.* 2004 Oct;78(20):11040-50.  
PMID: 15452224 [PubMed - indexed for MEDLINE]
- 8: Hoyt CC, Bouchard RJ, Tyler KL. Novel nuclear herniations induced by nuclear localization of a viral protein.  
*J Virol.* 2004 Jun;78(12):6360-9.  
PMID: 15163729 [PubMed - indexed for MEDLINE]
- 9: Tyler KL, Barton ES, Ibach ML, Robinson C, Campbell JA, O'Donnell SM, Valyi-Nagy T, Clarke P, Wetzel JD, Dermody TS. Isolation and molecular characterization of a novel type 3 reovirus from a child with meningitis.  
*J Infect Dis.* 2004 May 1;189(9):1664-75. Epub 2004 Apr 15.  
PMID: 15116303 [PubMed - indexed for MEDLINE]
- 10: Richardson-Burns SM, Tyler KL. Regional differences in viral growth and central nervous system injury correlate with apoptosis.

- J Virol. 2004 May;78(10):5466-75.  
PMID: 15113925 [PubMed - indexed for MEDLINE]
- 11: Edelmann KH, Richardson-Burns S, Alexopoulou L, Tyler KL, Flavell RA, Oldstone MB. Does Toll-like receptor 3 play a biological role in virus infections? *Virology*. 2004 May 1;322(2):231-8.  
PMID: 15110521 [PubMed - indexed for MEDLINE]
- 12: DeBiasi RL, Clarke P, Meintzer S, Jotte R, Kleinschmidt-Demasters BK, Johnson GL, Tyler KL. Reovirus-induced alteration in expression of apoptosis and DNA repair genes with potential roles in viral pathogenesis. *J Virol*. 2003 Aug;77(16):8934-47.  
PMID: 12885910 [PubMed - indexed for MEDLINE]
- 13: Cuevas BD, Abell AN, Witowsky JA, Yujiri T, Johnson NL, Kesavan K, Ware M, Jones PL, Weed SA, DeBiasi RL, Oka Y, Tyler KL, Johnson GL. MEKK1 regulates calpain-dependent proteolysis of focal adhesion proteins for rear-end detachment of migrating fibroblasts. *EMBO J*. 2003 Jul 1;22(13):3346-55.  
PMID: 12839996 [PubMed - indexed for MEDLINE]
- 14: Clarke P, Tyler KL. Reovirus-induced apoptosis: A minireview. *Apoptosis*. 2003 Mar;8(2):141-50.  
PMID: 12766474 [PubMed - indexed for MEDLINE]
- 15: Clarke P, Meintzer SM, Moffitt LA, Tyler KL. Two distinct phases of virus-induced nuclear factor kappa B regulation enhance tumor necrosis factor-related apoptosis-inducing ligand-mediated apoptosis in virus-infected cells. *J Biol Chem*. 2003 May 16;278(20):18092-100.  
PMID: 12637521 [PubMed - indexed for MEDLINE]
- 16: Tyler KL. Human herpesvirus 6 and multiple sclerosis: the continuing conundrum. *J Infect Dis*. 2003 May 1;187(9):1360-4.  
PMID: 12717616 [PubMed - indexed for MEDLINE]
- 17: Richardson-Burns SM, Kleinschmidt-DeMasters BK, DeBiasi RL, Tyler KL. Progressive multifocal leukoencephalopathy and apoptosis of infected oligodendrocytes in the central nervous system of patients with and without AIDS. *Arch Neurol*. 2002 Dec;59(12):1930-6.  
PMID: 12470182 [PubMed - indexed for MEDLINE]
- 18: DeBiasi RL, Kleinschmidt-DeMasters BK, Richardson-Burns S, Tyler KL. Central nervous system apoptosis in human herpes simplex virus and cytomegalovirus encephalitis. *J Infect Dis*. 2002 Dec 1;186(11):1547-57.  
PMID: 12447729 [PubMed - indexed for MEDLINE]
- 19: Weinberg A, Li S, Palmer M, Tyler KL. Quantitative CSF PCR in Epstein-Barr virus infections of the central nervous system. *Ann Neurol*. 2002 Nov;52(5):543-8.

PMID: 12402250 [PubMed - indexed for MEDLINE]

20: Richardson-Burns SM, Kominsky DJ, Tyler KL. Reovirus-induced neuronal apoptosis is mediated by caspase 3 and is associated with the activation of death receptors.

J Neurovirol. 2002 Oct;8(5):365-80.

PMID: 12402163 [PubMed - indexed for MEDLINE]

21: Kominsky DJ, Bickel RJ, Tyler KL. Reovirus-induced apoptosis requires mitochondrial release of Smac/DIABLO and involves reduction of cellular inhibitor of apoptosis protein levels.

J Virol. 2002 Nov;76(22):11414-24.

PMID: 12388702 [PubMed - indexed for MEDLINE]

22: Kominsky DJ, Bickel RJ, Tyler KL. Reovirus-induced apoptosis requires both death receptor- and mitochondrial-mediated caspase-dependent pathways of cell death.

Cell Death Differ. 2002 Sep;9(9):926-33.

PMID: 12181743 [PubMed - indexed for MEDLINE]

23: DeBiasi RL, Kleinschmidt-DeMasters BK, Weinberg A, Tyler KL. Use of PCR for the diagnosis of herpesvirus infections of the central nervous system.

J Clin Virol. 2002 Jul;25 Suppl 1:S5-11.

PMID: 12091076 [PubMed - indexed for MEDLINE]

24: Poggioli GJ, DeBiasi RL, Bickel R, Jotte R, Spalding A, Johnson GL, Tyler KL. Reovirus-induced alterations in gene expression related to cell cycle regulation. J Virol. 2002 Mar;76(6):2585-94.

PMID: 11861824 [PubMed - indexed for MEDLINE]

25 Tyler KL, Clarke P, DeBiasi RL, Kominsky D, Poggioli GJ. Reoviruses and the host cell.

Trends Microbiol. 2001 Nov;9(11):560-4.

PMID: 11825717 [PubMed - indexed for MEDLINE]

26: Clarke P, Meintzer SM, Widmann C, Johnson GL, Tyler KL. Reovirus infection activates JNK and the JNK-dependent transcription factor c-Jun.

J Virol. 2001 Dec;75(23):11275-83.

PMID: 11689607 [PubMed - indexed for MEDLINE]

27: Clarke P, Meintzer SM, Spalding AC, Johnson GL, Tyler KL. Caspase 8-dependent sensitization of cancer cells to TRAIL-induced apoptosis following reovirus-infection.

Oncogene. 2001 Oct 18;20(47):6910-9.

PMID: 11687970 [PubMed - indexed for MEDLINE]

28: Kleinschmidt-DeMasters BK, DeBiasi RL, Tyler KL. Polymerase chain reaction as a diagnostic adjunct in herpesvirus infections of the nervous system.

Brain Pathol. 2001 Oct;11(4):452-64.

PMID: 11556691 [PubMed - indexed for MEDLINE]

29: Poggioli GJ, Dermody TS, Tyler KL. Reovirus-induced sigma1s-dependent G(2)/M phase cell cycle arrest is associated with inhibition of p34(cdc2).

J Virol. 2001 Aug;75(16):7429-34.  
PMID: 11462015 [PubMed - indexed for MEDLINE]

30: DeBiasi RL, Edelstein CL, Sherry B, Tyler KL. Calpain inhibition protects against virus-induced apoptotic myocardial injury.  
J Virol. 2001 Jan;75(1):351-61.  
PMID: 11119604 [PubMed - indexed for MEDLINE]

31: Poggioli GJ, Keefer C, Connolly JL, Dermody TS, Tyler KL. Reovirus-induced G(2)/M cell cycle arrest requires sigma1s and occurs in the absence of apoptosis.  
J Virol. 2000 Oct;74(20):9562-70.  
PMID: 11000227 [PubMed - indexed for MEDLINE]

32: Clarke P, Meintzer SM, Gibson S, Widmann C, Garrington TP, Johnson GL, Tyler KL. Reovirus-induced apoptosis is mediated by TRAIL.  
J Virol. 2000 Sep;74(17):8135-9.  
PMID: 10933724 [PubMed - indexed for MEDLINE]

33: Connolly JL, Rodgers SE, Clarke P, Ballard DW, Kerr LD, Tyler KL, Dermody TS. Reovirus-induced apoptosis requires activation of transcription factor NF-kappaB.  
J Virol. 2000 Apr;74(7):2981-9.  
PMID: 10708412 [PubMed - indexed for MEDLINE]

34: DeBiasi RL, Tyler KL. Polymerase chain reaction in the diagnosis and management of central nervous system infections.  
Arch Neurol. 1999 Oct;56(10):1215-9.  
PMID: 10520937 [PubMed - indexed for MEDLINE]

35: DeBiasi RL, Squier MK, Pike B, Wynes M, Dermody TS, Cohen JJ, Tyler KL. Reovirus-induced apoptosis is preceded by increased cellular calpain activity and is blocked by calpain inhibitors.  
J Virol. 1999 Jan;73(1):695-701.  
PMID: 9847375 [PubMed - indexed for MEDLINE]

36: Pelosi E, Rozenberg F, Coen DM, Tyler KL. A herpes simplex virus DNA polymerase mutation that specifically attenuates neurovirulence in mice.  
Virology. 1998 Dec 20;252(2):364-72.  
PMID: 9878615 [PubMed - indexed for MEDLINE]

## **CONCLUSIONS**

Due in significant part to support provided by this grant, reoviruses have become one of the best understood models of virus-induced apoptosis. Viral genes and proteins involved in induction of apoptosis have been identified. The caspase activation pathways involved in apoptosis have been defined in both neuronal and non-neuronal cells, as has the role of specific mitochondrial pro-apoptotic factors. The capacity of the virus to activate specific MAPK cascades and their associated transcription factors has been characterized, and studies are currently underway to establish the entire network of genes that are up-regulated following viral infection. The importance of apoptosis in a variety of in vivo models of infection including encephalitis and myocarditis has been established, and studies are currently underway to determine whether key apoptotic pathways identified in vitro are also active in vivo. Targeted interventions that modulate apoptosis and enhance cell survival in vitro are being tested for efficacy as novel anti-viral strategies in vivo. The importance of apoptosis as a mechanism of CNS injury has also been established in a variety of key human viral infections, providing added significance to its study in both cell culture and experimental models of infection.

**Personnel receiving pay from the research effort at any point during the grant funding cycle:**

**Kenneth L. Tyler, M.D.      Penny Clarke, Ph.D.**

**Robin Goody, Ph.D.      Sarah Richardson-Burns, Ph.D.**

**Cristin Hoyt, Ph.D.      Suzanne Meintzer, B.S.**

**Bridget Robinson, M.S., B.S.**

**Inhibition of NF-κB Activity and cFLIP expression contribute to Viral-induced Apoptosis**

Penny Clarke,<sup>1, 2</sup> Roberta L. DeBiasi,<sup>1, 2, 3</sup> Suzanne M. Meintzer,<sup>1, 2</sup> Bridget A. Robinson<sup>1, 2</sup> and Kenneth L. Tyler.<sup>1, 3, 4, 5</sup>

Departments of Neurology,<sup>1</sup> Pediatrics,<sup>3</sup> Immunology,<sup>4</sup> Medicine and Microbiology,<sup>5</sup> University of Colorado Health Sciences Center, Denver, Colorado 80262, USA and Denver Veterans Affairs Medical Center, Denver, Colorado 80220, USA<sup>2</sup>

Abbreviated Title: NF-κB inhibition contributes to virus-induced apoptosis

Correspondence to: Penny Clarke, Department of Neurology (B 182), University of Colorado Health Sciences Center, 4200 East 9th Avenue, Denver CO 80262, USA. Tel: (+1) 303 393 4684; Fax: (+1) 303 393 4686; e-mail: Penny.Clarke@uchsc.edu

Virus-induced activation of nuclear factor-kappa B (NF- $\kappa$ B) is required for Type 3 (T3) reovirus-induced apoptosis. We now show that NF- $\kappa$ B is also activated by the prototypic Type 1 reovirus strain Lang (T1L), which induces significantly less apoptosis than T3 viruses, indicating that NF- $\kappa$ B activation alone is not sufficient for apoptosis in reovirus-infected cells. A second phase of virus-induced NF- $\kappa$ B regulation, where NF- $\kappa$ B activation is inhibited at later times following infection with T3 Abney (T3A), is absent in T1L-infected cells. This suggests that inhibition of NF- $\kappa$ B activation at later times post infection also contributes to reovirus-induced apoptosis. Reovirus-induced inhibition of stimulus-induced activation of NF- $\kappa$ B is significantly associated with apoptosis following infection of HEK293 cells with reassortant reoviruses and is determined by the T3 S1 gene segment, which is also the primary determinant of reovirus-induced apoptosis. Inhibition of stimulus-induced activation of NF- $\kappa$ B also occurs following infection of primary cardiac myocytes with apoptotic (8B) but not non-apoptotic (T1L) reoviruses. Expression levels of the NF- $\kappa$ B-regulated cellular FLICE inhibitory protein (cFLIP) reflect NF- $\kappa$ B activation in reovirus-infected cells. Further, inhibition of NF- $\kappa$ B activity and cFLIP expression promote T1L-induced apoptosis. These results demonstrate that inhibition of stimulus-induced activation of NF- $\kappa$ B and the resulting decrease in cFLIP expression promote reovirus-induced apoptosis.

*Keywords:* cFLIP, NF- $\kappa$ B, myocytes, reovirus

## Introduction

Reoviruses are non-enveloped viruses comprised of two concentric protein capsids surrounding a genome of 10 segments of double-stranded RNA. Mammalian reoviruses provide a well-established experimental system for studying mechanisms of virus-induced pathogenesis. Type 3 (T3) reoviruses can induce apoptosis in cultured cells *in vitro* and in target tissues *in vivo*, including the heart and central nervous system.<sup>1</sup> In these key target organs, viral infection, tissue injury and apoptosis co-localize suggesting that apoptosis is a critical mechanism by which disease is triggered in the host.<sup>2-5</sup> Further, support for this view comes from studies indicating that inhibition of apoptosis reduces reovirus-induced tissue injury.<sup>4</sup>

Reovirus-induced apoptosis is mediated by members of the tumor necrosis factor (TNF) family of ligands, which attach to cell surface death receptors to induce the activation of initiator (caspase 8) and effector (caspases 3 and 7) caspases.<sup>3, 6, 7</sup> Mitochondrial pathways of apoptosis, initiated following the caspase 8-dependent cleavage of Bid, contribute to effector caspase activation in virus-infected cells.<sup>7, 8</sup> In addition reovirus can sensitize cells to death receptor induced apoptosis.<sup>7, 9</sup>

The nuclear factor-kappa B (NF- $\kappa$ B) family of transcription factors plays a key role in the regulation of cell growth and survival. The prototypical form of NF- $\kappa$ B exists as a heterodimer of proteins p50 and p65 (RelA), which is sequestered in the cytoplasm of quiescent cells through its association with members of the I $\kappa$ B family of inhibitory proteins.<sup>10-13</sup> Site specific phosphorylation, followed by ubiquitination and proteosomal degradation of I $\kappa$ B, allows NF- $\kappa$ B to translocate to the nucleus and activate cellular gene expression.<sup>14-17</sup> Infection with T3 reoviruses induces the activation of NF- $\kappa$ B in a variety of cell types, including human embryonic kidney 293 (HEK293) and HeLa cells.<sup>18, 19</sup> This activation is required for T3 reovirus-induced apoptosis in these cells, which is inhibited by stable over-expression of an I $\kappa$ B super-repressor or treatment of cells with a proteosome inhibitor (Z-L<sub>3</sub>VS) that blocks I $\kappa$ B degradation.<sup>18, 19</sup> T3 reovirus-induced apoptosis is also inhibited in immortalized mouse embryo fibroblasts (MEFs) with targeted disruptions in the genes encoding the p50 or p65 subunits of

NF-κB.<sup>18</sup> Although required for apoptosis, T3 reovirus-induced activation of NF-κB is transient and at later times post infection (PI) the activation of NF-κB by a wide variety of stimuli is inhibited in infected cells.<sup>18,19</sup>

In this report we show that the initial NF-κB activation following infection with the Type 1 reovirus strain Lang (T1L), which induces apoptosis inefficiently in infected cells (APO-), parallels that of the strongly apoptotic (APO+) T3 reovirus strain Abney (T3A).<sup>20-22</sup> In contrast, T1L does not inhibit NF-κB activation at later times PI, whereas T3A does. Our results demonstrate that inhibition of stimulus-induced activation of NF-κB is associated with apoptosis following infection of both HEK293 cells and primary cardiac myocytes. We further show that the T3 S1 gene segment, which is the primary determinant of reovirus-induced apoptosis, also determines the ability of reovirus strains to inhibit stimulus-induced activation of NF-κB.<sup>20, 21, 23</sup> In addition, chemical inhibition of NF-κB was found to significantly enhance apoptosis in primary myocytes following infection T1L (APO-). Taken together these results demonstrate that inhibition of stimulus-induced activation of NF-κB following T3-reovirus infection promotes apoptosis in both HEK293 cells and primary myocytes, and therefore contributes to viral pathogenesis. Virus-induced regulation of the NF-κB dependent gene encoding the cellular inhibitor of caspase 8 (also known as FLICE inhibitory protein, cFLIP) provides a potential mechanism for these findings.

## Materials and methods

### Cells and Virus

HEK293 (ATCC CRL1573) were cultured in Dulbecco's modified Eagle's medium (DMEM) supplemented with 100 U/ml each of penicillin and streptomycin and containing 10% fetal bovine serum (FBS) and were maintained at 37°C with 5% CO<sub>2</sub>. HEK293 cells expressing a dominant negative (DN)

form of the Fas Associated Death Domain protein (FADD-DN) or the I $\kappa$ B super-repressor (I $\kappa$ B $\Delta$ N2) were gifts from Dr. Gary Johnson (University of North Carolina School of Medicine) Neonatal rat cardiac myocytes were generated in the laboratory of Dr. Carlin Long (University of Colorado Health Sciences Center). Myocytes were cultured in DMEM with Hanks salts supplemented with 5% FBS, 1 mg/ml bovine serum albumin, 50 U/ml penicillin, 2  $\mu$ g/ml vitamin B-12 (Sigma), 10  $\mu$ g/ml transferrin (Sigma), 10  $\mu$ g/ml insulin (Sigma) and 0.1 mM BrdU (Sigma) and were maintained at 37°C with 1% CO<sub>2</sub>. Reovirus strains Type 3 Abney (T3A) and Type 1 Lang (T1L) are laboratory stocks that have been plaque purified and passaged (twice) in L929 (ATCC CCL1) cells to generate working stocks. T1L x T3A reassortant viruses were grown from stocks originally isolated by Tricia Jandris, Lynda Morrison and Graeme Wilson in the laboratory of Bernard Fields.<sup>24</sup> Virus 8B is a reassortant virus derived from a mouse infected with T1L and T3D.<sup>25</sup> EB121 and E3 are reassortant viruses derived from T1L and T3 Dearing (T3D). All EW reassortants were derived from 8B x EB121, whereas all DW reassortants were derived from EW60 and E3. Reovirus EW and DW reassortants have been characterized for their myocarditic potential.<sup>25, 26</sup> All EW and DW reassortants and 8B were gifts from Dr. Barbara Sherry (North Carolina State University). Virus infections were performed using a multiplicity of infection (MOI) of 100.

### Apoptosis assays

Apoptotic nuclear morphology and cell viability were determined by staining with acridine orange and ethidium bromide at a final concentration of 1  $\mu$ g/ml each. Following staining, cells were examined by epifluorescence microscopy (Nikon Labophot-2: B-2A filter, excitation, 450-490 nm; barrier, 520 nm; dichroic mirror, 505 nm). The percentage of cells containing condensed nuclei and/or marginated chromatin in a population of 100 cells was recorded. The specificity of this assay has been previously established in reovirus-infected cells using DNA laddering techniques and electron microscopy.<sup>9, 20</sup> Cell

populations were also analyzed by flow cytometry to determine (i) the cell surface exposure of phosphatidylserine, using Annexin V-FITC (Trevigen), and (ii) intracellular levels of active caspase 3, using a fluorochrome inhibitor of caspases (FLICA, Immunochemistry Technologies).

## Reagents

Etoposide were purchased from Sigma and was used at a concentration of 100  $\mu$ M respectively. TNF $\alpha$  was purchased from Invitrogen and was used at a concentration of 100 ng/ml. The cell permeable, synthetic, peptide inhibitors of caspase 3 (Ac-DEVD-CHO; Ac-Asp-Glu-Val-Asp-CHO) and caspase 8 (Ac-IETD-CHO; Ac-Ile-Asp-Thr-Glu-CHO) were purchased from Calbiochem and were used at a concentration of 10  $\mu$ M, which we have shown to be effective at inhibiting caspase activity in HEK293 cells.<sup>7</sup> The cell permeable inhibitor of NF- $\kappa$ B translocation, SN50, was purchased from Calbiochem and was used at a concentration of 18  $\mu$ M. Staurosporine (Sigma) was used at a concentration of 5  $\mu$ M. Antisense and sense oligonucleotides were prepared by Integrated DNA Technologies (IDT) at a concentration of 1  $\mu$ M following HPLC purification. Phosphothionate bonds present between nucleotides were included to enhance cell permeability. Antisense cFLIP: 5'-gattcagcagacatccat-3' and sense cFLIP: 5'-catccatcagacgacttcag-3' sequences were used.<sup>27,28</sup> Oligonucleotides were added directly to the media (10 nM) and cells were incubated for 18h prior to viral infection. Oligonucleotides were then added back to the media following infections.

## Electrophoretic mobility shift assay (EMSA)

Nuclear extracts were prepared from treated cells ( $5 \times 10^6$ ) by washing cells in PBS followed by incubation in hypotonic lysis buffer (10 mM HEPES [pH 7.9], 10 mM KCl, 1.5 mM MgCl<sub>2</sub>, 0.5 mM dithiothreitol, 0.5 mM phenylmethylsulfonylfluoride, and a protease inhibitor cocktail [Boehringer Mannheim]) at 4°C for 15 min. One-twentieth volume 10% NP-40 was added to the cell lysate and the

sample was vortexed for 10 s and centrifuged at 10,000 x g for 5 min. The nuclear pellet was washed once in hypotonic buffer, resuspended in high-salt buffer (25% glycerol, 20 mM HEPES [pH 7.9], 0.42 M NaCl, 1.5 mM MgCl<sub>2</sub>, 0.2 mM EDTA, 0.5 mM dithiothreitol, 0.5 mM phenylmethylsulfonylfluoride, and protease inhibitor cocktail), and incubated at 4°C for 2 to 3 h. Samples were centrifuged at 10,000 x g for 10 min and the supernatant was used as the nuclear extract.

Nuclear extracts were assayed for NF-κB activation by EMSA using a [<sup>32</sup>P]-labeled oligonucleotide consisting of the NF-κB consensus binding sequence (Santa Cruz Biotechnology). Nuclear extracts (5 to 10 µg total protein) were incubated with a binding reaction buffer containing 2 µg poly-dI-dC (Sigma) in the presence of 20 mM HEPES (pH 7.9), 60 mM KCl, 1 mM EDTA, 1 mM dithiothreitol, and 5% glycerol at 4°C for 20 min. Radiolabeled NF-κB consensus oligonucleotide (0.1 to 1.0 ng) was added, and the mixture was incubated at room temperature for 20 min. For competition experiments, ten-fold excess unlabeled consensus oligonucleotide or an oligonucleotide containing the SP-1 consensus site (Santa Cruz Biotechnology) were added to reaction mixtures. Nucleoprotein complexes were subjected to electrophoresis on native 5% polyacrylamide gels at 180V, dried under vacuum, and exposed to Biomax MR film (Kodak).

## Western Blot Analysis

Following infection with reovirus, cells were pelleted by centrifugation, washed twice with ice-cold phosphate-buffered saline and lysed by sonication in 200 µl of a buffer containing 15 mM Tris, pH 7.5, 2 mM EDTA, 10 mM EGTA, 20% glycerol, 0.1% NP-40, 50 mM β-mercaptoethanol, 100 µg/ml leupeptin, 2 µg/ml aprotinin, 40 µM Z-D-DCB, and 1 mM PMSF. The lysates were then cleared by centrifugation at 16,000 g for 5 min, normalized for protein amount, mixed 1:1 with SDS sample buffer (100 mM Tris, pH 6.8, 2% SDS, 300 mM β-mercaptoethanol, 30% glycerol, and 5% pyronine Y), boiled for 5 min and stored at -70°C. Proteins were electrophoresed by SDS-PAGE (10% gels) and probed with antibodies directed against IκBα (Santa Cruz # 203) and cFLIP (GeneTex # GTX26144) which recognizes the 55kD

cFLIPL (FLIP alpha) protein. All lysates were standardized for protein concentration with antibodies directed against actin (Oncogene #CP01). Autoradiographs were quantitated by densitometric analysis using a Fluor-S MultiImager (BioRad Laboratories).

### Immunocytochemistry

Primary cardiac myocytes were grown on 8-well chamber slides coated with rat-tail collagen (Becton Dickenson 354630). Cells were infected with reovirus 24 -26 h prior to fixation with 3.7% formaldehyde/phosphate-buffered saline (PBS) for 15 min at room temperature. Cells were subsequently permeabilized and blocked with 5% normal goat serum (Vector S1000) in PBS with 0.1% Tween 20 for 2 – 4 h at room temperature. Cells were incubated overnight at 4°C with antibodies directed against NF-κB (Santa Cruz, sc-8008) at a 1:30 dilution in blocking solution. After washing in PBS/0.1% Tween 20, cells were incubated with secondary anti-rabbit IgG conjugated to FITC (Vector FI 1200) for 1 h at room temperature before being counterstained with Hoechst 33342 (Molecular Probes H 3570) for 3min at room temperature. Cells were then washed in PBS/.1% Tween 20 and mounted with vectashield (Vector H1000) and digitally imaged using a Zeiss Axioplan2 epifluorescence microscope.

### Statistical Analysis

One-way analysis of variance (ANOVA) was performed using GraphPad InStat software.

## Results

Activation of NF-κB is not sufficient for apoptosis induced by prototype reovirus strains

The T3 prototype reovirus strain, T3A (APO+) induces significantly more apoptosis in infected HEK293 cells than the T1 prototype reovirus strain, T1L, as determined by nuclear morphology ( $P < 0.001$  at 48 h)

and caspase 3 activation assays ( $P < 0.001$ ) (Figure 1). We have previously shown that T3A infection induces the transient activation of NF- $\kappa$ B in infected HEK293 cells.<sup>19</sup> Thus at early times PI with T3A NF- $\kappa$ B is activated and translocates to the nucleus. However, at later times PI activated NF- $\kappa$ B is no longer present in the nuclei of T3A-infected cells. The activation of NF- $\kappa$ B following reovirus infection is required for T3A-induced apoptosis in HEK293 cells.<sup>19</sup> In addition, the ability of reovirus to inhibit NF- $\kappa$ B activation at later times PI may sensitize cells to TRAIL-induced apoptosis and may be required for apoptosis in TRAIL-resistant cells.<sup>19</sup>

To determine the importance of NF- $\kappa$ B regulation in reovirus-induced apoptosis we investigated NF- $\kappa$ B activation following infection with T1L (APO-). EMSA analysis, using nuclear extracts from T1L-infected HEK293 cells, was used to demonstrate the presence of activated NF- $\kappa$ B in the nucleus of T1L (APO-)-infected cells as early as 2 h PI. As expected, activated NF- $\kappa$ B was also present in the nucleus of T3A (APO+)-infected cells at early times PI (Figure 2). However, at late time PI (24 h) levels of activated NF- $\kappa$ B were reduced in the nuclei of T3A (APO+)-infected cells whilst remaining high in the nuclei of T1 (APO-)-infected cells.

These results demonstrate that T1L (APO-), in addition to T3A (APO+) activates NF- $\kappa$ B following infection of HEK293 cells, indicating that, although required for reovirus-induced apoptosis, NF- $\kappa$ B activity is not sufficient for apoptosis in infected cells. Our results also suggest that the inhibition of NF- $\kappa$ B seen at late times following infection with T3A (APO+), but not T1L (APO-), may be an additional requirement for reovirus-induced apoptosis.

T3A (APO+), but not T1L (APO-), inhibits stimulus-induced activation of NF- $\kappa$ B at later times post infection

The ability of T3A (APO+) to inhibit NF- $\kappa$ B activity at later times PI accounts for both the transient nature of NF- $\kappa$ B activation in reovirus-infected cells and the inhibition of stimulus-induced activation of

NF- $\kappa$ B.<sup>19</sup> Since reovirus-induced apoptosis is mediated by death ligands and since death ligand-induced apoptosis is enhanced in cells where NF- $\kappa$ B activity is blocked, the ability of reovirus to inhibit stimulus-induced activation likely promotes reovirus-induced apoptosis.<sup>19</sup> Having shown that T1L (APO-) induced activation of NF- $\kappa$ B is not followed by a later inhibition phase, we next investigated whether T1L (APO-) infection inhibited stimulus-induced activation of NF- $\kappa$ B. Both TNF and the topoisomerase-II inhibitor, etoposide, which are strong inducers of NF- $\kappa$ B, were used as stimuli for our experiments. HEK293 cells were infected with T1L (APO-) for 12 h before being treated with TNF and were harvested for EMSA analysis after a further 1 h (Figure 3A). T1L (APO-) did not inhibit the ability of TNF to activate NF- $\kappa$ B compared to mock-infected cells. In comparison T3A (APO+) completely inhibited TNF-induced activation of NF- $\kappa$ B (Figure 3A). Similar results were obtained using etoposide as the stimulus for NF- $\kappa$ B activation (not shown).

The degradation of I $\kappa$ B is required for NF- $\kappa$ B activation. We therefore also investigated the ability of reovirus to inhibit stimulus-induced degradation of I $\kappa$ B. HEK293 cells were infected with reovirus for 12 h prior to treatment with etoposide and were harvested for western blot analysis after a further 3 h. T3A (APO+), but not T1L (APO-), was found to inhibit etoposide-induced degradation of I $\kappa$ B (Figure 3B). Similar results were obtained using TNF as the stimulus for I $\kappa$ B degradation (not shown).

Activation of NF- $\kappa$ B by two different stimuli is thus inhibited at later times PI in T3A (APO+), but not T1L (APO-) infected HEK293 cells, again suggesting that the inhibition of NF- $\kappa$ B seen at late times following infection with T3A (APO+) may be required for reovirus-induced apoptosis.

Inhibition of stimulus-induced activation of NF- $\kappa$ B is determined by the T3A S1 gene segment and correlates with apoptosis in reovirus-infected cells

Having shown that T3A inhibits stimulus-induced activation of NF- $\kappa$ B, whereas T1L does not, we next wished to identify whether a specific viral gene determined this difference. HEK293 cells were infected with a panel of T1L x T3A reassortant reoviruses. Twelve h PI cells were treated with etoposide. Cells were then harvested after a further 3 h for western blot analysis using antibodies directed against I $\kappa$ B. The ability of different reassortant viruses to inhibit the etoposide-induced degradation of I $\kappa$ B seen in mock-infected cells and the derivation of the various genome segments of each virus is shown in Table 1. The S1 gene segment alone was identified as being significantly associated with strain-specific differences in virus-induced inhibition of etoposide-induced I $\kappa$ B degradation (*t* test,  $P = 0.0008$ ; M-W test,  $P = 0.0159$ ). Although statistical analysis identified the T3A S1 gene segment as an important determining factor in the ability of reoviruses to inhibit stimulus-induced degradation of I $\kappa$ B it is important to note that reassortant viruses containing the T3A S1 gene segment in the presence of other gene segments derived from T1L show reduced apoptosis. This indicates that it is likely that other T3A gene segments also play a role in apoptosis following viral infections.

Since the T3 S1 gene segment has previously been shown to be the primary determinant of reovirus-induced apoptosis we next investigated the correlation between inhibition of etoposide-induced degradation of I $\kappa$ B and apoptosis following infection of HEK293 cells with the T3A X T1L reassortant viruses (Table 1, Figure 4A).<sup>20, 21</sup> Using linear regression analysis we obtained an  $R^2$  value of 0.89 ( $P = 0.0001$ ) indicating a significant correlation between apoptosis induction and inhibition of etoposide-induced degradation of I $\kappa$ B.

Infection of neonatal mice with the reassortant reovirus 8B<sup>25</sup> induces myocarditis.<sup>29, 30</sup> We have shown that apoptosis is a key mechanism by which 8B induces myocarditic cell death and tissue injury in infected animals.<sup>4, 31</sup> A second panel of reovirus reassortants that differ in myocarditic potential were therefore investigated for their ability to induce apoptosis and to inhibit stimulus-induced activation of NF- $\kappa$ B in HEK293 cells.<sup>24</sup> These viruses again revealed a significant correlation ( $R^2 = 0.91$ ,  $P = 0.0004$ ) between the ability to induce apoptosis and inhibition of stimulus-induced degradation of I $\kappa$ B (Table 2,

Figure 4B). Among the reassortants tested a high level of apoptosis and a high degree of inhibition of stimulus-induced activation of NF- $\kappa$ B were required for the myocarditic phenotype (Figure 4B).

These results demonstrate that inhibition of stimulus-induced activation of NF- $\kappa$ B is strongly correlated with apoptosis induction following reovirus-infection of HEK293 cells.

Reovirus-induced inhibition of stimulus-induced activation of NF- $\kappa$ B is associated with apoptosis in a pathogenic model of reovirus infection

Infection of primary cardiac myocytes has been used to investigate the mechanisms of cell death that result in viral-induced myocarditis.<sup>4, 32-35</sup> We used this model to explore the association of viral-induced inhibition of stimulus-induced activation of NF- $\kappa$ B and apoptosis during viral pathogenesis. Myocytes were mock-infected or were infected with either the strongly myocarditic reovirus reassortant 8B or the weakly myocarditic virus T1L. Twenty four h PI cells were then treated with staurosporine (NF- $\kappa$ B activating stimulus) and after a further 2 h the number of cells containing nuclear (active) NF- $\kappa$ B was determined by immunocytochemistry (Figure 5A). Following mock-infection staurosporine induced the nuclear translocation (activation) of NF- $\kappa$ B, as expected. Infection with 8B, but not T1L, inhibited staurosporine-induced activation of NF- $\kappa$ B. Consistent with our results in HEK293 cells, 8B, but not T1L, also induced apoptosis in primary cardiac myocytes (Figure 5B).

These results demonstrate that reovirus-induced inhibition of stimulus-induced activation of NF- $\kappa$ B is associated with apoptosis in primary cardiac myocytes.

Inhibition of NF- $\kappa$ B promotes apoptosis in reovirus-infected cells

Our results suggest that, in addition to the initial activation of NF- $\kappa$ B,<sup>18,19</sup> reovirus-induced apoptosis also requires a later phase of NF- $\kappa$ B regulation where stimulus-induced activation of NF- $\kappa$ B is inhibited in infected cells. To confirm the contribution of this later, inhibitory, phase to reovirus-induced apoptosis we investigated the effect of a cell permeable inhibitor of NF- $\kappa$ B (SN50), which functions to inhibit nuclear translocation of NF- $\kappa$ B, on reovirus-induced apoptosis. Primary cardiac myocytes were infected with 8B (APO+) or T1L (APO-) in the presence or absence of SN50 and were assayed for apoptosis after 48 h by nuclear morphology assays. As expected, 8B (APO+) induced high levels of apoptosis in infected primary cardiac myocytes at 48 h PI. This apoptosis was not inhibited following treatment of cells with SN50 (Figure 6A), suggesting that reovirus-induced apoptosis in primary cardiac myocytes does not require NF- $\kappa$ B activation. In fact, SN50-treatment resulted in a small increase in 8B-induced apoptosis. Also as expected, T1L did not induce apoptosis in infected primary cardiac myocytes (Figure 6A). However, in SN50-treated cells the ability of T1L-induced apoptosis increased significantly ( $P < 0.05$ ) from 11 to 42%. These results demonstrate that NF- $\kappa$ B inhibition promotes apoptosis following reovirus infection of primary cardiac myocytes and suggest that the ability of reoviruses to inhibit stimulus-induced activation of NF- $\kappa$ B is a pro-apoptotic event.

In contrast, apoptosis is not required for inhibition of stimulus-induced activation of NF- $\kappa$ B following T3 reovirus infection (Figure 6B). HEK293 cells were infected with reovirus for 12 h prior to treatment with etoposide. After a further 3 h cells were then harvested for western blot analysis using antibody directed against I $\kappa$ B. Inhibition of apoptosis by expression of FADD-DN or treatment with inhibitors of caspase 3 (Ac-DEVD-CHO) or caspase 8 (Ac-IETD-CHO) did not block inhibition of stimulus-induced degradation of I $\kappa$ B following reovirus infection.

### T3 reoviruses inhibit cFLIP expression

NF- $\kappa$ B regulates the expression of several cellular genes that function to inhibit apoptosis, including cFLIP, the cellular inhibitor of caspase 8.<sup>36</sup> To determine whether the inhibition of NF- $\kappa$ B-regulated genes following reovirus-infection contributed to an apoptotic phenotype we investigated cFLIP expression in reovirus-infected cells. HEK293 cells were infected with reovirus and were harvested at various times post infection for western blot analysis using antibodies directed against cFLIP. Following infection with both T1L (APO-) and T3A (APO+)-infection cFLIP levels increased, as would be expected consequent to the early activation of NF- $\kappa$ B in reovirus-infected cells (Figure 7A). This increase in cFLIP activation was not seen following T3A-infection of cells expressing the NF- $\kappa$ B super-repressor, I $\kappa$ B $\Delta$ N2. Since the expression of I $\kappa$ B $\Delta$ N2 prevents NF- $\kappa$ B activation, this indicated that activation of NF- $\kappa$ B was required for reovirus induced increases in cFLIP. The requirement of NF- $\kappa$ B for reovirus-induced activation of cFLIP was confirmed using the NF- $\kappa$ B inhibitor, SN50, which also inhibited up-regulation of cFLIP in T3A-infected cells (Figure 7B). At later times PI cFLIP levels dropped in T3A-infected cells, consistent with the shut-off of NF- $\kappa$ B activation in these cells (Figure 7A). In contrast, following T1L (APO-) infection levels of cFLIP increased and then remained stable. These results suggest that falling levels of cFLIP are associated with enhanced apoptosis in reovirus-infected cells (Figure 7A).

We next used antisense oligonucleotides directed against cFLIP<sup>28</sup> to determine the effect of reduced cFLIP expression on reovirus-induced apoptosis. At a concentration of 10  $\mu$ M antisense cFLIP oligonucleotides decreased T1L-induced up-regulation of cFLIP (Figure 7C) and significantly ( $P < 0.001$ ) increased T1L induced-apoptosis from 21% to 41% (Figure 7D). In contrast sense cFLIP oligonucleotides did not decrease T1L-induced up-regulation of cFLIP and did not increase T1L-induced apoptosis. Neither sense nor antisense cFLIP oligonucleotides changed apoptosis induced by T3A (Figure 7D).

## Discussion

The NF- $\kappa$ B pathway provides an attractive target to viral pathogens for modulating host cell events. Activation of NF- $\kappa$ B is a rapid immediate early response that occurs within minutes after exposure to a

relevant inducer, which does not require de novo protein synthesis and which can promote the expression of over 100 cellular genes, including genes that participate in the host immune response, oncogenesis and regulation of apoptosis. NF-κB is activated by many viruses, including human immunodeficiency virus-a (HIV-1),<sup>37</sup> human T cell leukemia virus-1,<sup>38</sup> hepatitis B virus,<sup>39</sup> hepatitis C virus (HCV),<sup>40,41</sup> Epstein Barr Virus,<sup>42</sup> rotavirus<sup>43</sup> and influenza virus<sup>44</sup> to promote viral replication, prevent virus-induced apoptosis, and mediate the immune response to the invading pathogen.<sup>45</sup> In contrast, activation of NF-κB by Sindbis<sup>46,47</sup> and Dengue virus<sup>48</sup> is associated with the induction of apoptosis, which may increase viral spread. In still other cases, proteins encoded by adenovirus,<sup>49</sup> HCV<sup>50</sup> and African swine fever virus<sup>51</sup> inhibit NF-κB activity to enhance replication or contribute to viral pathogenicity.

T3 strains of reovirus (APO+) induce the activation of NF-κB in epithelial cell lines and this activation is required for apoptosis in infected cells.<sup>18,19</sup> However, we now demonstrate that T1L, which induces significantly less apoptosis than T3A, activates NF-κB to a similar degree (Figure 2). This suggests that although required for apoptosis, reovirus-induced activation of NF-κB is not sufficient for apoptosis in infected cells.

Reovirus strain T3A (APO+) induces a second phase of NF-κB regulation in infected cells where the activation of NF-κB is inhibited at later times PI.<sup>19</sup> This inhibition results in both the transient nature of NF-κB activation following infection with T3A (APO+) and in the inhibition of NF-κB activation following treatment of cells with external stimuli, such as TNF or etoposide.<sup>19</sup> T1L (APO-) does not induce this second phase of NF-κB regulation. Thus T1L (APO-)-induced activation of NF-κB is sustained and activated NF-κB is present in the nucleus of infected cells at late times post infection (Figure 2). Further, T1L (APO-) does not inhibit stimulus-induced activation of NF-κB (Figure 3). These results suggest that reovirus-induced inhibition of NF-κB at later times PI is also required for apoptosis in infected cells and is supported by our demonstration that inhibition of stimulus-induced degradation of IκB is determined by the T3A S1 gene segment, which also determines reovirus-induced apoptosis.<sup>20,21</sup> In

addition, the ability of reoviruses to inhibit stimulus-induced degradation of I $\kappa$ B correlates with apoptosis following infection with two independent panels of reovirus reassortants (Figure 4).

The reovirus S1 gene segment encodes 2 viral proteins, the viral attachment protein  $\sigma$ 1 and the non-structural protein  $\sigma$ 1s both of which may contribute to the apoptosis in reovirus-infected cells.  $\sigma$ 1s is the determinant of reovirus-induced G<sub>2</sub>/M cell cycle arrest, an effect that results from inhibition of the G<sub>2</sub>/M regulatory kinase p34<sup>cdc2</sup>.<sup>52,53</sup>  $\sigma$ 1s contains a nuclear localization sequence and causes dramatic changes in nuclear architecture in infected cells.<sup>54</sup> Although it is not required for reovirus-induced apoptosis of L929 or HEK293 cells,<sup>52</sup>  $\sigma$ 1s enhances both the kinetics and extent of reovirus-induced apoptosis *in vivo* by as yet undefined mechanism.<sup>55</sup>

In virions, the reovirus  $\sigma$ 1 protein is a homotrimer comprised of an elongated fibrous tail, which inserts into the virion, and an externally facing globular head.<sup>56</sup> The heads of both reovirus T1 and T3  $\sigma$ 1 proteins contain a binding domain for junctional adhesion molecule (JAM), which serves as the primary reovirus receptor.<sup>57</sup> In addition, the fibrous tail of the T3 reovirus  $\sigma$ 1 protein contains a domain that binds  $\alpha$ -linked sialic acid.<sup>58</sup> Type 3 reovirus binding to both JAM and sialic acid are required for reovirus-induced activation of NF- $\kappa$ B and apoptosis.<sup>23</sup> The S1 gene segment of T3, but not T1L, reoviruses, is also associated with the ability to induce the activation of the c-Jun N-terminal kinase (JNK), which is also required for reovirus-induced apoptosis.<sup>59,60</sup> Together, these results suggest that reovirus-induced apoptosis is induced by the activation of cellular signaling pathways early in viral infection. We therefore predict that signaling pathways induced by reovirus binding will bring about the inhibition of NF- $\kappa$ B seen following T3 infection.

Reovirus-induced apoptosis is mediated in epithelial cells by TNF related death-inducing ligand (TRAIL) and is blocked by reagents that inhibit TRAIL binding to its apoptosis-associated receptors, death receptors (DRs) 4 and 5.<sup>6</sup> Reovirus-induced apoptosis is also blocked by reagents that inhibit signaling events downstream of TRAIL-receptor binding.<sup>6</sup> NF- $\kappa$ B has the ability to influence TRAIL-signaling pathways in two ways. Firstly, NF- $\kappa$ B can act in a pro-apoptotic manner by up-regulating the

expression of both TRAIL and its receptors.<sup>61-64</sup> The increase in levels of DR5 protein expression seen following reovirus infection of HEK293 cells and the release of TRAIL from infected cells may thus reflect virus-induced activation of NF-κB.<sup>6</sup>

Death receptor signaling pathways are commonly used by viruses to induce apoptosis. For example, HIV infection increases the expression of TRAIL and sensitizes T-cells to TRAIL-mediated apoptosis.<sup>65</sup> In addition, alteration of the cell surface expression of Fas may be involved in virus-induced, or viral regulation of, apoptosis in cells infected with influenza virus,<sup>66, 67</sup> herpes simplex virus type 2,<sup>68</sup> bovine herpesvirus 4 (BHV 4),<sup>69</sup> adenovirus<sup>70</sup> and HIV-1.<sup>71, 72</sup> Similarly, apoptosis induced by Hepatitis B virus,<sup>73</sup> HIV-1,<sup>74</sup> BHV 4<sup>69</sup> and parvovirus H-1<sup>75</sup> may involve the TNF receptor signaling pathway. NF-κB regulation is thus likely to have implications for death ligand-mediated apoptosis and disease resulting from a variety of viral infections.

NF-κB also regulates many genes encoding proteins with anti-apoptotic properties, including cFLIP,<sup>36</sup> which can inhibit DR-induced apoptosis. Our results show that cFLIP is regulated by NF-κB following reovirus infection and that inhibition of cFLIP can promote apoptosis in T1L-reovirus infected cells. We thus propose that following infection of HEK293 cells TRAIL-mediated apoptosis is first initiated by the activation of NF-κB and then enhanced by the later inhibition phase which results in the down-regulation of cFLIP. Inhibition of cFLIP in T1L infected cells does not increase apoptosis to levels seen following infection with T3A suggesting that additional pro-apoptotic mechanisms, are present in T3A, but not T1L-infected cells. These could include the down-regulation of additional NF-κB-dependent anti-apoptotic genes. Alternatively, it is possible that the sustained activation of NF-κB in T1L-infected cells, may prevent apoptosis through the up-regulation of as yet unidentified genes.

Reovirus infection of primary cardiac myocytes has been used to investigate the mechanisms of cell death that result in tissue injury.<sup>4, 32-35</sup> We have previously shown that apoptosis is a key mechanism by which reovirus induces myocarditic cell death and tissue injury in infected animals.<sup>4, 31</sup> We now show that in contrast to results in HEK293 cells, activation of NF-κB is not required for reovirus-induced

apoptosis in primary cardiac myocytes (Figure 6). In addition, 8B induces apoptosis in the hearts of infected p50<sup>-/-</sup> mice to a similar degree to that seen in wild type controls (not shown). The requirement of NF-κB activation for reovirus-induced apoptosis may therefore be cell-type specific. However, our demonstration that 8B (myocarditic), but not T1L (non-myocarditic), induces both the inhibition of stimulus-induced activation of NF-κB and apoptosis in infected primary cardiac myocytes (Figure 5) suggests that reovirus-induced inhibition of stimulus-induced activation of NF-κB contributes to viral-induced myocarditis. We further show that chemical inhibition of NF-κB enhances T1L-induced apoptosis in these cells (Figure 6).

### Acknowledgements

Work supported by the National Institute of Health (5K08AI52261-03, R. L. D.), the Department of Veterans Affairs (Merit and REAP grants, K. L. T.), the U.S. Army Medical Research and Material Command (DAMD17-98-1-8614, K. L. T.), the Reuler-Lewin Family Professorship of Neurology (K. L. T.) and the Ovarian Cancer Research Fund (P. C.).

### References

1. Clarke P, Tyler KL. Reovirus-induced apoptosis: A minireview. *Apoptosis* 2003; **8**: 141-150.
2. Oberhaus SM, Smith RL, Clayton GH, Dermody TS, Tyler KL. Reovirus infection and tissue injury in the mouse central nervous system are associated with apoptosis. *J. Virol.* 1997; **71**: 2100-2106.
3. Richardson-Burns SM, Kominsky DJ, Tyler KL. Reovirus-induced neuronal apoptosis is mediated by caspase 3 and is associated with the activation of death receptors. *J. Neuroviro.* 2002; **8**: 365-380.

4. DeBiasi RL, Edelstein CL, Sherry B, Tyler KL. Calpain inhibition protects against virus-induced apoptotic myocardial injury. *J. Virol.* 2001; **75**: 351-361.
5. Richardson-Burns SM, Tyler KL. Regional differences in viral growth and central nervous system injury correlate with apoptosis. *J. Virol.* 2004; **78**: 5466-5475.
6. Clarke P, Meintzer SM, Gibson S, et al. Reovirus-induced apoptosis is mediated by TRAIL. *J. Virol.* 2000; **74**: 8135-8139.
7. Kominsky DJ, Bickel RJ, Tyler KL. Reovirus-induced apoptosis requires both death receptor- and mitochondrial-mediated caspase-dependent pathways of cell death. *Cell Death Differ.* 2002; **9**: 926-933.
8. Kominsky DJ, Bickel RJ, Tyler KL. Reovirus-induced apoptosis requires mitochondrial release of Smac/DIABLO and involves reduction of cellular inhibitor of apoptosis protein levels. *J. Virol.* 2002; **76**: 11414-11424.
9. Clarke P, Meintzer SM, Spalding AC, Johnson GL, Tyler KL. Caspase 8-dependent sensitization of cancer cells to TRAIL-induced apoptosis following reovirus-infection. *Oncogene* 2001; **20**: 6910-6919.
10. Baeuerle PA, Baltimore D. A 65-kappaD subunit of active NF-kappaB is required for inhibition of NF-kappaB by I kappaB. *Genes Dev.* 1989; **3**: 1689-1698.
11. Ghosh S, Gifford AM, Riviere LR, Tempst P, Nolan GP, Baltimore D. Cloning of the p50 DNA binding subunit of NF-kappa B: homology to rel and dorsal. *Cell* 1990; **62**: 1019-1029.
12. Baeuerle PA, Baltimore D. I kappa B: a specific inhibitor of the NF-kappa B transcription factor. *Science* 1988; **242**: 540-546.

13. Verma IM, Stevenson JK, Schwarz EM, Van Antwerp D, Miyamoto S. Rel/NF-kappa B/I kappa B family: intimate tales of association and dissociation. *Genes Dev.* 1995; **9**: 2723-2735.
14. Brockman JA, Scherer DC, McKinsey TA. et al. Coupling of a signal response domain in I kappa B alpha to multiple pathways for NF-kappa B activation. *Mol. Cell Biol.* 1995; **15**: 2809-2818.
15. Brown K, Gerstberger S, Carlson L, Franzoso G, Siebenlist U. Control of I kappa B-alpha proteolysis by site-specific, signal-induced phosphorylation. *Science* 1995; **267**: 1485-1488.
16. Chen Z, Hagler J, Palombella VJ, et al. Signal-induced site-specific phosphorylation targets I kappa B alpha to the ubiquitin-proteasome pathway. *Genes Dev.* 1995; **9**: 1586-1597.
17. Traenckner EB, Pahl HL, Henkel T, Schmidt KN, Wilk S, Baeuerle PA. Phosphorylation of human I kappa B-alpha on serines 32 and 36 controls I kappa B-alpha proteolysis and NF-kappa B activation in response to diverse stimuli. *EMBO J.* 1995; **14**: 2876-2883.
18. Connolly JL, Rodgers SE, Clarke P, et al. Reovirus-induced apoptosis requires activation of transcription factor NF-kappaB. *J. Virol.* 2000; **74**: 2981-2989.
19. Clarke P, Meintzer SM, Moffitt LA, Tyler KL. Two distinct phases of virus-induced nuclear factor kappa B regulation enhance tumor necrosis factor-related apoptosis-inducing ligand-mediated apoptosis in virus-infected cells. *J. Biol. Chem.* 2003; **278**: 18092-18100.
20. Tyler KL, Squier MK, Rodgers SE, et al. Differences in the capacity of reovirus strains to induce apoptosis are determined by the viral attachment protein sigma 1. *J. Virol.* 1995; **69**: 6972-6979.
21. Tyler KL, Squier MK, Brown AL, et al. Linkage between reovirus-induced apoptosis and inhibition of cellular DNA synthesis: role of the S1 and M2 genes. *J. Virol.* 1996; **70**: 7984-7991.

22. Rodgers SE, Barton ES, Oberhaus SM, et al. Reovirus-induced apoptosis of MDCK cells is not linked to viral yield and is blocked by Bcl-2. *J. Virol.* 1997; **71**: 2540-2546.
23. Connolly JL, Barton ES, Dermody TS. Reovirus binding to cell surface sialic acid potentiates virus-induced apoptosis. *J. Virol.* 2001; **75**: 4029-4039.
24. Wilson GA, Morrison LA, Fields BN. Association of the reovirus S1 gene with serotype 3-induced biliary atresia in mice. *J. Virol.* 1994; **68**: 6458-6465.
25. Sherry B, Fields BN. The reovirus M1 gene, encoding a viral core protein, is associated with the myocarditic phenotype of a reovirus variant. *J. Virol.* 1989; **63**: 4850-4856.
26. Sherry B, Blum MA. Multiple viral core proteins are determinants of reovirus-induced acute myocarditis. *J. Virol.* 1994; **68**: 8461-8465.
27. Perlman H, Pagliari LJ, Georganas C, Mano T, Walsh K, Pope RM. FLICE-inhibitory protein expression during macrophage differentiation confers resistance to Fas-mediated apoptosis. *J. Exp. Med.* 1999; **190**: 1679-1688.
28. Okano H, Shiraki K, Inoue H, et al. Cellular FLICE/caspase-8-inhibitory protein as a principal regulator of cell death and survival in human hepatocellular carcinoma. *Lab. Invest.* 2003; **83**: 1033-1043.
29. Sherry B. Pathogenesis of reovirus myocarditis. In K. L. Tyler and M. B. A. Oldstone (ed.) *Reoviruses II: Cytopathogenicity and Pathogenesis*. Springer-Verlag, Berlin, Germany 1998: p51-66
30. Sherry B, Schoen FJ, Wenske E, Fields BN. Derivation and characterization of an efficiently myocarditic reovirus variant. *J. Virol.* 1989; **63**: 4840-4849.

31. DeBiasi RL, Robinson BA, Sherry B, et al. Caspase inhibition protects against reovirus-induced myocardial injury in vitro and in vivo. *J. Virol.* 2004; **78**: 11040-11050.
32. Stewart MJ, Blum MA, Sherry B. PKR's protective role in viral myocarditis. *Virology* 2003; **314**: 92-100.
33. Azzam-Smoak K, Noah DL, Stewart MJ, Blum MA, Sherry B. Interferon regulatory factor-1, interferon-beta, and reovirus-induced myocarditis. *Virology* 2002; **298**: 20-29.
34. Sherry B, Torres J, Blum MA. Reovirus induction of and sensitivity to beta interferon in cardiac myocyte cultures correlate with induction of myocarditis and are determined by viral core proteins. *J. Virol.* 1998; **72**: 1314-1323.
35. Noah DL, Blum MA, Sherry B. Interferon regulatory factor 3 is required for viral induction of beta interferon in primary cardiac myocyte cultures. *J. Virol.* 1999; **73**: 10208-10213.
36. Kreuz S, Siegmund D, Scheurich P, Wajant H. NF-kappaB inducers upregulate cFLIP, a cycloheximide-sensitive inhibitor of death receptor signaling. *Mol. Cell Biol.* 2001; **21**: 3964-3973.
37. Roulston A, Lin R, Beauparlant P, Wainberg MA, Hiscott J. Regulation of human immunodeficiency virus type 1 and cytokine gene expression in myeloid cells by NF-kappa B/Rel transcription factors. *Microbiol. Rev.* 1995; **59**: 481-505.
38. Sun SC, Ballard DW. Persistent activation of NF-kappaB by the tax transforming protein of HTLV-1: hijacking cellular IkappaB kinases. *Oncogene* 1999; **18**: 6948-6958.
39. Weil R, Sirma H, Giannini C, et al. Direct association and nuclear import of the hepatitis B virus X protein with the NF-kappaB inhibitor IkappaBalph. *Mol. Cell Biol.* 1999; **19**: 6345-6354.

40. You LR, Chen CM, Lee YH. Hepatitis C virus core protein enhances NF-kappaB signal pathway triggering by lymphotoxin-beta receptor ligand and tumor necrosis factor alpha. *J. Virol.* 1999; **73**: 1672-1681.
41. Tai DI, Tsai SL, Chen YM, et al. Activation of nuclear factor kappaB in hepatitis C virus infection: implications for pathogenesis and hepatocarcinogenesis. *Hepatology* 2000; **31**: 656-664.
42. Sylla BS, Hung SC, Davidson DM, et al. Epstein-Barr virus-transforming protein latent infection membrane protein 1 activates transcription factor NF-kappaB through a pathway that includes the NF-kappaB-inducing kinase and the IkappaB kinases IKKalpha and IKKbeta. *Proc. Natl. Acad. Sci. U. S. A.* 1998; **95**: 10106-10111.
43. Casola A, Garofalo RP, Crawford SE, et al. Interleukin-8 gene regulation in intestinal epithelial cells infected with rotavirus: role of viral-induced IkappaB kinase activation. *Virology* 2002; **298**: 8-19.
44. Pahl HL, Baeuerle PA. The ER-overload response: activation of NF-kappa B. *Trends Biochem. Sci.* 1997; **22**: 63-67.
45. Hiscott J, Kwon H, Genin P. Hostile takeovers: viral appropriation of the NF-kappaB pathway. *J. Clin. Invest.* 2001; **107**: 143-151.
46. Lin KI, Lee SH, Narayanan R, Baraban JM, Hardwick JM, Ratan RR. Thiol agents and Bcl-2 identify an alphavirus-induced apoptotic pathway that requires activation of the transcription factor NF-kappa B. *J. Cell Biol.* 1995; **131**: 1149-1161.
47. Lin KI, DiDonato JA, Hoffmann A, Hardwick JM, Ratan RR. Suppression of steady-state, but not stimulus-induced NF-kappaB activity inhibits alphavirus-induced apoptosis. *J. Cell Biol.* 1998; **141**: 1479-1487.

48. Jan JT, Chen BH, Ma SH, et al. Potential dengue virus-triggered apoptotic pathway in human neuroblastoma cells: arachidonic acid, superoxide anion, and NF-kappaB are sequentially involved. *J. Virol.* 2000; **74**: 8680-8691.
49. Shao R, Hu MC, Zhou BP, et al. E1A sensitizes cells to tumor necrosis factor-induced apoptosis through inhibition of IkappaB kinases and nuclear factor kappaB activities. *J. Biol. Chem.* 1999; **274**: 21495-21498.
50. Shrivastava A, Manna SK, Ray R, Aggarwal BB. Ectopic expression of hepatitis C virus core protein differentially regulates nuclear transcription factors. *J. Virol.* 1998; **72**: 9722-9728.
51. Powell PP, Dixon LK, Parkhouse RM. An IkappaB homolog encoded by African swine fever virus provides a novel mechanism for downregulation of proinflammatory cytokine responses in host macrophages. *J. Virol.* 1996; **70**: 8527-8533.
52. Poggioli GJ, Keefer C, Connolly JL, Dermody TS, Tyler KL. Reovirus-induced G<sub>2</sub>/M cell cycle arrest requires σ1s and occurs in the absence of apoptosis. *J. Virol.* 2000; **74**: 9562-9570.
53. Poggioli GJ, Dermody TS, Tyler KL. Reovirus-induced σ1s-dependent G2/M phase cell cycle arrest is associated with inhibition of p34cdc2. *J. Virol.* 2001; **75**: 7429-7434.
54. Hoyt CC, Bouchard RJ, Tyler KL. Novel nuclear herniations induced by nuclear localization of a viral protein. *J. Virol.* 2004; **78**: 6360-6369.
55. Hoyt CC, Richardson-Burns S M, Goody RJ, Robinson BA, Debiasis RL, Tyler KL. Non-structural protein σ1s is a determinant of reovirus virulence and influences the kinetics and severity of apoptosis in the heart and CNS. *J. Virol.* 2005; **79**, (In Press)
56. Chappell JD, Prota AE, Dermody TS, Stehle T. Crystal structure of reovirus attachment protein sigma 1 reveals evolutionary relationship to adenovirus fiber. *EMBO J.* 2002; **15**: 1-11.

57. Barton ES, Forrest JC, Connolly JL, et al. Junction adhesion molecule is a receptor for reovirus. *Cell* 2001; **104**: 441-451.
58. Chappell JD, Duong JL, Wright BW, Dermody TS. Identification of carbohydrate-binding domains in the attachment proteins of Type 1 and Type 3 reoviruses. *J. Virol.* 2000; **74**: 8472-8479.
59. Clarke P, Meintzer SM, Widmann C, Johnson GL, Tyler KL. Reovirus infection activates JNK and the JNK-dependent transcription factor c-Jun. *J. Virol.* 2001; **75**: 11275-11283.
60. Clarke P, Meintzer SM, Wang Y, et al. JNK regulates the release of proapoptotic mitochondrial factors in reovirus-infected cells. *J. Virol.* 2004; **78**: 13132-13138.
61. Gibson SB, Oyer R, Spalding AC, Anderson SM, Johnson GL. Increased expression of death receptors 4 and 5 synergizes the apoptosis response to combined treatment with etoposide and TRAIL. *Mol. Cell Biol.* 2000; **20**: 205-212.
62. Ravi R, Bedi GC, Engstrom LW, et al. Regulation of death receptor expression and TRAIL/Apo2L-induced apoptosis by NF-kappaB. *Nat. Cell Biol.* 2001; **3**: 409-416.
63. Spalding AC, Jotte RM, Scheinman RI, et al. TRAIL and inhibitors of apoptosis are opposing determinants for NF-kappaB-dependent, genotoxin-induced apoptosis of cancer cells. *Oncogene* 2002; **21**: 260-271.
64. Rivera-Walsh I, Waterfield M, Xiao G, Fong A, Sun SC. NF-kappaB signaling pathway governs TRAIL gene expression and human T-cell leukemia virus-I Tax-induced T-cell death. *J. Biol. Chem.* 2001; **276**: 40385-40388.
65. Jeremias I, Herr I, Boehler T, Debatin KM. TRAIL/Apo-2-ligand-induced apoptosis in human T cells. *Eur. J. Immunol.* 1998; **28**: 143-152.

66. Takizawa T, Matsukawa S, Higuchi Y, Nakamura S, Nakanishi Y, Fukuda R. Induction of programmed cell death (apoptosis) by influenza virus infection in tissue culture cells. *J. Gen. Virol.* 1993; **74**: 2347-2355.
67. Takizawa T, Fukuda R, Miyawaki T, Ohashi K, Nakanishi Y. Activation of the apoptotic Fas antigen-encoding gene upon influenza virus infection involving spontaneously produced beta-interferon. *Virology* 1995; **209**: 288-296.
68. Sieg S, Yildirim Z, Smith D, et al. Herpes simplex virus type 2 inhibition of Fas ligand expression. *J. Virol.* 1996; **70**: 8747-8751.
69. Wang GH, Bertin J, Wang Y, et al. Bovine herpesvirus 4 BORFE2 protein inhibits Fas- and tumor necrosis factor receptor 1-induced apoptosis and contains death effector domains shared with other gamma-2 herpesviruses. *J. Virol.* 1997; **71**: 8928-8932.
70. Tollefson AE, Hermiston TW, Lichtenstein DL, et al. Forced degradation of Fas inhibits apoptosis in adenovirus-infected cells. *Nature* 1998; **392**: 726-730.
71. Conaldi PG, Biancone L, Bottelli A, et al. HIV-1 kills renal tubular epithelial cells in vitro by triggering an apoptotic pathway involving caspase activation and Fas upregulation. *J. Clin. Invest* 1998; **102**: 2041-2049.
72. Kaplan D, Sieg S. Role of the Fas/Fas ligand apoptotic pathway in human immunodeficiency virus type 1 disease. *J. Virol.* 1998; **72**: 6279-6282.
73. Su F, Schneider RJ. Hepatitis B virus HBx protein sensitizes cells to apoptotic killing by tumor necrosis factor alpha. *Proc. Natl. Acad. Sci. U. S. A* 1997; **94**: 8744-8749.
74. Herbein G, Mahlknecht U, Batliwalla F, et al. Apoptosis of CD8+ T cells is mediated by macrophages through interaction of HIV gp120 with chemokine receptor CXCR4. *Nature* 1998; **395**: 189-194.

75. Johnson DE, Gastman BR, Wieckowski E, et al. Inhibitor of apoptosis protein hILP undergoes caspase-mediated cleavage during T lymphocyte apoptosis. *Cancer Res.* 2000; **60**: 1818-1823.

## Figure Legends

**Figure 1.** T3A induces significantly more apoptosis in infected HEK293 cells than T1L. HEK293 cells were infected with reovirus strains T3A (black bars) and T1L (gray bars). Cells were harvested 24 and 48 h PI. The graphs show the mean percentage of cells (above the percentage seen following mock-infection) containing apoptotic nuclei (A) and active caspase 3 (B) from three independent experiments. Error bars represent standard errors of the mean.

**Figure 2.** Activation of NF- $\kappa$ B following reovirus infection. HEK293 cells were infected with reovirus strains T3A or T1L for the indicated times. Nuclear extracts were then prepared and EMSA analysis was performed using a radiolabeled oligonucleotide probe comprising NF- $\kappa$ B binding sequences. Shifted bands, corresponding to activated NF- $\kappa$ B: DNA complexes are indicated. The specificity of the probe sequences was confirmed by including a 10-fold excess of cold oligonucleotides comprising NF- $\kappa$ B ( $\kappa$ B) or SP6 (SP) binding sequences in reactions using nuclear extracts from T3A-infected cells (4 h PI).

**Figure 3.** Inhibition of stimulus-induced activation of NF- $\kappa$ B following reovirus infection. HEK293 cells were infected with T3A and T1L strains of reovirus or were mock-infected. (A) Twelve h PI cells were treated with TNF or were left untreated. After a further 1 h cells were harvested for EMSA analysis using a radiolabelled oligonucleotide probe comprising NF- $\kappa$ B binding sequences. Shifted bands, corresponding to activated NF- $\kappa$ B: DNA complexes are indicated. (B) Twelve h PI cells were treated with etoposide or were left untreated. After a further 3 h cells were harvested for western blot analysis using antibodies directed against I $\kappa$ B. Antibodies directed against actin were used to control for protein loading.

**Figure 4.** Inhibition of stimulus-induced degradation of I $\kappa$ B is correlated with apoptosis in reovirus-infected cells. The ability of T3A x T1L (A) and 8B x T1L (B) reassortant reoviruses and the parental

strains to inhibit etoposide-induced degradation of I $\kappa$ B was plotted against their ability to induce apoptosis. Values were obtained from Tables 1 and 2. Each point represents a single virus strain or reassortant. Diamond shaped points indicate viruses with myocarditic potential.

**Figure 5.** The myocarditic reassortant 8B inhibits stimulus-induced activation of NF- $\kappa$ B and induces apoptosis in primary cardiac myocytes whereas the T1L (non-myocarditic) does not. Primary cardiac myocytes were mock-infected (clear bars) or were infected with either the myocarditic reovirus (Reo) reassortant 8B (black bars) or the non-myocarditic reovirus (Reo) T1L (gray bars). (A) Twenty four h PI cells were then treated with staurosporine (NF- $\kappa$ B activating stimulus) and after a further 2 h the number of cells containing nuclear (active) NF- $\kappa$ B was determined by immunocytochemistry. The graph shows the mean percentage of cells containing nuclear NF- $\kappa$ B for 3 different fields of view. Error bars represent standard deviations. (B) Forty eight h PI cells were assayed for apoptosis by annexin assays. The graph shows the mean percentage of annexin-positive cells (% apoptosis) for 3 individual populations of cells. Error bars represent standard deviations. Both graphs are representative of three independent experiments.

**Figure 6.** Inhibition of NF- $\kappa$ B promotes apoptosis following reovirus (Reo) infection. (A) Primary cardiac myocytes were either mock-infected (white bars) or were infected with T1L (gray bars) or 8B (black bars) with or without the NF- $\kappa$ B inhibitor SN50. Forty eight h PI cells were harvested and the percentage of cells with apoptotic nuclear morphology was determined. The graph shows the mean percentage of cells with apoptotic nuclear morphology (% apoptosis) for 3 individual populations of cells. Error bars represent standard deviations. The graph is representative of three independent experiments. (B) Untreated HEK293 cells, HEK293 cells expressing FADD-DN and HEK293 cells treated with inhibitors of caspase 3 (Ac-DEVD-CHO) or caspase 8 (Ac-IETD-CHO) were infected with T3A or were mock-infected. Twelve h PI cells were treated with etoposide and were harvested after a further 3 h for western blot analysis using antibodies directed against I $\kappa$ B. Antibodies directed against actin were used to control for protein loading.

**Figure 7.** Expression of cFLIP following reovirus infection. (A) HEK293 cells or HEK293 cells expressing I $\kappa$ B $\Delta$ N2 were either mock-infected or were infected with reovirus strains T1L or T3A. At various times PI cells were harvested for western blot analysis using antibodies directed against cFLIP. Antibodies directed against actin were used to control for protein loading (not shown). (B) HEK293 cells were mock-infected or were infected with T3A in the presence of the NF- $\kappa$ B inhibitor SN50. At 14 h PI cells were harvested for western blot analysis using antibodies directed against cFLIP and actin. HEK293 cells were also mock (M)-infected or were infected with T3A (A) or T1L (L) in the presence of antisense (AS) or sense (s) cFLIP oligonucleotides (cFLIP oligo). At 14 h PI cells were harvested for western blot analysis using antibodies directed against cFLIP and actin (C) and at 48 h PI cells for apoptosis assays (D). The graph shows the mean percentage of cells containing apoptotic nuclei from three independent experiments. Error bars represent standard errors of the mean.

**Table 1.** Ability of reassortant reoviruses (T1L x T3A) to induce apoptosis and to inhibit stimulus-induced degradation of I $\kappa$ B

Virus	Gene Segment						% Inhibition of etoposide-induced				% Apoptosis
	$\leftarrow$ L $\rightarrow$			$\leftarrow$ M $\rightarrow$			$\leftarrow$ S $\rightarrow$				
	1	2	3	1	2	3	1	2	3	4	I $\kappa$ B degradation
T3A	3	3	3	3	3	3	3	3	3	3	93
GW7	1	1	1	1	3	3	3	1	3	3	88
GW49	1	1	1	3	3	3	3	3	3	3	86
GW12	3	1	3	3	1	3	3	3	3	1	74
GW16	3	3	3	3	3	3	1	3	3	1	54
GW10	1	1	3	1	1	3	1	3	1	1	47

GW15	3	3	3	3	3	1	1	1	3	1	43	31
GW26	1	1	3	3	1	1	1	1	1	1	42	23
T1L	1	1	1	1	1	1	1	1	1	1	17	24

IIEK293 cells were infected with reovirus (MOI 100). Twelve h following infection cells were treated with etoposide (100μM). Cells were harvested after a further 3 h for western blot analysis. Results shown represent % inhibition of etoposide-induced IκB degradation in virus-infected cells compared to the amount of etoposide-induced degradation of IκB seen in mock-infected cells (column 3). This data is graphed against virus-induced apoptosis in Figure 4. Also shown is the mean % apoptosis for two independent experiments. Apoptosis was determined 48 h PI (MOI 100) by annexin assays.

**Table 2.** Ability of reassortant reoviruses (myocarditic and non-myocarditic) to induce apoptosis and to inhibit stimulus-induced degradation of IκB

Virus	% Apoptosis	% Apoptosis	% Inhibition of
	Annexin assay	Nucl. Morph Assay	etoposide-induced
			40 h PI
T3A	49 ± 2.0 *** <sup>c</sup>	81 ± 3.7 ***	72 ± 4.8 ***
8B	57 ± 3.2 ***	92 ± 3.2 ***	78 ± 4.4 ***
EW60	59 ± 2.7 ***	87 ± 1.6 ***	90 ± 7.5 ***
DB88	63 ± 2.1 ***	84 ± 2.4 ***	77 ± 8.7 ***
DB181	55 ± 3.1 ***	93 ± 1.9 ***	89 ± 4.7 ***
DB188	52 ± 1.5 ***	88 ± 3.2 ***	57 ± 3.7 **

EW93A	$48 \pm 1.7$ ***	$65 \pm 1.7$ ***	$60 \pm 6.4$ **
EW29B	$28 \pm 2.0$	$32 \pm 1.9$	$33 \pm 6.0$
T1L	$20 \pm 0.9$	$30 \pm 1.4$	$22 \pm 2.5$
Mock	$17 \pm 1.2$	$7 \pm 0.6$	0

HEK293 cells were infected with reovirus (MOI 100). Twelve h following infection cells were treated with etoposide (100 $\mu$ M). Cells were harvested after a further 3 h for western blot analysis. Results shown represent % inhibition of etoposide-induced I $\kappa$ B degradation in virus-infected cells compared to the amount of etoposide-induced degradation of I $\kappa$ B seen in mock-infected cells  $\pm$  the standard error of the mean (column 4). Means were calculated from three independent experiments. Also shown is the mean % apoptosis for three independent experiments. Apoptosis values obtained by nuclear morphology assays are graphed against ability to inhibit stimulus-induced degradation of I $\kappa$ B (Figure 4B). Results showing statistical deviation from those seen in mock-infected cells are indicated (\*\* represents P < 0.001, \*\* represents P < 0.01)



**FIGURE 1**

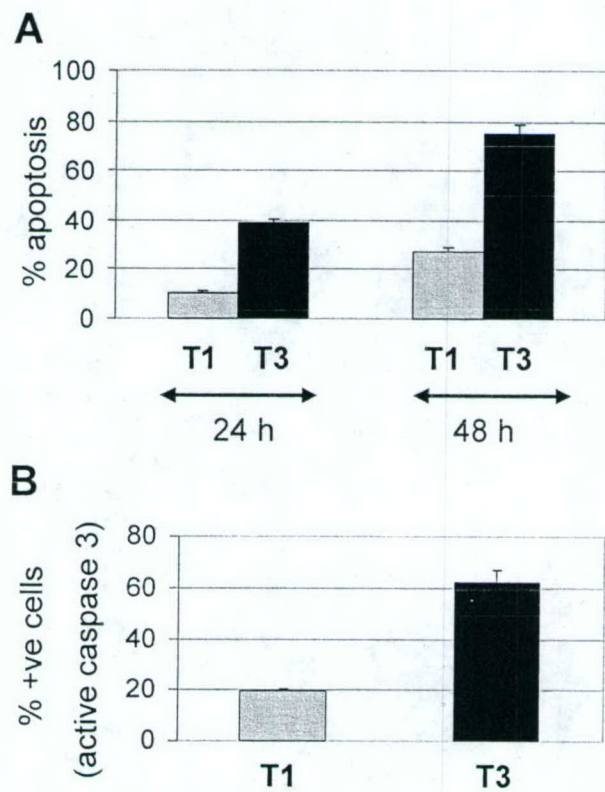


## FIGURE 2

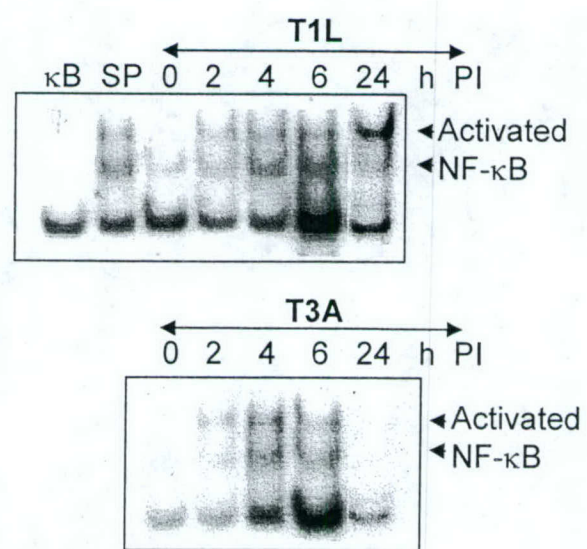


**FIGURE 3**

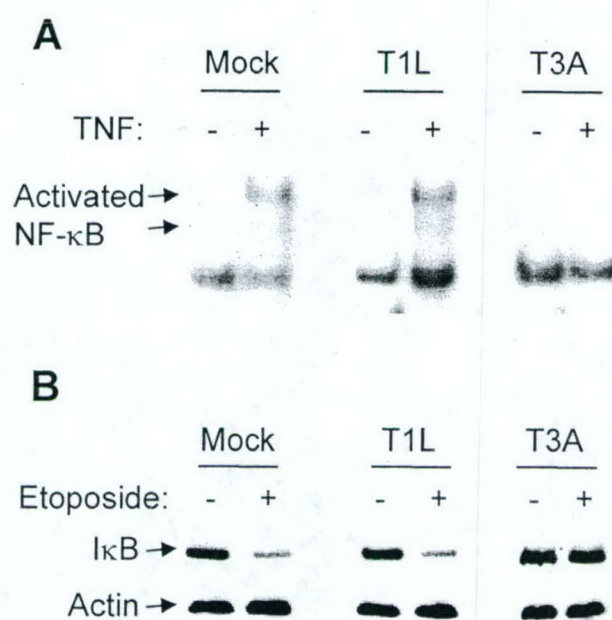
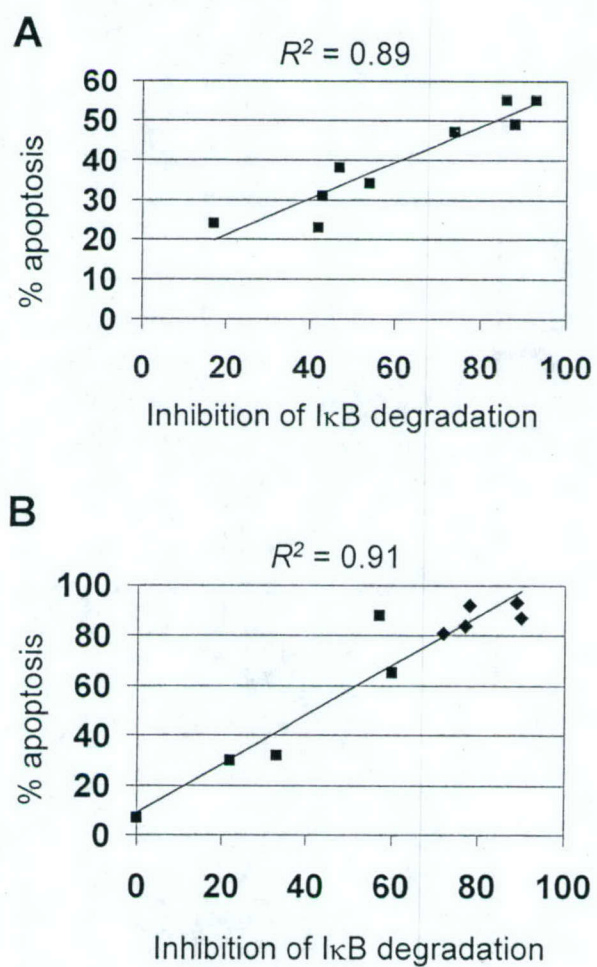
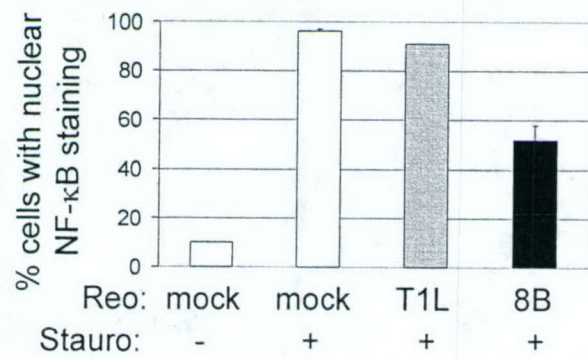


FIGURE 4



**FIGURE 5**

**A**



**B**

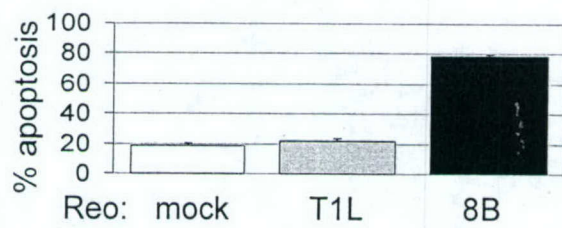


**FIGURE 6**

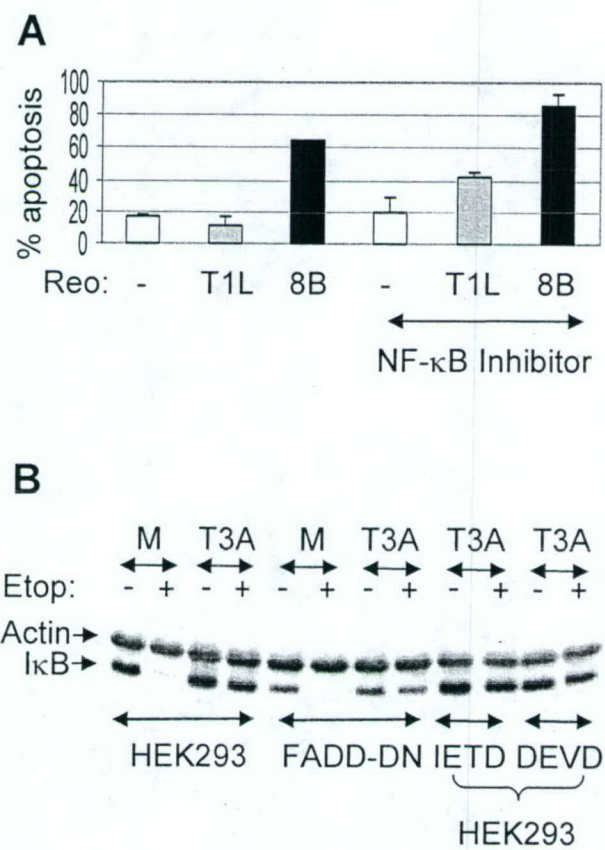
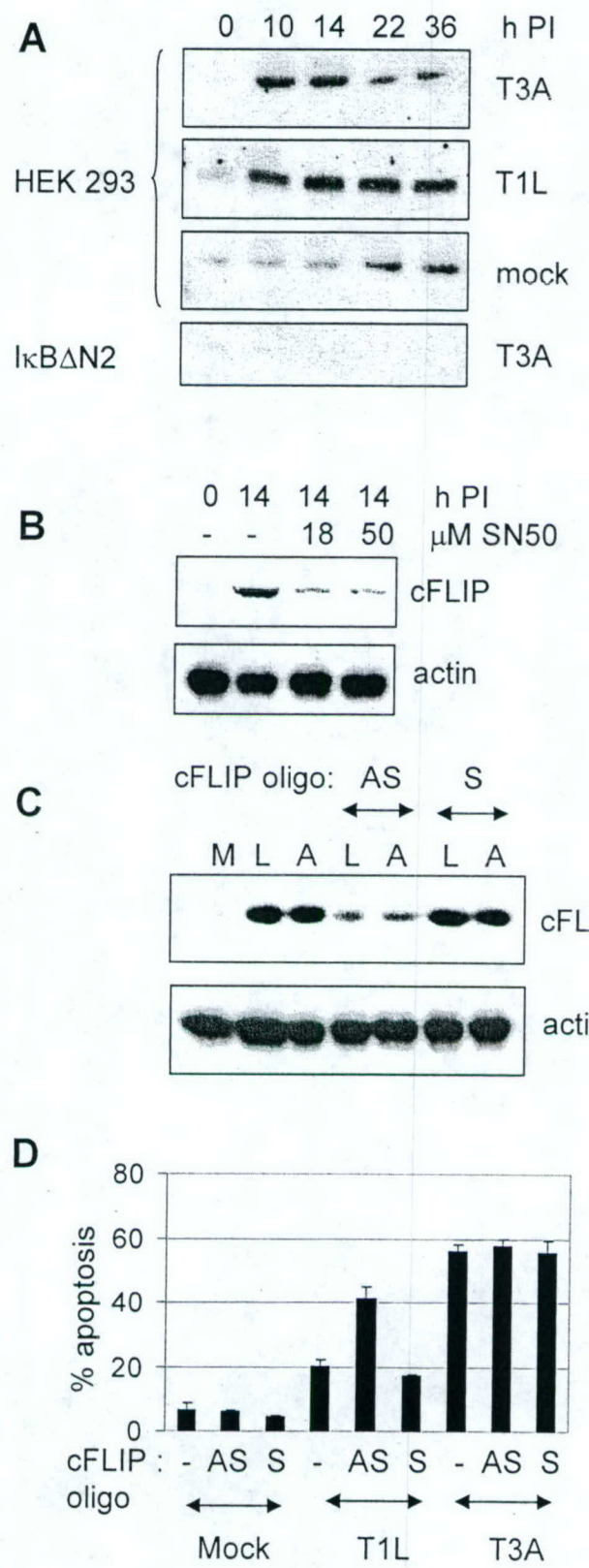


**FIGURE 7**



VIRAL IMMUNOLOGY  
 Volume 18, Number 1, 2005  
 © Mary Ann Liebert, Inc.  
 Pp. 000-000 1-24

## Review

# Mechanisms of Reovirus-Induced Cell Death and Tissue Injury: Role of Apoptosis and Virus-Induced Perturbation of Host-Cell Signaling and Transcription Factor Activation

P. CLARKE,<sup>1</sup> R.L. DEBIASI,<sup>1,5</sup> R. GOODY,<sup>1</sup> C.C. HOYT,<sup>1,4</sup>  
 S. RICHARDSON-BURNS,<sup>1,6</sup> and K.L. TYLER<sup>1-4,6,7</sup>

### ABSTRACT

Reoviruses have provided insight into the roles played by specific viral genes and the proteins they encode in virus-induced cell death and tissue injury. Apoptosis is a major mechanism of cell death induced by reoviruses. Reovirus-induced apoptosis involves both death-receptor and mitochondrial cell death pathways. Reovirus infection is associated with selective activation of mitogen activated protein kinase (MAPK) cascades including JNK/SAPK. Infection also perturbs transcription factor signaling resulting in the activation of c-Jun and initial activation followed by strain-specific inhibition of NF- $\kappa$ B. Infection results in changes in the expression of genes encoding proteins involved in cell cycle regulation, apoptosis, and DNA damage and repair processes. Apoptosis is a major mechanism of reovirus-induced injury to key target organs including the CNS and heart. Inhibition of apoptosis through the use of caspase or calpain inhibitors, minocycline, or in caspase 3  $-/-$  mice all reduce virus-associated tissue injury and enhance survival of infected animals. Reoviruses induce apoptotic cell death (oncrosis) in a wide variety of cancer cells and tumors. The capacity of reoviruses to grow efficiently in transformed cells is enhanced by the presence of an activated Ras signaling pathway likely through mechanisms involving inhibition of antiviral PKR signaling and activation of Ras/RalGEF/p38 pathways. The potential of reovirus-induced oncrosis in therapy of human cancers is currently being investigated in phase I/II clinical trials.

### INTRODUCTION

**A**POPTOSIS IS A PARTICULAR FORM of cell death distinguished from necrosis by the presence of characteristic morphological changes in host cell chromatin and the plasma membrane. Apoptotic cells show condensed nuclei, reduced cytoplasmic volume, and ruffling and/or

blebbing of the plasma membrane. Among the biochemical hallmarks of apoptosis are fragmentation of DNA into oligonucleosomal ladders, exteriorization (flipping) of phosphatidyl serine groups from the inner to the outer surface of the plasma membrane, and the activation of specific sets of cysteinyl aspartate proteases (caspases).

Viruses belonging to many different viral families are

Departments of <sup>1</sup>Neurology, <sup>2</sup>Medicine, <sup>3</sup>Microbiology, <sup>4</sup>Immunology, and <sup>5</sup>Pediatrics, and the <sup>6</sup>Program in Neuroscience, University of Colorado Health Sciences Center, and <sup>7</sup>Denver Veterans Affairs Medical Center, Denver, Colorado.

known to either induce or inhibit apoptosis (4,12,62,75). In the setting of viral infection apoptosis may either represent a part of the host's innate antiviral defense system, or a mechanism utilized by viruses to enhance pathogenesis by facilitating release from cells and dissemination in the host. For viruses that induce apoptosis, it is likely that there are cell-type and organ-specific differences in the pathways involved. Understanding the role of apoptosis in viral pathogenesis and cytopathicity is greatly facilitated by the availability of an experimental system with both *in vivo* models of disease involving a variety of organ systems, and cell culture models to facilitate detailed investigation of apoptosis-related cell signaling pathways. Experimental reovirus infection has these characteristics, and has become one of the most thoroughly investigated viral models of apoptosis (8,23,25,37,64,94).

## REOVIRUS STRUCTURE AND REPLICATION

Reoviruses are non-enveloped viruses with a genome comprised of ten discrete segments of double-stranded RNA (dsRNA) contained within two icosahedrally symmetric concentric protein shells (56). The virion outer shell (capsid) is composed of ~600 heterodimeric complexes of the  $\sigma_3$  and  $\mu_1$  proteins. Sixty copies of the  $\lambda 2$  "core spike" protein form twelve pentons located at each of the outer capsid's icosahedral vertices. The inner capsid (core) is composed predominantly of two additional structural proteins,  $\lambda 1$  and  $\sigma_2$ , and small numbers of the minor core proteins  $\mu 2$  and  $\lambda 3$  (68). Trimmers of the viral attachment protein  $\sigma 1$  sit in a channel in the outer face of the  $\lambda 2$  pentons (18).

Reovirus replication is purely cytoplasmic (56), although recent studies indicate that virally encoded proteins are

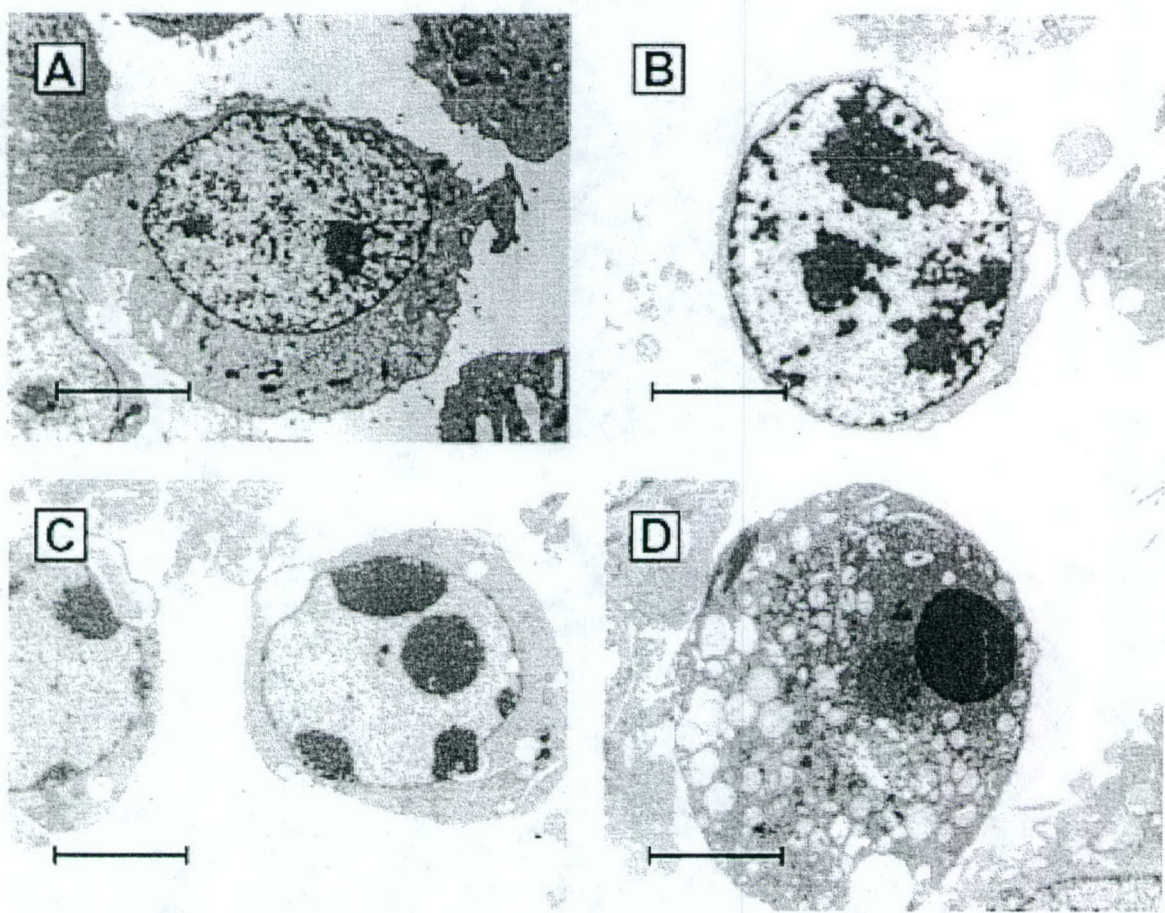


**FIG. 1.** Electron microscopic appearance of uninfected (A) and apoptotic T3D-infected L929 fibroblasts (B–D). Note the progressive margination and compaction of the nuclear chromatin (B,C) and the eventual complete consensation of the nucleus (D). Despite profound changes in nuclear chromatin the cell membrane remains intact. From Tyler et al. (92) with permission.

transported to the nucleus during infection (42). Viral entry occurs following receptor-mediated endocytosis after virions bind to cell surface molecules including junctional adhesion molecule 1 (JAM1) and sialic acids (9,10,37). Current models suggest that for serotype 3 (T3) reovirus strains capable of binding to both JAM1 and sialic acid, cell attachment is mediated by an initial low affinity binding to sialic acid followed by high-affinity binding to JAM1 in a multi-step adhesion strengthening process (9,37).

Once inside endosomes, virions are progressively uncoated through an acid-pH and cysteine-protease dependent process. Conversion to infectious subvirion particles (ISVPs) involves removal of the major outer capsid protein  $\sigma_3$ , cleavage of the major outer capsid protein  $\mu_1$  into smaller fragments, several of which ( $\delta$ ,  $\phi$ ) remain virion-associated, and changes in the conformation of the cell attachment protein  $\sigma_1$  (56).

ISVPs are infectious and can be formed either intracellularly within endosomes of infected cells or extracellularly through the action of proteolytic enzymes such as those present in the intestinal lumen. In the intestinal tract extracellularly produced ISVPs, rather than virions, are the major form of infectious particles. When ISVPs infect cells, they no longer require endosomal acidification for processing. Regardless of their site of initial generation, ISVPs are processed further within endosomes to form the non-infectious but transcriptionally active core particle. This conversion involves removal of  $\sigma_1$  and of the virion-associated  $\mu_1$  fragments and is associated with penetration of the core particle through the endosomal membrane into the host cell cytoplasm. A key event in this process is the exposure of residues on  $\mu_1$  that facilitate fusion of the ISVP with the endosomal membrane to facilitate delivery of the core particle into the cytoplasm (15,63). Transcription occurs within cores, and involves extrusion of distinct (+)-sense capped primary transcripts corresponding to each of the ten genomic dsRNA (+) strands from the core into the cytoplasm through channels in the  $\lambda_2$  core spike pentons (90). Protein self-assembly is likely to play a critical role in formation of viral capsids and cores, although the exact assembly steps are still not completely resolved. Similarly, the mechanisms that insure that each virion has exactly one copy of each of the ten dsRNA genome segments are not well understood. Following assembly of virus particles, release of mature virions accompanies cell death and disruption of the plasma membrane.

#### ROLE OF VIRAL GENES AND PROTEINS IN APOPTOSIS

**Genetics of strain-specific differences in apoptosis induction.** Reovirus strains differ in their capacity to in-

duce apoptosis in a variety of continuous and primary cell lines. This has been most thoroughly investigated in murine L929 fibroblasts, in these cells the T3 prototype strain Dearing (T3D) induces apoptosis much more efficiently than the serotype 1 prototype strain Lang (T1L) (92). Following infection with T3D, cells exhibit all the ultrastructural hallmarks of apoptosis including chromatin condensation and margination, and fragmentation into oligonucleosomal ladders (73,92) (Figs. 1 and 2). In L929 cells viral replication has nearly reached a plateau by 24 h post-infection. The completion of the one-step growth curve precedes the onset of apoptotic changes in nuclear chromatin morphology as identified by staining cells with a DNA intercalating dye (acridine orange) or measuring fragmentation of [ $^3$ H] thymidine-labeled DNA, which indicate that apoptosis increases progressively at 24–48 h post-infection (92).

Reassortant viruses containing different combinations of genes derived from the apoptosis inducing (APO $^+$ ) T3D strain and the minimally apoptogenic (APO $^-$ ) T1L strain were used to identify the S1 viral gene as a determinant of strain-specific differences in apoptosis in L929 (92), MDCK (73) and HeLa cells (28). The M2 gene, encoding the major outer capsid protein  $\mu_1$ , was also identified as a determinant of apoptosis in L929 and MDCK

F1,2

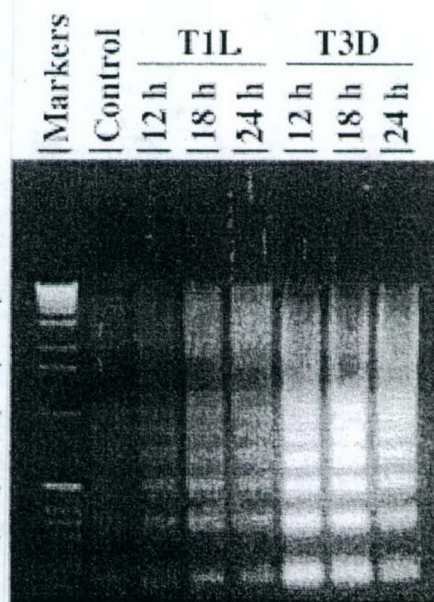


**FIG. 2.** Oligonucleosomal DNA ladders characteristic of apoptosis in reovirus-infected MDCK cells. Oligonucleosomal ladders of fragmented DNA are visible following electrophoresis of extracted total cellular DNA from infected cell lysates through 1.8% TBE/agarose gels stained with ethidium bromide and illuminated with ultraviolet light. From Rodgers et al. (73) with permission.

cells, but not HeLa cells. Studies using reassortants generated between another apoptosis-inducing prototypic strain T3 Abney (T3A) and the APO<sup>-</sup> T1L strain also identified the S1 and M2 genes as determinants of strain-specific differences in apoptosis (93). The S1 gene is bicistronic and encodes the viral cell attachment protein  $\sigma 1$  and a small non-structural protein,  $\sigma 1s$  from overlapping but out of sequence reading frames. The M2 gene encodes the major outer capsid protein  $\mu 1$ .

*Role of the S1 encoded  $\sigma 1$  and  $\sigma 1s$  proteins in apoptosis.* Both of the two S1 encoded proteins appear to play a role in regulation of apoptosis. A reovirus T3D mutant, variant K, with a single amino acid substitution (lysine for glutamine) at position 419 within the globular head of the  $\sigma 1$  protein (11) has reduced ability to grow and induce apoptosis compared to wild-type virus in both cultured primary hippocampal cortical neurons and in the hippocampus of infected neonatal mice (70). Augmentation of virus-induced apoptosis in variant K infected hippocampal neurons by treatment with Fas-activating antibody partially rescues the defect in viral growth (70). Variant K does not show defective growth or apoptosis induction in mouse cortical neurons, suggesting that cell-type specific factors influence  $\sigma 1$ -mediated effects on apoptosis (70).

A T3 reovirus mutant (clone 84-MA) has been isolated which contains a full-length  $\sigma 1$  protein but fails to express  $\sigma 1s$  in infected cells due to the presence of a premature stop codon in the  $\sigma 1s$  ORF (74). This mutant can still induce apoptosis in L929 cells in culture, indicating that  $\sigma 1s$  is dispensable for this process (74).  $\sigma 1s$  is a non-structural protein which first appears in infected cells at approximately 8 h post-infection and requires viral transcription. The failure of ribavirin to inhibit reovirus-induced apoptosis in L929 cells and the ability of UV-inactivated replication-incompetent T3D to still induce apoptosis in these cells is consistent with the lack of a requirement for  $\sigma 1s$  in apoptosis induction.

Despite the apparent lack of a requirement for  $\sigma 1s$  in apoptosis induction *in vitro*, this protein does appear to play a role in regulating apoptosis *in vivo* (43). Neonatal mice infected with  $\sigma 1s$  null virus (clone 84-MA) still develop apoptosis in the heart and central nervous system (CNS), however the magnitude and onset of this is greatly delayed compared to that seen with  $\sigma 1s+$  wild-type viruses, indicating that  $\sigma 1s$  is a regulator of apoptosis *in vivo* (43).

**Avian reovirus proteins and apoptosis.** For avian reoviruses the S1 gene encoded  $\sigma C$  protein is the cell attachment protein, and is functionally analogous to the S1 gene encoded  $\sigma 1$  protein in mammalian reoviruses. Despite this functional similarity, the avian and mammalian proteins do not have significant amino acid or nucleotide sequence homology. BHK-21 cells transiently transfected

with plasmids encoding the  $\sigma C$  protein undergo apoptosis as demonstrated by the appearance of oligonucleosomal DNA laddering and histone-associated DNA fragments detectable by ELISA (83). Deletion experiments suggest that the carboxy-terminus of  $\sigma C$  is important for induction of apoptosis (83). Interestingly, some C-terminal deletion mutants of  $\sigma C$  that lack the capacity to oligomerize into the trimeric form contained in virion particles can still induce apoptosis (83). The finding that transfected protein, which presumably acts at an intracellular site rather than through a cell surface receptor, still induces apoptosis suggests that this is triggered by intracellular protein-protein interactions and not by events triggered by cell surface receptor binding.

**Reovirus replication and apoptosis.** Replication-incompetent UV-irradiated T3D virions can induce apoptosis, but do so inefficiently compared to non-UV irradiated counterparts (92). Inhibition of viral binding also efficiently inhibits apoptosis (92). These results suggest that an early event occurring between viral receptor engagement and onset of transcriptional activation is required for apoptosis induction—a result which has been subsequently confirmed by studies of the relationship between stages in viral disassembly and apoptosis in reovirus-infected HeLa cells (29). In these studies, inhibition of viral processing into ISVPs in infected HeLa cells by the endosomal acidification inhibitor ammonium chloride or the protease inhibitor E64, blocked apoptosis induction. ISVPs remained able to induce apoptosis in the presence of these inhibitors (29). These results are also consistent with a model suggesting that apoptosis may be triggered by intracellular events during the reovirus replication cycle and not simply by association with cell surface receptors.

Treatment of ~~HeLa~~ cells with ribavirin, a guanosine nucleoside analog which inhibits the reovirus encoded dsRNA-dependent RNA polymerase and inhibits formation of both single-stranded (ss)-RNA and ds-RNA (66), does not inhibit apoptosis. Temperature sensitive (ts) mutants of T3D (30) with blocks in entry (tsA201), core assembly (tsC447) outer capsid assembly (tsB352, tsG453), and dsRNA synthesis (tsD357, tsE320) and reovirus particles devoid of dsRNA genome ("top component"), are all capable of inducing apoptosis in both HeLa and L929 cells at non-permissive temperatures (29). These studies clearly indicate that reovirus-induced apoptosis does not require viral replication and is triggered at a stage in the replication cycle prior to viral transcription. Interestingly, almost identical results have been found in studies of apoptosis induced by the avian reovirus strain 1133 in chicken embryo fibroblasts (52). Similar to its mammalian counterpart, UV-inactivated avian S1133 retains the ability to induce apoptosis, and apoptosis induced by wild-type virus is inhibited by ~~both~~ lysosomotropic agents and treatment of cells with ribavirin (52).

but not by

✓ ribavirin effect

**Role of reovirus binding to receptors and apoptosis induction.** The reovirus  $\sigma 1$  protein serves as the viral cell attachment protein. In virions, the protein forms homotrimers with an externally facing globular head domain and an interior long fibrous tail (18). Most T3 reoviruses, including the apoptosis-inducing prototype strains T3A and T3D, have the capacity to bind to both junctional adhesion molecule-1 (JAM1) (10) and sialic acid (SA) residues on the surface of host cells. Some T3 field isolates (e.g., T3C43, T3C44, and T3C84), although still able to bind to JAM1, fail to bind sialic acids. Serotype 1 (T1) reovirus strains, including the prototype strain type 1 Lang (T1L), also bind to JAM1 and to other as yet uncharacterized cell surface carbohydrate moieties, but not to sialic acid (17). The JAM1 binding region of  $\sigma 1$  involves a cluster of highly conserved amino acid residues in a loop-like structure in the globular head domain (10), while sialic acid binding is mediated by a discrete region in the fibrous tail of  $\sigma 1$  (16,17).

Despite the importance of intracellular events early in the reovirus replication cycle for apoptosis induction, it is important to recognize that initial virion binding to *both* JAM1 and sialic acid (SA) is essential for optimal expression of apoptosis in infected cells. In both HeLa and L929 cells, non-SA binding T3 strains (clones T3C43, T3C44, T3C84) are still able to induce apoptosis, but do so at a much lower level than their SA<sup>+</sup> revertant counterparts (T3C43-MA, T3C44-MA, T3C84-MA) (28). Substitution of a leucine for a proline at amino acid 204 of the  $\sigma 1$  protein in a reovirus monoreassortant with a T3D S1 gene on a T1L genetic background abrogates SA binding and dramatically inhibits apoptosis induction in L929 and HeLa cells (28). These results indicate that the addition of SA binding to JAM1 binding is required for the full induction of apoptosis. This result is supported by studies showing that pre-treatment of HeLa or L929 cells with *Arthrobacter ureafaciens* neuraminidase, which removes cell surface sialic acids, dramatically reduces apoptosis induced by SA<sup>+</sup> T3 strains (28). Apoptosis is also inhibited by pre-incubation of SA<sup>+</sup> T3 strains with  $\alpha$ -sialyllectose, a trisaccharide containing  $\alpha$ -linked terminal sialic acid residues which competitively inhibits binding of T3 viruses to SA, but not to JAM1 (28). The effects of SA binding on apoptosis are not simply due to enhanced viral growth, as in L929 cells both T3SA<sup>-</sup> and T3SA<sup>+</sup> strains grow equivalently (although SA<sup>+</sup> strains grow better than their SA<sup>-</sup> counterparts in HeLa cells) (28). Despite its importance, SA binding in and of itself is insufficient for apoptosis-induction by SA<sup>+</sup> T3 strains. In L929 cells, monoclonal antibodies that inhibit viral binding to JAM1 completely block apoptosis by SA<sup>+</sup> strains, and have only a modest impact on viral growth (10).

## CELLULAR PATHWAYS OF REOVIRUS-INDUCED APOPTOSIS

**Death receptor initiated apoptosis signaling pathways.** An increasingly more comprehensive picture of the cellular apoptotic pathways activated following reovirus infection has emerged from studies of continuous cell lines, cancer cell lines, and primary neuronal and cardiac myocyte cultures (8,23,25,64) (Fig. 3). Although the basic features of reovirus-induced apoptotic signaling are strikingly similar regardless of cell type, there are variations in the specific details. In all cell lines examined to date the initiating event appears to be activation of cell surface death receptors belonging to the tumor necrosis factor receptor (TNFR) superfamily. In HEK293, L929, and a variety of human cervical (HeLa), lung (H157, A549), and breast (MDA231, ZR75-1) cancer cell lines, apoptosis is initiated by the interaction of TRAIL (TNF-related apoptosis-inducing ligand) with death receptors 4 and 5 (DR4, DR5) (19,20). The supernatant derived from T3 reovirus-infected cells can induce apoptosis in TRAIL-sensitive indicator cells (HeLa), and this apoptosis-inducing activity can be inhibited by treatment of the supernatant with soluble Fc-coupled DR5, but not by anti-reovirus antibody (19). Apoptosis-inducing activity is detectable in the supernatant within 24 h post-infection and increases through 48 h post-infection (19). This suggests that TRAIL is released from infected cells through a yet undefined mechanism, and presumably acts to initiate apoptosis in both virus-infected cells (autocrine pathway) and uninfected neighboring bystander cells (paracrine pathway). Consistent with this model, treatment of infected cells with either antibodies against TRAIL or soluble DR4 or DR5 inhibits T3 reovirus-induced apoptosis (19) (Fig. 4). This activity appears to be specific for TRAIL; as antibodies against TNF or against Fas Ligand and soluble forms of non-TRAIL related death receptors (e.g. TNFR) all fail to inhibit T3 reovirus-induced apoptosis in HEK293 cells (19). Consistent with the key role for TRAIL, stable over-expression of a non-functional decoy receptor for TRAIL (DcR-1) in MDA231 breast cancer cells, inhibits T3 reovirus-induced apoptosis (20). Intriguingly, TRAIL has also been implicated in apoptosis mediated by a diverse group of viruses including measles (95), hepatitis (55), influenza (99), respiratory syncytial virus (50), cytomegalovirus (79), lyssavirus (45), Theiler's virus (44,76), HIV (54), and HTLV (72).

Death-receptor initiated pathways also play a key role in T3 reovirus-induced apoptosis in primary mouse cortical neuronal cultures (69,70). However, in these cells soluble forms of Fas-receptor and to a lesser extent of soluble forms of TNFR were more effective in inhibiting apoptosis than soluble DR5 (69). Interestingly, the neuroblastoma cell line NB41A3 shows an intermediate phe-

F3

F4

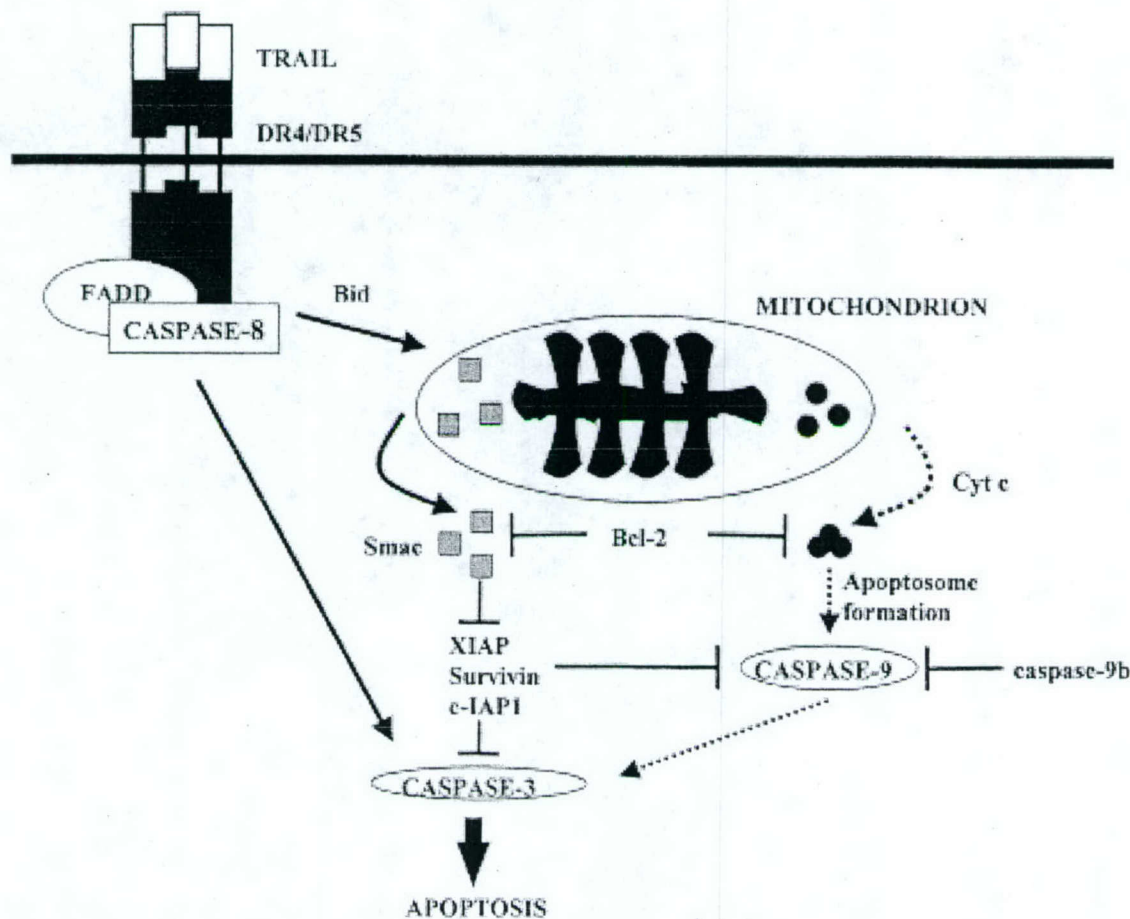


**FIG. 3.** A general outline of caspase pathways activated during reovirus T3 infection of epithelial and human cancer cell lines. Infection results in release of the death inducing ligand TRAIL which binds to cell death receptors DR4 and DR5 which are members of the TNFR superfamily of cell death receptors. Binding of TRAIL to DR4/DR5 activates caspase 8 through the death-inducing signaling complex (DISC). Cleavage of the Bcl-2 family protein Bid plays a key intermediary role in death-receptor initiated activation of mitochondrial apoptosis pathways. Pro-apoptotic factors released from mitochondria following reovirus infection include cytochrome *c* and Smac/Diablo. Smac/Diablo augments apoptosis by inhibiting the action of cellular inhibitor of apoptosis proteins (IAPs). From Kominsky et al. (49) with permission.

notype when compared to epithelial and cancer lines (see above) and primary neurons, with apoptosis inhibited by soluble DR5 and TNFR but not by soluble Fas-receptor (69).

Binding of apoptosis-inducing ligands such as TRAIL to their cognate cell surface death receptors results in receptor oligomerization and the apposition of the receptors' cytoplasmic death effector domains (DEDs). Death receptor oligomerization and DED apposition results in the recruitment of adapter molecules such as FADD (Fas-associated death domain), which also contain DEDs, to the receptor complex. The addition of pro-caspase 8, the death-receptor associated initiator caspase, completes the components of a "death-inducing signaling complex"

(DISC) and leads to the cleavage and activation of caspase 8 (6). Consistent with a model of death receptor-initiated apoptosis, T3 reovirus infection activates caspase 8 in infected epithelial and human cancer cells as well as in primary neuronal cultures (48,69) (Figs. 5 and 6). In addition, T3 reovirus-induced apoptosis is inhibited in HEK293 cells by stable over-expression of a dominant-negative form of FADD (19,49). Treatment with a soluble form of the caspase 8 inhibitory peptide IETD also inhibits T3 reovirus-induced apoptosis in HEK293 and neuronal cells (19,49,69).

**Mitochondrial apoptosis signaling pathways.** Over-expression of Bcl-2 in MDCK cells markedly reduces T3 reovirus-induced apoptosis (73) (Fig. 7). Over-ex-

F5,6

F7

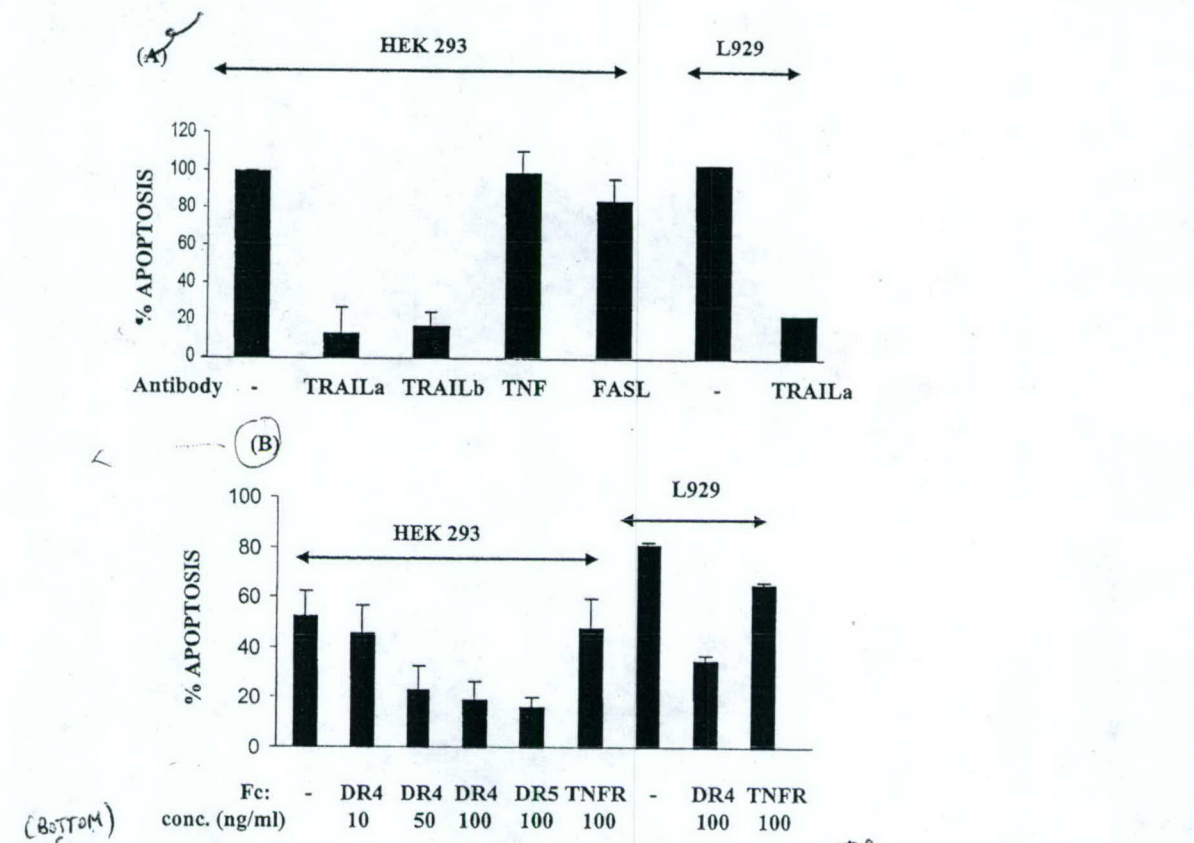


FIG. 4. Inhibition of TRAIL binding to reovirus-infected cells with either anti-TRAIL antibodies (▲) or soluble Fc-coupled death receptors (B). A/B inhibit T3 induced apoptosis in HEK293 and L929 cells. TRAILa and TRAILb are two different polyclonal anti-TRAIL antibodies. TNF and FASL are antibodies against these death ligands. DR4, DR5, and TNFR are Fc-coupled forms of these death receptors. From Clarke et al. (19) with permission.

pression of Bcl-2 also dramatically inhibits effector caspase activation in reovirus-infected HEK293 cells (48). Although the anti-apoptotic actions of Bcl-2 are heterogeneous, the capacity of Bcl-2 to inhibit apoptosis is generally considered a strong indicator that mitochondrial apoptotic pathways are involved (67). This is consistent with results showing that Bcl-2 over-expression blocks reovirus-induced release of a variety of mitochondrial pro-apoptotic factors including cytochrome *c*, and Smac/DIABLO (49).



FIG. 5. Caspase 8 is activated in T3A-infected HEK293 cells. The immunoblot shows progressive activation-associated disappearance of pro-caspase 8 with an initial phase beginning at ~8 h post-infection followed by sustained activation after 20 h. From Kominsky et al. (48) with permission.

Direct evidence for involvement of mitochondrial pathways in reovirus-induced apoptosis comes from studies in HEK293 cells indicating that mitochondrial pro-apoptotic factors including cytochrome *c* (24,48,49) and Smac/DIABLO (24,49) are released from mitochondria

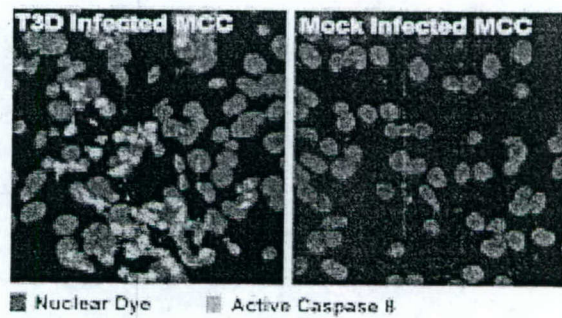
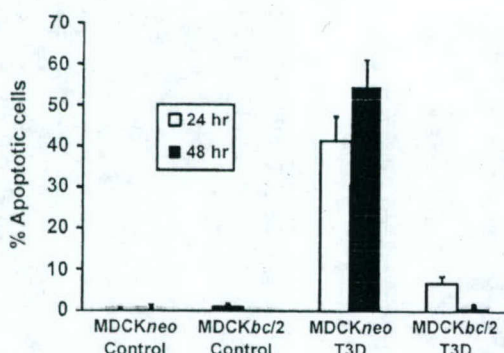


FIG. 6. Caspase 8 activation detected using an antibody specific for the activated form of caspase-8 (green staining) in mouse primary cortical neurons at 20 h post-infection with T3D.



**FIG. 7.** Stable over-expression of Bcl-2 inhibits apoptosis induced by T3D in MDCK cells. MDCKneo is a control plasmid lacking Bcl-2. From Rodgers et al. (73) with permission.

F8

into the cytoplasm of infected cells (Fig. 8). This release is selective, as AIF (apoptosis inducing factor) is not detected in either the cytoplasm or nucleus of infected cells (49). In distinction to the result seen in HEK293 cells, there appears to be only limited and late release of cytochrome *c* in primary neuronal cultures or NB41A3 cells (69).

In some settings, release of mitochondrial apoptotic factors may be associated with profound changes in mitochondrial transmembrane potential ( $\Delta\Psi_m$ ), likely reflecting the creation of pores in the outer mitochondrial membrane. Reovirus infection is not associated with alterations in mitochondrial  $\Delta\Psi_m$  in either HEK293 cells (49) or monkey kidney CV-1 cells (80), suggesting that significant disruption of mitochondrial integrity is not occurring.

Two prominent pathways by which mitochondrial pro-apoptotic factors facilitate or augment apoptosis are through their activation of caspase 9, and their effects on inhibitor of apoptosis proteins (IAPs). Released cytochrome *c* forms a complex known as the apoptosome with cytosolic factors including Apaf-1 and procaspase 9 and results in ATP-dependent activation of caspase 9. Caspase 9 activation can be detected in reovirus infected HEK293 cells (48,49). In NB41A3 cells, caspase 9 activation is a late event (>24 h pi) and may occur consequent to activation of caspase 3 rather than as a result of cytochrome *c* release (69). Even in HEK293 cells, where caspase 9 activation is robust and detectable within 12 h pi, inhibition of this activation by expression of a dominant negative form of caspase 9 (caspase 9b) has no effect on reovirus-induced apoptosis, suggesting that it is not caspase 9 activation, but rather other mitochondrial-dependent events that are critical in reovirus-induced apoptosis (49). Cell permeable caspase 9 inhibitors (LEHD) fail to inhibit reovirus-induced apoptosis in primary neuronal cultures, although both caspase 8 (IETD)

and caspase 3 (DEVD) inhibitors effectively inhibit apoptosis (69,70).

The recognition that reovirus infection results in the release of the mitochondrial pro-apoptotic factor Smac/DIABLO (24,49) provides an alternative candidate for the key mitochondrial signaling pathway in reovirus-induced apoptosis. Smac/DIABLO facilitates the activation of caspases by preventing the inhibitory interaction between caspases and IAPs. Selective degradation of specific IAPs, including XIAP, survivin, and cIAP1 (but not cIAP2), occurs in reovirus-infected cells (49) (Fig. 9), and is blocked by over-expression of Bcl-2, which also blocks mitochondrial release of Smac/DIABLO (49). Interestingly, gene expression studies using microarrays suggest that at least one IAP (SMN/NAIP) is up-regulated in T3A infected HEK293 cells by 2.5-fold, a result which is confirmed by RT-PCR and by immunocytochemical studies showing increased expression of SMN protein in the hearts of reovirus 8B-infected mice (34).

The pathways linking death-receptor initiated apoptotic signaling to activation of mitochondrial apoptotic pathways in reovirus-infected cells have become increasingly well understood. In reovirus T3-infected cells, caspase 8 activation leads to the cleavage of the Bcl-2 family protein Bid, producing a truncated form of the protein (tBid) (48) which translocates to the mitochondria and facilitate the release of pro-apoptotic mitochondrial factors. The generation of tBid is dependent on death-receptor activation as it can be effectively inhibited by stable over-expression of DN-FADD (48).

The JNK MAPK pathway also plays a key role in activation of mitochondrial apoptotic signaling in reovirus-infected cells (24). HEK293 cells pre-treated with JNK inhibitor 1 show significantly delayed release of both Smac/DIABLO and cytochrome *c* from mitochondria into the cytosol (24). Although the mechanism of action of JNK in facilitating reovirus-induced activation of the mitochondrial pathway remains unknown, it may be related to the phosphorylation and associated subcellular redistribution of Bcl-2 family proteins.

**Effector caspases.** The ultimate effect of the activation of death receptor and mitochondrial apoptotic pathways in T3 reovirus-infected cells and tissues is the activation of effector caspases. Caspase 3 activation is detectable in HEK293 cells and in both primary neuronal and cardiac myocyte cultures utilizing immunoblots, fluorescent substrate activity assays, immunohistochemical staining for activated caspase 3, and cleavage of the caspase 3 substrate PARP (35,48,69) (Fig. 10). Caspase 7 activation has also been detected in infected HEK293 cells by immunoblotting (48), although caspase 6, another effector caspase, does not appear to be activated (48). Caspase 3 activation precedes that of caspase 7 and appears at higher levels, suggesting that caspase 3, rather

F9

F10

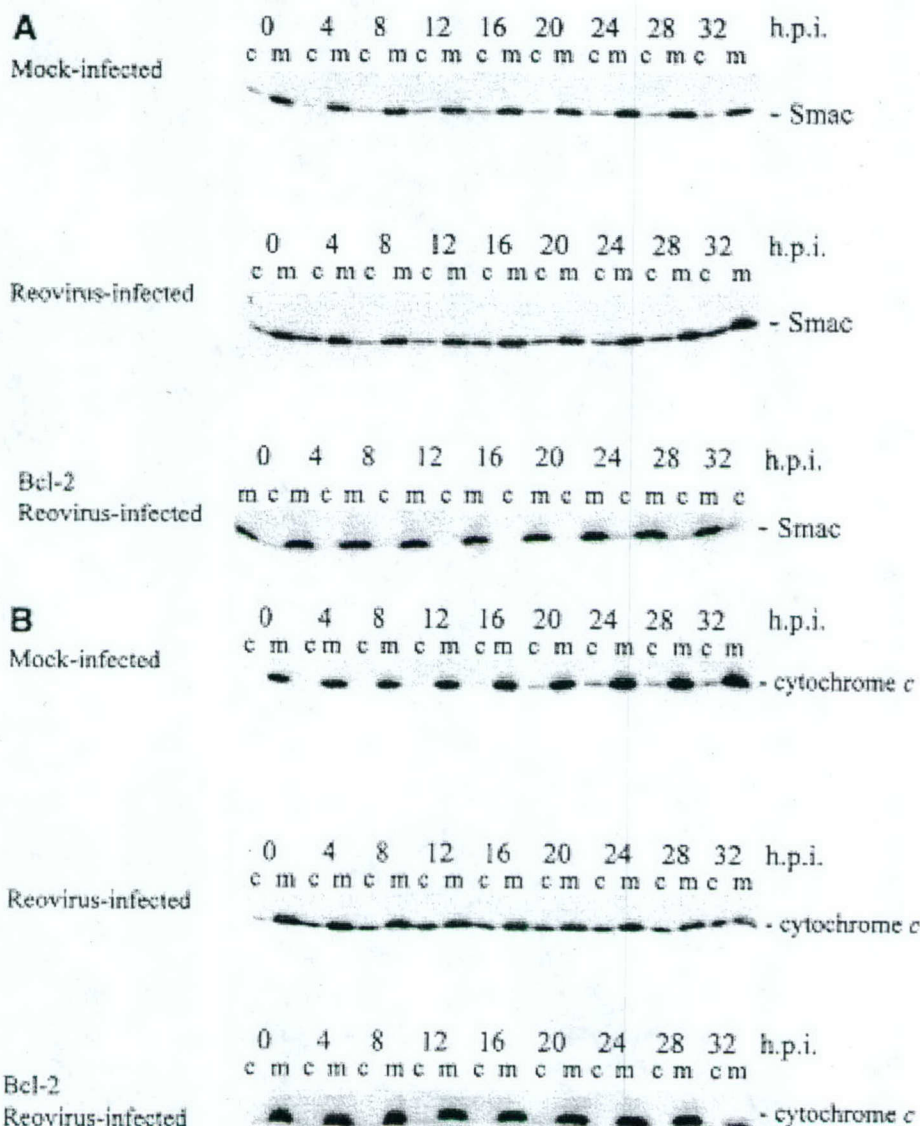


**FIG. 8.** Smac/DIABLO and cytochrome *c* are released from mitochondria into the cytosol of T3A-infected cells. HEK 293 cells. c, cytosolic fraction; m, mitochondrial fraction of cell lysates; h.p.i., hours post-infection. Both Smac (A) and cytochrome *c* (B) are released from the mitochondria into the cytosol of reovirus infected cells, and this release is almost completely prevented in cells stably expressing Bcl-2 (bottom immunoblot in each series). From Kominsky et al. (49) with permission.

than caspase 7, is the critical effector caspase following T3 reovirus infection (48). In addition to being activated, expression levels of both caspase 3 and 7 are substantially increased (2.6–3.2-fold) in T3A-infected HEK293 cells by 24 h post-infection (34), suggesting that regulation occurs both at the level of gene transcription and protein activation.

Caspase 3 activation is detectable in immunoblots from T3 reovirus-infected cells as early as 4 h post-infection, and has a biphasic activation pattern with early

initial activation at 4–12 h post-infection followed by a more robust and sustained secondary activation after 24 h post-infection (48). A dual-phase activation pattern is also detectable in fluorogenic substrate assays of caspase 3 activity (48). In these assays, DN-FADD inhibits all caspase 3 activation, whereas Bcl-2 inhibits predominantly the late phase activation. This dual phase activation of caspase 3 would be consistent with an initial transient death-receptor mediated caspase 3 activation phase, followed by a mitochondrially aug-

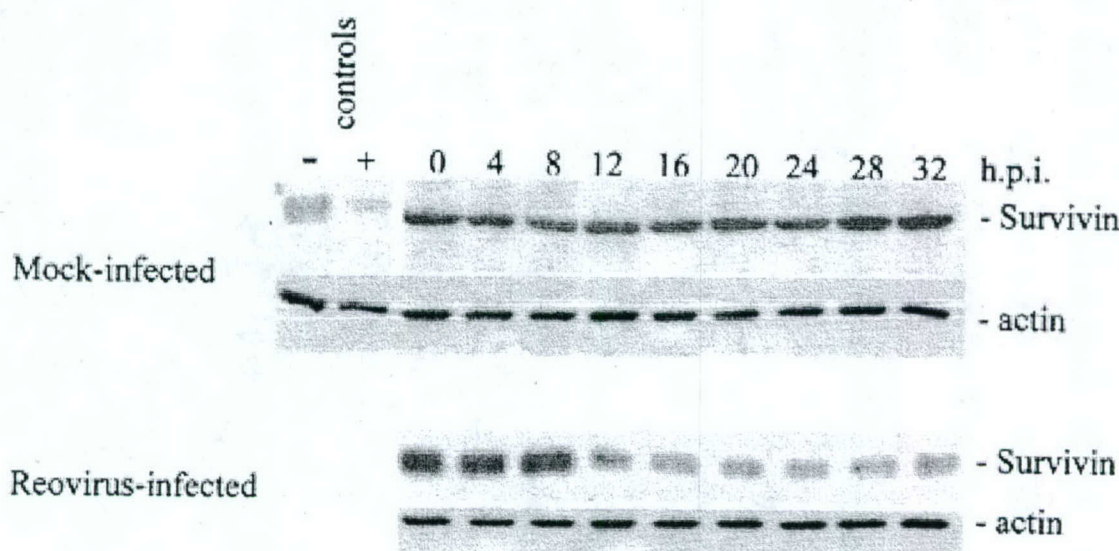


**FIG. 9.** Cellular levels of the inhibitor of apoptosis (IAP) protein survivin are reduced in T3A-infected HEK293 cells. Degradation first appears at 8–12 h post-infection and is inhibited in cells over-expressing Bcl-2 (not shown). From Kominsky et al. (49) with permission.

mented sustained activation phase. As would be predicted from these studies, cell permeable inhibitors of caspase 3 (DEVD) dramatically inhibit T3 reovirus induced apoptosis (48,69).

**Calpain.** In addition to caspases, the calcium-dependent neutral cysteine protease calpain has been implicated

in many models of apoptotic and non-apoptotic cell death (39). Calpains are ubiquitously expressed in the cytosol of many cells, with mu-calpain activated by calcium concentrations in the micromolar range and m-calpain by millimolar concentrations. Both enzymes are specifically inhibited by calpastatin as well as a variety of less spe-

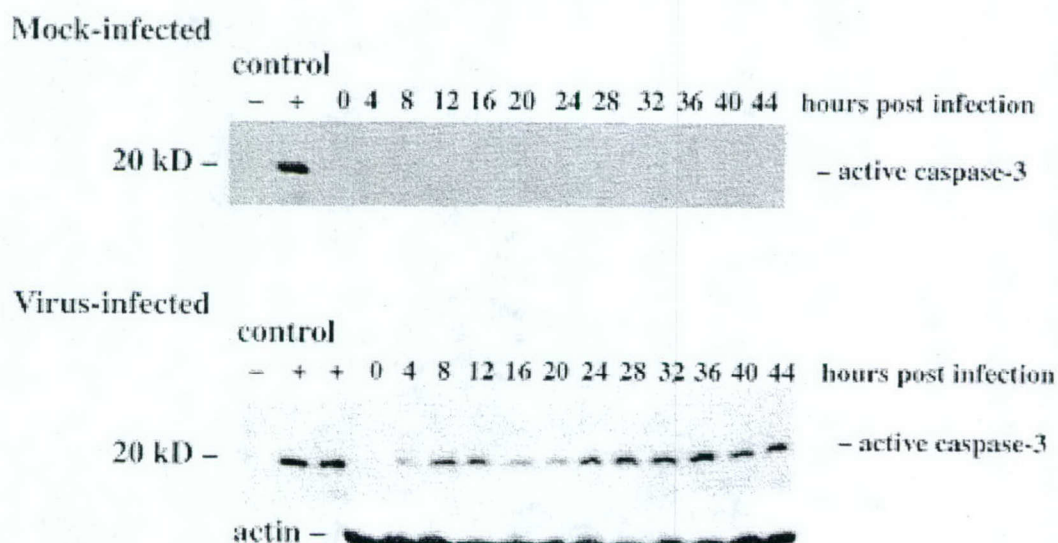


**FIG. 10.** Caspase 3 activation in T3A-infected HEK293 cells detected by immunoblotting using a monoclonal antibody specific for the active form of caspase 3. Note the appearance of an early activation phase at 8–12 h post-infection followed by more sustained activation after 20 h post-infection. From Kominsky et al. (48) with permission.

cific protease inhibitors. Calpains cleave a variety of proteins at a conformation-dependent rather than sequence specific site. Cellular targets of potential interest in apoptosis signaling include specific cytoskeletal proteins, kinases and phosphatases, caspases, and I- $\kappa$ B the cytosolic inhibitor of NF- $\kappa$ B (39).

T3A infection of L929 cells is associated with increase in calpain activity (1.6-fold) measured by fluorogenic substrate assay in live cells (32). At supra-physiologic multiplicities of infection (MOI 10,000), calpain activation could be detected as early as 30 min post-infection and increased steadily through 2 h post-infection (the last time-point assayed). Calpain activation can also be detected in reovirus 8B infected mouse primary cardiac myocytes as determined by the appearance of calpain-specific 150- and 145-kDa spectrin cleavage products (33). Peak activation (fourfold) occurred at 48 h after infection of cells at MOI 20. Interestingly, gene expression studies using microarrays suggest that calpain gene (GenBank X04366) expression is decreased by 2.6-fold in T3A-infected HEK293 cells at 24 h post-infection, (34) suggesting that activation may be associated with a negative feedback loop that reduces gene expression in infected cells.

Inhibition of calpain activation by pre-treatment of L929 cells with either calpain inhibitor I (aLLN), which blocks the active site, or by PD150606, an  $\alpha$ -mercaptopropionic acid derivative which blocks the  $\text{Ca}^{2+}$  binding site; inhibited apoptosis induced by T1L, T3D, and T3A (32). In 8B infected primary cardiac myocytes a similar effect was seen with CX295, a dipeptide  $\alpha$ -ketoamide compound that inhibits calpain at the active site (33). Apoptosis was also inhibited in L929 cells treated with calpain inhibitors and infected with replication-incompetent UV-inactivated virus, indicating that the anti-apoptotic effects of calpain inhibition were due to inhibition of viral replication (32).

The therapeutic efficacy of calpain inhibition was also examined in neonatal mice infected with the myocarditis-inducing reovirus 8B strain (33). Treatment of mice with six daily intraperitoneal injections of CTX 295 (70 mg/kg) beginning 30 min before challenge with 8B (1000 pfu IM) resulted in substantial reduction in the degree of myocardial injury as determined both by a blinded histopathological scoring system and reduction in serum creatine phosphokinase (CPK).

#### REOVIRUS-INDUCED MODULATION OF TRANSCRIPTION FACTOR ACTIVATION

**c-JUN and mitogen-activated protein kinase (MAPK) cascades.** Reovirus infection induces changes in several transcription factor systems, notably those involving c-Jun and NF- $\kappa$ B. Increased levels of active, phosphorylated c-Jun are detected in L929 cells infected by the prototypic reovirus strains T1L, T3A, and T3D (21) (Fig. 11). T3A also induces c-Jun phosphorylation in both HEK293 and HeLa cells (24). In L929 cells, phosphorylated c-Jun is first detected at 6–12 h post-infection (pi) and reaches a peak of 30–40-fold over baseline at about 18 h before declining to basal levels by 48 h post-infection (21). The kinetics of c-Jun activation are similar for T3A and T3D. However, T1L shows a slower and less robust activation of c-Jun in comparison to T3 strains (21).

F11

In L929 cells, a strong correlation exists between the capacity of the reovirus prototype strains to activate c-Jun and to induce apoptosis ( $R^2 = 0.93 - 0.96$  at 12 and 18 h pi), while a similar, but less robust correlation is observed using T1L  $\times$  T3D reassortant viruses ( $R^2 = 0.3$ ,  $p = 0.035$ ) (21). This suggests that the effects of c-Jun activation are pro-apoptotic. However, later studies, using an adenovirus vector (TAM67) expressing a dominant-negative form of c-Jun (DN-C-Jun) suggest that it is not c-Jun activation per se but likely an upstream event in the mitogen activated protein kinase (MAPK) pathway leading to c-Jun activation that is the key pro-apoptotic event (24).

JNK and ERK but not p38 MAPK are activated in reovirus infected cells by T3A and T3D but not by T1L, and contribute to reovirus-induced c-Jun activation (21). In HEK293 cells, inhibition of either JNK or ERK activity partially reduces T3A-induced c-Jun phosphorylation and the combination of both inhibitors completely blocks c-Jun phosphorylation (24). Inhibition of p38 and ERK activation with pharmacologic inhibitors does not effect reovirus-induced apoptosis (21,24), in contrast to the results seen with JNK inhibition (24), suggesting that JNK but not p38 or ERK, contribute to reovirus-induced apoptosis (see below). The kinetics of JNK activation parallels that of activation of c-Jun (21). Following infection with T3D, JNK activation is detectable as early as 10 hrs pi and increases steadily through 24 h (Fig. 12). T1L does not significantly induce JNK activity in these cells. Studies using reassortant T1L  $\times$  T3D viruses indicate that the same reovirus genes that determine strain-specific differences in apoptosis (S1, M2) also determine differences in the capacity of reoviruses to activate JNK (21). There is a stronger correlation between the capacity of T1L  $\times$  T3D reassortants to activate JNK and to induce apoptosis ( $R^2 = 0.61$ ,  $p = 0.003$ ), than for c-Jun activation ( $R^2 = 0.3$ ,  $p = 0.035$ ), suggesting that it is JNK rather than c-Jun activation that may be the key factor in modulating reovirus induced apoptosis.

F12

Additional evidence suggesting that JNK activation rather than c-Jun activation was the key factor in reovirus-induced apoptosis comes from studies with MAPK in-

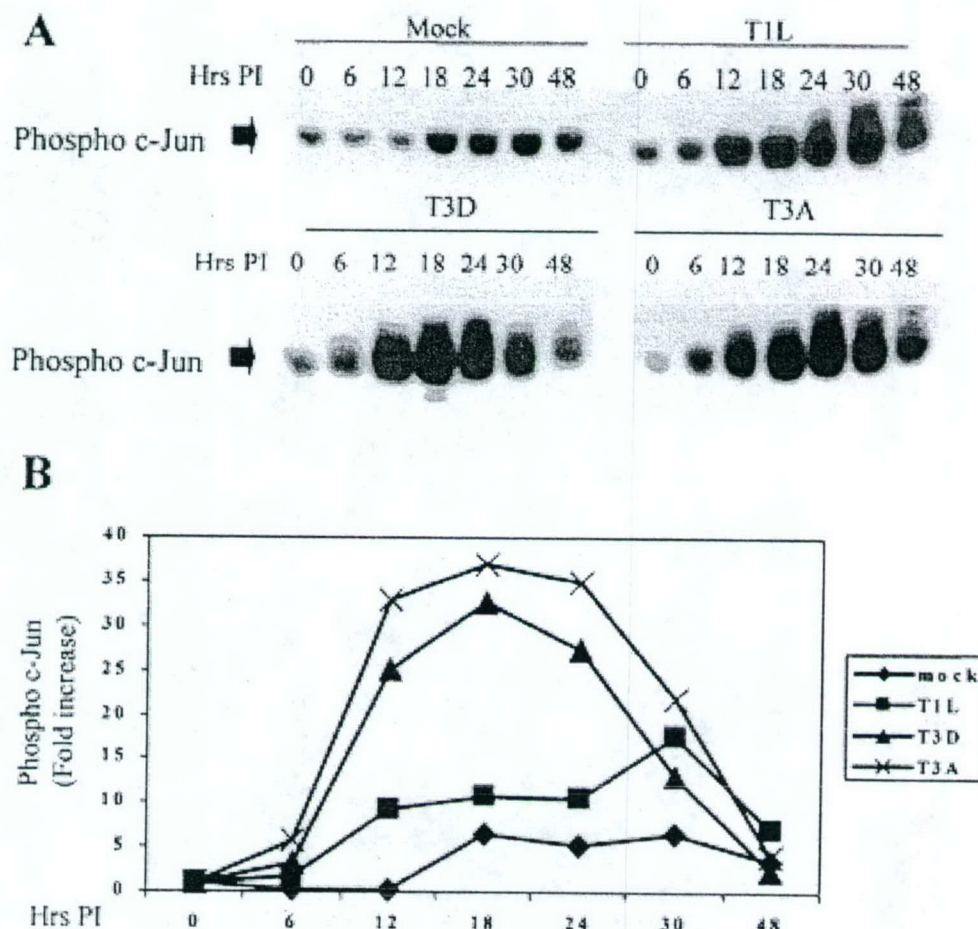


**FIG. 11.** Phosphorylated c-Jun is increased in reovirus-infected L929 cells as detected in immunoblots of infected cell lysates using a phospho-c-Jun specific antibody. Both T3A and T3D induce more robust activation of c-Jun than T1L. **B** is a graphical representation of the data shown in the immunoblots in **A**. From Clarke et al. (21) with permission.

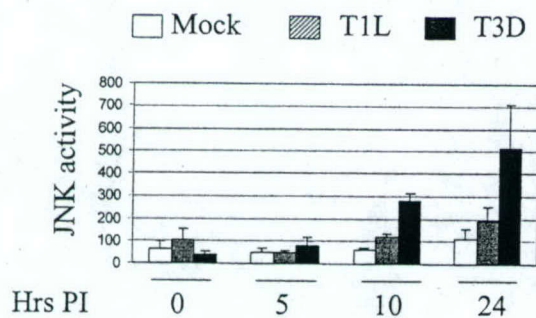


**FIG. 12.** Reovirus infection activates JNK in infected L929 cells. JNK activity was determined using an *in vitro* kinase assay measuring c-Jun phosphorylation. T3D infection results in significantly higher JNK activity in infected cells than T1L infection. From Clarke et al. (21) with permission.

hibitors. JNK inhibitor 1 (Alexis) is a cell permeable peptide inhibitor that contains the minimal inhibitory sequence of JNK inhibitory protein 1 (JIP-1/IB1) and inhibits downstream signaling events by inhibiting the interaction between JNK and its substrates. JNK inhibitor II (1,9-pyrazoloanthrone) (Calbiochem) is a cell permeable, selective and reversible competitive inhibitor of JNK. Pre-treatment of either HeLa or HEK293 cells with these inhibitors significantly reduces T3A-induced apoptosis at 24–48 h post infection (57–67% reduction), although this effect could be overcome with high multiplicity of infection (MOI = 100) at the late (48 h) time-point (24). Similar results were seen when caspase 3 activity was examined in T3A-infected HeLa cells. In HEK293 cells, inhibitors of MAPK p38 (SB203580) and ERK (PD98059) had no effect on apoptosis, while JNK

inhibitors decreased both caspase-3 induction and apoptosis. In contrast to the specificity of JNK inhibition on apoptosis in HEK293 cells, in HeLa cells the p38 inhibitor did inhibit apoptosis, suggesting that cell-type specific variations exist in MAPKs involved in reovirus-induced apoptosis. The effects of MAP kinase inhibitors on apoptosis and viral growth are distinct. Although JNK inhibition blocks apoptosis it does not affect viral yield in HEK293 cells (24) nor viral protein synthesis in *Ras*-transformed NIH 3T3 cells (59). Conversely, p38 inhibition does inhibit viral protein synthesis, at least in *Ras*-transformed NIH 3T3 cells (59).

The exact pathways by which JNK is activated in reovirus-infected cells have not been elucidated. JNK is phosphorylated by JNK kinase (JNKK), which in turn can be activated by the MAP kinase kinase kinase (MAP3K) MEKK1. MEKK1 preferentially activates the JNK pathway and also influences the activity of ERK but does not affect the p38-MAPK pathway. Embryonal stromal (ES) cells lacking MEKK1 show reduced T3A-induced JNK activation (103). MEKK1<sup>-/-</sup> mouse embryo fibroblasts show almost complete inhibition of T3A-induced apoptosis and caspase 3 activation (24), as do HEK293 cells expressing a kinase-dead mutant MEKK1 (24). These results suggest that MEKK1-dependent JNK activation may play a key role in reovirus-induced apoptosis.

The mechanism by which reovirus infection could potentially activate MEKK1 remains unknown. It has been shown that viral engagement of the JAM1 receptor and sialic acid co-receptor are critical for T3D-induced activation of NF- $\kappa$ B (28,29), but it is unknown if receptor engagement or early disassembly events are also critical for activation of MAPK pathways. MEKK1 can also be activated through pathways downstream of death receptors (see below). However inhibition of reovirus-induced TRAIL-mediated engagement of death receptors 4 and 5 (DR4, DR5) in L929 cells with soluble DR4/DR5 receptors (19,21), although dramatically inhibiting apoptosis, does not inhibit reovirus-induced phosphorylation of c-Jun, suggesting that activation of the DR-pathway is not the critical event in JNK activation (21).

**Ras signaling pathways.** The presence of an active Epidermal Growth Factor Receptor (EGF-R) on mouse fibroblasts enhances the efficiency of reovirus infection (87). This activity appears dependent on functional EGF-R tyrosine kinase activity. Studies in NIH-3T3 fibroblasts indicates that a similar enhanced efficiency of infection occurs in cells transfected with *v-erbB* oncogene constructs with active tyrosine kinase (TK) activity (88). Activation of EGF-R by ligand binding results in receptor autophosphorylation and subsequent recruitment of adapter molecules including Grb2 and the guanine nucleotide-exchange factor Sos. Grb2/Sos in turn activates

the Ras-GTP signaling pathway. Transfection of NIH-3T3 cells with either *Sos* or *Ras* also enhances susceptibility to reovirus infection (89). Activated Ras-GTP is involved in a wide variety of kinase signaling pathways including those involving PI3 kinase and Raf kinase, and may inhibit virus-induced PKR responses perhaps through a *Ras*-inducible PKR kinase inhibitor (RIKI). In NIH-3T3 cells reovirus replication appears to be normally restricted by reovirus-induced activation of PKR (89), suggesting that this may be a key antiviral pathway that is inactivated by activated *Ras*.

Recent studies suggest that the RalGEF signaling pathway may also play an important role in the enhanced replication efficiency of reovirus in *Ras*-transformed cells (59). *Ras* and RalGEFs have been associated with activation of NF- $\kappa$ B, cyclin D, and activation of both JNK and p38 MAP kinases. Although JNK activation has been associated with reovirus-induced apoptosis (21,24), inhibition of JNK with SB600125 did not inhibit reovirus protein synthesis in NIH 3T3 cells with activated *Ras* (59), nor does JNK inhibition reduce viral yield in HEK293 cells (24). Interestingly, inhibition of p38 with SB203580 did inhibit reovirus protein synthesis in NIH 3T3 cells (59) despite the absence of effects of this inhibitor on reovirus-induced apoptosis in HEK293 cells (24). These data suggest that cell signaling pathways involved in apoptosis and enhanced viral growth may be dissociable, consistent with results suggesting a lack of correlation between viral growth and apoptosis induction.

**Oncolysis.** Reovirus-induced killing of tumor cells, a property often referred to as "oncolysis," is due to induction of apoptosis in target cells (20). Tumors and tumor cells with an activated *Ras* pathway appear particularly susceptible to reovirus-induced cell death (26,59,89). Reovirus-induced oncolysis has been demonstrated in an extensive variety of tumor types both *in vitro* and *in vivo*, including gliomas (98), breast cancers (20,58,101), lung cancers (20), ovarian cancers (41), colon cancers (41), lymphoid malignancies (2), medulloblastoma (100), and bladder cancer (47). Based on these animal studies, a proprietary reovirus preparation ("reolysin," Oncolytics Biotech Inc., Calgary, Canada) has recently been tested in Phase I human clinical trials involving direct inoculation of virus into subcutaneous tumors, prostate cancers, and recurrent malignant gliomas. A trial of intravenous administration of reolysin in patients with advanced stage primary or metastatic solid tumors that have failed other chemotherapies has also recently been instituted (see [www.oncolyticsbiotech.com](http://www.oncolyticsbiotech.com)).

**NF- $\kappa$ B.** Reoviruses share with many other viruses the capacity to perturb regulation of the transcription factor NF- $\kappa$ B (14). All reovirus strains tested to date induce an initial early phase of NF- $\kappa$ B activation (22,27), with T3A

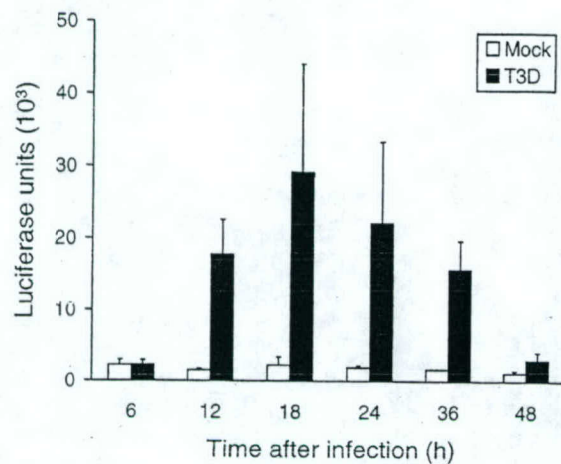


FIG. 13. T3D-induced expression of an NF-κB-dependent luciferase reporter gene in HeLa cells. From Connolly et al. (27) with permission.

and T3D strains having the capacity to subsequently inhibit NF-κB activation (22). Under resting conditions, NF-κB is complexed with its inhibitor, IκB, and retained in the cytoplasm. The canonical pathway of NF-κB activation involves the phosphorylation, ubiquitination, and proteosomal degradation of IκB, which exposes a nuclear localization signal on NF-κB, allowing it to translocate to the nucleus where it activates expression of genes containing promoters with NF-κB consensus binding sequences.

F13 → T3-induced NF-κB activation can be detected as early as 2–4 h post-infection, peaking at 4 h in HEK293 cells and at 8–10 h post-infection in HeLa cells as determined by electrophoretic mobility shift assays (EMSA) (22,27). Nuclear extracts from T3-infected HeLa cells contain both the p50 and p65 subunits of the NF-κB RelA heterodimer (27). In T3D-infected HeLa, NF-κB-dependent expression of a luciferase reporter gene is detected by 12 h pi, reaches a maximum at 18 h pi (27) (Fig. 13). Results are essentially similar in T3A-infected HEK293 cells with luciferase activity detected at 6 h, peaking at 12 h, and returning to baseline by 24 h pi (22). In HeLa cells, this initial phase of T3-induced NF-κB activation requires viral binding to sialic acid residues, as a T3SA<sup>-</sup> strain failed to activate NF-κB when compared to its isogenic SA<sup>+</sup> counterpart. Furthermore, pre-treatment of cells with neuraminidase, to remove cell surface sialic acid, abrogates NF-κB activation by SA<sup>+</sup> virus (28). The pathways by which T1 strains, such as the prototype T1L activate NF-κB (22) differ from those utilized by T3 strains as T1 strains fail to bind sialic acid.

NF-κB activation in HeLa cells does not require viral replication, as it is not inhibited by ribavirin (29). How-

ever, receptor binding alone is apparently insufficient to induce NF-κB activation, as it is inhibited in cells treated with lysosomotropic agents (ammonium chloride, E64) that prevent virion disassembly (29). These results indicate that it is a step in the disassembly process rather than just receptor engagement that triggers NF-κB activation.

The initial phase of NF-κB activation is followed by a later second phase of reovirus-induced inhibition of NF-κB activation (22). In HEK293 cells, both etoposide and TNFα are potent inducers of NF-κB activation. Cells infected with T3A and then stimulated with either etoposide or TNFα show markedly reduced levels of NF-κB activation compared to uninfected cells (Fig. 14). This inhibitory effect is associated with failure to degrade the cytoplasmic inhibitor of NF-κB, IκB. This effect is detectable as earlier as 4 h pi, and reaches a maximum by 12 hrs pi, by which time IκB levels are comparable to those seen in unstimulated control cells.

Reovirus-induced NF-κB inhibition in HEK293 cells requires viral replication. Following treatment with etoposide, cells infected with T3A and the reovirus replication inhibitor ribavirin show a normal pattern of NF-κB activation and associated degradation of the inhibitor, IκB (22). This suggests a model in which an early step (ribavirin insensitive) in viral replication results in NF-κB activation, whereas a later step (ribavirin sensitive) is required for the subsequent inhibition of NF-κB activation. Ribavirin treatment also inhibits the ability of reovirus to induce apoptosis in HEK293 cells (22), suggesting that in these cells the second inhibitory phase may be more critical to apoptosis induction than the initial NF-κB activation. This phenomenon may be cell type spe-

F14

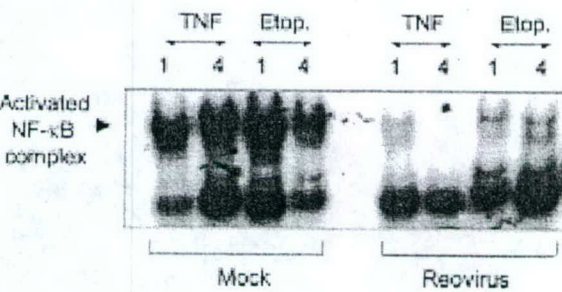


FIG. 14. T3A prevents TNF and etoposide-induced activation of NF-κB in HEK293 cells. Cells were infected with T3A and then 12 h later treated with TNF (100 ng/mL) or etoposide (100 μM). Nuclear extracts were prepared 1 or 4 h post-stimulus treatment as indicated in the figure. NF-κB activation was measured by electrophoretic mobility shift assay (EMSA) using an oligonucleotide probe with NF-κB binding sequences. Note the marked reduction in the size of the shifted (activated) NF-κB complex in the reovirus infected lanes compared to mock-infected controls. From Clarke et al. (22) with permission.

cific, as in contrast to the results seen in HEK293 cells, ribavirin inhibited apoptosis in HeLa cells (22,29).

Reovirus infection sensitizes many epithelial cells and human cancer cell lines, to killing by the apoptosis inducing ligand TRAIL (19,20). Cell lines vary in their sensitivity to TRAIL, and reovirus infection can make some previously TRAIL-resistant lines sensitive to killing by TRAIL (19,20). The capacity of reovirus to sensitize HEK293 cells to TRAIL killing was blocked by ribavirin treatment, suggesting that the TRAIL sensitization phenomenon required the late phase of NF- $\kappa$ B inhibition. Further evidence in support of this concept came from studies in HEK293 cells stably expressing a dominant negative I $\kappa$ B- $\Delta$ N2 that acts to inhibit activation of NF- $\kappa$ B. These cells show enhanced sensitivity to apoptotic killing by TRAIL, similar to that seen in wild-type cells in which NF- $\kappa$ B inhibition occurred as a consequence of reovirus infection.

Although reovirus-induced regulation of NF- $\kappa$ B is still a subject of active investigation, a unitary hypothesis would suggest that at an early stage following viral infection (prior to onset of viral RNA synthesis and therefore insensitive to ribavirin inhibition) virus induces the activation of NF- $\kappa$ B. This activation exerts a pro-apoptotic influence, presumably through NF- $\kappa$ B mediated regulation of expression of as yet unidentified pro-apoptotic genes. At a later step in replication, following RNA synthesis and therefore sensitive to inhibition by ribavirin, infection induces an inhibitory state that may be designed to prevent expression of NF- $\kappa$ B-dependent apoptosis-inhibitory genes (51).

#### REOVIRUS-INDUCED CHANGES IN EXPRESSION OF APOPTOSIS-RELATED HOST CELL GENES

Reovirus-induced alterations in activation of transcription factors, including c-Jun and NF- $\kappa$ B, suggests that virus-induced changes in host cell gene expression are likely to play an important role during viral pathogenesis in general and in apoptosis in particular. Reovirus T1L and T3A-induced changes in gene expression following infection of HEK293 cells have been examined using oligonucleotide microarrays (34,65). Using microarrays (Affymetrix HU95A) containing probes for over 12,000 human genes, T3A was found to induce altered expression (twofold or greater change) compared to mock infection of 18 genes at 6 h pi, 86 at 12 h pi, and 309 at 24 h pi (34). T1L produced more modest changes, inducing alteration in expression compared to mock of only 59 genes at 24 h pi. All of the changes induced by T3A at 6 h pi involved up-regulation of expression, although at 12 and 24 h there were

both up- and down-regulated genes (34). Categorization of these genes into functional groupings indicates that a significant number of affected genes encode proteins involved in apoptotic signaling including mitochondrial, endoplasmic reticulum, and death receptor signaling as well as proteases including calpain and caspases (Tables 1 and 2). An additional group of affected genes encode proteins involved in DNA damage repair pathways (34). Of 24 genes involved in apoptotic signaling pathways whose expression was altered following infection with the APO<sup>+</sup> T3A strain, only five were also found to be altered following infection with the APO<sup>-</sup> T1L strain (34). Similarly, of 14 identified genes involved in DNA damage and repair pathways whose expression was altered by APO<sup>+</sup> T3A, none were altered following infection with APO<sup>-</sup> T1L. Interestingly, the majority of T3A induced changes in expression involved up-regulation of apoptotic signaling genes (19 of 24 at 24 h pi) and down-regulation of DNA repair genes (11 of 14 at 12 or 24 h) (34). Taken together the patterns of gene expression suggest that infection of cells with APO<sup>+</sup> reovirus strains enhances expression of genes involved in ER stress and both death receptor and mitochondrial apoptotic signaling, and shifts the balance toward pro-apoptotic Bcl-2 family proteins (34). This was combined with a down-regulation by the APO<sup>+</sup> virus of genes encoding proteins involved in cellular DNA repair, which would be predicted to impair the cell's ability to repair DNA damage and thereby promote apoptosis induction.

T1,2

#### REOVIRUS APOPTOSIS *IN VIVO*

**Central nervous system (CNS).** In addition to inducing apoptosis in a variety of continuous cell lines, reovirus-induced apoptosis also occurs *in vivo* in both the central nervous system (CNS) (60,61,69,70,71) and heart (33,35), in addition to both primary neuronal cultures (69,70) and primary cardiac myocytes (33,35). Following intracerebral (ic) inoculation of reovirus T3D into 1-day-old Swiss Webster (Tac:(SW)fBR) mice neurons undergo morphological changes characteristic of apoptosis including cytoplasmic shrinkage, chromatin condensation, and nuclear pyknosis and fragmentation. Cells staining positive by TUNEL (terminal deoxynucleotidyl transferase (TdT)-mediated dUTP nick end-labeling) can be detected as early as 3 days pi and progressively increasing in both number and extent until the death of animals at ~day 8–10 (60,61). DNA extracted from whole brains at 8–9 days pi showed a characteristic laddering pattern consistent with oligonucleosomal DNA fragmentation pathognomonic of apoptosis (60,61). Staining for the activated form of the effector caspase, caspase 3, co-local-

TABLE 1. REOVIRUS-INDUCED ALTERATION IN EXPRESSION OF GENES ENCODING PROTEINS KNOWN TO REGULATE APOPTOTIC SIGNALING

Gene	GenBank accession no. <sup>a</sup>	Change in expression (n-fold) <sup>b</sup> at the indicated time (h) after infection with:			<i>T3A</i> 24	<i>TIL</i> 24
		6	12	24		
<b>QU4 Mitochondrial signaling</b>						
Pim-2 proto-oncogene homologue	U77735				-2.2 ±0.1	
MCL1 L08246	2.0±	2.2±			0.0	0.0
BAC 15E1-cytochrome C oxidase polypeptide	AL021546				2.1± 0.0	
Par-4	U63809				2.1± 0.0	
HSP-70 (heat shock protein 70 testis variant)	D85730				2.2± 0.1	
BNIP-1 (BCL-2 interacting protein)	U15172				2.3± 0.2	
SMN/Btfp44/NAIP (survival motor neuron/neuronal apoptosis inhibitor protein)	U80017				2.5± 0.1	
DRAK-2	AB011421				2.8± 0.2	
SIP-1	AF027150				3.0± 0.2	
DP5	D83699				5.5± 1.1	
<b>ER stress-induced signaling</b>						
ORP150	U65785				-2.4 ±0.2	
GADD 34	U83981	6.8±	3.7±	2.9±	0.2	
GADD45	M60974	3.3±	4.9±	4.4±	0.2	0.2
					0.1	0.1
<b>Death receptor signaling</b>						
Bcl-10	AJ006288				5.6± 1.1	
PML-2	M79463				3.4± 0.3	
Ceramide glucosyltransferase	D50840				4.0± 1.2	
Sp100	M60618				6.5± 0.3	
					5.8± 0.6	
<b>Proteases</b>						
Calpain (calcium-activated neutral protease)	X04366				-2.6 ±0.1	
Beta-4 adducin	U43959				-2.1 ±0.1	

TABLE 1. REOVIRUS-INDUCED ALTERATION IN EXPRESSION OF GENES ENCODING PROTEINS KNOWN TO REGULATE APOPTOTIC SIGNALING (CONTINUED)

Gene	GenBank accession no. <sup>a</sup>	Change in expression (n-fold) <sup>b</sup> at the indicated time (h) after infection with:			
		6	12	24	TIL 24
Caspase 7 (lice-2 beta cysteine protease	U67319			2.6 ± 0.2	
Caspase 3 (CPP32)	U13737	3.2 ±	2.8 ±	0.2	0.1
<u>Undefined</u>					
Frizzled related protein	AF056087		-2.5	-3.3 ± ± 0.1	0.5
TCBP (T cluster binding protein)	D64015			3.3 ± 0.2	
Cug-BP/hNAb50 RNA binding protein	U63289			6.6 ± 1.1	

<sup>a</sup>GenBank accession number corresponds to sequence from which the Affymetrix U95A probe set was designed.<sup>b</sup>Data are means ± standard errors of the means.

TABLE 2. REOVIRUS-INDUCED ALTERATION IN EXPRESSION OF GENES ENCODING PROTEINS KNOWN TO BE INVOLVED IN DNA REPAIR

Gene	GenBank accession no. <sup>a</sup>	Change in expression (n-fold) <sup>b</sup> at the indicated time (h) after infection with:			
		6	12	24	TIL 24
QU4 → DNA ligase I	M36067			-8.2 ± 1.1	
PARPL	AF057160			-6.3 ± 0.7	
XP-C repair complementing protein (p125)	D21089			-3.4 ± 0.1	
DNA polymerase gamma	U60325		-1.9 ± 0.1	-2.9 ± 0.1	
ERCC5	L20046		-2.7 ± 0.1		
DNA polymerase alpha	L24559			-2.5 ± 0.2	
HLP (helicase-like protein)	U09877		-2.4 ± 0.1		
GTBP	U28946		-2.0 ± 0.1	-2.1 ± 0.0	
DDB2 (p48 subunit)	U18300			-2.0 ± 0.0	
RAD 54 homologue	X97795			-2.0 ± 0.1	
Mi2 autoantigen	X86691		-1.3 ± 0.1	-2.0 ± 0.1	
MMS2	AF049140			2.1 ± 0.0	
Rad-51-interacting protein	AF006259			2.6 ± 0.2	
Rec-1	AF084513			2.4 ± 0.4	

<sup>a</sup>GenBank accession number corresponds to sequence from which the Affymetrix U95A probe set was designed.<sup>b</sup>Data are means ± standard errors of the means.

izes with TUNEL staining and is widespread in areas of virus injury by day 7 pi (69,70).

Within the CNS, the most significantly involved areas include the cingulate gyrus (notably layer V), thalamus, and hippocampus (CA1–CA3). The involved cells appear to be predominantly neurons as determined by their morphology (60,61), consistent with results in primary neuronal cultures derived from E20-P0 Swiss Webster mice in which cell-type specific markers confirm that it is neurons (neuron nuclear protein, NeuN-positive cells) rather than glial cells (GFAP positive) that are infected by T3D and that undergo apoptosis (70).

In the CNS, there is an excellent correlation between the areas of viral injury detected histopathologically, the sites of viral infection detected by immunocytochemistry for viral antigen, and regions of apoptosis detected by either TUNEL staining or staining for activated caspase 3 (60,61,69,70) (Fig. 15). Double staining of tissue sections for both viral antigen and apoptosis suggests that apoptosis occurs both in productively infected cells (direct apoptosis) and in uninfected cells in close proximity to infected cells (bystander apoptosis) (60,61). A similar phenomenon can be observed in primary neuronal cultures. In T3D-infected mouse cortical neuronal cultures at 48 h pi, 38% of cells are both antigen and TUNEL positive, and 12% TUNEL positive but antigen negative, suggesting that direct apoptosis accounts for three-fourths of the apoptotic neurons, and bystander apoptosis for the remainder. Essentially similar results were seen in the NB41A3 neuroblastoma cell line (69).

The co-localization of viral antigen, apoptosis, and tissue injury strongly suggests that apoptosis is an important mechanism of reovirus-induced CNA injury. Additional support for this idea comes from studies of an attenuated reovirus T3D variant, variant K (84). Variant K was selected from T3D stocks based on its capacity to resist neutralization by a monoclonal antibody (9BG5) directed against the viral  $\sigma 1$  protein (84). Nucleotide sequence analysis indicates that variant K differs from its T3D parent by a single amino acid substitution at amino acid position 419 (K419L) within the globular head domain of the S1 gene encoded sigma 1 (11). Variant K is of particular interest, as the S1 gene is a determinant of strain-specific differences in the ability of reovirus strains to induce apoptosis in a variety of cell lines. After intracerebral inoculation variant K has attenuated neurovirulence associated with reduced growth and a restricted pattern of tissue injury compared to T3D (84,85). Studies with a reassortant virus containing the Variant K S1 gene on a T1L ("1HAK") background confirm that it is the S1 gene mutation that accounts for these properties (46). Both variant K and T3D produce injury in the hippocampus, but only T3D produces significant injury in the thalamus, frontoparietal cortex and cingulate gyrus

(70,85). Variant K infected mice can survive infection and clear virus, although focal hippocampal lesions are still detectable in mice sacrificed >80 days pi (70).

Following IC inoculation, variant K and T3D show similar patterns of regional growth, apoptosis, and caspase 3 activation in the hippocampus (70). By contrast, the growth of variant K is markedly reduced in other brain regions, and apoptosis is not detectable. These results have been replicated in primary neuronal cultures derived from hippocampus and cortex. Variant K and T3D grow to identical titers hippocampal cultures and produce equivalent amounts of apoptosis. By contrast, in cortical cultures T3D grows significantly better and produces significantly more apoptosis and higher levels of caspase 3 activation than variant K (70).

Studies in non-neuronal cells indicate that the capacity of reovirus strains to grow in these cells does not correlate with its capacity to induce apoptosis. For example, both T3D and T1L grow to equivalent titers in L929 cells, yet T3D induces significantly more apoptosis than T1L (92). In MDCK cells, T1L grows significantly better than T3D, yet T3D induces significantly higher levels of apoptosis (73). This suggests that it might be the reduced capacity of variant K to induce apoptosis in cortical neurons that results in its impaired growth in these cells, rather than the impaired growth inhibiting apoptosis. Support for this hypothesis comes from studies in which inhibiting apoptosis reduced the growth of T3D in primary cortical neurons and augmenting apoptosis enhanced growth of variant K (70). T3D-infected cortical neurons were treated with the cell-permeable pancaspase inhibitor ZVAD-fmk, which reduces apoptosis and decreases viral titer in addition to viral yield to levels at or below those seen in variant K infected cultures. Similar results are seen with the caspase 3 inhibitor DEVD-fmk, but not with an irrelevant caspase inhibitor used as a negative control (YVAD-fmk an inhibitor of caspase 1, a caspase not involved in reovirus-induced apoptosis). These results clearly indicate that inhibition of apoptosis could inhibit viral growth in neuronal cultures. Conversely, treatment of variant K infected cortical neurons at 18 h pi with an antibody that augments apoptosis by binding to and activating the death receptor FAS, enhances apoptosis to levels similar to those seen following T3D infection and significantly augments viral titer and yield, although not to levels seen with T3D. Treatment of variant K infected cortical neuronal cultures with caspase inhibitors does not further reduce either apoptosis or viral yield, nor does treatment of T3D-infected cultures with FAS activating antibody further increase apoptosis or viral yield in T3D-infected cultures.

The variant K studies provide support for the importance of  $\sigma 1$  as a mediator of apoptosis, as at least in cortical neurons, variant K has attenuated apoptosis induc-

F15

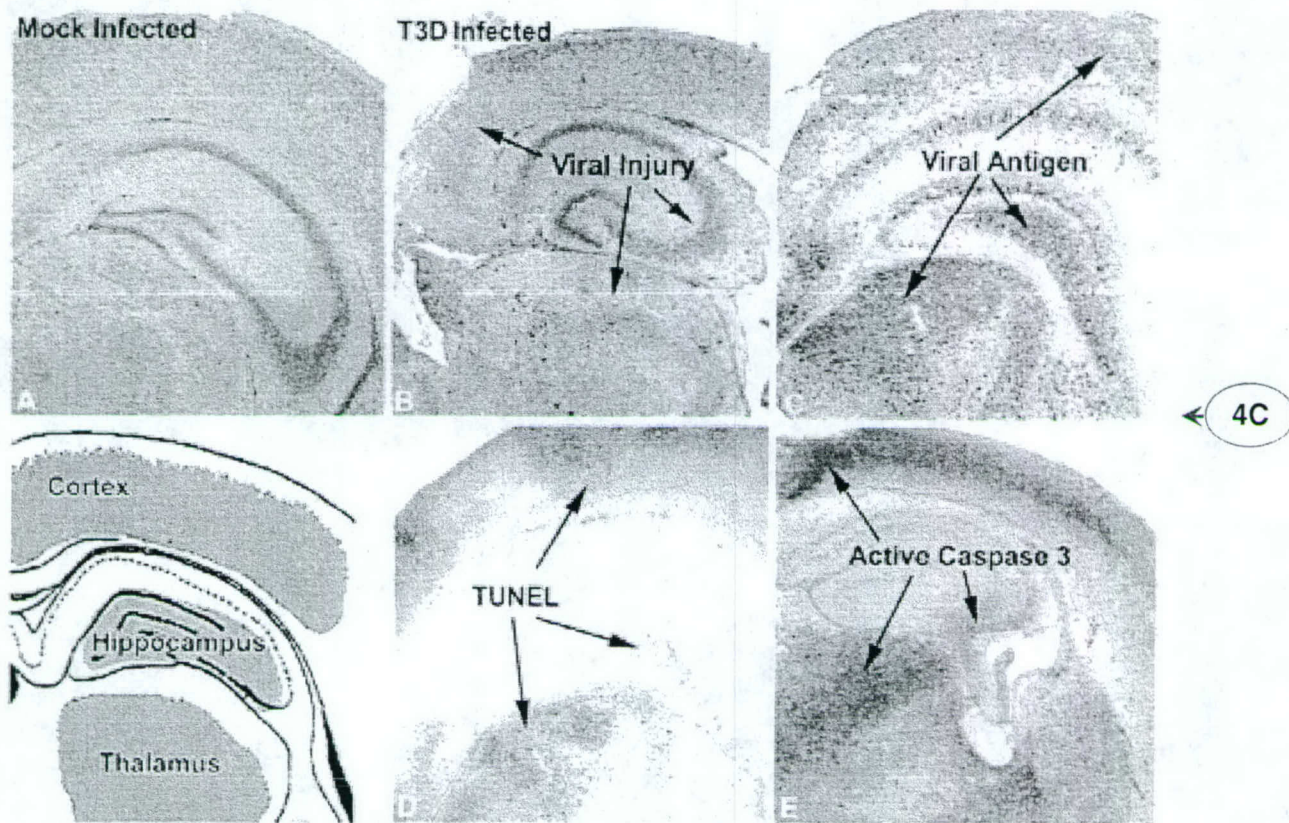


**FIG. 15.** Correlation between viral injury, viral antigen, apoptosis, and caspase-3 activation in the brains of neonatal mice 7 days after intracerebral inoculation with T3D. From Richardson-Burns et al. (69) with permission.

ing capacity. However, variant K remained fully capable of inducing apoptosis and activating caspase 3 in hippocampal neurons, indicating that apoptotic signaling pathways and requirements for induction differ within distinct populations of neurons. These studies also provide evidence that inhibiting apoptosis may decrease viral yield and augmenting apoptosis may increase viral yield in the CNS.

$\sigma 1$  is not the only reovirus protein that can influence CNS apoptosis *in vivo*. The reovirus S1 gene is bicistronic, encoding the viral attachment protein  $\sigma 1$  and a small non-structural protein,  $\sigma 1s$ , from overlapping but out-of-sequence reading frames. The reovirus T3  $\sigma 1s$  null mutant virus clone 84MA (C84MA) has attenuated neurovirulence after intracerebral inoculation (43). The  $\sigma 1s$  null virus grows to equivalent titer in the brain as  $\sigma 1s^+$  control viruses, indicating that its attenuated neurovirulence is not simply the result of reduced viral growth. By contrast, mice infected with  $\sigma 1s$  null virus show significantly delayed onset of caspase 3 activation and apoptosis compared to mice injected with control serotype 3  $\sigma 1s^+$  viruses (43). This suggests that  $\sigma 1s$  serves to mod-

ulate the efficiency with which T3 reoviruses induce CNS apoptosis, with the  $\sigma 1s$  null virus showing less severe and less extensive apoptosis than its  $\sigma 1s^+$  counterparts. The fact that mice infected with  $\sigma 1s$  null virus eventually developed significant apoptosis indicated that lack of this protein only delayed but did not prevent apoptosis induction in the CNS. In  $\sigma 1s$  null virus infected mice, the extent of CNS tissue injury and apoptosis were both delayed and paralleled each other in extent and severity, providing additional evidence that apoptosis is the major mechanism of tissue injury following T3 infection of the CNS.

Given the importance of apoptosis in the development of reovirus-induced CNS tissue injury, it is of great interest to determine whether inhibition of apoptosis could provide a novel strategy for antiviral therapy by influencing the pathogenesis of reovirus-induced CNS disease (71). The antibiotic minocycline, a synthetic tetracycline derivative, is known to be neuroprotective in several models of neurodegenerative disease, traumatic CNS injury, and CNS hypoxic-ischemic injury (5,38,97,104). The mechanisms by which minocycline exerts its neuro-

protective effects have not been definitively established, but can include inhibition of mitochondrially mediated apoptosis pathways through decreasing the release of mitochondrial pro-apoptotic factors including cytochrome *c* and Smac/DIABLO (78,104), and through up-regulation of Bcl-2 and IAPs (78,96). In addition, minocycline may inhibit microglial-mediated excitotoxic pathways that contribute to neuronal cell death (91). Minocycline delays but does not prevent CNS injury *and* the onset of death in a reovirus model of encephalitis, consistent with its effects in other models of neurodegeneration. In the reovirus studies, neonatal mice were injected intracerebrally with 3000 pfu of T3D ( $\sim 300 \times LD_{50}$ ) and then treated beginning at 48 hrs post infection with minocycline (35 mg/kg ip daily). Minocycline treated mice survived an average of three days longer than untreated controls (mean day of death  $11.6 \pm 0.9$  vs.  $8.6 \pm 0.7$ ,  $p < 0.01$ ) (71). A survival effect was even noted when the challenge dose was increased to 30,000 pfu ( $30,000 \times LD_{50}$ ). The prolonged survival in treated mice was associated with reduction and delay in onset of the extent of CNS viral injury in thalamus, hippocampus, and cingulate gyrus. Reduction in injury correlated with a decrease in the number of apoptotic neurons in each of these brain regions (71). This effect is likely due to an anti-apoptotic action of minocycline, as microglial activation and astrogliosis is not prominent at times when tissue injury has been dramatically reduced by minocycline (71). Consistent with earlier results with other apoptosis inhibitors, minocycline slowed the kinetics of viral replication in the CNS, although peak titers eventually reached those achieved in untreated animals (71). A similar beneficial effect of minocycline treatment has recently been described in a Sindbis-virus model of spinal motor neuron death (31).

The identification of mammalian Toll-like receptors (TLRs) was followed by the recognition that binding of microbial ligands to these receptors could trigger the activation of NF- $\kappa$ B, and the subsequent up-regulation of specific cytokines and related co-stimulatory molecules (1,13). TLR3 is of potential interest in the context of reovirus infection, as it is the only TLR that binds double-stranded RNA, and this leads to NF- $\kappa$ B activation and enhanced production of type 1 interferons ( $\alpha/\beta$ ) (3,53). TLR3  $(-/-)$  mice have been utilized to study the potential role of this TLR in viral pathogenesis (36). The extent and distribution of reoviral injury, antigen, apoptosis, and total brain titer are identical in wild-type (TLR 3  $(+/+)$ ) and TLR 3  $(-/-)$  mice, suggesting that this TLR does not play a critical role in either reovirus-induced CNS apoptosis or pathogenesis (36).

**Heart.** Reoviruses provide an important experimental model system for studying viral myocarditis (81). The most extensively characterized myocarditic strain is a re-

assortant virus, 8B, which was initially isolated following simultaneous inoculation of mice with reovirus strains T1L and T3D. When injected intramuscularly (im) into neonatal mice, 8B is efficiently myocarditic even at low doses, producing extensive cardiac tissue injury, that is the result of direct viral injury to mycardiocytes rather than immune-mediated mechanisms (81).

The myocardial injury induced by 8B is the result of apoptosis. At 7 days pi (im) sections from infected mice show extensive areas of TUNEL-positive nuclei which co-localize with regions of viral injury seen histologically, and viral infection as identified by antigen staining (33) (Fig. 16). DNA extracted from infected hearts shows characteristic oligonucleosomal DNA laddering (33). The kinetics of development of apoptosis and myocardial injury in the heart has been examined in detail (35). Apoptosis, as determined by TUNEL and staining for activated caspase 3, viral growth, and evidence of histologic injury develop in parallel. Injury and apoptosis are typically detectable as early as 4 days pi, and increases steadily in severity and extent thereafter. By day 7, the degree of involvement is extensive, involving 18% (TUNEL) to 23% (activated caspase 3) of the cross-sectional myocardial area.

Apoptosis is also clearly demonstrable using TUNEL, Annexin PI and activated caspase 3 staining in 8B-infected primary cardiac myocyte cultures derived from neonatal mice (35). The "flipping" of phosphatidylserine residues from the inner to the outer surface of the cell membrane, a marker of apoptosis-related changes in cell membranes, can be detected by binding of Annexin V. Using flow cytometric analysis of annexin V positivity, nearly 50% of virus-infected cells are positive at 48 h pi, increasing to  $>90\%$  by 72 h. Although the absolute numbers are lower (35–30% positive cells), there is also a significant increase at 48 h pi in the percentage of both TUNEL and activated caspase 3-positive cells in virus compared to mock infected cultures at 48 h pi (35).

The reovirus myocarditis model is a valuable system for testing the effects of apoptosis inhibition on viral pathogenesis (33,35). A variety of apoptosis inhibitors have been shown to reduce reovirus-induced cell death *in vitro*. This suggests that apoptosis inhibitors might also reduce the extent of virus-induced tissue injury *in vivo*, providing a potentially novel strategy for antiviral therapy. Proof of this principle came initially from studies of calpain inhibitor treatment of 8B-induced myocarditis. Calpain was initially shown to be activated following reovirus infection of L929 cells *in vitro*, and inhibition of this activation inhibits reovirus induced apoptosis (32). Calpain was subsequently shown to be activated in 8B-infected primary cardiac myocytes as detected by the appearance of calpain-specific spectrin cleavage products in infected cells (33). To test the ef-

F16

300,000

Superscript  
TLR3<sup>+</sup>  
TLR3<sup>-/-</sup>

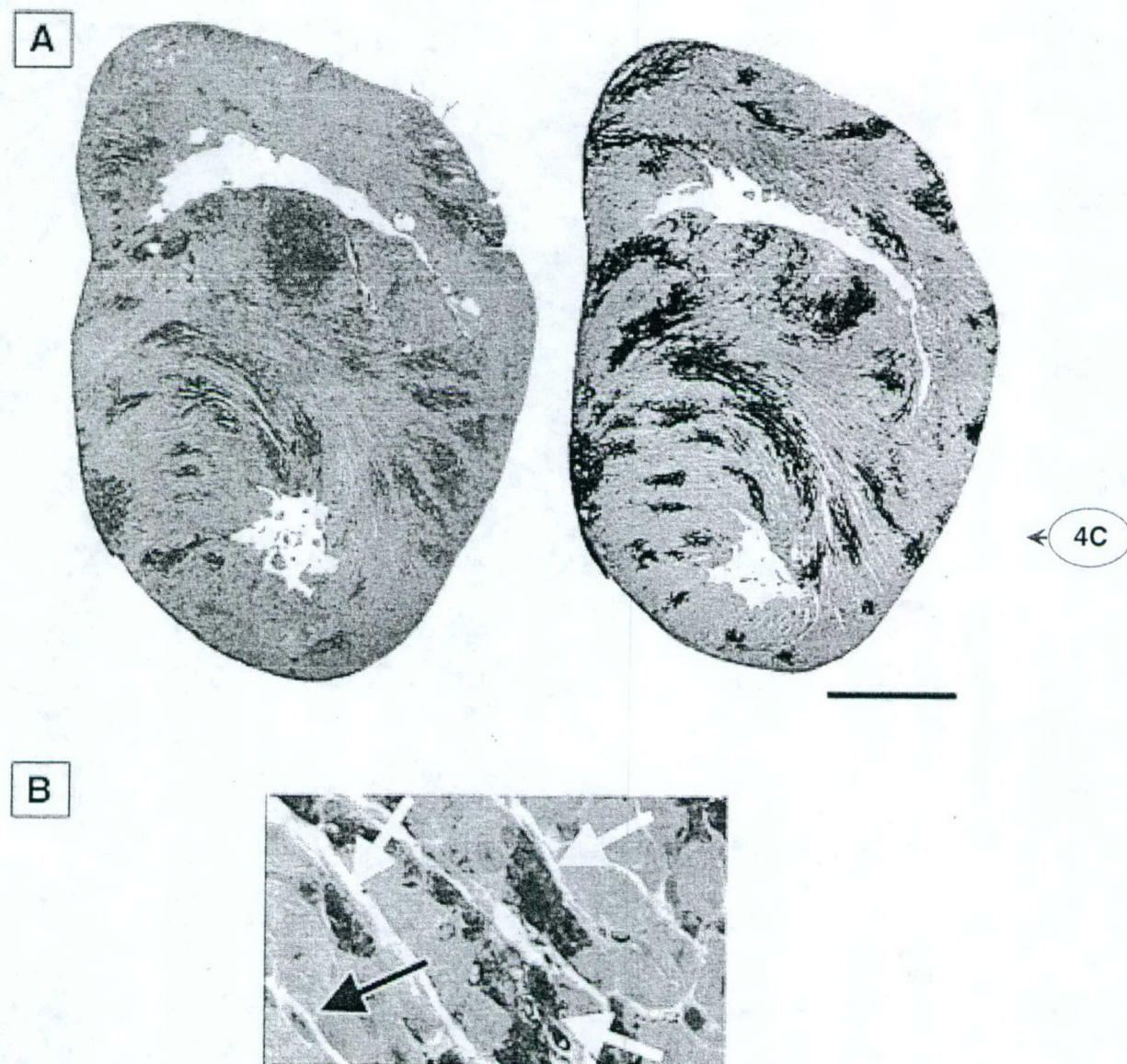


**FIG. 16.** Apoptosis in the hearts of neonatal mice 7 days after infection with the myocarditic reovirus strain 8B. (A) TUNEL staining (left) and staining for active caspase 3 (right). (B) Positive staining for active caspase 3 in cardiac myocytes (white arrows). A negative fibroblast is also shown (black arrow). From DeBiasi et al. (35) with permission.

fects of calpain inhibition on 8B-induced myocardial apoptosis *in vivo*, neonatal mice were treated with six daily intraperitoneal (ip) inoculations of the calpain inhibitor CX295 (Cortex Pharmaceuticals) beginning at 30 min prior to infection with 8B. CX295 is a specific inhibitor of calpain, and does not inhibit caspase 2 or 3 at doses tested (100  $\mu$ M) and was shown to inhibit reovirus-induced calpain activation in 8B-infected mouse primary cardiac myocytes (33). 8B-infected CX295-treated mice showed a significant reduction in the sever-

ity and extent of cardiac lesions using a standardized lesion scoring scale ( $3.0 \pm 0.1$  to  $0.6 \pm 0.1$ ,  $p < 0.0001$ ) (33). A significant reduction in serum CPK levels was also seen in treated compared to control mice. CPK is an intracellular enzyme found in cardiac myocytes that is released into serum in response to tissue injury. Staining of cardiac tissue sections from treated mice showed marked reduction in apoptosis as determined both by morphology of cardiac myocytes and almost complete absence of TUNEL staining (33).

Further evidence for the significance of apoptosis in the pathogenesis of 8B-induced reovirus myocarditis comes from studies using peptide caspase inhibitors (35). 8B-infected mice were treated at days 3–6 pi with daily ip inoculations of the irreversible broad spectrum peptide pancaspase inhibitors Q-VD-OPH or Z-VAD(OMe)-FMK (Enzyme Systems). Compared to controls, Q-VD-OPH reduced myocardial lesion score by 60% and cross-sectional lesion area by 89% (Fig. 17). The effects with Z-VAD(OMe)-FMK were similar but more modest (39% reduction in lesion score, 55% in cross-sectional lesion area). In Q-VD-OPH-treated mice, histological sections were also examined for apoptosis, and treated mice showed a significant decrease in both TUNEL and staining for activated caspase 3 compared to controls.

The studies with both calpain and caspase inhibitors indicated that apoptosis was a major mechanism of myocardial injury in 8B-infected mice. This result was confirmed in studies using transgenic C57B6 caspase-3-deficient mice (gift of Richard Flavell, Yale University) (35). 8B-infected caspase 3<sup>-/-</sup> deficient mice showed reduced cardiac lesion scores compared to both syngeneic caspase 3<sup>+/+</sup> heterozygotes and wild-type caspase 3<sup>++</sup> homozygotes. The caspase 3<sup>-/-</sup> mice had a 58% reduction in lesion score and a 56% reduction in cross-sectional lesion area compared to infected wild-type caspase 3<sup>+/+</sup> mice (35). Heterozygous caspase 3<sup>+/+</sup> mice showed an intermediate phenotype. As expected, staining for activated caspase 3 was not detectable in caspase-3<sup>-/-</sup> mice (although present in hearts of infected wild-type caspase 3<sup>+/+</sup> mice). Apoptosis was reduced in the hearts of infected caspase 3<sup>-/-</sup> mice as assayed by TUNEL (35). Long-term survival is not seen in 8B infected caspase 3<sup>+/+</sup> mice (100% mortality within 9 days pi after im inoculation of 2 day-old mice with 10<sup>4</sup> PFU of 8B). By contrast, 50% of caspase 3<sup>-/-</sup> survived at least 21 days pi, and 37.5% >50 days (Fig. 18). These long-term survivors did not show cardiac lesions when sacrificed (day 54 pi) (35).

Studies in the CNS of an attenuated T3 mutant virus had suggested that defects in apoptosis were associated with decreased viral yield and peak titer (70). Hearts of mice treated with calpain or pancaspase inhibitors showed modest (2–5-fold, 0.3–0.7 log<sub>10</sub>) reductions in viral titer compared to controls. Significantly more dramatic effects were seen in caspase 3<sup>-/-</sup> mice in which a 80-fold (1.9 log<sub>10</sub>) reduction in heart titer was seen compared to caspase 3<sup>+/+</sup> mice (35).

An additional signaling pathway of paramount importance in reovirus-induced myocarditis is the IFN- $\beta$  signaling pathway (77,81,82). Myocarditis can be induced by a normally non-myocarditic reovirus strain in mice depleted of IFN- $\alpha/\beta$ . In addition, non-myocarditic reovirus strains differ from their myocarditic counterparts

by both inducing higher levels of IFN- $\beta$  and by increased sensitivity to its action (82). IFN- $\beta$  induction in infected cardiac myocytes appears to require activation of the transcription factor interferon regulatory factor 3 (IRF3), as over-expression of a dominant negative IRF-3 in these cells blocks virus-induced IFN- $\beta$  (57). Although the actions of IFN- $\beta$  are pleiotropic, a major candidate for mediating its antiviral activity during reovirus infection is the ds-RNA activated protein kinase, PKR. After binding to dsRNA, PKR becomes activated and phosphorylates the eukaryotic initiation factor eIF2 $\alpha$ , which inhibits host cell protein translation. Activated PKR may also act as an I- $\kappa$ B kinase, with phosphorylated I- $\kappa$ B undergoing ubiquitination and degradation allowing cytosolic NF- $\kappa$ B to translocate to the nucleus and activate genes with  $\kappa$ B-responsive promoter elements, a group that includes the IFN- $\beta$  gene. As might be expected from this model, loss of PKR enhances the virulence of both myocarditic and non-myocarditic reovirus strains (86). Perhaps not surprisingly, both avian and mammalian strains of reovirus encode proteins that inhibit the activation of PKR (40,102). Reovirus infection of cardiac myocytes also induces IRF-1, likely through an indirect mechanism that requires prior induction of the IFN- $\alpha/\beta$  response, and mice lacking IRF-1 show more extensive cardiac lesions than wild-type mice (7).

## CONCLUSION

Reovirus infection has served as an experimental model system to understand how specific viral genes and the proteins they encode induce cell death *in vitro* and tissue injury *in vivo*. Recent studies indicate that apoptosis is a major mechanism by which reovirus T3 strains kill target cells. Apoptosis is triggered by early events in the viral replication cycle consequent to viral binding to JAM1 and sialic acid receptors, and not dependent on viral RNA synthesis. In a wide variety of continuous and primary cell lines reovirus-induced apoptosis is initiated by death-receptor activation. Activation of death-receptor signaling pathways results in activation of the death receptor associated initiator caspase 8, which is followed by cleavage of the Bcl-2 family protein Bid. Cleaved Bid translocates to the mitochondria where it is involved with other Bcl-2 family proteins in the activation of intrinsic mitochondrial-associated apoptotic signaling pathways. Activation of pro-apoptotic mitochondrial signaling pathways are also influenced by reovirus-induced activation of JNK which acts to phosphorylate specific Bcl-2 family proteins and may influence their redistribution from cytosol to mitochondria. Pro-apoptotic factors released from mitochondria following reovirus infection include cytochrome *c* and Smac/DIABLO. The mitochondrial-as-

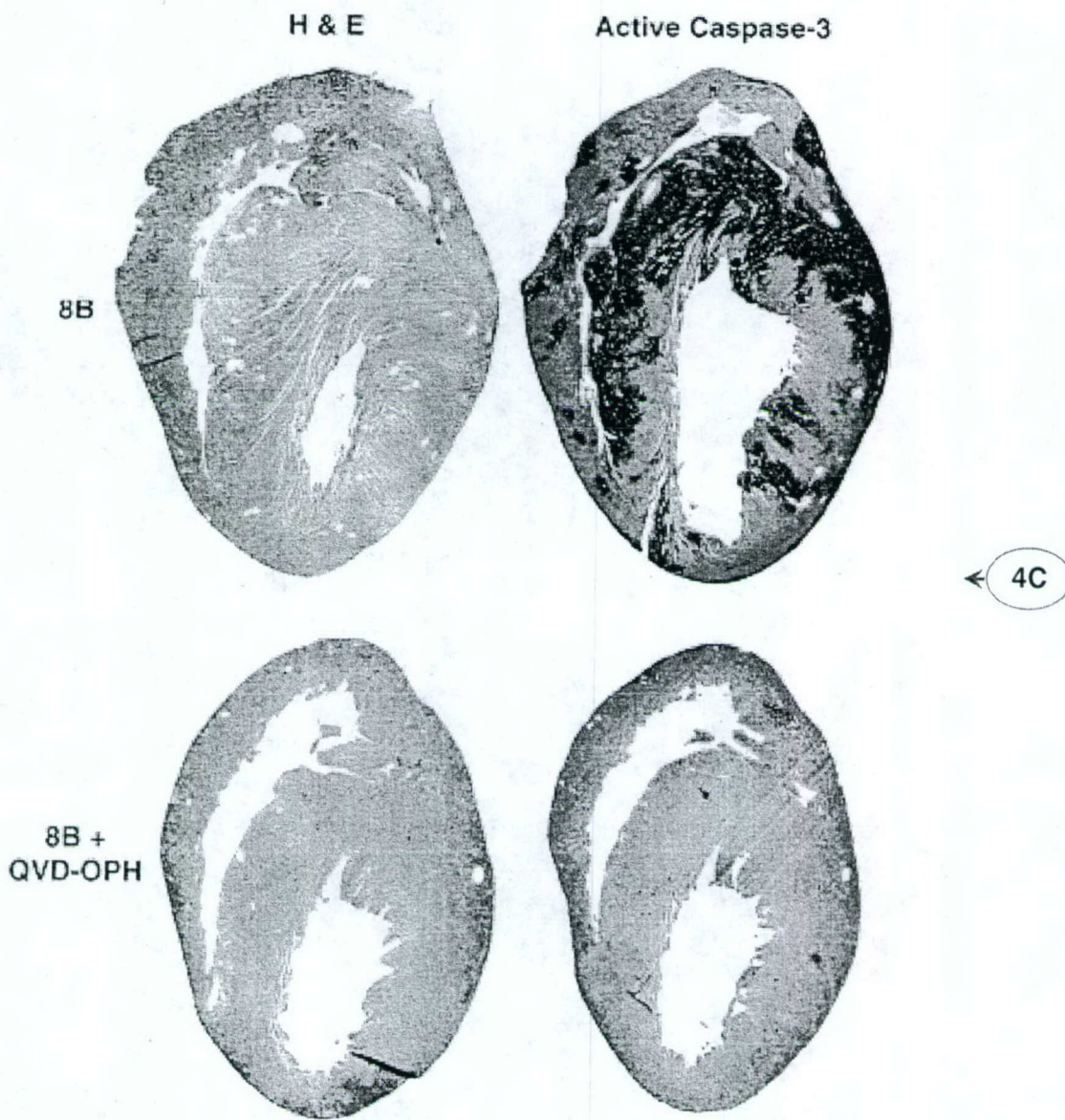
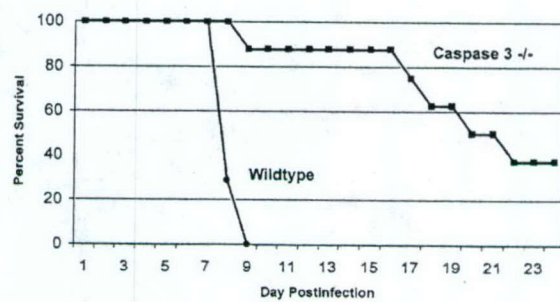


**FIG. 17.** Treatment of neonatal mice with the pancaspase inhibitor Q-VD-OPH inhibits reovirus 8B-induced apoptosis and myocardial injury. Day 7 post-infection. From DeBiasi et al. (35), with permission.

**FIG. 18.** Survival of caspase  $3^{-/-}$  (deficient) mice and their syngeneic caspase  $3^{+/+}$  (wild-type) counterparts following infection with the myocarditic reovirus strain 8B. The caspase 3-deficient mice show enhanced survival and markedly reduced cardiac lesions after infection. From DeBiasi et al. (35) with permission.



sociated initiator caspase 9 is activated following reovirus infection in some but not all cells. Recent studies suggest that Smac/DIABLO-associated degradation of cellular inhibitor of apoptosis proteins plays a critical role in the augmentation of apoptosis signaling pathways in many reovirus-infected cells. Activation of extrinsic and intrinsic cell death pathways leads ultimately to the activation of effector caspases including caspase 3. Inhibition of caspase cascades at multiple levels can inhibit reovirus-induced cell death in cell culture.

Apoptosis is not limited to reovirus-infected cells in culture, but also appears to be the major mechanism of reovirus-induced tissue injury in experimental models of reovirus-induced encephalitis and myocarditis. Apoptosis and activation of caspases can be detected in both the heart and CNS of reovirus-infected mice, and correlates with the localization of viral antigen and tissue injury. Inhibition of virus-induced apoptosis through use of peptide inhibitors of caspases, calpain inhibitors, or treatment of animals with minocycline all ameliorate reovirus-induced tissue injury and prolong survival of infected animals. Even more dramatic reductions in virus-induced tissue injury and beneficial effects on survival are seen in caspase 3<sup>-/-</sup> mice.

In addition to triggering activation of apoptosis signaling pathways, reovirus infection also results in the selective activation of mitogen activated protein kinase cascades including those involving JNK/SAPK. There is an excellent correlation between the capacity of reovirus strains to activate JNK and their capacity to induce apoptosis, and JNK inhibition results in inhibition of apoptosis. In many cells including a wide variety of cancer cell lines, the efficiency of reovirus infection is enhanced by the presence of activated Ras signaling pathways. This effect may be mediated by inhibition of the antiviral effects of PKR and by activation of Ras/RelGEF/p38 signaling. Interestingly, the signaling pathways involved in apoptosis and viral growth may be dissociable, as inhibition of JNK signaling can inhibit apoptosis without affecting efficiency of viral growth. Conversely, inhibition of p38 MAPK signaling may inhibit viral replication without affecting apoptosis.

Reovirus infection also results in selective changes in the regulation of specific transcription factors. Both ERK and JNK activation contribute to the subsequent activation of c-Jun. Reovirus infection also results in early activation of NF- $\kappa$ B, which is followed in the case of infection with T3 strains by subsequent inhibition of NF- $\kappa$ B activation. These alterations in transcription factor regulation play a key role in regulating reovirus-induced apoptosis, suggesting that virus-induced alterations in gene expression play a key role in regulating apoptosis. Oligonucleotide microarrays have been utilized to gain a more comprehensive picture of reovirus-induced alter-

ations in gene expression. These studies reveal significant alterations in genes encoding proteins involved in cell cycle regulation, apoptosis, and DNA damage and repair processes.

## ACKNOWLEDGMENTS

Work described in this paper has been supported by MERIT and REAP grants from the Department of Veterans Affairs (K.L.T.), Public Health Service/NIH grants R01 NS050138 (K.L.T.), 5K08AI52261 (R.L.D.), the U.S. Army Medical Research and Materiel Command Grant DAMD17-98-1-8614 (K.L.T.), the Ovarian Cancer Research Fund (P.C.), and the Reuler-Lewin Family Professorship of Neurology (K.L.T.).

## REFERENCES

1. Akira, S., and K. Takeda. 2004. Toll-like receptor signaling. *Nat. Rev. Immunol.* 4:499–511.
2. Alain, T., K. Hirasawa, K.J. Pon, et al. 2002. Reovirus therapy of lymphoid malignancies. *Blood* 100:4146–4153.
3. Alexopoulou, L., A.C. Holt, R. Medzhitov, et al. 2001. Recognition of double-stranded RNA and activation of NF- $\kappa$ B by Toll-like receptor 3. *Nature* 413:732–738.
4. Amiesen, J.C., O. Pleskoff, J.D. Lelievre, et al. 2003. Subversion of cell survival and cell death: viruses as enemies, tools, teachers, and allies. *Cell Death Diff.* 10 (Suppl 1):S3–S6.
5. Arvin, K.L., B.H. Han, Y. Du, et al. 2002. Minocycline markedly protects the neonatal brain against hypoxic-ischemic injury. *Ann. Neurol.* 52:54–61.
6. Ashkenazi, A., and V.M. Dixit. 1998. Death receptors: signaling and modulation. *Science* 281:1305–1308.
7. Azzam-Smoak, K., D.L. Noah, M.J. Stewart, et al. 2002. Interferon regulatory factor-1, interferon-beta, and reovirus-induced myocarditis. *Virology* 298:20–29.
8. Barton, E.S., J.D. Chappell, J.L. Connolly, et al. 2001. Reovirus receptors and apoptosis. *Virology* 290:173–180. ← QU2
9. Barton, E.S., J.L. Connolly, J.C. Forrest, et al. 2001. Utilization of sialic acid as a coreceptor enhances reovirus attachment by multistep adhesion strengthening. *J. Biol. Chem.* 276:2200–2211.
10. Barton, E.S., J.C. Forrest, J.L. Connolly, et al. 2001. Junction adhesion molecule is a receptor for reovirus. *Cell* 104:441–451.
11. Bassel-Duby, R., D.R. Spriggs, K.L. Tyler, et al. 1986. Identification of attenuating mutations on the reovirus type 3 S1 double-stranded RNA segment with a rapid sequencing technique. *J. Virol.* 60:64–67.

12. Benedict, C.A., P.S. Norris, and C.F. Ware. 2002. To kill or be killed: viral evasion of apoptosis. *Nat. Immunol.* 3:1013–1018.
13. Boehme, K.W., and T. Compton. 2004. Innate sensing of viruses by toll-like receptors. *J. Virol.* 78:7867–7873.
14. Bowie, A.G., J. Zhan, and W.L. Marshall. 2004. Viral appropriation of apoptotic and NF-κB signaling pathways. *J. Cell. Biochem.* 91:1099–1108.
15. Chandran, K., D.L. Farsetta, and M.L. Nibert. 2002. Strategy for nonenveloped virus entry: a hydrophobic conformer of the reovirus membrane penetration protein  $\mu 1$  mediates membrane disruption. *J. Virol.* 76: 9920–9933.
16. Chappell, J.D., V.L. Gunn, J.D. Wetzel, et al. 1997. Mutations in type 3 reovirus that determine binding to sialic acid are contained in the fibrous tail domain of viral attachment protein  $\sigma 1$ . *J. Virol.* 71:1834–1841.
17. Chappell, J.D., J. Duong, B.W. Wright, et al. 2000. Identification of carbohydrate-binding domains in the attachment proteins of type 1 and type 3 reoviruses. *J. Virol.* 74:8472–8479.
18. Chappell, J.D., A. Prota, T.S. Dermody, et al. 2002. Crystal structure of reovirus attachment protein  $\sigma 1$  reveals evolutionary relationship to adenovirus fiber. *EMBO J.* 21:1–11.
19. Clarke, P., S.M. Meintzer, S. Gibson, et al. 2000. Reovirus-induced apoptosis is mediated by TRAIL. *J. Virol.* 74:8135–8139.
20. Clarke, P., S.M. Meintzer, A.C. Spalding, et al. 2001. Caspase 8-dependent sensitization of cancer cells to TRAIL-induced apoptosis following reovirus-infection. *Oncogene* 20:6910–6919.
21. Clarke, P., S.M. Meintzer, C. Widmann, et al. 2001. Reovirus infection activates JNK and the JNK-dependent transcription factor c-Jun. *J. Virol.* 75:11275–11283.
22. Clarke, P., S.M. Meintzer, L.A. Moffitt, et al. 2003. Two distinct phases of virus-induced nuclear factor kappa B regulation enhance tumor necrosis factor-related apoptosis-inducing ligand-mediated apoptosis in virus-infected cells. *J. Biol. Chem.* 278:18092–18100.
23. Clarke, P., and K.L. Tyler. 2003. Reovirus-induced apoptosis: a minireview. *Apoptosis* 8:141–150.
24. Clarke, P., S.M. Meintzer, Y. Wang, et al. 2004. JNK regulates the release of pro-apoptotic mitochondrial factors in reovirus-infected cells. *J. Virol.* 78:13132–13138.
25. Clarke, P., S.M. Richardson-Burns, R.L. DeBiasi, et al. 2005. Mechanisms of apoptosis during reovirus infections. *Curr. Topics Microbiol. Immunol.* (in press). 289:1–24
26. Coffey, M.C., J.E. Strong, P.A. Forsyth, et al. 1998. Reovirus therapy of tumors with an activated Ras pathway. *Science* 282:1332–1334.
27. Connolly, J.L., S.E. Rodgers, P. Clarke, et al. 2000. Reovirus-induced apoptosis requires activation of transcription factor NF-κB. *J. Virol.* 74:2981–2989.
28. Connolly, J.L., E.S. Barton, and T.S. Dermody. 2001. Reovirus binding to cell surface sialic acid potentiates virus-induced apoptosis. *J. Virol.* 75:4029–4039.
29. Connolly, J.L., and T.S. Dermody. 2002. Virion disassembly is required for apoptosis induced by reovirus. *J. Virol.* 76:1632–1641.
30. Coombs, K.M. 1998. Temperature-sensitive mutants of reovirus. *Curr. Top. Microbiol. Immunol.* 233:69–107.
31. Darman, J., S. Backovic, S. Dike, et al. 2004. Viral-induced spinal motor neuron death is non-cell-autonomous and involves glutamate excitotoxicity. *J. Neurosci.* 24:7566–7575.
32. DeBiasi, R.L., M.K.T. Squier, B. Pike, et al. 1999. Reovirus-induced apoptosis is preceded by increased cellular calpain activity and is blocked by calpain inhibitors. *J. Virol.* 73:695–701.
33. DeBiasi, R.L., C. Edelstein, B. Sherry, et al. 2001. Calapin inhibition protects against virus-induced myocardial injury. *J. Virol.* 75:351–361.
34. DeBiasi, R.L., P. Clarke, S. Meintzer, et al. 2003. Reovirus-induced alteration in expression of apoptosis and DNA repair genes with potential roles in viral pathogenesis. *J. Virol.* 77:8934–8947.
35. DeBiasi, R.L., B.A. Robinson, B. Sherry, et al. 2004. Caspase inhibition protects against reovirus-induced myocardial injury *in vitro* and *in vivo*. *J. Virol.* 78:11040–11050.
36. Edelmann, K.H., S.M. Richardson-Burns, A. Alexopoulos, et al. 2004. Does Toll-like receptor 3 play a biological role in virus infections? *Virology* 322:231–238.
37. Forrest, J.C., and T.S. Dermody. 2003. Reovirus receptors and pathogenesis. *J. Virol.* 77:9109–9115.
38. Friedlander, R.M. 2003. Apoptosis and caspases in neurodegenerative diseases. *N. Engl. J. Med.* 348:1365–1375.
39. Goll, D.E., V.F. Thompson, H. Li, et al. 2003. The calpain system. *Physiol. Rev.* 83:731–801.
40. Gonzalez-Lopez, C., J. Martinez-Castas, M. Esteban, et al. 2003. Evidence that avian reovirus protein sigmaA is an inhibitor of the double-stranded RNA-dependent protein kinase. *J. Gen. Virol.* 84:1629–1639.
41. Hirasawa, K., S.G. Nishikawa, K.L. Norman, et al. 2002. Oncolytic reovirus against ovarian and colon cancer. *Cancer Res.* 62:1696–1701.
42. Hoyt, C.C., R.J. Bouchard, and K.L. Tyler. 2004. Novel nuclear herniations induced by nuclear localization of a viral protein. *J. Virol.* 78:6360–6369.
43. Hoyt, C.C., S.M. Richardson-Burns, R.J. Goody, et al. 2005. Reovirus non-structural protein  $\sigma 1$ s is a determinant of virulence and the efficiency of apoptosis induction in the heart and CNS. *J. Virol.* (in press). 79: 2743–53

AU1 →

← AU2

- AU3 ➔**
44. Jelachich, M.L., and H.L. Lipton. 2001. Theiler's murine encephalomyelitis virus induces apoptosis in gamma interferon-activated M1 differentiated myelomonocytic cells through a mechanism involving tumor necrosis factor-alpha (TNF-alpha) and TNF-alpha-related apoptosis-inducing ligand. *J. Virol.* 75:5930–5938.
  45. Kassis, R., F. Larrous, J. Estaquier, et al. 2004. Lyssavirus matrix protein induces apoptosis by a TRAIL-dependent mechanism involving caspase-8 activation. *J. Virol.* 78:6543–6555.
  46. Kaye, K.M., D.R. Spriggs, R. Bassel-Duby, et al. 1986. Genetic basis for altered pathogenesis of an immune-selected antigenic variant of reovirus type 3 (Dearing). *J. Virol.* 59:90–97.
  47. Kilani, R.T., Y. Tamimi, E.G. Panel, et al. 2003. Selective reovirus killing of bladder cancer in a co-culture spheroid model. *Virus Res.* 93:1–12.
  48. Kominsky, D.J., R.J. Bickel, and K.L. Tyler. 2002. Reovirus-induced apoptosis requires both death receptor- and mitochondrial-mediated caspase-dependent pathways of cell death. *Cell Death Diff.* 9:926–933.
  49. Kominsky, D.J., R.J. Bickel, and K.L. Tyler. 2002. Reovirus-induced apoptosis requires mitochondrial release of Smac/DIABLO and involves reduction of cellular inhibitor of apoptosis protein levels. *J. Virol.* 76:11414–11424.
  50. Kotelkin, A., E.A. Prikhod'ko, J.I. Cohen, et al. 2003. Respiratory syncytial virus infection sensitizes cells to apoptosis mediated by tumor necrosis factor-related apoptosis-inducing ligand. *J. Virol.* 77:9156–9172.
  51. Kucharczak, J., M.F. Simmons, Y. Fan, et al. 2003. To be, or not to be: NF-kappaB is the answer—the role of Rel/NF-kappaB in the regulation of apoptosis. *Oncogene* 22:8961–8982.
  52. Labrada, L., G. Bodelon, J. Vinuela, et al. 2002. Avian reoviruses cause apoptosis in cultured cells: viral uncoating, but not viral gene expression, is required for apoptosis induction. *J. Virol.* 76:7932–7941.
  53. Matsumoto, M., K. Funami, H. Oshiumi, et al. 2004. Toll-like receptor 3: a link between toll-like receptor, interferon, and viruses. *Microbiol. Immunol.* 48:147–154.
  54. Miura, Y., N. Misawa, Y. Kawano, et al. 2003. Tumor necrosis factor-related apoptosis-inducing ligand induces neuronal death in a murine model of HIV central nervous system infection. *Proc. Natl. Acad. Sci. USA* 100:2777–2782.
  55. Mundt, B., F. Kuhnel, L. Zender, et al. 2003. Involvement of TRAIL and its receptors in viral hepatitis. *FASEB J.* 17:94–96.
  56. Nibert, M.L., and L. Schiff. 2001. Reoviruses and their replication, pp. 1679–1728. In: B.N. Fields, D.M. Knipe, and P.M. Howley (eds.), *Fields Virology*. Lippincott-Raven, Philadelphia.
  57. Noah, D.L., M.A. Blum, and B. Sherry. 1999. Interferon regulatory factor 3 is required for viral induction of beta interferon in primary cardiac myocyte cultures. *J. Virol.* 73:10208–10213.
  58. Norman, K.L., M.C. Coffey, K. Hirasawa, et al. 2002. Reovirus oncolysis of human breast cancer. *Hum. Gene Ther.* 13:641–652.
  59. Norman, K.L., K. Hirasawa, A.D. Yang, et al. 2004. Reovirus oncolysis: the Ras/RalGEF/p38 pathway dictates host cell permissiveness to reovirus infection. *Proc. Natl. Acad. Sci. U.S.A.* 101:11099–11104.
  60. Oberhaus, S.M., R.L. Smith, G.H. Clayton, et al. 1997. Reovirus infection and tissue injury in the mouse central nervous system are associated with apoptosis. *J. Virol.* 71:2100–2106.
  61. Oberhaus, S.M., T.S. Dermody, and K.L. Tyler. 1998. Apoptosis and the cytopathic effects of reovirus. *Curr. Top. Microbiol. Immunol.* 233/II:23–49.
  62. O'Brien, V. 1998. Viruses and apoptosis. *J. Gen. Virol.* 79:1833–1845.
  63. Odegard, A.L., K. Chandran, X. Zhang, et al. 2004. Putative autocleavage of outer capsid protein  $\mu_1$ , allowing release of myristoylated peptide  $\mu_1N$  during particle uncoating, is critical for cell entry by reovirus. *J. Virol.* 78:8732–8745.
  64. O'Donnell, S.M., M.W. Hansberger, and T.S. Dermody. 2003. Viral and cellular determinants of apoptosis induced by mammalian reovirus. *Int. Rev. Immunol.* 22:477–503.
  65. Poggioli, G.J., R.L. DeBiasi, R. Bickel, et al. 2002. Reovirus-induced alterations in gene expression related to cell cycle regulation. *J. Virol.* 76:2585–2594.
  66. Rankin, J.T., Jr., S.B. Eppes, J.B. Antczak, et al. 1989. Studies on the mechanism of the antiviral activity of ribavirin against reovirus. *Virology* 168:147–158.
  67. Reed, J.C. 1998. Bcl-2 family proteins. *Oncogene* 17:3225–3236.
  68. Reinisch, K.M., M.L. Nibert, and S.C. Harrison. 2000. Structure of the reovirus core at 3.6 Å resolution. *Nature* 404:960–967.
  69. Richardson-Burns, S.M., D.J. Kominsky, and K.L. Tyler. 2002. Reovirus-induced neuronal apoptosis is mediated by caspase 3 and is associated with activation of death receptors. *J. Neurovirol.* 8:365–380.
  70. Richardson-Burns, S.M., and K.L. Tyler. 2004. Regional differences in viral growth and central nervous system injury correlate with apoptosis. *J. Virol.* 78:5466–5475.
  71. Richardson-Burns, S.M., and K.L. Tyler. 2005. Minocycline delays disease onset and mortality in a murine model of viral encephalitis. *Exp. Neurol.* (in press).
  72. Rivera-Walsh, I., M. Waterfield, G. Xiao, et al. 2001. NF-kappaB signaling pathway governs TRAIL gene expres-
- AU4 ←**
- 192:331-339

- sion and human T-cell leukemia virus-I Tax-induced T-cell death. *J. Biol. Chem.* 276:40385–40388.
73. Rodgers, S.E., E.S. Barton, S.M. Oberhaus, et al. 1997. Reovirus-induced apoptosis of MDCK cells is not linked to viral yield and is blocked by Bcl-2. *J. Virol.* 71:2540–2546.
74. Rodgers, S.E., J.L. Connolly, J.D. Chappell, et al. 1998. Reovirus growth in cell culture does not require the full complement of viral proteins: identification of a sigma $\lambda$ -null mutant. *J. Virol.* 72:8597–8604.
75. Roulston, A., R.C. Marcellus, and P.E. Branton. 1999. Viruses and apoptosis. *Annu. Rev. Microbiol.* 53:577–628.
76. Rubio, N., B. Martin-Clemente, and H.L. Lipton. 2003. High-neurovirulence GDVII virus induces apoptosis in murine astrocytes through tumor necrosis factor (TNF)-receptor and TNF-related apoptosis-inducing ligand. *Virology* 311:366–375.
77. Samuel, C.E. 1998. Reoviruses and the interferon system. *Curr. Top. Microbiol. Immunol.* 233:125–145.
78. Scarabelli, T.M., A. Stephanou, E. Pasini, et al. 2004. Minocycline inhibits caspase activation and reactivation, increases the ratio of XIAP to Smac/DIABLO, and reduces the mitochondrial leakage of cytochrome c and Smac/DIABLO. *J. Am. Coll. Cardiol.* 43:865–874.
79. Sedger, L.M., D.M. Shows, R.A. Blanton, et al. 1999. IFN-gamma mediates a novel antiviral activity through dynamic modulation of TRAIL and TRAIL receptor expression. *J. Immunol.* 163:920–926.
80. Sharpe, A.H., L.B. Chen, and B.N. Fields. 1982. The interaction of mammalian reoviruses with the cytoskeleton of monkey kidney CV-1 cells. *Virology* 120:399–411.
81. Sherry, B. 1998. Pathogenesis of reovirus myocarditis. *Curr. Top. Microbiol. Immunol.* 233/II:51–66.
82. Sherry, B., J. Torres, and M.A. Blum. 1998. Reovirus induction of and sensitivity to beta interferon in cardiac myocyte cultures correlate with induction of myocarditis and are determined by viral core proteins. *J. Virol.* 72:1314–1323.
83. Shih, W.L., H.W. Hsu, M.H. Liao, et al. 2004. Avian reovirus  $\sigma$ C protein induces apoptosis in cultured cells. *Virology* 321:65–74.
84. Spriggs, D.R., and B.N. Fields. 1982. Attenuated reovirus type 3 strains generated by selection of hemagglutinin antigenic variants. *Nature* 297:68–70.
85. Spriggs, D.R., R.T. Bronson, and B.N. Fields. 1983. Hemagglutinin variants of reovirus type 3 have altered central nervous system tropism. *Science* 220:505–507.
86. Stewart, M.J., M.A. Blum, and B. Sherry. 2003. PKR's protective role in viral myocarditis. *Virology* 314:92–100.
87. Strong, J.E., D. Tang, and P.W. Lee. 1993. Evidence that the epidermal growth factor receptor on host cells confers reovirus infection efficiency. *Virology* 197:405–411.
88. Strong, J.E., and P.W. Lee. 1996. The *v-erbB* oncogene confers enhanced cellular susceptibility to reovirus infection. *J. Virol.* 70:612–616.
89. Strong, J.E., M.C. Coffey, D. Tang, et al. 1998. The molecular basis of viral oncolysis: usurpation of the Ras signaling pathway by reovirus. *EMBO J.* 17:3351–3362.
90. Tao, Y., D.L. Farsetta, M.L. Nibert, et al. 2002. RNA synthesis in a cage—structural studies of reovirus polymerase lambda3. *Cell* 111:733–745.
91. Tilkka, T., B.L. Fiebich, G. Goldsteins, et al. 2001. Minocycline, a tetracycline derivative, is neuroprotective against excitotoxicity by inhibiting activation and proliferation of microglial. *J. Neurosci.* 21:258–2588. L258c
92. Tyler, K.L., M.K.T. Squier, S.E. Rodgers, et al. 1995. Differences in the capacity of reovirus strains to induce apoptosis are determined by the viral attachment protein  $\sigma$ 1. *J. Virol.* 69:6972–6979.
93. Tyler, K.L., M.K.T. Squier, A.L. Brown, et al. 1996. Linkage between reovirus-induced apoptosis and inhibition of cellular DNA synthesis: role of the S1 and M2 genes. *J. Virol.* 70:7984–7991.
94. Tyler, K.L., P. Clarke, R.L. DeBiasi, et al. 2001. Reoviruses and the host cell. *Trends Microbiol.* 9:560–564.
95. Vidalain, P.O., O. Azocar, B. Lamouille, et al. 2000. Measles virus induces functional TRAIL production by human dendritic cells. *J. Virol.* 74:556–559.
96. Wang, J., Q. Wei, C.Y. Wang, et al. 2004. Minocycline up-regulates Bcl-2 and protects against cell death in mitochondria. *J. Biol. Chem.* 279:19948–19954.
97. Wang, X., S. Zhu, M. Drozda, et al. 2003. Minocycline inhibits caspase-independent and -dependent mitochondrial cell death pathways in models of Huntington's disease. *Proc. Natl. Acad. Sci. USA* 100:10483–10487.
98. Wilcox, M.E., W. Yang, D. Senger, et al. 2001. Reovirus as an oncolytic agent against experimental human malignant gliomas. *J. Natl. Cancer Inst.* 93:903–912.
99. Wurzer, W.J., C. Ehrhardt, S. Pleschka, et al. 2004. NF-kappaB-dependent induction of tumor necrosis factor-related apoptosis-inducing ligand (TRAIL) and Fas/FasL is crucial for efficient influenza virus propagation. *J. Biol. Chem.* 279:30931–30937.
100. Yang, W.Q., D. Senger, H. Muzik, et al. 2003. Reovirus prolongs survival and reduces the frequency of spinal and leptomeningeal metastases from medulloblastoma. *Cancer Res.* 63:6162–6172.
101. Yang, W.Q., D.L. Saenger, X.Q. Lun, et al. 2004. Reovirus as an experimental therapeutic for brain and leptomeningeal metastases from breast cancer. *Gene Ther.* 11:1579–1589.
102. Yue, Z., and A.J. Shatkin. 1997. Double-stranded RNA-dependent protein kinase (PKR) is regulated by reovirus structural proteins. *Virology* 234:364–371.

QU3

103. Yujiri, T., M. Ware, C. Widmann, et al. 2000. MEK kinase 1 gene disruption alters cell migration and c-Jun NH<sub>2</sub>-terminal kinase regulation but does not cause a measurable defect in NF-κappaB activation. Proc. Natl. Acad. Sci. USA 97:7272-7277.

AU5 ➤

104. Zhu, S., I.G. Starvrovskaya, M. Drozda, et al. 2002. Minocycline inhibits cytochrome c release and delays progression of amyotrophic lateral sclerosis in mice. *Nature* 417: 74-8

Address reprint requests to:

Dr. K.L. Tyler

Neurology B-182

University of Colorado Health Sciences Center

4200 East 9<sup>th</sup> Ave.

Denver, CO 80262

E-mail: Ken.Tyler@uchsc.edu

## Mechanisms of Apoptosis During Reovirus Infection

P. Clarke<sup>1, 2</sup> (✉) · S. M. Richardson-Burns<sup>1, 2</sup> · R. L. DeBiasi<sup>1, 2</sup>  
K. L. Tyler<sup>1, 2</sup>

<sup>1</sup> Department of Neurology (B 182), University of Colorado Health Sciences Center,  
4200 East 9th Ave., Denver, CO 80262, USA  
*Penny.Clarke@uchsc.edu*  
<sup>2</sup> Denver VA Medical Center, 1055 Clermont St, Denver, CO 80220, USA

1	Introduction . . . . .	3
2	Reovirus-Induced Apoptosis Is Determined by the Type <sup>3</sup>	3
	Reovirus S1 and M2 Gene Segments . . . . .	3
2.1	Role of the S1 Gene Segment in Reovirus-Induced Apoptosis . . . . .	4
2.2	Role of the M2 Gene Segment and Viral Disassembly in Reovirus-Induced Apoptosis . . . . .	4
3	Reovirus-Induced Apoptosis Is Mediated by Death Receptor Signaling .	5
4	Mitochondrial Signaling Contributes to Reovirus-Induced Apoptosis .	7
4.1	Reovirus Induces the Cleavage of Bid . . . . .	8
4.2	Role of Smac in Reovirus-Induced Apoptosis . . . . .	8
4.3	Mitochondrial Pathways Amplify Death Receptor Apoptotic Signaling Following Reovirus Infection . . . . .	9
5	Role of NF-κB in Reovirus-Induced Apoptosis . . . . .	10
6	Reovirus-Induced Apoptosis Is Associated with Activation of JNK and the Transcription Factor c-Jun . . . . .	12
7	Reovirus-Induced Alteration in Expression of Genes with Potential Roles in Virus-Induced Apoptosis and Pathogenesis . . . . .	12
8	Reovirus Sensitizes Cells to TRAIL-Induced Apoptosis . . . . .	14
9	Reovirus-Induced Apoptosis in the Mouse CNS . . . . .	15
10	Reovirus-Induced Apoptosis in the Heart . . . . .	17
11	Apoptosis and Viral Growth . . . . .	17
11.1	The Effects of Virus Replication and Growth on Apoptosis . . . . .	19
11.2	Effect of Apoptosis on Viral Growth . . . . .	20
12	Conclusions and Future Directions . . . . .	21
	References . . . . .	21

**Abstract** Reovirus infection has proven to be an excellent experimental system for studying mechanisms of virus-induced pathogenesis. Reoviruses induce apoptosis in a wide variety of cultured cells *in vitro* and in target tissues *in vivo*, including the heart and central nervous system. *In vivo*, viral infection, tissue injury, and apoptosis colocalize, suggesting that apoptosis is a critical mechanism by which disease is triggered in the host. This review examines the mechanisms of reovirus-induced apoptosis and investigates the possibility that inhibition of apoptosis may provide a novel strategy for limiting virus-induced tissue damage following infection.

#### Abbreviations

AIF	Apoptosis-inducing factor
CNS	Central nervous system
DcR	Decoy receptor
DD	Death domain
DISC	Death-inducing signaling complex
DN	Dominant negative
DR	Death receptor
E	Embryonic
FADD/FADD	Fas-associated death domain
FMK	Fluoromethyl ketone
HTLV	Human T cell lymphoma virus
IAP	Inhibitor of apoptosis protein
IκB/IκB	Inhibitor κB
ISVP	Infectious subviron particle
JAM	Functional adhesion molecule
JNK/JNK	c-Jun N-terminal kinase
Mabs	Monoclonal antibodies
MCC	Mouse cortical cultures
MDCK	Madin-Darby canine kidney
MHC	Mouse hippocampal cultures
MEF	Mouse embryo fibroblasts
NF-κB	Nuclear factor κB
PCR	Polymerase chain reaction
PI	Postinfection
PFU	Plaque-forming unit
smac/smamac	Second mitochondrion-derived activator of caspases
SMN	Survival motor neuron
TIL	Type 1 reovirus, strain Lang
T3A	Type 3 reovirus, strain Abney
T3D	Type 3 reovirus, strain Dearing
TNF/TNF	Tumor necrosis factor
TNFR	TNF receptor
TRAIL/TRAIL	TNF-related apoptosis-inducing ligand
<i>ts</i>	Temperature sensitive
TUNEL	TdT-mediated dUTP nick-end labeling
UV	Ultraviolet
VarK	Variant K

## 1 Introduction

Reoviruses are ubiquitous, nonenveloped, cytoplasmically replicating viruses that have been isolated from a wide variety of mammalian species, including humans. In humans, reovirus has been associated with diarrheal illnesses, upper respiratory infections, hepatobiliary diseases including biliary atresia, and rare cases of central nervous system (CNS) infection. However, the viruses are still considered “orphan viruses” as they have not been definitively linked to disease. In contrast, natural and experimental infection of animals with reovirus produces a variety of diseases. The most extensively studied experimental system involves infection of neonatal mice where, depending on the viral strain and route of inoculation, reovirus infection can produce disease in a variety of organs (Tyler 1998; Tyler et al. 2001).

Reovirus infection has proven to be an excellent experimental system for studying mechanisms of virus-induced pathogenesis. Reoviruses induce apoptosis in a wide variety of cultured cells *in vitro* and in target tissues *in vivo*, including the heart and CNS (Clarke and Tyler 2003). *In vivo*, viral infection, tissue injury, and apoptosis colocalize, suggesting that apoptosis is a critical mechanism by which disease is triggered in the host (DeBiasi et al. 2001; Oberhaus et al. 1997; Richardson-Burns et al. 2002). This review examines the mechanisms of reovirus-induced apoptosis and investigates the possibility that inhibition of apoptosis may provide a novel strategy for limiting virus-induced tissue damage following infection.

## 2 Reovirus-Induced Apoptosis Is Determined by the Type 3 Reovirus S1 and M2 Gene Segments

The reovirus virion is comprised of two concentric protein capsids surrounding a genome of 10 segments of double-stranded (ds) RNA. Reovirus strains differ in their ability to induce apoptosis with prototype Type 3 (T3) reovirus strains, Dearing (T3D) and Abney (T3A), inducing significantly more apoptosis in L929 fibroblasts than the prototype Type 1 (T1) reovirus strain, Lang (T1L). The T3 S1 and M2 gene segments have been identified as the viral determinants of reovirus-induced apoptosis in L929 and Madin-Darby canine kidney (MDCK) cells and the S1 gene

segment alone as a determinant of apoptosis in HeLa cells (Tyler et al. 1995, 1996; Rodgers et al. 1997; Connolly et al. 2001).

### 2.1 Role of the S1 Gene Segment in Reovirus-Induced Apoptosis

The S1 gene segment encodes the viral attachment protein  $\sigma_1$  and the nonstructural protein  $\sigma_{1s}$ .  $\sigma_{1s}$  is the determinant of reovirus-induced G<sub>2</sub>/M cell cycle arrest, an effect that results from inhibition of the regulatory kinase p34<sup>cdc2</sup> and the resulting inhibition of cellular DNA synthesis (Tyler et al. 1996; Poggio et al. 2000, 2001). In vitro,  $\sigma_{1s}$  is not required for reovirus-induced apoptosis of L929 or HEK293 cells and cell cycle arrest and inhibitors of apoptosis do not prevent reovirus-induced cell cycle arrest, suggesting that these are distinct pathways (Poggio et al. 2000). The viral attachment protein  $\sigma_1$  must therefore be a determinant of reovirus-induced apoptosis.

In support of this, apoptosis can be induced at nonpermissive temperatures by a variety of reovirus temperature-sensitive (*ts*) mutants (Connolly and Dermody 2002), which are arrested at defined steps in viral replication and by ultraviolet (UV)-inactivated virus, all of which contain  $\sigma_1$  but lack  $\sigma_{1s}$  (Tyler et al. 1995).

In virions, the reovirus  $\sigma_1$  protein is a homotrimer comprised of an elongated fibrous tail, which inserts into the virion, and an externally facing globular head (Chappell et al. 2002). The heads of both reovirus T1L and T3D  $\sigma_1$  proteins contain a binding domain for junctional adhesion molecule (JAM), which serves as the primary reovirus receptor (Barton et al. 2001b). In addition, the fibrous tail of the T3 reovirus  $\sigma_1$  protein contains a domain that binds  $\alpha$ -linked sialic acid (Chappell et al. 2000). Sialic acid binding is not required for viral entry. However, the binding of sialic acid in addition to JAM at early times after attachment can enhance both reovirus attachment and growth in some cell types (Connolly et al. 2001; Barton et al. 2001a). Virus binding to both JAM and sialic acid are required for reovirus-induced activation of nuclear factor  $\kappa$ B (NF- $\kappa$ B) (see below) and apoptosis (Connolly et al. 2001).

### 2.2 Role of the M2 Gene Segment and Viral Disassembly in Reovirus-Induced Apoptosis

The M2 gene, which encodes the major viral outer capsid protein  $\mu_1/\mu_1C$  also contributes to the apoptotic phenotype. In fact, incubation of in-

fected cells with monoclonal antibodies (MAbs) directed against either the  $\sigma_1$  (viral attachment),  $\mu_1$ , or  $\sigma_3$  (outer capsid) proteins can inhibit apoptosis. In the case of the  $\sigma_1$  MAbs this almost certainly reflects their capacity to inhibit viral cell attachment. However, both anti- $\mu_1$  and anti- $\sigma_3$  MAbs, which do not inhibit viral cell attachment but do prevent viral uncoating, can inhibit apoptosis (Virgin et al. 1994; Tyler et al. 1995, 1996; Connolly et al. 2001; Rodgers et al. 1997).

After viral cell attachment and subsequent receptor-mediated endocytosis, reovirions are proteolytically disassembled to form infectious subvirion particles (ISVPs). This process is characterized by removal of the outer capsid protein  $\sigma_3$ , proteolytic cleavage of  $\mu_1/\mu_1C$ , and conformational changes in  $\sigma_1$ . Reovirus-induced apoptosis (and activation of NF- $\kappa$ B, see below) is blocked by inhibiting proteolysis of reovirus virions with ammonium chloride, which inhibits endosomal acidification, or E64, which inhibits cysteine-containing endocytic proteases, indicating that viral disassembly is required for apoptosis in infected cells (Connolly and Dermody 2002). Early events during viral entry, but subsequent to virus engagement of cellular receptors, thus appear to be required for reovirus-induced apoptosis, an interpretation that has subsequently been supported by experiments using *ts* mutants blocked at different stages in the reovirus replication cycle (Connolly and Dermody 2002).

## 3 Reovirus-Induced Apoptosis Is Mediated by Death Receptor Signaling

Tumor necrosis factor (TNF)-related apoptosis-inducing ligand (TRAIL) is a widely expressed type 2 membrane protein that was identified by its homology to Fas ligand (FasL) and TNF $\alpha$ . TRAIL induces apoptosis by binding to the cell surface death receptors (DRs) DR4 (also called TRAIL-R1) and DR5 (also called Apo2, TRAIL-R2, TRAIL-R2, or KILLER). In addition, TRAIL can bind to the decoy receptors DcR-1 (for decoy receptor 1) and DcR-2, which do not transduce apoptotic signals and which can prevent the induction of apoptosis in TRAIL-treated cells. TRAIL-mediated activation of DR4 and DR5 induces DR oligomerization and the close association of their cytoplasmic death domains (DDs). The cytosolic adapter molecule FADD (for Fas-associated death domain) and pro-caspases 8 and 10 are then recruited to the receptor to form the death-inducing signaling complex (DISC), where pro-caspase cleavage generates active initiator caspases, 8 and 10.

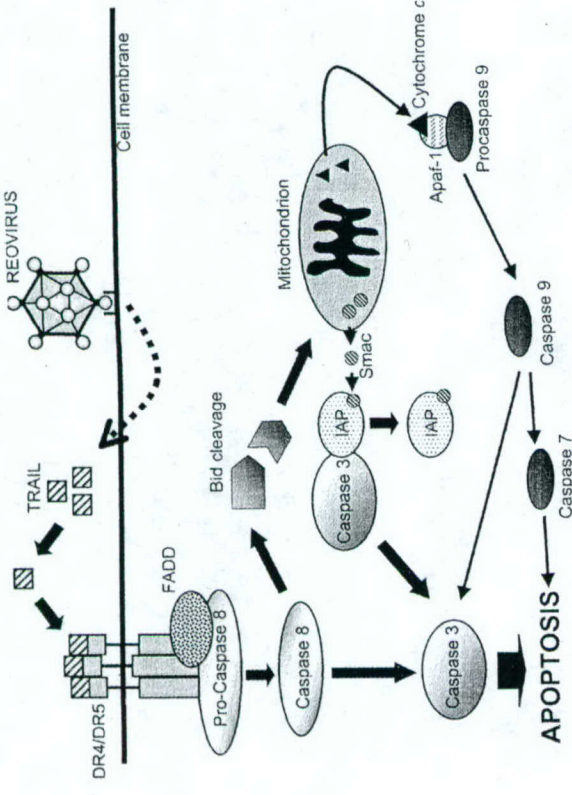


**Fig. 1** Model of reovirus-induced apoptosis. After virus infection, TRAIL is released into the supernatant, by an unknown mechanism, and initiates apoptosis by binding to cell surface death receptors DR4 and DR5. TRAIL-receptor binding induces the activation of caspase 8, which in turn activates the downstream effector caspase, caspase 3. Caspase 8 also activates mitochondrial apoptotic pathways in reovirus-infected cells through the cleavage of Bid, resulting in the release of mitochondrial apoptotic factors and the amplification of death receptor apoptotic signaling. The mitochondrial release of smac, rather than cytochrome *c*, is thought to have a more significant role in reovirus induced apoptosis. (With permission from Clarke and Tyler 2003)

Soluble TRAIL receptors, anti-TRAIL antibodies, and the overexpression of DcR-1 can all inhibit reovirus-induced apoptosis in a wide variety of cells including L929 cells, human embryonic kidney (HEK293) cells, and several human cancer cell lines (Clarke et al. 2000, 2001a). This suggests that reovirus-induced apoptosis is mediated by TRAIL signaling pathways. Reovirus-infected cells release soluble TRAIL into the supernate, providing a potential mechanism for initiating both autocrine and exocrine (bystander) apoptosis (Clarke et al. 2000).

Events downstream of TRAIL receptor binding are also activated after reovirus infection. Reovirus infection thus induces the cleavage and activation of pro-caspase 8. In HEK293 cells, the activation of caspase 8 oc-

curs in two phases. An initial phase occurs between 8 and 14 h post-infection (PI) and a later phase occurs between 24 and 34 h PI, by which time all pro-caspase 8 has been cleaved in infected cells (Kominsky et al. 2002a). Expression of dominant-negative (DN)-FADD or a peptide inhibitor of caspase 8 activity, IETD-FMK results in the inhibition of apoptosis in reovirus-infected cells, indicating that caspase 8 activity is required for reovirus-induced apoptosis (Clarke et al. 2000; Kominsky et al. 2002a). Caspase 8 activation is also required for the activation of caspase 3 in reovirus-infected cells (Kominsky et al. 2002a). Like caspase 8 activation, reovirus-induced activation of caspase 3 is biphasic, with a first phase of activation beginning around 8 h PI and a second phase of activation beginning at 24 h PI. The kinetics of caspase 8 and caspase 3 activation suggest that these two events occur in rapid succession in reovirus-infected cells. Reovirus-induced caspase 3 activity corresponds closely to the cleavage of the cellular substrate PARP, indicating that caspase 3 has biological activity in infected cells and can participate in the cleavage of cellular substrates to induce the morphological hallmarks of apoptosis (Connolly and Dermody 2002; Clarke et al. 2001a; Kominsky et al. 2002a). A model of reovirus-induced, TRAIL-mediated apoptosis is shown in Fig. 1.

#### 4 Mitochondrial Signaling Contributes to Reovirus-Induced Apoptosis

The first indication that mitochondrial signaling pathways are involved in reovirus-induced apoptosis came from the observation that reovirus-induced apoptosis is inhibited in MDCK cells that overexpress Bcl-2 (Rodgers et al. 1997). Bcl-2 belongs to a family of proteins that contain both proapoptotic (e.g., Bax and Bak) and antiapoptotic (e.g., Bcl-2 and Bcl-xL) members. During apoptosis the interactions of pro- and anti-apoptotic Bcl-2 family proteins are disrupted, resulting in the oligomerization of Bax and Bak, the formation of a pore within the mitochondrial membrane, and the release of proapoptotic mitochondrial factors, including cytochrome *c* and a second mitochondrion-derived activator of caspases (smac; also called DIABLO). Cytochrome *c* contributes to apoptosis by activating the initiator caspase 9, which functions to activate the effector caspases. Smac contributes to apoptosis by binding to cellular inhibitor of apoptosis proteins (IAPs), thereby preventing their inhibitory actions on caspase activity (Verhagen et al. 2000).

#### 4.1 Reovirus Induces the Cleavage of Bid

In some cell types, DR signaling activates mitochondrial apoptotic pathways through the caspase 8 (or 10)-dependent cleavage of the BH3-only Bcl-2 family protein Bid. This produces a C-terminal fragment of Bid, truncated (t) Bid, which translocates to the mitochondria and interferes with Bcl-2 protein interactions resulting in the release of cytochrome *c* and smac. Bid is cleaved in HEK293 cells after infection with reovirus (Kominsky et al. 2002a). Bid cleavage coincides with the release of cytochrome *c* from the mitochondria and the associated activation of caspase 9 (Kominsky et al. 2002a). Furthermore, both Bid cleavage and the release of cytochrome *c* are blocked in cells expressing DN-FADD and, like caspase 8 activation, Bid cleavage is biphasic. These results indicate that caspase 8 activity is required for activation of mitochondrial apoptotic pathways in reovirus-infected cells (Kominsky et al. 2002a).

#### 4.2 Role of Smac in Reovirus-Induced Apoptosis

Smac is also released from the mitochondria of reovirus-infected cells with kinetics similar to that of the release of cytochrome *c* and, like cytochrome *c*, smac release is blocked by the overexpression of Bcl-2 (Kominsky et al. 2002a). After reovirus infection, some cellular IAPs (survivin, cIAP1, and XIAP) undergo proteolytic cleavage and degradation (Kominsky et al. 2002b). This is prevented in cells overexpressing Bcl-2 (Kominsky et al. 2002b) and is consistent with a key role for smac in inhibiting IAP-mediated caspase inhibition (Verhagen et al. 2000). It is thought that this may be mediated through direct binding of smac with target IAPs (Verhagen et al. 2000; Chai et al. 2001; Huang et al. 2001; Riedl et al. 2001). Alternatively, IAP degradation has also been shown to represent an important apoptotic event both in mammalian cells and in *Drosophila*, where proteins with regions homologous to smac (Grim and REAPER) promote ubiquitin-mediated degradation of *Drosophila* IAP1 (Johnson et al. 2000; Deveraux et al. 1999; Yang et al. 2000; Palaga and Osborne 2002).

Smac release, rather than caspase 9 activation, plays a critical role in the mitochondrion-related augmentation of reovirus-induced, DR-mediated, apoptotic pathways (Kominsky et al. 2002b). Thus stable transfection of HEK293 cells with DN-caspase 9 (caspase 9b) only inhibits reovirus-induced activation of caspase 9, unlike Bcl-2 overexpression, which

blocks all mitochondrially mediated events. In addition, caspase 9b expression does not affect reovirus-induced activation of caspase 3 or reovirus-induced PARP cleavage, suggesting that, although caspase 9 is activated in reovirus-infected cells, other pathways are necessary for effector caspase activation (Kominsky et al. 2002b).

A variety of other mitochondrial apoptotic factors have been identified, including apoptosis-inducing factor (AIF). Reovirus infection is not associated with release of AIF in HEK293 cells (Kominsky et al. 2002b). Nor does it result in disruption of mitochondrial transmembrane potential, indicating that the release of proapoptotic factors from the mitochondria after reovirus infection is selective (Kominsky et al. 2002b). This is consistent with ultrastructural studies in reovirus-infected cells that suggest that disruption of mitochondrial architecture is not a typical feature of reovirus infection.

#### 4.3 Mitochondrial Pathways Amplify Death Receptor Apoptotic Signaling Following Reovirus Infection

As previously described, activation of both caspase 8 and Bid is biphasic (Kominsky et al. 2002a). In contrast, reovirus-induced release of smac is not biphasic, occurring just after the early phase and before the late phase of caspase 8 activation and Bid cleavage (Kominsky et al. 2002b). Overexpression of Bcl-2 inhibits the late phase of caspase 8 activation without affecting the early phase, suggesting that the late phase is mitochondrial dependent (Kominsky et al. 2002a). Together, these results are consistent with a model in which DR activation initiates reovirus apoptosis and results in early low-level activation of effector caspases. Mitochondrial events, likely initiated by Bid translocation and involving release of smac, then amplify the initial DR-initiated signal and dramatically augment effector caspase activation (Fig. 1).

In addition to caspase 3, the effector caspase 7 is also activated after reovirus infection (Kominsky et al. 2002a). This activation occurs later than the first phase of caspase 3 activity and is less robust, suggesting that caspase 7 activation may play a less critical role in reovirus-induced apoptosis than caspase 3. In addition, the observations that caspase 7 activation parallels that of caspase 9 and is not biphasic suggest that it may result from the activation of caspase 9.

## 5 Role of NF- $\kappa$ B in Reovirus-Induced Apoptosis

Nuclear factor  $\kappa$ B (NF- $\kappa$ B) is a transcription factor that is normally prevented from migrating to the nucleus and binding to DNA by its association in the cytoplasm with members of the inhibitor  $\kappa$ B (IkB) family of proteins. Site-specific phosphorylation, followed by ubiquitination and proteosomal degradation of IkB, allows for NF- $\kappa$ B activation. Reovirus infection transiently activates NF- $\kappa$ B in a variety of cell types, including L929, MDCK, and HeLa cells (Connolly et al. 2000). This activation can be detected in HeLa cells as early as 4 h PI, peaks at 10 h PI, and then declines (Connolly et al. 2000). Similarly, expression of an NF- $\kappa$ B-dependent luciferase reporter gene is transient in reovirus-infected cells (Connolly et al. 2000). Inhibition of NF- $\kappa$ B by stable overexpression of an IkB super-repressor or treatment of cells with a proteasome inhibitor that blocks IkB degradation (Z-L<sub>s</sub>V5) inhibits reovirus-induced apoptosis (Connolly et al. 2000). Apoptosis is also inhibited in immortalized mouse embryo fibroblasts (MEFs) with targeted disruptions in the genes encoding the p50 or p65 subunits of NF- $\kappa$ B (Connolly et al. 2000). These results suggest, in contradistinction to many other models of apoptosis, that after reovirus infection early activation NF- $\kappa$ B exerts a pro- rather than antiapoptotic influence.

The regulation of TRAIL and DR expression is upregulated by NF- $\kappa$ B in a variety of systems, including cells undergoing apoptosis induced by human T cell lymphoma virus (HTLV-1) Tax and the chemotherapeutic agents etoposide and doxorubicin (Ravi et al. 2001; Gibson et al. 2000; Spalding et al. 2002; Rivera-Walsh et al. 2001). Studies are now underway to determine the role of NF- $\kappa$ B in mediating TRAIL and DR expression during reovirus-induced apoptosis.

Several lines of evidence suggest that activation of NF- $\kappa$ B does not completely explain the involvement of NF- $\kappa$ B in reovirus-induced apoptosis. First, NF- $\kappa$ B activation is transient and occurs before the onset of apoptosis in reovirus-infected cells (Connolly et al. 2000; Clarke et al. 2003b). Second, our preliminary experiments indicate that both T1 and T3 reoviruses activate NF- $\kappa$ B to a similar extent in HeLa and HEK293 cells, although T3 reoviruses induce significantly more apoptosis, suggesting that NF- $\kappa$ B is required, but not sufficient, for apoptosis in these cells. Third, although activation of NF- $\kappa$ B may be required for apoptosis in both HeLa and HEK293 cells the difference in magnitude of the response is dramatic, whereas apoptosis occurs with similar efficiency. Thus weak NF- $\kappa$ B activation can be detected in HEK293 cells 2–4 h after

infection with T3A reovirus (Clarke et al. 2003b), whereas robust NF- $\kappa$ B activation is detected in HeLa cells 2–12 h PI (Connolly et al. 2000).

In addition to activating NF- $\kappa$ B at early times PI, reovirus has now been shown to induce a second phase of NF- $\kappa$ B regulation where NF- $\kappa$ B activity is inhibited in reovirus-infected cells at later times PI (Clarke et al. 2003a). This phase of regulation results in the transient nature of NF- $\kappa$ B activation in reovirus-infected cells and also inhibits stimulus-induced activation of NF- $\kappa$ B (Clarke et al. 2003a). Reovirus-induced inhibition of NF- $\kappa$ B activation in HEK293 cells is inhibited by the viral RNA synthesis inhibitor ribavirin, which is also required for efficient apoptosis in these cells and for the ability of reovirus to sensitize these cells to TRAIL-induced apoptosis (Clarke et al. 2003a). Because DR receptor-induced apoptosis is enhanced in many systems if NF- $\kappa$ B signaling is inhibited and because reovirus-induced apoptosis is mediated by DR signaling, it is likely that the inhibition of NF- $\kappa$ B at later times PI is necessary for efficient reovirus-induced apoptosis and for reovirus-induced apoptosis in TRAIL-resistant cells (Clarke et al. 2003a).

The mechanism by which NF- $\kappa$ B is regulated by reovirus is not fully understood. One possible activator of NF- $\kappa$ B in reovirus-infected cells is the calcium-dependent, papain-like, neutral cysteine protease calpain. Calpain is activated as early as 2 h after reovirus infection of L929 cells and myocytes and inhibition of this activation inhibits reovirus-induced apoptosis (DeBiasi et al. 1999, 2001). In most models of apoptosis calpains act upstream of caspases, and the early onset of calpain activity in reovirus-infected cells suggests that this may also be true for reovirus-induced apoptosis. However, calpain has also been implicated in the regulation of a variety of cellular transcription factors, including NF- $\kappa$ B (Chen et al. 1997; Watt and Molloy 1993). The early activation of calpain after reovirus infection makes this an attractive candidate for reovirus-induced activation of NF- $\kappa$ B. In addition, reovirus induces the upregulation of the proapoptotic protein par-4 (DeBiasi et al. 2003), which can inhibit the phosphorylation and degradation of I $\kappa$ B, thereby preventing NF- $\kappa$ B activation (Camandola and Mattson 2000; Diaz-Meco et al. 1999). This results in the downmodulation of Bcl-2 and can result in sensitization of cells to TNF- and FasL-induced apoptosis (Diaz-Meco et al. 1999).

## 6 Reovirus-Induced Apoptosis Is Associated with Activation of JNK and the Transcription Factor c-Jun

Reovirus infection results in a viral strain-specific pattern activation of the c-Jun N-terminal kinase (JNK) and the JNK-associated transcription factor c-Jun (Clarke et al. 2001b). The capacity of reovirus strains to activate JNK correlates closely with their capacity to induce apoptosis (Clarke et al. 2001b). In addition, experiments using T1L × T3D reassortants indicate that the same viral gene segments that determine apoptosis induction (S1 and M2) are also key determinants of JNK activation (Clarke et al. 2001b). Furthermore, our preliminary experiments indicate that reovirus-induced apoptosis is inhibited in cells deficient in MEK kinase 1, an upstream activator of JNK in reovirus-infected cells and in cells treated with inhibitors of JNK activity. These results indicate that JNK is required for reovirus-induced apoptosis.

Our recent experiments also indicate that JNK is required for the efficient release of smac and cytochrome *c* from the mitochondria of reovirus-infected cells, suggesting that JNK promotes mitochondrial pathways of apoptosis in reovirus-infected cells (Clarke et al. 2004). Both JNK-induced phosphorylation of Bcl-2 family proteins and c-Jun-induced expression of the BH3-only protein Bim have previously been shown to promote mitochondrial apoptotic signaling. Experiments to determine the mechanism by which JNK and c-Jun influence reovirus-induced apoptosis are currently under way.

## 7 Reovirus-Induced Alteration in Expression of Genes with Potential Roles in Virus-Induced Apoptosis and Pathogenesis

Reovirus infection induces the activation of transcription factors NF- $\kappa$ B and c-Jun (Clarke et al. 2001b, 2003a; Connolly et al. 2000). This suggests that activation of specific cellular genes contributes to virus-induced cellular signaling, including apoptotic signaling, in infected cells. High-density oligonucleotide microarrays used to perform a global analysis of virus-induced cellular gene expression after reovirus infection of HEK293 cells (DeBiasi et al. 2003; Poggioli et al. 2002) showed that the expression of 24 genes related to apoptosis were altered in cells infected with the apoptosis-inducing reovirus strain T3A (Table 1). These genes encode proteins with potential roles in DR, endoplasmic reticulum

**Table 1** Reovirus-induced alteration in expression of genes encoding proteins with known apoptotic involvement

Gene	GenBank accession no. <sup>a</sup>	T3A	T1L	Change in expression ( <i>n</i> -fold) <sup>b</sup>
<b>Mitochondrial signaling</b>				
Pim-2 proto-oncogene homolog	U77735	-2.2±0.1		
Mcl-1	L08246	2.0±0.0	2.2±0.0	
BAC 15E1-cytochrome <i>c</i> oxidase polypeptide Par4	AL021546	2.1±0.0		
HSP-70 (heat shock protein 70 testis variant)	U63809	2.1±0.0		
BNP-1 (Bcl-2 interacting protein)	U85730	2.2±0.1		
SMN/Btfp44/NAIP (survival motor neuron/neuronal apoptosis inhibitor protein)	U15172	2.3±0.2		
DRAK-2	U80017	2.5±0.1		
SIP-1	AB011421	2.8±0.2		
DP5	AF027150	3.0±0.2		
Death receptor signaling	D83699	5.5±1.1		
Bcl-10	AJ006288	5.6±1.1		
PML-2	M79463	3.4±0.3		
Ceramide glucosyltransferase	D50840	4.0±1.2		
Sp 100	M60618	6.1±0.5		
ER stress-induced signaling	U63785	-2.4±0.2		
ORP150	U83981	3.7±0.2		
GADD 34	M60974	4.9±0.1	4.4±0.1	
GADD 45				
Proteases				
Calpain	X04366	-2.6±0.1		
Beta-4 adducin	U43959	-2.1±0.1		
Caspase 7	U67319	2.6±0.2		
Caspase 3	U13737	3.2±0.2	2.8±0.1	
Frizzled-related protein	AF056087	-2.5±0.1	-3.3±0.5	
TCBP (T cluster binding protein)	D64015	3.3±0.2		
Cug-BP/hAb50 (RNA binding protein)	U63289	6.6±1.1		

<sup>a</sup> GenBank accession number corresponds to the sequence from which the Affymetrix microarray U95A probe set was designed.

<sup>b</sup> Data are means ± standard errors of the means.

stress, and mitochondrial apoptotic signaling and cysteine proteases (caspases and calpains) (DeBiasi et al. 2003). Only five of these genes were also differentially expressed after T1L (weakly apoptotic) infection, emphasizing their potential importance in reovirus-induced apoptosis.

To date the best-characterized example of a potentially apoptosis-inducing gene identified by microarray analysis to be differentially expressed after reovirus infection is the survival motor neuron (SMN) gene. This gene was found by polymerase chain reaction (PCR) analysis to be upregulated at the transcriptional level in reovirus-infected HEK293 cells and at the translational level in the hearts of reovirus-infected baby mice (DeBiasi et al. 2003). The SMN protein has been shown to interact with Bcl-2, conferring a synergistic protective effect against Bax-induced or Fas-mediated apoptosis that has been shown to underlie the pathogenesis of spinal muscular atrophy (Sato et al. 2000; Iwahashi et al. 1997).

Changes in the expression of genes encoding proteins known to be involved in DNA repair and cell cycle regulation were also identified in this study and may also affect virus-induced pathogenesis (DeBiasi et al. 2003).

## 8 Reovirus Sensitizes Cells to TRAIL-Induced Apoptosis

In addition to inducing TRAIL-mediated apoptosis, reovirus infection also sensitizes cells to TRAIL-induced apoptosis by a mechanism that results in an increase in the activation of caspases 8 and 3 and is blocked by the caspase 8 inhibitor IETD-FMK (Clarke et al. 2000, 2001a). Reovirus infection and TRAIL treatment have synergistic rather than merely additive effects on apoptosis, and infection can confer TRAIL sensitivity to previously TRAIL-resistant cells as well as increasing the TRAIL sensitivity of partially resistant lines (Clarke et al. 2000, 2001a). This finding may increase the potential utility of TRAIL as an agent for cancer therapy, which is currently limited by the fact that cancer cells of all types differ in sensitivity to TRAIL-induced apoptosis.

The ability of reovirus to sensitize cells to TRAIL receptors as assayed in several human cancer cell lines (Clarke et al. 2001a) and may instead be the result of inhibition of TRAIL-induced activation of NF- $\kappa$ B in reovirus-infected cells (Clarke et al. 2003a).

The ability of reovirus to sensitize cells to TRAIL also suggests that reovirus-infected cells in vivo are also susceptible to killing through the TRAIL pathway by immune cells such as natural killer and CD4 $^{+}$  cells that bear membrane-bound TRAIL.

## 9 Reovirus-Induced Apoptosis in the Mouse CNS

T3 reovirus strains infect neurons within specific regions of neonatal mouse brains, producing a lethal meningoencephalitis. Viral antigen and pathology colocalize in the brain and have a predilection for the cortex, hippocampus and thalamus (Fig. 2). T3 reovirus infection also induces apoptosis in the brains of newborn mice (Oberhaus et al. 1997; Richardson-Burns et al. 2002). Thus fragmentation of DNA into oligonucleosomal-length ladders can be detected in tissue samples prepared from T3D- but not mock-infected brains at 8–9 days PI, which coincides with maximal viral growth (Oberhaus et al. 1997). The presence of apoptotic cells also correlates with areas of tissue injury and viral infection in T3D-infected brain sections (Fig. 2) (Oberhaus et al. 1997; Richardson-Burns et al. 2002).

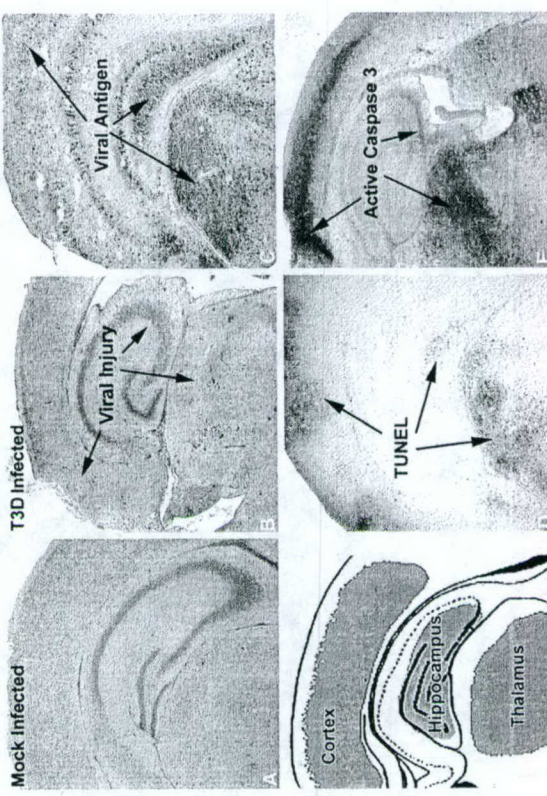


**Fig. 2** Coronal sections of neonatal mouse brain 7 days after intratrcranial inoculation of 10,000 plaque forming units (PFU) of reovirus strain T3D or mock inoculation. Hematoxylin and eosin-stained tissue reveals marked destruction of brain tissue in the T3D-infected brain (B) as compared to the uninfected brain (A). By immunohistochemistry, serial sections of T3D-infected brain tissue were stained for viral antigen (C), TUNEL/apoptosis marker (D), and active caspase 3 (E). Staining for viral antigen, TUNEL, and caspase 3 were undetectable in the mock-infected brains (data not shown). (With permission from Richardson-Burns et al. 2002)

Burns et al. 2002). Most cells in infected brain regions are both TUNEL (TdT-mediated dUTP nick-end labeling)-positive (apoptotic) and reovirus antigen-positive (infected). However, there are cells in these regions that are apoptotic but antigen negative, suggesting that apoptosis occurs both as a result of direct viral infection and in uninfected "bystander" cells (Oberhaus et al. 1997). Reovirus infection in a mouse neuroblastoma-derived cell line (NB41a3) and in primary mouse cortical cultures (MCC) derived from embryonic (E20) mice is also associated with increased levels of caspase 3 activity and is blocked with the caspase 3 inhibitor DEVD-FMK (Richardson-Burns et al. 2002). Studies of reovirus infection in neuronal cultures also provides further evidence of bystander apoptosis. In both MCC and NB4 cells dual labeling with immunocytochemistry and TUNEL showed that although a great majority of infected cells were undergoing apoptosis there was also a subset of apoptotic cells that were uninfected but located in proximity to virus-infected cells (Richardson-Burns et al. 2002). Bystander apoptosis could result from the release of TRAIL, or other death ligands, from reovirus-infected cells. If this is the case, the amount of bystander apoptosis would reflect the sensitivity of the surrounding cells to the released ligand.

Reovirus infection also induces increased caspase 8 activation in infected neurons, indicating that neuronal apoptosis, like that in its epithelial cell counterparts, involves DR activation (Richardson-Burns et al. 2002). However, the ligand-receptor trigger for this activation appears to be less specific. Thus, whereas reovirus-induced apoptosis in HEK293 cells is selectively inhibited by blocking TRAIL ligand-receptor interaction, reovirus-induced apoptosis in NB4 cells is inhibited by treating cells with both soluble TRAIL receptors (Fc:DR5) and soluble TNF receptors (TNFR) (Fc:TNFR-1), and reovirus-induced apoptosis in MCCs is inhibited by Fc:TNFR-1 and Fc:FasL.

Mitochondrial apoptotic pathways are also activated after reovirus infection of neurons. Preliminary studies indicate that proapoptotic Bcl-2 family proteins, including Bid, Bax, and Bim, are activated in virus-infected neurons, resulting in the release of proapoptotic mitochondrial factors. However, there are again differences between mitochondrial signaling pathways activated after reovirus infection of neuronal and epithelial cells. In HEK293 cells, reovirus infection is associated with robust release of cytochrome *c* and smac and the subsequent activation of caspase 9 and inhibition of cellular IAPs. In neuronal cultures, however, our preliminary results indicate that reovirus infection results in the discordant release of smac and cytochrome *c*. Smac is released around 17 h PI and coincides with the cleavage of cellular IAPs. In contrast, cytochrome

*c* release occurs only at low levels and at later times after infection, resulting in only low levels of activation of caspase 9 in these cells (Richardson-Burns et al. 2002). Consistent with these findings, the caspase 9 inhibitor Z-LEHD-FMK has little effect on reovirus-induced neuronal apoptosis, which is significantly inhibited by caspase 8 (Z-IETD-FMK), caspase 3 (Z-DEVD-FMK), or pan-caspase inhibitors.

## 10 Reovirus-Induced Apoptosis in the Heart

The T1L × T3D reassortant virus 8B efficiently produces myocarditis in infected neonatal mice. Similar to results seen in mouse brain, DNA extracted from the hearts of 8B-infected mice is fragmented into oligonucleosomal-length ladders, indicative of apoptosis (DeBiasi et al. 2001) and areas of TUNEL-positive cells in 8B-infected hearts correlates with areas of histological damage and reovirus antigen (DeBiasi et al. 2001). Injury to the heart following reovirus infection occurs in the absence of an inflammatory response, also suggesting that it results from apoptotic cell death (DeBiasi et al. 2001).

Treatment of mice with the calpain inhibitor CX295 [dipeptide  $\alpha$ -ketotamide calpain inhibitor z-Leu-aminobutyric acid-CONH(CH<sub>2</sub>)<sub>3</sub>-morpholine] is protective against reovirus-induced myocarditis and results in a dramatic reduction in histopathologic evidence of myocardial injury (Fig. 3), a reduction in serum creatine phosphokinase (an intracellular enzyme whose release into the serum is a quantitative marker of skeletal and cardiac muscle damage), and improved weight gain (DeBiasi et al. 2001).

Prevention of myocardial injury by apoptosis inhibitors is accompanied by a virtually complete inhibition of apoptotic myocardial cell death, strongly suggesting that virus-induced apoptosis is a key mechanism of cell death, tissue injury, and mortality in reovirus-infected mice and that inhibitors of apoptosis may prove useful in the treatment of virus-induced diseases (DeBiasi et al. 2001).

## 11 Apoptosis and Viral Growth

Early studies showed that there is little correlation in continuous non-neuronal cell lines between the efficiency with which reovirus strains

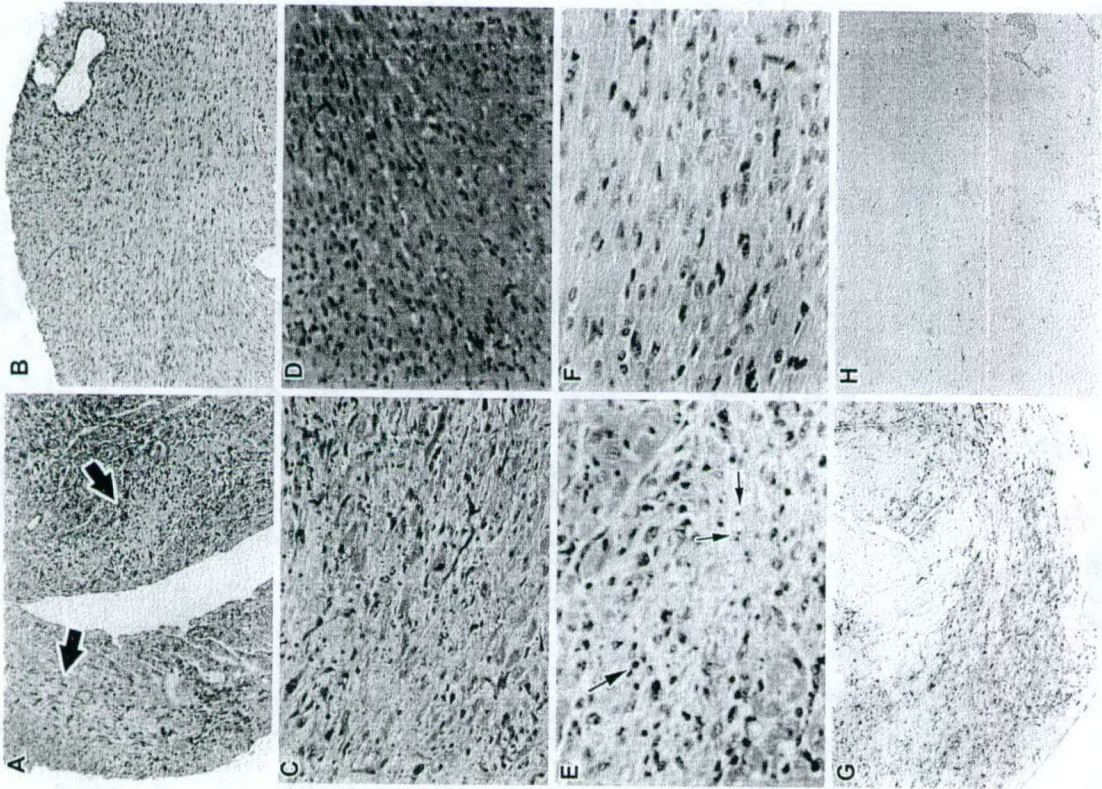


**Fig. 3** Cardiac midsections from reovirus 8B-infected neonatal mice treated with the calpain inhibitor CX295 (B, D, F, and H) compared to those from inactive diluent control mice (A, C, E, and G) 7 days after intramuscular inoculation with 1,000 PFU of reovirus 8B. Hematoxylin and eosin-stained sections at an original magnification of  $\times 25$  reveal extensive focal areas of myocardial injury (arrows) in the control ani-

replicate and their capacity to induce apoptosis. For example, T1L and T3D grow to approximately equivalent titers in L929 fibroblasts, yet T3D induces significantly more apoptosis (Tyler et al. 1995). Similarly, T1L grows better than T3D in MDCK cells, yet again T3D induces significantly more apoptosis (Rodgers et al. 1997).

### 11.1 The Effects of Virus Replication and Growth on Apoptosis

In HeLa cells, viral RNA synthesis is not required for reovirus-induced apoptosis because the viral RNA synthesis inhibitor ribavirin does not prevent apoptosis (Connolly and Dermody 2002). In addition, particles lacking genomic dsRNA can induce apoptosis in HeLa cells, and *ts* reovirus mutants with mutations resulting in defects in outer capsid assembly (*ts*B352/L2 gene), and in dsRNA synthesis (*ts*D357/L1 gene, *ts*E320/S3 gene), are capable of inducing similar levels of apoptosis at both nonpermissive (39°C) and permissive (32°C) temperatures. Temperature-sensitive mutants with defects in viral core (*ts*C447/S2 gene) and outer capsid assembly (*ts*G453/S4 gene) also still induce apoptosis at 39°C, but only about half as efficiently as they do at 32°C (Connolly and Dermody 2002).

Because all these *ts* mutants undergo endosomal processing, their ability to induce apoptosis is consistent with a key role for endosomal vesicle-related events in apoptosis induction. However, the fact that assembly defects can influence the efficiency of this process suggests that additional viral growth-related factors are also involved. Furthermore, UV-inactivated virions, which are not transcriptionally active, were 100 times less apoptotic than their T3D derivative in L929 cells (Tyler et al. 1995) and ribavirin inhibits reovirus-induced apoptosis after T3A-infection of HEK293 cells (Clarke et al. 2003a). Together these results suggest

◀

animal (A), which are absent in the CX295-treated animal (B), despite identical viral infections. Views at an original magnification of  $\times 50$  demonstrate minimal inflammatory cell infiltrate in the affected area (C), but myocardial architecture is dramatically disrupted, compared to that of a CX295-treated mouse (D). At an original magnification of  $\times 100$ , nuclei with apoptotic morphology are easily seen in the control animal (E) as are cells with pyknotic nuclei (*long arrows*) as well as apoptotic bodies (*short arrows*). These characteristics are absent in the drug-treated mouse (F). TUNEL analysis of the control animal reveals extensive areas of positively staining cells in the same regions of injury (G) but no TUNEL-positive areas in the drug-treated mouse. (With permission from DeBiasi et al. 2001)

that viral replication enhances, but is not absolutely required for, virus-induced apoptosis.

### 11.2 Effect of Apoptosis on Viral Growth

In several systems inhibition of apoptosis leads to a modest but reproducible decrease in viral titer in reovirus T3-infected cells. Thus a five-fold reduction in viral yield was observed in L929 cells treated with an inhibitor of calpain activity compared to untreated cells (DeBiasi et al. 1999). Similarly, in p50 or p65<sup>-/-</sup> immortalized fibroblasts, a two- to fivefold reduction in viral yield was seen, compared to wild-type cells (Connolly et al. 2000). Both of these treatments resulted in a significant inhibition of reovirus-induced apoptosis.

Treatment of mice with inhibitors of apoptosis also results in a reduction in viral growth. Ergo, after treatment with an inhibitor of calpain, a reduction of  $0.5 \log_{10}$  PFU/ml was observed at the site of primary replication primary (hindlimb), whereas a  $0.7 \log_{10}$  PFU/ml reduction was observed in the heart (DeBiasi et al. 2001). Our preliminary results indicate that chemical inhibition of caspase 3 produced similar effects on viral replication. However, in caspase 3-deficient mice, nearly a 2 log reduction was noted, compared to wild-type and heterozygous controls. As expected, treatment with these inhibitors and infection of caspase 3-deficient mice resulted in a marked decrease in apoptosis in infected tissues.

In a recent study, reovirus growth and apoptosis were determined after infection with reovirus variant K (VarK), which is an antigenic variant of T3D that has nearly a millionfold reduction in neurovirulence after intracerebral (IC) inoculation and a restricted pattern of CNS injury, with damage limited to the hippocampus (Richardson-Borns et al. 2004). It was found that VarK grew to similar titer as T3D in the hippocampus but had significantly lower titer in the cortex. Similarly, whereas the viruses grew to identical titers and infected the same percentage of cells in mouse primary hippocampal cultures (MHC), both the number of infected cells and the viral yield per infected cell were significantly lower for VarK than T3D in mouse primary cortical cultures (MCC). Like growth, VarK-induced apoptosis was limited to the hippocampus *in vivo* and to MHC *in vitro*. As expected (see above), growth of T3D in MCC was reduced to levels comparable to VarK after treatment of MCC with caspase inhibitors. However, also of note was the finding that induction of apoptosis in VarK-infected MCC with Fas-activating antibody

significantly enhanced viral yield. These results thus suggest that the decreased growth and neurovirulence of VarK may be due to its failure to efficiently induce apoptosis in cortical neurons.

Together these results suggest that reovirus-induced apoptosis is required for maximal viral growth.

## 12 Conclusions and Future Directions

Significant discoveries have been made regarding the mechanisms of and the requirement of apoptosis following reovirus infection. However, much still remains to be determined. For example, we now know that many individual apoptotic signaling pathways play a role in reovirus-induced apoptosis but our understanding of the regulation of these pathways and the way in which these pathways interact is much less clear. In addition, some apoptotic signaling events are cell type specific, making the confirmation of apoptotic signaling pathways in primary cells and infected tissues critical for our evaluation both of the role of reovirus-induced apoptosis *in vivo* and of the use of apoptosis inhibitors as a novel strategy for limiting virus-induced tissue damage.

**Acknowledgements** This work was supported by Merit and REAP grants from the Department of Veterans Affairs (KLT), R01NS050138 from the NIH/NINDS (KLT), the Revier-Lewin Family Professorship of Neurology (KLT), the Department of Defence/US Army Medical Research and Material Command (DAMD 17-98-8614) (KLT) and the Ovarian Cancer Research Fund (PC).

## References

- Barton ES, Connolly JL, Forrest JC, Chappell JD, Dermody TS (2001a) Utilization of sialic acid as a coreceptor enhances reovirus attachment by multistep adhesion strengthening. *J Biol Chem* 276:2200-2211
- Barton ES, Forrest JC, Connolly JL, Chappell JD, Liu Y, Schnell FI, Nusrat A, Parkos CA, Dermody TS (2001b) Junction adhesion molecule is a receptor for reovirus. *Cell* 104:441-451
- Camandola S, Mattson MP (2000) Pro-apoptotic action of PAR-4 involves inhibition of NF- $\kappa$ pB activity and suppression of BCL-2 expression. *J Neurosci Res* 61:134-139
- Chai J, Shiozaki E, Srinivasula SM, Wu Q, Datta P, Alnemri ES, Shi Y, Datta P (2001) Structural basis of caspase-7 inhibition by XIAP. *Cell* 104:769-780

- Chappell JD, Duong JL, Wright BW, Dermody TS (2000) Identification of carbohydrate-binding domains in the attachment proteins of type 1 and type 3 reoviruses. *J Virol* 74:8472-8479
- Chappell JD, Prota AE, Dermody TS, Siehle T (2002) Crystal structure of reovirus attachment protein sigma reveals evolutionary relationship to adenovirus fiber. *EMBO J* 21:1-11
- Chen F, Lu Y, Kuhn DC, Maki M, Shi X, Sun SC, Demers LM (1997) Calpain contributes to silica-induced I kappa B-alpha degradation and nuclear factor-kappa B activation. *Arch Biochem Biophys* 342:383-388
- Clarke P, Meintzer SM, Gibson S, Widmann C, Garrington TP, Johnson GL, Tyler KL (2000) Reovirus-induced apoptosis is mediated by TRAIL. *J Virol* 74:8135-8139
- Clarke P, Meintzer SM, Moffitt LA, Tyler KL (2003a) Two distinct phases of virus-induced nuclear factor kappa B regulation enhance tumor necrosis factor-related apoptosis-inducing ligand-mediated apoptosis in virus-infected cells. *J Biol Chem* 278:18092-18100
- Clarke P, Meintzer SM, Spalding AC, Johnson GL, Tyler KL (2001a) Caspase-8-dependent sensitization of cancer cells to TRAIL-induced apoptosis following reovirus-infection. *Oncogene* 20:6910-6919
- Clarke P, Meintzer SM, Wang Y, Moffitt LA, Richardson-Burns SM, Johnson GL, Tyler KL (2004) *J Virol* 78:13132-13138
- Clarke P, Meintzer SM, Widmann C, Johnson GL, Tyler KL (2001b) Reovirus infection activates JNK and the JNK-dependent transcription factor c-Jun. *J Virol* 75:11275-11283
- Clarke P, Tyler KL (2003) Reovirus-induced apoptosis: A minireview. *Apoptosis* 8:141-150
- Connolly JL, Barton ES, Dermody TS (2001) Reovirus binding to cell surface sialic acid potentiates virus-induced apoptosis. *J Virol* 75:4029-4039
- Connolly JL, Dermody TS (2002) Virion disassembly is required for apoptosis induced by reovirus. *J Virol* 76:1632-1641
- Connolly JL, Rodgers SE, Clarke P, Ballard DW, Kerr LD, Dermody TS (2000) Reovirus-induced apoptosis requires activation of transcription factor NF-kappaB. *J Virol* 74:2981-2989
- DeBiasi RL, Clarke P, Meintzer S, Jotter R, Kleinschmidt-Demasters BK, Johnson GL, Tyler KL (2003) Reovirus-induced alteration in expression of apoptosis and DNA repair genes with potential roles in viral pathogenesis. *J Virol* 77:8934-8947
- DeBiasi RL, Edelstein CL, Sherry B, Tyler KL (2001) Calpain inhibition protects against virus-induced apoptotic myocardial injury. *J Virol* 75:351-361
- DeBiasi RL, Squier MK, Pike B, Wynne M, Dermody TS, Cohen JJ, Tyler KL (1999) Reovirus-induced apoptosis is preceded by increased cellular calpain activity and is blocked by calpain inhibitors. *J Virol* 73:695-701
- Deveraux QL, Leo E, Stennicke HR, Welsh K, Salvesen GS, Reed JC (1999) Cleavage of human inhibitor of apoptosis protein XIAP results in fragments with distinct specificities for caspases. *EMBO J* 18:5242-5251
- Diaz-Meco MT, Lallena MJ, Monjas A, Frutos S, Moscat J (1999) Inactivation of the inhibitory kappaB protein kinase/nuclear factor kappaB signaling pathway potentiates tumor necrosis factor alpha-induced apoptosis. *J Biol Chem* 274:19606-19612
- Chappell JD, Duong JL, Wright BW, Dermody TS, Johnson GL (2000) Increased expression of death receptors 4 and 5 synergizes the apoptosis response to combined treatment with etoposide and TRAIL. *Mol Cell Biol* 20:205-212
- Huang Y, Park YC, Rich RL, Segal D, Myszka DG, Wu H (2001) Structural basis of caspase inhibition by XIAP: differential roles of the linker versus the BIR domain. *Cell* 104:781-790
- Iwahashi H, Eguchi Y, Yashihara N, Hanafusa T, Matsuzawa Y, Tsujimoto Y (1997) Synergistic anti-apoptotic activity between Bcl-2 and SMN implicated in spinal muscular atrophy. *Nature* 390:413-417
- Johnson DE, Gastman BR, Wieckowski E, Wang GQ, Amoscato A, Delach SM, Rabinowich H (2000) Inhibitor of apoptosis protein hIPL undergoes caspase-mediated cleavage during T lymphocyte apoptosis. *Cancer Res* 60:1818-1823
- Kominsky DJ, Bickel RJ, Tyler KL (2002a) Reovirus-induced apoptosis requires both death receptor- and mitochondrial-mediated caspase-dependent pathways of cell death. *Cell Death Differ* 9:926-933
- Kominsky DJ, Bickel RJ, Tyler KL (2002b) Reovirus-induced apoptosis requires mitochondrial release of Smac/DIABLO and involves reduction of cellular inhibitor of apoptosis protein levels. *J Virol* 76:11414-11424
- Oberhaus SM, Smith RL, Clayton GH, Dermody TS, Tyler KL (1997) Reovirus infection and tissue injury in the mouse central nervous system are associated with apoptosis. *J Virol* 71:2100-2106
- Palaga T, Osborne B (2002) The 3D's of apoptosis: death, degradation and DIAPS. *Nat Cell Biol* 4:E149-E151
- Poggiooli GI, DeBiasi RL, Bickel RJ, Jotter R, Spalding A, Johnson GL, Tyler KL (2002) Reovirus-induced alterations in gene expression related to cell cycle regulation. *J Virol* 76:2585-2594
- Poggiooli GI, Dermody TS, Tyler KL (2001) Reovirus-induced signals-dependent G<sub>2</sub>/M phase cell cycle arrest is associated with inhibition of p34 (cdc2). *J Virol* 75:7429-7434
- Poggiooli GI, Keefer C, Connolly JL, Dermody TS, Tyler KL (2000) Reovirus-induced G<sub>2</sub>/M cell cycle arrest requires signals and occurs in the absence of apoptosis. *J Virol* 74:9562-9570
- Ravi R, Bedi GC, Engstrom LW, Zeng Q, Mookerjee B, Gelinas C, Fuchs EJ, Bedi A (2001) Regulation of death receptor expression and TRAIL/Apo2L-induced apoptosis by NF-kappaB. *Nat Cell Biol* 3:409-416
- Richardson-Burns SM, Kominsky DJ, Tyler KL (2002) Reovirus-induced neuronal apoptosis is mediated by caspase 3 and is associated with the activation of death receptors. *J Neurovirol* 8:365-380
- Richardson-Burns SM, Tyler KL (2004) Regional differences in viral growth and central nervous system injury correlate with apoptosis. *J Virol* 78:5466-5475
- Riedl SJ, Renatus M, Schwarzenbacher R, Zhou Q, Sun C, Fesik SW, Liddington RC, Salvesen GS (2001) Structural basis for the inhibition of caspase-3 by XIAP. *Cell* 104:791-800
- Rivera-Walsh I, Waterfield M, Xiao G, Fong A, Sun SC (2001) NF-kappaB signaling pathway governs TRAIL gene expression and human T-cell leukemia virus-I Tax-induced T-cell death. *J Biol Chem* 276:40385-40388

- Rodgers SE, Barton ES, Oberhaus SM, Pike B, Gibson CA, Tyler KL, Dermody TS (1997) Reovirus-induced apoptosis of MDCK cells is not linked to viral yield and is blocked by Bcl-2. *J Virol* 71:2540–2546
- Saito K, Eguchi Y, Kodama TS, Tsujimoto Y (2000) Regions essential for the interaction between Bcl-2 and SMN, the spinal muscular atrophy disease gene product. *Cell Death Differ* 7:374–383
- Spalding AC, Jotte RM, Scheinman RI, Geraci MW, Clarke P, Tyler KL, Johnson GL (2002) TRAIL and inhibitors of apoptosis are opposing determinants for NF- $\kappa$ B-dependent, genotoxin-induced apoptosis of cancer cells. *Oncogene* 21:260–271
- Tyler KL (1998) Pathogenesis of reovirus infections of the central nervous system. *Curr Top Microbiol Immunol* 233: Reovir.ii:93–124
- Tyler KL, Clarke P, DeBiasi RL, Kominský D, Poggioli GJ (2001) Reoviruses and the host cell. *Trends Microbiol* 9:560–564
- Tyler KL, Squier MK, Brown AL, Pike B, Willis D, Oberhaus SM, Dermody TS, Cohen JJ (1996) Linkage between reovirus-induced apoptosis and inhibition of cellular DNA synthesis: role of the S1 and M2 genes. *J Virol* 70:7984–7991
- Tyler KL, Squier MK, Rodgers SE, Schneider BE, Oberhaus SM, Grdina TA, Cohen JJ, Dermody TS (1995) Differences in the capacity of reovirus strains to induce apoptosis are determined by the viral attachment protein sigma 1. *J Virol* 69:6972–6979
- Verhagen AM, Ekert PG, Pakusch M, Silke J, Connolly LM, Reid GE, Moritz RL, Simpson RJ, Vaux DL (2000) Identification of DIABLO, a mammalian protein that promotes apoptosis by binding to and antagonizing IAP proteins. *Cell* 102:43–53
- Virgin HW, Mann MA, Tyler KL (1994) Protective antibodies inhibit reovirus internalization and uncoating by intracellular proteases. *J Virol* 68:6719–6729
- Watt E, Molloy PL (1993) Specific cleavage of transcription factors by the thiol protease, m-calpain. *Nucleic Acids Res* 21:5092–5100
- Yang Y, Fang S, Jensen JP, Weissman AM, Ashwell JD (2000) Ubiquitin protein ligase activity of IAPs and their degradation in proteasomes in response to apoptotic stimuli. *Science* 288:874–877

## Poliovirus, Pathogenesis of Poliomyelitis, and Apoptosis

B. Blondel<sup>1</sup> (✉) · F. Colbère-Garapin<sup>1</sup> · T. Couderc<sup>2</sup> · A. Wirotius<sup>1</sup>

F. Guivel-Benhassine<sup>3</sup>

<sup>1</sup> Laboratoire des Virus Entérotropes et Stratégies Antivirales, Institut Pasteur, 75724 Paris Cedex 15, France  
**bblondel@pasteur.fr**

<sup>2</sup> Unité Postulante de Neuroimmunologie Virale, Institut Pasteur,

75724 Paris Cedex 15, France

<sup>3</sup> Groupe Virus et Immunité, Institut Pasteur,  
 75724 Paris Cedex 15, France

1	Poliovirus . . . . .	28
1.1	Structure of the Virion . . . . .	28
1.2	PV Receptor . . . . .	28
1.3	Viral Cycle . . . . .	32
1.4	Effect of PV Replication on the Host Cell . . . . .	34
2	Pathogenesis of Poliomyelitis and Post-Polio Syndrome . . . . .	35
3	Poliovirus and Apoptosis . . . . .	38
3.1	PV-Induced Apoptosis in Nerve Cells In Vivo and Ex Vivo . . . . .	39
3.2	PV-Induced Apoptosis In Vitro . . . . .	40
3.3	CD155 and Apoptosis . . . . .	42
4	Conclusion . . . . .	43
	References . . . . .	44

**Abstract** Poliovirus (PV) is the causal agent of paralytic poliomyelitis, an acute disease of the central nervous system (CNS) resulting in flaccid paralysis. The development of new animal and cell models has allowed the key steps of the pathogenesis of poliomyelitis to be investigated at the molecular level. In particular, it has been shown that PV-induced apoptosis is an important component of the tissue injury in the CNS of infected mice, which leads to paralysis. In this review the molecular biology of PV and the pathogenesis of poliomyelitis are briefly described, and then several models of PV-induced apoptosis are considered; the role of the cellular receptor of PV, CD155, in the modulation of apoptosis is also addressed.

Poliomyelitis (PV) is the causal agent of paralytic poliomyelitis, an acute disease of the central nervous system (CNS) resulting in flaccid paralysis. In addition, another neuromuscular pathology, called the post-polio



## Minocycline delays disease onset and mortality in reovirus encephalitis

Sarah M. Richardson-Burns<sup>a</sup>, Kenneth L. Tyler<sup>a,b,c,\*</sup>

<sup>a</sup>Neuroscience Program, University of Colorado Health Sciences Center, Denver, CO 80262, USA

<sup>b</sup>Departments of Neurology, Medicine, Immunology, and Microbiology, University of Colorado Health Sciences Center, Denver, CO 80262, USA

<sup>c</sup>Denver Veteran's Affairs Medical Center, Denver, CO 80220, USA

Received 7 September 2004; revised 2 November 2004; accepted 9 November 2004

### Abstract

Minocycline is neuroprotective in many experimental models of neurodegenerative diseases and central nervous system (CNS) injury but has not previously been tested in a model of viral encephalitis. Experimental infection of neonatal mice with neurotropic reoviruses is a classic model for studying the pathogenesis of viral encephalitis. Intracerebral inoculation of serotype 3 reovirus strain Dearing (T3D) in neonatal mice results in lethal encephalitis caused by neuronal apoptosis throughout the CNS. Minocycline significantly delayed death in mice to  $11.6 \pm 0.9$  days post-infection vs.  $8.6 \pm 0.7$  days post-infection in controls ( $P < 0.01$ ). Virus-induced CNS injury, apoptosis, viral titer and antigen expression were significantly decreased in the brains of minocycline-treated mice on 6 and 8 days post-infection compared to controls. Virus-induced injury and viral titer in minocycline-treated infected mice at 11 days post-infection were similar to those seen in untreated T3D-infected mice at 8 days post-infection. Little microglial or astrocytic invasion of brain regions with viral injury was found at any time-point in untreated or minocycline-treated mice, suggesting that in this model system the neuroprotective effect exerted by minocycline is more likely due to its anti-apoptotic properties rather than its capacity to inhibit microglial activation and limit gliosis. These findings, similar to those reported for neurodegenerative diseases, indicate that minocycline does not prevent development of fatal reovirus encephalitis but delays disease onset and progression, suggesting that minocycline treatment may provide a useful adjunctive therapy in viral CNS infections.

© 2004 Elsevier Inc. All rights reserved.

**Keywords:** Apoptosis; Central nervous system; Microglia; Neurons; Mouse

### Introduction

The antibiotic minocycline, a synthetic tetracycline derivative, is neuroprotective in a variety of experimental models of neurodegenerative diseases (Denovan-Wright et al., 2002; Erickson and Bernard, 2002; Friedlander, 2003; Kriz et al., 2002; Thomas et al., 2003), traumatic CNS injury (Wells et al., 2003), and cerebral hypoxia-ischemia (Arvin et al., 2002; Wang et al., 2003a; Yrjanheikki et al., 1999). However, the neuroprotective effects of minocycline have not yet been tested in experimental models of

CNS infection. Current studies suggest that minocycline may exert its neuroprotective effect by inhibiting apoptosis, a type of cell death common to these diverse CNS diseases. Apoptosis is mediated by complex cellular signaling processes resulting in new protein synthesis, altered gene expression, and activation of apoptosis-specific proteases called caspases (Hengartner, 2000). Although the mechanisms of minocycline's anti-apoptotic effects have not been unequivocally defined, several studies suggest that minocycline interferes with mitochondria-initiated death signaling preventing caspase activation (Friedlander, 2003; Scarabelli et al., 2004; Wang et al., 2004). Minocycline may also act to inhibit neuronal apoptosis by reducing microglial-mediated excitotoxic pathways (Shaw, 2002; Tikka et al., 2001a; Yrjanheikki et al., 1998).

\* Corresponding author. Department of Neurology (B-182), University of Colorado Health Sciences Center, 4200 E. 9th Avenue, Denver, CO 80262, USA. Fax: +1 303 393 4686.

E-mail address: ken.tyler@uchsc.edu (K.L. Tyler).

Experimental infection of neonatal mice with neurotropic reoviruses is a classic model for studying the pathogenesis of viral encephalitis. Serotype 3 (T3) reovirus infection causes widespread CNS injury highlighted by apoptosis in the hippocampus, cingulate gyrus, frontoparietal cortex, and thalamic nuclei with minimal inflammation (Oberhaus et al., 1997; Raine and Fields, 1973; Richardson-Burns and Tyler, 2004; Tyler, 2001). Reovirus infection of neurons activates death receptors leading to robust caspase activation that can be inhibited with specific tetrapeptide caspase inhibitors (Richardson-Burns et al., 2002b). Inhibiting virus-induced apoptosis by disrupting key molecules in pro-apoptotic signaling may protect neurons in the mouse CNS from virus-induced apoptosis and represents a novel strategy for anti-viral therapy. Since inhibition of apoptosis is a proposed mechanism by which minocycline exerts its protective effect in CNS disease, we investigated whether reovirus encephalitis could be ameliorated or prevented by treating infected mice with minocycline.

## Materials and methods

### Mouse viral infection and drug administration

Neonatal mice (2 days postnatal) were randomly separated into three treatment groups prior to infection; uninfected, phosphate-buffered saline (PBS; vehicle) + T3D, and minocycline + T3D. Average mouse weight at time of infection was 1.7 g. Minocycline (Sigma-Aldrich, St. Louis MO) was prepared fresh each day in PBS. Mice were intracerebrally (ic) inoculated with  $3 \times 10^3$  or  $3 \times 10^5$  plaque forming units (PFU) of serotype 3 reovirus strain Dearing (T3D) in 10  $\mu$ l with a 29-gauge needle. Mice were intraperitoneally (ip) injected each day starting 2 days post-infection with 35 mg/kg minocycline in 20  $\mu$ l with a 29-gauge needle. Mice were sacrificed either 6, 8, 11 days post-infection, or when incapacitated by disease. In untreated mice inoculated with  $3 \times 10^3$  or  $3 \times 10^5$  PFU, T3D encephalitis is 100% fatal by 9 days post-infection.

Data shown in Fig. 1 is representative of six studies, in Figs. 2 and 4 of three studies, and in Fig. 3 of one study. Each of these studies used 5 uninfected mice, 7 vehicle + T3D mice, and 9 minocycline + T3D mice for each study.

All animal experiments received institutional approval and were conducted in accordance with the United States Public Health Service Policy on Humane Care and Use of Laboratory Animals.

### Histology

For histopathologic and immunohistochemical staining, brains were removed and immediately fixed by immersion in 10% buffered formalin for 24–30 h at room temperature (RT), then coronally sectioned. Whole brains were transferred to 70% ethanol, paraffin-embedded, and sectioned at 4- $\mu$ m thickness. For histopathological analysis, coronal sections were stained with hematoxylin and eosin (H&E) then scored for severity of virus-induced CNS damage according to the Histopathology Score Chart shown in Fig. 1C. The scale is from 0 to 6 with higher numbers representing more severe viral injury. For analysis, brains were divided into five distinct brain regions that are susceptible to reovirus-induced injury; thalamic nuclei (THA), hippocampal regions CA1–3 (CA2/3 and CA1), and cortical regions, cingulate gyrus (CG) and frontoparietal cortex (FPX).

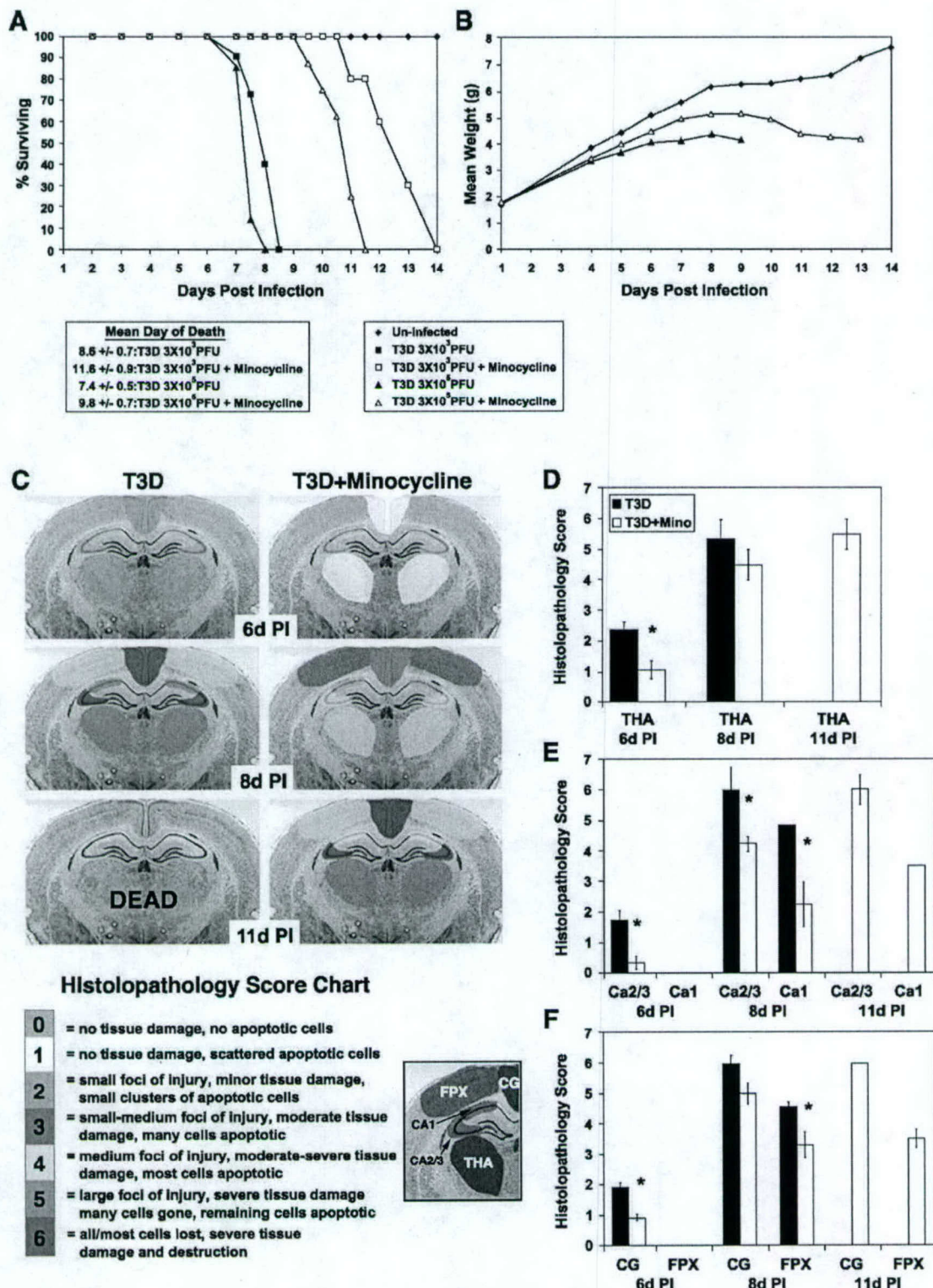
### Viral titer assays

Whole brains were removed, immediately placed in 2 ml ice-cold gel saline and frozen at  $-70^{\circ}\text{C}$  for at least 24 h. Tissues were lysed by three freeze ( $-70^{\circ}\text{C}$ )–thaw ( $37^{\circ}\text{C}$ ) cycles followed by homogenization by microtip sonication (Ultrasound Sonicator XL2020 Heat Systems-Misonix, Farmingdale, NY) for 4 s. Homogenates were then serially diluted and viral titer was determined by plaque assay using monolayers of L929 mouse fibroblasts, as previously described (Tyler et al., 1985).

### Immunohistochemistry and staining

Immunohistochemistry for activated caspase 3 was performed using the Ventana Automated Staining System as previously described (Richardson-Burns et al., 2002a). For TdT dUTP Nick-End Labeling (TUNEL), an anti-BrdU based kit was used (TACS-XL; Trevigen). Deparaffinized brain tissue sections were permeabilized with Neopore

**Fig. 1.** Minocycline delays disease onset and progression and mortality of reovirus encephalitis. (A) Survival curves for mice intracerebrally (ic) inoculated with either  $3 \times 10^3$  plaque-forming units (PFU) or  $3 \times 10^5$  PFU of reovirus serotype 3 strain Dearing (T3D) treated with either vehicle (PBS) or minocycline (35 mg/kg in PBS) intraperitoneally (ip). Mean day of death was significantly different between vehicle + T3D and minocycline + T3D for both  $3 \times 10^3$  PFU and  $3 \times 10^5$  PFU inoculations of T3D (data are mean  $\pm$  SEM;  $P < 0.01$  between T3D and T3D + minocycline for both doses of virus; Student's *t* test). (B) T3D-infected ( $3 \times 10^3$  PFU ic inoculation) mice do not gain weight normally. This failure to thrive is partially ameliorated by minocycline treatment. (C) The mean histopathological score for virus-induced injury in THA was significantly reduced in minocycline + T3D (white bars) on 6 days PI compared to vehicle + T3D (black bars) but by 11 days, PI thalamic injury in minocycline + T3D was similar to that seen in vehicle + T3D on 8 days PI (\* $P < 0.01$ ; Student's *t* test). (D) Virus-induced injury in the CA2/3 and CA1 regions of the hippocampus was also significantly reduced by minocycline treatment at 6 and 8 days PI but like results in THA by 11 days PI hippocampal injury in minocycline + T3D was similar to that seen in vehicle + T3D on 8 days PI (\* $P < 0.05$ ; Student's *t* test). (E) Minocycline significantly decreased viral injury in the CG and the FPX at 6 and 8 days PI, respectively (\* $P < 0.01$ ; Student's *t* test). (F) The mean histopathological score for each brain region in parts C–E (rounded to nearest whole number) is represented by a corresponding color on the histopathology scoring chart and is indicated on each representative brain section.



(Trevigen) then the remainder of the procedure was performed according to manufacturer's instructions. For viral antigen staining, deparaffinized, permeabilized (Neuro-pore, Trevigen, Gaithesburg, MD) brain tissue sections were blocked (5% BSA/PBS 0.1% triton X) 1 h at RT, then

incubated 1 h at 37°C with anti-T3D polyclonal antisera at 1:100 in 3% BSA/PBSX. Anti-T3D was detected by anti-rabbit Alexa Fluor594 (1:100) and counterstained with Hoechst 33342 (both from Molecular Probes, Eugene OR). For double labeling of astrocyte and microglia, deparaffi-

nized, permeabilized (1 h PBSX) sections were incubated ON at 4°C with rabbit anti-GFAP (1:100; Chemicon, Temecula, CA) and FITC-labeled *Griffonia simplicifolia* I isolectin B4 (Sigma, St. Louis MO) in 3% BSA/PBSX + 5 μM Ca<sup>2+</sup>. The GFAP was detected with anti-rabbit Alexa Fluor 594 (Molecular Probes) and the sections were counterstained with Hoechst. Fluorescently labeled sections were aqueous mounted with Vectashield (Vectorlabs, Burlingame, CA). All sections were digitally imaged using a Zeiss AxioPlan microscope with a Cooke Sensicam QE camera.

## Results

T3D infection in neonatal mice produces massive virus-induced neuronal apoptosis throughout the CNS resulting in fatal encephalitis by 7–9 days post-infection (Oberhaus et al., 1997; Richardson-Burns and Tyler, 2004; Richardson-Burns et al., 2002b). We tested the capacity of minocycline to protect neurons from reovirus-induced apoptosis and to prevent the development of fatal encephalitis in mice. Mice were intracerebrally (ic) infected with  $3 \times 10^3$  PFU (300 times LD<sub>50</sub>) of virus then treated daily with minocycline beginning 48 h post-infection. Minocycline significantly delayed but did not prevent death of infected mice. Mean day of death was  $11.6 \pm 0.9$  days post-infection for minocycline + T3D mice, which was significantly greater than that for vehicle + T3D mice ( $8.6 \pm 0.7$  days post-infection;  $P < 0.01$ ; Fig. 1A). Even with a higher dose (30,000 times LD<sub>50</sub>) of virus, minocycline treatment significantly delayed death (mean day of death  $7.4 \pm 0.5$  days post-infection vehicle + T3D vs.  $9.8 \pm 0.7$  days post-infection minocycline + T3D;  $P < 0.01$ ; Fig. 1A). In addition to delaying mortality, minocycline treatment ameliorated virus-induced “failure to thrive” in infected mice. Failure to gain weight is a sensitive indication of the severity of T3D-induced disease. Minocycline-treated mice grow better than untreated infected mice, although not as well as uninfected control animals (Fig. 1B).

Having shown that minocycline treatment delays progression of T3D encephalitis, we next investigated whether this is associated with a reduction in virus-induced CNS injury. In T3D-infected mice the earliest pathological signs of CNS injury are detectable at 5–6 days post-infection and by 8 days post-infection massive cell death, neuronal loss, and disruption of CNS cytoarchitecture is evident (Oberhaus et al., 1997; Richardson-Burns et al., 2002b). T3D encephalitis is fatal by 8–9 days post-infection. At 6 days post-infection, minocycline treatment of infected mice significantly reduces viral injury in thalamic nuclei (THA), Ca2/3 regions of the hippocampus, and in the cingulate gyrus (CG) compared to that seen in vehicle + T3D mice ( $P < 0.01$ ; Figs. 1C–F). At 8 days post-infection, there is a significant difference between minocycline + T3D and vehicle + T3D in both the CA1 and CA2/3 hippocampal regions and in the frontoparietal cortex (FPX) (Figs. 1C–F).

Interestingly, minocycline + T3D animals are still alive on 11 days post-infection; however, they show virus-induced CNS injury equivalent to that seen in vehicle + T3D at 8 days post-infection (see Fig. 1F).

Minocycline treatment of T3D-infected mice significantly decreased the total number of apoptotic cells in the five brain regions assessed on 6 days post-infection as detected by TUNEL assay ( $P < 0.01$ ; Fig. 2A). The total number of TUNEL positive cells in each brain region assessed was also decreased in minocycline + T3D mice as compared to vehicle + T3D mice (Figs. 2B–D). Similar results were obtained using immunohistochemical staining for activated caspase 3. An example of this stain is shown in Figs. 2E,F. The dorsal thalamic nuclei of brain tissue sections from vehicle + T3D mice (Fig. 2E) show numerous cells staining positive for activated caspase 3 (brown cells). In contrast, the dorsal thalamus from minocycline + T3D mice (Fig. 2F) has comparably fewer apoptotic cells (compare Figs. 2E–F).

We next analyzed whether microglial and/or astrocytes invade viral injury foci and whether minocycline-associated inhibition of microglial/glial activation may play a role in delaying T3D encephalitis. Using FITC-labeled *G. simplicifolia* I isolectin B4 (isolectin B4) as a marker for microglia and immunohistochemical labeling of GFAP to detect astrocytes, we found few GFAP or isolectin B4 positive cells throughout the brains of the neonatal mice (Fig. 3). However, in regions with viral injury on 8 days post-infection in vehicle + T3D mice and 11 days post-infection in minocycline + T3D mice, cells with GFAP-positive processes were detected near the lateral ventricles and migrating toward clusters of apoptotic cells. Rare isolectin B4-labeled cells were also found in the vicinity of viral injury (Figs. 3C). These phenomena were detected in a subset of brain regions injured by the virus, specifically the dorsal thalamus (shown in Fig. 3), subiculum, and cingulate gyrus.

Lastly, we investigated whether T3D growth in the CNS is affected by minocycline treatment. Viral antigen was detected by immunohistochemical staining for reovirus proteins in brains from vehicle + T3D at 6 and 8 days post-infection and minocycline + T3D at 6, 8, and 11 days post-infection. Viral antigen was found in all brain tissue sections from both vehicle + T3D mice and minocycline + T3D mice; however, the intensity and extent of antigen expression was decreased in the minocycline + T3D group as compared to vehicle + T3D group on both 6 and 8 days post-infection (compare Figs. 4A–D). By 11 days post-infection in minocycline + T3D mice, viral antigen intensity and expression pattern looked similar to that seen in vehicle + T3D mice at 8 days post-infection (compare Figs. 4D–F). CNS viral titers were determined at 8 days post-infection for both vehicle + T3D mice and minocycline + T3D mice and at 11 days post-infection for minocycline + T3D. We found that minocycline treatment significantly reduces T3D CNS titer at 8 days post-infection, but by 11 days post-infection CNS titers are similar to those seen in

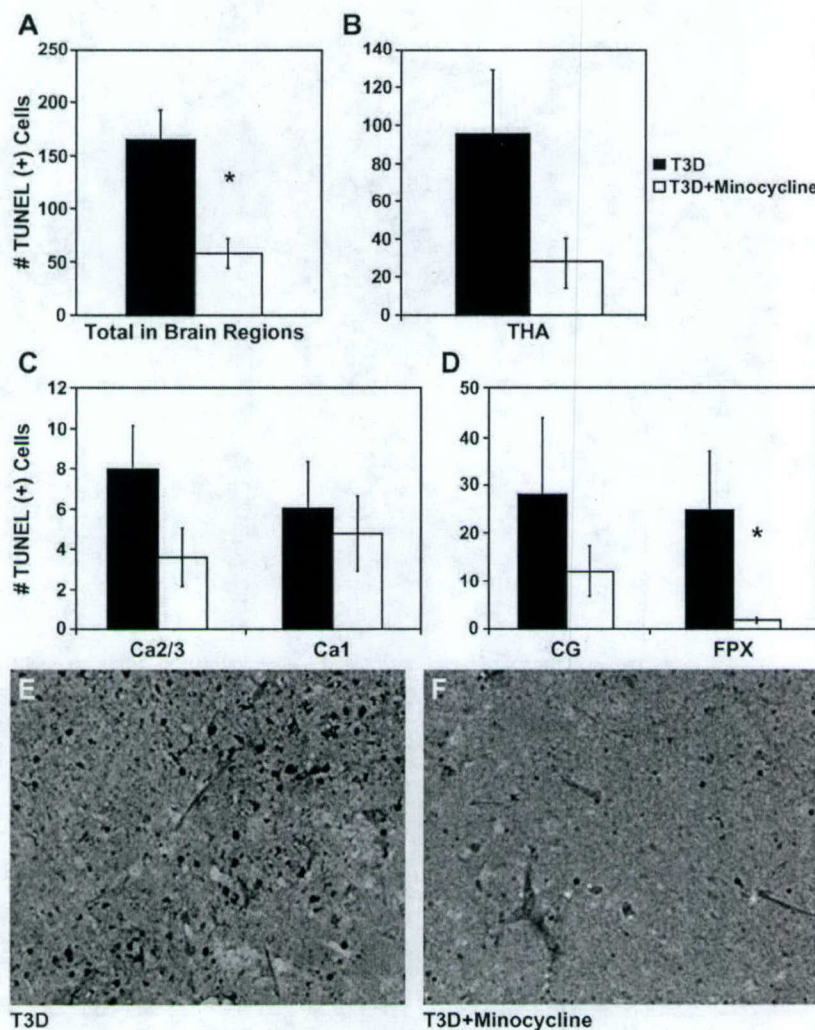


Fig. 2. Minocycline reduces virus-induced apoptosis in the CNS. (A) The total number of TdT-mediated dUTP Nick-End Label (TUNEL)-positive cells is significantly reduced in the brains of minocycline + T3D mice as compared to vehicle + T3D mice (\* $P < 0.01$ ; Student's *t* test. These data are the combined total from five brain regions assessed on 6 days post-infection). (B) Total number of TUNEL-positive cells in the (B) THA, (C) Ca2/3 and Ca1, (D) CG and FPX (\* $P < 0.01$  for B–D; Student's *t* test). (E) Numerous cells positive (brown staining) for activated caspase 3 can be seen in the dorsal thalamus of vehicle + T3D mice (100 $\times$  magnification). Similar results to that seen with TUNEL assay were found by staining for activated caspase 3. (F) Fewer activated caspase-3-positive cells are seen in tissue from minocycline + T3D mice (compare to part E).

vehicle + T3D mice at 8 days post-infection (Fig. 4E). Thus, minocycline treatment is associated with delayed viral growth paralleling the delay in injury and mortality.

## Discussion

The antibiotic minocycline has been shown to have neuroprotective properties in diverse models of neurodegeneration and CNS injury (Arvin et al., 2002; Chen et al., 2000; Du et al., 2001; Kriz et al., 2002; Thomas et al., 2003; Tikka and Koistinaho, 2001; Tikka et al., 2001b; Van Den et al., 2002; Wells et al., 2003; Yrjanheikki et al., 1998, 1999). However, until recently, this drug had not been tested in experimental models of CNS infection. Darman et al. (2004) reported that minocycline protects infected mice

from Neuroadapted Sindbis virus-induced spinal motor neuron death. Similarly, here we show that treatment of reovirus-infected neonatal mice with minocycline significantly delays the mortality of the resulting encephalitis with mean day of death extended from roughly 8 days post-infection to about 12 days post-infection. This is associated with a delay in onset and progression of reovirus-induced CNS injury and apoptosis.

Assessment of CNS injury by H&E analysis of brain tissue sections and whole brain viral titer assays from T3D-infected mice treated with either minocycline or vehicle revealed significant decreases in virus-induced CNS injury and CNS viral titer in minocycline-treated mice as compared to untreated mice. Brains from minocycline-treated mice at 11 days post-infection showed severity of viral injury and viral titer levels similar to that

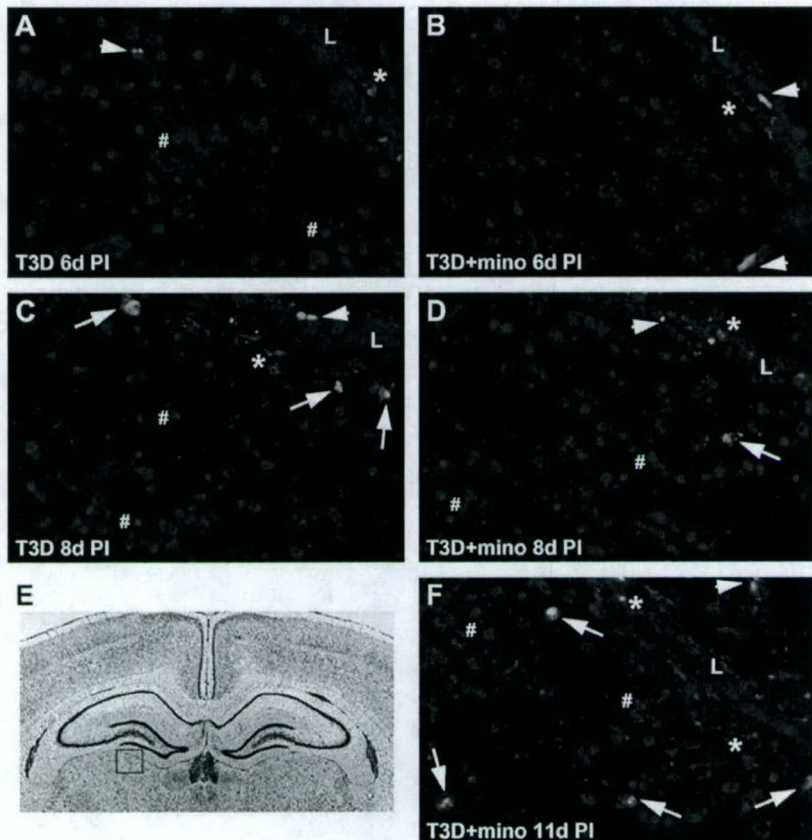


**Fig. 3.** There is no difference between untreated or minocycline-treated mice in microglial or astrocyte invasion of viral injury sites. The brain region represented in each panel is 400 $\times$  magnification of dorsal thalamus; location is indicated in panel E. L indicates the location of the lateral ventricle, white arrowheads indicate isolectin B4-labeled vascular endothelial cells, white arrows indicate isolectin B4-labeled microglia, \* indicate cells with GFAP-positive processes, and # indicate representative apoptotic cells. (A) The brains of untreated or (B) minocycline-treated T3D-infected mice at 6 days PI. (C) Untreated mice at 8 days PI show some isolectin B4-labeled microglia and GFAP-positive cells at the site of viral injury, near apoptotic cells. (D) Minocycline-treated mice at 8 days PI. (F) Minocycline-treated infected mice at 11 days PI.

seen in untreated mice on 8 days post-infection, indicating that minocycline is delaying the onset and progression of disease but not preventing it. Consistent with this result, the intensity and extent of viral antigen expression in the CNS of minocycline-treated T3D-infected mice was lower than that seen in untreated T3D-infected mice at 8 days post-infection, yet by 11 days post-infection viral antigen expression was similar to that seen in untreated T3D-infected mice at 8 days post-infection. Similar to its effects on disease progression, this suggests that minocycline may be hampering but not preventing viral growth. Further studies need to be performed to determine if this minocycline-associated inhibition of viral replication is due to direct interference in the replication cycle by minocycline or whether minocycline-mediated apoptosis inhibition results in reduced viral titers. The latter idea is supported by our previous research indicating that inhibition of reovirus-induced apoptosis results in reduced viral titers (Richardson-Burns and Tyler, 2004; Richardson-Burns et al., 2002b).

The mechanisms by which minocycline exerts its neuroprotective effects in CNS disease are thought to

be related to either its capacity to inhibit neuronal apoptosis (Chen et al., 2000; Sanchez Mejia et al., 2001; Wang et al., 2003b; Zhu et al., 2002) or its anti-inflammatory and microglial-inhibiting activity (He et al., 2001; Tikka and Koistinaho, 2001; Tikka et al., 2001a; Yrjanheikki et al., 1998). Studies on reovirus encephalitis indicate that CNS injury in infected mice results from neuronal apoptosis and that inflammation is minor; however, no studies have investigated whether microglial activity at viral injury foci contributes to the disease (Oberhaus et al., 1997; Richardson-Burns et al., 2002b). We found significantly fewer apoptotic cells in brain regions that are highly susceptible to reovirus-induced injury in minocycline-treated T3D-infected mice as compared to vehicle-treated T3D-infected mice as indicated by two markers for apoptosis, TUNEL staining, and immunohistochemical detection of activated caspase 3.

These data suggested that minocycline is anti-apoptotic in this model; however, we also analyzed whether minocycline's microglial/astrocyte-inhibiting activity may play a role in delaying T3D encephalitis. In many models of CNS injury, microglial activation and invasion of the damaged

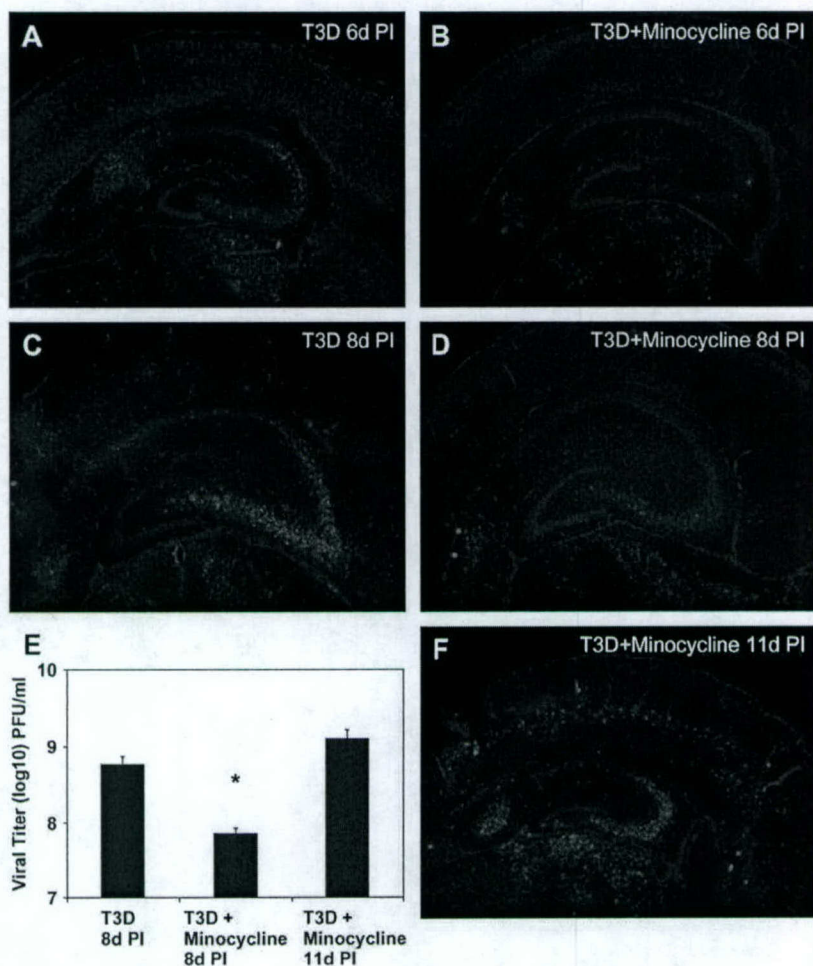


Fig. 4. Minocycline treatment of infected mice resulted in inhibition of viral growth as indicated by a decrease in viral titer and viral antigen expression. Immunohistochemical staining for reovirus antigen was used to detect viral proteins in brain tissue ( $25\times$  magnification) sections from T3D-infected vehicle-treated mice at 6 days PI (A) and 8 days PI (C) and T3D-infected minocycline-treated mice at 6 days PI (B), 8 days PI (D), and (F) 11 days PI. (E) Viral titer determined by plaque assay indicated that minocycline significantly reduced CNS viral titer at 8 days PI as compared to untreated T3D-infected mice (\* $P < 0.01$ ; Student's  $t$  test).

tissue is an early response to injury followed by sustained local astrogliosis or scar formation. In mounting of the immune response, activated microglia release numerous agents that are toxic to CNS cells, including inflammatory cytokines and glutamate. This can aggravate tissue injury and attract astrocytes resulting in gliosis (Chao et al., 1996; Lee et al., 1995, 2000; Srebro and Dziobek, 2001). More microglia were detected in the brains of T3D-infected mice on 8 days post-infection compared to 6 days post-infection; however, there was no significant difference between untreated and minocycline-treated animals. We found few microglia and astrocytes at viral injury sites at all times assayed following infection. This is supported by studies on CNS immune responses reporting that the severity of microglial and astrocyte activation is age dependent, occurring to a greater extent in adult compared to developing animals (Kyrkanides et al., 2001; Milligan et al., 1991). Our data show that microglial and astrocytic invasion of the regions of viral injury is not a major feature of T3D

encephalitis in neonatal mice and that minocycline treatment does not inhibit the minor microglial/glial activation seen in this model system.

This study indicates that minocycline delays but does not prevent development of fatal viral encephalitis and associated CNS injury. Similar results have been found in mouse models of neurodegenerative disease including amyotrophic lateral sclerosis (ALS) and Huntington's disease (Chen et al., 2000; Van Den et al., 2002; Zhu et al., 2002) and virus-associated neurodegeneration (Darman et al., 2004). Numerous studies suggest that the minocycline-mediated neuroprotective effects may be due to its capacity to inhibit apoptotic signaling (Chen et al., 2000; Sanchez Mejia et al., 2001; Wang et al., 2003b; Zhu et al., 2002). Given that apoptosis is a major mechanism of virus-induced injury in reovirus encephalitis, minocycline-mediated inhibition of virus-induced apoptosis may be resulting in the delayed onset, progression, and mortality of the disease. In conclusion, our findings suggest that minocycline treatment

is an effective strategy for protecting the CNS from viral injury and may represent a novel and possibly adjunctive antiviral therapy.

### Acknowledgments

The authors would like to thank Dr. Roberta DeBiasi for her expert advice regarding mouse infections, dissections, and drug administration. This work would have been impossible without the histology services of the University of Colorado Cancer Center. This work was supported by MERIT and REAP grants from the Department of Veterans Affairs, Public Health Service grant 1R01NS050138 from the National Institute of Neurological Disorders and Stroke (NINDS), and a U.S. Army Medical Research Acquisition Activity Grant No. DAMD 17-98-1-8614. Dr. Tyler is also supported by the Reuler-Lewin Family Professorship of Neurology. Some of these results were published in a doctoral thesis at University of Colorado Health Sciences Center (author: Sarah Richardson-Burns).

### References

- Arvin, K.L., Han, B.H., Du, Y., Lin, S.Z., Paul, S.M., Holtzman, D.M., 2002. Minocycline markedly protects the neonatal brain against hypoxic-ischemic injury. *Ann. Neurol.* 52, 54–61.
- Chao, C.C., Hu, S., Sheng, W.S., Bu, D., Burkinsky, M.I., Peterson, P.K., 1996. Cytokine-stimulated astrocytes damage human neurons via a nitric oxide mechanism. *Glia* 16, 276–284.
- Chen, M., Ona, V.O., Li, M., Ferrante, R.J., Fink, K.B., Zhu, S., Bian, J., Guo, L., Farrell, L.A., Hersch, S.M., Hobbs, W., Vonsattel, J.P., Cha, J.H., Friedlander, R.M., 2000. Minocycline inhibits caspase-1 and caspase-3 expression and delays mortality in a transgenic mouse model of Huntington disease. *Nat. Med.* 6, 797–801.
- Darman, J., Backovic, S., Dike, S., Maragakis, N.J., Krishnan, C., Rothstein, J.D., Irani, D.N., Kerr, D.A., 2004. Viral-induced spinal motor neuron death is non-cell-autonomous and involves glutamate excitotoxicity. *J. Neurosci.* 24, 7566–7575.
- Denovan-Wright, E.M., Devarajan, S., Dursun, S.M., Robertson, H.A., 2002. Maintained improvement with minocycline of a patient with advanced Huntington's disease. *J. Psychopharmacol.* 16, 393–394.
- Du, Y., Ma, Z., Lin, S., Dodel, R.C., Gao, F., Bales, K.R., Triarhou, L.C., Chernet, E., Perry, K.W., Nelson, D.L., Luecke, S., Phebus, L.A., Bymaster, F.P., Paul, S.M., 2001. Minocycline prevents nigrostriatal dopaminergic neurodegeneration in the MPTP model of Parkinson's disease. *Proc. Natl. Acad. Sci. U. S. A.* 98, 14669–14674.
- Erickson, R.P., Bernard, O., 2002. Studies on neuronal death in the mouse model of Niemann-Pick C disease. *J. Neurosci. Res.* 68, 738–744.
- Friedlander, R.M., 2003. Apoptosis and caspases in neurodegenerative diseases. *N. Engl. J. Med.* 348, 1365–1375.
- He, Y., Appel, S., Le, W., 2001. Minocycline inhibits microglial activation and protects nigral cells after 6-hydroxydopamine injection into mouse striatum. *Brain Res.* 909, 187–193.
- Hengartner, M.O., 2000. The biochemistry of apoptosis. *Nature* 407, 770–776.
- Kriz, J., Nguyen, M.D., Julien, J.P., 2002. Minocycline slows disease progression in a mouse model of amyotrophic lateral sclerosis. *Neurobiol. Dis.* 10, 268–278.
- Kyrkanides, S., O'Banion, M.K., Whiteley, P.E., Daeschner, J.C., Olschowka, J.A., 2001. Enhanced glial activation and expression of specific CNS inflammation-related molecules in aged versus young rats following cortical stab injury. *J. Neuroimmunol.* 119, 269–277.
- Lee, S.C., Dickson, D.W., Brosnan, C.F., 1995. Interleukin-1, nitric oxide and reactive astrocytes. *Brain Behav. Immun.* 9, 345–354.
- Lee, J.M., Grabb, M.C., Zipfel, G.J., Choi, D.W., 2000. Brain tissue responses to ischemia. *J. Clin. Invest.* 106, 723–731.
- Milligan, C.E., Levitt, P., Cunningham, T.J., 1991. Brain macrophages and microglia respond differently to lesions of the developing and adult visual system. *J. Comp. Neurol.* 314, 136–146.
- Oberhaus, S.M., Smith, R.L., Clayton, G.H., Dermody, T.S., Tyler, K.L., 1997. Reovirus infection and tissue injury in the mouse central nervous system are associated with apoptosis. *J. Virol.* 71, 2100–2106.
- Raine, C.S., Fields, B.N., 1973. Reovirus type 3 encephalitis—a virologic and ultrastructural study. *J. Neuropathol. Exp. Neurol.* 32, 19–33.
- Richardson-Burns, S.M., Tyler, K.L., 2004. Regional differences in viral growth and central nervous system injury correlate with apoptosis. *J. Virol.* 78, 5466–5475.
- Richardson-Burns, S.M., Kleinschmidt-DeMasters, B.K., DeBiasi, R.L., Tyler, K.L., 2002a. Progressive multifocal leukoencephalopathy and apoptosis of infected oligodendrocytes in the central nervous system of patients with and without AIDS. *Arch. Neurol.* 59, 1930–1936.
- Richardson-Burns, S.M., Kominsky, D.J., Tyler, K.L., 2002b. Reovirus-induced neuronal apoptosis is mediated by caspase 3 and is associated with the activation of death receptors. *J. Neurovirol.* 8, 365–380.
- Sanchez Mejia, R.O., Ona, V.O., Li, M., Friedlander, R.M., 2001. Minocycline reduces traumatic brain injury-mediated caspase-1 activation, tissue damage, and neurological dysfunction. *Neurosurgery* 48, 1393–1399.
- Scarabelli, T.M., Stephanou, A., Pasini, E., Gitti, G., Townsend, P., Lawrence, K., Chen-Scarabelli, C., Saravolatz, L., Latchman, D., Knight, R., Gardin, J., 2004. Minocycline inhibits caspase activation and reactivation, increases the ratio of XIAP to smac/DIABLO, and reduces the mitochondrial leakage of cytochrome c and smac/DIABLO. *J. Am. Coll. Cardiol.* 43, 865–874.
- Shaw, P.J., 2002. Toxicity of CSF in motor neurone disease: a potential route to neuroprotection. *Brain* 125, 693–694.
- Srebro, Z., Dziobek, K., 2001. Neuroprotection: the role of neuroglia. *Folia Med. Crac.* 42, 113–121.
- Thomas, M., Le, W.D., Jankovic, J., 2003. Minocycline and other tetracycline derivatives: a neuroprotective strategy in Parkinson's disease and Huntington's disease. *Clin. Neuropharmacol.* 26, 18–23.
- Tikka, T.M., Koistinaho, J.E., 2001. Minocycline provides neuroprotection against N-methyl-D-aspartate neurotoxicity by inhibiting microglia. *J. Immunol.* 166, 7527–7533.
- Tikka, T., Fiebich, B.L., Goldsteins, G., Keinanen, R., Koistinaho, J., 2001a. Minocycline, a tetracycline derivative, is neuroprotective against excitotoxicity by inhibiting activation and proliferation of microglia. *J. Neurosci.* 21, 2580–2588.
- Tikka, T., Usenius, T., Tenhunen, M., Keinanen, R., Koistinaho, J., 2001b. Tetracycline derivatives and ceftazidime, a cephalosporin antibiotic, protect neurons against apoptosis induced by ionizing radiation. *J. Neurochem.* 78, 1409–1414.
- Tyler, K., 2001. In: Knipe, D., Howley, P. (Eds.), *Fields Virology: Mammalian Reoviruses*. Lippincott-Williams and Wilkins, Philadelphia, PA, USA, pp. 1729–1746.
- Tyler, K.L., Bronson, R.T., Byers, K.B., Fields, B., 1985. Molecular basis of viral neurotropism: experimental reovirus infection. *Neurology* 35, 88–92.
- Van Den, B.L., Tilkin, P., Lemmens, G., Robberecht, W., 2002. Minocycline delays disease onset and mortality in a transgenic model of ALS. *NeuroReport* 13, 1067–1070.
- Wang, C.X., Yang, T., Shuaib, A., 2003a. Effects of minocycline alone and in combination with mild hypothermia in embolic stroke. *Brain Res.* 963, 327–329.
- Wang, X., Zhu, S., Drozda, M., Zhang, W., Stavrovskaya, I.G., Cattaneo, E., Ferrante, R.J., Kristal, B.S., Friedlander, R.M., 2003b. Minocycline

- cline inhibits caspase-independent and -dependent mitochondrial cell death pathways in models of Huntington's disease. Proc. Natl. Acad. Sci. U. S. A. 100, 10483–10487.
- Wang, J., Wei, Q., Wang, C.Y., Hill, W.D., Hess, D.C., Dong, Z., 2004. Minocycline up-regulates Bcl-2 and protects against cell death in mitochondria. J. Biol. Chem. 279, 19948–19954.
- Wells, J.E., Hurlbert, R.J., Fehlings, M.G., Yong, V.W., 2003. Neuroprotection by minocycline facilitates significant recovery from spinal cord injury in mice. Brain 126, 1628–1637.
- Yrjanheikki, J., Keinanen, R., Pellikka, M., Hokfelt, T., Koistinaho, J., 1998. Tetracyclines inhibit microglial activation and are neuroprotective in global brain ischemia. Proc. Natl. Acad. Sci. U. S. A. 95, 15769–15774.
- Yrjanheikki, J., Tikka, T., Keinanen, R., Goldsteins, G., Chan, P.H., Koistinaho, J., 1999. A tetracycline derivative, minocycline, reduces inflammation and protects against focal cerebral ischemia with a wide therapeutic window. Proc. Natl. Acad. Sci. U. S. A. 96, 13496–13500.
- Zhu, S., Stavrovskaya, I.G., Drozda, M., Kim, B.Y., Ona, V., Li, M., Sarang, S., Liu, A.S., Hartley, D.M., Wu, d.C., Gullans, S., Ferrante, R.J., Przedborski, S., Kristal, B.S., Friedlander, R.M., 2002. Minocycline inhibits cytochrome *c* release and delays progression of amyotrophic lateral sclerosis in mice. Nature 417, 74–78.

## Nonstructural Protein $\sigma$ 1s Is a Determinant of Reovirus Virulence and Influences the Kinetics and Severity of Apoptosis Induction in the Heart and Central Nervous System

Cristen C. Hoyt,<sup>1</sup> Sarah M. Richardson-Burns,<sup>2</sup> Robin J. Goody,<sup>3</sup> Bridget A. Robinson,<sup>3</sup> Roberta L. DeBiasi,<sup>3,4</sup> and Kenneth L. Tyler<sup>1,2,3,5,6,7\*</sup>

Departments of Immunology,<sup>1</sup> Neurology,<sup>3</sup> Pediatrics,<sup>4</sup> Microbiology,<sup>5</sup> and Medicine<sup>6</sup> and Program in Neurosciences,<sup>2</sup> University of Colorado Health Sciences Center, and Denver Veterans Affairs Medical Center,<sup>7</sup> Denver, Colorado

Received 25 May 2004/Accepted 11 October 2004

The mechanisms by which viruses kill susceptible cells in target organs and ultimately produce disease in the infected host remain poorly understood. Dependent upon the site of inoculation and strain of virus, experimental infection of neonatal mice with reoviruses can induce fatal encephalitis or myocarditis. Reovirus-induced apoptosis is a major mechanism of tissue injury, leading to disease development in both the brain and heart. In cultured cells, differences in the capacity of reovirus strains to induce apoptosis are determined by the S1 gene segment, which also plays a major role as a determinant of viral pathogenesis in both the heart and the central nervous system (CNS) *in vivo*. The S1 gene is bicistronic, encoding both the viral attachment protein sigma-1 and the nonstructural protein sigma-1-small ( $\sigma$ 1s). Although  $\sigma$ 1s is dispensable for viral replication *in vitro*, we wished to investigate the expression of  $\sigma$ 1s in the infected heart and brain and its potential role in reovirus pathogenesis *in vivo*. Two-day-old mice were inoculated intramuscularly or intracerebrally with either  $\sigma$ 1s<sup>-</sup> or  $\sigma$ 1s<sup>+</sup> reovirus strains. While viral replication in target organs did not differ between  $\sigma$ 1s<sup>-</sup> and  $\sigma$ 1s<sup>+</sup> viral strains, virus-induced caspase-3 activation and resultant histological tissue injury in both the heart and brain were significantly reduced in  $\sigma$ 1s<sup>-</sup> reovirus-infected animals. These results demonstrate that  $\sigma$ 1s is a determinant of the magnitude and extent of reovirus-induced apoptosis in both the heart and CNS and thereby contributes to reovirus pathogenesis and virulence.

Experimental infection of neonatal mice with reovirus has provided important new insights into the mechanisms of viral entry, spread, tissue tropism, and disease pathogenesis in the infected host. Reoviruses infect and produce tissue injury in multiple organ systems, including the heart and central nervous system (CNS) (28, 31). Reovirus-induced apoptosis is a major mechanism of cell death, tissue injury, and ensuing disease in infected neonatal mice (8, 9, 19, 24, 25). In both the infected heart and brain, reovirus antigen, areas of histological injury, and apoptosis all colocalize (8, 19, 25). In the brain, type 3 (T3) reoviruses cause fatal encephalitis associated with neuronal injury and virus-induced apoptosis in neurons of the cortex, thalamus, and hippocampus (19, 24, 25). The viral S1 gene is a key determinant of the pattern of viral injury in the CNS (37, 38), although other viral genes play contributory roles as well (14). In the heart, reovirus-induced apoptosis appears to be the major mechanism for virus-induced myocardial injury and consequential death (8, 9). Reovirus genetics has identified multiple viral genes, including M1, L1, L2, and S1, as determinants of reovirus-induced acute myocarditis (28). S1 has been implicated as a major determinant of cytopathic effects in cardiomyocytes (3). The S1 gene is also a major determinant of differences in the capacity of reovirus strains to induce apoptosis in a variety of cultured cells (33, 34).

The S1 double-stranded RNA gene segment is bicistronic, encoding both the viral attachment protein sigma-1 ( $\sigma$ 1) and the nonstructural protein sigma-1-small ( $\sigma$ 1s) from overlapping but out-of-sequence open reading frames (11, 15, 27).  $\sigma$ 1 is a structural protein located at the icosahedral vertices of the viral outer capsid and functions as the viral cell attachment protein (17).  $\sigma$ 1 may influence virulence through its role in host cell receptor binding to mediate viral entry or through receptor-triggered intracellular signaling pathways (6, 20, 32). The second S1-encoded protein,  $\sigma$ 1s, is a nonstructural protein and is a key determinant of the capacity of reoviruses to induce a G<sub>2</sub>/M cell cycle arrest in infected cells (22, 23). We have recently shown that  $\sigma$ 1s contains a functional nuclear localization signal and undergoes active signal-mediated nuclear import in both transfected and infected cells, resulting in profound disruption of nuclear architecture (13). Although a  $\sigma$ 1s-null mutant replicates as well as wild-type T3 reovirus in cultured L929 and MDCK cells (26), the fact that  $\sigma$ 1s is conserved in all known reovirus field isolates (5, 10) suggests that it plays an important role during viral pathogenesis *in vivo*. In order to evaluate the potential role of  $\sigma$ 1s during pathogenesis, we compared heart and CNS disease following infection of neonatal mice with a  $\sigma$ 1s-null reovirus mutant (C84-MA) to that following infection with  $\sigma$ 1s-positive control strains.

We show that a  $\sigma$ 1s deficiency does not affect viral growth in target tissues but profoundly reduces the capacity of reovirus to induce apoptosis and tissue injury in both the heart and the CNS. These studies indicate that although  $\sigma$ 1s may not be

\* Corresponding author. Mailing address: Department of Neurology (B-182), University of Colorado Health Sciences Center, 4200 E. 9th Ave., Denver, CO 80262. Phone: (303) 393-2874. Fax: (303) 393-4686. E-mail: Ken.Tyler@uchsc.edu.

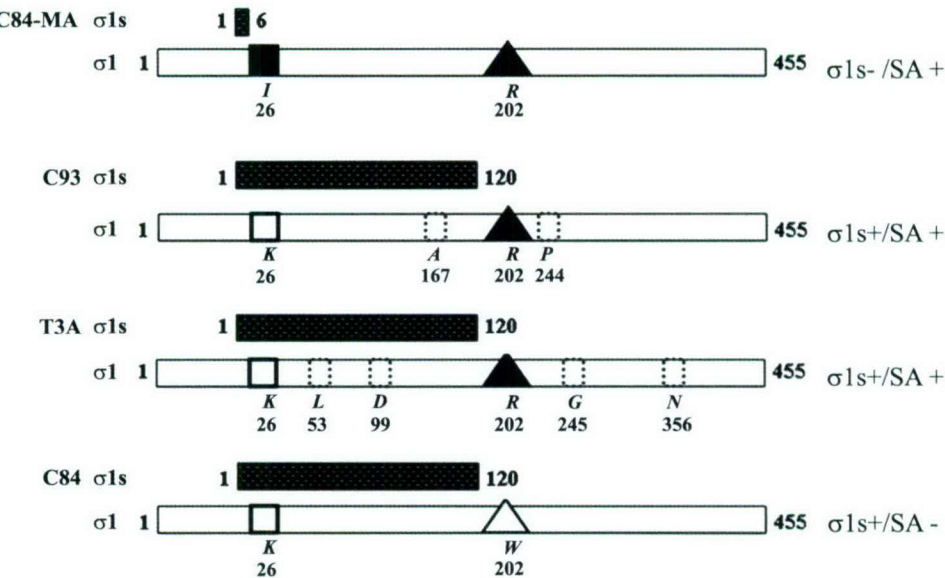


FIG. 1.  $\sigma 1s^-$  and  $\sigma 1s^+$  T3 reoviruses used in this study. Shown are representations of the 120-amino-acid  $\sigma 1s$  protein sequence (stippled bars) and the 455-amino-acid  $\sigma 1$  protein sequence (white bars) for each viral strain used. C84-MA does not express  $\sigma 1s$  due to an S1 gene mutation (black square). C84-MA, C93, and T3A bind SA (black triangles). C84 does not bind SA due to a mutation in  $\sigma 1$  (open triangle). C93 and T3A contain differences in the  $\sigma 1$  protein sequence compared to C84-MA (dotted boxes). Noted to the right is the  $\sigma 1s$  expression status and SA binding ability of each strain.

required for viral replication in cultured cells, it plays a major role in viral virulence and disease outcome *in vivo*.

#### MATERIALS AND METHODS

**Mice.** Swiss-Webster mouse litters were housed in individual filter-topped cages in an American Association for Laboratory Animal Care-accredited animal facility. All animal procedures were performed under protocols approved by the appropriate institutional animal care and use committees.

**Mouse inoculations.** Two-day-old Swiss-Webster mice (Harlan Sprague-Dawley, Indianapolis, Ind.) were inoculated either intramuscularly (hind limb) or intracranially (right cerebral hemisphere) with  $10^5$  or  $10^3$  PFU (as specified) of the indicated reovirus strain in a 20- $\mu$ l (intramuscular inoculation) or 10- $\mu$ l (intracranial inoculation) volume of gel saline (137 mM NaCl, 0.2 mM CaCl<sub>2</sub>, 0.8 mM MgCl<sub>2</sub>, 19 mM H<sub>3</sub>BO<sub>3</sub>, 0.1 mM Na<sub>2</sub>B<sub>4</sub>O<sub>7</sub>, 0.3% gelatin).

**Viruses.** The  $\sigma 1s$  and  $\sigma 1$  protein sequences of the viruses used are diagrammed in Fig. 1. All viruses utilized were from laboratory stocks. T3C84 and T3C84-MA were originally provided by T. Dermody (Vanderbilt University, Nashville, Tenn.). T3 C84-MA is a  $\sigma 1s$ -null mutant that was originally isolated following serial passage of the T3C84 (C84) strain through murine erythroleukemia cells (26). C84-MA contains a tryptophan (W)-to-arginine (R) mutation at position 202 which enables it to bind terminal sialic acid (SA) on glycosylated cellular proteins (SA<sup>+</sup>), whereas C84 cannot (SA<sup>-</sup>) (Fig. 1). C84-MA also contains an S1 gene mutation which results in a lysine (K)-to-isoleucine (I) substitution at amino acid 26 in  $\sigma 1$  (Fig. 1). This mutation also introduces a premature stop codon in  $\sigma 1s$ . Since SA binding plays a significant role in reovirus pathogenesis (1, 2, 7), we used reovirus T3 clone 93 (C93) and the prototype T3 reovirus strain Abney (T3A), both of which bind SA, as additional controls for C84-MA. C93 expresses  $\sigma 1s$ , binds SA coreceptors, and is the most closely related SA<sup>+</sup> field isolate to C84-MA in terms of its  $\sigma 1$  amino acid sequence. T3A expresses  $\sigma 1s$  and binds to SA residues on target cells (Fig. 1).

**Viral titer.** Mice were sacrificed at the indicated times postinfection, and whole hearts or brains were placed in gel saline and immediately frozen at -70°C. After three freeze (-70°C)-thaw (37°C) cycles, tissues were sonicated for 30 s with a microtip probe (Heat Systems model XL2020) until a homogenate solution was formed. Viral suspensions were serially diluted in gel saline in 10-fold steps. Monolayers of L929 cells were infected with diluted virus in duplicate for plaque assay as previously described (36).

**Histological analysis.** Mice were sacrificed at the indicated times postinfection, and individual organs were immediately immersed in 10% buffered formalin solution for 24 h and then transferred to 70% ethanol for histological preparation. For the brain, paraffin-embedded tissues were cut to 4- $\mu$ m coronal sections, showing cingulate cortex, frontoparietal cortex, hippocampus, and thalamus. Sections were stained with hematoxylin and eosin (H&E) for analysis of tissue pathology and quantitative scoring. Scoring of the extent of neuropathologic damage was based on a previously validated blinded grading system in which the extent of morphological changes and the area affected within specific brain regions were graded on a scale of 0 to 4 (30) (Table 1). For the heart, paraffin-embedded tissues were transversely cut to 4- $\mu$ m sections. Quantitative scoring of histological injury in the heart was based on a previously validated blinded grading system in which the number and size of specific heart lesions were evaluated on a scale of 0 to 4 (8, 29) (Table 1). Histological injury in both the heart and brain was evaluated and scored from either a single coronal H&E-stained section per mouse or a single H&E-stained transverse heart section per mouse from multiple animals. For caspase-3 immunohistochemistry, 4- $\mu$ m paraffin-embedded tissue sections were retrieved in a deblocker (BioCare, Vista, Calif.) in citrate buffer, followed by staining with rabbit anti-mouse polyclonal antibody directed against activated caspase-3 (Cell Signaling Technologies, Beverly, Mass.) at a 1:25 dilution, followed by detection by using an automated staining system with the Ventana (Tucson, Ariz.) detection system. Quantitative scoring of caspase-3-stained tissue sections was based on a blinded grading system in which the number of caspase-3-positive cells and the size of caspase-3-positive areas were graded on a scale of 0 to 3 (Table 1). For  $\sigma 1s$  immunohistochemistry in the brain, 4- $\mu$ m paraffin-embedded coronal tissue sections were deparaffinized and retrieved in antigen-unmasking solution (Vector Laboratories, Burlingame, Calif.) according to the high-temperature unmasking technique provided by the manufacturer. After an overnight permeabilization with Neopore at 4°C (Trevigen, Gaithersburg, Md.), goat anti-mouse monoclonal antibody directed against  $\sigma 1s$  (3E2) was used at 200  $\mu$ g/ml diluted into 3% bovine serum albumin (BSA)-Tris-buffered saline (TBS) plus 0.1% Tween (TBST) overnight at 4°C. As a secondary antibody, biotinylated goat anti-mouse antibody (Vector Laboratories) was used at 1:100 in 3% BSA-TBST for 2 h at 25°C. Detection was monitored by a diaminobenzidine tetrahydrochloride-based immunohistochemistry protocol according to the suggestions of the manufacturer (Vector Laboratories). Dehydration was carried out in a series of graded ethanol solutions, followed by clarification in xylene. Slides were mounted with

TABLE 1. Tissue section grading systems for apoptosis and histopathological damage in  $\sigma 1s^-$  and  $\sigma 1s^+$  reovirus-infected animals

Condition scored	Criteria for score of:				
	0	1	2	3	4
Apoptosis (CNS and heart)	No caspase-3-positive cells in tissue area	Scattered caspase-3-positive cells in tissue area	Groups of caspase-3-positive cells occupying up to 30% of affected tissue area	Groups of caspase-3-positive cells found in >30% of affected tissue area	
CNS histopathology <sup>a</sup>	No lesions	Affected area $\leq 10\%$ of total section with morphological changes of individual dead neurons and small patchy areas of tissue destruction	Affected area approximately 10–40% of total section with partly confluent areas of tissue destruction	Affected area approximately 40–75% of total section with large confluent areas of tissue destruction	Affected area >75% of total section with total disintegration of cortical tissue, large complete areas of tissue destruction in the thalamus, and neuronal death in the hippocampus
Cardiac histopathology <sup>b</sup>	No lesions	One or a few small lesions	Many small or a few large lesions	Multiple small and large lesions	Massive lesions

<sup>a</sup> As described in reference 30.<sup>b</sup> As described in references 8 and 29.

Vectamount (Vector Laboratories) and stored at 25°C. A similar procedure was used to evaluate  $\sigma 1s$  expression in cardiac tissue sections, with the following exceptions: monoclonal antibody 2F4 was used as the primary antibody at a concentration of 100  $\mu$ g/ml, diluted into 3% BSA-TBST, overnight at 4°C. The hybridoma cell lines synthesizing the anti- $\sigma 1s$  antibodies, 2F4 and 3E2, were generous gifts (26). Anti- $\sigma 1s$  antibodies were purified on protein A columns based on the recommended protocol described by the manufacturer (Pierce, Rockford, Ill.). For reovirus antigen detection (reovirus structural proteins), deparaffinized tissue sections were retrieved in antigen-unmasking solution (Vector Laboratories) according to the high-temperature unmasking technique provided by the manufacturer and permeabilized in Neupore (Trevigen) at 4°C overnight. Rabbit polyclonal reovirus antiserum was used at 1:200 in 5% normal goat serum-TBST at 25°C for 1 h. Extensive washing in TBST was followed by incubation in fluorescein isothiocyanate-conjugated goat anti-rabbit immunoglobulin G (Vector Laboratories) diluted at 1:100 in 3% BSA-TBST. After extensive washing in TBST and TBS, nuclei were visualized with Hoechst 33342 (Molecular Probes, Eugene, Oreg.). Stained sections were mounted with Vectashield (Vector Laboratories) and stored at 4°C.

**Statistics.** All statistical analyses were performed with In Stat version 3.0 (Graph Pad, San Diego, Calif.).

## RESULTS

**$\sigma 1s$  enhances reovirus virulence following intramuscular inoculation.** In order to evaluate the role of  $\sigma 1s$  in the induction of reovirus-induced myocarditis, 2-day-old neonatal mice were inoculated intramuscularly with 10<sup>5</sup> PFU of reovirus strain C84-MA ( $\sigma 1s^-$  SA<sup>+</sup>), C93 ( $\sigma 1s^+$  SA<sup>+</sup>), T3A ( $\sigma 1s^+$  SA<sup>+</sup>), or C84 ( $\sigma 1s^+$  SA<sup>-</sup>). Infected animals were examined daily to assess health and progression of disease (Fig. 2). All C84-MA ( $\sigma 1s^-$  SA<sup>+</sup>)-infected mice survived virus challenge, whereas all mice infected with the control T3A ( $\sigma 1s^+$  SA<sup>+</sup>) or C93 ( $\sigma 1s^+$  SA<sup>+</sup>) strain appeared to be sick at approximately 6 days postinfection and died within 14 days of infection (mean day of death  $\pm$  standard error of the mean, 9.9  $\pm$  1.2 days or 10.4  $\pm$  0.5, respectively) (Fig. 2). The  $\sigma 1s^+$  SA<sup>-</sup> strain C84 showed an intermediate phenotype, with 30% mortality (Fig. 2). The observed differences in patterns of lethality between  $\sigma 1s^-$  and  $\sigma 1s^+$  strains indicated that  $\sigma 1s$  was an important

determinant of virulence following peripheral intramuscular inoculation. The intermediate phenotype of the SA<sup>-</sup> strain C84 indicated that in addition to the presence or absence of  $\sigma 1s$ , SA binding is likely to be an important determinant of reovirus virulence following intramuscular inoculation.

**$\sigma 1s$  is not required for viral replication in the heart.** Following intramuscular inoculation of either  $\sigma 1s^-$  or  $\sigma 1s^+$  reovirus strains, the viral titer in the hearts of infected animals was determined at 8 days postinfection. There were no significant differences in titer observed between virus strains in the heart ( $P > 0.05$  for all interstrain comparisons) (Fig. 3).  $\sigma 1s$  was therefore not required for either efficient spread to or growth within the heart. Similarly, no significant differences in titer were observed between SA<sup>+</sup> and SA<sup>-</sup> viruses (Fig. 3), suggesting that SA binding was also not a significant determinant of

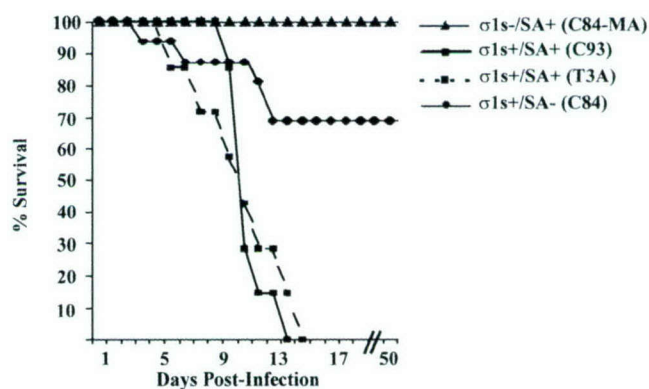


FIG. 2.  $\sigma 1s$  confers enhanced virulence following intramuscular reovirus inoculation. Neonatal mice ( $n = 7$  to 16) were inoculated intramuscularly with C84-MA ( $\sigma 1s^-$  SA<sup>+</sup>), C93 ( $\sigma 1s^+$  SA<sup>+</sup>), T3A ( $\sigma 1s^+$  SA<sup>+</sup>), or C84 ( $\sigma 1s^+$  SA<sup>-</sup>).

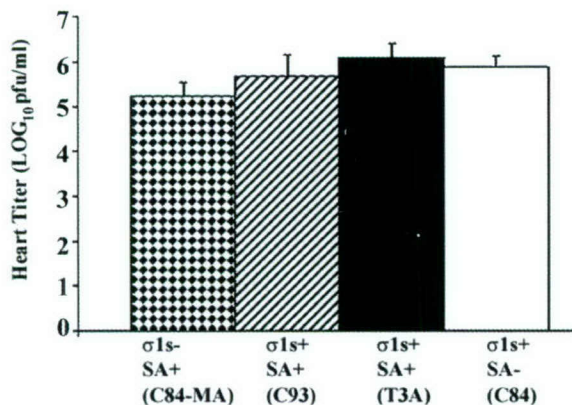


FIG. 3.  $\sigma 1s$  does not influence viral growth in the heart. Viral titers in infected hearts were not significantly different ( $P > 0.05$ ) between  $\sigma 1s^-$  and all  $\sigma 1s^+$  viral strains. Each bar represents the average viral titer from 5 to 10 mice at 8 days post-intramuscular inoculation. Error bars indicate standard errors of the means.

spread to or growth within the heart in infected animals following intramuscular peripheral inoculation.

**$\sigma 1s$  is a determinant of apoptosis and pathogenesis in the heart.** Having shown that  $\sigma 1s$  is a determinant of lethality following intramuscular reovirus inoculation, we next determined the effect of  $\sigma 1s$  on viral pathogenesis in hearts of reovirus-infected animals. To evaluate overall myocardial tissue injury, H&E-stained transverse cardiac sections were evaluated via light microscopy, and the degree of injury was quantified by using a previously validated scoring system (8, 29) (Table 1 and Fig. 4). At 8 days postinfection, prominent myocardial disruption, numerous apoptotic bodies, and evidence of pyknotic nuclei were observed in hearts of  $\sigma 1s^+$  virus-infected mice regardless of SA binding ability, while very minor myocardial injury was noted in  $\sigma 1s^-$  reovirus-infected animals (Fig. 4).

Immunohistochemical detection of the activated form of caspase-3 was used as a marker of apoptosis in reovirus-in-

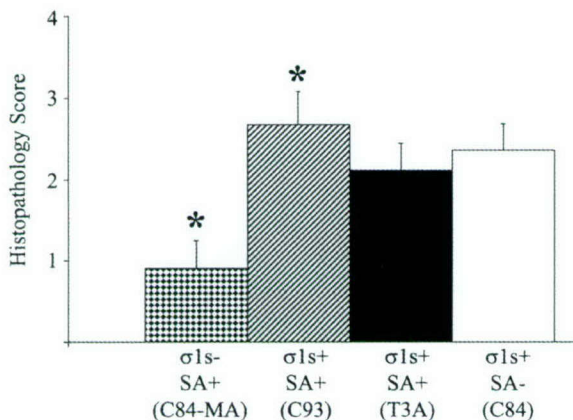


FIG. 4.  $\sigma 1s$  is required for maximal myocardial tissue injury. The degree of injury in the myocardium, as measured by quantifying H&E-stained heart sections, was significantly reduced in  $\sigma 1s^-$  (C84-MA) virus-infected mice. Each bar represents the average score from 10 to 13 mice. Error bars indicate standard errors of the means. \*,  $P < 0.05$ .

fected hearts. Dark brown staining indicates active caspase-3 apoptotic lesions within the myocardium (Fig. 5B and C). Mice infected with the  $\sigma 1s^-$  strain C84-MA showed a significant decrease in both the number and size of apoptotic lesions in the heart compared to each of the  $\sigma 1s^+$  control viruses at 8 days postinfection (Fig. 5A). In contrast, all  $\sigma 1s^+$  reoviruses produced severe myocardial injury with extensive areas of apoptosis analogous to those we have previously described for the prototypic myocarditis-inducing strain, 8B (8). The rare apoptotic lesions that were observed in  $\sigma 1s^-$  virus-infected hearts appeared similar in cellular composition and caspase-3 staining to heart lesions seen in  $\sigma 1s^+$  virus-infected hearts (data not shown).

Animals which survived C84-MA ( $\sigma 1s^-$  SA $^+$ ) virus challenge were sacrificed at 50 days postinfection and evaluated for myocardial injury. H&E-stained heart sections did not show any myocarditic damage, and no infectious virus was detectable by plaque assay in the heart or other organs (data not shown).

Taken together, these studies indicate that  $\sigma 1s$  was a determinant of the extent and severity of myocardial injury and apoptosis but not of viral growth in the hearts of infected mice. We next wished to determine whether these same features occurred in CNS infection.

**$\sigma 1s$  is a determinant of T3 reovirus virulence following intracranial inoculation.** In order to study the role of  $\sigma 1s$  in pathogenesis of reovirus-induced CNS disease, 2-day-old mice were intracerebrally inoculated with  $10^3$  PFU of reovirus strain C84-MA ( $\sigma 1s^-$  SA $^+$ ), C93 ( $\sigma 1s^+$  SA $^+$ ), T3A ( $\sigma 1s^+$  SA $^+$ ), or C84 ( $\sigma 1s^+$  SA $^-$ ). Mortality was monitored for 30 days following inoculation (Fig. 6). One hundred percent of mice infected with either C93 or T3A died (mean day of death  $\pm$  standard error of the mean,  $9.1 \pm 0.8$  and  $8.9 \pm 0.3$ , respectively), compared to only 67% of C84-MA-infected mice (mean day of death  $\pm$  standard error of the mean,  $14.3 \pm 1.2$ ) ( $P < 0.001$ ). The SA $^-$  strain C84 also showed enhanced survival compared to T3A and C93 (Fig. 6).

In an effort to see whether the attenuated phenotype of C84-MA ( $\sigma 1s^-$  SA $^+$ ) would persist after massive viral challenge, mice were injected intracranially with  $10^5$  PFU (approximately 10,000 times the intracranial 50% lethal dose) of the test viruses per mouse. All mice died at this high challenge dose, although the mean day of death for  $\sigma 1s^-$  virus (C84-MA)-infected mice was significantly ( $P < 0.001$ ) prolonged ( $11.2 \pm 0.3$  days) compared to that for either  $\sigma 1s^+$  T3A ( $8.3 \pm 0.3$  days)- or  $\sigma 1s^+$  C93 ( $9 \pm 0$  days)-infected animals.

These results indicate that  $\sigma 1s$  is a determinant of neurovirulence following intracerebral inoculation of reovirus. The enhanced survival in mice infected with the SA $^-$  strain C84 compared to the SA $^+$  strains T3A and C93 also indicate that SA binding plays a role in neurovirulence.

**$\sigma 1s$  is not required for viral replication in the brain.** Having shown that  $\sigma 1s$  influenced neurovirulence after intracranial inoculation, we next wished to determine whether this was due to an effect on viral growth in the CNS. Neonatal mice were intracerebrally infected with  $10^5$  PFU of the various reovirus strains. At 8 days postinfection brain tissue was removed from euthanized animals, and the viral titer was determined by plaque assay of brain homogenates (Fig. 7). As seen in the heart model, the presence or absence of  $\sigma 1s$  did not significantly affect viral growth in the brain ( $P > 0.05$  for all inter-

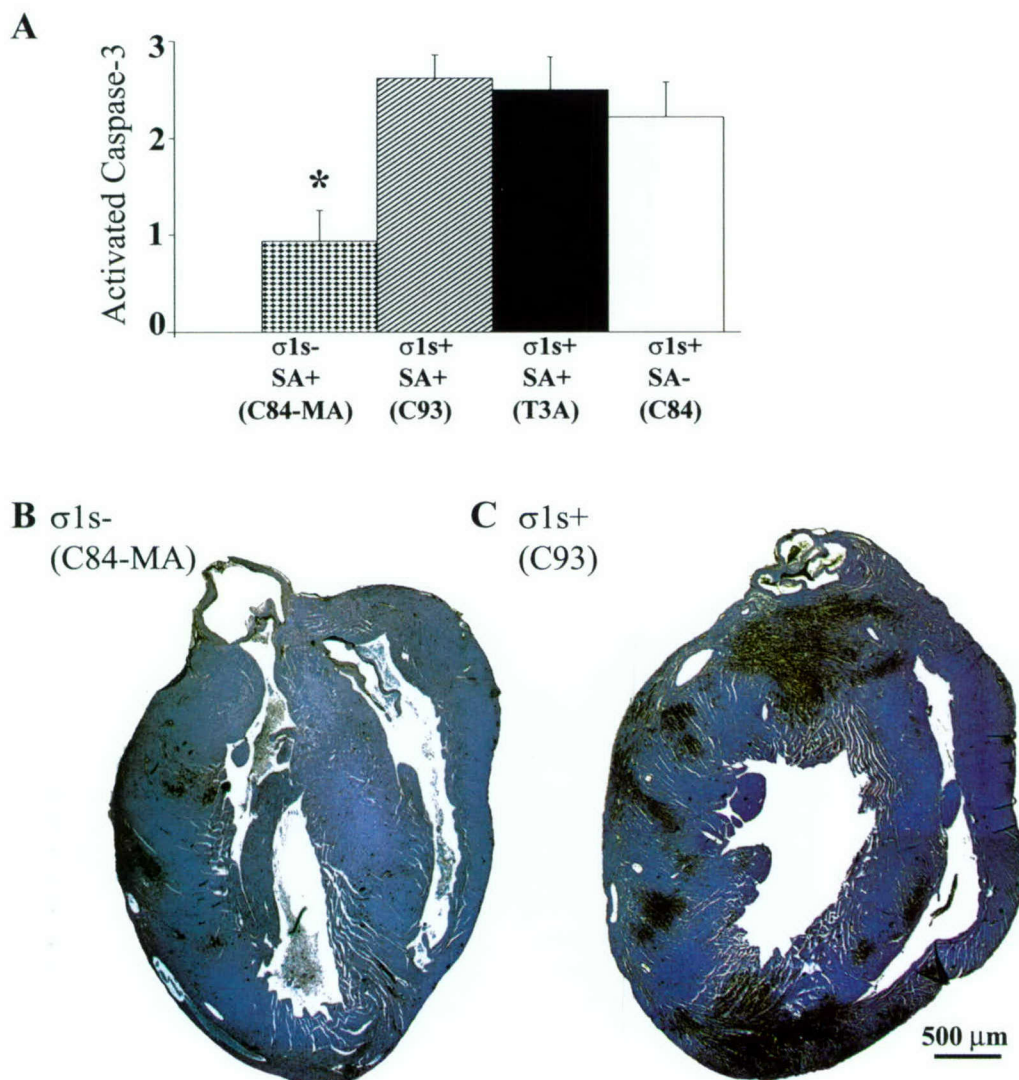


FIG. 5.  $\sigma 1s$  is required for maximal apoptosis induction in the heart. Immunohistochemical staining of activated caspase-3 in whole hearts (B and C) (original magnification,  $\times 25$ ) demonstrates that loss of  $\sigma 1s$  expression significantly reduces reovirus-induced apoptosis (A). In panel A, each bar represents the average score from four to eight mice. Error bars indicate standard errors of the means. \*,  $P < 0.05$ .

strain comparisons except that between the  $SA^-$  virus C84 and the  $SA^+$  virus T3A, for which  $P < 0.01$ ). These results indicate that  $\sigma 1s$  does not influence viral growth in the brain.

**$\sigma 1s$  is a determinant of apoptosis and pathogenesis in the brain.** We next wished to determine whether  $\sigma 1s$  influenced the extent of viral injury in the CNS. At 8 days following infection, mice were sacrificed and neuropathologic injury was evaluated. The  $\sigma 1s^-$  strain C84-MA (Fig. 8A to C and J) induced significantly less tissue injury in the cortex, thalamus, and hippocampus than its  $\sigma 1s^+$   $SA^+$  counterparts (Fig. 8D to I and J). By contrast, large areas in the thalamus and cortex of  $\sigma 1s^+$   $SA^+$  (C93 and T3A) virus-infected animals were destroyed and contained numerous apoptotic bodies (Fig. 8D and E). Extensive neuronal death was also evident in the hippocampi of these animals (Fig. 8F).  $\sigma 1s^-$  (C84-MA) virus-infected mice, examined when moribund (day 11), did show substantial CNS injury (data not shown), indicating that loss of

$\sigma 1s$  delayed but did not prevent the appearance of CNS injury following high-dose virus challenge. The  $SA^-$  virus (C84) also showed markedly reduced tissue injury (Fig. 8G to J) compared to  $SA^+$   $\sigma 1s^+$  virus C93 (Fig. 8D to F) or T3A (data not shown). When moribund, C84-infected mice displayed delayed CNS injury (data not shown).

Immunohistochemical detection of the activated form of caspase-3 was used as a marker for reovirus-induced apoptosis in the brain. Mice infected with  $\sigma 1s^-$  virus (C84-MA) had no detectable apoptosis in the cortex, thalamus, or hippocampus at 8 days postinfection (Fig. 9B). Conversely,  $\sigma 1s^+$  control strains C93 (Fig. 9D) and T3A (data not shown) displayed high levels of caspase-3 activation in all three areas. The  $SA^-$  virus C84 also displayed substantially reduced apoptosis in the cortex, thalamus, and hippocampus (Fig. 9C). As was the case for histological injury, C84-MA-infected mice examined when moribund (day 11) showed substantial caspase-3 activation

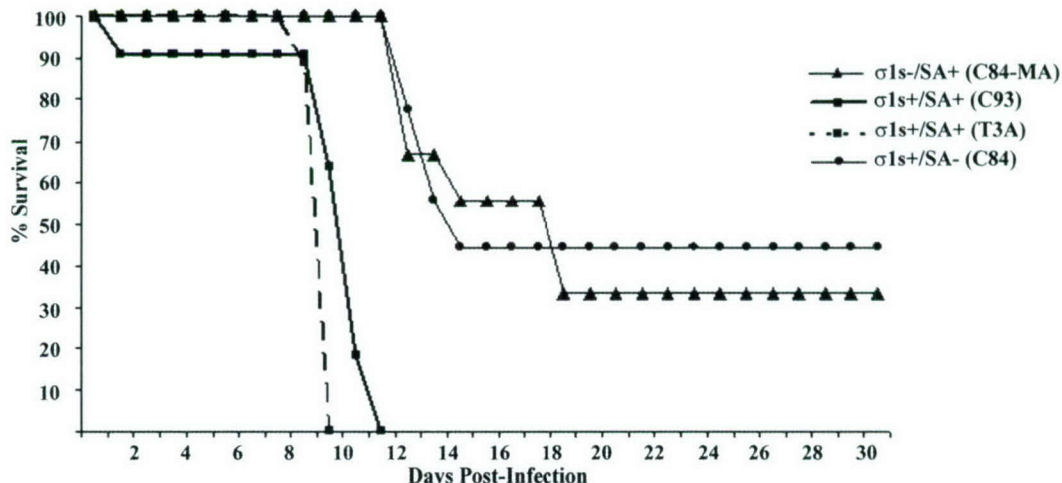


FIG. 6.  $\sigma$ 1s confers enhanced virulence following intracranial inoculation. Neonatal mice ( $n = 7$  to 11) were inoculated intracerebrally with  $10^3$  PFU of C84-MA ( $\sigma$ 1s<sup>-</sup> SA<sup>+</sup>), C93 ( $\sigma$ 1s<sup>+</sup> SA<sup>+</sup>), T3A ( $\sigma$ 1s<sup>+</sup> SA<sup>+</sup>), or C84 ( $\sigma$ 1s<sup>+</sup> SA<sup>-</sup>) per mouse.

(data not shown), indicating that loss of  $\sigma$ 1s served to delay but not prevent apoptosis following high-dose viral challenge.

By contrast to the results seen following high-dose viral challenge, long-term survivors of low-dose intracerebral challenge with  $\sigma$ 1s<sup>-</sup> reovirus (Fig. 6) sacrificed at 30 days postinfection did not show any histopathological indication of viral damage, and no infectious virus was detectable by plaque assay in the brain or other organs (data not shown). Similar results were obtained with survivors of SA<sup>-</sup> (C84) infection as well (data not shown).

**Expression of  $\sigma$ 1s in vivo by reovirus strains.** We next wished to evaluate  $\sigma$ 1s expression by C84-MA ( $\sigma$ 1s<sup>-</sup> SA<sup>+</sup>) and the  $\sigma$ 1s<sup>+</sup> strains T3A, C93, and C84 following both intramuscular (Fig. 10A to F) and intracranial (Fig. 10G to L) inoculation of neonatal mice. In vivo  $\sigma$ 1s expression was evaluated by staining cardiac and coronal sections from  $\sigma$ 1s<sup>-</sup> and  $\sigma$ 1s<sup>+</sup>

virus-infected animals with monoclonal antibodies directed against T3  $\sigma$ 1s. Expression of reovirus structural proteins was evaluated by using polyclonal antisera in adjacent sections.

As expected, both heart and brain tissues from C84-MA ( $\sigma$ 1s<sup>-</sup> SA<sup>+</sup>)-infected mice did not show positive  $\sigma$ 1s staining (Fig. 10C and I) despite detectable expression of reovirus structural proteins (Fig. 10F and L). These data indicate that reovirus was present in both the infected hearts and brains of C84-MA mice but was not expressing  $\sigma$ 1s.

In contrast, coronal sections from  $\sigma$ 1s<sup>+</sup> SA<sup>+</sup> (T3A) virus-infected mice displayed prominent expression of  $\sigma$ 1s (Fig. 10G) and structural proteins (Fig. 10J) within the cortex, as well as the thalamus and hippocampus (data not shown). In the heart, the  $\sigma$ 1s<sup>+</sup> strain T3A displayed high levels of  $\sigma$ 1s staining (Fig. 10A) and structural proteins (Fig. 10D) within areas of cardiac lesions. The  $\sigma$ 1s<sup>+</sup> SA<sup>+</sup> strain C93 displayed staining patterns similar to those of T3A in both the heart and brain (data not shown). In contrast to the exclusively cytoplasmic localization of reovirus structural proteins in infected cardiomyocyte neurons,  $\sigma$ 1s was observed in both the cytoplasm and nuclei of infected cells, thus corroborating in vivo our previous in vitro data indicating that  $\sigma$ 1s localizes to both the cytoplasm and nuclei of infected cells (13).

The  $\sigma$ 1s<sup>+</sup> SA<sup>-</sup> strain C84 expressed  $\sigma$ 1s in both the heart and CNS (Fig. 10B and H). In the brain, reovirus structural proteins were observed throughout the cortex (Fig. 10K), thalamus (data not shown), and hippocampus (data not shown). The relative amount of  $\sigma$ 1s expression compared to structural protein expression appeared to be lower in C84-infected mice than in T3A- or C93-infected mice, particularly in the CNS (Fig. 10G, J, H, and K). In the heart, the ratio of  $\sigma$ 1s expression to expression of reovirus structural proteins seemed to approximate that for T3A (Fig. 10 A, D, B, and E). Although these data are not quantitative, the reduced level of  $\sigma$ 1s expression compared to that of reovirus structural protein expression observed in C84 infected tissues suggests that C84 may express  $\sigma$ 1s at reduced levels compared to  $\sigma$ 1s<sup>+</sup> SA<sup>+</sup> strains, a result also noted in vitro (26).

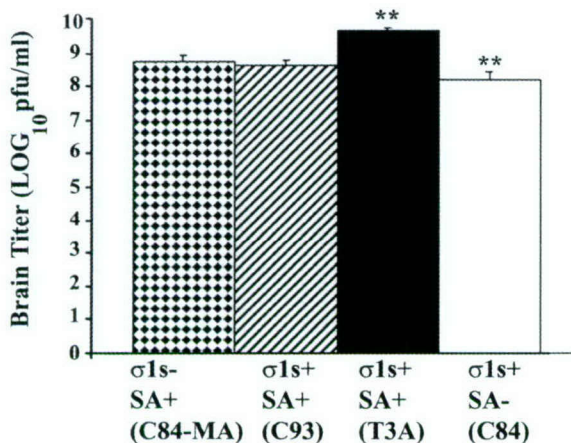


FIG. 7.  $\sigma$ 1s does not influence viral growth in the brain. Viral titers were not significantly different between  $\sigma$ 1s<sup>-</sup> and all  $\sigma$ 1s<sup>+</sup> viral strains ( $P > 0.05$ ). T3A and C84 viral titers were significantly different (\*\*,  $P < 0.01$ ). Each bar represents the average viral titer from three to six mice 8 days post-intracranial inoculation. Error bars indicate standard errors of the means.

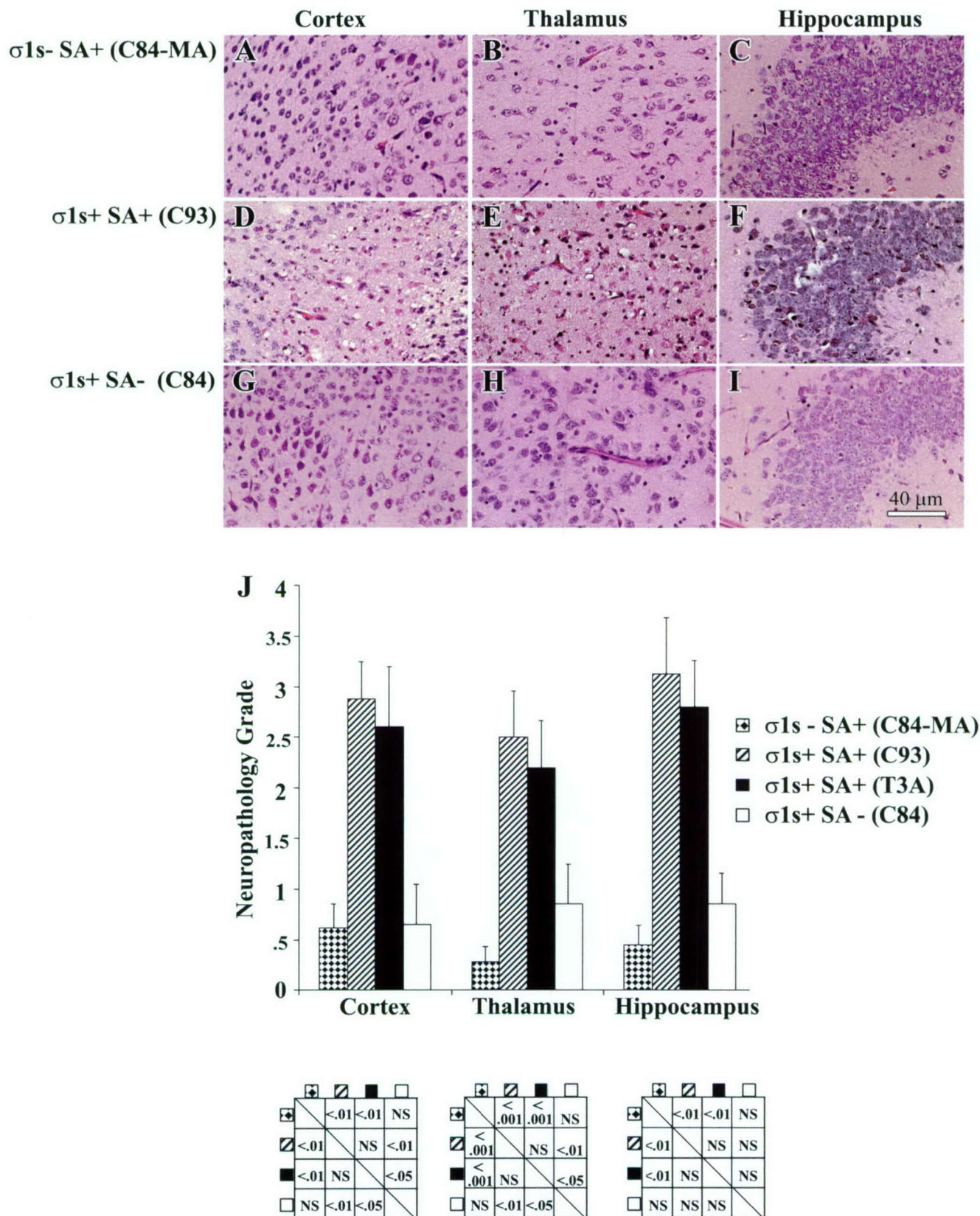


FIG. 8.  $\sigma 1s$  determines the extent and severity of reovirus-induced CNS injury. Representative H&E-stained coronal sections of the cortex, thalamus, and hippocampus are shown for C84-MA (A to C), C93 (D to F), and C84 (G to I) (original magnification,  $\times 400$ ). Tissue injury was quantified by using a previously validated neuropathology grading system (J). Each bar represents the average score from four to nine mice. Error bars indicate standard errors of the means. Statistical comparisons are shown in below the corresponding areas of the graph. NS, not significant.

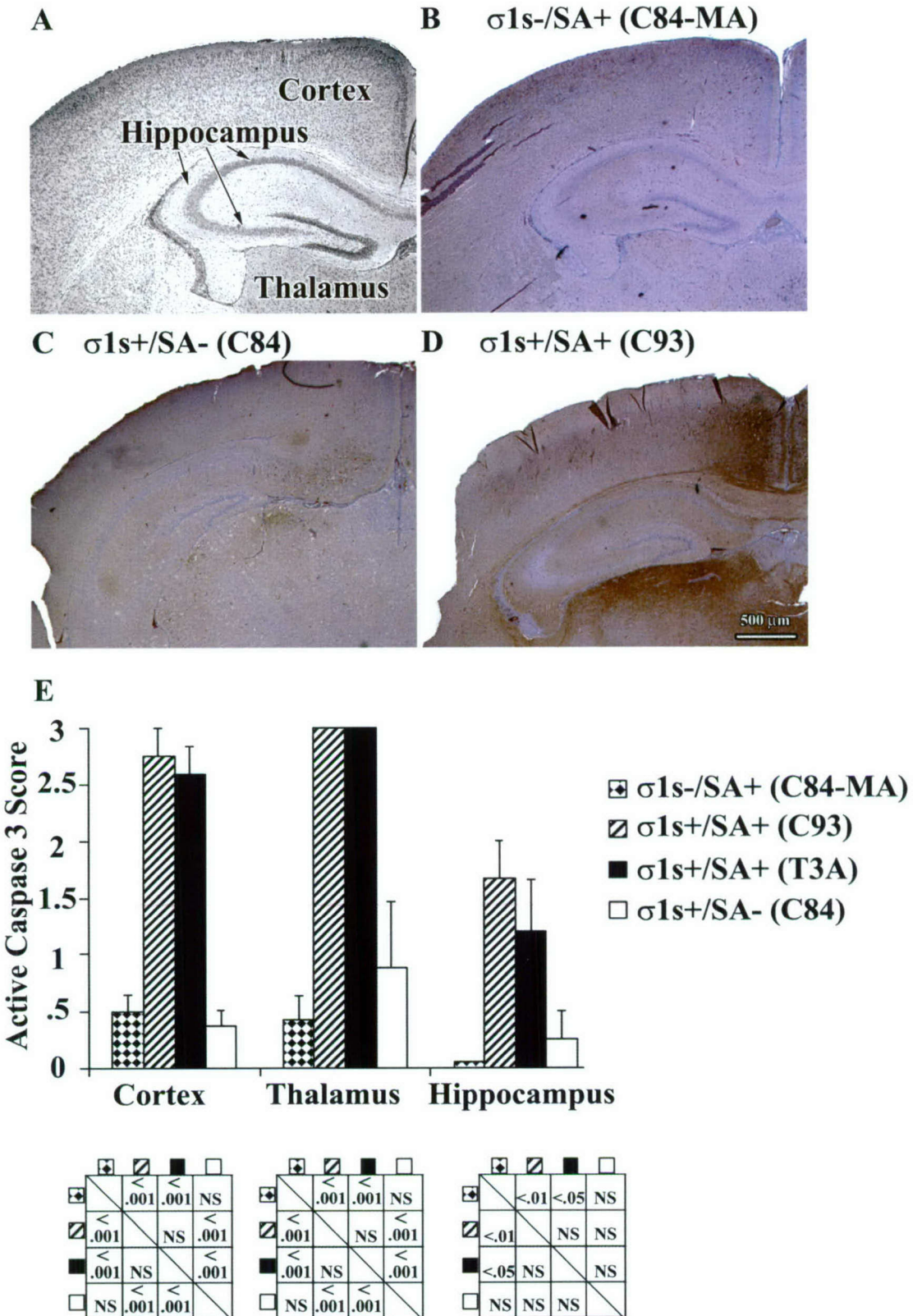


FIG. 9.  $\sigma 1s$  determines the extent and severity of reovirus-induced apoptosis in the brain. The cortex, hippocampus, and thalamus were examined at 8 days post-intracranial inoculation (A). Active, cleaved caspase-3 was quantified by the number and size of caspase-3-positive apoptotic areas (E). C84-MA ( $\sigma 1s^-$  SA $^+$ )-infected mice displayed reduced caspase-3 activation in the brain compared to  $\sigma 1s^+$  control viruses (B to E) (original magnification,  $\times 25$ ). In panel E, each bar represents the average score from four to seven mice. Error bars indicate standard errors of the means. Statistical comparisons are shown in below the corresponding areas of the graph. NS, not significant.

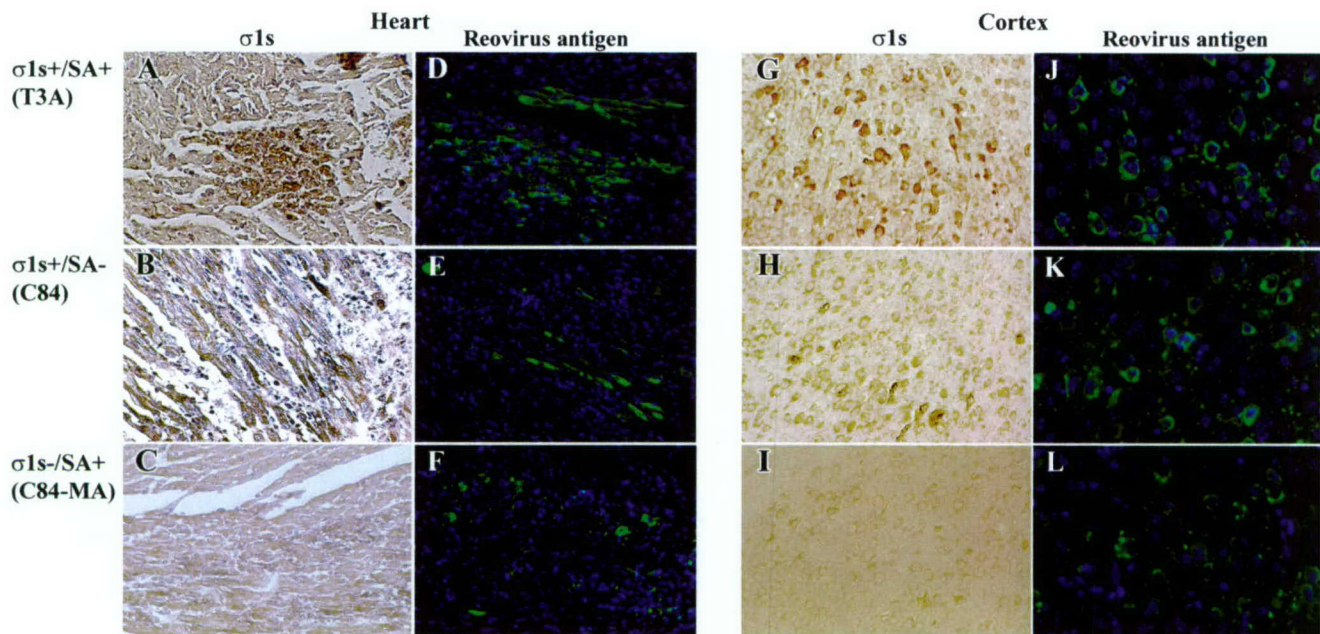


FIG. 10.  $\sigma 1s$  is expressed in vivo following both intramuscular and intracranial inoculation with  $10^5$  PFU of T3A ( $\sigma 1s^+ SA^+$ ) (A and G) and C84 ( $\sigma 1s^+ SA^-$ ) (B and H), but not C84-MA ( $\sigma 1s^- SA^+$ ) (C and I), per mouse. In vivo  $\sigma 1s$  expression in both the hearts and brains of infected animals was evaluated by diaminobenzidine tetrahydrochloride immunohistochemistry with monoclonal antibodies specific for T3  $\sigma 1s$ . Cardiac sections from intramuscularly inoculated mice (T3A, C84, and C84-MA) were stained with monoclonal antibody 2F4 directed against  $\sigma 1s$  (A to C) (original magnification,  $\times 200$ ) and polyclonal antisera directed against reovirus structural proteins (D to F) (original magnification,  $\times 100$ ). Coronal sections from intracranially inoculated mice (T3A, C84, and C84-MA) were stained with monoclonal antibody 3E2 directed against  $\sigma 1s$  (G to I) (original magnification,  $\times 200$ ) and polyclonal antisera directed against reovirus structural proteins (J to L) (original magnification,  $\times 400$ ). Polyclonal antiserum directed against T3 reovirus structural proteins was used as a control for the presence of reovirus in both cardiac (D to F) and brain (J to L) tissues.

## DISCUSSION

We now show that the reovirus nonstructural  $\sigma 1s$  protein is a determinant of viral injury in the hearts and brains of infected neonatal mice. Although viral growth in the brain and heart was not affected by the presence or absence of  $\sigma 1s$ , the extent of reovirus-induced apoptosis induction and severity of ensuing tissue damage in both organs was significantly influenced by  $\sigma 1s$  expression. In addition,  $\sigma 1s^- SA^+$  (C84-MA) virus-infected animals displayed enhanced survival following either intramuscular or intracranial challenge compared to mice injected with  $\sigma 1s^+ SA^+$  viral strains. These studies provide the first demonstration that  $\sigma 1s$  is expressed following intramuscular or intracranial inoculation and plays a significant role in reovirus pathogenesis in vivo.

Our results demonstrate that  $\sigma 1s$  expression does not influence viral growth in the heart or brain and supports previous in vitro data indicating that  $\sigma 1s$  is not required for reovirus replication in either L929 or MDCK cells (26). We further demonstrate that  $\sigma 1s$  influences the rate and extent of apoptosis induction in vivo, a phenomenon not obvious in vitro (26). This is not surprising, as there are many host factors that may operate in concert with  $\sigma 1s$  or other reovirus proteins to affect reovirus-induced disease in vivo (35). For example,  $\sigma 1s$  elicits a strong and specific cytotoxic-T-lymphocyte response (12) which may contribute to the ability of  $\sigma 1s$  to modulate the extent and severity of apoptosis induction that we observed in vivo. The conservation of  $\sigma 1s$  open reading frames in all reo-

virus field isolates provides further support for the conclusion that  $\sigma 1s$  plays an important role during viral pathogenesis in vivo.

We have recently shown that  $\sigma 1s$  actively localizes to the nucleus in infected cells and induces severe disruptions in nuclear architecture, including perturbation of the A-type nuclear lamina network (LaA/C) and induction of nuclear herniations (13). The relationship, if any, between  $\sigma 1s$ -induced nuclear architecture changes observed in vitro and the described effects on pathogenesis in vivo are unknown. However, recent studies report that disruption of LaA/C in mycardiocytes weakens nuclear structural mechanics and renders cells more sensitive to apoptosis following mechanical stress, such as that generated by the beating myocardium (16). This suggests the possibility that  $\sigma 1s$ -induced LaA/C defects may also function in vivo to render infected mycardiocytes more susceptible to apoptosis induction by reovirus.

The apoptosis-enhancing effects of LaA/C disruption are less likely the potential mechanism of action for  $\sigma 1s$  in the CNS due to the lack of mechanical strain in brain tissue. Other cytopathic effects of  $\sigma 1s$  may possibly influence the extent and severity of apoptosis induction in the brain. A growing body of evidence suggests that aberrant reentry into the cell cycle or abnormal expression of key cell cycle regulatory proteins represents a common mechanism of neuronal apoptosis (4).  $\sigma 1s$  modulates induction of reovirus-induced G<sub>2</sub>/M cell cycle arrest in infected cells and inhibits p34 (cdc2) kinase activity (22). In

addition, reovirus infection alters the expression profiles of key cell cycle proteins (21). Given these data, it is plausible that in reovirus-infected neurons,  $\sigma$ 1s perturbation of cell cycle regulatory proteins may exacerbate reovirus-induced neuronal apoptosis.

SA binding optimizes induction of apoptosis in a variety of cultured cells (7, 20) and is required for full expression of certain disease phenotypes, including reovirus-induced biliary atresia (2). Our studies suggest that SA binding is not essential for reovirus spread to and growth within the heart following peripheral inoculation. SA binding is not required for apoptosis induction in the heart or development of myocarditis, as the SA<sup>-</sup> strain (C84) was efficiently myocarditic and induced apoptosis. SA binding may be more important in CNS pathogenesis than in the heart, as the SA<sup>-</sup> strain (C84) showed reduced CNS tissue injury and apoptosis compared to the control  $\sigma$ 1s<sup>+</sup> SA<sup>+</sup> strains (T3A and C93).

An additional factor that may influence pathogenesis is differences in the amount of  $\sigma$ 1s expression in vivo. C84-MA ( $\sigma$ 1s<sup>-</sup> SA<sup>+</sup>) does not express  $\sigma$ 1s in vivo and is significantly less pathogenic in both the heart and the CNS. The SA<sup>-</sup> strain C84 also appeared to have lower levels of  $\sigma$ 1s expression in vivo than other  $\sigma$ 1s<sup>+</sup> strains. Although not quantitative, our data support previous in vitro data (26) and suggest that the altered phenotype of C84 could also reflect reduced  $\sigma$ 1s expression.

Our findings represent the first evidence of a role for the nonstructural reovirus protein  $\sigma$ 1s in viral pathogenesis in vivo. The onset of apoptosis induction and severity of virus-induced tissue injury are both dependent on the expression of  $\sigma$ 1s. The evidence presented here is all the more provocative considering the implication of a role for  $\sigma$ 1s in virus-induced pathogenesis independent of any effects on viral growth.

#### ACKNOWLEDGMENTS

This work was supported by Merit and REAP grants from the Department of Veterans Affairs NIH NINDS 1R01NS050138 (to K.L.T.), U.S. Army Medical Research and Material Command grant DAMD17-98-1-8614 (to K.L.T.), and the Reuler-Lewin Family Professorship of Neurology (to K.L.T.).

We acknowledge the University of Colorado Health Sciences Center Histology Services for assisting with histological preparation.

#### REFERENCES

- Barton, E. S., J. L. Connolly, J. C. Forrest, J. D. Chappell, and T. S. Dermody. 2001. Utilization of sialic acid as a coreceptor enhances reovirus attachment by multistep adhesion strengthening. *J. Biol. Chem.* **276**:2200–2211.
- Barton, E. S., B. E. Youree, D. H. Ebert, J. C. Forrest, J. L. Connolly, T. Valyi-Nagy, K. Washington, J. D. Wetzel, and T. S. Dermody. 2003. Utilization of sialic acid as a coreceptor is required for reovirus-induced biliary disease. *J. Clin. Investig.* **111**:1823–1833.
- Baty, C. J., and B. Sherry. 1993. Cytopathogenic effect in cardiac myocytes but not in cardiac fibroblasts is correlated with reovirus-induced acute myocarditis. *J. Virol.* **67**:6295–6298.
- Becker, E. B., and A. Bonni. 2004. Cell cycle regulation of neuronal apoptosis in development and disease. *Prog. Neurobiol.* **72**:1–25.
- Cashdollar, L. W., R. A. Chmelo, J. R. Wiener, and W. K. Joklik. 1985. Sequences of the S1 genes of the three serotypes of reovirus. *Proc. Natl. Acad. Sci. USA* **82**:24–28.
- Clarke, P., and K. L. Tyler. 2003. Reovirus-induced apoptosis. *Apoptosis* **8**:141–150.
- Connolly, J. L., E. S. Barton, and T. S. Dermody. 2001. Reovirus binding to cell surface sialic acid potentiates virus-induced apoptosis. *J. Virol.* **75**:4029–4039.
- DeBiasi, R. L., C. L. Edelstein, B. Sherry, and K. L. Tyler. 2001. Calpain inhibition protects against virus-induced apoptotic myocardial injury. *J. Virol.* **75**:351–361.
- DeBiasi, R. L., B. A. Robinson, B. Sherry, R. Bouchard, R. D. Brown, M. Rizeq, C. Long, and K. L. Tyler. 2004. Caspase inhibition is protective against reovirus-induced myocardial injury in vitro and in vivo. *J. Virol.* **78**:11040–11050.
- Dermody, T. S., M. L. Nibert, R. Bassel-Duby, and B. N. Fields. 1990. Sequence diversity in S1 genes and S1 translation products of 11 serotype 3 reovirus strains. *J. Virol.* **64**:4842–4850.
- Ernst, H., and A. J. Shatkin. 1985. Reovirus hemagglutinin mRNA codes for two polypeptides in overlapping reading frames. *Proc. Natl. Acad. Sci. USA* **82**:48–52.
- Hoffman, L. M., K. T. Hogan, and L. W. Cashdollar. 1996. The reovirus nonstructural protein  $\sigma$ 1NS is recognized by murine cytotoxic T lymphocytes. *J. Virol.* **70**:8160–8164.
- Hoyt, C. C., R. J. Bouchard, and K. L. Tyler. 2004. Novel nuclear herniations induced by nuclear localization of a viral protein. *J. Virol.* **78**:6360–6369.
- Hrdy, D. B., D. H. Rubin, and B. N. Fields. 1982. Molecular basis of reovirus neurovirulence: role of the M2 gene in virulence. *Proc. Natl. Acad. Sci. USA* **79**:1298–1302.
- Jacobs, B. L., and C. E. Samuel. 1985. Biosynthesis of reovirus-specified polypeptides: the reovirus s1 mRNA encodes two primary translation products. *Virology* **143**:63–74.
- Lammerding, J., P. C. Schulze, T. Takahashi, S. Kozlov, T. Sullivan, R. D. Kamm, C. L. Stewart, and R. T. Lee. 2004. Lamin A/C deficiency causes defective nuclear mechanics and mechanotransduction. *J. Clin. Investig.* **113**:370–378.
- Nibert, M. L., and L. A. Schiff. 2001. Reoviruses and their replication, p. 793–842. In D. M. Knipe and P. M. Howley (ed.), *Fundamental virology*. Lippincott Williams & Wilkins, Philadelphia, Pa.
- Oberhaus, S. M., T. S. Dermody, and K. L. Tyler. 1998. Apoptosis and the cytopathic effects of reovirus. *Curr. Top. Microbiol. Immunol.* **233**:23–49.
- Oberhaus, S. M., R. L. Smith, G. H. Clayton, T. S. Dermody, and K. L. Tyler. 1997. Reovirus infection and tissue injury in the mouse central nervous system are associated with apoptosis. *J. Virol.* **71**:2100–2106.
- O'Donnell, S. M., M. W. Hansberger, and T. S. Dermody. 2003. Viral and cellular determinants of apoptosis induced by mammalian reovirus. *Int. Rev. Immunol.* **22**:477–503.
- Poggiali, G. J., R. L. DeBiasi, R. Bickel, R. Jotte, A. Spalding, G. L. Johnson, and K. L. Tyler. 2002. Reovirus-induced alterations in gene expression related to cell cycle regulation. *J. Virol.* **76**:2585–2594.
- Poggiali, G. J., T. S. Dermody, and K. L. Tyler. 2001. Reovirus-induced  $\sigma$ 1s-dependent G<sub>(2)</sub>/M phase cell cycle arrest is associated with inhibition of p34 (cdc2). *J. Virol.* **75**:7429–7434.
- Poggiali, G. J., C. Keefer, J. L. Connolly, T. S. Dermody, and K. L. Tyler. 2000. Reovirus-induced G<sub>(2)</sub>/M cell cycle arrest requires  $\sigma$ 1s and occurs in the absence of apoptosis. *J. Virol.* **74**:9562–9570.
- Richardson-Burns, S. M., D. J. Kominsky, and K. L. Tyler. 2002. Reovirus-induced neuronal apoptosis is mediated by caspase 3 and is associated with the activation of death receptors. *J. Neurovirol.* **8**:365–380.
- Richardson-Burns, S. M., and K. L. Tyler. 2004. Regional differences in viral growth and central nervous system injury correlate with apoptosis. *J. Virol.* **78**:5466–5475.
- Rodgers, S. E., J. L. Connolly, J. D. Chappell, and T. S. Dermody. 1998. Reovirus growth in cell culture does not require the full complement of viral proteins: identification of a  $\sigma$ 1s-null mutant. *J. Virol.* **72**:8597–8604.
- Sarkar, G., J. Pelletier, R. Bassel-Duby, A. Jayasuriya, B. N. Fields, and N. Sonenberg. 1985. Identification of a new polypeptide coded by reovirus gene S1. *J. Virol.* **54**:720–725.
- Sherry, B. 1998. Pathogenesis of reovirus myocarditis. *Curr. Top. Microbiol. Immunol.* **233**:51–66.
- Sherry, B., F. J. Schoen, E. Wenske, and B. N. Fields. 1989. Derivation and characterization of an efficiently myocarditic reovirus variant. *J. Virol.* **63**:4840–4849.
- Thoresen, M., K. Haaland, E. M. Loberg, A. Whitelaw, F. Apricena, E. Hanko, and P. A. Steen. 1996. A piglet survival model of posthypoxic encephalopathy. *Pediatr. Res.* **40**:738–748.
- Tyler, K. L. 1998. Pathogenesis of reovirus infections of the central nervous system. *Curr. Top. Microbiol. Immunol.* **233**:93–124.
- Tyler, K. L., P. Clarke, R. L. DeBiasi, D. Kominsky, and G. J. Poggiali. 2001. Reoviruses and the host cell. *Trends Microbiol.* **9**:560–564.
- Tyler, K. L., M. K. Squier, A. L. Brown, B. Pike, D. Willis, S. M. Oberhaus, T. S. Dermody, and J. J. Cohen. 1996. Linkage between reovirus-induced apoptosis and inhibition of cellular DNA synthesis: role of the S1 and M2 genes. *J. Virol.* **70**:7984–7991.
- Tyler, K. L., M. K. Squier, S. E. Rodgers, B. E. Schneider, S. M. Oberhaus, T. A. Grdina, J. J. Cohen, and T. S. Dermody. 1995. Differences in the capacity of reovirus strains to induce apoptosis are determined by the viral attachment protein sigma 1. *J. Virol.* **69**:6972–6979.
- Virgin, H. W., T. S. Dermody, and K. L. Tyler. 1998. Cellular and humoral

- immunity to reovirus infection, p. 147–162. In K. L. Tyler and M. B. A. Oldstone (ed.), Reoviruses II. Cytopathogenicity and pathogenesis. Springer-Verlag, New York, N.Y.
36. Virgin, H. W., R. Bassel-Duby, B. N. Fields, and K. L. Tyler. 1988. Antibody protects against lethal infection with the neurally spreading reovirus type 3 (Dearing). *J. Virol.* **62**:4594–4604.
37. Weiner, H. L., D. Drayna, D. R. Averill, Jr., and B. N. Fields. 1977. Molecular basis of reovirus virulence: role of the S1 gene. *Proc. Natl. Acad. Sci. USA* **74**:5744–5748.
38. Weiner, H. L., M. L. Powers, and B. N. Fields. 1980. Absolute linkage of virulence and central nervous system cell tropism of reoviruses to viral hemagglutinin. *J. Infect. Dis.* **141**:609–616.

## Caspase Inhibition Protects against Reovirus-Induced Myocardial Injury In Vitro and In Vivo

Roberta L. DeBiasi,<sup>1,2,3\*</sup> Bridget A. Robinson,<sup>1</sup> Barbara Sherry,<sup>4</sup> Ron Bouchard,<sup>5</sup> R. Dale Brown,<sup>6</sup> Mona Rizeq,<sup>3,7</sup> Carlin Long,<sup>6</sup> and Kenneth L. Tyler<sup>2,3,6,8,9</sup>

*Departments of Pediatrics,<sup>1</sup> Neurology,<sup>2</sup> Medicine,<sup>6</sup> Pathology,<sup>7</sup> Microbiology,<sup>8</sup> Immunology,<sup>9</sup> and Pharmacology,<sup>5</sup> University of Colorado Health Sciences Center, and Veterans Administration Medical Center,<sup>3</sup> Denver, Colorado, and Departments of Microbiology, Pathology, and Parasitology, College of Veterinary Medicine, North Carolina State University, Raleigh, North Carolina<sup>4</sup>*

Received 25 February 2004/Accepted 13 July 2004

Viral myocarditis is a disease with a high morbidity and mortality. The pathogenesis of this disease remains poorly characterized, with components of both direct virus-mediated and secondary inflammatory and immune responses contributing to disease. Apoptosis has increasingly been viewed as an important mechanism of myocardial injury in noninfectious models of cardiac disease, including ischemia and failure. Using a reovirus murine model of viral myocarditis, we characterized and targeted apoptosis as a key mechanism of virus-associated myocardial injury in vitro and in vivo. We demonstrated caspase-3 activation, in conjunction with terminal deoxynucleotidyltransferase-mediated dUTP-biotin nick end labeling and annexin binding, in cardiac myocytes after myocarditic viral infection in vitro. We also demonstrated a tight temporal and geographical correlation between caspase-3 activation, histologic injury, and viral load in cardiac tissue after myocarditic viral infection in vivo. Two pharmacologic agents that broadly inhibit caspase activity, Q-VD-OPH and Z-VAD(OMe)-FMK, effectively inhibited virus-induced cellular death in vitro. The inhibition of caspase activity in vivo by the use of pharmacologic agents as well as genetic manipulation reduced virus-induced myocardial injury by 40 to 60% and dramatically improved survival in infected caspase-3-deficient animals. This study indicates that apoptosis plays a critical role in mediating cardiac injury in the setting of viral myocarditis and is the first demonstration that caspase inhibition may serve as a novel therapeutic strategy for this devastating disease.

Viral myocarditis remains a disease without a reliable or effective treatment, resulting in chronic dilated cardiomyopathy or death in up to 20% of affected children and 50% of affected adults (18). Unfortunately, the events following viral attachment and replication that produce the cytopathic effect and lead to myocarditis are not clearly understood. Several mechanisms have been suggested (32), including direct viral injury and persistence (10, 40, 58), autoimmune phenomena (6, 17, 25, 38, 52), cytokine fluxes (20, 28, 39), and T-cell-mediated inflammatory responses (27, 33, 53). Direct damage to cardiac myocytes plays a key role in the pathogenesis of nearly all models of viral myocarditis. A clearer understanding of the pathogenic mechanisms of virus-induced cardiac myocyte death is crucial for the development of effective therapeutic strategies since currently employed antiviral agents do not result in a significantly improved clinical outcome.

Murine models of viral infection utilizing coxsackievirus, murine encephalomyocarditis virus, and reovirus have been utilized to define key events in the pathogenesis of viral myocarditis. Reovirus strain 8B produces lethal myocarditis in infected neonatal mice (55, 56, 58). SCID mice still develop myocarditis, and the passive transfer of reovirus-specific immune cells is protective, rather than harmful, to 8B-infected

mice (57). These findings indicate that myocardial damage is a direct effect of viral infection of cardiac myocytes and that immune mechanisms contribute to amelioration rather than an induction of reovirus-induced viral injury. Reoviral myocarditis therefore allows dissection of the events leading to direct myocardial injury.

Apoptosis is an important mechanism of active cellular death that is distinct from necrosis and has been implicated in the pathogenesis of a variety of degenerative, ischemic, toxin-induced, and infectious human diseases (34, 41, 64). Increasing evidence indicates that apoptosis plays a central role in microbial pathogenesis, particularly in viral infections (54), and it is now recognized as an important mechanism of virus-induced tissue injury (14, 15, 47). Apoptosis has been increasingly implicated in multiple forms of cardiac pathology (reviewed in references 4, 30, and 46), including in vivo models of hypertrophic and dilated failure (5, 16, 49, 59), myocardial infarction (3), ischemia-reperfusion (23, 43), and beta-adrenergic stimulation (59). Apoptosis of cardiac myocytes in vitro has also been demonstrated in response to serum and glucose deprivation (components of ischemia in vivo) (3) as well as during cardiac myocyte differentiation (37). Although there have been sporadic reports suggesting the importance of apoptosis in the pathogenesis of viral myocarditis (1, 11, 13, 14, 61, 63), this mechanism of cellular death has not previously been extensively characterized for models of viral myocarditis.

It was shown previously that apoptosis occurs in cardiac tissue after the infection of animals with reovirus 8B (14). In

\* Corresponding author. Mailing address: Pediatrics (Infectious Diseases), University of Colorado Health Sciences Center, 4200 East 9th Ave., Box B055, Denver, CO 80262. Phone: (303) 393-4684. Fax: (303) 393-5271. E-mail: roberta.debiasi@uchsc.edu.

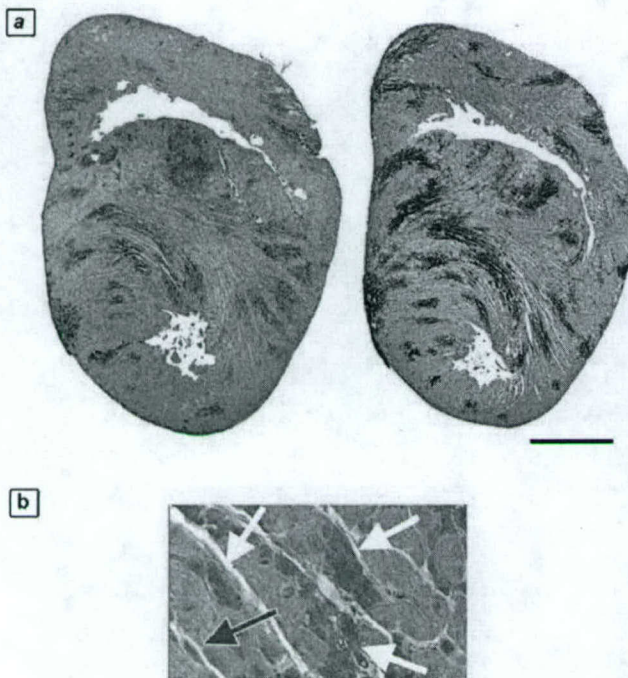


**FIG. 1.** Markers of apoptosis in virus-injured myocardium. Consecutive 4- $\mu\text{m}$ -thick sections of hearts from reovirus-infected mice were analyzed at 7 days postinfection by two independent assays for evidence of apoptosis. (a) TUNEL (left, blue staining) and active caspase-3 staining (right, brown staining) of 4- $\mu\text{m}$ -thick sections of a representative infected animal. It was calculated that 17.8% of the myocardial tissue was TUNEL positive and 23.3% was active caspase-3 positive. (b) Higher-magnification view of active caspase-3-positive area of myocardium. The black arrow indicates an example of a negatively stained cardiac fibroblast. White arrows indicate examples of positively stained cardiac myocytes. Bar = 2.5 mm.

that study, the *in vivo* inhibition of calpain, a cysteine protease implicated in apoptotic signaling, was protective against virus-induced myocardial injury. Taken together, these results indicated that apoptosis is potentially an important mechanism of virus-induced tissue damage, as has been suggested for at least one other animal model of viral myocarditis (61). In the present study, we demonstrate the importance of apoptosis, and specifically caspase activation, as a critical determinant in the pathogenesis of virus-induced myocarditis and show that caspase inhibition is protective in an animal model of viral myocarditis. These results shed light on the basic pathogenesis of viral myocarditis and may have direct therapeutic implications for the treatment of this and other diseases involving apoptotic tissue damage.

#### MATERIALS AND METHODS

**Virus and cells.** The reovirus 8B strain was passaged twice in L929 cells prior to use. 8B infectious subvirion particles (ISVPs) were generated by treating purified 8B virions with alpha-chymotrypsin at a final concentration of 150  $\mu\text{g}/\text{ml}$  (from a 2-mg/ml stock solution in 150 mM NaCl and 15 mM sodium citrate diluted to 300  $\mu\text{g}/\text{ml}$  in dialysis buffer) for 35 min at 37°C. Digestion was stopped by the addition of 2  $\mu\text{M}$  (final concentration) phenylmethylsulfonyl fluoride on ice. ISVP preparations were verified by Western blot analysis of viral proteins. Neonatal murine cardiac myocytes were cultured in Dulbecco's modified Eagle's medium with Hanks salts supplemented with 5% fetal bovine serum, 1 mg of bovine serum albumin/ml, 50 U of penicillin G (Sigma)/ml, 2  $\mu\text{g}$  of vitamin B<sub>12</sub>

(Sigma)/ml, 10  $\mu\text{g}$  of transferrin (Sigma)/ml, 10  $\mu\text{g}$  of insulin (Sigma)/ml, and 0.1 mM bromodeoxyuridine (Sigma) and were maintained at 37°C with 1% CO<sub>2</sub> (50, 51).

**Mice and inoculations.** For inhibitor experiments, Swiss-Webster mice were purchased from Transduction Laboratories. Caspase-3 knockout mice and C57B6 wild-type mice were a generous gift from Richard Flavell, Yale University. Two-day-old mice were infected intramuscularly (in the left hind limb) with 10<sup>4</sup> PFU of virus administered in 20  $\mu\text{l}$  of gel saline (137 mM NaCl, 0.2 mM CaCl<sub>2</sub>, 0.8 mM MgCl<sub>2</sub>, 19 mM H<sub>3</sub>BO<sub>3</sub>, 0.1 mM Na<sub>2</sub>B<sub>4</sub>O<sub>7</sub>, 0.3% gelatin).

**Histologic analysis.** Hearts were immersed in 10% buffered formalin for 12 h, embedded in paraffin, and sectioned transversely into 4- $\mu\text{m}$ -thick sections. Hematoxylin and eosin (H&E)-stained mid-cardiac sections were examined by light microscopy, photographed at a magnification of  $\times 2.5$ , and scored in a blinded fashion by two independent scorers, using a previously validated myocardial injury scoring system (58). Injury was also quantified by determining the area of injured myocardial tissue and expressing it as a percentage of the total myocardial tissue area (Adobe Photoshop Magnetic Lasso tool).

**Immunohistochemistry.** (i) **Viral antigen detection.** After antigen retrieval and a blockade of nonspecific binding, tissues were incubated with a rabbit polyclonal anti-T3D reovirus antiserum (1:100 dilution overnight at 4°C). After washes in Tris-buffered saline-0.1% Tween 20, the tissues were incubated with fluorescein isothiocyanate-conjugated goat anti-rabbit immunoglobulin G (Vector) (1:100 dilution for 1 h at room temperature [RT]) and were subsequently counterstained for nuclear detection with Hoechst 33342 (Molecular Probes) (5 min at RT). Sections were mounted with Vectashield (Vector) and then analyzed by fluorescence microscopy.

(ii) **Activation of caspase-3.** Antigen unmasking was performed as described above, and the endogenous peroxidase activity of the tissues was blocked. Sections were incubated with a rabbit polyclonal antibody detecting cleaved (active) caspase-3 (Cell Signaling) (1:100 dilution overnight at 4°C) and then with goat anti-rabbit immunoglobulin-biotin (Vector) (1:100 dilution for 1 h at RT) and were subsequently probed with avidin-horseradish peroxidase. Cleaved caspase-3 was detected with a diaminobenzidine peroxidase substrate (Trevigen). A blue counterstain (Trevigen) was used to visualize the tissue architecture.

**Immunocytochemistry.** Cells were fixed with 3.7% paraformaldehyde (20 min at RT) and then stored in a mild cell permeabilizer, Cytonin (Trevigen), at 4°C for up to 1 week. The cells were probed for reovirus antigens and cleaved caspase-3 (Cell Signaling), as described above. Fluorescence microscopy was used to visualize staining at a magnification of  $\times 20$ .

**Apoptosis assays and reagents.** Cardiac myocytes were harvested by using a 50-50 mixture of trypsin-EDTA (BioSource) and Accutase (Innovative Cell Technologies).

**Acridine orange and ethidium bromide stains.** Cells were stained with acridine orange for determinations of nuclear morphology and with ethidium bromide to distinguish cell viability, at a final concentration of 1  $\mu\text{g}/\text{ml}$  for each, as previously described (14).

**Flow cytometry.** Cells were analyzed by flow cytometry for the binding of annexin V-fluorescein isothiocyanate to phosphatidylserine and were simultaneously analyzed for propidium iodide incorporation. Data were collected for populations of 10,000 cells.

**TUNEL.** Tissues and cells were analyzed for evidence of DNA fragmentation by *in situ* terminal deoxynucleotidyltransferase-mediated dUTP-biotin nick end labeling (TUNEL) (TACS XL-Blue label; Trevigen). Terminal deoxynucleotidyltransferase was utilized to incorporate biotinylated nucleotides at the sites of DNA breaks. TUNEL in the tissues was detected with the TACS blue label, and the cells were counterstained with nuclear fast red for visualization of the background cellular architecture.

**Caspase inhibition.** The pan-caspase inhibitors Q-VD-OPH [quinoline-Val-Asp(OMe)-CH<sub>2</sub>-PH; Enzyme Systems] and Z-VAD(OMe)-FMK [Z-Val-Ala-Asp(OMe)-FMK; Enzyme Systems] were utilized to determine the effect of caspase inhibition on cardiac myocyte death *in vitro* and on myocardial injury *in vivo* following viral infection. Both drugs are potent irreversible broad-spectrum caspase inhibitors (7, 42). Neonatal mice received daily intraperitoneal injections of Q-VD-OPH or Z-VAD(OMe)-FMK (50 mg/kg of body weight in a 10- $\mu\text{l}$  volume) or of the corresponding diluent (70 or 15% dimethyl sulfoxide, respectively, in phosphate-buffered saline) on days 3 to 6 postinfection and were sacrificed on day 7. For *in vitro* experiments, inhibitors (50  $\mu\text{M}$ ) were added to primary cardiac myocytes 1 h prior to infection with virus.

**Viral titer determination.** Viral titers of the tissue homogenates were determined as previously described (14) and are reported as mean titers of two or three independently infected tissues or cell lysates  $\pm$  standard errors of the means.

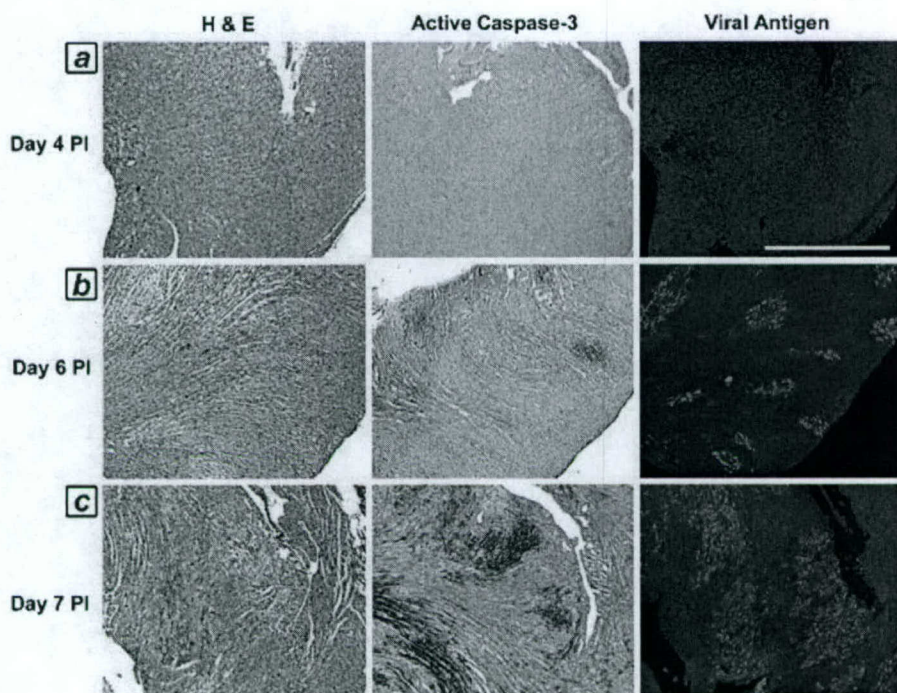


FIG. 2. Time course of injury, apoptosis, and viral load in virus-infected myocardium. Consecutive 4-μm-thick sections of hearts from reovirus-infected mice were analyzed on days 3 to 7 postinfection (PI) for evidence of apoptosis (active caspase-3, brown staining) in conjunction with histological injury (H&E stain) and viral load (green fluorescent staining). (a) Day 4; (b) day 6; (c) day 7. Sections are from single representative animals from each day ( $n = 26$ ; two to six mice were studied from each day postinfection). See Tables 1 and 2 for quantitation and correlation coefficients. Bar = 625 μm.

## RESULTS

**Apoptosis is an important mechanism in the pathogenesis of myocardial injury after viral infection.** (i) **Apoptosis and caspase-3 activation in myocardial tissue in vivo.** We wished to define the temporal relationship of apoptosis to tissue injury in order to confirm that apoptotic injury is an integral component of this damage. We analyzed 4-μm-thick consecutive sections from reovirus 8B-infected hearts on serial days postinfection (days 1 to 7 postinfection) for evidence of apoptosis (active caspase-3 immunohistochemistry and TUNEL), in conjunction with H&E staining for determinations of tissue injury and immunohistochemistry for viral antigens. TUNEL and active caspase-3 staining colocalized and were equally sensitive mark-

ers of apoptosis in the analyzed sections, as determined by the quantification of positive staining as a percentage of the total myocardial tissue from 4-μm-thick consecutive sections of infected hearts (Fig. 1a; 17.8% of the myocardium was TUNEL positive, and 23.3% was positive for active caspase-3). Caspase-3 activity was only noted within areas of injured myocardium and was completely absent from uninfected animals. Using high-magnification imaging of myocardial tissue with active caspase-3 positivity, we observed that the cell population undergoing apoptosis was composed of cardiac myocytes rather than fibroblasts (Fig. 1b). Using a previously validated scoring system, we determined average scores for injury and caspase-3 activation (by numerically scoring and averaging replicate sections from each day postinfection) and compared them. Myocardial tissue viral titers were also determined in parallel experiments on days 3 to 6 postinfection. On days 1 to 3 postinfection, the myocardial architecture appeared normal, viral antigen was undetectable, and neither the TUNEL nor active caspase-3 apoptotic marker was positive. Beginning on

TABLE 1. Quantitation of histologic injury, caspase-3 activation, and viral load in virus-infected myocardium over time postinfection<sup>a</sup>

Day postinfection	Myocardial injury score	Caspase-3 activation score	Viral titer in Tissue ( $\log_{10}$ PFU/ml)
3	0.0 ± 0.0	0.0 ± 0.0	4.4 ± 0.1
4	0.8 ± 0.5	0.5 ± 0.0	5.6 ± 0.4
5	1.0 ± 0.5	1.0 ± 0.0	7.5 ± 0.1
6	2.6 ± 0.3	2.2 ± 0.2	7.6 ± 0.5
7	3.3 ± 0.3	3.2 ± 0.2	ND

<sup>a</sup> Consecutive 4-μm-thick sections of hearts from reovirus-infected mice on days 3 to 7 postinfection ( $n = 26$ ) were scored quantitatively for histologic injury (0 to 4) and caspase-3 activation (0 to 4). Myocardial viral titers were also determined on days 3 to 6 postinfection. Mean scores ( $\pm$  standard errors of the means) for histologic injury, caspase-3 activation, and viral titers are reported for each day (derived from 2 to 6 mice per day). ND, not done.

TABLE 2. Correlation coefficients for histologic injury, caspase-3 activation, and viral load in virus-infected myocardium over time postinfection

Variable	Myocardial injury score	Caspase-3 activation score	Viral titer in tissue ( $\log_{10}$ PFU/ml)	R (P value)
Myocardial injury score			0.99 (<0.001)	0.79 (<0.02)
Caspase-3 activation score	0.99 (<0.001)		0.85 (<0.01)	

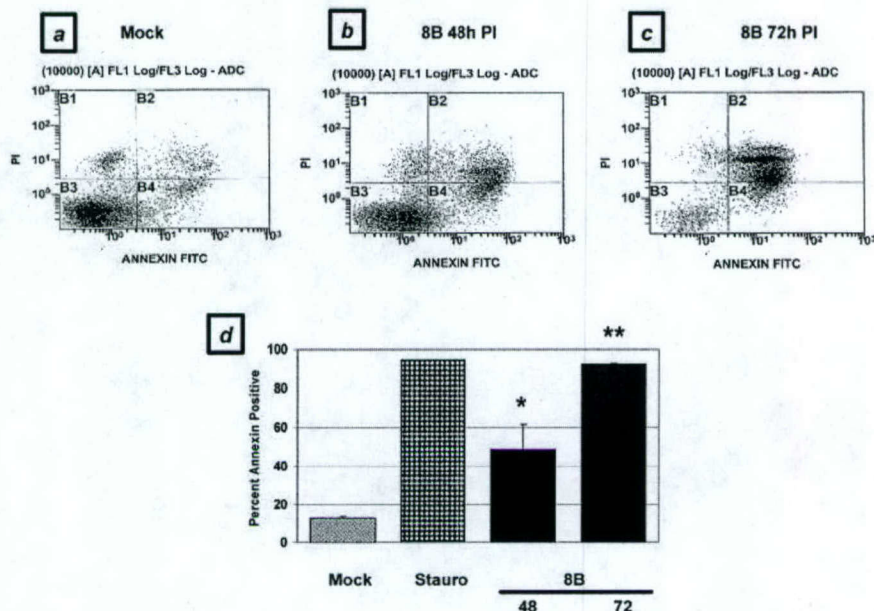


FIG. 3. Apoptosis in virus-infected primary cardiac myocytes in vitro, as measured by annexin binding. Primary cardiac myocytes were analyzed by flow cytometry for evidence of annexin binding (representing phosphatidylserine inversion) and propidium iodide incorporation (representing cellular viability) at 48 and 72 h postinfection (PI) with reovirus and were compared to mock-infected cells. (a) Mock-infected cells; (b) 48 h after virus infection; (c) 72 h after virus infection. (d) Quantitation of replicate flow cytometry experiments, including 5  $\mu$ M staurosporine treatment as a positive control. \*,  $P < 0.05$ ; \*\*,  $P < 0.001$ .

day 4 and continuing through day 7 postinfection, we detected a gradually increasing and highly correlated degree of histologic injury, apoptosis, and viral load on each day postinfection ( $R = 0.79$  to  $0.99$ ) (Fig. 2 and Tables 1 and 2). Importantly, there was no observed discrepancy or time lag between detectable histologic injury and the presence of apoptosis (caspase-3 activity). Taken together, these results indicate that apoptosis is an integral part of the pathological response to viral infection.

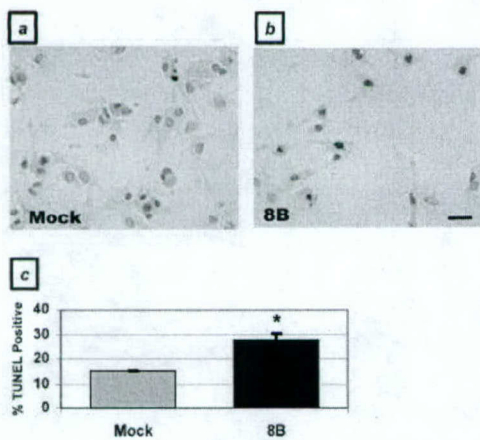


FIG. 4. Apoptosis in virus-infected primary cardiac myocytes, as determined by TUNEL. Primary cardiac myocytes were analyzed by TUNEL at 48 h postinfection. Blue-stained nuclei indicate TUNEL positivity. (a) Mock-infected myocytes; (b) 8B-infected myocytes. (c) Quantitation of staining. \*,  $P < 0.05$ . Bar = 160  $\mu$ m.

**(ii) Apoptosis and caspase-3 activation in infected cardiac myocytes in vitro.** To confirm that the representative cell population undergoing apoptosis in response to viral infection in vivo was cardiac myocytes, we infected primary cardiac myocytes with the 8B virus and analyzed them for evidence of apoptosis at several time points postinfection. In a flow cytometric analysis of annexin V positivity, cardiac myocytes showed a 3.8-fold increase over basal levels of apoptosis at 48 h postinfection ( $48.8\% \pm 12.6\%$  [8B infection] versus  $13.0\% \pm 1.0\%$  [mock infection];  $P < 0.05$ ), which increased to 7.1-fold at 72 h postinfection ( $92.3\% \pm 0.3\%$ ;  $P < 0.001$ ) (Fig. 3). This level of apoptosis was similar to that induced by exposure to a well-characterized apoptotic stimulus, 5  $\mu$ M staurosporine (94.6%). Using a TUNEL assay, we demonstrated a nearly twofold increase in apoptotic myocytes 48 h after 8B infection ( $28\% \pm 2.1\%$  versus  $15\% \pm 0\%$ ;  $P < 0.05$ ) (Fig. 4). Similar results were obtained by analyses of nuclear morphology and cell viability by ethidium bromide and acridine orange staining (data not shown). Virus-infected cells also demonstrated a 10.3-fold increase in active caspase-3 activity compared to mock-infected cells at 48 h postinfection ( $25.7\% \pm 0.3\%$  versus  $2.5\% \pm 0.3\%$ ;  $P < 0.001$ ) (Fig. 5a and b).

Taken together, both the in vivo and in vitro data suggest that cardiac myocytes undergo significant levels of apoptosis associated with caspase-3 activation in response to infection with myocarditic virus. As such, the apoptotic response in this cell population is likely to be an integral component of the myocardial damage observed after viral infection.

**Caspase inhibition protects cardiac myocytes from virus-induced apoptosis in vitro.** Having demonstrated significant caspase-3 activation in virus-infected cardiac myocytes, we next

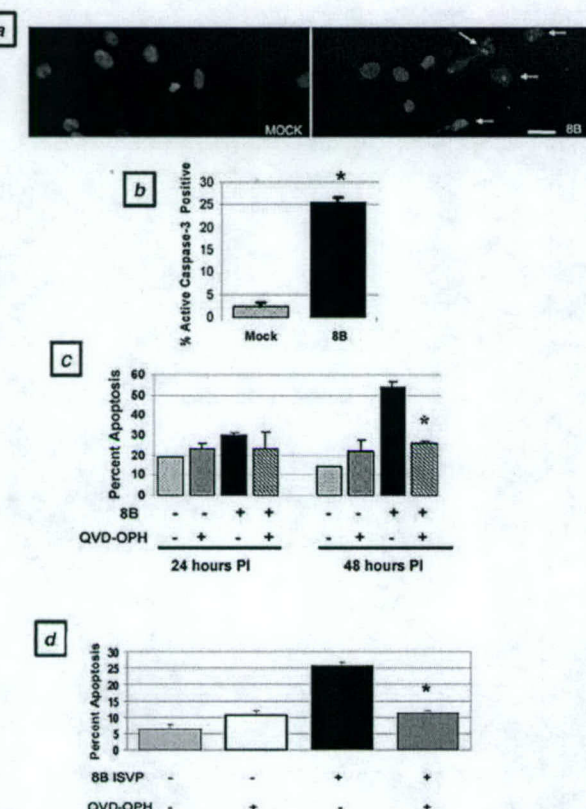


FIG. 5. Caspase-3 activation in virus-infected primary cardiac myocytes in vitro and effect of caspase inhibition on virus- and ISVP-induced apoptosis. Infected and mock-infected primary cardiac myocytes were doubly labeled to allow the simultaneous detection of caspase-3 activity (red) and nuclear morphology (Hoechst staining; blue) by immunocytochemistry at 48 h postinfection. (a) Mock-infected and 8B-infected myocytes. (b) Quantitation of replicate experiments. \*,  $P < 0.001$ . (c) Effect of Q-VD-OPH treatment ( $50 \mu\text{M}$ ) on apoptosis (assessed by acridine orange and ethidium bromide staining) of mock-infected and 8B virus-infected cardiac myocytes at 24 and 48 h postinfection. \*,  $P < 0.01$ . (d) Effect of Q-VD-OPH treatment ( $50 \mu\text{M}$ ) on apoptosis of mock- and 8B ISVP-infected cardiac myocytes at 48 h postinfection. \*,  $P < 0.01$ . Bar =  $160 \mu\text{m}$ .

determined the effect of caspase inhibition on virus-induced cardiac myocyte death. Using ethidium bromide and acridine orange staining, we quantified apoptosis after viral infection in the presence and absence of two broadly acting caspase inhibitors, Q-VD-OPH and Z-VAD(OMe)-FMK. Q-VD-OPH significantly protected cardiac myocytes from virus-induced apoptosis at 48 h postinfection, with a 50% ( $P < 0.01$ ) reduction in the levels of apoptosis compared to untreated infected cells (Fig. 5c). Z-VAD(OMe)-FMK also provided protection, with a 33% reduction in the levels of apoptosis. To address the possibility that caspase inhibitors confer protection by interfering with viral uncoating (by nonspecifically inhibiting lysosomal cathepsins), we also performed identical experiments with 8B ISVP infections of cardiac myocytes in the presence and absence of Q-VD-OPH. Q-VD-OPH significantly protected cardiac myocytes from ISVP-induced apoptosis at 48 h postinfection, with a 50% ( $P < 0.01$ ) reduction in the levels of apoptosis compared to untreated, ISVP-infected cells (Fig. 5d). These

results suggest that caspase inhibition protects infected cardiac myocytes against virus-induced apoptotic death by a mechanism other than the inhibition of viral uncoating.

**Caspase inhibition is protective against virus-induced myocardial injury in vivo.** (i) **Pharmacologic inhibitors.** Since pharmacologic caspase inhibition was protective against virus-induced apoptosis in cardiac myocytes in vitro, we next investigated whether administering these same inhibitors to infected mice in vivo would be effective at preventing myocardial tissue injury. Two-day-old Swiss-Webster mice were infected with  $10^4$  PFU of myocarditic virus, followed by the administration of Q-VD-OPH, Z-VAD(OMe)-FMK, or their diluent controls on days 3 to 6 postinfection. Mice receiving caspase inhibitors showed statistically significant reductions in myocardial injury scores compared to controls, as measured by two independent myocardial injury scoring systems. Treatment with Q-VD-OPH resulted in a 60% reduction in the myocardial lesion score (from  $2.9 \pm 0.3$  to  $1.2 \pm 0.2$ ;  $P < 0.0001$ ;  $n = 22$ ) compared to untreated infected mice (Fig. 6a, d, and g), corresponding to a reduction in the injured myocardial area from  $12.8\% \pm 2.0\%$  to  $1.4\% \pm 0.9\%$  ( $P < 0.0001$ ). Z-VAD(OMe)-FMK treatment also offered protection from virus-induced myocardial injury, resulting in a 39% reduction in the myocardial lesion score, from  $3.1 \pm 0.3$  to  $1.9 \pm 0.6$ , compared to that for untreated mice, which corresponded to a reduction in the injured myocardial area from  $16.4\% \pm 1.2\%$  to  $7.4\% \pm 3.3\%$  ( $P < 0.05$ ;  $n = 16$ ).

An analysis of 4- $\mu\text{m}$ -thick consecutive sections from Q-VD-OPH-treated mice revealed a significant decrease in apoptosis, as measured by active caspase-3 staining (Fig. 6b and e) and TUNEL (data not shown), as well as a reduction in tissue viral antigen staining (Fig. 6c and f) compared to that in untreated animals. Since the viral load appeared to be reduced, as observed by immunohistochemical techniques, a further analysis of tissue viral titers was undertaken in order to determine if the protection conferred by Q-VD-OPH caspase inhibition was explained by a significant inhibition of viral replication within the primary site of inoculation (limb) or the target tissue (myocardium). Viral titers in tissue homogenates of limbs and hearts, as well as of brains and livers, were compared for treated and untreated animals. Small but insignificant reductions in the viral titer were observed at the primary site of inoculation (0.7-log reduction, from  $8.4 \pm 0.1$  to  $7.7 \pm 0.3 \log_{10}$  PFU/ml;  $P > 0.05$ ) and in the heart (0.5-log reduction, from  $8.4 \pm 0.3$  to  $7.9 \pm 0.1 \log_{10}$  PFU/ml;  $P > 0.05$ ) after treatment with Q-VD-OPH (Fig. 6h). Notably, these reduced titers still represented a 3- to 4-log increase over the input viral titer at the time of infection. We also assessed the effect of both Q-VD-OPH and Z-VAD(OMe)-FMK on the growth of the virus in infected cardiac myocytes in vitro. No reduction in viral titer was observed in Z-VAD(OMe)-FMK-treated infected myocytes compared to untreated myocytes (from  $8.2 \pm 0.1$  to  $7.9 \pm 0.1 \log_{10}$  PFU/ml at 48 h postinfection;  $P > 0.05$ ). A modest reduction was observed following Q-VD-OPH treatment (1.2-log reduction, to  $7.0 \pm 0.1 \log_{10}$  PFU/ml;  $P = 0.01$ ) (Fig. 6i).

Taken together, these results suggest that pharmacologic caspase inhibition provides protection from virus-induced myocardial injury, with a significant reduction in caspase-3 activity within the infected myocardium in conjunction with minimal to modest reductions in the myocardial viral burden.

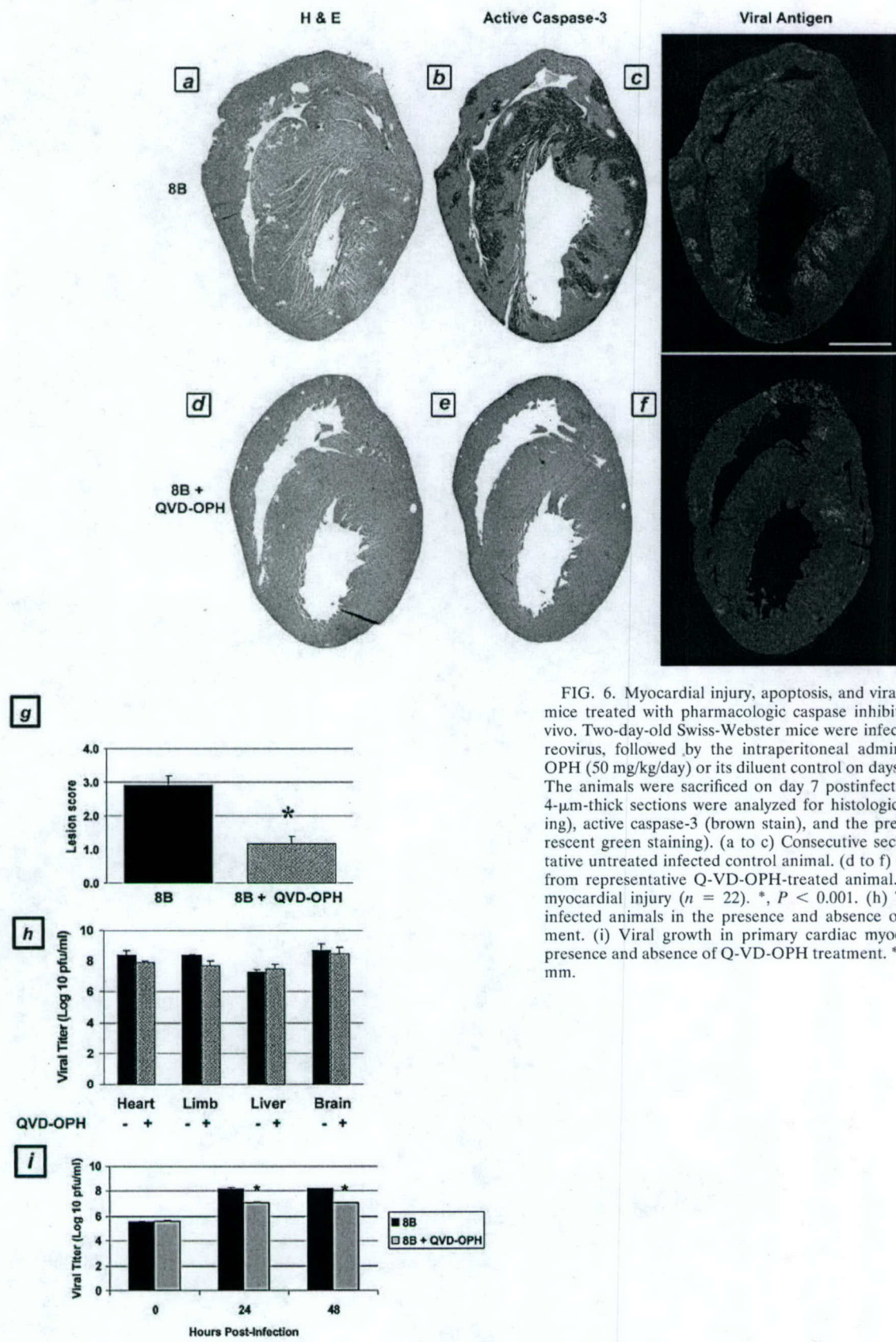
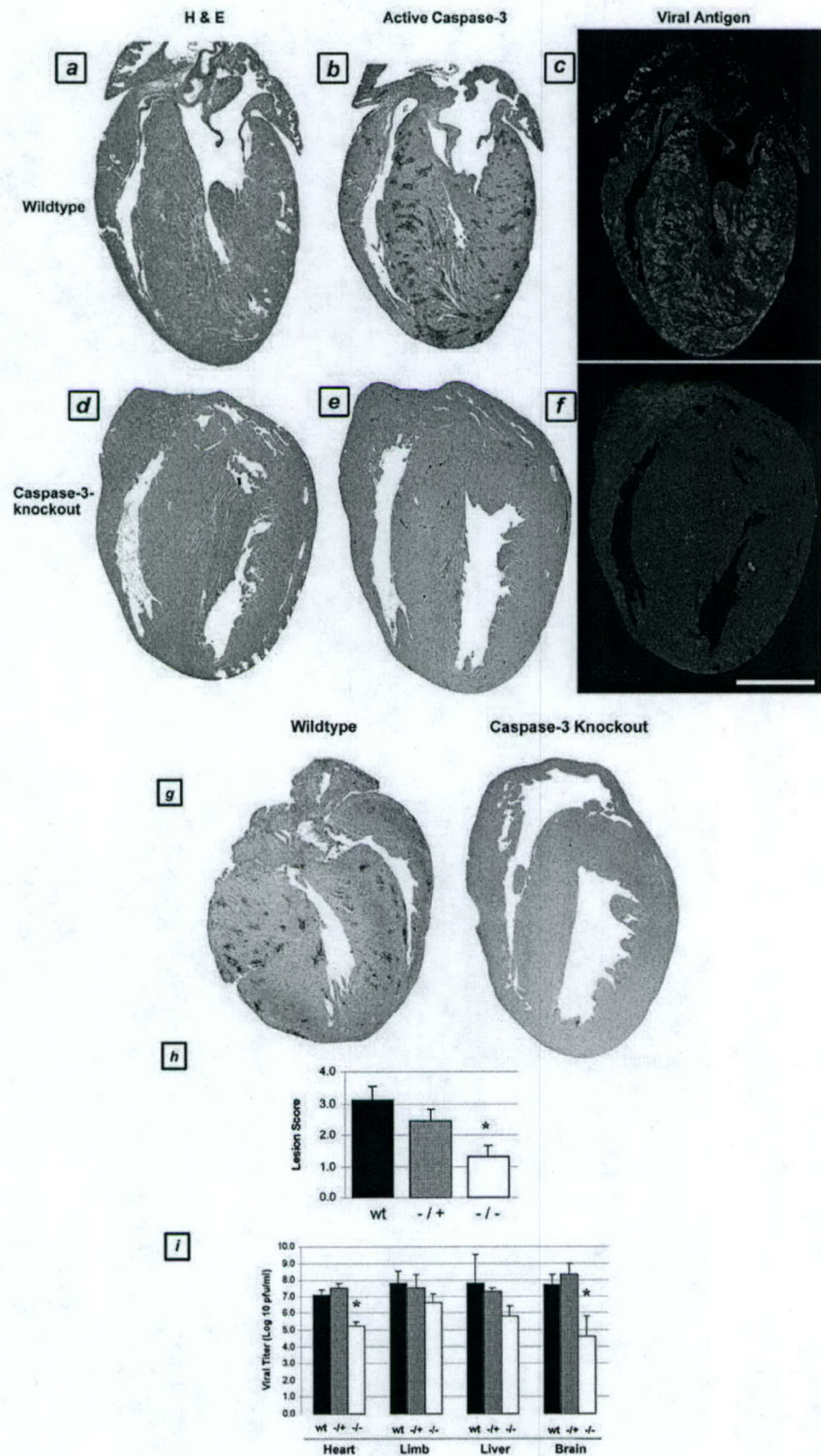


**FIG. 6.** Myocardial injury, apoptosis, and viral load in 8B-infected mice treated with pharmacologic caspase inhibitor (Q-VD-OPH) in vivo. Two-day-old Swiss-Webster mice were infected with myocarditic reovirus, followed by the intraperitoneal administration of Q-VD-OPH (50 mg/kg/day) or its diluent control on days 3 to 6 postinfection. The animals were sacrificed on day 7 postinfection, and consecutive 4- $\mu$ m-thick sections were analyzed for histologic injury (H&E staining), active caspase-3 (brown stain), and the presence of virus (fluorescent green staining). (a to c) Consecutive sections from representative untreated infected control animal. (d to f) Consecutive sections from representative Q-VD-OPH-treated animal. (g) Quantitation of myocardial injury ( $n = 22$ ). \*,  $P < 0.001$ . (h) Tissue viral titers in infected animals in the presence and absence of Q-VD-OPH treatment. (i) Viral growth in primary cardiac myocytes in vitro in the presence and absence of Q-VD-OPH treatment. \*,  $P = 0.01$ . Bar = 2.5 mm.



**(ii) Transgenic (caspase-3-deficient) mice.** Since pharmacologic caspase inhibition was protective against virus-induced myocardial injury, we performed identical experiments with transgenic mice who were deficient in caspase-3 as well as with matched wild-type controls (littermates). Infected transgenic mice exhibited statistically significant reductions in myocardial injury after viral infection compared to wild-type and heterozygous controls, as measured by both scoring systems. Hearts from caspase-3-deficient mice showed a 58% reduction in the cardiac lesion score (from  $3.1 \pm 0.4$  to  $1.3 \pm 0.4$ ;  $P < 0.05$ ;  $n = 32$ ) compared to untreated infected mice (Fig. 7a, d, and h), corresponding to a reduction in the injured myocardial area from  $13.3\% \pm 4.6\%$  to  $5.8\% \pm 2.5\%$  ( $P < 0.05$ ). Heterozygous mice demonstrated an intermediate injury phenotype, with a trend toward less injury than wild-type mice (lesion score,  $2.5 \pm 0.4$ ; not significant) but more injury than homozygous mice ( $P < 0.05$ ). Caspase-3 activation (Fig. 7b and e) and TUNEL staining (Fig. 7g) were both absent and the degree of viral antigen staining was reduced (Fig. 7c and f) in infected homozygous caspase-3-deficient mice compared to wild-type control animals. In contrast to the case in pharmacologic inhibition experiments, tissue viral titers were significantly reduced in caspase-3-deficient mice compared to wild-type and heterozygous controls, particularly in cardiac tissues. A nearly 2-log reduction was noted in the hearts of infected caspase-3-deficient mice compared to those of wild-type and heterozygous controls (from  $7.1 \pm 0.3$  to  $5.2 \pm 0.3 \log_{10}$  PFU/ml;  $P < 0.01$ ) (Fig. 7i). A reduction in titer at the primary site of inoculation (limb) was also noted, although it was of a lesser magnitude (1.2-log reduction, from  $7.8 \pm 0.7$  to  $6.6 \pm 0.5 \log_{10}$  PFU/ml). Notably, these reduced titers still represented 1- to 2-log increases over the input viral titer at the time of inoculation.

In addition to exhibiting reduced levels of injury at 7 days postinfection, caspase-3-deficient animals were also noted to have substantially prolonged survival times after viral infection (Fig. 8). Although wild-type animals exhibited 100% mortality by 9 days postinfection, 100% of the caspase-3-deficient mice were alive and well at that time. Fifty percent of the caspase-3-deficient mice were still alive at 21 days postinfection, and 37.5% of them survived indefinitely. Cardiac tissues from long-term survivors appeared normal (at 54 days postinfection).

## DISCUSSION

Apoptosis has been increasingly appreciated as an important mechanism of cardiac injury in noninfectious models of cardiac disease. We now have demonstrated the importance of apoptosis, and specifically caspase activation, as a critical determinant in the pathogenesis of virus-induced myocarditis by ma-

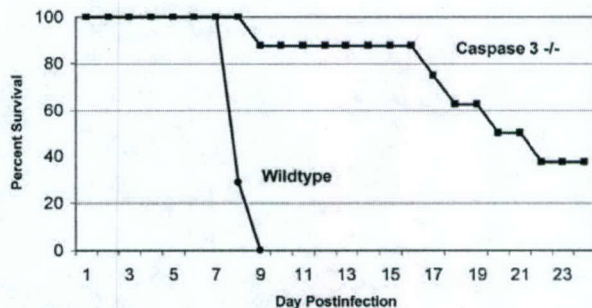


FIG. 8. Survival in infected caspase-3-deficient transgenic animals. The survival of wild-type and caspase-3-deficient transgenic animals was assessed daily after 8B infection ( $n = 8$ ).

nipulating this process in vitro and in vivo. Our study is the first to demonstrate that caspase inhibition by pharmacologic inhibitors or genetic alteration protects cardiac myocytes from virus-induced apoptotic death and infected mice from virus-induced myocardial injury.

In contrast to the paucity of data available regarding the role of apoptosis in infectious myocarditis, there is substantial evidence suggesting that apoptosis plays an important role in the settings of myocardial ischemia-infarction and heart failure. In the case of ischemia, myocardial apoptosis has been documented by many groups, utilizing a variety of animal models (murine, porcine, canine, and lagomorph) and experimental paradigms in vitro and in vivo (reviewed extensively in reference 46). In vivo models utilizing coronary ligation and reperfusion have suggested that both the initial ischemic insult and the reperfusion phase may independently contribute to the initiation and execution of apoptosis (3, 19, 21, 31, 35). The relative contributions of apoptosis and necrosis, the role of reactive oxygen species, specific depleted energy substrates, and molecular chaperones, and the delineation of specific apoptotic signaling pathways are areas of active research in this setting. The manipulation of caspases (the effector proteases of apoptosis) has been investigated previously with ischemic models of cardiac disease in vitro (2) and in vivo (12, 26, 44, 48, 62). Numerous groups have investigated the contribution of apoptosis to the pathogenesis of heart failure in various animal models (including transgenic constructs) as well as in human tissues from patients undergoing transplantation (9, 22, 36, 45; reviewed extensively in reference 31). Although the results vary depending on the model employed, the bulk of the evidence suggests an association of cardiac myocyte apoptosis with heart failure. Recent studies provided evidence that myocyte apoptosis may be a causal mechanism of heart failure and that the inhibition of cardiac apoptosis by the manipulation of

FIG. 7. Myocardial injury, apoptosis, and viral load in 8B-infected caspase-3-deficient transgenic animals. Two-day-old homozygous and heterozygous caspase-3-deficient transgenic mice and wild-type controls were infected with myocarditis reovirus. The animals were sacrificed on day 7 postinfection, and consecutive 4- $\mu$ m-thick sections were analyzed for histologic injury (H&E staining), activated caspase-3 (brown staining), and the presence of virus (fluorescent green staining). (a to c) Consecutive sections from a representative wild-type control animal. (d to f) Consecutive sections from a representative homozygous caspase-3-deficient transgenic animal. (g) TUNEL staining (brown) in representative wild-type and caspase-3-deficient infected animals. (h) Quantitation of myocardial injury in infected wild-type, homozygous, and heterozygous transgenic animals ( $n = 32$ ). \* $P < 0.05$ . (i) Tissue viral titers in infected wild-type, homozygous, and heterozygous transgenic animals at 7 days postinfection ( $n = 11$ ).  $P < 0.01$ . Bar = 2.5 mm.

caspases largely prevents the development of cardiac dilation and contractile dysfunction (24, 60). Evidence has accumulated to indicate an important role for the activation of the adrenergic system in the regulation of cardiomyocyte apoptosis (8, 29, 65). The extent to which apoptosis occurs and its contribution as a determinant of the severity and progression of heart failure, such as in the transition from compensated hypertrophy, warrant further study.

It was previously demonstrated that apoptosis is present within cardiac lesions after reovirus infection (14). We have now shown that caspase-3 activation is detected in tight temporal and spatial association with the development of tissue injury, indicating that apoptosis is an integral mechanism of the pathological injury itself rather than a delayed effect after virus-induced tissue injury. We did not detect caspase activation preceding the time points at which histological injury was evident, suggesting that caspase activation coincided with or occurred less than 24 h preceding injury. The demonstration that cardiac myocytes underwent significant increases in baseline levels of apoptosis and caspase-3 activity after viral infection *in vitro* was consistent with the degree of apoptotic damage observed in the myocardium after viral infection *in vivo*.

Caspase inhibition may be achieved by means of pharmacologic inhibitors or genetic manipulation. Both interventional approaches resulted in significant reductions in virus-induced myocardial injury, with more efficacy observed in genetically altered animals. Caspase inhibition could potentially interfere with virus-induced tissue damage on several fronts. One possibility is that protection is conferred by inhibition of the apoptotic program itself, independent of the effects on viral replication. Alternatively, apoptosis might be required for optimal viral replication and spread (as a means of evading the host immune response's viral clearance mechanisms), and the inhibition of apoptosis might result in a reduction in the ability of the virus to replicate and spread to target tissues. Data from our experiments suggest that both mechanisms may be operative. In the case of pharmacologic inhibition, substantial reductions in myocardial injury occurred in treated animals and were accompanied by only small reductions in organ viral titers (0.5 to 0.7 log<sub>10</sub> PFU/ml). Although they were modestly reduced, the titers achieved in all organs, including the heart, were still 3 to 4 log higher than the input viral titer at the primary site of inoculation in these animals, which is indicative of active viral replication and spread despite caspase inhibition. In caspase-3-deficient mice, more dramatic reductions in viral titers were observed in the limb and heart (1.2 and 1.9 log<sub>10</sub> PFU/ml, respectively), suggesting the possibility that apoptosis may be a requirement for optimal viral replication and spread. The specific mechanism by which caspase activity contributes to optimal viral replication and spread is not known, but it does not appear to be at the level of viral uncoating, since the efficacy of caspase inhibitors was not diminished in the setting of infection with ISVPs.

Increased survival was observed for infected caspase-3-deficient mice, but not for those who were treated with pharmacologic inhibitors. This may be due, at least in part, to the fact that the continued dosing of pharmacologic inhibitors was not feasible beyond day 6 postinfection because of the toxicities of the drugs and/or vehicles. Although a significant proportion of caspase-3-deficient mice lived indefinitely, the majority exhib-

ited substantially prolonged survival after infection with myocarditic virus but subsequently died. It is not clear if the mice with delayed death succumbed to delayed cardiac injury or to an alternate cause such as virus-induced hepatic injury, which may be unaffected by caspase-3 manipulation. Further study is required to identify the organ-specific signaling processes by which these diseases occur. In the case of caspase-3-deficient mice, it is possible that virus-induced apoptotic myocardial injury still occurred but was significantly delayed or blunted pending compensation by potential substitute effector caspases. From a therapeutic standpoint, such a delay in the tempo of tissue destruction would be advantageous to the host, allowing a broader window of opportunity for the development of immune responses and viral clearance.

In summary, these experiments shed light on the basic pathogenesis of viral myocarditis and have direct therapeutic implications for the treatment of this and other diseases involving apoptotic tissue damage. Studies are in progress to identify the intermediary signaling pathways leading to apoptosis after viral infection in cardiac cells and tissues. The inhibition of apoptotic signaling may provide a novel therapeutic strategy to prevent or limit cell death and to minimize tissue damage in the infected host. The development of new treatment approaches is urgently needed for serious viral infections, such as myocarditis, which result in irreversible cell damage and loss, since effective specific antiviral therapies are currently unavailable.

#### ACKNOWLEDGMENTS

Research support was provided by the National Institutes of Health (5K08AI052261-02 to R.D.B.; HL66399 to C.S.L.), the U.S. Army Medical Research Acquisition Activity grant DAMD 17-98-1-8614 to K.L.T., Merit and REAP grants from the Department of Veterans Affairs (K.L.T.), and the Reuler-Lewin Family Professorship of Neurology (K.L.T.).

#### REFERENCES

- Alter, P., M. Jobmann, E. Meyer, S. Pankuweit, and B. Maisch. 2001. Apoptosis in myocarditis and dilated cardiomyopathy: does enterovirus genome persistence protect from apoptosis? An endomyocardial biopsy study. *Cardiovasc. Pathol.* **10**:229-234.
- Bialik, S., V. L. Cryns, A. Drincic, S. Miyata, A. L. Wollowick, A. Srinivasan, and R. N. Kitsis. 1999. The mitochondrial apoptotic pathway is activated by serum and glucose deprivation in cardiac myocytes. *Circ. Res.* **85**:403-414.
- Bialik, S., D. L. Geenen, I. E. Sasson, R. Cheng, J. W. Horner, S. M. Evans, E. M. Lord, C. J. Koch, and R. N. Kitsis. 1997. Myocyte apoptosis during acute myocardial infarction in the mouse localizes to hypoxic regions but occurs independently of p53. *J. Clin. Investig.* **100**:1363-1372.
- Bishopric, N. H., P. Andreka, T. Slepak, and K. A. Webster. 2001. Molecular mechanisms of apoptosis in the cardiac myocyte. *Curr. Opin. Pharmacol.* **1**:141-150.
- Bueno, O. F., L. J. De Windt, K. M. Tymitz, S. A. Witt, T. R. Kimball, R. Klevitsky, T. E. Hewett, S. P. Jones, D. J. Lefer, C. F. Peng, R. N. Kitsis, and J. D. Molkentin. 2000. The MEK1-ERK1/2 signaling pathway promotes compensated cardiac hypertrophy in transgenic mice. *EMBO J.* **19**:6341-6350.
- Caforio, A. L., N. J. Mahon, F. Tona, and W. J. McKenna. 2002. Circulating cardiac autoantibodies in dilated cardiomyopathy and myocarditis: pathogenic and clinical significance. *Eur. J. Heart Fail.* **4**:411-417.
- Caserta, T. M., A. N. Smith, A. D. Gultee, M. A. Reedy, and T. L. Brown. 2003. Q-VD-OPh, a broad spectrum caspase inhibitor with potent antiapoptotic properties. *Apoptosis* **8**:345-352.
- Chesley, A., M. S. Lundberg, T. Asai, R. P. Xiao, S. Ohtani, E. G. Lakatta, and M. T. Crow. 2000. The beta(2)-adrenergic receptor delivers an antiapoptotic signal to cardiac myocytes through G(i)-dependent coupling to phosphatidylinositol 3'-kinase. *Circ. Res.* **87**:1172-1179.
- Chiu, H. C., A. Kovacs, D. A. Ford, F. F. Hsu, R. Garcia, P. Herrero, J. E.

- Saffitz, and J. E. Schaffer.** 2001. A novel mouse model of lipotoxic cardiomyopathy. *J. Clin. Investig.* **107**:813–822.
10. **Chow, L. H., K. W. Beisel, and B. M. McManus.** 1992. Enteroviral infection of mice with severe combined immunodeficiency. Evidence for direct viral pathogenesis of myocardial injury. *Lab Investig.* **66**:24–31.
  11. **Colston, J. T., B. Chandrasekar, and G. L. Freeman.** 1998. Expression of apoptosis-related proteins in experimental coxsackievirus myocarditis. *Cardiovasc. Res.* **38**:158–168.
  12. **Condorelli, G., R. Roncarati, J. Ross, Jr., A. Pisani, G. Stassi, M. Todaro, S. Trocha, A. Drusco, Y. Gu, M. A. Russo, G. Frati, S. P. Jones, D. J. Lefer, C. Napoli, and C. M. Croce.** 2001. Heart-targeted overexpression of caspase-3 in mice increases infarct size and depresses cardiac function. *Proc. Natl. Acad. Sci. USA* **98**:9977–9982.
  13. **DeBiasi, R. L., P. Clarke, S. Meintzer, R. Jotte, B. K. Kleinschmidt-Demasters, G. L. Johnson, and K. L. Tyler.** 2003. Reovirus-induced alteration in expression of apoptosis and DNA repair genes with potential roles in viral pathogenesis. *J. Virol.* **77**:8934–8947.
  14. **DeBiasi, R. L., C. L. Edelstein, B. Sherry, and K. L. Tyler.** 2001. Calpain inhibition protects against virus-induced apoptotic myocardial injury. *J. Virol.* **75**:351–361.
  15. **DeBiasi, R. L., B. K. Kleinschmidt-Demasters, S. Richardson-Burns, and K. L. Tyler.** 2002. Central nervous system apoptosis in human herpes simplex virus and cytomegalovirus encephalitis. *J. Infect. Dis.* **186**:1547–1557.
  16. **De Windt, L. J., H. W. Lim, T. Taigen, D. Wencker, G. Condorelli, G. W. Dorn, R. N. Kitsis, and J. D. Molkentin.** 2000. Calcineurin-mediated hypertrophy protects cardiomyocytes from apoptosis in vitro and in vivo: an apoptosis-independent model of dilated heart failure. *Circ. Res.* **86**:255–263.
  17. **Fairweather, D., Z. Kaya, G. R. Shellam, C. M. Lawson, and N. R. Rose.** 2001. From infection to autoimmunity. *J. Autoimmun.* **16**:175–186.
  18. **Feldman, A. M., and D. McNamara.** 2000. Myocarditis. *N. Engl. J. Med.* **343**:1388–1398.
  19. **Fliss, H., and D. Gattinger.** 1996. Apoptosis in ischemic and reperfused rat myocardium. *Circ. Res.* **79**:949–956.
  20. **Freeman, G. L., J. T. Colston, M. Zabalgoitia, and B. Chandrasekar.** 1998. Contractile depression and expression of proinflammatory cytokines and iNOS in viral myocarditis. *Am. J. Physiol.* **274**:H249–H258.
  21. **Freude, B., T. N. Masters, F. Robicsek, A. Fokin, S. Kostin, R. Zimmermann, C. Ullmann, S. Lorenz-Meyer, and J. Schaper.** 2000. Apoptosis is initiated by myocardial ischemia and executed during reperfusion. *J. Mol. Cell Cardiol.* **32**:197–208.
  22. **Frustaci, A., J. Kajstura, C. Chimenti, I. Jakoniuk, A. Leri, A. Maseri, B. Nadal-Ginard, and P. Anversa.** 2000. Myocardial cell death in human diabetes. *Circ. Res.* **87**:1123–1132.
  23. **Fujio, Y., T. Nguyen, D. Wencker, R. N. Kitsis, and K. Walsh.** 2000. Akt promotes survival of cardiomyocytes in vitro and protects against ischemia-reperfusion injury in mouse heart. *Circulation* **101**:660–667.
  24. **Hayakawa, Y., M. Chandra, W. Miao, J. Shirani, J. H. Brown, G. W. Dorn, R. C. Armstrong, and R. N. Kitsis.** 2003. Inhibition of cardiac myocyte apoptosis improves cardiac function and abolishes mortality in the peripartum cardiomyopathy of Galphac(q) transgenic mice. *Circulation* **108**:3036–3041.
  25. **Hill, S. L., and N. R. Rose.** 2001. The transition from viral to autoimmune myocarditis. *Autoimmunity* **34**:169–176.
  26. **Holly, T. A., A. Drinicic, Y. Byun, S. Nakamura, K. Harris, F. J. Klocke, and V. L. Cryns.** 1999. Caspase inhibition reduces myocyte cell death induced by myocardial ischemia and reperfusion in vivo. *J. Mol. Cell Cardiol.* **31**:1709–1715.
  27. **Huber, S. A., R. C. Budd, K. Rossner, and M. K. Newell.** 1999. Apoptosis in coxsackievirus B3-induced myocarditis and dilated cardiomyopathy. *Ann. N. Y. Acad. Sci.* **887**:181–190.
  28. **Huber, S. A., C. J. Gauntt, and P. Saksinen.** 1998. Enteroviruses and myocarditis: viral pathogenesis through replication, cytokine induction, and immunopathogenicity. *Adv. Virus Res.* **51**:35–80.
  29. **Iwai-Kanai, E., K. Hasegawa, M. Araki, T. Kakita, T. Morimoto, and S. Sasayama.** 1999. Alpha- and beta-adrenergic pathways differentially regulate cell type-specific apoptosis in rat cardiac myocytes. *Circulation* **100**:305–311.
  30. **James, T. N.** 1999. Apoptosis in cardiac disease. *Am. J. Med.* **107**:606–620.
  31. **Kajstura, J., W. Cheng, K. Reiss, W. A. Clark, E. H. Sonnenblick, S. Krajewski, J. C. Reed, G. Olivetti, and P. Anversa.** 1996. Apoptotic and necrotic myocyte cell deaths are independent contributing variables of infarct size in rats. *Lab. Investig.* **74**:86–107.
  32. **Kawai, C.** 1999. From myocarditis to cardiomyopathy: mechanisms of inflammation and cell death: learning from the past for the future. *Circulation* **99**:1091–1100.
  33. **Knowlton, K. U., and C. Badorff.** 1999. The immune system in viral myocarditis: maintaining the balance. *Circ. Res.* **85**:559–561.
  34. **Krammer, P. H.** 2000. CD95's deadly mission in the immune system. *Nature* **407**:789–795.
  35. **Kurrelmeyer, K. M., L. H. Michael, G. Baumgarten, G. E. Taffet, J. J. Peschon, N. Sivasubramanian, M. L. Entman, and D. L. Mann.** 2000. Endogenous tumor necrosis factor protects the adult cardiac myocyte against ischemic-induced apoptosis in a murine model of acute myocardial infarction. *Proc. Natl. Acad. Sci. USA* **97**:5456–5461.
  36. **Latif, N., M. A. Khan, E. Birks, A. O'Farrell, J. Westbrook, M. J. Dunn, and M. H. Yacoub.** 2000. Upregulation of the Bcl-2 family of proteins in end stage heart failure. *J. Am. Coll. Cardiol.* **35**:1769–1777.
  37. **Liu, Y., and R. N. Kitsis.** 1996. Induction of DNA synthesis and apoptosis in cardiac myocytes by E1A oncoprotein. *J. Cell Biol.* **133**:325–334.
  38. **Maisch, B., A. D. Ristic, G. Hufnagel, and S. Pankuweit.** 2002. Pathophysiology of viral myocarditis: the role of humoral immune response. *Cardiovasc. Pathol.* **11**:112–122.
  39. **Matsumori, A., and S. Sasayama.** 2001. The role of inflammatory mediators in the failing heart: immunomodulation of cytokines in experimental models of heart failure. *Heart Fail. Rev.* **6**:129–136.
  40. **McManus, B. M., L. H. Chow, J. E. Wilson, D. R. Anderson, J. M. Gulizia, C. J. Gauntt, K. E. Klingel, K. W. Beisel, and R. Kandolf.** 1993. Direct myocardial injury by enterovirus: a central role in the evolution of murine myocarditis. *Clin. Immunol. Immunopathol.* **68**:159–169.
  41. **Meier, P., A. Finch, and G. Evan.** 2000. Apoptosis in development. *Nature* **407**:796–801.
  42. **Melnikov, V. Y., S. Faubel, B. Siegmund, M. S. Lucia, D. Ljubanovic, and C. L. Edelstein.** 2002. Neutrophil-independent mechanisms of caspase-1- and IL-18-mediated ischemic acute tubular necrosis in mice. *J. Clin. Investig.* **110**:1083–1091.
  43. **Miao, W., Z. Luo, R. N. Kitsis, and K. Walsh.** 2000. Intracoronary, adenovirus-mediated Akt gene transfer in heart limits infarct size following ischemia-reperfusion injury in vivo. *J. Mol. Cell Cardiol.* **32**:2397–2402.
  44. **Mocanu, M. M., G. F. Baxter, and D. M. Yellon.** 2000. Caspase inhibition and limitation of myocardial infarct size: protection against lethal reperfusion injury. *Br. J. Pharmacol.* **130**:197–200.
  45. **Narula, J., P. Pandey, E. Arbustini, N. Haider, N. Narula, F. D. Kolodgie, B. Dal Bello, M. J. Semigran, A. Bielsa-Masdeu, G. W. Dec, S. Israels, M. Ballester, R. Virmani, S. Saxena, and S. Kharbanda.** 1999. Apoptosis in heart failure: release of cytochrome c from mitochondria and activation of caspase-3 in human cardiomyopathy. *Proc. Natl. Acad. Sci. USA* **96**:8144–8149.
  46. **Neuss, M., M. T. Crow, A. Chesley, and E. G. Lakatta.** 2001. Apoptosis in cardiac disease—what is it—how does it occur. *Cardiovasc. Drugs Ther.* **15**:507–523.
  47. **Oberhaus, S. M., R. L. Smith, G. H. Clayton, T. S. Dermody, and K. L. Tyler.** 1997. Reovirus infection and tissue injury in the mouse central nervous system are associated with apoptosis. *J. Virol.* **71**:2100–2106.
  48. **Okamura, T., T. Miura, G. Takemura, H. Fujiwara, H. Iwamoto, S. Kawamura, M. Kimura, Y. Ikeda, M. Iwatake, and M. Matsuzaki.** 2000. Effect of caspase inhibitors on myocardial infarct size and myocyte DNA fragmentation in the ischemia-reperfused rat heart. *Cardiovasc. Res.* **45**:642–650.
  49. **Olivetti, G., R. Abbi, F. Quaini, J. Kajstura, W. Cheng, J. A. Nitahara, E. Quaini, C. Di Loreto, C. A. Beltrami, S. Krajewski, J. C. Reed, and P. Anversa.** 1997. Apoptosis in the failing human heart. *N. Engl. J. Med.* **336**:1131–1141.
  50. **Palmer, J. N., W. E. Hartogensis, M. Patten, F. D. Fortuin, and C. S. Long.** 1995. Interleukin-1 beta induces cardiac myocyte growth but inhibits cardiac fibroblast proliferation in culture. *J. Clin. Investig.* **95**:2555–2564.
  51. **Patten, M., W. Wang, S. Aminololama-Shakeri, M. Burson, and C. S. Long.** 2000. IL-1 beta increases abundance and activity of the negative transcriptional regulator yin yang-1 (YY1) in neonatal rat cardiac myocytes. *J. Mol. Cell Cardiol.* **32**:1341–1352.
  52. **Rose, N. R.** 2000. Viral damage or “molecular mimicry”—placing the blame in myocarditis. *Nat. Med.* **6**:631–632.
  53. **Seko, Y., N. Takahashi, M. Azuma, H. Yagita, K. Okumura, and Y. Yazaki.** 1998. Expression of costimulatory molecule CD40 in murine heart with acute myocarditis and reduction of inflammation by treatment with anti-CD40L/B7-1 monoclonal antibodies. *Circ. Res.* **83**:463–469.
  54. **Shen, Y., and T. E. Shenk.** 1995. Viruses and apoptosis. *Curr. Opin. Genet. Dev.* **5**:105–111.
  55. **Sherry, B.** 1998. Pathogenesis of reovirus myocarditis. *Curr. Top. Microbiol. Immunol.* **233**:51–66.
  56. **Sherry, B., C. J. Baty, and M. A. Blum.** 1996. Reovirus-induced acute myocarditis in mice correlates with viral RNA synthesis rather than generation of infectious virus in cardiac myocytes. *J. Virol.* **70**:6709–6715.
  57. **Sherry, B., X. Y. Li, K. L. Tyler, J. M. Cullen, and H. W. Virgin.** 1993. Lymphocytes protect against and are not required for reovirus-induced myocarditis. *J. Virol.* **67**:6119–6124.
  58. **Sherry, B., F. J. Schoen, E. Wenske, and B. N. Fields.** 1989. Derivation and characterization of an efficiently myocarditic reovirus variant. *J. Virol.* **63**:4840–4849.
  59. **Shizukuda, Y., P. M. Buttrick, D. L. Geenen, A. C. Boreczuk, R. N. Kitsis, and E. H. Sonnenblick.** 1998. Beta-adrenergic stimulation causes cardiocyte apoptosis: influence of tachycardia and hypertension. *Am. J. Physiol.* **275**:H961–H968.
  60. **Wencker, D., M. Chandra, K. Nguyen, W. Miao, S. Garantziotis, S. M. Factor, J. Shirani, R. C. Armstrong, and R. N. Kitsis.** 2003. A mechanistic

- role for cardiac myocyte apoptosis in heart failure. *J. Clin. Investig.* **111**: 1497–1504.
61. Yang, D., J. Yu, Z. Luo, C. M. Carthy, J. E. Wilson, Z. Liu, and B. M. McManus. 1999. Viral myocarditis: identification of five differentially expressed genes in coxsackievirus B3-infected mouse heart. *Circ. Res.* **84**:704–712.
  62. Yaoita, H., K. Ogawa, K. Maehara, and Y. Maruyama. 1998. Attenuation of ischemia/reperfusion injury in rats by a caspase inhibitor. *Circulation* **97**:276–281.
  63. Yeh, E. T. 1997. Life and death in the cardiovascular system. *Circulation* **95**:782–786.
  64. Yuan, J., and B. A. Yankner. 2000. Apoptosis in the nervous system. *Nature* **407**:802–809.
  65. Zhu, W. Z., M. Zheng, W. J. Koch, R. J. Lefkowitz, B. K. Kobilka, and R. P. Xiao. 2001. Dual modulation of cell survival and cell death by beta(2)-adrenergic signaling in adult mouse cardiac myocytes. *Proc. Natl. Acad. Sci. USA* **98**:1607–1612.



Available online at [www.sciencedirect.com](http://www.sciencedirect.com)

SCIENCE @ DIRECT®

Virology 322 (2004) 231–238

VIROLOGY

[www.elsevier.com/locate/yviro](http://www.elsevier.com/locate/yviro)

## Does Toll-like receptor 3 play a biological role in virus infections?

Kurt H. Edelmann,<sup>a</sup> Sarah Richardson-Burns,<sup>b</sup> Lena Alexopoulou,<sup>c</sup> Kenneth L. Tyler,<sup>d</sup> Richard A. Flavell,<sup>c</sup> and Michael B.A. Oldstone<sup>a,\*</sup>

<sup>a</sup>Division of Virology, Department of Neuropharmacology, The Scripps Research Institute, La Jolla, CA 92037, USA

<sup>b</sup>Program in Neuroscience, University of Colorado Health Sciences Center, Denver, CO 80262, USA

<sup>c</sup>Section of Immunobiology and the Howard Hughes Medical Institute, Department of Internal Medicine, Yale University School of Medicine, New Haven, CT 06520-8056, USA

<sup>d</sup>Departments of Neurology, Medicine, Microbiology and Immunology, University of Colorado Health Sciences Center, Denver, CO 80262, USA

Received 4 September 2003; returned to author for revision 31 December 2003; accepted 27 January 2004

### Abstract

The Toll-like receptor (TLR) family functions to recognize conserved microbial and viral structures with the purpose of activating signal pathways to instigate immune responses against infections by these organisms. For example, in vitro studies reveal that the TLR3 ligand is a double-stranded RNA (dsRNA), a product of viral infections. From this observation, it has been proposed that TLR3 is likely an important first signal for virus infections. We approached this issue by investigating the role of TLR3 in four different infectious viral models (lymphocytic choriomeningitis virus (LCMV), vesicular stomatitis virus (VSV), murine cytomegalovirus (MCMV), and reovirus) and in TLR3 genetically deficient ( $-/-$ ) mice. Our results indicate that TLR3 is not universally required for the generation of effective antiviral responses because the absence of TLR3 does not alter either viral pathogenesis or impair host's generation of adaptive antiviral responses to these viruses.

© 2004 Elsevier Inc. All rights reserved.

**Keywords:** Toll-like receptor 3; Virus; Mice

### Introduction

Ten distinct mammalian Toll-like receptors (TLRs) have been described, most of which have been shown to function as receptors for pathogen-associated molecular patterns (Akira and Hemmi, 2003; Takeda et al., 2003). These receptors aid the host to combat infection as microbial ligands upon binding to various TLRs on antigen-presenting cells (APCs) trigger NF- $\kappa$ B leading to the upregulation of cytokines and co-stimulatory molecules with the presumed purpose of initially enhancing innate immune attack against the pathogen from which that ligand is derived (Aderem and Ulevitch, 2000; Anderson, 2000; Hallman et al., 2001; Kopp and Medzhitov, 1999). It has been hypothesized that loss of function of particular TLRs causes the host to become more susceptible to infections with TLR-reactive pathogens. Evidence supporting this concept comes from observations

where the loss of TLR2 has resulted in increased susceptibility to *Staphylococcus aureus* infections (Takeuchi et al., 2000), loss of TLR9 resulted in ablation of the immunostimulatory properties of bacterial DNA (Hemmi et al., 2000), and loss of TL4 resulted in increased susceptibility to respiratory syncytial virus (Kurt-Jones et al., 2000). These results led to the proposal that TLR3, a receptor demonstrated to be reactive to double-stranded (ds) RNA (Alexopoulou et al., 2001; Matsumoto et al., 2002), a frequent byproduct of virus replication, functions as a universal virus receptor for priming the innate immune system to viral infections.

Of the TLRs studied, only TLR3 has been identified to respond to dsRNA (Alexopoulou et al., 2001) by specifically recognizing poly (I:C) and purified Lang reovirus genomic dsRNA, both of which resulted in the induction of IFN- $\beta$ , IL-12, IL-6, and TNF $\alpha$  from macrophages obtained from TLR3-sufficient mice. The ability of TLR3 to induce IFN- $\beta$  has been attributed to at least two factors: its MyD88-independent activation of IRF3 and to its induction of the traditional dsRNA-dependent protein kinase (PKR) pathway (Doyle et al., 2002; Horng et al., 2001; Oshiumi et al., 2003). Recognition of dsRNA ligand has been demonstrated to

\* Corresponding author. Division of Virology, Department of Neuropharmacology, The Scripps Research Institute, 10550 N. Torrey Pines Road, IMM-6, La Jolla, CA 92037-1092. Fax: +1-858-784-9981.

E-mail address: [mbaobo@scripps.edu](mailto:mbaobo@scripps.edu) (M.B.A. Oldstone).

occur extracellularly by TLR3-blocking antibodies that prevented TLR3-mediated responses to poly (I:C) in vitro (Matsumoto et al., 2002). In vivo studies using TLR3-deficient ( $-/-$ ) mice showed protection of such mice from shock induced by poly (I:C) treatment, suggesting this receptor contributed to the in vivo recognition of and responses to extracellular dsRNA (Alexopoulou et al., 2001). Furthermore, it was shown that the effector responses elicited by TLR3–poly (I:C) interaction can inhibit murine  $\gamma$  herpesvirus 68 replication in bone marrow-derived macrophage cultures (Doyle et al., 2002). Based on the above findings, it has been repeatedly assumed that TLR3 likely played an important role in host defense against virus infections (Akira and Hemmi, 2003; Alexopoulou et al., 2001; Doyle et al., 2002; Harte et al., 2003; Matsumoto et al., 2002; Renshaw et al., 2002). However, it has not yet been determined if the physiologic amounts of dsRNA naturally made during viral infections per se were sufficient to trigger through TLR3 a biologically meaningful response to alter the outcome of disease. We set out to experimentally determine if TLR3 is essential for antiviral immunity or if TLR3 represents an expendable level of redundancy built into the dsRNA recognition system. Here we report our work that directly tests this hypothesis by studying both host immune responses and control of infection by a dsRNA virus, reovirus; two ssRNA viruses that make dsRNA intermediates, lymphocytic choriomeningitis virus (LCMV) and vesicular stomatitis virus (VSV); and a DNA virus, murine cytomegalovirus (MCMV), in TLR3 gene-disrupted mice. Our results indicate that TLR3 does not play a critical role in the host antiviral adaptive immune response to reovirus, LCMV, VSV, or MCMV as susceptibility to infection and generation of CD4 and CD8 T cell immune responses to these viruses are equivalent in TLR3-deficient and -sufficient mice.

## Results and discussion

Our initial experiments studied the primary adaptive immune responses to LCMV infection in TLR3 $-/-$  mice. LCMV is an arenavirus containing a genome consisting of two negative-stranded RNAs and like the other viruses investigated in this report is able to trigger Type-I IFNs. Control of acute LCMV infection is totally mediated by virus-specific CD8 $+$  T cells through a perforin-mediated pathway (Anderson et al., 1985; Kagi et al., 1995). To test if TLR3 plays a role in the immune response to LCMV, TLR3 $-/-$  mice and control C57Bl/6 (B6)  $\times$  129 mixed background mice bred at TSRI vivarium were inoculated intraperitoneally with  $1 \times 10^5$  pfu LCMV ARM53b. IFN $\gamma$  responses from LCMV-specific T cells were assessed 8 days postinfection via intracellular cytokine staining and flow cytometry following a 5-h culture of splenocytes with brefeldin A, rIL2, and CD8 and CD4 LCMV-specific H-2 $b$ -specific peptide epitopes, GP61 (aa GP61–80) and GP33 (aa GP33–41), respectively

(Hudrisier et al., 1997; Murali-Krishna et al., 1998; Whitmire et al., 1998). TLR3 $-/-$  mice showed no difference compared to controls in their ability to generate both a robust CD8 $+$  and CD4 $+$  IFN $\gamma$  response to LCMV (Fig. 1A). Furthermore, LCMV-specific CD8 $+$  T cells from TLR3 $-/-$  mice also displayed normal lysis of GP33 peptide-coated H-2 $b$ -MC57 targets cells (Fig. 1B).

Hosts usually encounter pathogens during natural infections at significantly lower concentrations than utilized in many laboratory infectious models. To investigate a role for TLR3 during a low-level infection, we conducted experiments in which both the dose and route of inoculation of LCMV were varied. A series of ip and foot pad inoculations with doses of LCMV ranging from as little as  $1 \times 10^2$  to  $5 \times 10^5$  pfu LCMV were carried out and CD8 $+$  T cell IFN $\gamma$  responses from both the draining lymph nodes and spleen were analyzed (Fig. 1C). Intravenous injection of a very high dose of LCMV ( $2 \times 10^6$  pfu) was also analyzed (data not shown); however, irrespective of the route and dose of virus inoculation, the absence of TLR3 did not affect the generation of the primary cellular response to LCMV.

We next assayed the primary T cell responses to a RNA virus, VSV, and a DNA virus, MCMV, in TLR3 $-/-$  mice. VSV, a member of the Rhabdovirus family, contains a single-stranded negative-sense RNA genome, and control of VSV in mice is dependent on the generation of virus-specific antibodies and complement (Lefrancois, 1984; Steinhoff et al., 1995). Furthermore, VSV infection leads to induction of Type-I IFNs triggered, in part, by the prevalence of structured dsRNA-defective interfering particles found during VSV infection (Holland, 1987). We found that TLR3 $-/-$  mice handle VSV infection as well as B6  $\times$  129 control mice. Mice infected with VSV generated both CD4 $+$  and CD8 $+$  VSV-specific T cell responses to peptides NP415 and NP52, respectively (Fig. 2A), and were able to clear the virus (data not shown). MCMV is a dsDNA herpes virus that, like LCMV, is a natural pathogen of mice. MCMV infection of susceptible strains of mice results in lifelong latent infection punctuated by spontaneous reactivation from the latent state. Protection of the host from lethal MCMV infection is complex requiring contributions from both the innate and adaptive immune response (Koszinowski et al., 1990). The effect of the loss of TLR3 on the T cell response to MCMV in TLR3 $-/-$  mice was analyzed day 9 postinfection with  $1 \times 10^4$  pfu ip. T cell IFN $\gamma$  responses were measured after 5-h culture in  $\alpha$ CD3-coated wells because there are no currently defined H-2 $b$  T cell peptide epitopes for MCMV. These analyses did not identify differences between control and TLR3 $-/-$  mice in the primary T cell response to MCMV (Fig. 2B). Furthermore, the spleens from these mice were free of virus, indicating that the absence of TLR3 did not increase the susceptibility to MCMV (data not shown).

Next we determined the role TLR3 played in functional T cell memory responses. Intravenous inoculation of naive or immunosuppressed mice with LCMV variant Cl 13 ( $2 \times 10^6$  pfu) leads to establishment of persistent infection

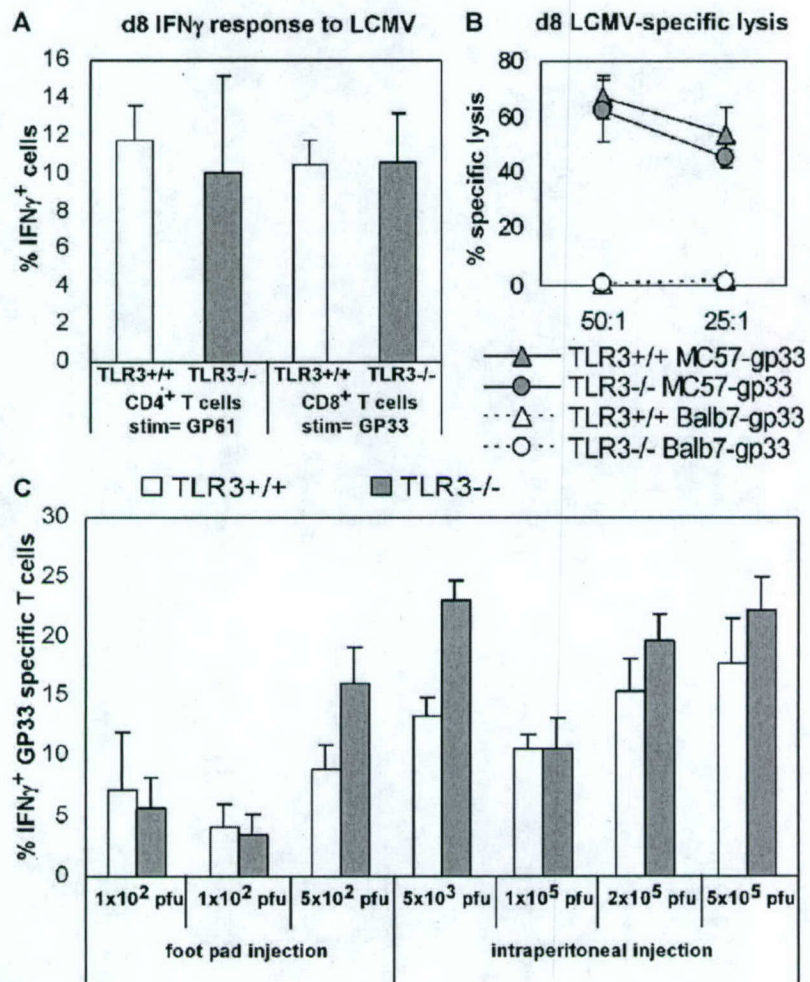


Fig. 1. Absence of TLR3 does not affect primary CD4<sup>+</sup> or CD8<sup>+</sup> T cell responses to LCMV. TLR3<sup>-/-</sup> mice and control mice ( $n = 3$  mice per group) were infected with LCMV ARM53b ( $1 \times 10^5$  pfu ip), infection with TLR3<sup>-/-</sup> and control splenocytes was obtained 8 days later. (A) Cells were stimulated in vitro with either LCMV-specific CD4<sup>+</sup> or CD8<sup>+</sup> T cell peptide epitopes in the presence of brefeldin A. IFN $\gamma$  responses were measured by intracellular cytokine staining in combination with CD8<sup>+</sup> and CD4<sup>+</sup> surface staining. Results are represented as percentage of IFN $\gamma$ -positive cells within respective CD4<sup>+</sup> or CD8<sup>+</sup> populations. (B) Measurement of CD8<sup>+</sup> T cell lytic function was assessed via standard chromium release assay against GP33 peptide-coated syngeneic and allogeneic cells; MC57 and BALB17 cells respectively. (C) TLR3<sup>-/-</sup> mice respond efficiently to LCMV irrespective of route and dose of inoculation. TLR3<sup>-/-</sup> and control mice ( $n = 3$ –4 mice per group per condition) were inoculated with LCMV ARM 53b using either foot pad or ip injection and varying doses as indicated. IFN $\gamma$  responses from GP-33-specific T cells were analyzed 8 days postinfection from draining lymph nodes in foot pad-injected mice and splenocytes from ip-injected mice. Results are represented as percent IFN $\gamma$ + CD8<sup>+</sup> T cells of total CD8<sup>+</sup> T cell population. Data represented in A and B are derived from individual experiments while those for C are compiled from several experiments.

(Ahmed et al., 1984). In contrast, mice previously immunized with LCMV ARM53b develop T cell memory responses that are able to prevent establishment of persistent infection by subsequent LCMV Cl 13 challenge (Arbour et al., 2002). TLR3<sup>-/-</sup> mice were tested for the ability to generate a lasting functional memory response to LCMV infection. LCMV immune TLR3<sup>-/-</sup> and control mice ( $1 \times 10^5$  pfu LCMV ARM53b ip) were inoculated 3 months after primary challenge with  $2 \times 10^6$  pfu LCMV Cl 13 via iv injection. The CD4<sup>+</sup> and CD8<sup>+</sup> T cell responses of these mice were analyzed 3 days after inoculation. All mice showed levels of IFN- $\gamma$ + LCMV-specific T cells that were not statistically different, indicating normal induction of the T cell memory response (Fig. 2C).

The last series of studies employed a double-stranded RNA virus infection of neonatal TLR3<sup>-/-</sup> and control mice using Type 3 reovirus strain Dearing (T3D). Intracerebral inoculation of neonatal mice is the classic experimental model for evaluating virulence of neurotropic viruses such as reovirus. We therefore compared mortality, viral titer, antigen distribution, and neuropathology in newborn TLR3<sup>-/-</sup> and control TLR3<sup>+/+</sup> injected intracerebrally with T3D. There was no difference between T3D-infected TLR3<sup>+/+</sup> control mice and T3D-infected TLR3<sup>-/-</sup> mice in virus-induced CNS injury. The localization and the severity of viral CNS pathology were similar in both strains of mice, with the brunt of virus-induced injury present in the CA2–3 region of the hippocampus, cingulate gyrus, fronto-parietal cortex, and

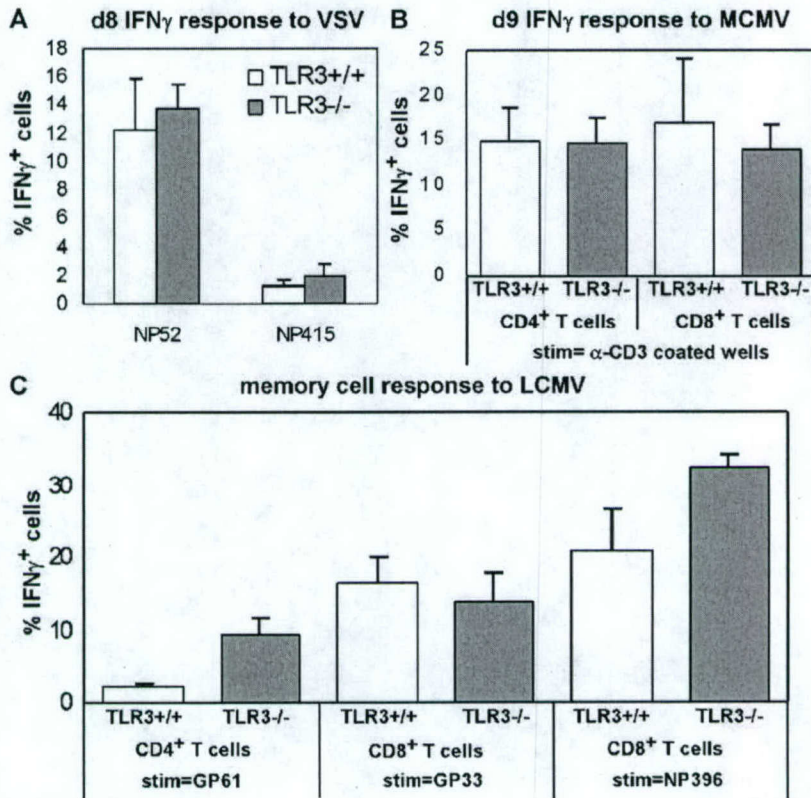


Fig. 2. (A–B) Primary T cell responses to VSV and MCMV are normal in TLR3 $^{-/-}$  mice. Splenocytes were isolated from TLR3 $^{-/-}$  and control mice 8 days postinfection with VSV ( $2 \times 10^6$  pfu iv) or 9 days postinfection with MCMV ( $1 \times 10^4$  pfu ip). Cells from VSV-infected mice were stimulated for 5 h with either CD8-specific peptide epitope NP52 or CD4-specific peptide epitope NP415, while cells from MCMV-infected mice were stimulated with  $\alpha$ -CD3. Groups consisted of 3–4 mice. All data represent averages of results from individual mice derived from three experiments and are represented as percent IFN $\gamma$  $^{+}$  T cells of respective CD8 $^{+}$  or CD4 $^{+}$  T cell populations. (C) TLR3 $^{-/-}$  mice have functional T cell memory responses. TLR3 $^{-/-}$  and control mice ( $n = 2$  per group) were immunized with LCMV Arm 53b ( $1 \times 10^5$  pfu ip). These mice were challenged with LCMV Cl 13 ( $2 \times 10^6$  pfu iv) 3 months after immunization. Splenocytes were isolated 3 days post-secondary challenge, and responses to CD4 peptide epitope GP61 and CD8 peptide epitopes GP33 and NP396 were measured. Results are presented as percent IFN $\gamma$  $^{+}$  cells of either CD4 $^{+}$  or CD8 $^{+}$  cell populations.

dorsal thalamus as previously reported (Figs. 3B–C) (Oberhaus et al., 1997; Raine and Fields, 1973; Richardson-Burns et al., 2002). CNS injury is evidenced by the presence of numerous pyknotic and apoptotic cells, some infiltrating inflammatory cells, disruption of cytoarchitecture, and loss of tissue integrity (see Fig. 3). The viral antigen co-localized with areas of CNS injury with anti-T3D immunohistochemical staining present in the hippocampus, cortex, and thalamus. Fig. 4 shows viral antigen staining in the dorsal thalamus and CA3 region of the hippocampus from T3D-infected TLR3 $^{+/+}$  and TLR3 $^{-/-}$  mice (Fig. 4). There was no difference in survival between T3D-infected TLR3 $^{+/+}$  and control mice. Mortality was 40% by day 7 in TLR3 $^{-/-}$  mice, with all six survivors appearing moribund. Mortality was 37.5% in control TLR3 $^{+/+}$  mice, with all five survivors appearing moribund. Mean weight of mice on day of sacrifice (d7) was 3.53 g for TLR3 $^{-/-}$  mice and 3.90 g for TLR3 $^{+/+}$  control mice. Viral titer in the brain at time of sacrifice was the same in the two groups of mice ( $8.94 \pm 0.06 \log_{10}$  pfu/ml in TLR3 $^{-/-}$  mice compared to  $9.00 \pm 0.13$  in control TLR3 $^{+/+}$  mice).

In summary, our data indicate that the TLR3 signaling pathway does not appear to influence the generation of effective antiviral responses for a range of virus infections, thereby calling into question whether it represents a universal element in antiviral immunity. Although we did not observe enhanced susceptibility with our strain and dose of MCMV, others (Hoebe et al., 2003) using mice deficient in lps2, a downstream component of the TLR3 signaling pathway, noted increased susceptibility to MCMV at higher doses of virus. So it appears that there may be some conditions where TLR3 does enhance immunity, and that it may be restricted to the early control of an overwhelming viral infection requiring a fast and strong IFN type-I innate response to prevent host death. One question that arises from the current studies is whether TLR3 can in fact recognize any component of these viruses. Using an *in vitro* assay where the various TLR genes are transfected and expressed in HeLa and HEK cells, UV-inactivated LCMV Arm 53b and other arenaviruses were unable to activate cells expressing TLR3 while control poly I:C did, again indicating that TLR3 is unlikely to play a role in the

pathogenesis of arenaviruses. However, several of these arenaviruses did activate other TLR receptors (de Silva and Kunz, unpublished observations). It is also possible that TLR3 is not capable of recognizing the viral RNA intermediates of LCMV, VSV, and MCMV. This is not true for reovirus where Alexopoulou et al. (2001) identified TLR3 recognition of purified reovirus genomic dsRNA. Hence, it is possible that during these viral infections, TLR3

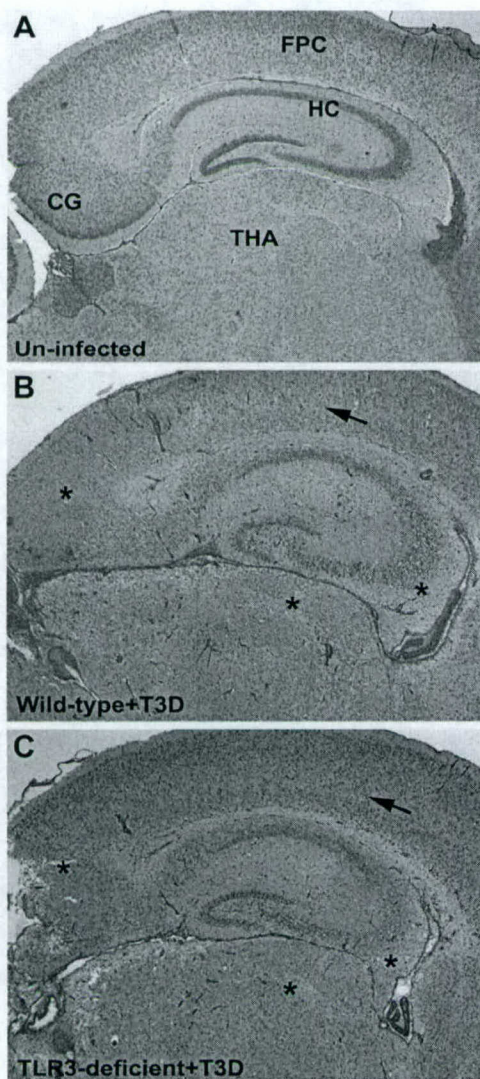


Fig. 3. There is no difference between TLR3-deficient mice and wild-type mice in T3 reovirus-induced injury or T3 reovirus antigen expression in the CNS. (A) Uninfected control mouse brain stained with hematoxylin and eosin (H&E) shows normal CNS cytoarchitecture and normal appearing nuclei of viable cells. (B) H&E-stained brain from T3D-infected TLR3<sup>+/+</sup> wild-type mouse shows characteristic T3 reovirus-associated injury throughout the brain evidenced by cell death, loss of normal cytoarchitecture, and loss of tissue integrity in the cingulate gyrus (CG), fronto-parietal cortex (FPC), hippocampus (HC), and thalamus (THA). (C) H&E-stained brain from T3D-infected TLR3-deficient (TLR3<sup>-/-</sup>) mouse shows T3 reovirus-induced CNS injury comparable to that seen in T3D-infected TLR3<sup>+/+</sup> wild-type mice. \* = brain region with viral injury, cell loss, apoptotic cells, and loss of cytoarchitecture; arrow = brain region with cell loss.

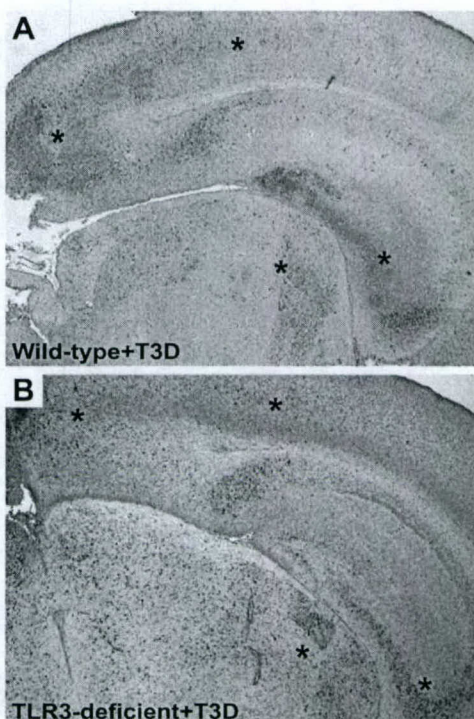


Fig. 4. There is no difference between TLR3-deficient mice and wild-type control mice in T3 reovirus-induced injury in the CNS. (A) Immunohistochemistry (IHC) for T3 reovirus antigen shows numerous T3D-positive cells (dark brown) in brains of T3D-infected TLR3<sup>+/+</sup> wild-type control mice. Antigen staining is evident in the same brain regions in which T3 reovirus injury is present (compare to Fig. 3). (B) IHC for T3 reovirus antigen in brain of T3D-infected TLR3<sup>-/-</sup> mouse shows similar antigen levels to that seen in the T3D-infected TLR3<sup>+/+</sup> wild-type control mouse brains.

never comes in contact with unsequestered or exposed viral RNAs. Alternatively and a more likely scenario is that the concentrations of dsRNA made during natural infection are not sufficient to bind to and significantly influence TLR3 signalling when compared to the high concentrations used for in vitro studies.

## Materials and methods

### Mice

TLR3<sup>-/-</sup> mice on C57BL/6 × B129 mixed background and matched control mice were derived at Yale University and bred at The Scripps Research Institute. Mice were bred and maintained under specific pathogen-free conditions.

### Virus strains

Stocks of both LCMV ARM 53b and variant LCMV Cl 13 were grown up via single passage in baby hamster kidney (BHK) cells from stocks that had been previously triple plaque purified in Vero cells (Ahmed et al., 1984; Dutko and Oldstone, 1983). VSV stocks were generated by collection of

supernatants from 100% CPE VSV-infected BHK-21 cells (Lyles et al., 1992). Stocks of the Smith strain of MCMV of virus derived from in vivo propagation in salivary glands of Balb/c mice were obtained from Dr. Raymond Welsh at the University of Massachusetts Medical School, Worcester, MA (Bukowski et al., 1984). Reovirus strain type 3 Dearing (T3D) was identified, passaged, and quantitated as previously reported (Tyler et al., 1985, 1989).

#### *LCMV, VSV, and MCMV methods*

LCMV ARM 53b was inoculated into mice intraperitoneally with either  $5 \times 10^3$ ,  $1 \times 10^5$ , or  $5 \times 10^5$  pfu where noted. Footpad injection experiments with LCMV ARM 53b were conducted with  $1 \times 10^2$  or  $5 \times 10^2$  pfu virus. Secondary challenges with LCMV Cl 13 were performed intravenously with a dose of virus previously demonstrated to result in persistent infection in naive mice ( $2 \times 10^6$  pfu). In experiments using VSV, the virus was injected intravenously at a dose of  $2 \times 10^6$  pfu. Mice infected with MCMV were inoculated intraperitoneally with  $1 \times 10^4$  pfu virus.

#### *Reovirus methods*

Two-day-old neonatal mice (weight: 1.5–2 g) were used in reovirus T3D studies. Eight control (C57BL/6 × 129) and 10 TLR3<sup>-/-</sup> mice on the same background were infected with  $10^7$  pfu of T3D intracerebrally in a 10-μl volume using a 29-gauge needle connected to a Hamilton microsyringe. Animals were sacrificed for tissue collection at day 7 postinfection, by which time all animals were moribund. Tissue was collected for histology, immunocytochemistry, and determination of viral titer by plaque assay. T3D infected and 5 were not virally infected (uninfected control). Nine TLR3<sup>-/-</sup> mice were T3D infected. Mice were inoculated with T3D ( $1 \times 10^5$  PFU) via intracerebral or intracranial (ic) injection with each mouse pup weighing about 1.7 g. Injections were made using a 29-gauge needle in a 10-μl volume. Animals were sacrificed by decapitation 7 days after infection.

#### *Analysis of T cell responses*

All data represent averages of results from individual mice with 3–5 per group. Splenocytes from LCMV- or VSV-infected mice were cultured for 5 h in RPMI 7% FCS with 50 U/ml rIL2 and 1 μg/ml MHC class-I or class-II restricted peptides. T cells from MCMV mice were cultured for 5 h in α-CD3-coated wells in RPMI 7% FCS + 50 U/ml rIL2. Brefeldin A (1 μg/ml) was added to all cultures at least 3 h before staining. Surface and intracellular staining procedures were performed as previously described using CD4-FITC, CD8-PE, and IFNγ-APC antibodies (Homann et al., 1998). Antibodies used in these experiments were obtained from Pharmingen. CD8<sup>+</sup> T cell cytolytic function was measured by standard 5 h <sup>51</sup>Cr release assay using MC57

and BALB17 mouse fibroblasts coated with LCMV peptide GP33–41 (1-h incubation with 1 μg/ml peptide followed by three washes).

#### *MHC H-2<sup>b</sup> restricted peptides*

Peptides were obtained from PeptidoGenic Research. Peptides used were LCMV MHC Class-I: GP33–41, NP396–404; LCMV MHC Class-II: GP61–80; VSV MHC Class-I: NP52–59; VSV MHC Class-II GP 415–433.

#### *Histology*

For histopathologic and immunohistochemical staining, five or six whole mouse brains per treatment group were fixed by immersion in 10% buffered formalin for 24–30 h at room temperature (RT), then cut in half along the mid-coronal line for sectioning. Fixed tissues were transferred to 70% ethanol, paraffin embedded, and sectioned at 4-μm thickness. For each animal, two coronal sections were stained with hematoxylin and eosin (H&E) for studies of the extent of virus-induced pathology. Paraffin-embedded sections were baked at 57 °C for 5 min to enhance antigen retrieval, then de-paraffinized by immersion in mixed xylenes followed by rehydration in a series of descending ethanol concentrations followed by PBS.

#### *Immunohistochemistry*

Brain tissue sections were de-paraffinized by baking for 5 min at 57 °C, immersion in mixed xylenes, then rehydration in graded alcohols. For viral antigen staining, de-paraffinized tissues were permeabilized in PBS/0.1% Triton X (PBSX) for 1 h at room temperature (RT), then non-specific binding was blocked in 3% BSA/PBS for 1 h at RT. Tissue was incubated with primary antibody anti-T3D polyclonal (laboratory stock) diluted (1:200) in 3% BSA/PBSX for 1 h at 37 °C, then washed in PBSX. Secondary antibody anti-rabbit-Alexafluor594 (Molecular Probes, Eugene OR) diluted 1:100 in 1.5% BSA/PBSX was incubated with tissue for 1 h at RT in the dark. Tissues were washed in PBSX, exposed to Hoechst 33342 (Molecular Probes), diluted in PBS for 5 min at RT, washed in PBSX, then aqueous mounted with Vectashield (Vector Laboratories Inc, Burlingame, CA). All images were captured by digital bright-field or fluorescence microscopy at  $\times 25$ –100 magnification using a Zeiss AxioPlan 2 Digital Microscope with Cooke SensiCam 32 bit Camera.

#### *Determination of viral titer*

Reovirus T3 titer in brain tissue was determined by standard plaque assay techniques on confluent monolayers of L929 fibroblasts. Specimens were frozen ( $-70$  °C) and thawed (RT) three times, briefly sonicated, and then diluted into gelatinized saline. Duplicate aliquots were serially di-

luted in 10-fold steps and samples from at least three consecutive dilutions were inoculated onto L929 cell monolayers. Monolayers were stained with neutral red dye at day 6 postinfection and plaques counted. Viral titer was determined by averaging the number of plaques seen at the most informative dilution and correcting for inoculum size and dilution factor. Results are presented as  $\log_{10}$  plaque forming units (pfu)/ml  $\pm$  SEM.

### Acknowledgments

This work is supported by US Public Health grants from the NIH AI09484 and AI45927 (KHE, MBAO), VA MERIT and REAP Awards (KLT) and Department of Defense Grant DAMD 17-98-1-8614 (SR-B, KLT), Howard Hughes Investigator award (RAF), and NIH training grant NS41219 (KHE). The authors thank Bruce Beutler and Philippe Georgel at TSRI for helpful comments.

### References

- Aderem, A., Ulevitch, R.J., 2000. Toll-like receptors in the induction of the innate immune response. *Nature* 406, 782–787.
- Ahmed, R., Salmi, A., Butler, L.D., Chiller, J.M., Oldstone, M.B., 1984. Selection of genetic variants of lymphocytic choriomeningitis virus in spleens of persistently infected mice. Role in suppression of cytotoxic T lymphocyte response and viral persistence. *J. Exp. Med.* 160, 521–540.
- Akira, S., Hemmi, H., 2003. Recognition of pathogen-associated molecular patterns by TLR family. *Immunol. Lett.* 85, 85–95.
- Alexopoulou, L., Holt, A.C., Medzhitov, R., Flavell, R.A., 2001. Recognition of double-stranded RNA and activation of NF- $\kappa$ B by Toll-like receptor 3. *Nature* 413, 732–738.
- Anderson, K.V., 2000. Toll signaling pathways in the innate immune response. *Curr. Opin. Immunol.* 12, 13–19.
- Anderson, J., Byrne, J.A., Schreiber, R., Patterson, S., Oldstone, M.B., 1985. Biology of cloned cytotoxic T lymphocytes specific for lymphocytic choriomeningitis virus: clearance of virus and in vitro properties. *J. Virol.* 53, 552–560.
- Arbour, N., Naniche, D., Homann, D., Davis, R.J., Flavell, R.A., Oldstone, M.B., 2002. c-Jun NH(2)-terminal kinase (JNK)1 and JNK2 signaling pathways have divergent roles in CD8(+) T cell-mediated antiviral immunity. *J. Exp. Med.* 195, 801–810.
- Bukowski, J.F., Woda, B.A., Welsh, R.M., 1984. Pathogenesis of murine cytomegalovirus infection in natural killer cell-depleted mice. *J. Virol.* 52, 119–128.
- Doyle, S., Vaidya, S., O'Connell, R., Dadgostar, H., Dempsey, P., Wu, T., Rao, G., Sun, R., Haberland, M., Modlin, R., Cheng, G., 2002. IRF3 mediates a TLR3/TLR4-specific antiviral gene program. *Immunity* 17, 251–263.
- Dutko, F.J., Oldstone, M.B., 1983. Genomic and biological variation among commonly used lymphocytic choriomeningitis virus strains. *J. Gen. Virol.* 64, 1689–1698.
- Hallman, M., Ramet, M., Ezekowitz, R.A., 2001. Toll-like receptors as sensors of pathogens. *Pediatr. Res.* 50, 315–321.
- Harte, M.T., Haga, I.R., Maloney, G., Gray, P., Reading, P.C., Bartlett, N.W., Smith, G.L., Bowie, A., O'Neill, L.A., 2003. The poxvirus protein A52R targets Toll-like receptor signaling complexes to suppress host defense. *J. Exp. Med.* 197, 343–351.
- Hemmi, H., Takeuchi, O., Kawai, T., Kaisho, T., Sato, S., Sanjo, H., Matsumoto, M., Hoshino, K., Wagner, H., Takeda, K., Akira, S., 2000. A Toll-like receptor recognizes bacterial DNA. *Nature* 408, 740–745.
- Hoebe, K., Du, X., Georgel, P., Janssen, E., Tabata, K., Kim, S.O., Goode, J., Lin, P., Mann, N., Mudd, S., Crozat, K., Sovath, S., Han, J., Beutler, B., 2003. Identification of Lps2 as a key transducer of MyD88-independent TIR signalling. *Nature* 424, 743–748.
- Holland, J., 1987. Defective-interfering rhabdoviruses. In: Wagner, R. (Ed.), *The Rhabdoviruses*. Plenum, New York, pp. 297–360.
- Homann, D., Tishon, A., Berger, D.P., Weigle, W.O., Von Herrath, M.G., Oldstone, M.B., 1998. Evidence for an underlying CD4 helper and CD8 T-cell defect in B-cell-deficient mice: failure to clear persistent virus infection after adoptive immunotherapy with virus-specific memory cells from muMT/muMT mice. *J. Virol.* 72, 9208–9216.
- Horng, T., Barton, G.M., Medzhitov, R., 2001. TIRAP: an adapter molecule in the Toll signaling pathway. *Nat. Immunol.* 2, 835–841.
- Hudrisier, D., Oldstone, M.B., Gairin, J.E., 1997. The signal sequence of lymphocytic choriomeningitis virus contains an immunodominant cytotoxic T cell epitope that is restricted by both H-2D(b) and H-2K(b) molecules. *Virology* 234, 62–73.
- Kagi, D., Seiler, P., Pavlovic, J., Ledermann, B., Burki, K., Zinkernagel, R.M., Hengartner, H., 1995. The roles of perforin- and Fas-dependent cytotoxicity in protection against cytopathic and noncytopathic viruses. *Eur. J. Immunol.* 25, 3256–3262.
- Kopp, E.B., Medzhitov, R., 1999. The Toll-receptor family and control of innate immunity. *Curr. Opin. Immunol.* 11, 13–18.
- Koszinowski, U.H., Del Val, M., Reddehase, M.J., 1990. Cellular and molecular basis of the protective immune response to cytomegalovirus infection. *Curr. Top. Microbiol. Immunol.* 154, 189–220.
- Kurt-Jones, E.A., Popova, L., Kwinn, L., Haynes, L.M., Jones, L.P., Tripp, R.A., Walsh, E.E., Freeman, M.W., Golenbock, D.T., Anderson, L.J., Finberg, R.W., 2000. Pattern recognition receptors TLR4 and CD14 mediate response to respiratory syncytial virus. *Nat. Immunol.* 1, 398–401.
- Lefrancois, L., 1984. Protection against lethal viral infection by neutralizing and nonneutralizing monoclonal antibodies: distinct mechanisms of action in vivo. *J. Virol.* 51, 208–214.
- Lyles, D.S., McKenzie, M., Parce, J.W., 1992. Subunit interactions of vesicular stomatitis virus envelope glycoprotein stabilized by binding to viral matrix protein. *J. Virol.* 66, 349–358.
- Matsumoto, M., Kikkawa, S., Kohase, M., Miyake, K., Seya, T., 2002. Establishment of a monoclonal antibody against human Toll-like receptor 3 that blocks double-stranded RNA-mediated signaling. *Biochem. Biophys. Res. Commun.* 293, 1364–1369.
- Murali-Krishna, K., Altman, J.D., Suresh, M., Sourdive, D.J., Zajac, A.J., Miller, J.D., Slansky, J., Ahmed, R., 1998. Counting antigen-specific CD8 T cells: a reevaluation of bystander activation during viral infection. *Immunity* 8, 177–187.
- Oberhaus, S.M., Smith, R.L., Clayton, G.H., Dermody, T.S., Tyler, K.L., 1997. Reovirus infection and tissue injury in the mouse central nervous system are associated with apoptosis. *J. Virol.* 71, 2100–2106.
- Oshiumi, H., Matsumoto, M., Funami, K., Akazawa, T., Seya, T., 2003. TICAM-1, an adaptor molecule that participates in Toll-like receptor 3-mediated interferon-beta induction. *Nat. Immunol.* 4, 161–167.
- Raine, C.S., Fields, B.N., 1973. Reovirus type 3 encephalitis—A virologic and ultrastructural study. *J. Neuropathol. Exp. Neurol.* 32, 19–33.
- Renshaw, M., Rockwell, J., Engleman, C., Gewirtz, A., Katz, J., Sambhara, S., 2002. Cutting edge: impaired Toll-like receptor expression and function in aging. *J. Immunol.* 169, 4697–4701.
- Richardson-Burns, S.M., Kominsky, D.J., Tyler, K.L., 2002. Reovirus-induced neuronal apoptosis is mediated by caspase 3 and is associated with the activation of death receptors. *J. Neurovirol.* 8, 365–380.
- Steinhoff, U., Muller, U., Schertler, A., Hengartner, H., Aguet, M., Zinkernagel, R.M., 1995. Antiviral protection by vesicular stomatitis vi-

- rus-specific antibodies in alpha/beta interferon receptor-deficient mice. *J. Virol.* 69, 2153–2158.
- Takeda, K., Kaisho, T., Akira, S., 2003. Toll-like receptors. *Annu. Rev. Immunol.* 9, 9.
- Takeuchi, O., Hoshino, K., Akira, S., 2000. Cutting edge: TLR2-deficient and MyD88-deficient mice are highly susceptible to *Staphylococcus aureus* infection. *J. Immunol.* 165, 5392–5396.
- Tyler, K.L., Bronson, R.T., Byers, K.B., Fields, B., 1985. Molecular basis of viral neurotropism: experimental reovirus infection. *Neurology* 35, 88–92.
- Tyler, K.L., Virgin, H.W.T., Bassel-Duby, R., Fields, B.N., 1989. Antibody inhibits defined stages in the pathogenesis of reovirus serotype 3 infection of the central nervous system. *J. Exp. Med.* 170, 887–900.
- Whitmire, J.K., Asano, M.S., Murali-Krishna, K., Suresh, M., Ahmed, R., 1998. Long-term CD4 Th1 and Th2 memory following acute lymphocytic choriomeningitis virus infection. *J. Virol.* 72, 8281–8288.

## JNK Regulates the Release of Proapoptotic Mitochondrial Factors in Reovirus-Infected Cells

Penny Clarke,<sup>1\*</sup> Suzanne M. Meintzer,<sup>1</sup> Yibing Wang,<sup>2</sup> Lisa A. Moffitt,<sup>2</sup>  
Sarah M. Richardson-Burns,<sup>3</sup> Gary L. Johnson,<sup>4</sup>  
and Kenneth L. Tyler<sup>1,2,5,6</sup>

Departments of Neurology,<sup>1</sup> Immunology,<sup>2</sup> Neuroscience,<sup>3</sup> and Medicine and Microbiology,<sup>5</sup> University of Colorado Health Sciences Center, and Denver Veteran's Affairs Medical Center,<sup>6</sup> Denver, Colorado, and Department of Pharmacology and Lineberger Comprehensive Cancer Center, University of North Carolina School of Medicine, Chapel Hill, North Carolina<sup>4</sup>

Received 25 March 2004/Accepted 19 July 2004

**Reovirus-induced apoptosis is associated with activation of the proapoptotic mitogen-activated protein kinase c-Jun N-terminal kinase (JNK) and the JNK-associated transcription factor c-Jun. Here we show that reovirus-induced apoptosis and activation of caspase 3 are inhibited in cells deficient in MEK kinase 1, an upstream activator of JNK in reovirus-infected cells. Inhibition of JNK activity following reovirus infection delays the release of proapoptotic mitochondrial factors and the subsequent onset of apoptosis. In contrast, reovirus-induced apoptosis is not blocked by infection with adenovirus expressing dominant-negative c-Jun, and c-Jun activation does not correlate with apoptosis in reovirus-infected cells. This is the first report demonstrating that JNK is associated with regulation of mitochondrial pathways of apoptosis following viral infection.**

The c-Jun N-terminal kinases (JNKs) (also called stress-activated protein kinases) are mitogen-activated protein kinases (MAPKs) that are activated by stress stimuli, such as growth factor withdrawal and UV irradiation, and which function to communicate growth-inhibitory and apoptotic signals within cells (11, 14, 23). Members of the JNK family phosphorylate and activate members of the AP-1 group of transcription factors (c-Jun, JunB, and JunD) and the AP-1-related transcription factor ATF2, events which are likely to mediate, at least in part, the effects of JNK signaling pathways (9).

Gene disruption studies have shown that JNK is required for the release of proapoptotic molecules from the mitochondria in response to UV irradiation, indicating a role for JNK in mitochondrial pathways of apoptosis, although the exact mechanisms by which JNK facilitates this process remain incompletely understood (39). Mitochondrial apoptotic pathways are regulated by the Bcl-2 family of proteins. During mitochondrial-dependent apoptosis, the proapoptotic multidomain Bcl-2 family members (Bax and Bak) undergo a conformational change and redistribute from the cytoplasm to the mitochondria, where they are thought to mediate the release of proapoptotic molecules, including cytochrome *c* and Smac (15). The finding that Bax and Bak are essential for JNK-stimulated release of cytochrome *c* and apoptosis suggests that JNK influences mitochondrial apoptotic pathways through Bcl-2 family proteins (26).

Reovirus is a double-stranded RNA virus that induces apoptosis both in cultured cells and in target tissues (6). In the central nervous system and heart, virus-induced apoptosis correlates with pathology and is a critical mechanism by which disease is triggered in the host (10, 27, 32). In a variety of

human epithelial cell lines and in primary neuronal cultures, reovirus-induced apoptosis is mediated by death ligands, including tumor necrosis factor, tumor necrosis factor-related apoptosis-inducing ligand, and Fas ligand (3, 4, 32). Ligand binding induces the activation of the initiator caspase, caspase 8, and the subsequent activation of the effector caspases (3, 20). Mitochondrial apoptotic pathways are also activated following reovirus infection by the caspase 8-dependent cleavage of Bid (20, 21). Consequently, reovirus-induced apoptosis is inhibited by overexpression of Bcl-2 (33), which blocks the release of proapoptotic mitochondrial factors, including cytochrome *c* and Smac, and the activation of caspase 3 in reovirus-infected cells (21). Although both Smac and cytochrome *c* function to promote caspase 3 activity, it is the release of Smac and the subsequent inhibition of cellular inhibitors of apoptosis that play the most significant role during reovirus-induced apoptosis (21).

We have shown that JNK and its associated transcription factor, c-Jun, are activated following reovirus infection and that JNK activation is mediated by MEK kinase I (MEKK1) (43). Activation of JNK and c-Jun are associated with reovirus-induced apoptosis (5). Thus, apoptotic viral strains induce the activation of JNK and c-Jun, whereas nonapoptotic viral strains do not (5). In addition, strain-specific differences in JNK activation are determined by the reovirus S1 and M2 gene segments, which encode viral outer capsid proteins ( $\sigma 1$  and  $\mu 1c$ ) involved in receptor binding and host cell membrane penetration (5). These same gene segments also determine differences in the capacity of reovirus strains to induce apoptosis (40, 41). We now show that inhibition of JNK activity inhibits apoptosis in reovirus-infected cells. In contrast, inhibition of c-Jun does not affect reovirus-induced apoptosis, and c-Jun phosphorylation does not correlate with apoptosis in reovirus-infected cells. We further show that JNK inhibition delays the release of the proapoptotic mitochondrial factors

\* Corresponding author. Mailing address: Dept. of Neurology (B182), University of Colorado Health Sciences Center, 4200 East 9th Ave., Denver, CO 80262. Phone: (303) 393-3684. Fax: (303) 393-4686. E-mail: penny.clarke@uchsc.edu.

Smac and cytochrome *c* from the mitochondria of infected cells. This report represents the first demonstration of JNK-induced regulation of mitochondrial apoptotic pathways in virus-infected cells.

#### MATERIALS AND METHODS

**Cells and virus.** HEK293 cells (ATCC CRL1573) were grown in Dulbecco's modified Eagle's medium supplemented with 100 U each of penicillin and streptomycin/ml and containing 10% fetal bovine serum. HeLa cells (ATCC CCL2) were grown in Eagle's minimal essential medium supplemented with 2.4 mM L-glutamine, nonessential amino acids, and 60 U each of penicillin and streptomycin/ml and containing 10% fetal bovine serum (Gibco BRL). MEKK1<sup>-/-</sup> and wild-type (WT) embryonic stem (ES) cells and HEK293 cells expressing kinase-inactive MEK kinase 1, MEKK1KM (13), have previously been described. Reovirus strain type 3 Abney was used for all experiments. Reovirus strain type 3 Abney is a laboratory stock that has been plaque purified and passaged (twice) in L929 (ATCC CCL1) cells to generate working stocks. Virus infections and growth assays were performed as previously described (3, 41). Adenovirus expressing dominant-negative (DN) c-Jun (28) was provided by K. Heidenreich (University of Colorado).

**Reagents.** JNK inhibitor I (JNKII) was obtained from Alexis, and JNK inhibitor II (420119), PD98059 (MEK inhibitor), and SB203580 (p38 inhibitor) were purchased from Calbiochem. Each inhibitor was used at a concentration of 10  $\mu$ M. Cells were pretreated with inhibitors for 2 h before viral infection and were added back to media following infection.

**Apoptosis assays.** Cells were assayed for apoptosis by staining them with acridine orange, for determination of nuclear morphology, and ethidium bromide, to distinguish cell viability, at a final concentration of 1  $\mu$ g/ml each. Following staining, cells were examined by epifluorescence microscopy (Labophot-2; B-2A filter, excitation, 450 to 490 nm; barrier, 520 nm; dichroic mirror, 505 nm; Nikon). The percentage of cells containing condensed nuclei and/or marginated chromatin in a population of 100 cells was recorded. The specificity of this assay has been previously established with reovirus-infected cells by using DNA laddering techniques and electron microscopy (4, 41).

**Caspase 3 activity assays.** Caspase 3 activation assays were performed by using a kit obtained from Clontech. Cells ( $10^6$ ) were centrifuged at 200  $\times g$  for 10 min, supernatants were removed, and cell pellets were frozen at -70°C until collections were made for all time points. Assays were performed with 96-well plates, and analysis was done by using a fluorescence plate reader (CytoFluor 4000; PerSeptive Biosystems). Cleavage of DEVD-AFC, a synthetic caspase-3 substrate, was used to measure caspase 3 activation in reovirus-infected cells. Cleavage after the second Asp residue produces free AFC that can be detected using a fluorescence plate reader. The amount of fluorescence detected is directly proportional to the amount of caspase 3 activity.

**Western blot analysis.** Following infection with reovirus, cells were pelleted by centrifugation and washed twice with ice-cold phosphate-buffered saline (PBS). For whole-cell extracts, the cell pellet was lysed by sonication in 150  $\mu$ l of a buffer containing 1% Triton X-100, 10 mM triethanolamine-HCl, 150 mM NaCl, 5 mM EDTA (pH = 8.0), 1 mM phenylmethylsulfonyl fluoride, and 2.5  $\mu$ l of 25× complete protease inhibitor cocktail mix (catalog no. 1-697-498; Roche)/ml. The lysates were then cleared by centrifugation at 14,000  $\times g$  for 3 min, mixed 1:1 with 2× Laemmli buffer (catalog no. S-3401; Sigma), boiled for 5 min, and stored at -70°C. For mitochondrial extracts, the cell pellet was resuspended in 300  $\mu$ l of a buffer containing 220 mM mannitol, 68 mM sucrose, 50 mM piperazine-N,N'-bis(2-ethanesulfonic acid)-KOH (pH = 7.4), 50 mM KCl, 5 mM EGTA, 2 mM MgCl<sub>2</sub>, and 1 mM dithiothreitol. The resuspended pellet was incubated on ice for 30 min and then homogenized with a B-pestle in a 2-ml dounce homogenizer for 40 strokes. The lysates were then cleared by centrifugation at 14,000  $\times g$  for 15 min. The supernatant, the mitochondrial-free fraction, was mixed 1:1 with 2× Laemmli Buffer (Sigma catalog no. S-3401), boiled for 5 min, and stored at -70°C. The pellet, the cytoplasmic fraction, was then lysed by sonication in 100  $\mu$ l of whole-cell lysis buffer (above), mixed 1:1 with 2× Laemmli buffer, boiled for 5 min, and stored at -70°C.

Proteins were electrophoresed by sodium dodecyl sulfate-polyacrylamide gel electrophoresis, either through 10% Tris-tricine gels (phospho-c-Jun and c-Jun) or through 15% Tris-tricine gels (Smac and cytochrome *c*), and probed with antibodies directed against phospho-c-Jun (catalog no. 9261; 1:1,000 in 1% nonfat dry milk-Tris-buffered saline [TBS]; Cell Signaling), c-Jun (catalog no. 9162; 1:1,000 in 1% nonfat dry milk-TBS; Cell Signaling), Smac (catalog no. 567365; 1:1,000 in 1% nonfat dry milk-TBS; Calbiochem), and cytochrome *c* (catalog no. 556433; 1:1,000 in 1% nonfat dry milk-TBS; BD Pharmingen). All lysates were standardized for protein concentration with antibodies directed

against actin (catalog no. CP-01; 1:10,000 in 1% nonfat dry milk-TBS; Calbiochem).

**Immunocytochemistry.** Cells were plated in eight-well chamber slides. After infection, cells were fixed (3.7% formaldehyde-PBS) for 30 min at room temperature (RT). Cells were then washed with PBS and made permeable with PBS-0.1% Triton X-100 (PBSX) for 1 h at RT, blocked in 5% bovine serum albumin-PBSX for 2 h at RT, and then incubated overnight (4°C) with primary antibody (1:100) in 3% bovine serum albumin-PBSX. Primary antibodies used were directed against cleaved (active) caspase 3 (catalog no. 9661L; Cell Signaling). Following incubation, cells were washed three times (3 min each wash) with PBSX before being incubated with antirabbit or antirat immunoglobulin G conjugated with fluorescein isothiocyanate (1:100) for 1 h at RT. Fluorescent immunoglobulin Gs were obtained from Vector Laboratories. Incubation with secondary antibody and all subsequent steps were performed in the dark. Cells were then washed with PBSX (three times, 3 min each wash), incubated for a further 5 min with Hoechst-PBS (1:1000; Molecular Probes), washed again with PBSX (three times, 3 min each wash), and mounted with Vectashield (Vector Laboratories). After mounting, slides were sealed with clear nail polish and stored at 4°C. Labeling of mitochondria was performed using Cy3-labeled streptavidin (ImmunoResearch Laboratories) for 15 to 20 min prior to Hoechst staining.

#### RESULTS

**MEKK1 is required for reovirus-induced apoptosis.** Reovirus-induced activation of JNK and c-Jun is associated with apoptosis in infected cells (5). We have shown that MEKK1 acts as an upstream activator of JNK signaling (43). We thus investigated the role of MEKK1 in reovirus-induced apoptosis. MEKK1<sup>-/-</sup> mouse embryo fibroblasts were infected with reovirus (multiplicity of infection [MOI], 10). At 48 h postinfection (p.i.), 48% of reovirus-infected wild-type (WT) cells contained apoptotic nuclei (Fig. 1A). This number was significantly reduced ( $P < 0.05$ ) to 11% in MEKK1<sup>-/-</sup> cells (Fig. 1A). We next looked at reovirus-induced activation of caspase 3 in MEKK1<sup>-/-</sup> cells, using fluorogenic substrate assays. In WT cells, increases in caspase 3 activity were seen as early as 18 h p.i. and peaked at 30 h p.i., after which times levels remained high (Fig. 1B). In contrast, there was no increase in caspase 3 activity in MEKK1<sup>-/-</sup> cells following reovirus infection.

Reovirus-induced apoptosis was also investigated in HEK293 cells expressing a kinase-inactive form of MEKK1 (MEKK1KM). Cells were infected with reovirus (MOI of 100). Forty-eight hours p.i., reovirus induced 65% apoptosis in cells expressing vector alone. This was significantly ( $P < 0.05$ ) reduced to 20% in cells expressing MEKK1KM (Fig. 1C). These results indicate that reovirus-induced apoptosis is inhibited in MEKK1<sup>-/-</sup> cells and in cells expressing MEKK1KM, compared to the case with controls expressing WT MEKK1.

**JNK is required for efficient apoptosis in reovirus-infected cells.** Having shown that reovirus-induced apoptosis requires MEKK1 and is inhibited in MEKK1<sup>-/-</sup> cells, which show reduced reovirus-induced JNK activation (43), we next investigated the effects of specific JNK inhibitors on reovirus-induced apoptosis. Two different inhibitors were used. The first, JNKI1, is a peptide inhibitor that blocks JNK binding to its substrate, and the second, JNK inhibitor II, inhibits JNK kinase activity. Since both HEK293 cells and HeLa cells have been used extensively in the analysis of reovirus-induced apoptosis, we used both of these cell lines in our experiments. Cells were treated with JNK inhibitors for 2 h before being infected with reovirus at a MOI of 10 or 100. Cells were harvested 24 and 48 h p.i., and the percentage of cells with apoptotic nuclear morphology was determined (Fig. 2A and B). In HEK293 cells, an inhibitor

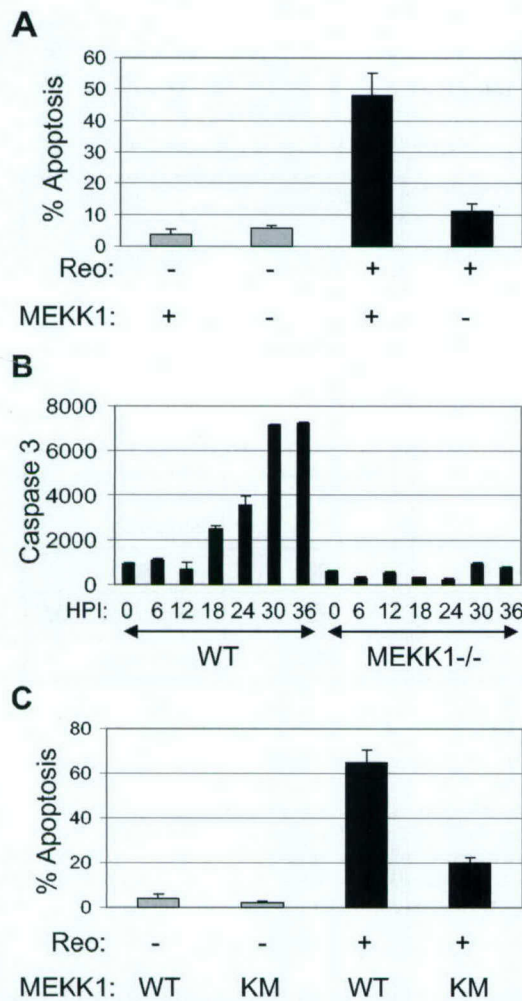


FIG. 1. Reovirus-induced apoptosis is inhibited in MEKK1<sup>-/-</sup> cells and in cells expressing MEKK1KM. MEKK1<sup>-/-</sup> cells were infected with reovirus (MOI of 10; black bars) or were mock infected (gray bars), and the percentage of cells containing apoptotic nuclei at 48 h p.i. was determined (A). The graph shows the mean percentage of apoptotic cells from three independent experiments. Error bars represent standard errors of the mean. Reovirus-induced activation of caspase 3 was also determined for MEKK1<sup>-/-</sup> cells and controls (WT) at various times p.i. by fluorogenic substrate assay (B). The graph shows the mean fluorescence (arbitrary units) from three wells of an individual experiment, which represents caspase 3 activity, and is representative of three separate experiments. Cells expressing MEKK1KM and controls were infected with reovirus (MOI of 100; black bars) or were mock infected (gray bars), and the percentage of cells containing apoptotic nuclei at 48 h p.i. was determined (C). The graph shows the mean percentage of apoptotic cells from three independent experiments. Error bars represent standard errors of the mean.

of JNK binding (JNK1) inhibited reovirus (MOI of 10)-induced apoptosis at both 24 (a 67% reduction) and 48 (a 47% reduction;  $P < 0.001$ ) h p.i. At a MOI of 100, inhibition of JNK binding delayed reovirus-induced apoptosis in HEK293 cells. Thus, at 24 h p.i., a 57% ( $P < 0.001$ ) reduction in reovirus (MOI of 100)-induced apoptosis was observed. However, at 48 h p.i., JNK1 was not able to protect HEK293 cells from reovirus (MOI of 100)-induced apoptosis, and high (>70%) levels of apoptosis were seen in both treated and untreated cells. Similar results were obtained by inhibition of JNK kinase

activity. In contrast, inhibitors of the proapoptotic MAPK P38 (16, 24, 34) and the antiapoptotic extracellular signal-related kinases (ERK) (7) had no effect on reovirus-induced apoptosis (Fig. 2A and B), as previously shown (5). These results indicate that JNK, but not P38 or ERK, is required for efficient apoptosis in reovirus-infected HEK293 cells. Apoptosis in mock-infected cells, with or without inhibitor, was less than 5%. A similar effect on apoptosis was seen after treatment of HeLa cells with JNK and ERK inhibitors (data not shown). However, an inhibitor of P38 was able to reduce reovirus-induced apoptosis in these cells at 24 h p.i. (data not shown).

The effect of JNK inhibition on apoptosis was also investigated by immunocytochemistry, using antibody directed against the cleaved (active) form of caspase 3. HeLa cells were incubated with JNK1 for 2 h before being infected with reovirus. Cells were then incubated for a further 18 h before immunocytochemistry was performed (Fig. 2C). Active caspase 3 staining was seen in 39% of cells infected with reovirus, compared to 3% of mock-infected controls. Activation of caspase 3 was significantly ( $P < 0.001$ ) reduced in the presence of JNK1. These experiments suggest that JNK activity is required for efficient apoptosis and activation of caspase 3 in reovirus-infected cells.

The observed differences in the ability of reovirus to induce apoptosis were not caused by differences in viral growth, since one-step growth curves indicated that reovirus grows efficiently and equivalently in HEK293 cells in the presence or absence of JNK1 (Fig. 2D).

**c-Jun activation is not required for reovirus-induced apoptosis.** JNK activates members of the AP-1 group of transcription factors, including c-Jun, JunB, and JunD (9). We have previously shown that c-Jun is activated after reovirus infection, and this activation has been associated with reovirus-induced apoptosis. In other systems, JNK has been shown to influence apoptosis by its ability to activate the AP-1 transcription factor. We therefore investigated the role of AP-1 in reovirus-induced apoptosis. First, the role of MAPKs, including JNK, in c-Jun phosphorylation was determined in reovirus-infected cells. c-Jun is activated by 12 h p.i. in reovirus-infected HEK293 cells, and activation peaks around 18 h p.i. (5). We therefore investigated c-Jun phosphorylation in reovirus-infected HEK293 cells at 18 h p.i. in the presence or absence of inhibitors of JNK binding and P38 and ERK activity. Cells were pretreated with inhibitor for 2 h prior to infection (MOI of 100). Eighteen hours p.i., cells were harvested and screened by Western blot analysis for the presence of both the phosphorylated (active) and nonphosphorylated form of c-Jun. Reovirus infection resulted in the phosphorylation of c-Jun (Fig. 3A), as has previously been shown (5). The detection of multiple bands by the c-Jun antibodies indicates the multiple phosphorylation sites present on the c-Jun protein. Reovirus-induced activation of c-Jun was partially blocked by inhibition of JNK or ERK and was completely blocked when both JNK and ERK inhibitors were used together. In contrast, an inhibitor of P38 appeared to increase c-Jun phosphorylation after reovirus infection (Fig. 3A). Levels of total c-Jun indicated that reovirus also induced an increase in levels of total c-Jun in HEK293 cells (Fig. 3A). The presence of multiple bands again indicated that c-Jun was phosphorylated at multiple sites following reovirus infection. Increased c-Jun levels were not affected by

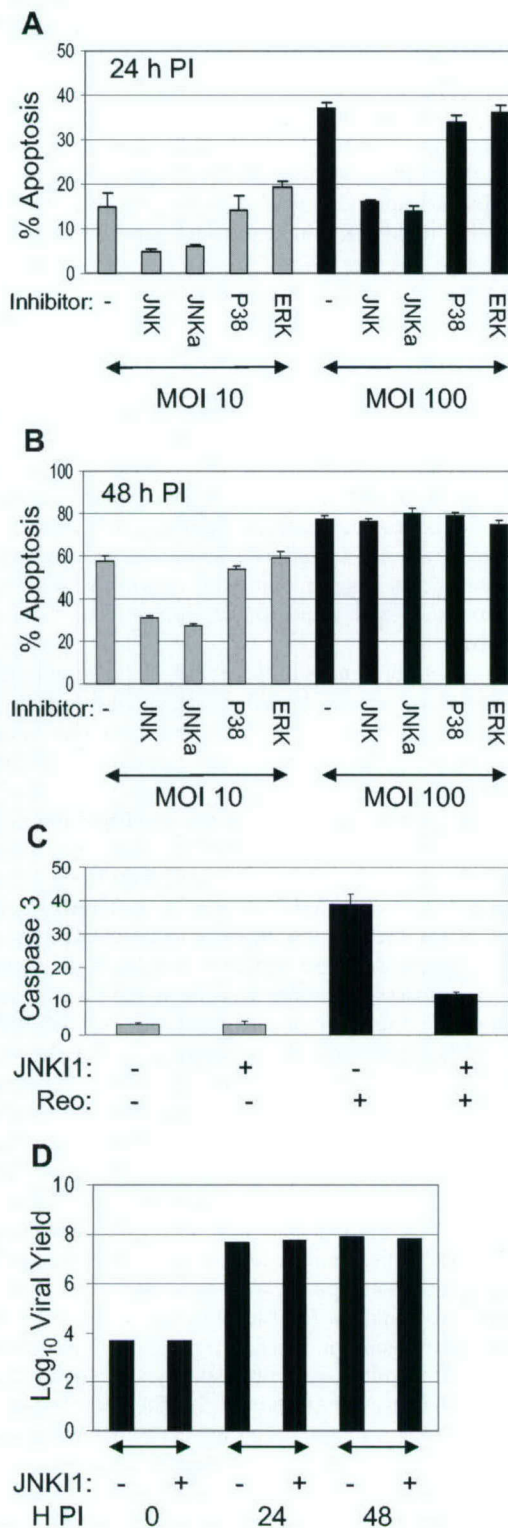


FIG. 2. Reovirus-induced apoptosis requires JNK. HEK293 cells were treated with inhibitors of JNK (JNK, JNKA), P38 (P38), or ERK (ERK) for 2 h before being infected with reovirus (MOI of 10 [grey bars] or MOI of 100) ([black bars]). Specifically, JNKI1 (JNK) blocks JNK binding to its substrate, and JNK inhibitor II (JNKA) inhibits JNK kinase activity. Cells were harvested 24 (A) or 48 (B) h p.i., and the percentage of cells with apoptotic nuclear morphology was determined. The graphs show the mean percentages of apoptotic cells from

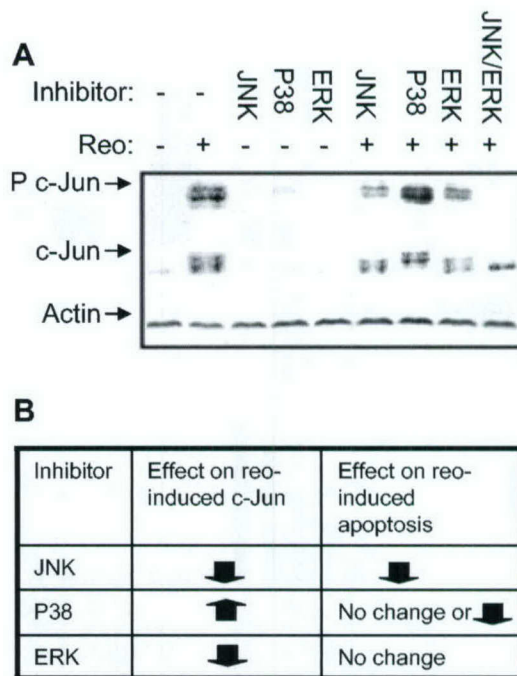


FIG. 3. c-Jun is activated by JNK and ERK following reovirus infection. Cells were pretreated for 2 h with inhibitor of JNK binding (JNK) or p38 (p38) or ERK (ERK). In addition, a combination of JNK and ERK inhibitors was used. Cells were then infected with reovirus (MOI of 100). Eighteen hours after infection, cells were harvested for Western blot analysis, using antibodies directed against phosphorylated c-Jun (P c-Jun), c-Jun, and actin (A). The effects of inhibitors of JNK, p38, and ERK on reovirus-induced activation and apoptosis were compared (B).

inhibition of MAPK activity. Similar results were seen in HeLa cells (results not shown).

These results indicate that JNK and ERK, but not P38, contribute to c-Jun activation following reovirus infection. They also suggest that c-Jun activation does not correlate with apoptosis in reovirus-infected cells, since JNK inhibition reduces c-Jun phosphorylation and decreases apoptosis, ERK inhibition reduces c-Jun phosphorylation and has no effect on apoptosis, and P38 inhibition increases c-Jun phosphorylation yet has no effect on apoptosis in HEK293 cells and decreases apoptosis in HeLa cells (Fig. 3B).

To conclusively determine the role of c-Jun/AP-1 in reovirus-induced apoptosis, we used adenovirus expressing domi-

three independent experiments. Error bars represent standard errors of the mean. Cells harvested at 18 h p.i. were fixed and stained with Hoechst 33342 (blue) to identify nuclei and with fluorescein isothiocyanate-labeled antibodies directed against active caspase 3 (green) to detect active caspase 3. The percentages of mock-infected (grey bars) and reovirus (Reo)-infected (black bars) cells with active caspase 3 staining were determined (C). The graph shows the mean percentages of apoptotic cells of three independent fields. Error bars represent standard errors of the means. One-step growth curves of reovirus in the presence or absence of JNKI1 are also presented (D). HEK293 cells were infected with reovirus (MOI of 1) and were harvested and assayed for growth at 24 and 48 h p.i. The graph shows the  $\log_{10}$  virus yield over time.

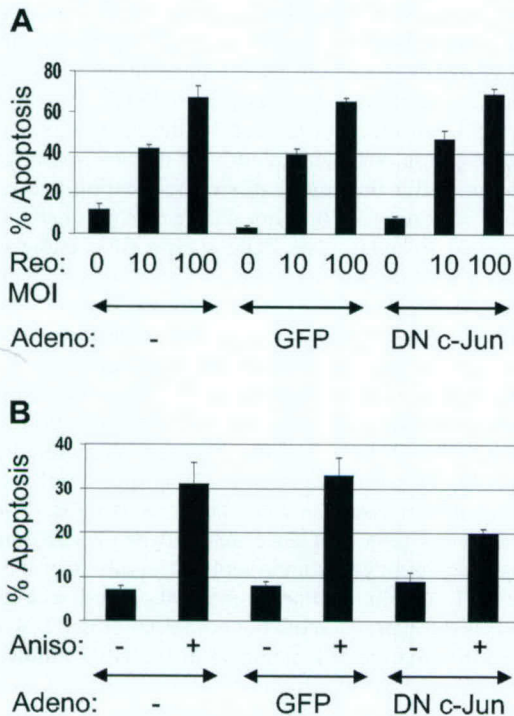


FIG. 4. c-Jun is not required for reovirus-induced apoptosis. Cells were infected with adenovirus (Adeno) expressing GFP or DN c-Jun (MOI of 50) for 36 h. Cells were then infected with reovirus (MOI of 10 or 100) and were assayed for apoptosis after a further 48 h (A). Alternatively, cells were treated with anisomycin (1  $\mu$ M) and were assayed for apoptosis after a further 24 h (B). The graphs show the mean percentages of apoptotic cells from three independent experiments. Error bars represent standard errors of the mean.

nant-negative (DN) c-Jun, which blocks AP-1 activity (28). HEK293 cells were infected with adenovirus (MOI of 50) expressing either DN c-Jun or green fluorescent protein (GFP) under the control of the cytomegalovirus promoter and were incubated for 36 h to allow expression of the DN c-Jun phenotype. Cells were then infected with reovirus (MOI of 10 and 100) for 48 h before being harvested. Reovirus infection at both a MOI of 10 and a MOI of 100 resulted in apoptosis (42 and 67%, respectively) in HEK293 cells that had not been previously treated with adenovirus (Fig. 4A). Reovirus induced apoptosis was not affected by treatment with adenovirus expressing either GFP or DN c-Jun (Fig. 4A). In contrast, anisomycin-induced apoptosis, which requires c-Jun, was reduced in HEK293 cells infected with adenovirus expressing DN c-Jun (Fig. 4B), indicating that c-Jun expression is not required for reovirus-induced apoptosis and suggesting that JNK exerts its proapoptotic effects in reovirus-infected cells through an alternate mechanism.

**JNK is required for efficient release of Smac and cytochrome *c* after reovirus infection.** JNK is required for the release of proapoptotic molecules from the mitochondria in response to UV irradiation (39). Reovirus also activates mitochondrial apoptotic pathways following infection, resulting in the release of the proapoptotic mitochondrial factors cytochrome *c* and Smac (21). We thus investigated the role of JNK in the release of Smac and cytochrome *c* from the mitochondria during reovirus-induced apoptosis. HeLa cells were incu-

bated with JNK1 for 2 h before being infected with reovirus. Cells were then harvested at 8 and 24 h p.i. Mitochondrial pellet and mitochondrion-free fractions were prepared and analyzed by Western blot analysis, using antibodies directed against Smac and cytochrome *c*. Reovirus induced the release of both Smac and cytochrome *c* from the mitochondria of infected cells (Fig. 5A), as previously described (20, 21). Levels of Smac and cytochrome *c* thus dropped in mitochondrial pellet fractions and rose in mitochondrion-free fractions. JNK1 delayed the release of both mitochondrial Smac and cytochrome *c* following reovirus infection.

## DISCUSSION

We have previously shown that reovirus-induced activation of JNK and its associated transcription factor, c-Jun, is associated with reovirus-induced apoptosis (5). We now show that reovirus-induced apoptosis is blocked in MEKK1<sup>-/-</sup> cells, in which reovirus-induced JNK activation is inhibited (43), and in cells in which MEKK1 kinase activity is blocked. In addition, specific inhibitors of JNK that block JNK-substrate binding or kinase activity block reovirus-induced apoptosis at a low MOI and significantly delay reovirus-induced apoptosis at a high MOI. These results indicate that JNK is required for efficient apoptosis in reovirus-infected cells (Fig. 6). The more-effective reduction in apoptosis seen in MEKK1<sup>-/-</sup> cells and cells expressing MEKK1KM compared to that in cells treated with an inhibitor of JNK suggests that MEKK1 may influence reovirus-induced apoptosis by JNK-independent, as well as JNK-dependent, pathways. Inhibition of P38 had no effect on reovirus-induced apoptosis in HEK293 cells, as has been previously shown (5). However, in HeLa cells, P38 inhibition decreased reovirus-induced apoptosis, suggesting cell type differences in MAPK involvement in reovirus-induced apoptosis. In contrast,

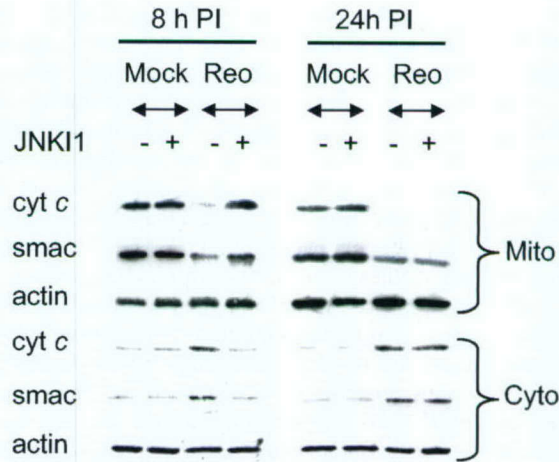


FIG. 5. JNK is required for the release of Smac and cytochrome *c* from the mitochondria of reovirus (Reo)-infected cells. Cells were pretreated with an inhibitor of JNK activity (JNK1) for 2 h before being infected with reovirus (MOI of 100). Eight and twenty-four hours p.i., cells were harvested. Mitochondrial (Mito) and mitochondrion-free (Cyto) fractions were then prepared and used as lysates for Western blot analysis. Lysates were probed with antibodies directed against Smac and cytochrome *c*. Levels of actin were used to control for protein loading.

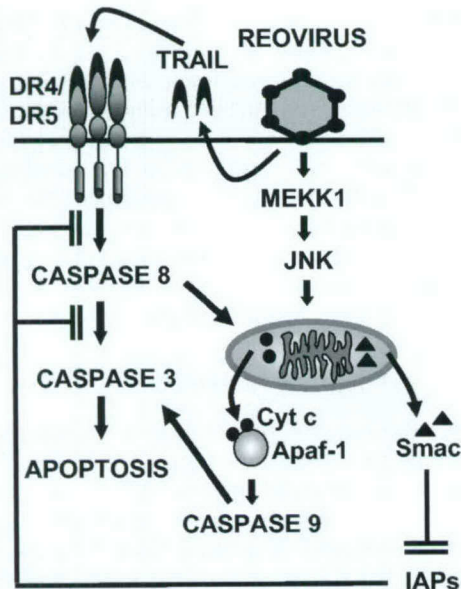


FIG. 6. Model of apoptotic signaling pathways triggered by reovirus infection. Following reovirus infection, MEKK1 activates JNK, which promotes the release of the proapoptotic factors Smac and cytochrome *c* (Cyt *c*) from the mitochondria. Smac influences apoptosis by inhibiting cellular inhibitors of apoptosis (IAPs), whereas cytochrome *c* influences apoptosis by activating caspase 9 in conjunction with Apaf-1. Tumor necrosis factor-related apoptosis-inducing ligand (TRAIL) receptor signaling is also induced following reovirus infection, and the reovirus-induced caspase 8-dependent cleavage of Bid also promotes the mitochondrial release of Smac and cytochrome *c* (20, 21).

inhibition of ERK had no effect on reovirus-induced apoptosis in either cell line, indicating specificity in the role of MAPKs in reovirus-induced apoptosis.

It is possible that JNK regulation of the AP-1 transcription factor mediates, in part, the effects of JNK signaling pathways (9). JNK-mediated regulation of AP-1 has been reported to increase the expression of the BH3-only proteins Bim and HRK, which are critical for Bax-dependent cytochrome *c* release, caspase activation, and apoptosis in neurons (17, 30, 42), although in fibroblasts JNK does not increase Bim expression (25). To investigate the role of AP-1 in reovirus-induced apoptosis, we used adenovirus expressing DN c-Jun (TAM67), which prevents formation of a functional AP-1 transcription factor (28). Our studies indicate that expression of DN c-Jun does not block reovirus-induced apoptosis in fibroblasts. The expression of Bim also remains unaltered in reovirus-infected cells (data not shown). In addition, c-Jun phosphorylation does not correlate with reovirus-induced apoptosis. These results indicate that JNK-mediated activation of the c-Jun/AP-1 transcription factor is not required for reovirus-induced apoptosis and that other JNK-dependent pathways are involved.

We have previously demonstrated that caspase 8 activity is required for cleavage of the proapoptotic Bcl-2 family member, Bid, following reovirus infection (20). We now show that JNK activity is also required for the efficient release of the proapoptotic mitochondrial factors Smac and cytochrome *c* following reovirus infection. Since JNK activity in reovirus-infected cells does not appear to require death receptor sig-

naling (5), caspase 8-dependent cleavage of Bid and the subsequent redistribution of Bcl-2 family proteins in the mitochondrial membrane provide a mechanism for Smac and cytochrome *c* release in the presence of JNK1 (Fig. 6).

Apoptosis is a mechanism used by the host as part of the antiviral response, and deregulation of this host-pathogen interaction can alter the course of viral replication and explain aspects of viral disease. It is not surprising that many viruses have evolved to manipulate cellular apoptotic pathways. In many cases, inhibition of apoptosis by viruses serves to prevent premature death of the host cell. Inhibitors of apoptosis also may enhance virus production, enable efficient emergence from latency, facilitate persistent infection, and contribute to the avoidance of immune surveillance (8). Since mitochondrial apoptotic pathways are activated following infection with a wide variety of viruses, including human immunodeficiency virus (12, 18, 19), influenza A virus (2), herpes simplex virus 1 (44), human herpesvirus 8 (35), hepatitis B virus (38), and West Nile virus (29), and since many forms of virus-induced apoptosis are inhibited by antiapoptotic members of the Bcl-2 family (1, 31, 36, 37), a common method of viral inhibition of apoptosis is the expression of viral homologs of Bcl-2 (8) or the induction of antiapoptotic members of the Bcl-2 family (22).

In addition to contributing to the host's antiviral response, apoptosis can also influence viral pathogenesis and may facilitate rapid virus release and cell-to-cell spread. Reovirus-induced apoptosis requires both death receptor and mitochondrial apoptotic pathways (6). Here we show that efficient activation of mitochondrial apoptotic pathways in reovirus-infected cells requires JNK. This is the first report linking JNK to the activation of mitochondrial apoptotic pathways in virus-infected cells. Since the proapoptotic Bcl-2 proteins Bax and Bak are essential for JNK-stimulated release of cytochrome *c* and apoptosis (26), further investigation of reovirus-induced mitochondrial apoptotic pathways may provide valuable insight into the pathogenesis of viruses that utilize Bcl-2 family proteins to promote apoptosis (22) or that are blocked by the overexpression of Bcl-2 (1, 31, 36, 37).

#### ACKNOWLEDGMENTS

This work was supported by Public Health Service grant 1R01AG14071 from the National Institutes of Health (K.L.T.), Merit and REAP grants from the Department of Veterans Affairs (K.L.T.), a U.S. Army Medical Research and Materiel Command grant, DAMD17-98-1-8614 (K.L.T.), the Reuler-Lewin Family Professorship of Neurology (K.L.T.), and the Ovarian Cancer Research Fund (P.C.). Microscope assistance was provided by Ron Bouchard.

#### REFERENCES

1. Carthy, C. M., B. Yanagawa, H. Luo, D. J. Granville, D. Yang, P. Cheung, C. Cheung, M. Esfandiari, C. M. Rudin, C. B. Thompson, D. W. Hunt, and B. M. McManus. 2003. Bcl-2 and Bcl-xL overexpression inhibits cytochrome *c* release, activation of multiple caspases, and virus release following coxsackievirus B3 infection. *Virology* 313:147–157.
2. Chen, W., P. A. Calvo, D. Malide, J. Gibbs, U. Schubert, I. Bacik, S. Basta, R. O'Neill, J. Schickli, P. Palese, P. Henklein, J. R. Bennink, and J. W. Yewdell. 2001. A novel influenza A virus mitochondrial protein that induces cell death. *Nat. Med.* 7:1306–1312.
3. Clarke, P., S. M. Meintzer, S. Gibson, C. Widmann, T. P. Garrington, G. L. Johnson, and K. L. Tyler. 2000. Reovirus-induced apoptosis is mediated by TRAIL. *J. Virol.* 74:8135–8139.
4. Clarke, P., S. M. Meintzer, A. C. Spalding, G. L. Johnson, and K. L. Tyler. 2001. Caspase 8-dependent sensitization of cancer cells to TRAIL-induced apoptosis following reovirus-infection. *Oncogene* 20:6910–6919.
5. Clarke, P., S. M. Meintzer, C. Widmann, G. L. Johnson, and K. L. Tyler.

2001. Reovirus infection activates JNK and the JNK-dependent transcription factor c-Jun. *J. Virol.* **75**:11275–11283.
6. Clarke, P., and K. L. Tyler. 2003. Reovirus-induced apoptosis: a minireview. *Apoptosis* **8**:141–150.
  7. Cobb, M. H., J. E. Hepler, M. Cheng, and D. Robbins. 1994. The mitogen-activated protein kinases, ERK1 and ERK2. *Semin. Cancer Biol.* **5**:261–268.
  8. Cuconati, A., and E. White. 2002. Viral homologs of BCL-2: role of apoptosis in the regulation of virus infection. *Genes Dev.* **16**:2465–2478.
  9. Davis, R. J. 2000. Signal transduction by the JNK group of MAP kinases. *Cell* **103**:239–252.
  10. DeBiasi, R. L., C. L. Edelstein, B. Sherry, and K. L. Tyler. 2001. Calpain inhibition protects against virus-induced apoptotic myocardial injury. *J. Virol.* **75**:351–361.
  11. Derijard, B., M. Hibi, I. H. Wu, T. Barrett, B. Su, T. Deng, M. Karin, and R. J. Davis. 1994. JNK1: a protein kinase stimulated by UV light and Ha-Ras binds and phosphorylates the c-Jun activation domain. *Cell* **76**:1025–1037.
  12. Ferri, K. F., E. Jacotot, J. Blanco, J. A. Este, N. Zamzami, S. A. Susin, Z. Xie, G. Brothers, J. C. Reed, J. M. Penninger, and G. Kroemer. 2000. Apoptosis control in syncytia induced by the HIV type 1-envelope glycoprotein complex: role of mitochondria and caspases. *J. Exp. Med.* **192**:1081–1092.
  13. Gibson, S. B., R. Oyer, A. C. Spalding, S. M. Anderson, and G. L. Johnson. 2000. Increased expression of death receptors 4 and 5 synergizes the apoptosis response to combined treatment with etoposide and TRAIL. *Mol. Cell. Biol.* **20**:205–212.
  14. Graves, J. D., J. S. Campbell, and E. G. Krebs. 1995. Protein serine/threonine kinases of the MAPK cascade. *Ann. N. Y. Acad. Sci.* **766**:320–343.
  15. Gross, A., J. M. McDonnell, and S. J. Korsmeyer. 1999. BCL-2 family members and the mitochondria in apoptosis. *Genes Dev.* **13**:1899–1911.
  16. Han, J., J. D. Lee, L. Bibbs, and R. J. Ulevitch. 1994. A MAP kinase targeted by endotoxin and hyperosmolarity in mammalian cells. *Science* **265**:808–811.
  17. Harris, C. A., and E. M. Johnson, Jr. 2001. BH3-only Bcl-2 family members are coordinately regulated by the JNK pathway and require Bax to induce apoptosis in neurons. *J. Biol. Chem.* **276**:37754–37760.
  18. Jacotot, E., K. F. Ferri, C. El Hamel, C. Brenner, S. Druilennec, J. Hoebeke, P. Rustin, D. Metivier, C. Lenoir, M. Geuskens, H. L. Vieira, M. Loeffler, A. S. Belzacq, J. P. Briand, N. Zamzami, L. Edelman, Z. H. Xie, J. C. Reed, B. P. Roques, and G. Kroemer. 2001. Control of mitochondrial membrane permeabilization by adenine nucleotide translocator interacting with HIV-1 viral protein R and Bcl-2. *J. Exp. Med.* **193**:509–519.
  19. Jacotot, E., L. Ravagnan, M. Loeffler, K. F. Ferri, H. L. Vieira, N. Zamzami, P. Costantini, S. Druilennec, J. Hoebeke, J. P. Briand, T. Irinopoulou, E. Daugas, S. A. Susin, D. Cointe, Z. H. Xie, J. C. Reed, B. P. Roques, and G. Kroemer. 2000. The HIV-1 viral protein R induces apoptosis via a direct effect on the mitochondrial permeability transition pore. *J. Exp. Med.* **191**:33–46.
  20. Kominsky, D. J., R. J. Bickel, and K. L. Tyler. 2002. Reovirus-induced apoptosis requires both death receptor- and mitochondrial-mediated caspase-dependent pathways of cell death. *Cell Death Differ.* **9**:926–933.
  21. Kominsky, D. J., R. J. Bickel, and K. L. Tyler. 2002. Reovirus-induced apoptosis requires mitochondrial release of Smac/DIABLO and involves reduction of cellular inhibitor of apoptosis protein levels. *J. Virol.* **76**:11414–11424.
  22. Kotelkin, A., E. A. Prikhod'ko, J. I. Cohen, P. L. Collins, and A. Bukreyev. 2003. Respiratory syncytial virus infection sensitizes cells to apoptosis mediated by tumor necrosis factor-related apoptosis-inducing ligand. *J. Virol.* **77**:9156–9172.
  23. Kyriakis, J. M., P. Banerjee, E. Nikolakaki, T. Dai, E. A. Rubie, M. F. Ahmad, J. Avruch, and J. R. Woodgett. 1994. The stress-activated protein kinase subfamily of c-Jun kinases. *Nature* **369**:156–160.
  24. Lee, J. C., J. T. Laydon, P. C. McDonnell, T. F. Gallagher, S. Kumar, D. Green, D. McNulty, M. J. Blumenthal, J. R. Heys, S. W. Landvatter, et al. 1994. A protein kinase involved in the regulation of inflammatory cytokine biosynthesis. *Nature* **372**:739–746.
  25. Lei, K., and R. J. Davis. 2003. JNK phosphorylation of Bim-related members of the Bcl2 family induces Bax-dependent apoptosis. *Proc. Natl. Acad. Sci. USA* **100**:2432–2437.
  26. Lei, K., A. Nimnuan, W.-X. Zong, N. J. Kennedy, R. A. Flavell, C. B. Thompson, D. Bar-Sagi, and R. J. Davis. 2002. The Bax subfamily of Bcl2-related proteins is essential for apoptotic signal transduction by c-Jun NH<sub>2</sub>-terminal kinase. *Mol. Cell. Biol.* **22**:4929–4942.
  27. Oberhaus, S. M., R. L. Smith, G. H. Clayton, T. S. Dermody, and K. L. Tyler. 1997. Reovirus infection and tissue injury in the mouse central nervous system are associated with apoptosis. *J. Virol.* **71**:2100–2106.
  28. Park, J. S., L. Qiao, Z. Z. Su, D. Hinman, K. Willoughby, R. McKinstry, A. Yacoub, G. J. Duigou, C. S. Young, S. Grant, M. P. Hagan, E. Ellis, P. B. Fisher, and P. Dent. 2001. Ionizing radiation modulates vascular endothelial growth factor (VEGF) expression through multiple mitogen activated protein kinase dependent pathways. *Oncogene* **20**:3266–3280.
  29. Parquet, M. C., A. Kumatori, F. Hasebe, K. Morita, and A. Igarashi. 2001. West Nile virus-induced bax-dependent apoptosis. *FEBS Lett.* **500**:17–24.
  30. Putcha, G. V., K. L. Moulder, J. P. Golden, P. Bouillet, J. A. Adams, A. Strasser, and E. M. Johnson. 2001. Induction of BIM, a proapoptotic BH3-only BCL-2 family member, is critical for neuronal apoptosis. *Neuron* **29**:615–628.
  31. Razvi, E. S., and R. M. Welsh. 1995. Apoptosis in viral infections. *Adv. Virus Res.* **45**:1–60.
  32. Richardson-Burns, S. M., D. J. Kominsky, and K. L. Tyler. 2002. Reovirus-induced neuronal apoptosis is mediated by caspase 3 and is associated with the activation of death receptors. *J. Neurovirol.* **8**:365–380.
  33. Rodgers, S. E., E. S. Barton, S. M. Oberhaus, B. Pike, C. A. Gibson, K. L. Tyler, and T. S. Dermody. 1997. Reovirus-induced apoptosis of MDCK cells is not linked to viral yield and is blocked by Bcl-2. *J. Virol.* **71**:2540–2546.
  34. Rouse, J., P. Cohen, S. Trigon, M. Morange, A. Alonso-Llamazares, D. Zamanillo, T. Hunt, and A. R. Nebreda. 1994. A novel kinase cascade triggered by stress and heat shock that stimulates MAPKAP kinase-2 and phosphorylation of the small heat shock proteins. *Cell* **78**:1027–1037.
  35. Sharp, T. V., H. W. Wang, A. Koumi, D. Hollyman, Y. Endo, H. Ye, M. Q. Du, and C. Boshoff. 2002. K15 protein of Kaposi's sarcoma-associated herpesvirus is latently expressed and binds to HAX-1, a protein with antiapoptotic function. *J. Virol.* **76**:802–816.
  36. Shen, Y., and T. E. Shenk. 1995. Viruses and apoptosis. *Curr. Opin. Genet. Dev.* **5**:105–111.
  37. Teodoro, J. G., and P. E. Branton. 1997. Regulation of apoptosis by viral gene products. *J. Virol.* **71**:1739–1746.
  38. Terradillos, O., A. de la Coste, T. Pollicino, C. Neuveut, D. Sitterlin, H. Lecoeur, M. L. Gougeon, A. Kahn, and M. A. Buendia. 2002. The hepatitis B virus X protein abrogates Bcl-2-mediated protection against Fas apoptosis in the liver. *Oncogene* **21**:377–386.
  39. Tournier, C., P. Hess, D. D. Yang, J. Xu, T. K. Turner, A. Nimnuan, D. Bar-Sagi, S. N. Jones, R. A. Flavell, and R. J. Davis. 2000. Requirement of JNK for stress-induced activation of the cytochrome c-mediated death pathway. *Science* **288**:870–874.
  40. Tyler, K. L., M. K. Squier, A. L. Brown, B. Pike, D. Willis, S. M. Oberhaus, T. S. Dermody, and J. J. Cohen. 1996. Linkage between reovirus-induced apoptosis and inhibition of cellular DNA synthesis: role of the S1 and M2 genes. *J. Virol.* **70**:7984–7991.
  41. Tyler, K. L., M. K. Squier, S. E. Rodgers, B. E. Schneider, S. M. Oberhaus, T. A. Grdina, J. J. Cohen, and T. S. Dermody. 1995. Differences in the capacity of reovirus strains to induce apoptosis are determined by the viral attachment protein sigma 1. *J. Virol.* **69**:6972–6979.
  42. Whitfield, J., S. J. Neame, L. Paquet, O. Bernard, and J. Ham. 2001. Dominant-negative c-Jun promotes neuronal survival by reducing BIM expression and inhibiting mitochondrial cytochrome c release. *Neuron* **29**:629–643.
  43. Yujiro, T., M. Ware, C. Widmann, R. Oyer, D. Russell, E. Chan, Y. Zaitzu, P. Clarke, K. Tyler, Y. Oka, G. R. Fanger, P. Henson, and G. L. Johnson. 2000. MEK kinase 1 gene disruption alters cell migration and c-Jun NH<sub>2</sub>-terminal kinase regulation but does not cause a measurable defect in NF-κappa B activation. *Proc. Natl. Acad. Sci. USA* **97**:7272–7277.
  44. Zhou, G., and B. Roizman. 2000. Wild-type herpes simplex virus 1 blocks programmed cell death and release of cytochrome c but not the translocation of mitochondrial apoptosis-inducing factor to the nuclei of human embryonic lung fibroblasts. *J. Virol.* **74**:9048–9053.

## Novel Nuclear Herniations Induced by Nuclear Localization of a Viral Protein

Cristen C. Hoyt,<sup>1</sup> Ron J. Bouchard,<sup>2</sup> and Kenneth L. Tyler<sup>1,2,3,4,5,6\*</sup>

Departments of Immunology,<sup>1</sup> Microbiology,<sup>6</sup> Neurology,<sup>3</sup> and Medicine<sup>4</sup> and Program in Neurosciences,<sup>5</sup>  
University of Colorado Health Sciences Center, and Denver Veterans Affairs Medical Center,<sup>2</sup>  
Denver, Colorado 80262

Received 15 December 2003/Accepted 5 February 2004

**A common consequence of viral infection is perturbation of host cell nuclear functions. For cytoplasmically replicating viruses, this process may require regulated transport of specific viral proteins into the nucleus. Here, we describe a novel form of virus-induced perturbation of host cell nuclear structures. Active signal-mediated nuclear import of the reovirus  $\sigma$ 1s protein results in redistribution of nuclear pore complexes and nuclear lamins and formation of nuclear herniations. These herniations represent a previously undescribed mechanism by which cytoplasmic viral infection can perturb nuclear architecture and induce cytopathic effects, which ultimately lead to disease pathogenesis in the infected host.**

Mammalian reoviruses provide an important experimental model for understanding viral pathogenesis and virus-host interactions at a cellular level (40). Although reovirus replication occurs in the cytoplasm, infection disrupts a variety of host cell nuclear functions, resulting in a virus-induced cytopathic effect in infected cells and tissue injury in the infected host. For example, reovirus infection results in activation of specific cellular signaling pathways and their associated transcription factors (4–6), alteration of host cell gene expression (9, 30), perturbation of cell cycle regulation (31, 32), and induction of apoptosis (40, 41).

The mechanisms responsible for reovirus-induced alteration of nuclear function and the viral genes and proteins involved are only beginning to be characterized. For example, reovirus-induced inhibition of host cellular proliferation results from a cell cycle arrest at the G<sub>2</sub>/M checkpoint (32). Studies using a mutant reovirus and protein expression studies indicate that  $\sigma$ 1s, a nonstructural protein encoded by the reovirus S1 gene, is necessary and sufficient for reovirus-induced G<sub>2</sub>/M cell cycle arrest (32).  $\sigma$ 1s-mediated changes in cell cycle regulation are associated with changes in the activities and phosphorylation states of key G<sub>2</sub>/M-regulatory kinases, including p34 (cdc2) (31).

Like reoviruses, many other viruses perturb cell cycle regulation and other host cell nuclear functions, presumably in order to promote an optimal environment for viral replication. These viral effects on host cell nuclear functions can be mediated through a variety of mechanisms, including alteration of nuclear architecture (17, 18, 26, 37), disruption of nucleocytoplasmic transport pathways (12, 14, 27, 28), and induction of nuclear herniations (10). For cytoplasmically replicating viruses, the nuclear envelope (NE) acts as a protective boundary preventing indiscriminate interaction between cytoplasmic viral proteins and the nucleus. The NE consists of the outer and

inner nuclear membranes, nuclear pore complexes (NPCs), and the underlying nuclear lamina. The nuclear lamina organizes the distribution of NPCs (20), provides shape to the nucleus (39), and plays a role in chromatin organization (16). Embedded within the NE are large multiprotein NPC structures that regulate bidirectional macromolecular traffic between the nucleus and cytoplasm in eukaryotic cells. One mechanism by which viral proteins can traverse the NE is through active nucleocytoplasmic transport. This process can be mediated by the binding of cellular nuclear transport receptors (importins) to specific nuclear localization signals (NLS) in viral proteins. The viral protein complex docks at the cytoplasmic face of the NPC, following which the viral cargo is imported through the NPC and into the nucleus. Once inside the nucleus, viral proteins can interact with specific nuclear structures (15, 28, 44), nuclear proteins (19, 45), or chromatin (22, 35) to alter nuclear function.

Early immunocytochemical studies suggested that  $\sigma$ 1s could be detected in the nucleus during reovirus infection (1, 34); however, definitive evidence of  $\sigma$ 1s nuclear localization, the mechanism by which this occurs, and its potential effects on nuclear function have been lacking. We now show that reovirus  $\sigma$ 1s is actively localized to the nucleus, utilizing a previously unrecognized NLS. Nuclear localization of  $\sigma$ 1s induces profound structural defects in chromatin, disrupts nuclear lamina, and induces clustering of NPCs and the formation of nuclear herniations. These effects represent a novel type of virus-induced damage to host cell nuclear architecture, which provides a previously undescribed mechanism by which a cytoplasmically replicating virus can perturb nuclear function.

### MATERIALS AND METHODS

**Cells and viruses.** Mouse L929 cells were grown in minimal essential medium (Gibco/Invitrogen, Carlsbad, Calif.) supplemented to contain 5% heat-inactivated fetal bovine serum (Gibco/Invitrogen), 1 mM nonessential amino acids (Gibco/Invitrogen), and 2 mM L-glutamine (Gibco/Invitrogen). Human HeLa cells were grown in minimal essential medium (Gibco/Invitrogen) supplemented to contain 10% fetal bovine serum (Gibco/Invitrogen), 1 mM nonessential amino acids (Gibco/Invitrogen), and 2 mM L-glutamine (Gibco/Invitrogen). Cell monolayers were grown on eight-well glass chamber slides. Type 3 Abney (T3A)

\* Corresponding author. Mailing address: Department of Neurology (B-182), University of Colorado Health Sciences Center, 4200 E. 9th Ave., Denver, CO 80262. Phone: (303) 393-2874. Fax: (303) 393-4686. E-mail: Ken.Tyler@uchsc.edu.

reovirus was used as wild-type reovirus and is a laboratory stock. Type 3 reovirus clone 84-MA (T3C84-MA) was used as  $\sigma 1s$  null mutant reovirus and was originally isolated via serial passage of T3C84 through murine erythroleukemia cells (34).

**Plasmids.** A cDNA of reovirus T3A  $\sigma 1s$  was generated by reverse transcriptase PCR amplification from purified T3A double-stranded RNA by using primers specific for the  $\sigma 1s$  ORF. Chicken pyruvate kinase fused to green fluorescent protein (pEGFP-PK) was a generous gift (38). T3A  $\sigma 1s$  cDNA was cloned between green fluorescent protein (GFP) and chicken pyruvate kinase by using HindIII and BglII restriction sites to generate the GFP- $\sigma 1s$ -PK vector. Mutation constructs GFP-No NLS  $\sigma 1s$ -PK and  $\sigma 1s$  NLS-GFP-PK were derived from GFP- $\sigma 1s$ -PK by introducing specific amino acid changes via site-directed mutagenesis.

**Transfection.** L929 and HeLa cells were grown on glass chamber slides to 80% confluence. L929 cell DNA transfections were carried out with the Lipofectamine 2000 reagent by a method based on the recommended protocol described by the manufacturer (Gibco/Invitrogen). HeLa cell DNA transfections were carried out with the CalPhos mammalian transfection kit (BD Biosciences Clontech, Palo Alto, Calif.) by a method based on the recommended protocol described by the manufacturer.

**Immunocytochemistry.** Posttransfection, cells were washed in phosphate-buffered saline and fixed in fresh 3.7% paraformaldehyde in phosphate-buffered saline for 15 min (Fischer). Nuclei were visualized with Hoechst 33342 double-stranded DNA (dsDNA) stain (Molecular Probes, Eugene, Oreg.). GFP fusion proteins were visualized directly by digital fluorescence microscopy. For indirect immunofluorescence analysis, L929 or HeLa cells plated on glass chamber slides were fixed in 3.7% paraformaldehyde for 15 min, permeabilized with 0.1% Triton X-100–3 to 5% bovine serum albumin overnight at 4°C, blocked in 3 to 5% bovine serum albumin at 25°C for 1 h, and incubated with primary antibody overnight at 4°C. The antibodies used were as follows: mouse monoclonal anti-C23 antibody (1:100; Santa Cruz Biotechnology, Santa Cruz, Calif.), mouse monoclonal anti-nuclear transport factor p97/importin  $\beta$  antibody (1:1,000; Affinity BioReagents, Golden, Colo.), mAb414 (antinucleoporin antibody) (1:1,000; Covance/BabCo, Richmond, Calif.), and mouse monoclonal anti-lamin A and C (anti-LaA/C) (1:500; Covance/BabCo). The hybridoma cell line synthesizing the anti- $\sigma 1s$  antibody, 2F4, was a generous gift (34). Anti- $\sigma 1s$  was purified on a protein A column by a method based on the recommended protocol described by the manufacturer (Pierce, Rockford, Ill.). After being washed, cells were incubated with secondary horse anti-mouse immunoglobulin G conjugated to Texas red (1:100; Vector Laboratories, Inc., Burlingame, Calif.) for 1 h at 25°C. Cells were washed, and nuclei were visualized with Hoechst 33342 dsDNA stain and examined via deconvolution microscopy. Cellular expression patterns were quantified by examining approximately 100 cells/field. Three independent cell counts from different fields were normalized for graphing and statistically analyzed with In Stat version 3.0 (GraphPad, San Diego, Calif.).

**Microscopy.** Cells for transmission electron microscopy were fixed in 2.5% glutaraldehyde, postfixed in 2% osmium tetroxide, dehydrated in a graded series of alcohol solutions, and embedded in epoxy resin. Sections, approximately 80 nm in thickness, were stained with uranyl acetate and lead citrate prior to examination at 60 kV with a transmission electron microscope (Zeiss EM-10). Cells for digital fluorescence microscopy were imaged under oil immersion with a 63 $\times$  Plan-Apochromate objective (Zeiss AxioPlan 2 digital microscope with Cooke sensiCam 12-bit camera). Cells for digital deconvolution microscopy were imaged under oil immersion with a 63 $\times$  Plan-Apochromate objective, and by using nearest neighbor (Slidebook software; Intelligent Imaging Innovations, Denver, Colo.), multiple 0.5- $\mu$ m planes were deconvolved into an image in which blur and artifact had been digitally removed. Three-view images ( $x$  and  $y$  cross-sections) are expansions of deconvolved images in which orthogonal planes can be seen simultaneously.

**Nucleotide sequence accession numbers.** The NCBI accession number for T3A ( $\sigma 1s^+$  reovirus) is L37677, and the NCBI accession number for T3 C84-MA ( $\sigma 1s^-$  reovirus) is U74291.

## RESULTS

**$\sigma 1s$  localization during reovirus infection.** The subcellular localization of T3A  $\sigma 1s$  was determined by immunocytochemistry and deconvolution microscopy with the  $\sigma 1s$ -specific monoclonal antibody 2F4. Deconvolution of multiple planes through  $x$ ,  $y$ , and  $z$  axes of reovirus-infected L929 cells (Fig. 1A to C) and reovirus-infected HeLa cells (Fig. 1D to F) at 24 h postinfection clearly demonstrates the presence of  $\sigma 1s$  in the

cytoplasm and within nuclear boundaries as evidenced by the  $x$  and  $y$  plane cross-section images (Fig. 1A and D).  $\sigma 1s$  occupies discrete nuclear subareas as evidenced by the appearance of separate zones of  $\sigma 1s$  interlaced with distinct areas of chromatin in the  $x$  and  $y$  cross-sections (Fig. 1A and D). In infected L929 cells the distributions of  $\sigma 1s$  in the nucleus and cytoplasm are approximately equivalent (Fig. 1B). However, in HeLa cells  $\sigma 1s$  appears to preferentially localize to the nucleus (Fig. 1E). The  $\sigma 1s$  localization patterns shown persist through 48 h postinfection.

**Active signal-mediated nuclear import of  $\sigma 1s$ .** We expressed the 14-kDa  $\sigma 1s$  protein as a fusion with the cytoplasmic reporter protein, GFP-PK (38) (GFP- $\sigma 1s$ -PK) (Fig. 2E). The large size of the GFP- $\sigma 1s$ -PK fusion protein ensured that nuclear localization was dependent upon active  $\sigma 1s$  signal-mediated nuclear import and was not a result of passive diffusion. L929 cells were transiently transfected with either GFP-PK (Fig. 2B to D) or GFP- $\sigma 1s$ -PK (Fig. 2F to H) and analyzed at 24 h posttransfection via digital fluorescence microscopy. Constructs lacking  $\sigma 1s$  were restricted to the cytoplasm (Fig. 2B). Insertion of  $\sigma 1s$  resulted in significant redistribution of GFP-PK to the nucleus (Fig. 2F).  $\sigma 1s$  also imparted nuclear localization to GFP-PK in HeLa cells (data not shown). The percentage of cells exhibiting nuclear localization of the reporter construct compared to exclusively cytoplasmic localization is shown in Fig. 2I.

Examination of the  $\sigma 1s$  nuclear localization pattern in both reovirus-infected and  $\sigma 1s$ -transfected cells suggested that the protein was not uniformly distributed throughout the nucleus (Fig. 2H). We used an antibody against nucleolin to define nucleolar boundaries during GFP- $\sigma 1s$ -PK transfection of L929 cells. The nuclear expression pattern of GFP- $\sigma 1s$ -PK was distinctly segregated from nucleolar regions (Fig. 2J to L). Using deconvolution microscopy to image multiple sections through L929 cells expressing GFP- $\sigma 1s$ -PK in the  $x$ ,  $y$ , and  $z$  planes, we found that GFP- $\sigma 1s$ -PK was located both in the cytoplasm and within nuclear boundaries but was excluded from nucleolar regions of cell nuclei (Fig. 2 M, top and side panels). These studies indicate that both transfected  $\sigma 1s$  and virion-encoded  $\sigma 1s$  synthesized in cells during natural infection can translocate to the nucleus and that the  $\sigma 1s$  protein contains an NLS that can mediate nuclear localization of a cytoplasmic reporter protein.

**A novel  $\sigma 1s$  NLS.** Sequence analysis of  $\sigma 1s$  suggested the presence of a putative  $\sigma 1s$  NLS,  $^{15}$ RSRRRLK<sup>21</sup>, within a conserved arginine-rich region (11) near the N terminus of the protein. In order to ascertain whether this putative  $\sigma 1s$  NLS was functional, site-directed mutagenesis was performed to remove residues  $^{15}$ RSRRRLK<sup>21</sup> from  $\sigma 1s$  in the context of the GFP- $\sigma 1s$ -PK construct (Fig. 3C, schematic) (GFP-No NLS  $\sigma 1s$ -PK). L929 cells were transiently transfected with GFP-PK (Fig. 3A), GFP- $\sigma 1s$ -PK (Fig. 3B), or GFP-No NLS  $\sigma 1s$ -PK (Fig. 3C) and analyzed at 24 posttransfection via digital fluorescence microscopy. Removal of the putative  $\sigma 1s$  NLS significantly disrupted  $\sigma 1s$ -mediated nuclear localization of GFP- $\sigma 1s$ -PK (Fig. 3C and E). Similar results were found for GFP- $\sigma 1s$ -PK-transfected HeLa cells (data not shown).  $\sigma 1s$  amino acids  $^{15}$ RSRRRLK<sup>21</sup> were then added to the cytoplasmic GFP-PK protein to determine whether the  $\sigma 1s$  NLS alone was sufficient to mediate nuclear localization of the reporter protein (Fig. 3D) ( $\sigma 1s$  NLS-GFP-PK). Transfection of L929 cells with  $\sigma 1s$  NLS-GFP-PK resulted in significant nuclear localiza-

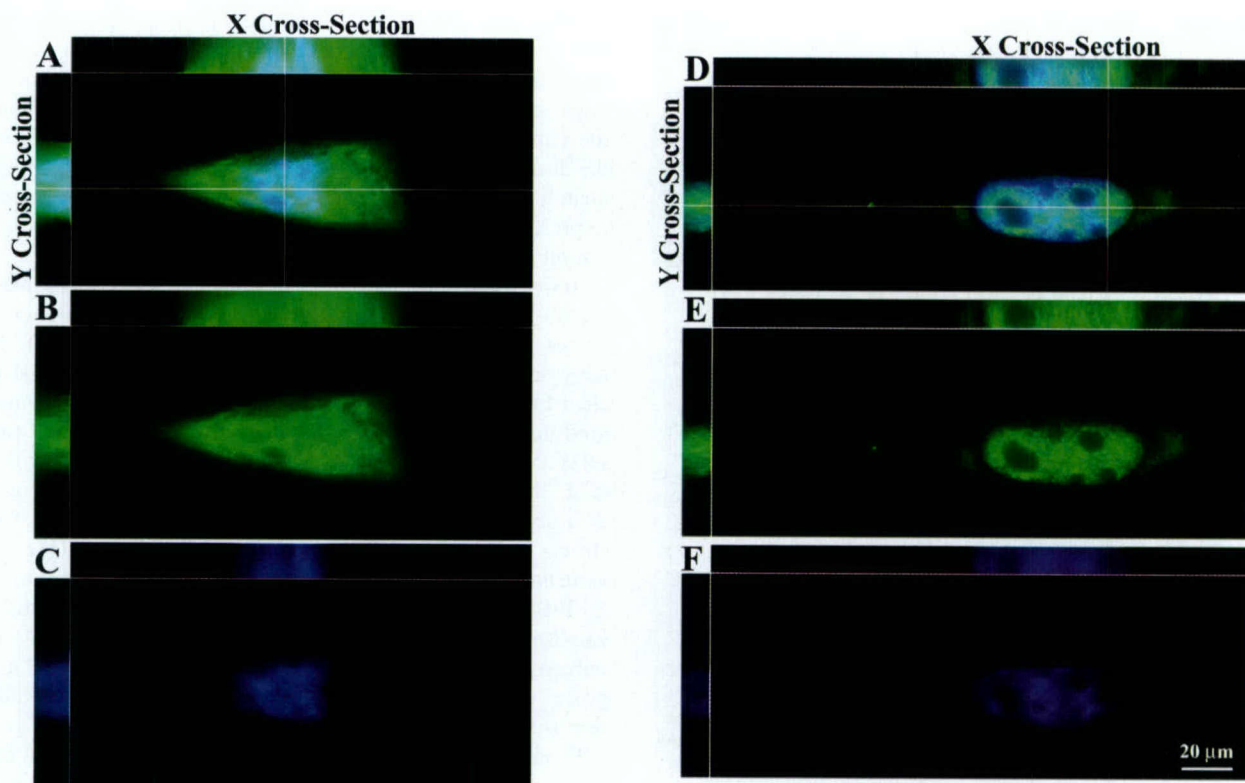


FIG. 1.  $\sigma 1s$  localizes to the nucleus and cytoplasm during natural virus infection. L929 cells (A to C) and HeLa cells (D to F) were infected with reovirus for 24 h and stained with a monoclonal antibody directed against  $\sigma 1s$ . (B and E) Monoclonal antibody staining was followed by a fluorescein isothiocyanate-conjugated secondary antibody. (C and F) Hoechst 33342 dsDNA stain was used to define the misshapen nuclei of  $\sigma 1s$ -expressing cells. (A and D) Deconvolution microscopy was used to analyze  $\sigma 1s$  subcellular and subnuclear localization in multiple  $x$ ,  $y$ , and  $z$  planes in the merged images.  $\sigma 1s$  localizes to the nucleus in infected cells but does not colocalize with chromatin (A and D).

tion of GFP-PK compared to cells transfected with reporter protein alone (Fig. 3F). These results indicate that  $\sigma 1s$  residues  $^{15}\text{RSRRRLK}^{21}$  comprise a novel  $\sigma 1s$  NLS which is both necessary and sufficient for nuclear localization.

**$\sigma 1s$ -induced nuclear herniations and infection.** In our studies of  $\sigma 1s$  localization we observed that infection of cells with wild-type reovirus was associated with dramatic alterations in the shape and distribution of nuclear chromatin (Fig. 1C and F). In order to determine whether  $\sigma 1s$  was required for these effects, we tested a  $\sigma 1s$  null mutant reovirus ( $\sigma 1s^-$  virus) for the presence of similar chromatin abnormalities during viral infection. The  $\sigma 1s$  null mutant reovirus is unable to express  $\sigma 1s$  due to a mutation in the S1 gene segment which introduces a premature stop codon at amino acid 6 in the  $\sigma 1s$  sequence (34). In cell culture  $\sigma 1s$ -deficient reovirus grows as well as its  $\sigma 1s^+$  parent virus and induces equivalent levels of apoptosis (34) but does not induce G<sub>2</sub>/M cell cycle arrest due to the loss of  $\sigma 1s$  expression (32).

Following infection of HeLa cells with wild-type reovirus ( $\sigma 1s^+$  virus), chromatin appeared to be misshapen and decompactored as indicated by heterogeneity in Hoechst 33442 staining (Fig. 4A). These changes were not seen following  $\sigma 1s^-$  virus infection, during which Hoechst 33442 staining remained homogenous and with an undistorted shape (Fig. 4D). These data suggested that the presence of  $\sigma 1s$  in the nucleus was the cause of the observed changes in nuclear architecture and chromatin organization.

Consistent with the observed irregularities in chromatin organization, examination of  $\sigma 1s^+$  virus-infected cell nuclei by differential interference contrast (DIC) microscopy revealed structural alterations in nuclear shape, which were not seen during  $\sigma 1s^-$  virus infection (Fig. 4, B and E). In  $\sigma 1s^-$  virus-infected cells, nuclei were generally round or ovoid with smooth nuclear contours (Fig. 4E), whereas cells infected with  $\sigma 1s^+$  virus contained nuclei of irregular shape with marked nuclear herniations containing DNA (Fig. 4A and B).

Thin-section electron microscopy was used to further examine the relationship between  $\sigma 1s$  and the nuclear morphology of reovirus-infected cells. Consistent with DIC microscopy, nuclei of  $\sigma 1s^+$  virus-infected HeLa cells were highly lobulated and misshapen, with prominent nuclear herniations evident (Fig. 5A). The cytoplasm of both  $\sigma 1s^+$  virus-infected and  $\sigma 1s^-$  virus-infected cells showed no changes other than the presence of replicating reovirus (Fig. 5). The chromatin of both  $\sigma 1s^+$  virus-infected and  $\sigma 1s^-$  virus-infected HeLa cells was surrounded by an intact NE and did not appear to be undergoing margination or compaction as is characteristic of later stages of reovirus-induced apoptosis (41).

Since disruption of the NE affects nuclear shape (20), we used an antibody against importin- $\beta$  to examine the consistency of the NE framework. The nuclear import receptor importin- $\beta$  defines both the contoured boundaries of the nuclear envelope and the integrity of specific nuclear import components within the NE by its ability to form an import complex

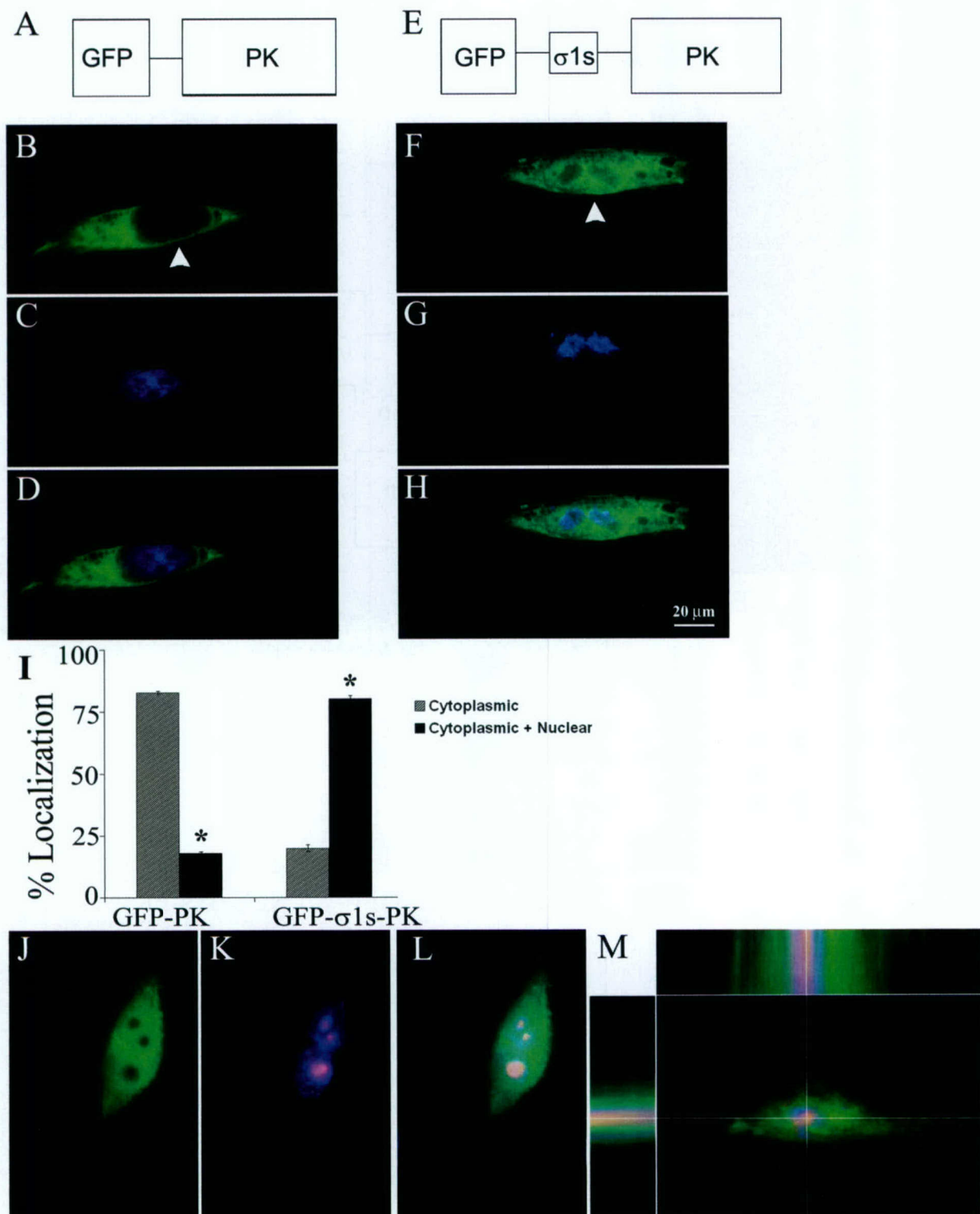


FIG. 2. σ1s imparts nuclear localization to a cytoplasmic reporter protein and does not localize to the nucleolus. (A) Schematic of GFP-PK fusion protein. (E) Schematic of GFP-σ1s-PK fusion protein. (B to D and F to H) L929 cells were transiently transfected with GFP-PK (B to D) or GFP-σ1s-PK (F to H). Hoechst 33342 dsDNA stain was used to define nuclei (C and G). Arrowheads indicate localization of fusion proteins. GFP-σ1s-PK significantly (\*) ( $P < 0.001$ ) localized to the nucleus (I) and did not colocalize with misshapen chromatin (G and H). (J to M) GFP-σ1s-PK-transfected L929 cells were stained with a monoclonal antibody directed against nucleolin followed by a Texas-red conjugated secondary antibody to demonstrate that GFP-σ1s-PK does not localize to nucleolar regions. Deconvolution microscopy was used to analyze subcellular and subnuclear localization in multiple  $x$ ,  $y$ , and  $z$  planes (top and side bars in panel M).

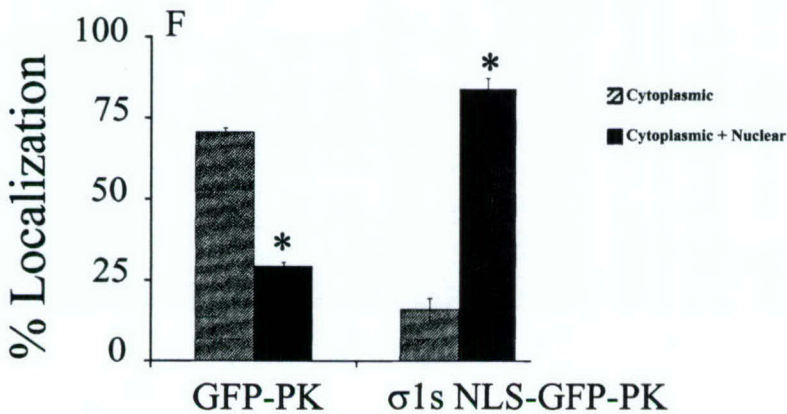
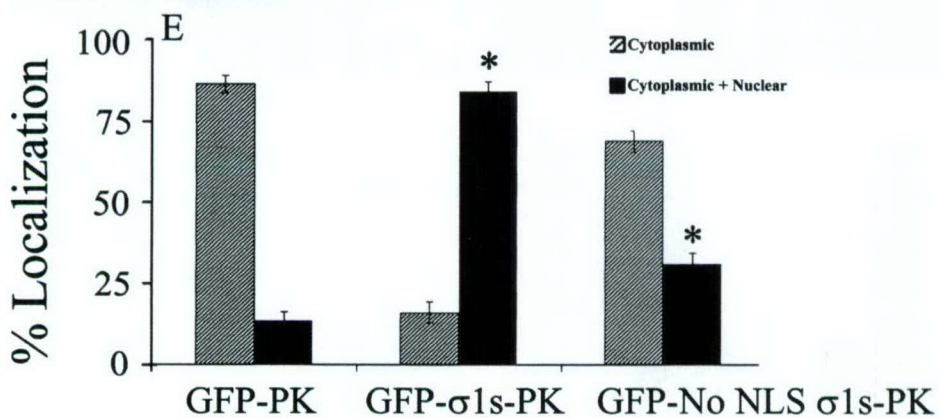
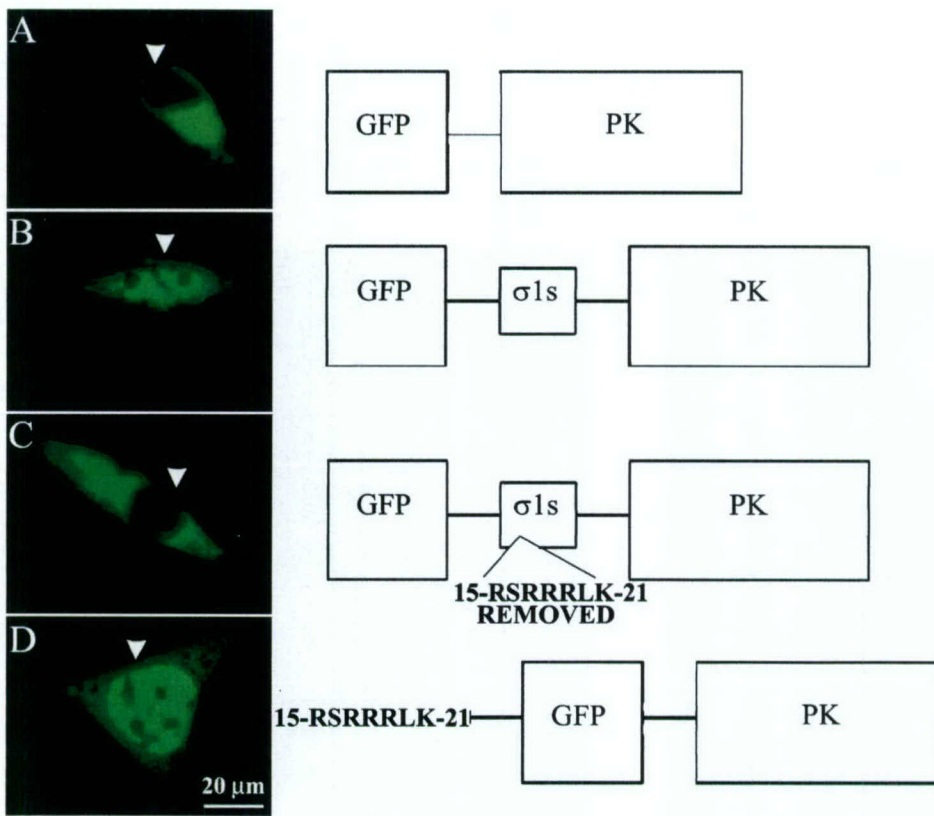
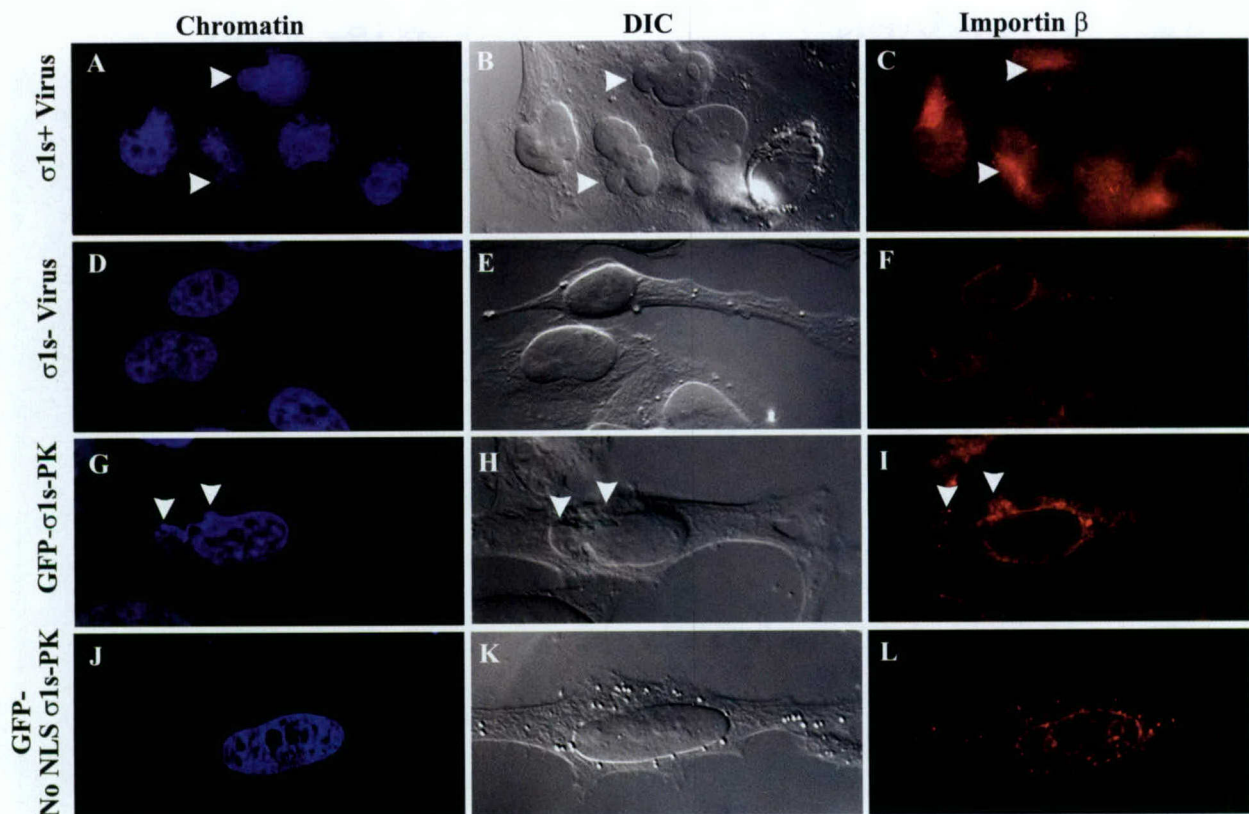


FIG. 3.  $\sigma$ 1s contains a novel NLS ( $^{15}$ RSRRRLK $^{21}$ ) that is necessary and sufficient for nuclear import. L929 cells were transiently transfected with GFP-PK (A), GFP- $\sigma$ 1s-PK (B), GFP-No NLS  $\sigma$ 1s-PK (C), or  $\sigma$ 1s-NLS-GFP-PK (D) and analyzed via digital fluorescence microscopy. Removal of the  $\sigma$ 1s NLS from GFP- $\sigma$ 1s-PK resulted in significant (\*) ( $P < 0.001$ ) loss of nuclear localization (E) while addition of the  $\sigma$ 1s NLS resulted in significant translocation to the nucleus (F).  $\sigma$ 1s amino acids  $^{15}$ RSRRRLK $^{21}$  comprise a previously undiscovered NLS.



**FIG. 4.**  $\sigma 1s$  nuclear localization induces nuclear herniations during natural virus infection and  $\sigma 1s$  transfection. HeLa cells were infected with wild-type reovirus ( $\sigma 1s^+$  virus) (A to C) or  $\sigma 1s$  null reovirus ( $\sigma 1s^-$  virus) (D to F) for 24 h. Hoechst 33342 dsDNA stain was used to define nuclei (A, D, G, and J).  $\sigma 1s^+$  virus-infected cells induced localized disruption in nuclear morphology (arrowheads in panel B) and chromatin staining (arrowheads in panel A) compared to cells infected with the mutant reovirus that does not produce  $\sigma 1s$  (D and E). The nuclear envelope remained intact in  $\sigma 1s^+$  virus-infected cells and displayed areas of importin- $\beta$  clustering, suggestive of NPC clustering (arrowheads in panel C) while  $\sigma 1s^-$  virus-infected cells retained typical nuclear morphology, chromatin, and importin- $\beta$  staining (D to F). GFP- $\sigma 1s$ -PK-transfected HeLa cells displayed identical alterations in nuclear morphology, chromatin staining, and importin- $\beta$  clustering (arrowheads in panels G to I) compared to cells expressing  $\sigma 1s$  only in the cytoplasm (J to L).  $\sigma 1s$  induces disruption in nuclear morphology (arrowheads in panel H), chromatin staining (arrowheads in panel G), and importin- $\beta$  (arrowheads in panel I) only when localized in the nucleus.

containing NLS-containing protein cargo, dock the import complex at the cytoplasmic face of the NPC, and release it at the nucleoplasmic face of the NE (7). In  $\sigma 1s^+$  virus-infected cells, importin- $\beta$  staining showed that the NE remained intact and encompassed the altered nuclear contour (Fig. 4C). Consistent with spacing of NPCs throughout the NE, importin- $\beta$  staining maintained a punctate pattern throughout the NEs of  $\sigma 1s^-$  virus-infected cells (Fig. 4F). In contrast, in  $\sigma 1s^+$  virus-infected cells, importin- $\beta$  staining showed a pattern of areas of dense positive staining localized to the cytoplasmic face of nuclear herniations, which is suggestive of clustered NPCs at nuclear herniation sites (Fig. 4C).

**$\sigma 1s$  nuclear import and nuclear herniations.** The conclusion that virally encoded  $\sigma 1s$  expressed during infection induces nuclear herniations is further strengthened by the finding that identical alterations in NE morphology were seen when  $\sigma 1s$  was expressed alone. As seen with viral infection, GFP- $\sigma 1s$ -PK transfection of L929 cells (Fig. 2G) and HeLa cells (Fig. 4G) induces chromatin abnormalities. When  $\sigma 1s$  was inhibited from entering the nucleus due to removal of the  $\sigma 1s$  NLS (GFP-No NLS  $\sigma 1s$ -PK) the nucleus maintained the smooth contour and unaltered symmetric morphology of nontrans-

fected cells and the chromatin remained of a uniform and undistorted shape (Fig. 4J and K). By contrast, nuclear expression of  $\sigma 1s$  grossly altered the nuclear contour and chromatin staining intensity and shape (Fig. 4G and H). Despite the presence of an altered nuclear shape seen in the DIC image induced by  $\sigma 1s$  nuclear localization (Fig. 4H), the NEs of GFP- $\sigma 1s$ -PK-expressing cell nuclei remained intact and encompassed the altered nuclear contour (Fig. 4I). Similarly to  $\sigma 1s^+$  virus-infected cells, GFP- $\sigma 1s$ -PK-expressing cells exhibited cytoplasmic clustering of importin- $\beta$  in areas of nuclear herniations (Fig. 4I), again suggesting that although NPCs are positioned throughout the NE, they appear to be clustered within areas of nuclear herniations. In summary, both  $\sigma 1s$  transfection and  $\sigma 1s$  expression during natural virus infection induced nuclear herniations distinguished by misshapen chromatin, abnormal nuclear morphology, and importin- $\beta$  clustering. These data indicate that  $\sigma 1s$  is both necessary and sufficient for herniation development and that the appearance of nuclear herniations required the presence of  $\sigma 1s$  in the nuclei of cells.

**NPC clustering and nuclear lamina disruption.** As suggested by the pattern of importin- $\beta$  staining, antibodies to NPC

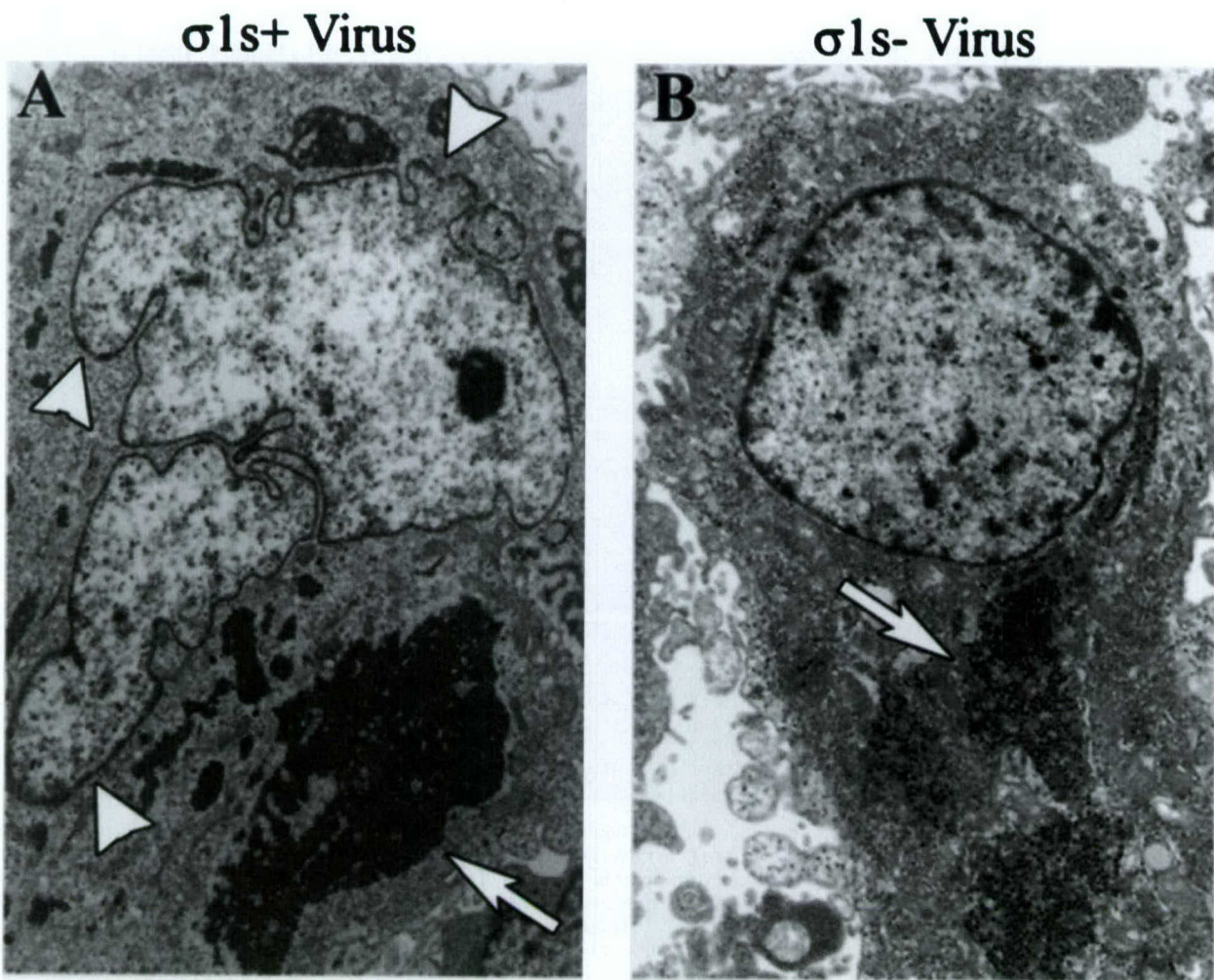


FIG. 5.  $\sigma 1s$  induces nuclear herniations during natural virus infection. HeLa cells were infected with wild-type reovirus ( $\sigma 1s^+$  virus) (A) or  $\sigma 1s$  null reovirus ( $\sigma 1s^-$  virus) (B) for 24 h. Thin-section electron microscopy was used to image nuclear architecture changes induced by  $\sigma 1s$  expression.  $\sigma 1s$  induces nuclear herniations (arrowheads in panel A). Both wild-type and  $\sigma 1s$  null reovirus are present in the cytoplasm (arrows).

proteins (nucleoporins) confirmed clustering of NPCs in areas of  $\sigma 1s$ -induced nuclear herniations. Nucleoporin labeling of cells lacking  $\sigma 1s$  in the nucleus (GFP-No NLS  $\sigma 1s$ -PK) showed uninterrupted punctate NE rim and NE surface staining characteristic of the regular distribution of NPC (2) throughout the NE (Fig. 6D to F and J to L). Conversely, cells in which  $\sigma 1s$  was expressed in the nucleus (GFP- $\sigma 1s$ -PK) exhibited clustering of NPC in areas of  $\sigma 1s$ -induced nuclear herniations seen at both the rim and the surface of the NE (Fig. 6B and H). Although some rim-like NPC staining was apparent in nuclei of these cells (Fig. 6B), the remainder of the NE was usually barren of NPC (Fig. 6B). This can be seen more directly by looking at the surface of the nucleus in which the NE was depleted of NPCs in specific areas (Fig. 6H) balanced by others areas with clustered NPCs near herniation sites (Fig. 6I), while minor regions of the NE appeared to have NPCs in a regular distribution.

An intact nuclear lamina helps govern correct spacing of NPCs and helps maintain normal nuclear shape (13, 21, 23). The type V intermediate filament proteins lamins A and C are

major components of the nuclear lamina and polymerize in various ratios to form a filamentous scaffold which maintains nuclear shape and integrity (24, 39). The observed  $\sigma 1s$ -mediated abnormalities in nuclear shape and  $\sigma 1s$ -induced clustering of NPC and herniation development could result from perturbation of the nuclear lamina organization. A monoclonal antibody against A-type nuclear LaA/C was used to stain HeLa cells transfected with GFP- $\sigma 1s$ -PK (Fig. 7A to C) or GFP-No NLS  $\sigma 1s$ -PK (Fig. 7D to F) constructs. In contrast to the round or ovoid nuclei of nontransfected cells (data not shown) or to GFP-No NLS  $\sigma 1s$ -PK-transfected cells, which display normal continuous nuclear rim LaA/C staining (Fig. 7F), GFP- $\sigma 1s$ -PK-expressing cell nuclei displayed marked abnormalities in the A-type lamina network (Fig. 7C). Within the nucleus,  $\sigma 1s$  induced highly localized defects in the nuclear lamina at sites of herniations, which appeared as LaA/C gaps (Fig. 7C). In addition, LaA/C accumulated at other points throughout the nucleus, sometimes at the base of herniations, as seen by increased intensity of LaA/C staining (Fig. 7C). Thus, both the

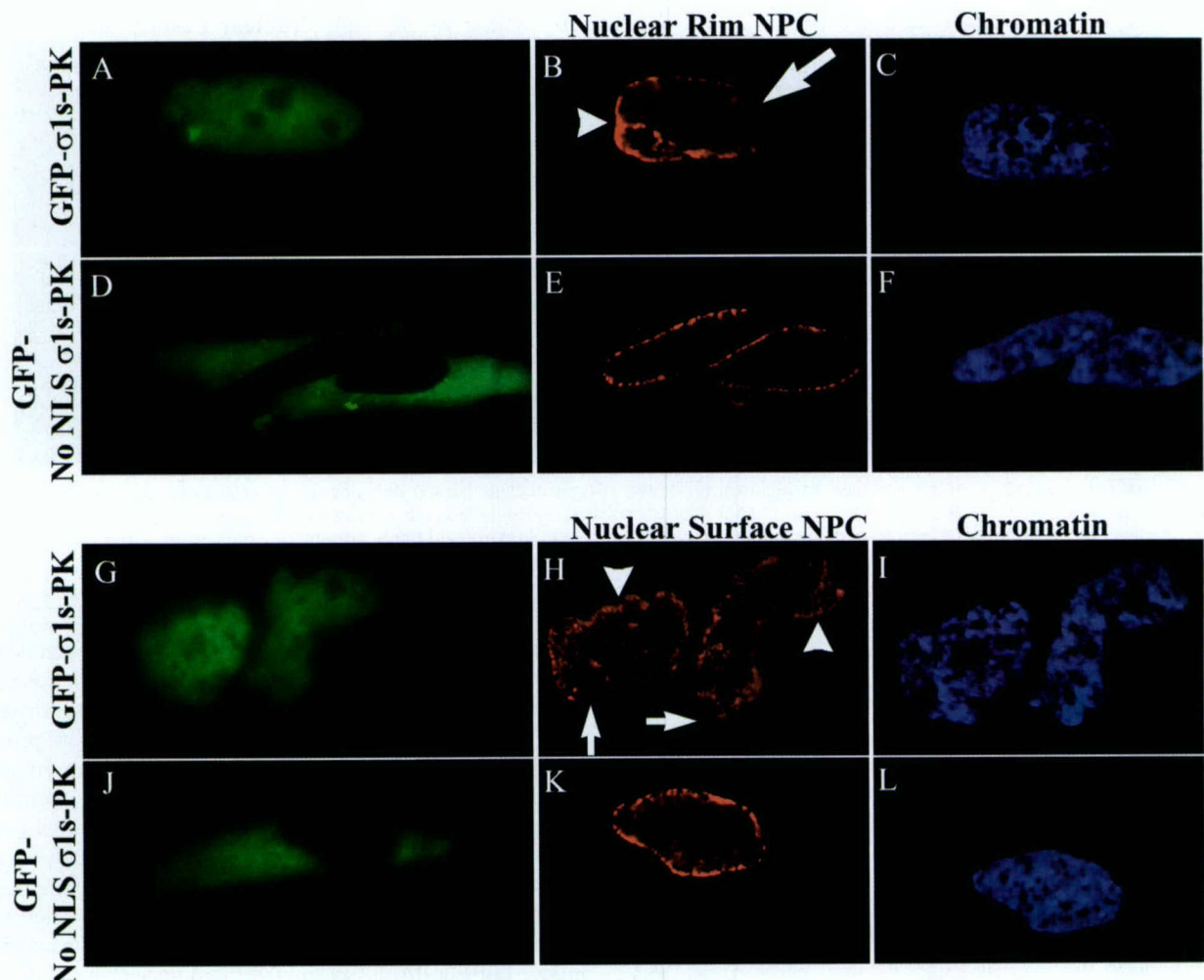


FIG. 6. Nuclear localization of  $\sigma$ 1s induces NPC clustering. HeLa cells were transfected with GFP- $\sigma$ 1s-PK (A to C and G to I) or GFP-No NLS  $\sigma$ 1s-PK (D to F and J to L). Digital microscopy of NPC nucleoporin-labeled cells expressing GFP- $\sigma$ 1s-PK (A and G) showed clustering of NPCs at the surface of the nucleus (arrowheads in panel H) and at the nuclear rim (arrowheads in panel B), while some areas of the NE were depleted of NPC (arrows in panels B and H). Cells in which  $\sigma$ 1s is expressed but is not able to translocate to the nucleus (D and J) showed conventional NPC staining (E and K). Hoechst 33342 dsDNA stain was used to define nuclei (C, F, I, and L).

A-type lamina network and NPCs are perturbed by the translocation of  $\sigma$ 1s into the host cell nucleus.

## DISCUSSION

Cytoplasmic reovirus infection profoundly affects the host cell nucleus and its functions (9, 30–32, 41). Recently, we have shown that  $\sigma$ 1s plays a key role in determining host cell nuclear function by its capacity to modulate virus-induced G<sub>2</sub>/M cell cycle arrest in infected cells (31, 32). We now show that the  $\sigma$ 1s protein localizes to the nucleus in both infected and transfected cells. Nuclear import of  $\sigma$ 1s occurs by an active, NLS-mediated mechanism involving a novel  $\sigma$ 1s NLS, <sup>15</sup>RSRRRLK<sup>21</sup>, that is both necessary and sufficient for  $\sigma$ 1s nuclear localization.

Upon entering the nucleus,  $\sigma$ 1s induces disruptions in chromatin organization, NPC distribution, and nuclear lamina organization, which result in profound distortion of nuclear morphology and in the appearance of a novel type of nuclear

herniation containing both  $\sigma$ 1s and cellular DNA (Fig. 6A and G and 7A). Both NPCs and the A-type lamina network lose their normal homogenous distribution and become irregularly clustered in specific areas of the NE and subsequently absent from others. It is unclear which of these two disturbances is primary. Although the primary means of herniation development has yet to be determined,  $\sigma$ 1s-induced nuclear herniations represent a novel type of virus-induced perturbation of nuclear structure.

Perturbation of the nuclear lamina can grossly alter nuclear shape, induce nuclear herniations and NPC clustering, and alter chromatin organization (10, 13, 21, 23, 36, 42). Vigouroux et al. reported that skin fibroblasts from patients bearing mutations in LaA/C possess nuclei with prominent NE herniations deficient in NPCs and exhibit aberrant chromatin staining (42). Loss of lamin expression in *Caenorhabditis elegans* or *Drosophila* mutants results in spatial disorganization of NPCs, nuclear herniations, chromatin disorganization, and cell cycle inhibi-

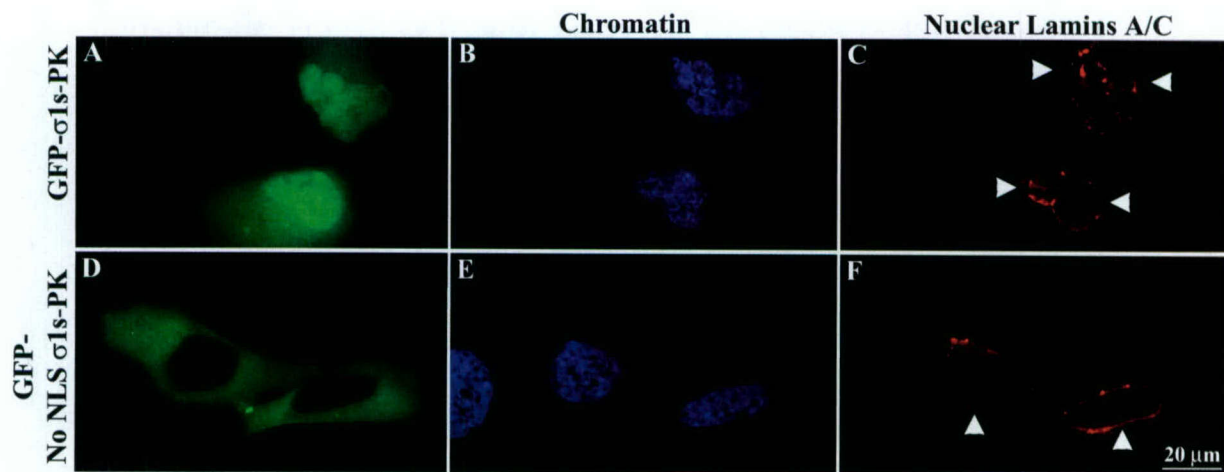


FIG. 7. Nuclear localization of  $\sigma$ 1s induces disorganization of the A-type nuclear lamina network. HeLa cells were transfected with GFP- $\sigma$ 1s-PK (A to C) or GFP-No NLS  $\sigma$ 1s-PK (D to F). Digital microscopy of LaA/C-labeled cells expressing GFP- $\sigma$ 1s-PK showed delamination of the A-type nuclear lamina network (arrowheads in panel C). Cells in which  $\sigma$ 1s is expressed but is not able to translocate to the nucleus showed conventional LaA/C staining (F). Hoechst 33342 dsDNA stain was used to define nuclei (B and E).

tion (21, 23). Like these lamin-based nuclear herniations,  $\sigma$ 1s-induced nuclear herniations display similar patterns of lamina disorganization, chromatin staining, and NE shape abnormalities. However, NPC clustering is a prominent feature of  $\sigma$ 1s-induced herniations, and although NPC clustering is a result of lamin-based nuclear architecture abnormalities in the *C. elegans* and *Drosophila* systems (21, 23), this has not yet been described for mammalian cells.

An alternative explanation for our findings is that altered NPC structure and distribution may trigger disorganization of the nuclear lamina and its attached chromatin, resulting in the development of nucleoporin-based nuclear herniations. NPCs form an immobile network within the NE and are tethered by the nuclear lamina (8, 21, 23, 39). Wente and Blobel suggested a model in which perturbation of the N terminus of nucleoporin 145p (nup145p) resulted in an irregular NPC distribution, NPC clustering, and multilobulated nuclei with irregular chromatin organization (43). They suggested that loss of the N terminus of nup145p left the NPC unanchored and allowed it to diffuse into the NE, resulting in NPC clustering and nuclear shape abnormalities (43). In yeast two-hybrid experiments, we found that  $\sigma$ 1s interacted with mammalian nucleoporin p54 (nup54) (unpublished observation). This suggests the possibility that  $\sigma$ 1s may interact with nup54 and destabilize the NPC structure within the NE, allowing the unanchored NPC to migrate and cluster with other destabilized NPCs within the NE. One consequence of the abnormal migration of NPCs is that the attached lamina could become strained and disorganized, in turn altering nuclear morphology and chromatin organization. This model is supported by our data, which show that, similar to the case for nup145p $\Delta$ N herniations,  $\sigma$ 1s expression induces misshapen lobulated nuclei with prominent nuclear herniations, clustered NPCs, and aberrant chromatin staining.

Regardless of whether  $\sigma$ 1s-induced nuclear herniations arise from a primary lamina disorganization event or from a primary disturbance in NPC structure, it is interesting to speculate about their potential biological significance. Reovirus infection

leads to a G<sub>2</sub>/M cell cycle arrest in infected cells and is associated with alteration of the activity and phosphorylation status of key G<sub>2</sub>/M regulatory proteins (31). The phosphorylation state and consequent enzymatic activity of many G<sub>2</sub>/M proteins are in part dependent upon their subcellular compartmentalization (29). Interestingly, even though reoviruses (which undergo cytoplasmic viral replication) and retroviruses (which undergo nuclear viral replication) differ dramatically in their replicative strategies and structural organizations, the human immunodeficiency virus type 1 Vpr protein has many functional parallels with reovirus  $\sigma$ 1s, including the capacity to induce both G<sub>2</sub>/M cell cycle arrest and nuclear herniations in infected and transfected cells (10, 31–33). It has recently been suggested that Vpr-induced nuclear herniations may serve to dysregulate the compartmentalization of G<sub>2</sub>/M cell cycle proteins (10). Perhaps  $\sigma$ 1s plays an analogous role in reovirus-infected cells. Both Vpr (10)- and  $\sigma$ 1s-induced nuclear herniations are characterized by the disorganization of the nuclear lamina and chromatin architecture, yet  $\sigma$ 1s-induced nuclear herniations consistently display clustering of NPCs at or near herniation sites, establishing them as a unique type of virus-induced nuclear alteration. It is possible that this disorganization itself plays a role in disrupting cell cycle regulation. *C. elegans* lamin mutants have both abnormal nuclear morphology and the inability to complete the cell cycle (23), and *Xenopus* extracts with disrupted nuclear lamin organization undergo DNA synthesis arrest, in turn prohibiting mitotic progression (25). Taken together, these findings suggest that  $\sigma$ 1s may alter nuclear architecture to affect G<sub>2</sub>/M arrest by either herniating the nucleus or disrupting nuclear lamina organization.

Mechanisms of virus-induced cytopathic effects in infected host cells are complex and only partially defined. Our work presented here identifies a new type of virus-mediated alteration of nuclear architecture and a novel form of virus-induced cytopathic effect. Virus-induced nuclear herniations may well influence regulation of cellular behavior and gene expression

from the nucleus and ultimately disease pathogenesis in the infected host.

#### ACKNOWLEDGMENTS

We thank Gary W. Mierau for electron microscopy collaboration. We also thank Warner C. Greene for the generous gift of the pEGFP-PK vector, which was invaluable in our studies, and Terry Dermody for the 2F4 hybridoma cell line.

This work was supported by Public Health Service grant 1RO1AG14071 from the National Institutes of Health (to K.L.T.), Merit and REAP grants from the Department of Veterans Affairs (to K.L.T.), U.S. Army Medical Research and Material Command grant DAMD17-98-1-8614 (to K.L.T.), and the Reuler-Lewin Family Professorship of Neurology (to K.L.T.).

#### REFERENCES

- Belli, B. A., and C. E. Samuel. 1991. Biosynthesis of reovirus-specified polypeptides: expression of reovirus S1-encoded sigma 1NS protein in transfected and infected cells as measured with serotype specific polyclonal antibody. *Virology* **185**:698–709.
- Bodoor, K., S. Shaikh, P. Enarson, S. Chowdhury, D. Salina, W. H. Raharjo, and B. Burke. 1999. Function and assembly of nuclear pore complex proteins. *Biochem. Cell Biol.* **77**:321–329.
- Bogerd, A. M., J. A. Hoffman, D. C. Amberg, G. R. Fink, and L. I. Davis. 1994. nup1 mutants exhibit pleiotropic defects in nuclear pore complex function. *J. Cell Biol.* **127**:319–332.
- Clarke, P., S. M. Meintzer, L. Moffitt, and K. L. Tyler. 2003. Two distinct phases of virus-induced NF- $\kappa$ B-regulation enhance TRAIL-mediated apoptosis in virus-infected cells. *J. Biol. Chem.* **278**:18092–18100.
- Clarke, P., S. M. Meintzer, C. Widmann, G. L. Johnson, and K. L. Tyler. 2001. Reovirus infection activates JNK and the JNK-dependent transcription factor c-Jun. *J. Virol.* **75**:11275–11283.
- Connolly, J. L., S. E. Rodgers, P. Clarke, D. W. Ballard, L. D. Kerr, K. L. Tyler, and T. S. Dermody. 2000. Reovirus-induced apoptosis requires activation of transcription factor NF- $\kappa$ B. *J. Virol.* **74**:2981–2989.
- Conti, E. 2002. Structures of importins, p. 93–113. In K. Weis (ed.), Nuclear transport. Springer-Verlag, Heidelberg, Germany.
- Daigle, N., J. Beaudouin, L. Hartnell, G. Imreh, E. Hallberg, J. Lippincott-Schwartz, and J. Ellenberg. 2001. Nuclear pore complexes form immobile networks and have a very low turnover in live mammalian cells. *J. Cell Biol.* **154**:71–84.
- DeBiasi, R. L., P. Clarke, S. Meintzer, R. Jotte, B. K. Kleinschmidt-Demasters, G. L. Johnson, and K. L. Tyler. 2003. Reovirus-induced alteration in expression of apoptosis and DNA repair genes with potential roles in viral pathogenesis. *J. Virol.* **77**:8934–8947.
- de Noronha, C. M., M. P. Sherman, H. W. Lin, M. V. Cavrois, R. D. Moir, R. D. Goldman, and W. C. Greene. 2001. Dynamic disruptions in nuclear envelope architecture and integrity induced by HIV-1 Vpr. *Science* **94**:1105–1108.
- Dermody, T. S., M. L. Nibert, R. Bassel-Duby, and B. N. Fields. 1990. Sequence diversity in S1 genes and S1 translation products of 11 serotype 3 reovirus strains. *J. Virol.* **64**:4842–4850.
- Enninga, J., D. E. Levy, G. Blobel, and B. M. Fontoura. 2002. Role of nucleoporin induction in releasing an mRNA nuclear export block. *Science* **295**:1523–1525.
- Favreau, C., E. Dubosclard, C. Ostlund, C. Vigouroux, J. Capeau, M. Wehnert, D. Higuet, H. J. Worman, J. C. Courvalin, and B. Buendia. 2003. Expression of lamin A mutated in the carboxyl-terminal tail generates an aberrant nuclear phenotype similar to that observed in cells from patients with Dunnigan-type partial lipodystrophy and Emery-Dreifuss muscular dystrophy. *Exp. Cell Res.* **282**:14–23.
- Fortes, P., A. Beloso, and J. Ortín. 1994. Influenza virus NS1 protein inhibits pre-mRNA splicing and blocks mRNA nucleocytoplasmic transport. *EMBO J.* **13**:704–712.
- Fouchier, R. A., B. E. Meyer, J. H. Simon, U. Fischer, A. V. Albright, F. Gonzalez-Scarano, and M. H. Malim. 1998. Interaction of the human immunodeficiency virus type 1 Vpr protein with the nuclear pore complex. *J. Virol.* **72**:6004–6013.
- Glass, J. R., and L. Gerace. 1990. Lamins A and C bind and assemble at the surface of mitotic chromosomes. *J. Cell Biol.* **111**:1047–1057.
- Gustin, K. E., and P. Sarnow. 2001. Effects of poliovirus infection on nucleocytoplasmic trafficking and nuclear pore complex composition. *EMBO J.* **20**:240–249.
- Gustin, K. E., and P. Sarnow. 2002. Inhibition of nuclear import and alteration of nuclear pore complex composition by rhinovirus. *J. Virol.* **76**:8787–8796.
- Hirano, M., S. Kaneko, T. Yamashita, H. Luo, W. Qin, Y. Shirota, T. Nomura, K. Kobayashi, and S. Murakami. 2003. Direct interaction between nucleolin and hepatitis C virus NS5B. *J. Biol. Chem.* **278**:5109–5115.
- Hutchison, C. J. 2002. Lamins: building blocks or regulators of gene expression? *Nat. Rev. Mol. Cell Biol.* **3**:848–858.
- Lenz-Bohme, B., J. Wismar, S. Fuchs, R. Reifegerste, E. Buchner, H. Betz, and B. Schmitt. 1997. Insertional mutation of the *Drosophila* nuclear lamin Dm0 gene results in defective nuclear envelopes, clustering of nuclear pore complexes, and accumulation of annulate lamellae. *J. Cell Biol.* **137**:1001–1016.
- Lim, C., D. Lee, T. Seo, C. Choi, and J. Choe. 2003. Latency-associated nuclear antigen of Kaposi's sarcoma-associated herpesvirus functionally interacts with heterochromatin protein 1. *J. Biol. Chem.* **278**:7397–7405.
- Liu, J., T. R. Ben Shahar, D. Riemer, M. Treinin, P. Spann, K. Weber, A. Fire, and Y. Gruenbaum. 2000. Essential roles for *Caenorhabditis elegans* lamin gene in nuclear organization, cell cycle progression, and spatial organization of nuclear pore complexes. *Mol. Biol. Cell.* **11**:3937–3947.
- Moir, R. D., and T. P. Spann. 2001. The structure and function of nuclear lamins: implications for disease. *Cell Mol. Life Sci.* **58**:1748–1757.
- Moir, R. D., T. P. Spann, H. Herrmann, and R. D. Goldman. 2000. Disruption of nuclear lamin organization blocks the elongation phase of DNA replication. *J. Cell Biol.* **149**:1179–1192.
- Muranyi, W., J. Haas, M. Wagner, G. Krohne, and U. H. Koszinowski. 2002. Cytomegalovirus recruitment of cellular kinases to dissolve the nuclear lamina. *Science* **297**:854–857.
- Petersen, J. M., L. S. Her, and J. E. Dahlberg. 2001. Multiple vesiculoviral matrix proteins inhibit both nuclear export and import. *Proc. Natl. Acad. Sci. USA* **98**:8590–8595.
- Petersen, J. M., L. S. Her, V. Varvel, E. Lund, and J. E. Dahlberg. 2000. The matrix protein of vesicular stomatitis virus inhibits nucleocytoplasmic transport when it is in the nucleus and associated with nuclear pore complexes. *Mol. Cell. Biol.* **20**:8590–8601.
- Pines, J. 1999. Four-dimensional control of the cell cycle. *Nat. Cell Biol.* **1**:E73–E79.
- Poggiali, G. J., R. L. DeBiasi, R. Bickel, R. Jotte, A. Spalding, G. L. Johnson, and K. L. Tyler. 2002. Reovirus-induced alterations in gene expression related to cell cycle regulation. *J. Virol.* **76**:2585–2594.
- Poggiali, G. J., T. S. Dermody, and K. L. Tyler. 2001. Reovirus-induced  $\sigma$ 1s-dependent  $G_{(2)}/M$  phase cell cycle arrest is associated with inhibition of p34 (cdc2). *J. Virol.* **75**:7429–7434.
- Poggiali, G. J., C. Keefer, J. L. Connolly, T. S. Dermody, and K. L. Tyler. 2000. Reovirus-induced  $G_{(2)}/M$  cell cycle arrest requires  $\sigma$ 1s and occurs in the absence of apoptosis. *J. Virol.* **74**:9562–9570.
- Poon, B., K. Gravitz-Ferbas, S. A. Stewart, and I. S. Chen. 1998. Cell cycle arrest by Vpr in HIV-1 virions and insensitivity to antiretroviral agents. *Science* **281**:266–269.
- Rodgers, S. E., J. L. Connolly, J. D. Chappell, and T. S. Dermody. 1998. Reovirus growth in cell culture does not require the full complement of viral proteins: identification of a  $\sigma$ 1s-null mutant. *J. Virol.* **72**:8597–8604.
- Rohr, O., D. Lecestre, S. Chasserot-Golaz, C. Marban, D. Avram, D. Aunis, M. Leid, and E. Schaeffer. 2003. Recruitment of Tat to heterochromatin protein HP1 via interaction with CTIP2 inhibits human immunodeficiency virus type 1 replication in microglial cells. *J. Virol.* **77**:5415–5427.
- Schirmer, E. C., T. Guan, and L. Gerace. 2001. Involvement of the lamin rod domain in heterotypic lamin interactions important for nuclear organization. *J. Cell Biol.* **153**:479–489.
- Scott, E. S., and P. O'Hare. 2001. Fate of the inner nuclear membrane protein lamin B receptor and nuclear lamins in herpes simplex virus type 1 infection. *J. Virol.* **75**:8818–8830.
- Sherman, M. P., C. M. de Noronha, M. I. Heusch, S. Greene, and W. C. Greene. 2001. Nucleocytoplasmic shuttling by human immunodeficiency virus type 1 Vpr. *J. Virol.* **75**:1522–1532.
- Stuurman, N., S. Heins, and U. Aebi. 1998. Nuclear lamins: their structure, assembly, and interactions. *J. Struct. Biol.* **122**:42–66.
- Tyler, K. L., P. Clarke, R. L. DeBiasi, D. Kominsky, and G. J. Poggiali. 2001. Reoviruses and the host cell. *Trends Microbiol.* **9**:560–564.
- Tyler, K. L., M. K. Squier, S. E. Rodgers, B. E. Schneider, S. M. Oberhaus, T. A. Grdina, J. J. Cohen, and T. S. Dermody. 1995. Differences in the capacity of reovirus strains to induce apoptosis are determined by the viral attachment protein sigma 1. *J. Virol.* **69**:6972–6979.
- Vigouroux, C., M. Auclair, E. Dubosclard, M. Pouchelet, J. Capeau, J. C. Courvalin, and B. Buendia. 2001. Nuclear envelope disorganization in fibroblasts from lipodystrophic patients with heterozygous R482Q/W mutations in the lamin A/C gene. *J. Cell Sci.* **114**:4459–4468.
- Wente, S. R., and G. Blobel. 1994. NUP145 encodes a novel yeast glycine-leucine-phenylalanine-glycine (GLFG) nucleoporin required for nuclear envelope structure. *J. Cell Biol.* **125**:955–969.
- Wurm, T., H. Chen, T. Hodgson, P. Britton, G. Brooks, and J. A. Hiscox. 2001. Localization to the nucleolus is a common feature of coronavirus nucleoproteins, and the protein may disrupt host cell division. *J. Virol.* **75**:9345–9356.
- Zolotukhin, A. S., and B. K. Felber. 1999. Nucleoporins nup98 and nup214 participate in nuclear export of human immunodeficiency virus type 1 Rev. *J. Virol.* **73**:120–127.

## Regional Differences in Viral Growth and Central Nervous System Injury Correlate with Apoptosis

Sarah M. Richardson-Burns<sup>1,2</sup> and Kenneth L. Tyler<sup>1,2,3,4\*</sup>

*Neuroscience Program<sup>1</sup> and Departments of Neurology, Medicine, Immunology, and Microbiology,<sup>3</sup> University of Colorado Health Sciences Center,<sup>2</sup> and Denver Veteran's Affairs Medical Center,<sup>4</sup> Denver, Colorado 80262*

Received 2 October 2003/Accepted 8 January 2004

**Infection of neonatal mice with reovirus T3 Dearing (T3D), the prototypic neurotropic reovirus, causes fatal encephalitis associated with neuronal injury and virus-induced apoptosis throughout the brain. T3D variant K (VarK) is an antigenic variant that has a nearly 1 million-fold reduction in neurovirulence following intracerebral (i.c.) inoculation compared to T3D and a restricted pattern of central nervous system injury with damage limited to the hippocampus, sparing other brain regions. We wished to determine whether the restricted pattern of VarK-induced injury was due to a reduced capacity to replicate in or injure cortical, as opposed to hippocampal, tissue. We found that following i.c. inoculation, VarK grew to similar titers as T3D in the hippocampus but had significantly lower titers in the cortex. Both viruses grew to identical titers and infected the same percentage of cells in mouse primary hippocampal cultures (MHC). In mouse primary cortical cultures (MCC) both the number of infected cells and the viral yield per infected cell were significantly lower for VarK than T3D. VarK-induced apoptosis was limited to the hippocampus *in vivo*, and *in vitro* both viruses induced apoptosis equally in MHC but VarK induced significantly less apoptosis than T3D in MCC. Growth of T3D in MCC was reduced to levels comparable to those of VarK following treatment of MCC with caspase inhibitors. Conversely, induction of apoptosis in VarK-infected MCC with fatty acid synthase-activating antibody significantly enhanced viral yield. These results suggest that the decreased neurovirulence of VarK may be due to its failure to efficiently induce apoptosis in cortical neurons.**

Experimental reovirus infection is used as a model for studying the roles of viral genes and the proteins they encode in virus-cell interactions *in vitro* and during pathogenesis *in vivo*. Type 3 (T3) reoviruses are highly neurovirulent, causing fatal encephalitis in neonatal mice that is associated with massive central nervous system (CNS) apoptosis (13, 16). Differences in the capacity of reovirus strains to infect discrete populations of cells within the CNS and to induce apoptosis are determined by the viral S1 gene (22, 23, 25). Antigenic variants of T3 strain Dearing (T3D) have been generated by incubating T3D with anti-sigma 1 neutralizing monoclonal antibodies (19). Following intracerebral (i.c.) inoculation into newborn mice, the prototypic reovirus antigenic variant K (VarK) has markedly reduced neurovirulence and decreased CNS growth and induces a restricted pattern of CNS injury when compared to the parental virus from which it was derived, T3D (10, 18). These dramatic phenotypic differences are reproduced by a reassortant virus containing the VarK S1 gene, indicating that mutations in this gene alone account for the variant phenotype (10). Nucleotide sequence analysis of the S1 gene indicate that VarK and T3D differ by a single nucleotide change which results in a single amino acid substitution in VarK (K419L) in the globular head domain of sigma 1 (3).

Prior studies indicate that VarK was not restricted for growth in mouse L929 fibroblasts *in vitro* and that it was able to grow to equivalent titers as T3D in a wide variety of non-neuronal organs *in vivo* (18, 19). VarK also retains the capacity to

spread within the CNS through neural pathways, another property linked to the S1 gene (10). The mutation in VarK is not associated with either the sialic acid or JAM1 receptor binding domains of sigma 1 (5). The basis for the restricted pattern of CNS injury by VarK and its attenuated growth within the CNS were unknown. We now show that VarK has a selectively reduced capacity to induce apoptosis in the mouse cortex and diencephalon *in vivo* and in cortical neuronal cultures *in vitro*. This results in reduced viral growth of VarK in the cortex and diencephalon *in vivo* and in cortical neurons *in vitro* compared to that of the wild-type parent strain T3D. Together, these data help explain the restricted pattern of CNS injury and reduced CNS viral growth of VarK.

### MATERIALS AND METHODS

**Viral infection of mice.** Postnatal day 2 neonatal Swiss-Webster mice were infected with either T3D or variant K via i.c. injection with a 29-gauge needle in a 10-μl volume. Animals were sacrificed 7 days after infection. Control mice were not injected.

**Primary neuronal cultures.** Primary cortical and hippocampal cultures were prepared from embryonic day 20 or postnatal day 0 Swiss-Webster mice. Mouse pups were decapitated, brains were removed, and the cingulate frontal cortex and hippocampus were dissected, immediately submerged in ice-cold sterile Hanks buffer (without calcium chloride, magnesium chloride, magnesium sulfate, and phenol red; GibcoBRL, Invitrogen, Carlsbad, Calif.), and then manually dissociated with a 1-ml pipette tip. The percentage of viable cells was quantified by trypan blue staining with a hemocytometer. Cells were plated at densities of  $10^5$  cells per ml in poly-D-lysine (PDL)-coated 12-well polystyrene plates or on PDL-laminin 12-mm glass coverslips placed in 6-well plates (BioCoat; BD Biosciences, San Jose, Calif.). Mouse cortical cultures (MCC) were maintained in neurobasal A media (2% B27 [GibcoBRL], 10% fetal bovine serum, 0.5 mM L-glutamine) at 37°C in 5% CO<sub>2</sub>, and mouse hippocampal cultures (MHC) were maintained in the same media with the addition of 100 μM glutamic acid (Sigma) for the first 4 days in culture. Four days after plating, a 50% medium change was performed, adding fresh media. Cells were allowed to mature for 7 to 10 days

\* Corresponding author. Mailing address: Department of Neurology (B-182), University of Colorado Health Sciences Center, 4200 E. 9th Ave., Denver, CO 80262. Phone: (303) 393-2874. Fax: (303) 393-4686. E-mail: ken.tyler@uchsc.edu.

before use in experiments. The neuronal and astroglial contents of MCC and MHC were assessed by immunocytochemistry for cell type-specific markers (other CNS cells are present at negligible levels in the cortex and hippocampus of day 0 newborn or day 20 embryonic mice).

**Viral growth assays.** Viral growth in mouse brains, MCC, and MHC was assayed by determining virus titers at various times postinfection (p.i.) with a multiplicity of infection (MOI) of 10 by plaque assay on a monolayer of L929 mouse fibroblasts as previously described (10, 14, 21). For some experiments with MCC and MHC, the pan caspase inhibitor ZVAD-FMK (15  $\mu$ M; Calbiochem, San Diego, Calif.) was added to the cultures immediately following viral infection and was maintained in the media throughout the infection. For some experiments, the apoptosis-inducing activating antibody anti-fatty acid synthase (FAS) (0.5  $\mu$ g/ml; Upstate Biotech, Waltham, Mass.) was added to the cultures immediately following viral infection and was maintained in the media throughout the infection.

**Histology.** For histologic analysis, mouse brains were fixed by immersion in 10% buffered formalin for 18 to 30 h at room temperature (RT), transferred to 70% ethanol, paraffin embedded, and sectioned at a 4- $\mu$ m thickness. For each animal, a coronal section that showed cingulate gyrus, hippocampus, and thalamus was stained with hematoxylin and eosin for studies to determine the extent of virus-induced pathology.

**Apoptosis assays.** Cell monolayers were virus infected with an MOI of 100. Apoptotic cells were identified by evaluating nuclear morphology at various times following reovirus infection by staining fixed cells with the fluorescent nuclear DNA intercalating dye Hoechst 33342 (Molecular Probes, Eugene, Oreg.) as previously described (16). A biotin-streptavidin-based terminal deoxynucleotidyltransferase-mediated dUTP-biotin nick end labeling (TUNEL) kit optimized for neuronal tissues and cells was used (NeuroTACS II; Trevigen, Gaithersburg, Md.). At 48 h following reovirus infection, cells were fixed with 3.7% formaldehyde-phosphate-buffered saline (PBS) for 10 min, postfixed in methanol for 20 min, and then permeabilized in Neupore (Trevigen) for 30 min at RT under hydrophobic coverslips. For each condition, the percentage of TUNEL-positive cells was determined by counting 300 cells in at least three individual samples. Caspase 3 activity in reovirus-infected (MOI, 100) and mock-infected primary cortical and hippocampal cultures was detected via the ApoAlert caspase 3 activity fluorometric assay (Clontech, Palo Alto, Calif.) as previously described (11). Samples were transferred to 96-well enzyme-linked immunosorbent assay plates for detection of fluorescent activity with a fluorimeter (Cytofluor series 4000; PerSeptive Biosystems) set with a 400-nm excitation filter and a 505-nm emission filter.

**Immunocytochemistry and immunohistochemistry.** For viral antigen detection, T3D- and VarK-infected (MOI, 100) MCC and MHC were grown on PDL-coated glass coverslips, fixed at various times following virus infection with 3.7% formaldehyde-PBS for 30 min at RT, and permeabilized with PBS-0.1% Triton X-100 (PBSX). Primary antibody (diluted 1:100 in 3% bovine serum albumin [BSA]-PBSX) was incubated at 4°C overnight, washed in PBSX, and then incubated with secondary antibody for 1 h at RT in the dark. After immunocytochemistry, nuclei of cells were labeled with Hoechst 33342-PBS, aqueous mounted with Vectashield, sealed with nail polish, and stored at 4°C until imaging as described for TUNEL. Double labeling of cultures was as previously described (16).

For immunohistochemistry, mouse brains were fixed in 10% buffered formalin, paraffin embedded, processed, and sectioned (4- $\mu$ m thickness), and then sections were deparaffinized by baking at 57°C for 5 min followed by immersion in mixed xylenes and rehydration in a series of descending ethanol concentrations followed by PBS. For viral antigen staining, brain tissue sections were permeabilized with Neupore (Trevigen) for 30 min at RT, blocked for 1 h in 5% BSA-PBSX (PBS with 0.1% Triton X-100), and then incubated for 1 h at 37°C with anti-T3D polyclonal antisera at a 1:100 dilution in 3% BSA-PBSX (21). Sections were washed twice in PBSX, incubated for 30 min in the dark with secondary antibody anti-rabbit Alexa Fluor 594 (1:100; Molecular Probes) and Neurotrace Alexa Fluor 430 Nissl (1:50; Molecular Probes) in 1.5% BSA-PBSX. Sections were washed three times in PBSX, aqueous mounted with Vectashield (Vectorlabs, Burlingame, Calif.), sealed with nail polish, and stored at 4°C until imaging. Immunohistochemistry for activated caspase 3 was as previously described (15, 16).

## RESULTS

**VarK injures only a subset of neurons that are susceptible to T3D-induced injury.** T3D causes neuronal injury and death throughout the neonatal mouse CNS, with particularly severe

injury seen in the cingulate gyrus, frontoparietal cortex, subiculum, CA1 to CA4 regions of the hippocampus, and several thalamic nuclei (20). In contrast, previous studies found that VarK-induced injury is almost exclusively restricted to the hippocampus (Fig. 1A to C) (18). VarK is much less neurovirulent than T3D, which causes fatal encephalitis in 100% of infected neonatal mice at doses as low as 10 PFU by 14 days p.i. by i.c. inoculation. In contrast, 90% of mice i.c. infected with the highest possible dose of VarK (greater than  $3 \times 10^7$  PFU) never develop encephalitis and survive beyond 14 days p.i. (19). We now report that VarK-infected neonatal mice survive into adulthood with no observable neurologic deficits and no detectable virus in the brain at 6 or 12 weeks after infection, indicated by the absence of reovirus antigen as detected by immunohistochemistry (data not shown). Histologic analysis of brains from these mice revealed prominent lesions in the CA2 to CA4 regions of the hippocampus associated with cellular debris and evidence of some infiltrating immune cells but no gliosis (identified by morphology) (Fig. 1E). This indicates that VarK-induced injury remains restricted to the hippocampus throughout the course of the infection and that virus has been cleared from the brain by 6 weeks p.i.

**VarK grows as well as T3D in the hippocampus but does not grow in other brain regions that support robust growth of T3D.** The hippocampal restriction of VarK-induced CNS injury could result either from an enhanced susceptibility of hippocampal compared to cortical neurons to VarK-induced injury or by the reduced capacity of VarK to grow in the cortex compared to the hippocampus. Therefore, to better understand the altered pattern of CNS pathogenesis of VarK, we evaluated VarK growth in various brain regions and expression of VarK antigen throughout the brain. VarK has attenuated growth in whole-brain lysates compared to T3D (10, 18); however, differences in the capacity of VarK and T3D to grow in individual brain regions have not been previously assessed. We therefore compared growth of T3D and VarK in tissue microdissected from the hippocampus and cortex (frontoparietal cortex and cingulate gyrus combined) at 7 days following i.c. inoculation of viruses into newborn mice. T3D grew well in all brain regions, reaching viral titers of  $10^9$  PFU/ml in the cortex and  $>10^8$  PFU/ml in the hippocampus and cerebellum (Fig. 2A). VarK grew to nearly the same titer as T3D in the hippocampus but reached a peak titer of  $<10^6$  PFU/ml in the cortex, >1,000-fold less than that achieved by T3D.

We next compared the distribution of viral antigen in the brain by immunocytochemistry. In VarK-infected brains, viral antigen was found exclusively in the CA2-CA4 region of the hippocampus (Fig. 2B) in striking contrast to T3D infection, following which antigen was detected throughout the cortex, CA2-CA4 region of the hippocampus, thalamus (Fig. 2C), and cerebellum (data not shown). Taken together, these data indicate that although both T3D and VarK grow almost equally well in the hippocampus, by contrast, growth of VarK is markedly attenuated in other brain regions that are readily infected by T3D.

**VarK induces apoptosis in the hippocampus but not in other regions of the CNS in infected mice.** It has previously been shown that apoptosis is the major mechanism by which T3D reoviruses induce injury in the CNS (13, 16). We therefore wished to determine whether VarK and T3D differed in their

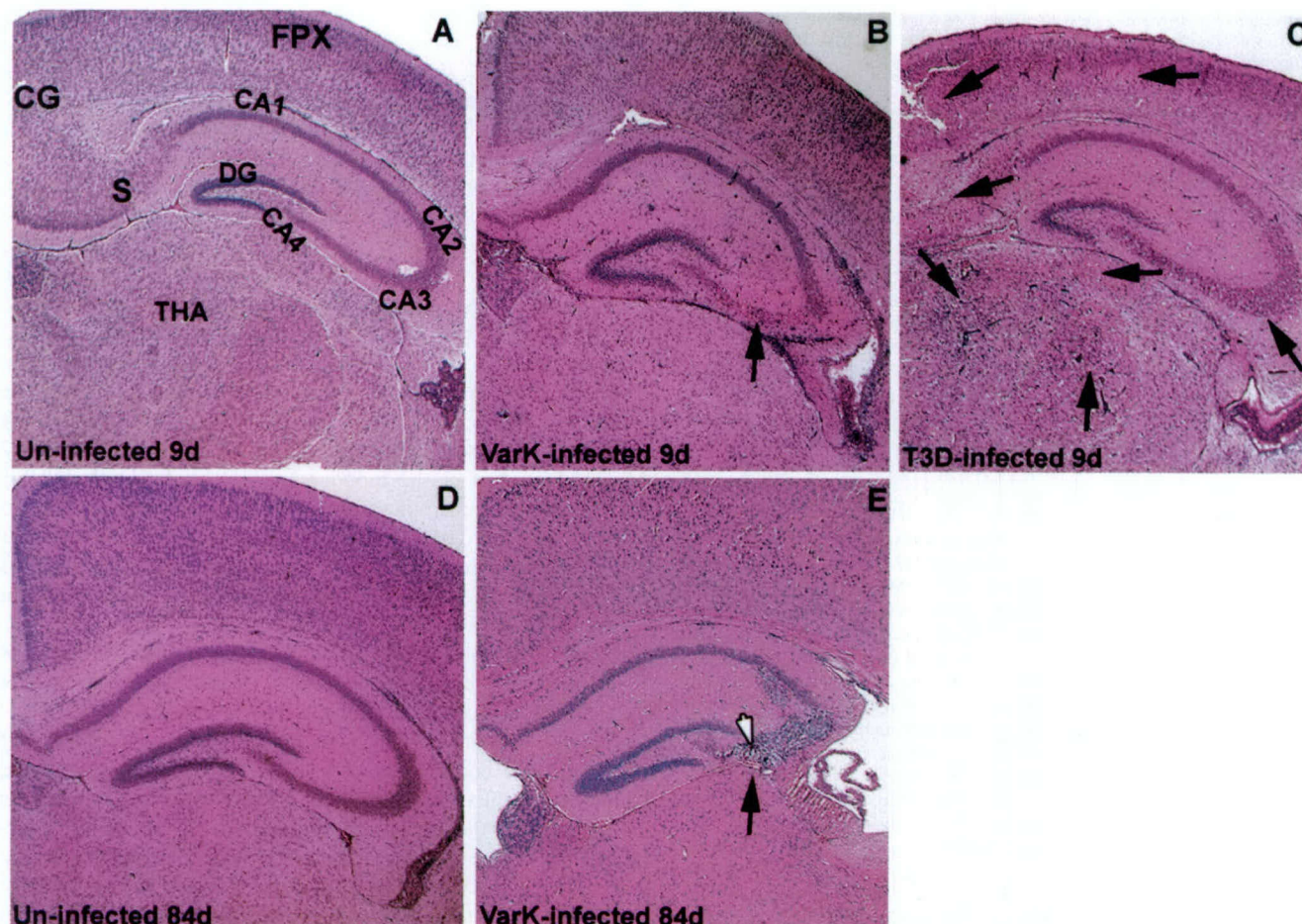


**FIG. 1.** VarK injures only a subset of neurons that are susceptible to T3D-induced injury, resulting in long-term loss of hippocampal cells after clearance of the virus. (A) Coronal brain section from an uninfected mouse 9 days (d) postnatal shows normal cytoarchitecture with hematoxylin and eosin histologic stain. (B) Brain section from VarK-infected mouse 7 days p.i. and 9 days postnatal shows normal cytoarchitecture and no evidence of neuronal loss in the cortical and thalamic areas but shows viral injury in the CA2 to CA3 region of the hippocampus, indicated by neuronal death and minor inflammation. (C) Brain section from a T3D-infected mouse 7 days p.i. and 9 days postnatal shows abnormal cytoarchitecture, massive cell loss, and minor inflammation throughout the cortical, hippocampal, and thalamic regions. T3D-infected mice die 7 to 9 days p.i. (D) Brain section from an uninfected mouse at 12 weeks (84 days) postnatal shows normal brain cytoarchitecture. (E) Brain section from a VarK-infected mouse 82 days p.i. and 84 days postnatal. CG, cingulate gyrus; FPX, frontoparietal cortex; S, subiculum; DG, dentate gyrus; THA, thalamic nuclei. Arrows point to areas of severe viral injury. These tissue sections are representative of data from the results of 4 studies with at least 8 mice per treatment group in each study.

capacity to induce apoptosis *in vivo* and whether this correlated with differences in their patterns of replication. At 7 days following i.c. inoculation of neonatal mice with T3D or VarK, we analyzed the brains of infected mice for evidence of apoptosis by TUNEL staining and staining for the activated form of the key apoptotic effector caspase, caspase 3. In VarK-infected brains, apoptosis was limited to the CA2-CA4 region of the hippocampus, the identical anatomic site in which the largest amount of viral antigen was detected by immunocytochemistry (compare Fig. 2B to 3B). By contrast, as previously reported (13, 16), T3D produced apoptosis throughout the cortex, thalamus, and hippocampus, again corresponding to regions of peak viral antigen detection (Fig. 3C). Since VarK was clearly able to induce apoptosis in the hippocampus, it did not have a global defect in its capacity to induce neuronal apoptosis. However, in comparison to T3D, VarK showed a

striking regional restriction in apoptosis induction, failing to induce apoptosis in the cortex, thalamus, or cerebellum.

**The capacity of VarK to induce apoptosis and grow in primary hippocampal and cortical neuronal cultures parallels its *in vivo* phenotype.** Our results *in vivo* indicated that there was an almost perfect correlation between the growth of VarK and its capacity to induce apoptosis but did not indicate which was the key causal factor. Thus, this correlation may have resulted from the fact that apoptosis is required for optimal viral growth and that a reduced capacity of VarK to induce apoptosis in the cortex and other regions may have resulted in impaired replication, thus limiting viral growth and virus-induced injury to that brain region. Conversely, optimal viral growth may be required for apoptosis induction, with VarK's impaired replication in the cortex and other regions resulting in an attenuated capacity to induce apoptosis and produce histopatholog-

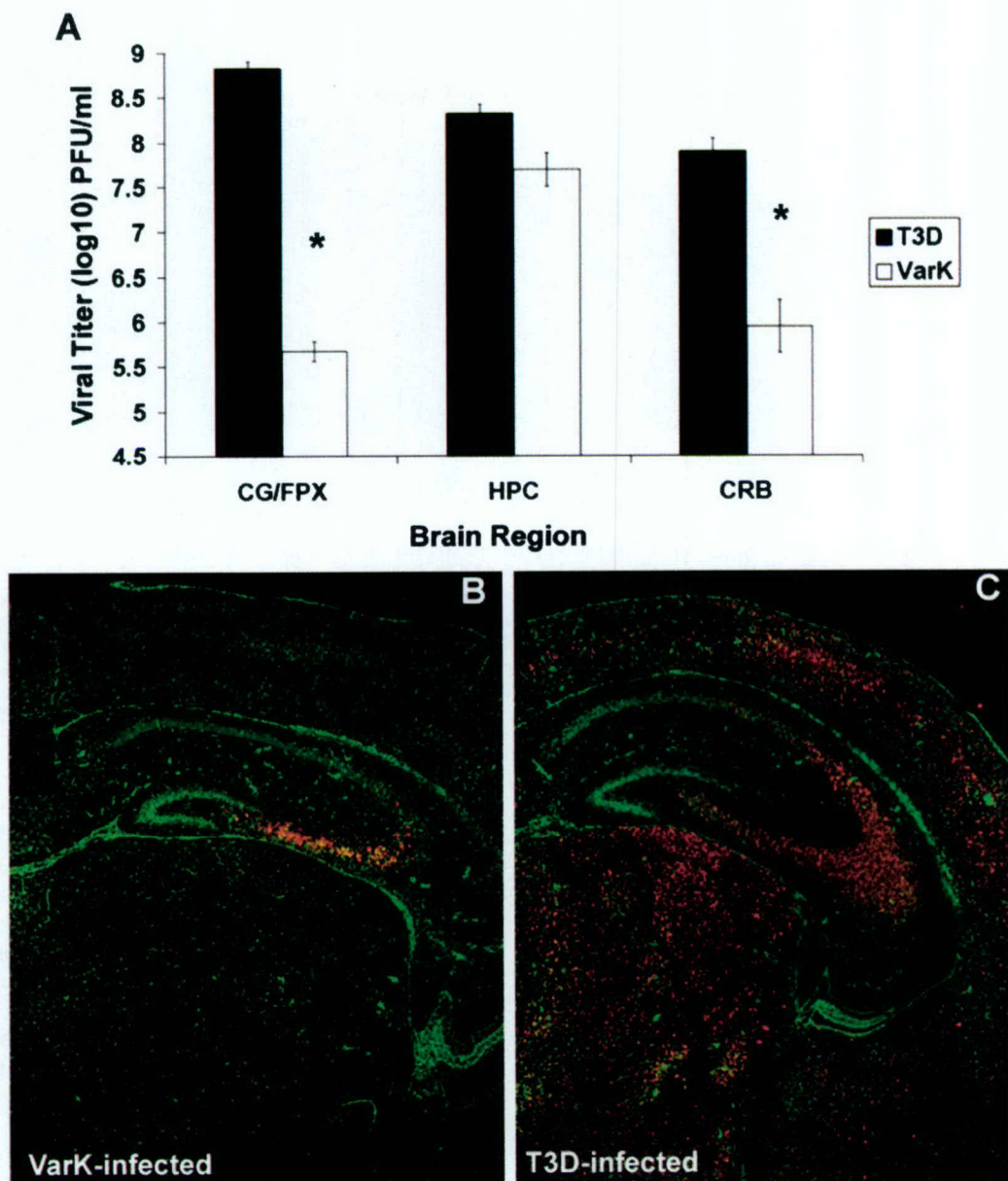


**FIG. 2.** VarK grows as well as T3D in the hippocampus but does not grow in other brain regions that support robust growth of T3D. (A) VarK did not grow as well as wild-type T3D in the cortex (cingulate gyrus [CG] combined with frontoparietal cortex [FPX]) or cerebellum (CRB), however VarK and T3D grew to similar titers in the hippocampus (HPC). These data are brain region viral titers from day 7 p.i. \*,  $P < 0.01$  for T3D compared to VarK titer by Tukey-Kramer. These tissue sections are representative of data from 2 studies with 3 mice per treatment group in each study. (B) The coronal section of the brain from a mouse i.c. inoculated with VarK 7 days p.i. immunohistochemically stained for reovirus antigen shows that viral antigen is restricted to the CA2 to CA4 regions of the hippocampus (red staining is positive). (C) A brain section from a mouse i.c. inoculated with T3D 7 days p.i. stained for reovirus antigen shows strong positive staining (red cells) throughout the cortical, hippocampal, and thalamic regions of the brain. All neurons in brain tissue sections were counterstained with fluorescent Nissl stain (green cells). These tissue sections are representative of data from 4 studies with at least 8 mice per treatment group in each study.

ical injury. To investigate this issue further, we examined the capacity of VarK and T3D to grow and induce apoptosis in primary neuronal cultures derived from the hippocampus and cortex.

Primary neuronal cultures derived from the hippocampus (MHC) and cortex (MCC) of postnatal day 0 mice were prepared as described (see Materials and Methods) and infected at 7 to 10 days postisolation with either T3D or VarK at an

MOI of 10. Both MCC and MHC have 75 to 95% neuronal content as quantified by dual immunocytochemical staining for microtubule-associated protein 2 (MAP2), a neuronal marker, and glial fibrillary acidic protein (GFAP), an astroglial marker (Fig. 4A to H). Other CNS cells such as oligodendrocytes and microglia (identified morphologically) are not present in these cultures; furthermore, neuronal cultures are maintained in serum-free media to inhibit the growth of nonneuronal cells.

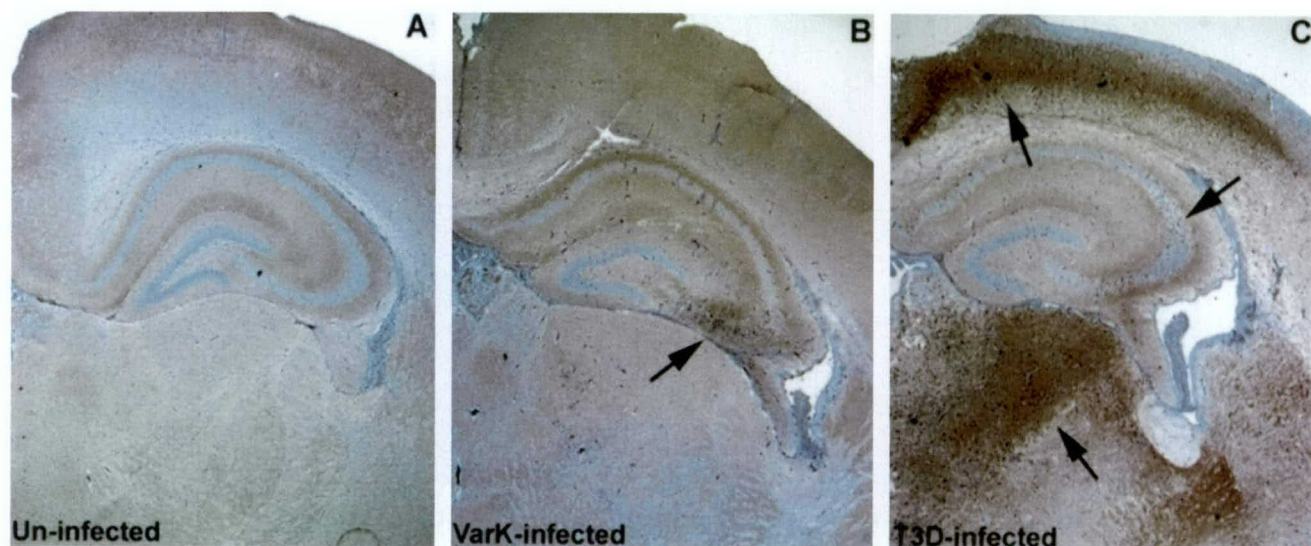


FIG. 3. VarK induces apoptosis in the hippocampus but not in other regions of the CNS in infected mice. (A) A coronal section from an uninfected mouse at 9 days postnatal shows few apoptotic cells as detected by immunohistochemistry for activated caspase 3. (B) A brain section from a VarK-infected mouse 7 days p.i. shows apoptotic neurons positive for activated caspase 3 (brown cells) in the CA2 to CA4 regions of the hippocampus with very few apoptotic cells present in the cortical or thalamic regions. (C) A brain section from a T3D-infected mouse 7 days p.i. shows massive apoptosis throughout the brain regions displayed, as indicated, by cells positive for activated caspase 3 staining in the cortical, hippocampal, and thalamic areas. In both T3D- and VarK-infected mice, regions of apoptotic cells correspond to the regions of viral injury and those positive for viral antigen as seen in Fig. 1 and 2, respectively. All brain sections were counterstained with a blue stain. Arrows point to areas of strong activated caspase 3 staining. These tissue sections are representative of data from the results from 3 studies with at least 8 mice per treatment group in each study.

Both T3D and VarK infected only neurons in both MCC and MHC, as seen previously in MCC prepared for studies by Richardson-Burns et al. (16). Here we show dual label immunocytochemistry for the neuronal nuclei marker (NeuN) and reovirus antigen (Fig. 4I to L) (16). Both T3D and VarK grew with identical kinetics and reached identical peak titers in MHC (Fig. 5A). Conversely, in MCC, VarK grew to significantly lower titers (>10-fold less) than T3D (Fig. 5B). We found similar viral titers at 0 h p.i. (cells were exposed to virus for 1 h and washed three times, and then viral titer was measured) in MCC infected with either VarK or T3D, suggesting that VarK is not deficient in its capacity to attach to cellular receptors on MCC compared to MHC.

To determine whether differences in virus titer were the result of fewer infected cells per culture or lower viral yield per infected cell, we performed immunocytochemistry on infected cultures. Both T3D and VarK infected a similar percentage of cells in MHC; however, in MCC, VarK infected approximately 50% fewer cells than T3D (Fig. 5C). This represents a significantly different percentage of infected MCC for T3D versus VarK, yet this does not completely account for the >10-fold (1 log) difference in virus titer seen between the two viruses in MCC (Fig. 5B). These results suggest that the yield of VarK per infected cell was identical to that of T3D in the hippocampal cultures but lower than that of T3D in the cortical cultures.

We next wished to compare the capacity of VarK and T3D to induce apoptosis in MCC and MHC by TUNEL. We found that VarK and T3D induced almost identical levels of apoptosis in MHC; however, VarK induced significantly less apoptosis than T3D in MCC (Fig. 6A). To confirm these results, we measured levels of activated caspase 3, the key apoptosis ef-

fector caspase, in infected cell lysates (Fig. 6B). We found that VarK induced significantly less caspase 3 activation than did T3D in MCC but not MHC. Thus, our results in primary neuronal cultures replicated our findings *in vivo*. VarK and T3D grow to identical titers and induce similar amounts of apoptosis in MHC, but VarK has both reduced growth and decreased apoptosis in MCC.

**Inhibiting apoptosis reduces growth of T3D and augmenting apoptosis enhances growth of VarK in cortical neurons.** Having shown that VarK is associated with reduced growth and decreased apoptosis induction both *in vitro* and *in vivo*, it was still not clear whether this was due to an impaired capacity of VarK to induce apoptosis, resulting in reduced viral growth, or vice versa. Therefore, we wished to determine whether inhibiting the apoptosis-inducing capacity of T3D would attenuate its growth and, conversely, whether augmenting the apoptosis-inducing capacity of VarK would enhance its growth. Previous studies on T3D-induced neuronal apoptosis indicated that peptide caspase inhibitors are potent blockers of T3D-induced apoptosis in neurons; hence, ZVAD-FMK, a pancaspase inhibitor, was used to inhibit apoptosis in this experiment. Since it had previously been shown that the death receptor FAS-FAS ligand system was important in mediating reovirus-induced apoptosis in primary neuronal cultures (16), we tested whether an antibody which binds and activates the death receptor FAS (anti-FASactiv), inducing apoptosis in MCC, can function as a possible reagent for augmenting virus-induced apoptosis.

As previously reported (16), T3D-induced apoptosis in MCC is significantly inhibited by the pancaspase inhibitor ZVAD-FMK ( $P < 0.001$ ) (Fig. 6C). ZVAD treatment decreases percentage of apoptosis in T3D-infected MCC to levels

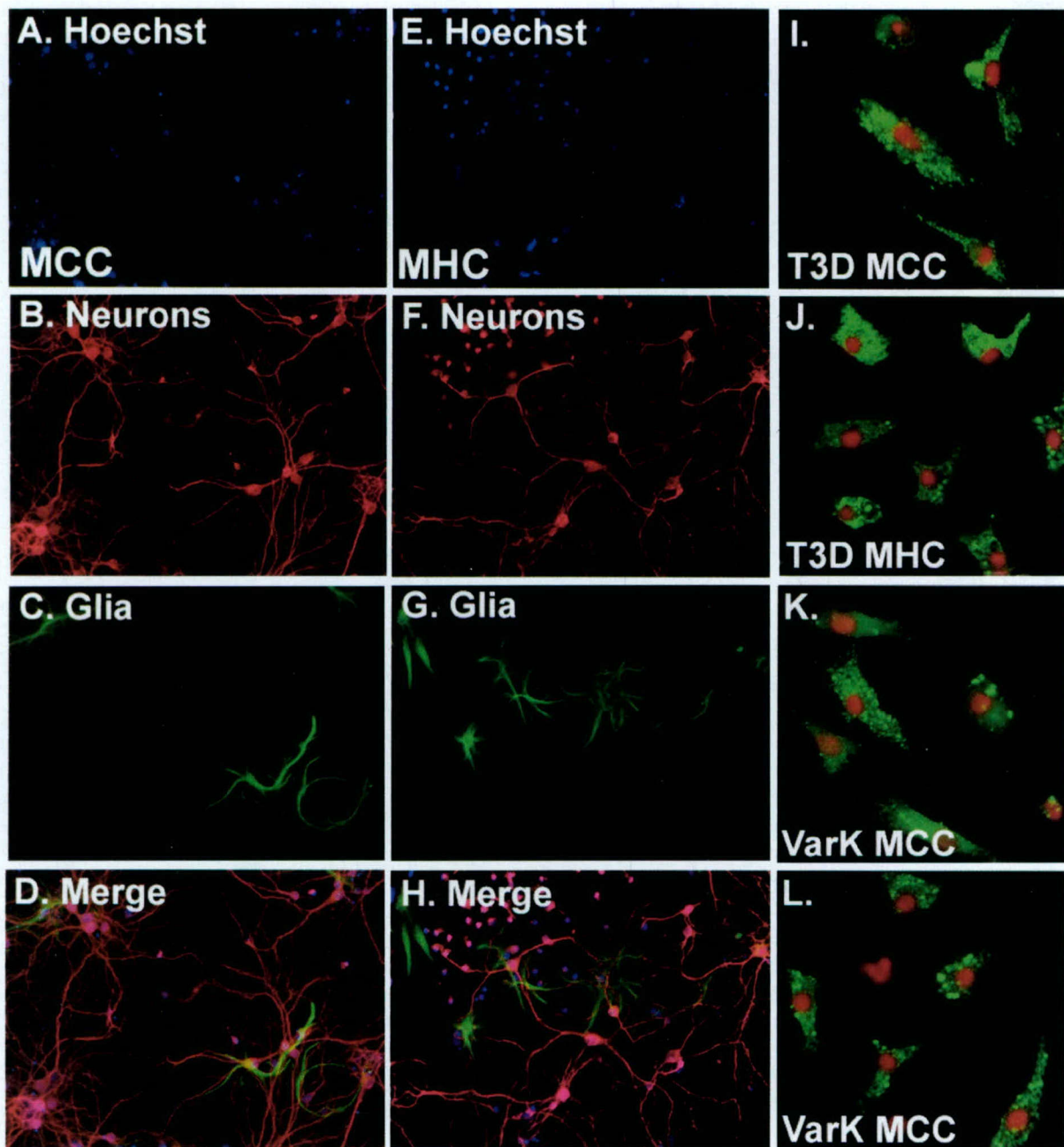


FIG. 4. MCC and MHC are 75 to 95% neuronal, and only neurons are infected by T3D or VarK. (A) Nuclei in MCC prepared from E20-P0 stained with the fluorescent nuclear dye Hoechst 33342. Magnification,  $\times 100$ . (B) Neurons in MCC immunocytochemically detected with anti-MAP2 (Alexa Fluor 594; red staining) show both pyramidal neurons (larger with long processes) and interneurons (smaller with little or no processes). (C) Astroglia in MCC stained with anti-GFAP (green staining) show a few positive cells. (D) The merged image shows that most cells in the culture are neurons. (E) Nuclei in MHC prepared from E20-P0 stained with the fluorescent nuclear dye Hoechst 33342. (F) Neurons in MHC immunocytochemically detected with anti-MAP2 (Alexa Fluor 594; red staining) show both pyramidal neurons (larger with long processes) and interneurons (smaller with little or no processes). (G) Astroglia in MHC stained with anti-GFAP (green staining) show a few positive cells. (H) The merged image shows that most cells in the culture are neurons. (I) T3D-infected MCC dual labeled for reovirus antigen (anti-T3D polyclonal, green staining) and the neuronal nucleus marker NeuN (Cy3; red staining) shows that infected cells (antigen in cytoplasm) are neurons. Magnification,  $\times 400$ . (J) T3D-infected MHC dual labeled for reovirus antigen (green) and the neuronal nucleus marker NeuN (red). (K) VarK-infected MCC dual labeled for reovirus antigen (green) and the neuronal nucleus marker NeuN (red). (L) VarK-infected MHC dual labeled for reovirus antigen (green) and the neuronal nucleus marker NeuN (red).

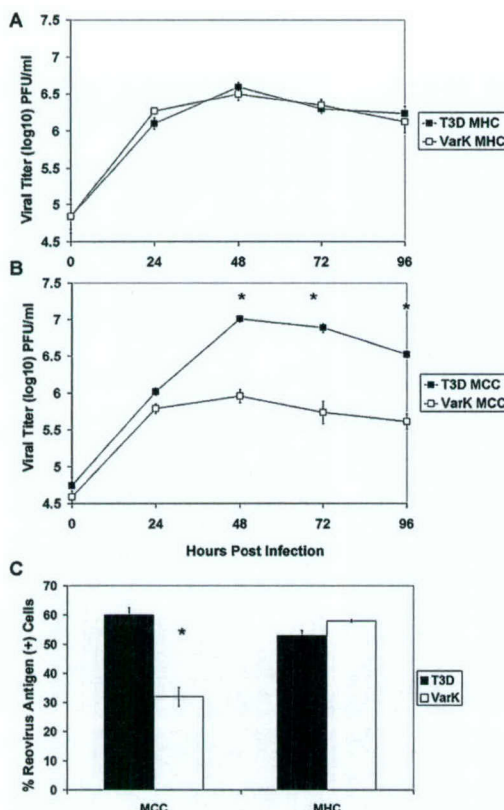


FIG. 5. Capacity of VarK to infect and grow in primary hippocampal and cortical neuronal cultures parallels its in vivo phenotype. (A) T3D and VarK grow to similar titers in MHC; (B) in MCC, T3D grows significantly better than VarK. \*,  $P < 0.05$  by Tukey-Kramer. (C) MCC and MHC were infected with either T3D or VarK, and immunocytochemistry was performed to detect the percentage of virus-infected cells at 48 h p.i. The percentage of cells positive for viral antigen was quantified in each culture. \*,  $P < 0.01$  by Tukey-Kramer. These data are representative of viral growth assays performed for at least three individual samples of primary cultures from three to four different culture preparations.

closer to that seen in VarK-infected MCC; however, treatment of VarK-infected MCC with ZVAD does not further reduce the level of virus-induced apoptosis. Anti-FASactiv induces apoptosis in MCC similarly to levels seen with T3D infection (data not shown) and significantly increases the level of apoptosis in both T3D- and VarK-infected MCC compared to either virus alone ( $P < 0.05$ ) (Fig. 6C) or virus-plus-control nonactivating FAS antibody (anti-FASNeg) (data not shown). Therefore, we used anti-FASactiv as an apoptosis-inducing reagent in VarK-infected MCC to determine whether increasing the capacity of VarK to induce apoptosis in MCC could increase VarK titer.

We found that treatment with ZVAD (25  $\mu$ M) significantly reduced T3D virus titer and viral yield in MCC but had no effect on viral growth in VarK-infected MCC (Fig. 7A and C). The virus titer in ZVAD-treated T3D-infected MCC was virtually identical to that seen following VarK infection, and viral yield per cell was actually lower than that seen following VarK infection (Fig. 7C). The T3D titer in infected MCC was also significantly reduced by DEVD-FMK (15  $\mu$ M), a caspase 3-specific peptide inhibitor, but not by YVAD-FMK (15  $\mu$ M),

a caspase 1-specific inhibitor (Fig. 7E). This is consistent with previous studies indicating that T3D reovirus-induced apoptosis is not associated with caspase 1 activation, further supporting the idea that reovirus-induced apoptosis is mediated by specific virus-activated cellular signaling (11). These results clearly indicate that inhibition of apoptosis can inhibit growth and yield of T3D in neurons (Fig. 7E). No caspase inhibitor changed the VarK titer in MCC (Fig. 7A and E).

Having shown that inhibition of apoptosis could decrease viral growth and yield in cortical cultures, we next wished to see whether augmentation of apoptosis would enhance the replication of VarK in MCC. Infected MCC were exposed to the

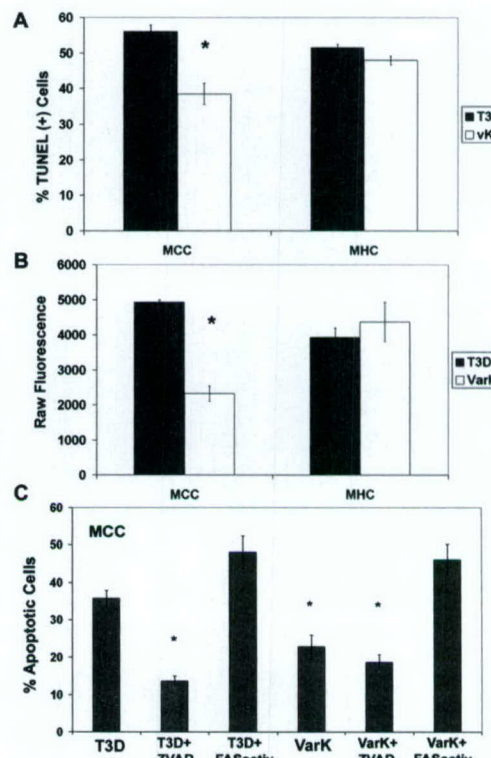


FIG. 6. VarK induced significantly less apoptosis than T3D in MCC, but in MHC, VarK and T3D kill an equal percentage of cells. (A) TUNEL, a marker for apoptosis-associated DNA fragmentation, was performed on MCC, and MHC were infected with either T3D or VarK at 48 h p.i. Significantly fewer MCC were TUNEL positive after VarK infection than after T3D infection, whereas T3D- and VarK-infected MHC had similar percentages of TUNEL-positive cells. (B) Another assay for apoptosis which detects the total level of activated caspase 3, an apoptosis-specific protease in cell lysate, by fluorogenic substrate cleavage. Increases in raw fluorescence of the cell lysate correspond to increases in levels of activated caspase 3 present in the lysate. By 24 h p.i., there was significantly more activated caspase 3 in T3D-infected MCC than in VarK-infected MCC. At the same time, activated caspase 3 levels in MHC infected with T3D or VarK were the same. \*,  $P < 0.01$  by Tukey-Kramer. These data are representative of apoptosis assays performed with at least three individual samples of primary cultures from three to four different culture preparations. (C) Apoptosis morphology assay (percent apoptosis in mock-infected control MCC subtracted from all treatments) at 48 h p.i. in MCC infected with either T3D or VarK (MOI of 100) and treated with caspase inhibitor ZVAD (25  $\mu$ M in dimethyl sulfoxide), anti-FASactiv (0.25  $\mu$ g/ml), or dimethyl sulfoxide (vehicle control). \*,  $P < 0.01$  by Tukey-Kramer.

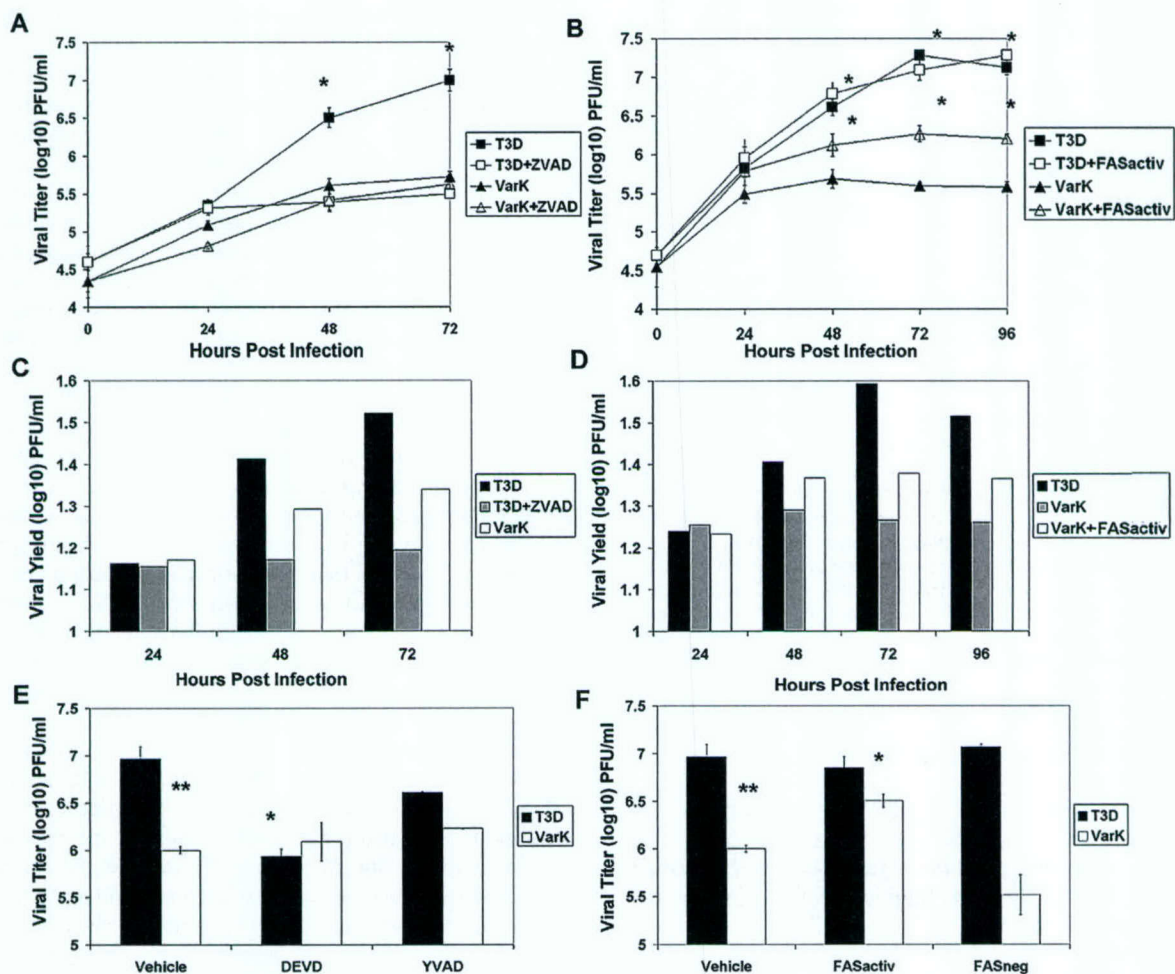


FIG. 7. Inhibiting apoptosis reduces growth of T3D, and augmenting apoptosis enhances growth of VarK in cortical neurons. (A) ZVAD treatment of T3D-infected MCC but not VarK-infected MCC results in a significant reduction in viral titer by 48 h p.i. Viral titer and the growth kinetics of ZVAD-treated T3D-infected MCC resembled those of VarK-infected MCC. \*,  $P < 0.01$  for T3D versus T3D plus ZVAD by Tukey-Kramer. (B) Anti-FASactiv (0.25  $\mu$ g/ml) added at 18 h p.i. to T3D- or VarK-infected MCC significantly increased VarK viral titer in MCC but did not increase titer to levels seen in T3D-infected MCC. \*,  $P < 0.05$  for T3D versus VarK plus FASactiv and VarK plus FASactiv versus VarK by Tukey-Kramer. (C) ZVAD treatment of T3D-infected MCC reduces viral yield in MCC compared to untreated T3D-infected cells. Viral yield was calculated by dividing the total viral titer at one time point by the viral titer at time 0 h p.i. (D) Anti-FASactiv treatment increased VarK viral yield compared to untreated VarK-infected MCC at all times p.i. after addition to the cultures. (E) Viral titer at 48 h p.i. for T3D- and VarK-infected MCC treated with either vehicle (2  $\mu$ l of dimethyl sulfoxide), caspase 3 inhibitor DEVD (15  $\mu$ M in dimethyl sulfoxide), or caspase 1 inhibitor YVAD (15  $\mu$ M in dimethyl sulfoxide). As previously seen, T3D and VarK have significantly different titers at 48 h p.i. in MCC. \*\*,  $P < 0.01$ . DEVD but not YVAD treatment significantly reduced T3D viral titer at 48 h p.i., bringing the T3D titer to the same level as the VarK titer. \*,  $P < 0.05$ . Neither treatment has an effect on VarK titer. (F) Viral titers of T3D and VarK at 48 h p.i. in MCC treated with either vehicle (2  $\mu$ l of PBS), anti-FASactiv or anti-FASnegative antibody (control antibody, 0.25  $\mu$ g in 2  $\mu$ l of PBS). Anti-FASactiv but not FASneg antibody significantly increased VarK viral titer in MCC at 48 h p.i. \*,  $P < 0.05$  for VarK plus FASactiv versus VarK. Neither antibody had an effect on the T3D viral titer. These data are representative of viral growth assays performed with primary cultures from at least four different culture preparations and apoptosis assays performed with two MCC preparations.

FAS-activating antibody, anti-FASactiv (0.25  $\mu$ g/ml), at 18 h p.i., a time p.i. at which previous studies indicate that virus-induced neuronal apoptosis is under way in T3D-infected MCC (16). Treatment of VarK-infected cells with anti-FASactiv significantly increased both titer and viral yield of VarK (Fig. 7B and D). Despite an increasing percentage of apoptosis in T3D-infected MCC (Fig. 6C), anti-FASactiv did not further increase T3D titer, suggesting that T3D is already growing maximally in MCC (Fig. 7B and F). A FAS-negative control antibody which binds the FAS receptor but does not activate associated apoptotic signaling cascades did not increase VarK

or T3D virus titer in MCC, indicating that the increased VarK titer seen in MCC treated with FAS activator is not nonspecifically associated with treatment of MCC with a FAS antibody (Fig. 7F). Taken together, these results suggest that differences in the capacity of T3D and VarK to induce apoptosis may be responsible for differences in their patterns of growth in specific neuronal populations. This idea is further supported by our data showing that a higher percentage of virus-induced apoptosis in MCC corresponds with increased viral yields (Fig. 8A and B). Treatments that reduce virus-induced apoptosis, such as exposure to caspase inhibitors, reduce viral yield, and

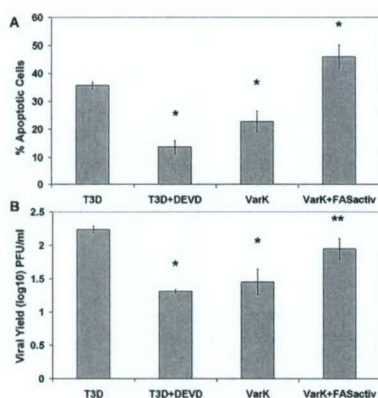


FIG. 8. Higher percentage of apoptosis in MCC corresponds to higher viral yield. (A) The percentage of apoptosis was quantified at 48 h p.i. in T3D, T3D plus DEVD, VarK, or VarK plus FASactivating antibody-treated MCC. T3D induced significantly greater levels of apoptosis than T3D plus DEVD or VarK alone. \*,  $P < 0.01$ . T3D alone was not different than VarK plus FASactiv. T3D plus DEVD was not different than VarK alone. The percentage of apoptosis in control mock-infected MCC was subtracted from each treatment prior to graphing. Apoptosis was measured by staining fixed cells with Hoechst 3342 and counting cells with condensed and/or fragmented nuclei. (B) The viral yield in MCC at 48 h p.i. was quantified for each treatment: T3D, T3D plus DEVD, VarK, or VarK plus FASactiv. DEVD treatment significantly inhibited T3D growth, making T3D plus DEVD titers similar to that of VarK alone. \*,  $P < 0.01$ . VarK grew significantly better in the presence of FASactiv, growing to titers similar to those with T3D. \*\*,  $P < 0.05$ .

on the other hand, the attenuated virus VarK that normally produces low viral yields grows significantly better in the presence of an apoptosis inducer.

## DISCUSSION

In this study, we investigated whether the neurovirulence of T3 reoviruses is linked to the capacity to induce apoptosis by examining two reovirus strains that differ greatly in neurovirulence. VarK, a reovirus antigenic variant, differs from its parent strain T3D by only a single amino acid change in the viral cell attachment protein, sigma 1. Several key differences in the pathogenesis of reovirus strains have been linked to the sigma 1 protein, including differences in the patterns of tropism within and spread to the CNS (24, 26), the capacity to induce apoptosis (1, 2, 4, 8), and differences in the capacity to bind to cell surface receptors, including sialic acid. Prior studies of VarK indicate that the striking differences in neuropathogenesis between this virus and T3D are not likely due to the inability of this virus to spread to or within the CNS (10) or to bind to either sialic acid-containing or JAM1 reovirus receptors, despite proximity of the VarK mutation to the JAM receptor binding site (5).

T3D administered by either intraperitoneal or i.c. injection causes severe neuronal injury and death throughout the neonatal mouse CNS, whereas VarK induces CNS injury only after i.c. injection and the injury is restricted to the CA2 to CA4 regions of the hippocampus (10, 18, 19, 25). Since VarK is not deficient in its capacity to spread within the CNS or in its potential to bind cellular receptors, we asked whether the restricted pattern of tissue injury by VarK was due to either its

inability to grow in or injure cortical as opposed to hippocampal neurons. We found in both infected mouse brain and in primary neuronal cultures that VarK was as competent as T3D to grow in and injure hippocampal neurons. By contrast, both in vivo and in vitro VarK had a markedly reduced capacity to grow in and injure cortical neurons compared to T3D. It was previously shown that CNS injury induced by T3 reoviruses results from apoptosis and that apoptotic injury was limited to regions of viral growth, as determined by immunocytochemical detection of viral antigen (13, 16), and a similar correlation in VarK-infected brains was found. These results clearly indicate that the restricted CNS injury induced by VarK is associated with both decreased viral replication and impaired apoptosis.

Since VarK showed both impaired growth and decreased capacity to induce apoptosis, it is not possible to definitively determine which of these two phenomena is the key causal event. Decreased growth may have resulted in decreased capacity to induce apoptosis, or conversely, decreased capacity to induce apoptosis may have inhibited viral growth and spread. It was previously shown that apoptosis induction does not require viral growth (17), and in fact, there is little correlation in continuous nonneuronal cell lines between the efficiency of reovirus replication and the capacity of viruses to induce apoptosis. For example, both T1L and T3D grow to approximately equivalent titers in L929 fibroblasts, yet T3D induces apoptosis far more efficiently in these cells than T1L (23). Similarly, T1L grows better than T3D in MDCK cells, yet T3D induces significantly more apoptosis (17). However, in several systems, inhibition of apoptosis has led to a modest but reproducible decrease in virus titer in reovirus T3-infected cells, suggesting that apoptosis may be required for maximal replication efficiency of T3 reoviruses both in vitro and in vivo.

We found that inhibiting apoptosis in primary cortical cultures by treatment of cells with a pancaspase inhibitor or a caspase 3 inhibitor significantly reduced T3D viral growth, making the T3D growth curve resemble that of VarK. These results provide the clearest evidence to date, suggesting that apoptosis is required for maximal replication of T3 reoviruses. Interestingly, treatment of T3D-infected cortical cultures with a caspase 1 inhibitor did not significantly reduce virus titer. Previous studies in our laboratory indicate that caspase 3, but not caspase, plays a key role in T3 reovirus-induced apoptotic signaling; thus, our findings here further support the idea that virus-activated apoptotic signaling has a role in viral growth (11, 16). In contrast to that seen with apoptosis inhibitors in T3D-infected cortical cultures, treating VarK-infected cortical cultures with an apoptosis-inducing agent significantly enhanced the VarK titer in the cells, although this treatment did not restore the yield of VarK to wild-type (T3D) levels. These data support the idea that VarK has a defect in its capacity to induce apoptosis which is associated with reduced growth in certain types of neurons and support the idea that induction of apoptosis is an important mechanism of viral neuropathogenesis. A similar phenomenon has been seen following Sindbis virus infection, in which coincident overexpression of the antiapoptotic protein Bcl-2 inhibits viral growth and reduces neurovirulence (12).

The explanation for the cell type specificity of VarK's effects remains to be established, as the defects in replication and apoptosis do not occur in hippocampal neurons but are clearly

manifested in cortical neurons. The sigma 1 protein plays a key role in the activation of cellular signaling pathways, leading to the activation of specific cellular transcription factors, including NF- $\kappa$ B (6, 9) and c-Jun (7), and to the selective activation of mitogen-activated protein kinase cascades that play a critical role in apoptosis induction (27). It remains to be seen whether the mutant sigma 1 protein is only capable of inducing these events in hippocampal as opposed to cortical cultures. Perhaps the mutant protein is defective in its capacity to interact with key host signaling proteins that either differ or are only required in one type of cells but not another.

In conclusion, we show that the altered neurovirulence of VarK is associated with a reduced capacity to induce apoptosis and grow in selected populations of neurons compared with the wild-type parent strain T3D. Our findings suggest that the deficiency in the capacity of VarK to induce apoptosis in cortical as opposed to hippocampal neurons may in turn reduce the efficiency of viral replication. Induction of apoptosis is likely to be an important mechanism for efficient production of viral progeny following T3D infection in the CNS. Further elucidation of the basis for the selective vulnerability of specific neuronal populations to reovirus-induced apoptosis may help shed light on the key cellular proteins and signaling pathways involved in neuronal cell death.

#### ACKNOWLEDGMENTS

This work was supported by Merit and REAP grants from the Department of Veterans Affairs, a U.S. Army Medical Research and Material Command (USAMRMC) grant (DAMD17-98-1-8614), and the Reuler-Lewin Family Professorship of Neurology (K.L.T.).

#### REFERENCES

- Barton, E. S., J. L. Connolly, J. C. Forrest, J. D. Chappell, and T. S. Dermody.** 2001. Utilization of sialic acid as a coreceptor enhances reovirus attachment by multistep adhesion strengthening. *J. Biol. Chem.* **276**:2200-2211.
- Barton, E. S., J. C. Forrest, J. L. Connolly, J. D. Chappell, Y. Liu, F. J. Schnell, A. Nusrat, C. A. Parkos, and T. S. Dermody.** 2001. Junction adhesion molecule is a receptor for reovirus. *Cell* **104**:441-451.
- Bassel-Duby, R., D. R. Spriggs, K. L. Tyler, and B. N. Fields.** 1986. Identification of attenuating mutations on the reovirus type 3 S1 double-stranded RNA segment with a rapid sequencing technique. *J. Virol.* **60**:64-67.
- Chappell, J. D., V. L. Gunn, J. D. Wetzel, G. S. Baer, and T. S. Dermody.** 1997. Mutations in type 3 reovirus that determine binding to sialic acid are contained in the fibrous tail domain of viral attachment protein sigma1. *J. Virol.* **71**:1834-1841.
- Chappell, J. D., A. E. Prota, T. S. Dermody, and T. Stehle.** 2002. Crystal structure of reovirus attachment protein sigma1 reveals evolutionary relationship to adenovirus fiber. *EMBO J.* **21**:1-11.
- Clarke, P., S. M. Meintzer, L. Moffitt, and K. L. Tyler.** 2003. Two distinct phases of virus-induced NF- $\kappa$ B regulation enhance TRAIL-mediated apoptosis in virus-infected cells. *J. Biol. Chem.* **278**:18092-18100.
- Clarke, P., S. M. Meintzer, C. Widmann, G. L. Johnson, and K. L. Tyler.** 2001. Reovirus infection activates JNK and the JNK-dependent transcription factor c-Jun. *J. Virol.* **75**:11275-11283.
- Connolly, J. L., E. S. Barton, and T. S. Dermody.** 2001. Reovirus binding to cell surface sialic acid potentiates virus-induced apoptosis. *J. Virol.* **75**:4029-4039.
- Connolly, J. L., S. E. Rodgers, P. Clarke, D. W. Ballard, L. D. Kerr, K. L. Tyler, and T. S. Dermody.** 2000. Reovirus-induced apoptosis requires activation of transcription factor NF- $\kappa$ B. *J. Virol.* **74**:2981-2989.
- Kaye, K. M., D. R. Spriggs, R. Bassel-Duby, B. N. Fields, and K. L. Tyler.** 1986. Genetic basis for altered pathogenesis of an immune-selected antigenic variant of reovirus type 3 (Dearing). *J. Virol.* **59**:90-97.
- Kominsky, D. J., R. J. Bickel, and K. L. Tyler.** 2002. Reovirus-induced apoptosis requires both death receptor- and mitochondrial-mediated caspase-dependent pathways of cell death. *Cell Death Differ.* **9**:926-933.
- Lewis, J., S. L. Wesselingh, D. E. Griffin, and J. M. Hardwick.** 1996. Alphavirus-induced apoptosis in mouse brains correlates with neurovirulence. *J. Virol.* **70**:1828-1835.
- Oberhaus, S. M., R. L. Smith, G. H. Clayton, T. S. Dermody, and K. L. Tyler.** 1997. Reovirus infection and tissue injury in the mouse central nervous system are associated with apoptosis. *J. Virol.* **71**:2100-2106.
- Poggio, G. J., C. Keefer, J. L. Connolly, T. S. Dermody, and K. L. Tyler.** 2000. Reovirus-induced  $G_2/M$  cell cycle arrest requires  $\sigma 1$ s and occurs in the absence of apoptosis. *J. Virol.* **74**:9562-9570.
- Richardson-Burns, S. M., B. K. Kleinschmidt-DeMasters, R. L. DeBiasi, and K. L. Tyler.** 2002. Progressive multifocal leukoencephalopathy and apoptosis of infected oligodendrocytes in the central nervous system of patients with and without AIDS. *Arch. Neurol.* **59**:1930-1936.
- Richardson-Burns, S. M., D. J. Kominsky, and K. L. Tyler.** 2002. Reovirus-induced neuronal apoptosis is mediated by caspase 3 and is associated with the activation of death receptors. *J. Neurovirol.* **8**:365-380.
- Rodgers, S. E., E. S. Barton, S. M. Oberhaus, B. Pike, C. A. Gibson, K. L. Tyler, and T. S. Dermody.** 1997. Reovirus-induced apoptosis of MDCK cells is not linked to viral yield and is blocked by Bcl-2. *J. Virol.* **71**:2540-2546.
- Spriggs, D. R., R. T. Bronson, and B. N. Fields.** 1983. Hemagglutinin variants of reovirus type 3 have altered central nervous system tropism. *Science* **220**:505-507.
- Spriggs, D. R., and B. N. Fields.** 1982. Attenuated reovirus type 3 strains generated by selection of haemagglutinin antigenic variants. *Nature* **297**:68-70.
- Tyler, K. L.** 1998. Pathogenesis of reovirus infections of the central nervous system. *Curr. Top. Microbiol. Immunol.* **233**:93-124.
- Tyler, K. L., R. T. Bronson, K. B. Byers, and B. Fields.** 1985. Molecular basis of viral neurotropism: experimental reovirus infection. *Neurology* **35**:88-92.
- Tyler, K. L., P. Clarke, R. L. DeBiasi, D. Kominsky, and G. J. Poggio.** 2001. Reoviruses and the host cell. *Trends Microbiol.* **9**:560-564.
- Tyler, K. L., M. K. Squier, S. E. Rodgers, B. E. Schneider, S. M. Oberhaus, T. A. Grdina, J. J. Cohen, and T. S. Dermody.** 1995. Differences in the capacity of reovirus strains to induce apoptosis are determined by the viral attachment protein  $\sigma 1$ . *J. Virol.* **69**:6972-6979.
- Tyler, K. L., H. W. Virgin, R. Bassel-Duby, and B. N. Fields.** 1989. Antibody inhibits defined stages in the pathogenesis of reovirus serotype 3 infection of the central nervous system. *J. Exp. Med.* **170**:887-900.
- Tyler, K. L.** 2001. Mammalian reoviruses, p. 1307-1328. In D. M. Knipe and P. M. Howley (ed.), *Fields virology*, 4th ed. Lippincott-Williams & Wilkins, Philadelphia, Pa.
- Virgin, H. W., R. Bassel-Duby, B. N. Fields, and K. L. Tyler.** 1988. Antibody protects against lethal infection with the neurally spreading reovirus type 3 (Dearing). *J. Virol.* **62**:4594-4604.
- Yujiri, T., M. Ware, C. Widmann, R. Oyer, D. Russell, E. Chan, Y. Zaitsev, P. Clarke, K. Tyler, Y. Oka, G. R. Fanger, P. Henson, and G. L. Johnson.** 2000. MEK kinase 1 gene disruption alters cell migration and c-Jun NH<sub>2</sub>-terminal kinase regulation but does not cause a measurable defect in NF- $\kappa$ B activation. *Proc. Natl. Acad. Sci. USA* **97**:7272-7277.

# Isolation and Molecular Characterization of a Novel Type 3 Reovirus from a Child with Meningitis

Kenneth L. Tyler,<sup>1,2,3,4</sup> Erik S. Barton,<sup>6,9,a</sup> Maria L. Ibach,<sup>5</sup> Christine Robinson,<sup>1,4</sup> Jacquelyn A. Campbell,<sup>6,9</sup> Sean M. O'Donnell,<sup>8,9</sup> Tibor Valyi-Nagy,<sup>7,9,a</sup> Penny Clarke,<sup>1,4</sup> J. Denise Wetzel,<sup>8,9</sup> and Terence S. Dermody,<sup>6,8,9</sup>

Departments of <sup>1</sup>Neurology, <sup>2</sup>Medicine, and <sup>3</sup>Microbiology and Immunology, University of Colorado Health Science Center, <sup>4</sup>Denver Veterans Affairs Medical Center, and <sup>5</sup>Department of Pathology, Children's Hospital, Denver, Colorado; Departments of <sup>6</sup>Microbiology and Immunology, <sup>7</sup>Pathology, and <sup>8</sup>Pediatrics, and <sup>9</sup>Elizabeth B. Lamb Center for Pediatric Research, Vanderbilt University School of Medicine, Nashville, Tennessee

**Mammalian reoviruses are nonenveloped viruses that contain a segmented, double-stranded RNA genome. Reoviruses infect most mammalian species, although infection with these viruses in humans is usually asymptomatic. We report the isolation of a novel reovirus strain from a 6.5-week-old child with meningitis. Hemagglutination and neutralization assays indicated that the isolate is a serotype 3 strain, leading to the designation T3/Human/Colorado/1996 (T3C/96). Sequence analysis of the T3C/96 S1 gene segment, which encodes the viral attachment protein, σ1, confirmed the serotype assignment for this strain and indicated that T3C/96 is a novel reovirus isolate. T3C/96 is capable of systemic spread in newborn mice after peroral inoculation and produces lethal encephalitis. These results suggest that serotype 3 reoviruses can cause meningitis in humans.**

Mammalian reoviruses are nonenveloped viruses that contain a genome of 10 discrete segments of double-stranded RNA (dsRNA) [1]. There are 3 major reovirus serotypes, which are differentiated by the capacity of antisera to neutralize viral infectivity and inhibit hemagglutination [2, 3]. Reoviruses have a wide geographic distribution and can infect virtually all mammals, including humans [4].

Reoviruses were originally called respiratory enteric orphans on the basis of their repeated isolation from

respiratory and enteric tracts of children with asymptomatic illness [2]. Only mild respiratory or gastrointestinal symptoms are observed when infection is symptomatic [4–7]. There are few studies of human reovirus-associated neurological disease [8]. These studies generally relied on serological analysis or isolation of reovirus from stool samples for diagnosis, which is diagnostically inconclusive, because of the frequency of asymptomatic reovirus infections. Three studies have described the isolation of reovirus directly from cerebrospinal fluid (CSF) or neural tissue samples obtained from individuals with meningitis or encephalitis, as described elsewhere [9–11]. In these studies, there was no molecular or virological analysis of the isolated strain performed. Therefore, little is known about the biologic characteristics of reovirus strains that cause human CNS disease.

In contrast to human reovirus infection, infection of newborn mice is highly pathogenic. After oral inoculation in mice, reovirus is taken up by intestinal M cells [12] and undergoes primary replication in lymphoid tissue of Peyer's patches. T1 reovirus spreads to the CNS hematogenously and infects ependymal cells [13, 14], which results in hydrocephalus [15]. In contrast, T3 reovirus spreads to the CNS neurally, infects neurons [13, 14, 16], and causes lethal encephalitis [15, 17]. The pathways of viral spread in the host [13] and pattern

Received 28 August 2003; accepted 17 October 2003; electronically published 15 April 2004.

Financial support: National Science Foundation (support to E.S.B.); Public Health Service (grants T32 CA09385 to J.A.C., T32 AI07474 to S.M.O. and T.V.-N., R01 AI38296 to T.S.D., CA68485 to Vanderbilt-Ingram Cancer Center, and DK20593 to Vanderbilt Diabetes Research and Training Center); Department of Veterans Affairs (REAP and MERIT awards to K.L.T.); US Army Medical Research and Material Command (grant DAMD17-98-1-8614 to K.L.T.); Vanderbilt University Research Council (support to E.S.B.); Elizabeth B. Lamb Center for Pediatric Research; Revlew-Lewin Family Professorship of Neurology (support to K.L.T.).

<sup>a</sup> Present affiliations: Department of Pathology, Washington University School of Medicine, St. Louis, Missouri (E.S.B.); Department of Pathology, University of Illinois, Chicago (T.V.-N.).

Reprints or correspondence: Dr. Terence Dermody, Elizabeth B. Lamb Center for Pediatric Research, D7235 MCN, Vanderbilt University School of Medicine, Nashville, TN 37232 (terry.dermody@vanderbilt.edu); Dr. Kenneth Tyler, Neurology B-182, University of Colorado Health Sciences Center, 4200 E. 9th Ave., Denver, CO 80262 (ken.tyler@uchsc.edu).

**The Journal of Infectious Diseases** 2004;189:1664–75

© 2004 by the Infectious Diseases Society of America. All rights reserved.  
0022-1899/2004/18909-0015\$15.00

**Table 1.** Reovirus strains used for T3C/96 S1 gene sequence analysis.

Virus strain <sup>a</sup>	Abbreviation	GenBank accession no.	Reference(s)
T1/Human/Ohio/Lang/1953	T1L/53	M35963	[2, 66]
T2/Human/Ohio/Jones/1955	T2J/55	M35964	[2, 67]
T3/Human/Ohio/Dearing/1955	T3D/55	NC_004277	[2, 67]
T3/Human/Washington, DC/clone 93/1955	T3C93/55	L37675	[68]
T3/Human/Washington, DC/Abney/1957	T3A/57	L37677	[69]
T3/Human/Washington, DC/clone 84/1957	T3C84/57	L37678	[44]
T3/Bovine/Maryland/clone 31/1959	T3C31/59	L37683	[68]
T3/Bovine/Maryland/clone 43/1960	T3C43/60	L37682	[68]
T3/Bovine/Maryland/clone 44/1960	T3C44/60	L37681	[44]
T3/Bovine/Maryland/clone 45/1960	T3C45/60	L37680	[44]
T3/Human/Tahiti/clone 8/1960	T3C8/60	L37679	[68]
T3/Bovine/Maryland/clone 18/1961	T3C18/61	L37684	[68]
T3/Murine/France/clone 9/1961	T3C9/61	L37676	[68]
T3/Human/Colorado/1996	T3C/96	AY 302467	Present study

<sup>a</sup> Strains are named according to the following scheme: serotype/species of origin/place of origin/strain designation/year of isolation [70].

of neurotropism [14, 18] segregate with the viral S1 gene, which encodes the viral attachment protein [19, 20]. The  $\sigma$ 1 protein which determines the CNS cell types that serve as targets for reovirus infection, presumably by its capacity to bind receptors expressed on specific CNS cells.

The  $\sigma$ 1 protein is a fibrous trimer with an elongated tail domain that inserts into the virion and a globular head domain that projects away from the virion surface [21–23]. T1 and T3  $\sigma$ 1 contain receptor-binding domains in both the tail and head regions. A domain in the T3  $\sigma$ 1 tail binds  $\alpha$ -linked sialic acid [24, 25], and another domain in the head of both T1 and T3  $\sigma$ 1 binds junctional adhesion molecule 1 (JAM1) [26]. The T1  $\sigma$ 1 tail also binds cell-surface carbohydrate [25]. As a consequence of a sequence polymorphism in the tail of T3D/55  $\sigma$ 1, the sialic acid- and JAM1-binding domains are dissociable by treatment of virions with intestinal proteases, such as trypsin or chymotrypsin [27, 28], which may determine the attenuated virulence of T3D/55 after oral inoculation [29].

Engagement of reovirus receptors also induces postbinding signaling events that influence disease pathogenesis. Reovirus induces apoptosis in cultured cells [30–33], including neurons [34], and in vivo [35, 36]. Neurovirulent strains induces apoptosis to a greater extent than nonneurovirulent strains [30, 31, 34, 37]. Analysis of T1L/53  $\times$  T3D/55 reassortant viruses indicates that differences in apoptosis efficiency are determined primarily by the  $\sigma$ 1-encoding S1 gene [30, 31, 37], which suggests that receptor engagement influences the magnitude of the apoptotic response. In concordance with this idea, the most apoptogenic reovirus strains bind to both sialic acid [37] and JAM1 [26].

In the present study, we report the isolation of a T3 reovirus designated T3/Human/Colorado/1996 (T3C/96) from the CSF

of a 6.5-week-old child with meningitis. The T3C/96 S1 gene sequence was determined and compared to all previously reported T3 reovirus S1 gene sequences. The capacity of T3C/96 to bind sialic acid and JAM1 and to cause encephalitis in mice was assessed. The results indicate that T3C/96 is a novel T3 reovirus capable of systemic spread to the CNS after peroral inoculation of newborn mice and provide direct evidence that T3 reovirus can be neurovirulent in humans.

## MATERIALS AND METHODS

**Cells, viruses, and antibodies.** Spinner-adapted murine L929 (L) cells grown in suspension or on monolayer cultures and HeLa cell monolayers were maintained as described elsewhere [30, 32]. Prototype reovirus strains T1L/53 and T3D/55 and reovirus field isolate strains (table 1) are laboratory stocks. Virus titers were determined by use of plaque assay [38], and purified virus and particle concentrations were determined, as described elsewhere [21, 39]. Antibodies used included murine  $\sigma$ 1-specific monoclonal antibody (MAb) 5C6 (T1  $\sigma$ 1) [40], MAb 9BG5 (T3  $\sigma$ 1) [41], and JAM1-specific MAb J10.4 [42].

**Electron microscopy.** Supernatant of infected rhesus monkey kidney (RMK) cells was clarified by centrifugation at 1000 g for 10 min at 22°C. Clarified supernatant was placed in an Airfuge EM-90 rotor (Beckman Coulter) containing a Formvar-coated grid (Electron Microscopy Sciences) and was centrifuged at 100,000 g for 30 min at 22°C. The grid was stained with 2% phosphotungstic acid (1 min) and was examined by use of a Zeiss EM10 electron microscope.

**Hemagglutination (HA) assays.** Purified reovirus virions ( $10^{11}$  particles) were serially diluted in 50  $\mu$ L of PBS in 96-well round-bottom microtiter plates (Corning-Costar). Calf eryth-

rocytes (Colorado Serum) were washed twice with PBS and were resuspended at a concentration of 1% (vol/vol) in PBS. Erythrocytes (50 µL) were added to wells containing virus and incubated for 2 h at 4°C.

**Neutralization assays.** T1 and T3  $\sigma$ 1-specific MAbs were serially diluted 2-fold in gelatin saline and were incubated with 10<sup>3</sup> pfu/mL of T3C/96 virions for 1 h at 37°C. Samples were titrated in duplicate on L-cell monolayers by use of plaque assay [38]. Data are presented as the percentage of control plaque-forming units (virions untreated by antibody).

**Sequence analysis of the S1 gene.** The S1 gene segment of T3C/96 was amplified by use of reverse-transcriptase polymerase chain reaction (RT-PCR), using primers complementary to the 5' and 3' nontranslated regions (NTRs) [43], and then was cloned into the pCR 2.1 vector (Invitrogen) and sequenced by use of T4 DNA polymerase (Sequenase 2.0; United States Biochemical). Sequences of the NTRs were determined by use of direct dsRNA sequencing, using purified viral genomic RNA [44]. The S1 gene nucleotide sequences of independent isolates of T3C/96 were determined in independent laboratories and were found to be identical.

**Phylogenetic analysis of S1 gene nucleotide sequences.** Phylogenetic trees were constructed from variation in the  $\sigma$ 1-encoding S1 gene nucleotide sequences by use of the neighbor-joining algorithm (phylogenetic analysis program; MacVector 2001, version 7.1.1; Accelrys). Branching orders of the phylogenograms were verified statistically by resampling the data 1000 times in a bootstrap analysis, using the branch and bound algorithm (MacVector).

**Fluorescent-focus assays of viral infectivity.** HeLa cell monolayers ( $2 \times 10^5$  cells/well) were pretreated with PBS, coxsackie and adenovirus receptor (CAR)-specific MAb RmcB (20 µg/mL) [45, 46], *Arthrobacter ureafaciens* neuraminidase (40 mU/mL; ICN Biomedicals), or JAM1-specific MAb J10.4 (20 µg/mL) [42] before adsorption of virus for 1 h at room temperature. Inoculum was removed, and cells were washed with PBS and were incubated for 20 h at 37°C, to permit completion of a single round of viral replication. Cells were fixed with 1 mL of methanol for 30 min at -20°C. Fixed monolayers were washed twice with PBS, blocked with 5% immunoglobulin-free bovine serum albumin (Sigma-Aldrich) in PBS, and incubated for 30 min at 37°C with protein-A-affinity-purified polyclonal rabbit antireovirus serum [47] at a 1:800 dilution in PBS/0.5% Triton X-100. Monolayers were washed twice with PBS/0.5% Triton X-100 and were incubated with a 1:1000 dilution of goat anti-rabbit immunoglobulin serum conjugated with Alexa Fluor 546 fluorophore (Molecular Probes). Monolayers were washed twice with PBS/0.5% Triton X-100, and infected cells were visualized by indirect immunofluorescence by use of a Zeiss Photomicroscope III microscope modified for fluorescence microscopy. Infected cells were identified by the presence of intense

cytoplasmic fluorescence that was excluded from the nucleus. No background staining of uninfected control monolayers was detected. Reovirus antigen-positive cells were quantitated by counting fluorescent cells in 3 random fields of view/well in triplicate at a 20 $\times$  magnification.

**Mice and inoculations.** ND4 Swiss Webster mice aged 2–3 days with an average weight of 2 g (Harlan) were inoculated either intracranially or perorally with purified virus. Before inoculation, all mice from simultaneously delivered litters were pooled and randomly subdivided into litters of 8–11 mice/dam. For intracranial inoculations, 5 µL of purified virus diluted in gelatin saline was delivered into the right cerebral hemisphere by use of a Hamilton syringe and a 30-gauge needle [48]. For peroral inoculations, 50 µL of purified virus diluted in gelatin saline was delivered into the stomach by passage of a polyethylene catheter 0.61 mm in diameter (BD Biosciences) through the esophagus [49]. At various times after inoculation, mice were killed, and brains were harvested into 2 mL of gelatin saline. Brains were homogenized by freezing (-70°C) and thawing (37°C), which was then followed by sonication. Virus titer in brain homogenates was determined by plaque assay [38].

The LD<sub>50</sub> of reovirus was determined by use of ND4 Swiss Webster mice aged 2–3 days. Litters of mice were inoculated either intracranially or perorally with a single dose of reovirus and were checked daily for survival. Moribund mice were killed. The LD<sub>50</sub> of reovirus was calculated by use of the method of Reed and Muench [50]. All animal experiments were performed under institutionally approved protocols in Association for Assessment and Accreditation of Laboratory Animal Care-approved facilities.

**Histological and immunohistochemical staining for reovirus antigen.** At various times after intracranial inoculation of neonatal mice, mice were killed. Brains were fixed in 10% buffered formaldehyde for 24–48 h at 4°C, paraffin embedded, and thin sectioned. Deparaffinized tissue samples were stained with hematoxylin-eosin.

For immunohistochemical staining, deparaffinized tissue samples were rehydrated by incubation in PBS for 20 min at room temperature. Endogenous peroxidase was quenched by incubation in 0.3% hydrogen peroxide in methanol for 30 min. Tissue samples were blocked by incubation in PBS containing 1.5% normal goat serum for 20 min. After the blocking solution was removed, tissue samples were incubated for 30 min in rabbit antireovirus serum (1:800 in blocking solution) that was first purified by protein-A affinity chromatography and was preadsorbed against methanol-fixed L-cell monolayers. Antigen-positive cells were visualized by use of avidin-biotin-conjugated horseradish peroxidase (Vectastain ABC) and 3,3'-diaminobenzidine (DAB) substrate, according to the manufacturer's instructions (Vector Laboratories). After DAB staining, tissue samples were rinsed in deionized water and were counterstained

for 45 s with hematoxylin, dehydrated in 95% ethanol, air dried, and mounted under coverslips by use of Accu-Mount 60 reagent (Baxter Healthcare).

## RESULTS

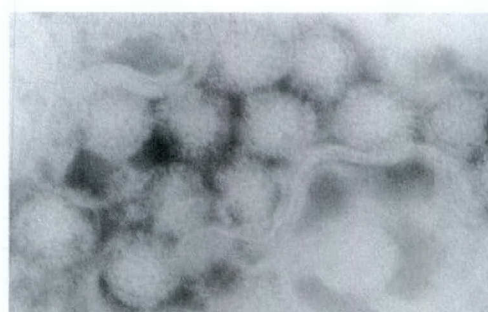
**Case report.** A 6.5-week-old female infant who was delivered vaginally at 35 weeks gestation had a 3-day history of irritability, decreased appetite, vomiting, and high-pitched cry. After vital signs were notable for temperature of 38.8°C (pr), heart rate of 166 beats/min, respiratory rate of 36 breaths/min, and blood pressure of 72/30 mmHg. The child was in mild respiratory distress, with grunting while breathing room air. Her neck was supple, chest and cardiac examinations were normal, and her abdomen was soft and nontender. Neurological examination was remarkable for lethargy, normal cranial nerves, muscle tone, and reflexes. An episode consistent with a generalized seizure was noted in the emergency department.

Her hematocrit was 27.7%, white blood cell (WBC) count was 9500 cells/mm<sup>3</sup>, and platelet count was 412,000 platelets/mm<sup>3</sup>. CSF contained a WBC count of 22 cells/mm<sup>3</sup> (77% neutrophils, 9% bands, and 14% lymphocytes), a protein level of 67 mg/dL, and a glucose level of 44 mg/dL. The serum glutamate oxaloacetate transaminase level was 64 IU/L (normal, <60 IU/L), and the conjugated bilirubin level was 0.5 mg/dL (normal, <0.3 mg/dL). Alkaline phosphatase, serum glutamate pyruvate transaminase, and gamma glutamyltransferase levels were normal. Bacterial cultures of blood and CSF were sterile. CSF PCR assay was negative for enteroviruses and herpes simplex virus. During her 5 days of hospitalization, the patient developed transient abdominal distension and watery diarrhea. No erythrocytes or leukocytes were observed after microscopy of stool samples, and stool cultures were negative for enteric pathogens, as were tests for rotavirus antigen and electron microscopy for rotavirus particles. She gradually recovered and was discharged from the hospital without obvious neurological sequelae.

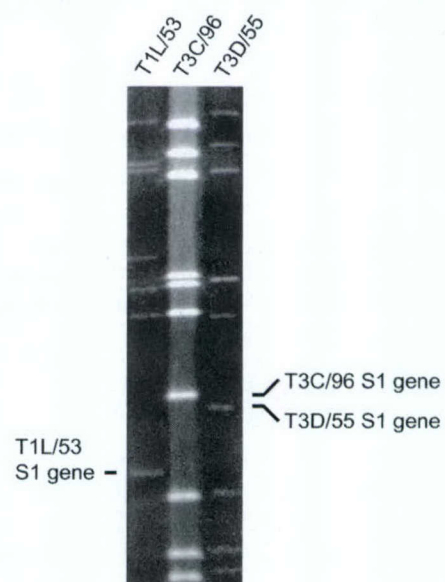
**Isolation and virological characterization of a novel T3 reovirus strain.** CSF was inoculated onto primary human diploid fibroblast (MRC-5), human epithelial carcinoma (Hep-2), and primary RMK cell monolayers. The RMK cell cultures developed a granular, nonsloughing pattern of cytopathic effect (CPE). Supernatant of these cells was used to infect MRC-5 cells, which developed similar CPE. Electron microscopy of infected cells demonstrated icosahedral nonenveloped viral particles characteristic of mammalian reovirus (figure 1A).

The original RMK cell lysate was used to inoculate flasks of murine L cells, which developed a characteristic reovirus CPE. Plaque assay of lysates demonstrated round 1–2 mm plaques. Electrophoretic analysis of infected L-cell lysates demonstrated the presence of 10 viral gene segments (figure 1B). The largest

A



B



C

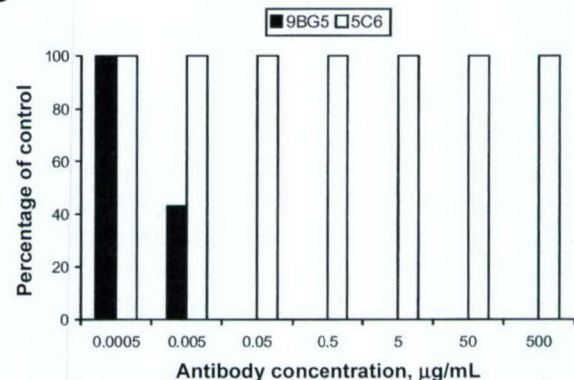


**Figure 1.** Strain characterization of T3C/96. A, Electron micrograph of T3C/96 after growth in primary rhesus monkey kidney cells. B, Electrophoretic analysis of reovirus strains T1L/53, T3C/96, and T3D/55. Approximately equal numbers of reovirus particles were resolved by acrylamide gel electrophoresis. Viral double-strand RNA (dsRNA) gene segments were visualized after staining of the gel with ethidium bromide. Position of the serotype-determining S1 gene segment is indicated for each strain. C, Neutralization of T3C/96 with  $\sigma$ 1-specific monoclonal antibodies (MAbs). T3C/96 virions were incubated for 1 h at 37°C with either the T1 $\sigma$ 1-specific MAb 5C6 or the T3  $\sigma$ 1-specific MAb 9BG5 at the concentrations shown. Viral titer was determined by plaque assay, using L cells. Data are the mean of 2 experiments.

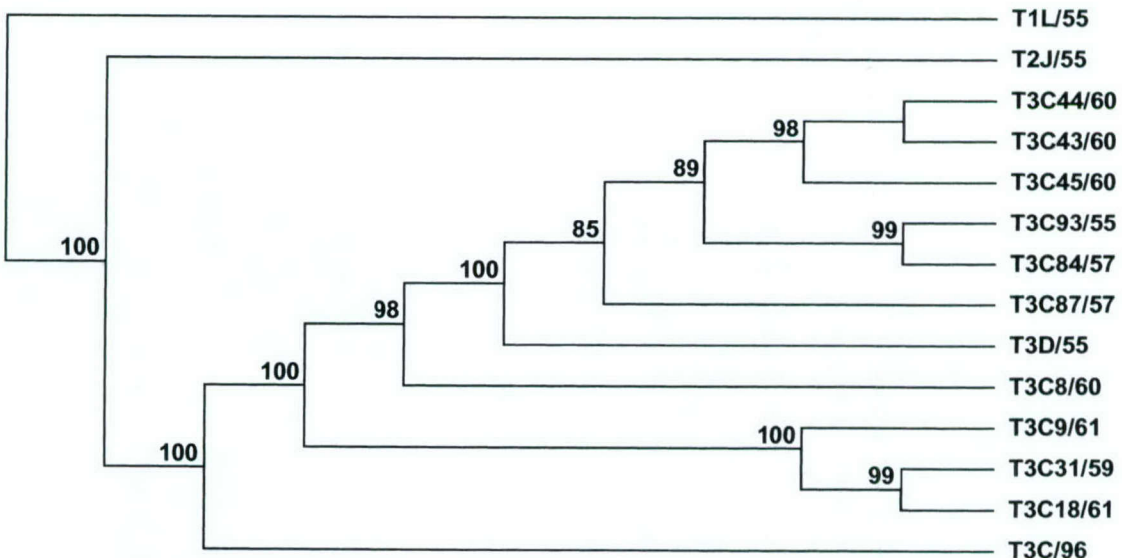


**Figure 2.** Phylogenetic tree based on S1 gene nucleotide sequences of 14 reovirus strains. Phylogenetic tree for 1416 nt of the S1 gene (nt 12–1370) of the strains shown in table 1 was constructed by use of the neighbor-joining algorithm of MacVector (version 7.1.1; Accelrys). Bootstrap values >50% (indicated as a percentage of 1000 repetitions) for major branches are shown at the nodes. The tree is unrooted.

of the S-class gene segments (S1) migrated slowly in the acrylamide gel, a characteristic of T3 reovirus strains (figure 1B). Virus produced after infection of L cells agglutinated bovine erythrocytes (HA observed at virus concentrations  $\geq 6.25 \times 10^4$  pfu/well), which is characteristic of HA produced by T3 reovirus (data not shown) [51, 52]. The CSF isolate was efficiently neutralized by T3  $\sigma 1$ -specific MAb 9BG5 (>50% plaque reduction at 5 ng/mL), but not by T1  $\sigma 1$ -specific MAb 5C6 (no plaque reduction at  $\leq 500$   $\mu$ g/mL) (figure 1C). The new reovirus isolate was designated T3C/96.

**Sequence analysis of the T3C/96 S1 gene.** The reovirus S1 gene, encoding viral attachment protein  $\sigma 1$  [19, 20], is the major genetic determinant of neurovirulence in infected mice [14, 15]. Therefore, we determined the sequence of the T3C/96 S1 gene (GenBank accession no. AY302467). The 5' and 3' NTRs of all T3 reovirus S1 genes sequenced to date are highly conserved [44]. RT-PCR primers complementary to the NTRs were designed to permit amplification of the entire T3C/96 S1 gene from infected L-cell lysates. A PCR product of the expected size (~1.4 kb) was obtained. The S1 gene cDNA was cloned and sequenced. NTRs of the T3C/96 S1 gene were directly sequenced by use of dsRNA as template. Nucleotide sequences of the prototype T3D/55 and the novel T3C/96 S1 genes shared 69% positional identity, which provided sequence confirmation of the assignment of this new isolate as a T3 strain.

To define the evolutionary relationship of the T3C/96 S1 gene with the S1 genes of other reovirus strains sequenced to date, we constructed phylogenetic trees by use of variation in the S1 gene nucleotide sequences and the neighbor-joining algorithm (figure 2). The most noteworthy feature of the S1

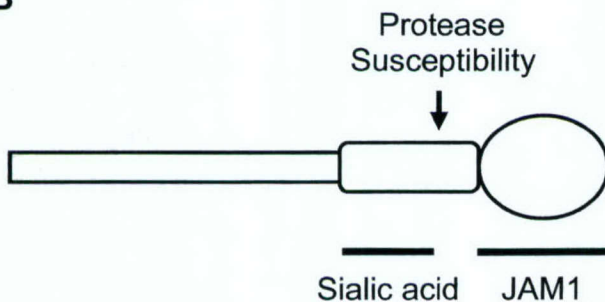
phylogenetic tree is that the S1 gene sequence of T3C/96 is substantially divergent from all other T3 strains analyzed. However, the T3C/96 S1 gene is more closely related to the S1 genes of the other T3 strains than to those of either T1 or T2 strains. A phylogenetic tree generated by use of the maximum likelihood method (Phylogeny Inference Package) [53] had a topology identical to the tree generated by using the neighbor-joining algorithm (data not shown). Therefore, T3C/96 is the first member of a highly divergent clade of T3 reovirus.

Comparison of the deduced amino acid sequences of the T3D/55 and T3C/96  $\sigma 1$  proteins confirms their evolutionary relationship, with the sequences sharing 74.3% positional identity (figure 3A). Secondary structure predictions for the 2 proteins are strikingly similar (data not shown). Notably, both T3D/55 and T3C/96  $\sigma 1$  possess amino-terminal regions with high  $\alpha$ -helical predictions and contain regions of sequence between amino-terminal residues 200–300 with high  $\beta$ -sheet predictions.

The deduced aa sequence of T3C/96  $\sigma 1$  protein was compared with that of T3D/55 across known functional domains (figure 3B). The region between aa residues 198 and 204 has been linked genetically [24, 52, 54] and biochemically [25] to the capacity of T3D/55 to bind sialic acid. The sequence of T3C/96  $\sigma 1$  was identical to that of T3D/55 across this region, which is consistent with the capacity of T3C/96 to produce HA and suggests that T3C/96 uses  $\alpha$ -linked sialic acid as a coreceptor. Sequence polymorphism at aa 249 influenced the susceptibility of T3  $\sigma 1$  protein to cleavage by intestinal proteases [28]. T3C/96 encoded a hydrophobic isoleucine at aa 249, which is a characteristic of all T3 strains that possess protease-resistant

**A**

1	T3 D/55	MDPRLREEVRLIIALTSDNGASLSKGLESRVSALEKTSQIHSDTILRIT
T3 C/96	-----T-----I-I-VLT--G---TTK--DF--IQ---Q---K---TSL--L-	
51	T3 D/55	QGLDDANKRIIALEQSRDDLVASVSDAQLAISRLESSIGALQTVVNGLDS
T3 C/96	-Q-----R-----S-----DAVASVKNTTD--ST	
101	T3 D/55	SVTQLGARVGQLETGLADVRVDHDLNVARVDTAERNIGSLTTELSTLTLR
T3 C/96	-----E---GV---FEGL-H-Y-A-IT---A---KVDA----A----	
151	T3 D/55	VTSIQADFESRISTLERTAUTSAGAPLSIRNNRMTMG LND GLTL SGNNLA
T3 C/96	--TMETGI---L-----TS-----I-I-----NVQ-----	
201	T3 D/55	IRLPGNITGLNIQNQGLQFRFNTDQFQIVNNNLTKTTVFD SINS RIGA
T3 C/96	-----S-----ID-T-----S--L-PLI--LD-I-	0
251	T3 D/55	QSYVAVSNTPLRLNSSTKVLDMIDSSTLEINSSQQLTVRSTSPNLRYPI
T3 C/96	H----VAA----PT-R--L-T--AA--V-----K-LT-A-K---	
301	T3 D/55	ADVSGGIGMSPNYRFRQSMWIGIVSYSGSGLNWRVQVN
T3 C/96	--I--S-----S----A--V-L-----I--A-----	5
351	T3 D/55	CLPAFDGFSIADGGDLSLNFVTGLLLPPLL/TGDTEPAFHNDVVTYGAQTV
T3 C/96	-----N--T-----S-----T-----R---	
401	T3 D/55	IGLSSGGAPQYMSKNLW
T3 C/96	-----A-----VC-----I--L-----A-----L--	0
451	T3 D/55	PRSFT
T3 C/96	-----	

**B**

**Figure 3.** Sequence analysis of the T3C/96  $\sigma 1$  protein. *A*, Alignment of deduced amino acid sequences of the  $\sigma 1$  proteins of T3D/55 and T3C/96. T3D/55  $\sigma 1$  protein aa residues 1–455 are shown by use of the single-letter aa code. aa Residues in T3C/96  $\sigma 1$  that are identical to the T3D/55 sequence are indicated by dashes. aa Positions are numbered above the sequences. aa Residues in the predicted sialic acid-binding domain [24, 25, 52, 54] are underlined. A sequence that confers sensitivity to cleavage by intestinal proteases [28] is circled. aa Residues identified to be important for neuronal tropism [55, 56] are boxed. *B*, Functional domains of  $\sigma 1$  protein. JAM1, junctional adhesion molecule 1.

$\sigma 1$  proteins [28]. Two aa residues in the  $\sigma 1$  head domain (aa 340 and 419) have been genetically implicated in reovirus neurotropism [55, 56]. These aa residues are identical in the T3D/55 and T3C/96  $\sigma 1$  proteins, and aa residues in the immediate vicinity of these 2 sites are highly conserved. Thus, the divergent strain T3C/96 conserves several domains of  $\sigma 1$  known to be important for reovirus neurovirulence.

**T3C/96 receptor utilization.** To determine whether T3C/96 is capable of using sialic acid and JAM1 as functional receptors, HeLa cells were treated with neuraminidase, JAM1-specific MAb J10.4, or both neuraminidase and MAb J10.4 before adsorption with T3C/96. Infected cells were quantitated by use of indirect immunofluorescence, using an antireovirus serum (figure 4). Compared to either untreated cells or cells treated with CAR-specific MAb RmcB as a control, treatment of cells with neuraminidase to remove cell-surface sialic acid resulted in a 61% reduction in the number of infected cells. Treatment of cells with JAM1-specific MAb J10.4 resulted in a 47% reduction in the number of infected cells. However, when cells were treated with both neuraminidase and MAb J10.4, infection by T3C/96 was virtually abolished. Therefore, T3C/96 is capable of using both sialic acid and JAM1 as receptors, which confirms predictions made by analysis of its  $\sigma 1$  protein sequence.

**Pathogenesis of T3C/96 in mice.** To test the capacity of T3C/96 to infect CNS tissue, newborn mice were inoculated intracranially with either T3C/96 or T3D/55 and were killed at various times after inoculation. Infectious virus present in homogenized brain tissue samples was quantitated by use of plaque assay (figure 5). Similar to T3D/55, T3C/96 replicated efficiently in CNS tissues, producing yields 10,000-fold greater than input 4 days after inoculation and sustaining high titers in the brain up to 12 days after infection. These data indicate that T3C/96 can infect and grow to high titer in the murine CNS.

To assess the neurovirulence of T3C/96, litters of newborn mice were inoculated intracranially with increasing doses ( $10^1$ – $10^4$  pfu/mouse) of either T3D/55 or T3C/96, and mortality was monitored daily for 21 days after inoculation (figure 6A). T3D/55 is neurovirulent after intracranial infection, displaying an LD<sub>50</sub> of ~100 pfu, which is consistent with previously studies, as described elsewhere [38, 57, 58]. Infection with T3C/96 also resulted in lethality, although with somewhat reduced virulence, compared with T3D/55 (LD<sub>50</sub>, ~3000 pfu). These results indicate that T3C/96 is virulent after direct inoculation of the virus into the brain.

To determine whether T3C/96 is virulent after a natural route of infection, newborn mice were inoculated perorally with  $10^5$ ,  $10^6$ , or  $10^7$  pfu/mouse of either T3D/55 or T3C/96 and were monitored daily for mortality (figure 6B). In contrast to results obtained after intracranial inoculation, we found that only T3C/96 was virulent after peroral inoculation. At the highest dose of virus used, no mice survived infection with T3C/96, whereas 90% of T3D-infected mice survived. Thus, T3C/96 can disseminate from the murine intestine to the CNS and produce a lethal infection.

To assess pathologic changes associated with T3C/96 infection in the CNS, brain section samples derived from mice killed 2, 4, and 6 days after intracranial inoculation with either  $10^4$

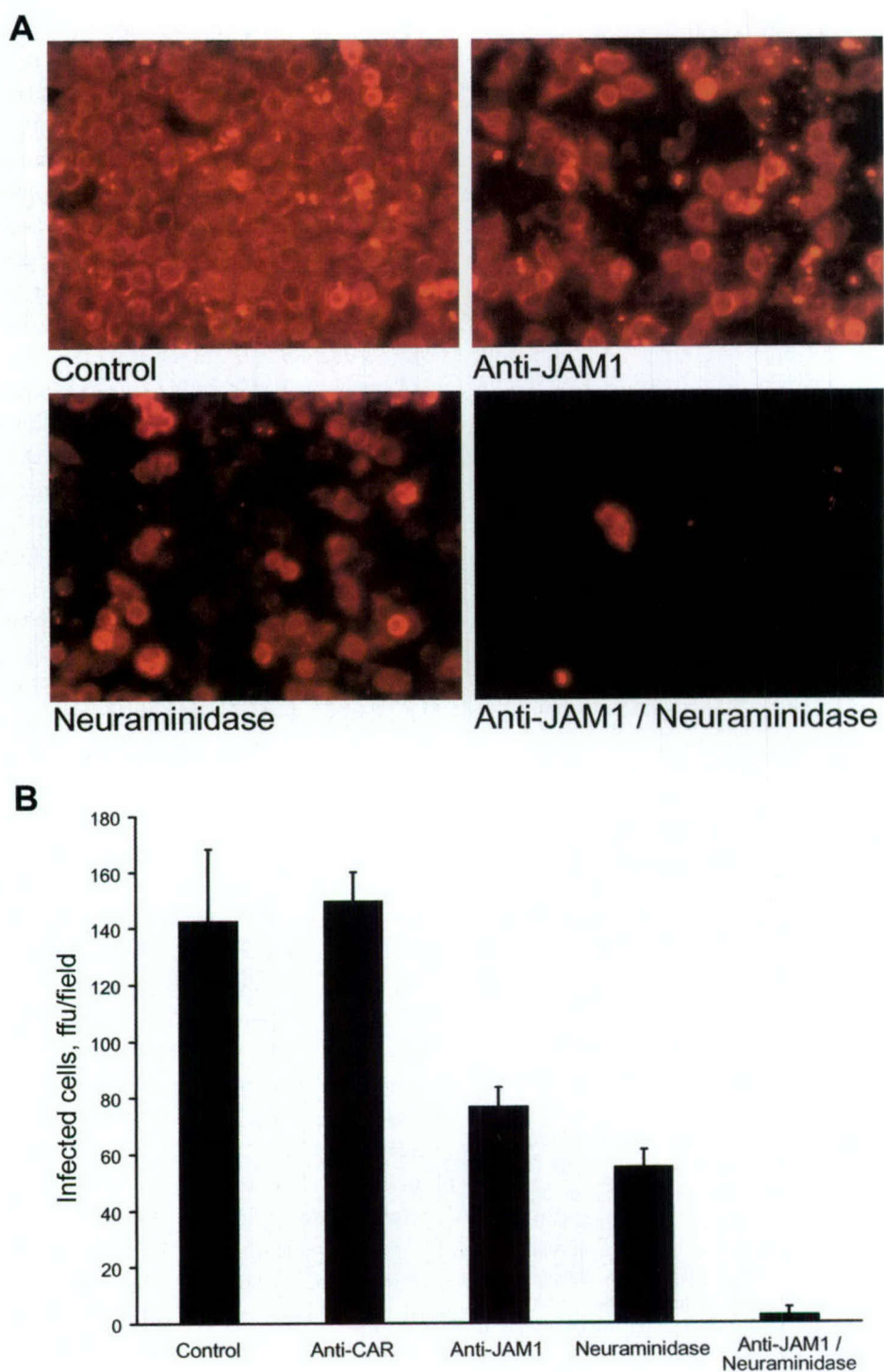


**Figure 4.** Effect of neuraminidase and junctional adhesion molecule 1 (JAM1)-specific monoclonal antibody (MAb) on growth of T3C/96. HeLa cells ( $2 \times 10^5$  cells) were pretreated with PBS, coxsackie and adenovirus receptor (CAR)-specific MAb RmcB (20 µg/mL) [45, 46], neuraminidase (40 mU/mL), JAM1-specific MAb J10.4 (20 µg/mL) [42], or neuraminidase and MAb J10.4 before adsorption with T3C/96 at an MOI of 1 fluorescent focus unit (ffu)/cell. After incubation for 20 h, cells were fixed and permeabilized with methanol. Newly synthesized viral proteins were detected by incubating cells with polyclonal rabbit antireovirus serum, followed by incubation with anti-rabbit immunoglobulin Alexa-546 serum for visualization of infected cells by indirect immunofluorescence. *A*, Representative fields of view are shown. *B*, Reovirus antigen-positive cells were quantitated by enumerating fluorescent cells in 3 random fields of view/well in triplicate. Data are mean fluorescent focus units for 3 wells. Error bars indicate SDs. ffu, Fluorescent-forming units.

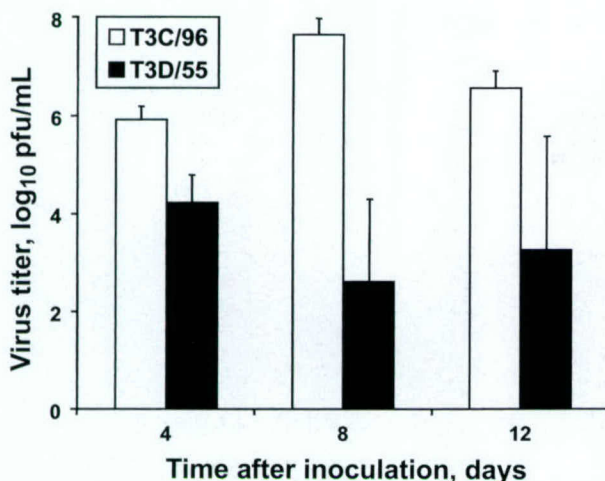


**Figure 5.** Growth of T3C/96 in mice after intracranial inoculation. ND4 Swiss Webster mice (aged 2–3 days) were inoculated intracranially with 100 plaque-forming units (pfu) of either T3C/96 or T3D/55. At the indicated days after inoculation, mice were killed, and brains were collected. Brain tissue samples were homogenized by sonication, and titers of virus present in homogenates were determined by use of plaque assay. Each data point represents the average virus titer of 2–4 brains. Error bars indicate SD.

pfu of T3C/96 or gelatin saline were examined after staining with hematoxylin-eosin (figure 7A, 7C, 7E, and 7G; data not shown). Brain section samples derived from mice infected with T3C/96 demonstrated evidence of meningoencephalitis (figure 7A and 7E; data not shown). Inflammatory infiltrates were detected primarily in the cerebral cortex, hippocampus, diencephalon, and brain stem. Morphologically, inflammatory cells were mostly lymphocytes and macrophages/microglia, with some plasma cells and neutrophils. The extent of inflammation increased with time after virus inoculation, with the most extensive inflammation observed 6 days after inoculation (data not shown).

To define the extent and location of reovirus antigen in the CNS of T3C/96-infected mice, section samples derived from mice killed 2, 4, and 6 days after inoculation with either 10<sup>4</sup> pfu of T3C/96 or gelatin saline were examined after staining with a reovirus-specific antiserum (figure 7B, 7D, 7F, and 7H; data not shown). Immunohistochemical staining for reovirus protein demonstrated immunoreactive neurons in brain section samples derived from T3C/96-infected, but not mock-infected, mice. Antigen-positive neurons were detected primarily in the cerebral cortex, hippocampus, diencephalon, and brain stem. Similar to the observed inflammatory changes, the number of antigen-positive cells increased with time after virus inoculation (data not shown). Most cells demonstrating immunohistochemical evidence of reovirus protein were detected in inflamed foci. These observations indicate that intracranial inoculation of T3C/96 leads to encephalitis and reovirus protein expression

in newborn mice. Therefore, T3C/96 is capable of neurovirulent infection.

## DISCUSSION

The present study is the first molecular characterization of a reovirus strain isolated directly from the CSF of an infant with symptoms and signs consistent with meningitis. The strain isolated, T3C/96, is a novel T3 reovirus, as determined by its HA capacity, neutralization profile, and S1 gene sequence. Molecular analysis of the T3C/96 S1 gene indicates that this strain is the most divergent T3 reovirus isolated to date. Despite this divergence, key functional domains of σ1 are conserved in this strain. T3C/96 encodes an isoleucine at position 249 in σ1, a polymorphism that has been linked to the capacity of T3 reovirus strains to infect the murine intestine and to spread from the intestine to the CNS [28]. In addition, key aa residues in the σ1 head domain implicated in T3 neural tropism and neu-

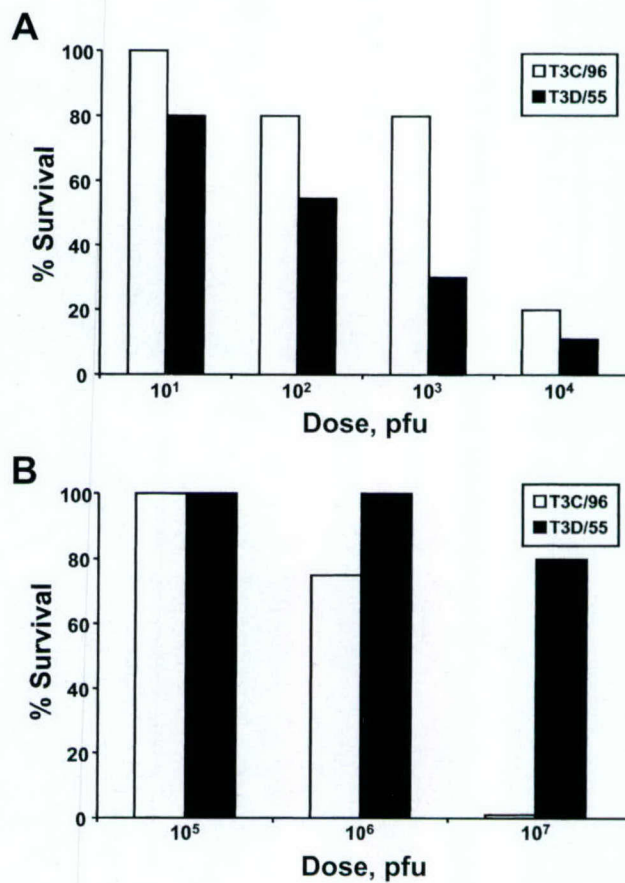


**Figure 6.** Lethality of T3D/55 and T3C/96 after either intracranial (A) or peroral inoculation (B). ND4 Swiss Webster mice (2–3 days) were inoculated with various doses of either T3D/55 or T3C/96. Each dose was inoculated into single litters of mice. Survival was monitored daily for 21 days. pfu, Plaque-forming units.

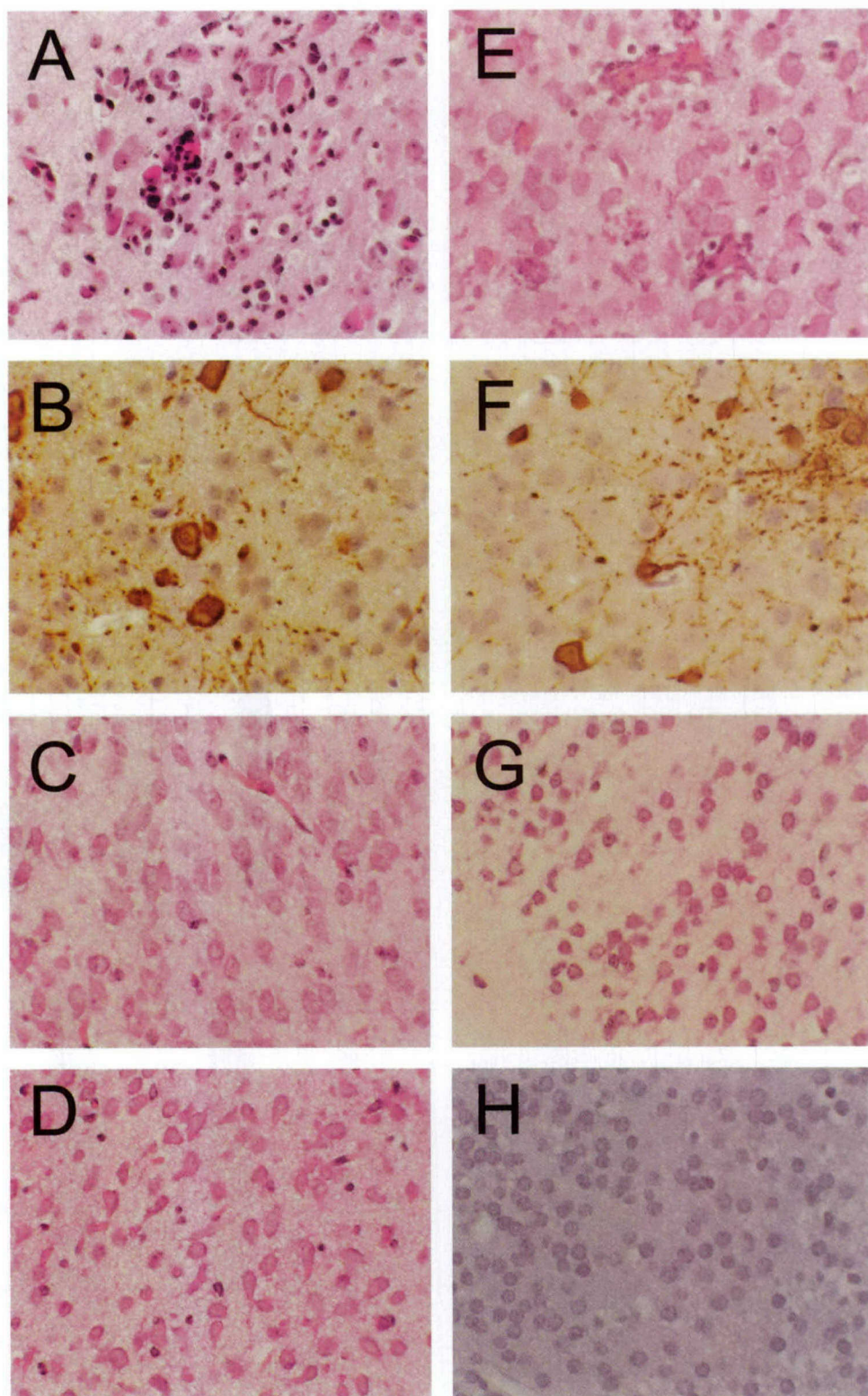


**Figure 7.** Inflammation and reovirus protein expression in the brain of newborn mice infected with T3C/96. ND4 Swiss Webster mice (2–3 days) were inoculated intracranially with either  $10^4$  pfu of T3C/96 (*A*, *B*, *E*, and *F*) or gelatin saline (*C*, *D*, *G*, and *H*). At 6 days after inoculation, brain tissue samples were harvested, paraffin embedded, sectioned, and stained with hematoxylin-eosin (*A*, *C*, *E*, and *G*) or stained for reovirus antigen by use of a polyclonal antireovirus serum (*B*, *D*, *F*, and *H*). Sections are from the upper brain stem (*A*–*D*) and the cortex (*E*–*H*). Brown staining indicates reovirus antigen.

rovirulence [55, 56] are conserved. The conservation of aa residues involved in sialic acid binding [24, 25, 52, 54] in T3C/96  $\sigma$ 1 suggests that binding to this carbohydrate may be important in neurovirulence, a hypothesis supported by the finding that the capacity to bind sialic acid enhances reovirus spread from the murine intestine to the CNS [59].

Experimental infections of mice indicate that T3C/96 is neurotropic and neurovirulent. T3C/96 productively infects the murine CNS, producing lethal infection after direct intracranial inoculation. However, in striking contrast to T3D/55, T3C/96 is also virulent after peroral inoculation, which may be related to a sequence polymorphism in  $\sigma$ 1 at aa 249.

Why do reovirus infections of humans rarely produce disease? Analysis of the T3C/96 S1 sequence suggests that the low incidence of serious illness associated with reovirus infection may be caused, in part, by a requirement for a discrete set of viral biochemical characteristics that permit neural spread of enteric reovirus infections. Specifically, a protease-resistant  $\sigma$ 1 molecule may be required for both efficient growth in the intestine and spread to secondary sites of replication, including the CNS. In addition, the capacity to bind sialic acid also may function to enhance spread to the CNS in infected humans [59]. Finally, specific sequences may be required in receptor-binding domains of the  $\sigma$ 1 head to permit efficient infection of CNS neurons. It is conceivable that viral strains lacking any of these characteristics would be nonpathogenic in humans.

Host factors also play an important role in determining the outcome of reovirus infection. Studies using mice indicate that reovirus virulence strongly correlates with host age. Newborn mice are exquisitely susceptible to reovirus CNS infection, whereas adult mice support limited viral growth and show no histopathological evidence of CNS injury even after intracranial inoculation of large doses of virus [17]. The capacity of reovirus to invade the CNS from a peripheral site of inoculation also declines rapidly with age [60]. In addition to host age, host immune responses can influence susceptibility to reovirus infection. Administration of reovirus-specific antibodies by either transplacental transfer [61] or intraperitoneal inoculation [38, 57, 58] protects newborn mice against fatal reovirus infection of the CNS. The rarity of human neurological infection with reoviruses could reflect the fact that exposure to nonneurovirulent reovirus generates protective immune responses, which, in turn, prevent neurological disease after subsequent exposure to "neurovirulent" strains. Neurological disease would occur only when a nonimmune susceptible individual was exposed to a virus containing the appropriate set of neurovirulence determinants.

In addition to reovirus, other members of the *Reoviridae* family have been associated with CNS disease in humans. Rotavirus, an important cause of gastroenteritis in children (reviewed in [62]) has been implicated in a few cases of encephalitis [63, 64], as has Colorado tick fever virus, a member of

the *Coltivirus* genus of the *Reoviridae* [65]. The patient reported in the present study provides evidence that reovirus also can cause human CNS disease.

## Acknowledgments

We appreciate the virology skills of Elaine Dowell and the willingness of Gary Mierau to perform electron microscopy on unusual viruses isolated at the Children's Hospital in Denver. We thank Kelly Parman (Vanderbilt Mouse Pathology Core Laboratory) and Sandy Olson (Vanderbilt Pathology Department) for tissue sectioning and staining and Greg Hanley and Joan Richerson for expert veterinary care. We are grateful to Jim Chappell, Tim Peters, and Bryan Youree for review of the manuscript; and Brent Weedman for preparation of the histology figures. We thank Chuck Parkos (Emory University) for providing monoclonal antibody J10.4.

## Reference

1. Nibert ML, Schiff LA. Reoviruses and their replication. In: Knipe DM, Howley PM, eds. *Fields virology*. 4th ed. Philadelphia: Lippincott-Raven, 2001:1679–728.
2. Sabin AB. Reoviruses: a new group of respiratory and enteric viruses formerly classified as ECHO type 10 is described. *Science* 1959; 130: 1387–9.
3. Rosen L. Serologic grouping of reovirus by hemagglutination-inhibition. *Am J Hyg* 1960; 71:242–9.
4. Tyler KL. Mammalian reoviruses. In: Knipe DM, Howley PM, eds. *Fields virology*. 4th ed. Philadelphia: Lippincott-Raven, 2001:1729–945.
5. Jackson GG, Muldoon RL, Cooper RS. Reovirus type 1 as an etiologic agent of the common cold. *J Clin Invest* 1961; 40:1051.
6. Lerner AM, Cherry JD, Klein JO, Finland M. Infections with reoviruses. *N Engl J Med* 1962; 267:947–52.
7. Leers WD, Rozee KR. A survey of reovirus antibodies in sera of urban children. *Can Med Assoc J* 1966; 94:1040–2.
8. Tyler KL. Pathogenesis of reovirus infections of the central nervous system. *Curr Top Microbiol Immunol* 1998; 233:93–124.
9. Krainer L, Aronson BE. Disseminated encephalomyelitis in humans with recovery of hepatoencephalitis virus. *J Neuropathol Exp Neurol* 1959; 18:339–42.
10. Joske RA, Keall DD, Leak PJ, Stanley NF, Walters MN. Hepatitis-encephalitis in humans with reovirus infections. *Arch Intern Med* 1964; 113:811–6.
11. Johansson PJ, Sveger T, Ahlfors K, Ekstrand J, Svensson L. Reovirus type 1 associated with meningitis. *Scand J Infect Dis* 1996; 28:117–20.
12. Wolf JL, Rubin DH, Finberg R, et al. Intestinal M cells: a pathway of entry of reovirus into the host. *Science* 1981; 212:471–2.
13. Tyler KL, McPhee DA, Fields BN. Distinct pathways of viral spread in the host determined by reovirus S1 gene segment. *Science* 1986; 233: 770–4.
14. Weiner HL, Powers ML, Fields BN. Absolute linkage of virulence and central nervous system tropism of reoviruses to viral hemagglutinin. *J Infect Dis* 1980; 141:609–16.
15. Weiner HL, Drayna D, Averill DR Jr, Fields BN. Molecular basis of reovirus virulence: role of the S1 gene. *Proc Natl Acad Sci USA* 1977; 74: 5744–8.
16. Morrison LA, Sidman RL, Fields BN. Direct spread of reovirus from the intestinal lumen to the central nervous system through vagal autonomic nerve fibers. *Proc Natl Acad Sci USA* 1991; 88:3852–6.
17. Tardieu M, Powers ML, Weiner HL. Age-dependent susceptibility to

- reovirus type 3 encephalitis: role of viral and host factors. *Ann Neurol* **1983**; 13:602–7.
18. Dichter MA, Weiner HL. Infection of neuronal cell cultures with reovirus mimics in vitro patterns of neurotropism. *Ann Neurol* **1984**; 16:603–10.
  19. Weiner HL, Ault KA, Fields BN. Interaction of reovirus with cell surface receptors. I. Murine and human lymphocytes have a receptor for the hemagglutinin of reovirus type 3. *J Immunol* **1980**; 124:2143–8.
  20. Lee PW, Hayes EC, Joklik WK. Protein  $\sigma 1$  is the reovirus cell attachment protein. *Virology* **1981**; 108:156–63.
  21. Furlong DB, Nibert ML, Fields BN. Sigma 1 protein of mammalian reoviruses extends from the surfaces of viral particles. *J Virol* **1988**; 62:246–56.
  22. Banerjea AC, Brechling KA, Ray CA, Erikson H, Pickup DJ, Joklik WK. High-level synthesis of biologically active reovirus protein  $\sigma 1$  in a mammalian expression vector system. *Virology* **1988**; 167:601–12.
  23. Fraser RDB, Furlong DB, Trus BL, Nibert ML, Fields BN, Steven AC. Molecular structure of the cell-attachment protein of reovirus: correlation of computer-processed electron micrographs with sequence-based predictions. *J Virol* **1990**; 64:2990–3000.
  24. Chappell JD, Gunn VL, Wetzel JD, Baer GS, Dermody TS. Mutations in type 3 reovirus that determine binding to sialic acid are contained in the fibrous tail domain of viral attachment protein  $\sigma 1$ . *J Virol* **1997**; 71:1834–41.
  25. Chappell JD, Duong JL, Wright BW, Dermody TS. Identification of carbohydrate-binding domains in the attachment proteins of type 1 and type 3 reoviruses. *J Virol* **2000**; 74:8472–9.
  26. Barton ES, Forrest JC, Connolly JL, et al. Junction adhesion molecule is a receptor for reovirus. *Cell* **2001**; 104:441–51.
  27. Nibert ML, Chappell JD, Dermody TS. Infectious subviral particles of reovirus type 3 Dearing exhibit a loss in infectivity and contain a cleaved  $\sigma 1$  protein. *J Virol* **1995**; 69:5057–67.
  28. Chappell JD, Barton ES, Smith TH, et al. Cleavage susceptibility of reovirus attachment protein  $\sigma 1$  during proteolytic disassembly of virions is determined by a sequence polymorphism in the  $\sigma 1$  neck. *J Virol* **1998**; 72:8205–13.
  29. Bodkin DK, Fields BN. Growth and survival of reovirus in intestinal tissue: role of the L2 and S1 genes. *J Virol* **1989**; 63:1188–93.
  30. Tyler KL, Squier MK, Rodgers SE, et al. Differences in the capacity of reovirus strains to induce apoptosis are determined by the viral attachment protein  $\sigma 1$ . *J Virol* **1995**; 69:6972–9.
  31. Rodgers SE, Barton ES, Oberhaus SM, et al. Reovirus-induced apoptosis of MDCK cells is not linked to viral yield and is blocked by Bcl-2. *J Virol* **1997**; 71:2540–6.
  32. Connolly JL, Rodgers SE, Clarke P, et al. Reovirus-induced apoptosis requires activation of transcription factor NF- $\kappa$ B. *J Virol* **2000**; 74:2981–9.
  33. Clarke P, Meintzer SM, Gibson S, et al. Reovirus-induced apoptosis is mediated by TRAIL. *J Virol* **2000**; 74:8135–9.
  34. Richardson-Burns SM, Kominsky DJ, Tyler KL. Reovirus-induced neuronal apoptosis is mediated by caspase 3 and is associated with the activation of death receptors. *J Neurovirol* **2002**; 8:365–80.
  35. Oberhaus SM, Smith RL, Clayton GH, Dermody TS, Tyler KL. Reovirus infection and tissue injury in the mouse central nervous system are associated with apoptosis. *J Virol* **1997**; 71:2100–6.
  36. DeBiasi R, Edelstein C, Sherry B, Tyler K. Calpain inhibition protects against virus-induced apoptotic myocardial injury. *J Virol* **2001**; 75:351–61.
  37. Connolly JL, Barton ES, Dermody TS. Reovirus binding to cell surface sialic acid potentiates virus-induced apoptosis. *J Virol* **2001**; 75:4029–39.
  38. Virgin HW 4th, Bassel-Duby R, Fields BN, Tyler KL. Antibody protects against lethal infection with the neurally spreading reovirus type 3 (Dearing). *J Virol* **1988**; 62:4594–604.
  39. Smith RE, Zweerink HJ, Joklik WK. Polypeptide components of virions, top component and cores of reovirus type 3. *Virology* **1969**; 39: 791–810.
  40. Virgin HW 4th, Mann MA, Fields BN, Tyler KL. Monoclonal antibodies to reovirus reveal structure/function relationships between capsid proteins and genetics of susceptibility to antibody action. *J Virol* **1991**; 65:6772–81.
  41. Burstin SJ, Spriggs DR, Fields BN. Evidence for functional domains on the reovirus type 3 hemagglutinin. *Virology* **1982**; 117:146–55.
  42. Liu Y, Nusrat A, Schnell FJ, et al. Human junction adhesion molecule regulates tight junction resealing in epithelia. *J Cell Sci* **2000**; 113: 2363–74.
  43. Wilson GJ, Wetzel JD, Puryear W, Bassel-Duby R, Dermody TS. Persistent reovirus infections of L cells select mutations in viral attachment protein  $\sigma 1$  that alter oligomer stability. *J Virol* **1996**; 70:6598–606.
  44. Dermody TS, Nibert ML, Bassel-Duby R, Fields BN. Sequence diversity in S1 genes and S1 translation products of 11 serotype 3 reovirus strains. *J Virol* **1990**; 64:4842–50.
  45. Hsu KH, Lonberg-Holm K, Alstein B, Crowell RL. A monoclonal antibody specific for the cellular receptor for the group B coxsackieviruses. *J Virol* **1988**; 62:1647–52.
  46. Bergelson JM, Cunningham JA, Drogue G, et al. Isolation of a common receptor for coxsackie B viruses and adenoviruses 2 and 5. *Science* **1997**; 275:1320–3.
  47. Wetzel JD, Chappell JD, Fogo AB, Dermody TS. Efficiency of viral entry determines the capacity of murine erythroleukemia cells to support persistent infections by mammalian reoviruses. *J Virol* **1997**; 71: 299–306.
  48. Tyler KL, Bronson RT, Byers KB, Fields BN. Molecular basis of viral neurotropism: experimental reovirus infection. *Neurology* **1985**; 35:88–92.
  49. Rubin DH, Fields BN. Molecular basis of reovirus virulence: role of the M2 gene. *J Exp Med* **1980**; 152:853–68.
  50. Reed LJ, Muench H. A simple method of estimating fifty percent end-points. *Am J Hyg* **1938**; 27:493–97.
  51. Lerner AM, Cherry JD, Finland M. Haemagglutination with reoviruses. *Virology* **1963**; 19:58–65.
  52. Dermody TS, Nibert ML, Bassel-Duby R, Fields BN. A  $\sigma 1$  region important for hemagglutination by serotype 3 reovirus strains. *J Virol* **1990**; 64:5173–6.
  53. Felsenstein J. PHYLIP 3.2 manual. Berkeley: University of California Herbarium, 1989.
  54. Rubin DH, Weiner DB, Dworkin C, Greene MI, Maul GG, Williams WV. Receptor utilization by reovirus type 3: distinct binding sites on thymoma and fibroblast cell lines result in differential compartmentalization of virions. *Microb Pathog* **1992**; 12:351–65.
  55. Kaye KM, Spriggs DR, Bassel-Duby R, Fields BN, Tyler KL. Genetic basis for altered pathogenesis of an immune-selected antigenic variant of reovirus type 3 Dearing. *J Virol* **1986**; 59:90–7.
  56. Bassel-Duby R, Spriggs DR, Tyler KL, Fields BN. Identification of attenuating mutations on the reovirus type 3 S1 double-stranded RNA segment with a rapid sequencing technique. *J Virol* **1986**; 60:64–7.
  57. Tyler KL, Virgin HW, Bassel-Duby R, Fields BN. Antibody inhibits defined stages in the pathogenesis of reovirus serotype 3 infection of the central nervous system. *J Exp Med* **1989**; 170:887–900.
  58. Tyler KL, Mann MA, Fields BN, Virgin HW 4th. Protective anti-reovirus antibodies and their effects on viral pathogenesis. *J Virol* **1993**; 67: 3446–53.
  59. Barton ES, Youree BE, Ebert DH, et al. Utilization of sialic acid as a coreceptor is required for reovirus-induced biliary disease. *J Clin Invest* **2003**; 111:1823–33.
  60. Mann MA, Knipe DM, Fischbach GD, Fields BN. Type 3 reovirus neuroinvasion after intramuscular inoculation: direct invasion of nerve terminals and age-dependent pathogenesis. *Virology* **2002**; 303:222–31.
  61. Cuff CF, Lavi E, Cebrak CK, Rubin DH. Passive immunity to fatal reovirus serotype 3-induced meningoencephalitis mediated by both secretory and transplacental factors in neonatal mice. *J Virol* **1990**; 64:1256–63.
  62. Kapikian A, Hoshino Y, Chanock R. Rotaviruses. In: Knipe DM, Howley PM, eds. *Fields virology*. 4th ed. Philadelphia: Lippincott-Raven, 2001:1787–833.
  63. Lynch M, Lee B, Azimi P, et al. Rotavirus and central nervous system

- symptoms: cause or contaminant? Case reports and review. *Clin Infect Dis* **2001**; *33*:932–8.
64. Wong CJ, Price Z, Bruckner DA. Aseptic meningitis in an infant with rotavirus gastroenteritis. *Pediatr Infect Dis* **1984**; *3*:244–6.
  65. Klasco R. Colorado tick fever. *Med Clin North Am* **2002**; *86*:435–40, ix.
  66. Ramos-Alvarez M, Sabin AB. Characteristics of poliomyelitis and other enteric viruses recovered in tissue culture from healthy American children. *Proc Soc Exp Biol Med* **1954**; *87*:655–61.
  67. Ramos-Alvarez M, Sabin AB. Enteropathogenic viruses and bacteria: role in summer diarrheal diseases of infancy and early childhood. *JAMA* **1958**; *167*:147–58.
  68. Hrdy DB, Rosen L, Fields BN. Polymorphism of the migration of double-stranded RNA segments of reovirus isolates from humans, cattle, and mice. *J Virol* **1979**; *31*:104–11.
  69. Rosen L, Hovis JF, Mastrota FM, Bell JA, Huebner RJ. Observations on a newly recognized virus (Abney) of the reovirus family. *Am J Hyg* **1960**; *71*:258–65.
  70. Goral MI, Mochow-Grundy M, Dermody TS. Sequence diversity within the reovirus S3 gene: reoviruses evolve independently of host species, geographic locale, and date of isolation. *Virology* **1996**; *216*:265–71.

# MEKK1 regulates calpain-dependent proteolysis of focal adhesion proteins for rear-end detachment of migrating fibroblasts

Bruce D.Cuevas<sup>1,2</sup>, Amy N.Abell<sup>1</sup>,  
James A.Witowsky<sup>1</sup>, Toshiaki Yujiri<sup>3</sup>,  
Nancy Lassignal Johnson<sup>1</sup>,  
Kamala Kesavan<sup>1</sup>, Marti Ware<sup>1</sup>,  
Peter L.Jones<sup>4,5</sup>, Scott A.Weed<sup>5,6</sup>,  
Roberta L.DeBiasi<sup>4,7,8</sup>, Yoshitomo Oka<sup>3</sup>,  
Kenneth L.Tyler<sup>7,8,9</sup> and Gary L.Johnson<sup>1,2,9</sup>

Departments of <sup>1</sup>Pharmacology, <sup>4</sup>Pediatrics, <sup>8</sup>Neurology, <sup>9</sup>Medicine,  
<sup>5</sup>Cell & Structural Biology, <sup>6</sup>Craniofacial Biology, University of  
Colorado Health Sciences Center, Denver, CO 80262, <sup>7</sup>Denver  
Veterans Affairs Medical Center, Denver, CO 80220, USA and <sup>3</sup>Third  
Department of Internal Medicine, Yamaguchi University of Medicine,  
Yamaguchi, Japan

<sup>2</sup>Corresponding authors

e-mail: bruce.cuevas@uchsc.edu or glj@med.unc.edu

Herein, we define how MEKK1, a MAPK kinase kinase, regulates cell migration. MEKK1 is associated with actin fibers and focal adhesions, localizing MEKK1 to sites critical in the control of cell adhesion and migration. EGF-induced ERK1/2 activation and chemotaxis are inhibited in MEKK1<sup>-/-</sup> fibroblasts. MEKK1 deficiency causes loss of vinculin in focal adhesions of migrating cells, increased cell adhesion and impeded rear-end detachment. MEKK1 is required for activation of the cysteine protease calpain and cleavage of spectrin and talin, proteins linking focal adhesions to the cytoskeleton. Inhibition of ERK1/2 or calpain, but not of JNK, mimics MEKK1 deficiency. Therefore, MEKK1 regulates calpain-mediated substratum release of migrating fibroblasts.

**Keywords:** calpain/MEKK1/rear-end detachment

## Introduction

Cell migration involves at least four basic components: extension of the leading edge, adherence to the substratum, release of adherence at the trailing edge and retraction of the trailing uropod. While adherence is necessary to exert force on a surface and produce forward movement, release of adherence at the uropod must occur for cell migration to continue. Control of adherence, and release thereof, is thus a critical regulatory function for migrating cells. Whereas extension and adherence have been studied extensively, few proteins have been characterized as regulators of the adhesion-release process during cell migration. Recently, the cysteine proteinase calpain has emerged as an important regulator of cell adhesion (Huttenlocher *et al.*, 1997; Bialkowska *et al.*, 2000). Originally referred to as Ca<sup>2+</sup>-dependent neutral protease (Beckerle *et al.*, 1987), the calpain family includes two ubiquitously expressed isoforms, μ- and m-calpain (murine calpains 1 and 2, respectively) (Huang and Wang, 2001). Calpains have

been suspected to regulate cell adhesion due to their ability to cleave several focal adhesion and cytoskeletal proteins (Pfaff *et al.*, 1999; Wang and Yuen, 1999). Further, calpain has been shown to be associated with cell adhesion complexes (Beckerle *et al.*, 1987), and calpain-deficient fibroblasts display inhibited migration (Arthur *et al.*, 2000; Dourdin *et al.*, 2001). Overexpression of the calpain inhibitor calpastatin also impairs cell detachment and migration (Potter *et al.*, 1998). Calpain has been proposed to regulate cell detachment through proteolytic cleavage of adhesion complex proteins in the trailing edge of migrating cells (Palecek *et al.*, 1998). An understanding of calpain regulation during migration has remained elusive. Recently, the MEK/ERK1/2 signaling pathway has been linked to calpain activation as the pharmacological MEK inhibitor PD98059 was shown to inhibit EGF-induced calpain activation (Glading *et al.*, 2000). Subsequent studies revealed that membrane-proximal ERK1/2 activity is required for EGF-induced m-calpain activation and cell migration (Glading *et al.*, 2001).

MEKK1 is a MAPK kinase kinase that is activated in response to changes in cell shape and the microtubule cytoskeleton (Yujiri *et al.*, 1999). Dual regulation of JNK and ERK1/2 pathways by low concentrations of growth factors like EGF and by microtubule-disrupting agents like nocodazole is mediated by MEKK1 (Yujiri *et al.*, 1998). Targeted gene disruption of MEKK1 demonstrated that it functionally regulates cell migration both *in vivo* and *in vitro* (Yujiri *et al.*, 2000). Our results reveal an association of MEKK1 with focal adhesions and actin fibers entering the focal adhesions. MEKK1 regulates the limited proteolysis of the focal adhesion proteins talin and spectrin. Characterization of MEKK1-null mouse embryo fibroblasts demonstrates that MEKK1 regulates the ERK1/2 pathway for control of calpain-catalyzed rear-end detachment.

## Results

### MEKK1 regulates cell adhesion

Comparison of wild-type and MEKK1<sup>-/-</sup> fibroblasts readily defines a function for MEKK1 in regulating cell adhesion and migration. We found that MEKK1<sup>-/-</sup> fibroblasts have a marked increase in adherence to the culture substratum relative to wild-type fibroblasts (Figure 1A). Using wild-type and MEKK1<sup>-/-</sup> cells that had been serum starved and then challenged with or without serum, the culture plates were inverted and centrifuged. The remaining attached cells were counted as a measure of adherence, with greater number of cells after centrifugation being indicative of increased adherence (Lotz *et al.*, 1989). This simple assay clearly demonstrates the increased adherence of MEKK1<sup>-/-</sup> cells relative to wild-type fibroblasts. Even though

MEKK1<sup>-/-</sup> cells show an increased adherence in the centrifugation assay, their rate of attachment on fibronectin or tissue culture plastic alone is similar to the rate of attachment of wild-type cells (Figure 1B). The increased adherence in the centrifugation assay, but similar attachment rate of MEKK1<sup>-/-</sup> compared with wild-type fibroblasts, suggested MEKK1 regulates release of cell adhesion. We used live cell microscopy to show that MEKK1<sup>-/-</sup> fibroblasts are, indeed, inhibited in random migration and rear-end detachment (see Supplementary data available at *The EMBO Journal Online*). Both wild-type and MEKK1<sup>-/-</sup> fibroblasts are capable of extending lamellipodia necessary for forward movement, and both cell types develop tails or uropods at the trailing edge as the cell moves in the direction of the leading edge. However, as wild-type fibroblasts have the ability to detach and retract their trailing edge, MEKK1<sup>-/-</sup> cell forward progress is impeded by an inability of the uropod to detach from the substrate, thereby giving the appearance that MEKK1<sup>-/-</sup> cells are tethered at their trailing end. Thus, the increased adherence of MEKK1<sup>-/-</sup> cells is, at least in part, a result of defective detachment from the substratum.

#### MEKK1 regulates directed cell migration

Inhibited movement of MEKK1<sup>-/-</sup> fibroblasts was readily demonstrated using both transwell migration and *in vitro* wound response assays. Chemotaxis toward serum is inhibited in MEKK1<sup>-/-</sup> compared with wild-type fibroblasts (Figure 2A), consistent with a defect in cell movement that would be observed with a loss of rear-end detachment. Further, when soluble fibronectin is used as a chemotactic agent, migration is reduced by 50% in MEKK1<sup>-/-</sup> versus wild-type cells (Figure 2B). Although EGF by itself is a weak chemotactic agent, EGF combined with fibronectin produces a synergistic effect relative to fibronectin alone to induce chemotaxis (Maheshwari *et al.*, 1999) (Figure 2B). This synergistic effect is completely absent in MEKK1-deficient cells, thus demonstrating that MEKK1 is required for the EGF/fibronectin-induced fibroblast migration.

When a confluent contact-inhibited fibroblast culture is 'wounded' using a razor swipe, the cells along the edge of the wound are contact inhibited on all sides save one, and will migrate into the wound opening. Wild-type fibroblasts will migrate into the wound space within 5 h after initiation of the wound (Figure 2C). In contrast, MEKK1<sup>-/-</sup> fibroblast migration into the open area of the wound is markedly inhibited. Indeed, the time required by MEKK1<sup>-/-</sup> fibroblasts to completely close a standardized wound (24.5 h) is significantly ( $P < 0.05$ ) prolonged compared with the MEKK1<sup>+/+</sup> cells (11 h) (Figure 2D). By 12 h post-wounding, some MEKK1<sup>-/-</sup> fibroblasts have migrated into the wound site but do not reach numbers or distances achieved by MEKK1<sup>+/+</sup> fibroblasts. This indicates that MEKK1<sup>-/-</sup> fibroblasts are markedly defective, but not completely inhibited in directed migration. The loss of migration is a direct consequence of MEKK1 deficiency because MEKK1 add-back by transfection of MEKK1<sup>-/-</sup> cells restores migration into the wound (Figure 2C and D). It is possible that the migration defect of MEKK1<sup>-/-</sup> cells was due to the loss of expression of a secreted factor such as a cytokine, protease or extracellular

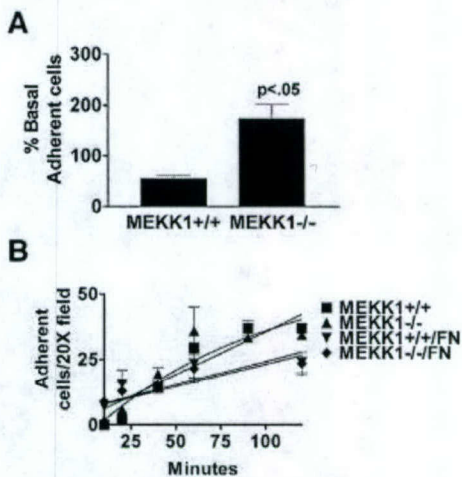


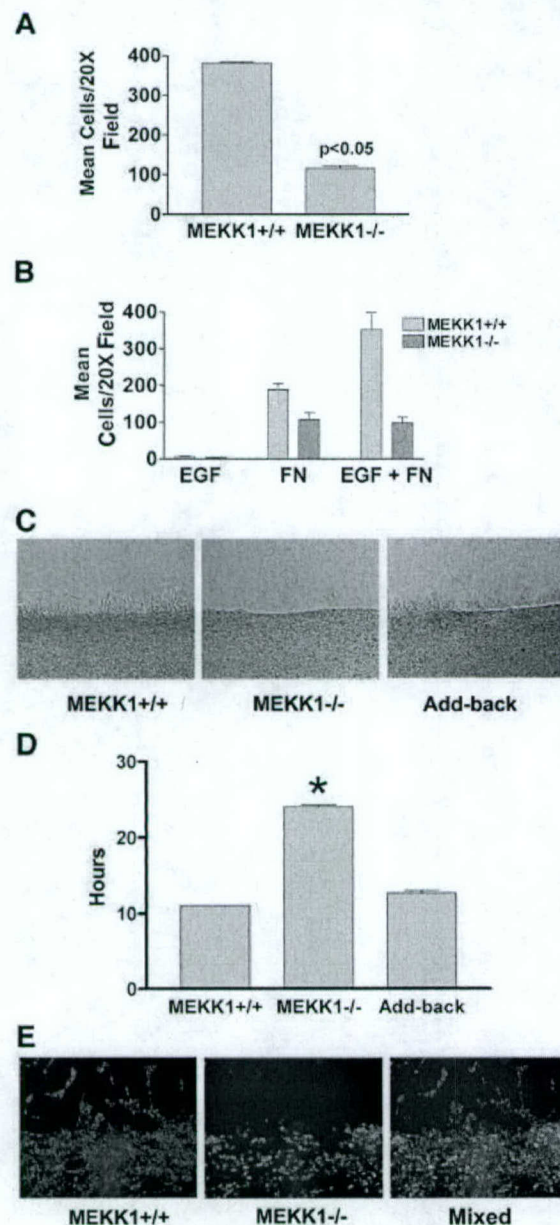
**Fig. 1.** MEKK1-deficient fibroblasts show increased adherence characteristic of a defect in rear-end detachment. (A) Wild-type or MEKK1<sup>-/-</sup> MEFs were serum starved for 8 h, then treated with media with or without 10% fetal bovine serum (FBS). The plates were then inverted and centrifuged at 2300 g for 5 min. Adherent cells remaining attached to the well surface were stained with Wright's stain and quantitated. Cell adherence is represented as the percent of the total serum-treated cells compared with the non-treated cells; 100% was taken as the number of wild-type cells in the dish before serum challenge, inversion and centrifugation. MEKK1<sup>-/-</sup> cells with serum challenge is >100% because more cells are retained after centrifugation than for the non-serum-stimulated wild-type cells, indicative of the increased adherence of MEKK1<sup>-/-</sup> cells. Results shown are the mean  $\pm$  SEM of at least three independent experiments, and the statistical significance was determined by Student's *t*-test. (B) Fibroblasts were resuspended in complete media and allowed to attach to either untreated or fibronectin-coated tissue culture plates. Cells were monitored for 2 h and the number of attached cells determined by phase microscopy. A digital movie of migrating MEKK1<sup>+/+</sup> and MEKK1<sup>-/-</sup> fibroblasts is available as Supplementary data.

matrix protein. To determine whether the migration defect in MEKK1<sup>-/-</sup> cells was due to loss of a secreted factor, MEKK1<sup>-/-</sup> and wild-type fibroblasts were co-cultured (Figure 2E) and their respective migration analyzed by the *in vitro* wound healing assay. MEKK1<sup>-/-</sup> and wild-type fibroblasts were stained with different vital fluorescent dyes so they could be readily distinguished when co-cultured. Strikingly, after 5 h post-wounding, wild-type but not MEKK1<sup>-/-</sup> fibroblasts have extensively moved into the wound space. Virtually no MEKK1<sup>-/-</sup> fibroblasts in co-culture with MEKK1<sup>+/+</sup> fibroblasts have migrated into the wound space, demonstrating that co-culture with wild-type cells can not restore migration to MEKK1<sup>-/-</sup> fibroblasts. Thus, the migration defect of MEKK1<sup>-/-</sup> fibroblasts is not rescued by secreted factors from wild-type cells. This result strongly suggests that the defective migration of MEKK1<sup>-/-</sup> fibroblasts is not due to an inability to secrete a required protein.

#### Vinculin content in focal adhesions is diminished in migrating MEKK1<sup>-/-</sup> fibroblasts

The MEKK1<sup>-/-</sup> phenotype is characterized by increased adherence, defective rear-end detachment and inhibited migration, suggesting a defect in the regulation of focal adhesions. To address the consequence of MEKK1 deficiency in the regulation of focal adhesions of migrating cells, we used quantitative immunofluorescence analysis

to measure vinculin content in focal adhesions of migrating wild-type (Figure 3A) and MEKK1<sup>-/-</sup> (Figure 3C) fibroblasts. The experiment required a 12 h incubation after inflicting the razor swipe to allow migration of MEKK1<sup>-/-</sup> cells into the wound site, and a larger wound than that of Figure 2D. Analysis of 58 wild-type and 97 MEKK1<sup>-/-</sup> fibroblasts migrating into the scrape wound of confluent monolayers indicated 2.8-fold ( $P < 0.0001$ ) less vinculin in focal adhesions of MEKK1<sup>-/-</sup> versus wild-type fibroblasts (Figure 3D). This result is consistent with the inability of migrating MEKK1<sup>-/-</sup> fibroblasts to properly organize the complex of proteins in focal adhesions. While vinculin may also be organized at cell-to-cell contacts, we have found that vinculin consistently co-localizes with the focal adhesion protein talin in mouse embryo fibroblasts (data not shown) and as such serves as a surrogate assay for focal adhesion formation. Further, as



organized vinculin staining is indicative of focal adhesions, loss of vinculin staining indicates that the increased adherence of MEKK1-deficient cells is not due to an increased number or size of focal adhesions as has been observed in FAK<sup>-/-</sup> fibroblasts. This indicates that the change in adherence and focal adhesion composition resulting from MEKK1 deficiency is different from that observed with loss of FAK expression. Importantly, the add-back of MEKK1 expression restores vinculin content to focal adhesions in migrating fibroblasts (Figure 3B and D). Stationary MEKK1<sup>-/-</sup> and wild-type fibroblasts in confluent monolayers have similar vinculin staining (data not shown), consistent with MEKK1 signaling being important for regulation of the turnover of focal adhesions during migration and not in the ability to form focal adhesions. The partial restoration of vinculin to focal adhesions is likely due to the level of MEKK1 expressed in the add-back clone, which is only 20% of MEKK1 protein in wild-type fibroblasts. Stable expression of MEKK1 by add-back to MEKK1<sup>-/-</sup> cells is extremely difficult. This is predictably due to the regulation of MEKK1 expression during the cell cycle that is not mimicked by using other promoters or viral LTRs to express MEKK1, and the toxicity of MEKK1 overexpression (Yujiri *et al.*, 1999). Despite intensive effort, we have not been able to achieve stable add-back clones that express >20% of wild-type MEKK1 protein. Interestingly, our preliminary findings suggest that the level of talin and FAK, unlike vinculin, may be similar in MEKK1<sup>-/-</sup> and wild-type fibroblasts (data not shown). To determine whether MEKK1 does indeed differentially regulate protein composition in focal adhesions, it will be necessary to perform quantitative immunofluorescence analysis of several focal adhesion proteins in stationary and migrating wild-type, MEKK1<sup>-/-</sup> and add-back fibroblasts.

#### **EGF stimulates the formation of MEKK1-FAK complexes**

Figure 4A shows that when serum-starved fibroblasts are stimulated with EGF, MEKK1 is co-immunoprecipitated with FAK. Co-expression of MEKK1 and FAK in

**Fig. 2.** MEKK1 expression is necessary for fibroblast migration. (A) Fibroblasts were seeded into the upper chamber of a Transwell migration plate with 5% FBS in the lower chamber. Cells traversed after 5 h to the lower surface of the membrane were quantitated. The results shown are the mean  $\pm$  SEM of at least three independent experiments. (B) Fibroblasts were treated as in (A) except that the bottom well of the Transwell contained either 1 nM EGF, 100  $\mu$ g/ml fibronectin or the combination of EGF and fibronectin. (C and E) Wild-type or MEKK1<sup>-/-</sup> fibroblasts were seeded onto coverslips and allowed to grow overnight. In addition, MEKK1<sup>-/-</sup> fibroblasts stably transfected with full-length MEKK1 (Add-back) were analyzed. Each confluent culture was 'wounded' with a razor and observed over the course of 5 h for migration into the wound space (*in vitro* wound healing assay). (C) is a DIC image of migrating cells. (D) The time required for confluent fibroblasts in a tissue culture plate to close a standardized wound (200  $\mu$ m) is represented by the graph. Results shown are the mean  $\pm$  SEM of at least three independent experiments, and the statistical significance was determined by Student's *t*-test (\* $P < 0.05$ ). (E) Cells were first stained with the fluorescent vital dyes PKH26 (red; MEKK1<sup>+/+</sup>) or PKH67 (green; MEKK1<sup>-/-</sup>) and then mixed in equal numbers before seeding onto coverslips, and treated as described above. The fluorescence image depicts the migration of MEKK1<sup>+/+</sup> (wild type) and MEKK1<sup>-/-</sup> cells in co-culture. The data are representative samples from at least three independent experiments.

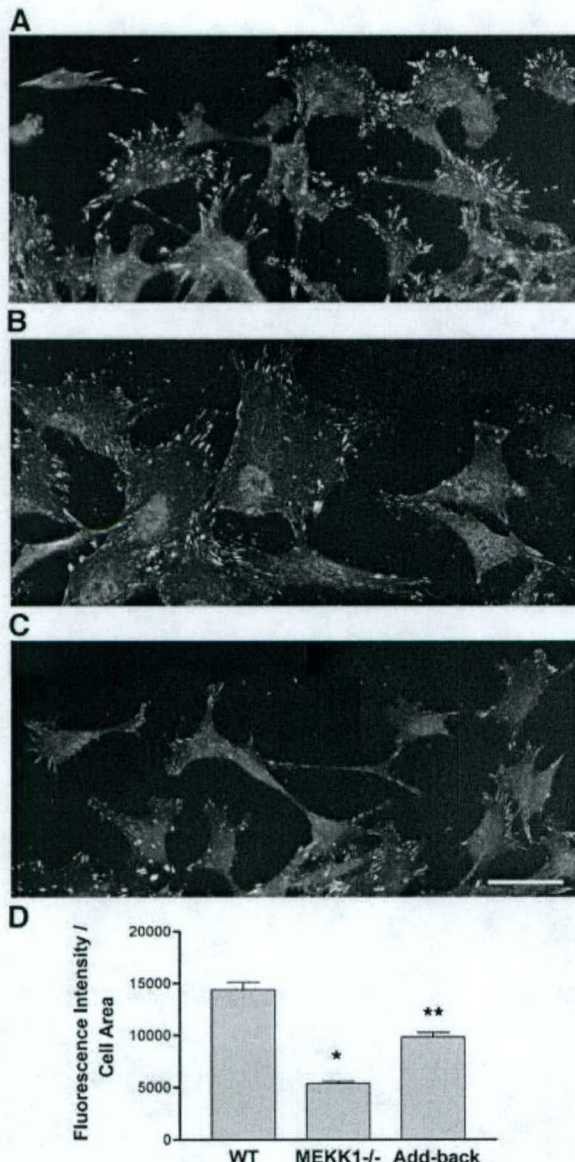


**Fig. 3.** Vinculin content in focal adhesions is diminished in migrating MEKK1<sup>-/-</sup> fibroblasts. A 0.4  $\mu$ m deconvolved image section of the cell having the brightest focal adhesion staining was used for the measurement of integrated intensity of vinculin content for MEKK1+/+ (A), add-back (B) and MEKK1<sup>-/-</sup> (C) fibroblasts. The intensity of vinculin staining was measured per cell area of the section. The add-back clone stably expresses full-length MEKK1 and was derived from the MEKK1<sup>-/-</sup> fibroblasts. The bar graph in (D) shows the analysis from three experiments where 58 wild-type, 97 MEKK1<sup>-/-</sup> and 96 add-back cells were analyzed for integrated vinculin staining intensity per cell area. Vinculin content in the MEKK1<sup>-/-</sup> clone is diminished at a statistically significant level from wild-type MEKK1+/+ cells (\* $P < 0.0001$ ) and add-back cells (\*\* $P < 0.001$ ). Bar = 50  $\mu$ m.

HEK293 cells by transient transfection demonstrated that they could be reciprocally co-immunoprecipitated (Yujiri *et al.*, 2003). These findings demonstrate the interaction of MEKK1 with FAK-associated protein complexes and that endogenous MEKK1 recruitment into FAK complexes is regulated by a growth factor that stimulates both FAK and MEKK1 kinase activities (Fanger *et al.*, 1997). Thus, EGF

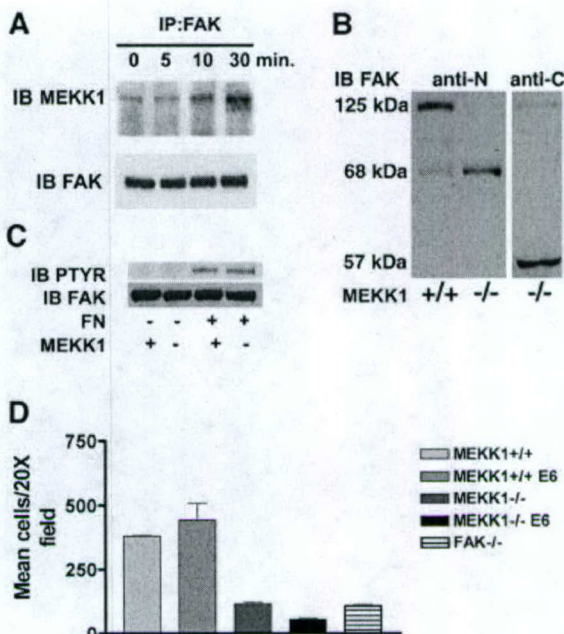


**Fig. 4.** MEKK1 and FAK form a complex in EGF-stimulated fibroblasts. (A) Wild-type mouse embryo fibroblasts were treated with 100 ng/ml EGF for the indicated times. After cell lysis, endogenous FAK was immunoprecipitated with anti-FAK antibody, and associated MEKK1 detected by MEKK1 immunoblotting. Total immunoprecipitated FAK was measured by anti-FAK immunoblotting using the same blots as that for MEKK1 analysis. (B) Wild-type (MEKK1<sup>+/+</sup>) and MEKK1<sup>-/-</sup> fibroblasts stably expressing papilloma virus E6/E7 proteins were immunoblotted for FAK protein expression using an antibody recognizing the N- or C-terminal domain of FAK. FAK is a 125 kDa protein with N- and C-terminal cleavage fragments of 68 and 57 kDa, respectively. (C) Serum-starved MEKK1<sup>+/+</sup> or MEKK1<sup>-/-</sup> MEFs were allowed to adhere to fibronectin-coated bacterial plates for 30 min, and then lysed. Endogenous FAK was immunoprecipitated with anti-FAK antibodies, and the level of tyrosine-phosphorylated FAK determined by phosphotyrosine immunoblotting. The membrane was then stripped and total FAK was assessed by FAK immunoblotting. (D) MEKK1<sup>+/+</sup> and MEKK1<sup>-/-</sup> fibroblasts  $\pm$  E6/E7 protein expression were analyzed for migration in Transwell assays using 5% FBS as described for Figure 2A. \*Inhibition of MEKK1<sup>-/-</sup> E6/E7 cell migration is statistically significant relative to FAK<sup>-/-</sup> cells ( $P < 0.05$ ) and MEKK1<sup>-/-</sup> cells ( $P < 0.001$ ).

induces the stable association of MEKK1 with FAK, altering the protein composition of focal adhesions.

Focal adhesion turnover, and therefore cell adhesion, is proposed to be modulated not only by signaling pathways involving protein phosphorylation, but by proteolysis of focal adhesion components as well. Interestingly, FAK and MEKK1 are regulated both by phosphorylation and proteolytic cleavage (Cooray *et al.*, 1996; Schlesinger *et al.*, 1998; Cary *et al.*, 2002). The discovery that MEKK1 becomes stably associated with FAK suggested that MEKK1 functions in focal adhesion signaling. The increased adherence and inhibition of migration resulting from MEKK1 deficiency also demonstrates that MEKK1 has an important role in the function of focal adhesions.

#### MEKK1 localizes with focal adhesions

Expression of EGFP-MEKK1 in MEKK1<sup>-/-</sup> MEFs demonstrates its association with focal adhesions and actin fibers entering the focal adhesions (Figure 5). The localization of EGFP-MEKK1 with focal adhesions is

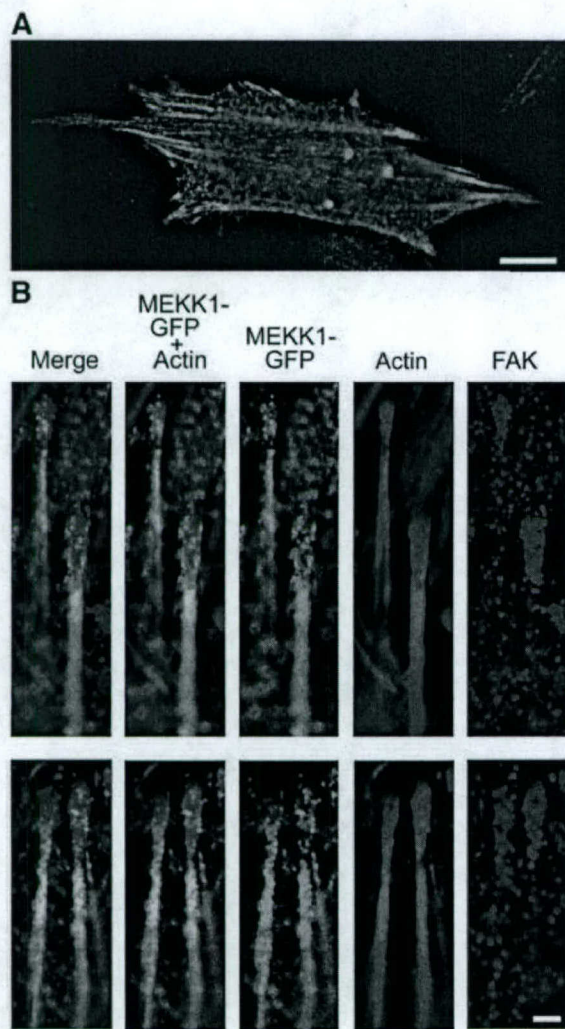


**Fig. 5.** MEKK1 localizes to focal adhesions. MEKK1 $^{-/-}$  fibroblasts were transfected with EGFP-MEKK1, incubated in serum-free media for 12 h, then processed as described in Materials and methods and subjected to immunofluorescence analysis. (A) An MEKK1 $^{-/-}$  MEF transfected with EGFP-MEKK1 and treated with anti-FAK antibodies (FAK displayed as red fluorescence). Bar = 10  $\mu$ m. (B) Displayed are two representative examples of co-localization of EGFP-MEKK1 with endogenous FAK (purple) and actin (red). Bar = 1  $\mu$ m.

consistent with its co-immunoprecipitation with FAK (Figure 4). We did not observe a measurable increase of EGFP-MEKK1 in focal adhesions of EGF-stimulated cells despite an increased stable association of MEKK1 in FAK immunoprecipitates. This suggests that the EGF stimulation of MEKK1-FAK co-immunoprecipitation may be related to increased stabilization of the complex, possibly due to phosphorylation-related responses, rather than a re-localization of MEKK1 to focal adhesions. It should also be noted that caspase-mediated cleavage of MEKK1 compelled us to use a mutant MEKK1 protein for these studies. The caspase-cleavage site residues had been mutated to alanines (Widmann *et al.*, 1998). The caspase-cleaved fragments do not appear to localize to focal adhesions. Cumulatively, the co-immunoprecipitation and immunofluorescence studies demonstrate that MEKK1

localizes, in part, to focal adhesions and actin filaments entering focal adhesions for the control of cell adherence.

#### **E6/E7 papilloma virus proteins induce FAK proteolysis in MEKK1 $^{-/-}$ fibroblasts**

E6/E7 expression immortalizes primary fibroblasts by inducing the degradation of p53. We had used E6/E7 for immortalization of both wild-type and MEKK1 $^{-/-}$  mouse embryo fibroblasts. We quickly realized that there was a significant difference in the phenotype of MEKK1 $^{-/-}$  fibroblasts but not wild-type fibroblasts that had been immortalized with papillomavirus E6/E7 proteins versus immortalization by serial passage. In addition to stimulating p53 degradation, the E6 oncoprotein binds to the focal adhesion protein paxillin (Turner, 2000). One outcome of E6 expression is the disruption of paxillin association with vinculin and FAK (Tong *et al.*, 1997; Turner, 2000). Relative to primary MEKK1 $^{-/-}$  fibroblasts, or MEKK1 $^{-/-}$  fibroblasts immortalized by serial passage, MEKK1 $^{-/-}$  fibroblasts expressing E6/E7 were extremely flat and highly adherent to the substratum, reminiscent of FAK $^{-/-}$  cells (Ilic *et al.*, 1995). In contrast, E6/E7-expressing wild-type fibroblasts were more rounded and less adherent to substratum. Figure 4B shows that E6/E7 expression in MEKK1 $^{-/-}$  fibroblasts causes a near quantitative cleavage of FAK. This contrasts with E6/E7-expressing MEKK1 $^{+/+}$  fibroblasts where FAK remains intact. This result is consistent with MEKK1 being associated with FAK-paxillin-vinculin complexes and playing a protective role against E6/E7-induced FAK degradation. This suggests that EGF-induced MEKK1 association with focal adhesions alters the organization and interaction of focal adhesion proteins.

Functionally, MEKK1 protects FAK from E6/E7-mediated degradation, but MEKK1 expression is not required for fibronectin binding-induced stimulation of FAK tyrosine phosphorylation (Figure 4C). With MEKK1 $^{-/-}$  fibroblasts immortalized by serial passage, fibronectin stimulation of FAK tyrosine phosphorylation is similar to that observed with MEKK1 $^{+/+}$  fibroblasts. This result indicates that FAK tyrosine phosphorylation is largely independent of the role MEKK1 plays in organization, signaling and proteolytic susceptibility of focal adhesion proteins.

E6/E7-induced FAK cleavage in MEKK1 $^{-/-}$  fibroblasts causes a migration defect more severe than that observed with FAK $^{-/-}$  or MEKK1 $^{-/-}$  fibroblasts not expressing the E6/E7 oncoproteins (Figure 4D). FAK $^{-/-}$  fibroblasts, like MEKK1 $^{-/-}$  fibroblasts, exhibit a marked reduction in migration in transwell assays (Figure 4D). Unlike E6/E7 wild-type fibroblasts that readily migrate toward serum, E6/E7 MEKK1 $^{-/-}$  fibroblasts display a migration defect more severe than either MEKK1 $^{-/-}$  or FAK $^{-/-}$  fibroblasts that do not express the E6/E7 proteins (Figure 4D). Thus, MEKK1 is important in maintaining the integrity and protein composition of focal adhesion complexes and is functionally required for fibroblast migration. The combined loss of MEKK1 and FAK exacerbates the migration defect resulting from the loss of either kinase alone.

#### **MEKK1 regulates calpain activation**

Previous studies have suggested that the intracellular cysteine protease calpain is involved in the regulation of

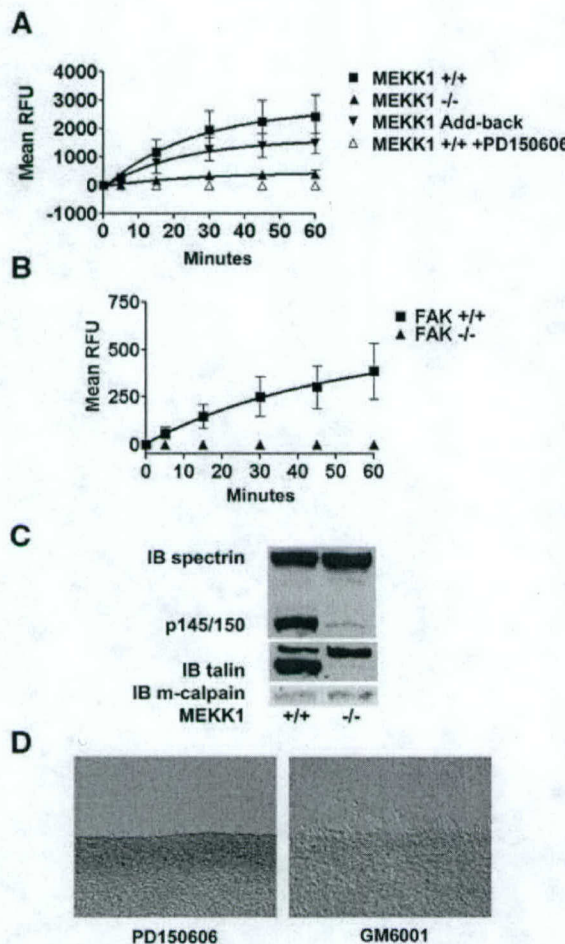


**Fig. 6.** MEKK1-deficient fibroblasts show reduced calpain activity, and calpain inhibition mimics MEKK1 deficiency. *In vivo* calpain activity was assessed in fibroblasts using the cell-permeable, fluorescent calpain substrate SLLVY-AMC (A and B) and by anti-spectrin or anti-talin immunoblotting (C). (A) MEKK1<sup>+/+</sup> cells in the presence and absence of the calpain inhibitor PD150606 (50  $\mu$ M), MEKK1<sup>-/-</sup> and MEKK1 add-back cells were used for measurement of calpain activity. (B) FAK<sup>+/+</sup> and FAK<sup>-/-</sup> cells were used to measure calpain activity as in (A). (C) The anti-spectrin and anti-talin immunoblots were stripped and reprobed with anti-m-calpain antibodies to verify protein levels. The immunoblots are representative of at least three independent experiments. (D) Wild-type fibroblasts grown to confluence on coverslips were pre-treated for 1 h with 50  $\mu$ M PD150606 (left panel) or 2  $\mu$ M GM6001, a matrix metalloproteinase inhibitor (right panel), and then analyzed for migration using the *in vitro* wound healing assay following a razor swipe in the continuous presence of inhibitor. Results are representative of at least three independent experiments for each set of experiments in (A–D).

rear-end detachment of migrating cells (Huttenlocher *et al.*, 1997; Frame *et al.*, 2002; Glading *et al.*, 2002), the migration defect of MEKK1<sup>-/-</sup> fibroblasts. Using a cell-permeable fluorogenic calpain substrate, we discovered that MEKK1<sup>-/-</sup> cells have significantly less calpain proteinase activity than wild-type fibroblasts (Figure 6A). Similarly, in culture conditions identical to the *in vitro* wound assay, MEKK1<sup>-/-</sup> fibroblasts have significantly less calpain activity than wild-type fibroblasts. Cleavage of the fluorogenic substrate is blocked using a calpain-specific inhibitor, PD150606, which prevents Ca<sup>2+</sup> binding

to calpain and does not significantly inhibit either cathepsins or caspases (Wang *et al.*, 1996), confirming that the assay is specifically measuring calpain activity (Figure 6A). Just as add-back of MEKK1 protein by transfection of MEKK1<sup>-/-</sup> fibroblasts rescued adherence and migration, add-back of MEKK1 also restored calpain regulation (Figure 6A). Even though the add-back clone expresses MEKK1 protein at only 20% of the MEKK1 expression of wild-type fibroblasts, it is sufficient to at least partially restore calpain activation, and rescue both migration and adherence. As we had demonstrated that MEKK1 is associated with focal adhesions (Figures 4 and 5), we asked whether FAK was necessary for calpain activation. Since FAK-deficient fibroblasts have been found to have severe migration defects (Ilic *et al.*, 1995), we wanted to determine whether loss of FAK from the signaling complex affected calpain activity. Strikingly, calpain activity in serum-treated FAK-deficient fibroblasts was dramatically reduced compared with that of FAK-expressing cells (Figure 6B). Taken together, our data support the existence of a complex containing FAK and MEKK1 that is required for calpain control of cell adherence and migration.

$\alpha_2\beta_2$  spectrin (fodrin) is a structural protein linking the cytoskeleton to membranes and is a defined calpain substrate (Wang and Yuen, 1999; Wang, 2000). Calpain cleavage of spectrin produces a specific pattern of proteolytic peptide fragments of 145–150 kDa (Wang and Yuen, 1999; Wang, 2000) that are unique to calpain and are different in size from those generated by caspases (Wang and Yuen, 1999; Wang, 2000). We found that calpain-specific spectrin fragments generated in wild-type fibroblasts were nearly undetectable in MEKK1<sup>-/-</sup> fibroblasts (Figure 6C). This finding demonstrates the loss of cleavage of an endogenous calpain substrate in MEKK1<sup>-/-</sup> fibroblasts. Cleavage of another calpain substrate, talin, was similarly reduced in the MEKK1-deficient cells (Figure 6C). While calpain activity was diminished in MEKK1<sup>-/-</sup> fibroblasts, immunoblotting indicated that total calpain protein expression was similar in wild-type and MEKK1<sup>-/-</sup> fibroblasts (Figure 6C). This result is consistent with the existence of a MEKK1-dependent signaling complex that regulates calpain activity but not calpain expression. Together, the loss of both spectrin and talin cleavage, coupled with reduced hydrolysis of the fluorogenic calpain-specific substrate, clearly demonstrates a loss of calpain activation in MEKK1<sup>-/-</sup> cells. Importantly, PD150606, the calpain-specific inhibitor, blocks the migration of wild-type fibroblasts in the *in vitro* wound assay (Figure 6D). However, GM6001, an inhibitor of metalloproteinases that function to remodel the extracellular matrix, did not inhibit fibroblast migration into the wound space, thereby demonstrating the specific requirement of calpain inhibition for disrupted migration in this assay. The findings demonstrate that the MEKK1-dependent regulation of calpain activity is required for cell migration.

#### MEKK1 regulates ERK1/2 activity

The MEK inhibitor PD98059 blocks ERK1/2 activation, inhibits calpain activation and cell motility (Glading *et al.*, 2000). However, as PD98059 may influence Ca<sup>2+</sup> influx independently of MEK activity (Pereira *et al.*, 2002), and

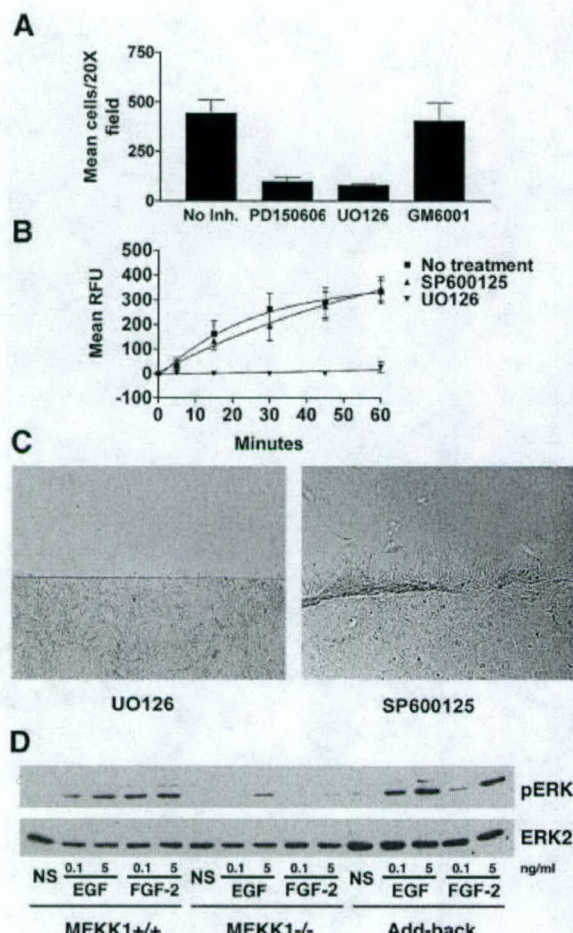


**Fig. 7.** Fibroblast migration and calpain activity are dependent on MEK, but not JNK activity. (A) Wild-type fibroblasts were loaded into Transwell migration chambers ( $10^5$  cells/well) and allowed to migrate for 5 h, using 5% serum as a chemoattractant. Calpain inhibitor PD150606 (50  $\mu$ M), MEK inhibitor UO126 (10  $\mu$ M) or matrix metalloproteinase inhibitor GM6001 (2  $\mu$ M) were added to both the upper and lower chambers of the designated wells. (B) Wild-type fibroblasts were pre-incubated for 1 h with JNK inhibitor SP600125 (10  $\mu$ M) or MEK inhibitor UO126 (10  $\mu$ M), and calpain activity was assessed by SLLVY-AMC cleavage, and compared with that of non-treated cells. The results of both (A) and (B) are the mean  $\pm$  SEM of at least three independent experiments. (C) Wild-type fibroblasts were pre-incubated with 10  $\mu$ M SP600125 or 10  $\mu$ M UO126 for 1 h and then analyzed for migration using the *in vitro* wound healing assay in the continuous presence of inhibitor. (D) Serum-starved wild-type, MEKK1<sup>-/-</sup> or MEKK1 add-back fibroblasts were treated with EGF or FGF-2 for 10 min and then lysed. ERK1/2 activation was then assessed by phospho-ERK immunoblotting. The membrane was then stripped and the total ERK2 level determined by ERK2 immunoblotting. The data are representative of at least three independent experiments. NS, no stimulus.

thereby possibly alter calpain activity, we tested the effect of UO126, an unrelated MEK inhibitor that does not non-specifically alter  $\text{Ca}^{2+}$  levels (Pereira *et al.*, 2002) (Figure 7). UO126 inhibits calpain activation (Figure 7B) and dramatically reduces fibroblast chemotaxis towards serum (Figure 7A). In contrast, SP600125, a JNK inhibitor, does not diminish fibroblast migration or calpain activity (Figure 7B and C). Thus, while MEKK1 has been shown to regulate both the ERK1/2 and JNK signaling

pathways, calpain activation and consequent cell migration may be attributed specifically to MEKK1 regulation of ERK1/2 signaling.

Given that numerous studies have identified Raf as the MAPK kinase kinase responsible for growth factor-mediated ERK1/2 activation, what role might MEKK1 play in EGF-induced ERK1/2 activation? We asked whether a portion of EGF-induced ERK1/2 activation might actually be attributable to MEKK1. By treating the cells with low (0.1–5 ng/ml) concentrations of EGF or FGF-2, we found that induced ERK1/2 phosphorylation and consequent activation by low levels of growth factors in mouse embryo fibroblasts is significantly dependent on MEKK1 expression (Figure 7D), while at higher levels of growth factor (100 ng/ml or higher), ERK1/2 phosphorylation levels of MEKK1<sup>+/+</sup> and MEKK1<sup>-/-</sup> MEFs were similar (data not shown). Thus, MEKK1 control of ERK1/2 activation is readily apparent at low growth factor concentrations and verified by comparison of wild-type and MEKK1<sup>-/-</sup> fibroblasts. Further, densitometric analysis of Figure 7D reveals that MEKK1<sup>+/+</sup> cells stimulated with the level of EGF used in our migration experiments (5 ng/ml) (Figure 2B) display a 2.5-fold greater level of pERK than the MEKK1<sup>-/-</sup> MEFs. Our data show that the loss of MEKK1 regulation of ERK1/2 signaling in MEKK1<sup>-/-</sup> fibroblasts contributes significantly to inhibition of calpain activation required for regulation of adherence and rear-end detachment of migrating cells. Importantly, the add-back of MEKK1 completely restores ERK1/2 activation by low doses of growth factor.

## Discussion

Cell adhesion to the extracellular matrix is mediated by integrins, which, in turn, are linked to the cytoskeleton through proteins in focal adhesion complexes (Yamada and Miyamoto, 1995). The strength of cell adherence to the extracellular matrix is modulated by signal transduction pathways involving proteins within focal adhesions (Yamada and Miyamoto, 1995). One such pathway of particular importance to adhesion-mediated signaling is the ERK1/2 pathway. v-Src, a potent activator of ERK1/2 signaling, has been shown to drive MEK-dependent ERK activation and localization to focal adhesions in chicken embryo fibroblasts (Fincham *et al.*, 2000). One explanation for the importance of membrane-localized ERK activity in cell adhesion, and by extension cell migration, is that ERK1/2 signaling is required for efficient release of cellular adhesion to the matrix substratum (Glading *et al.*, 2000). We have previously reported that MEKK1 regulates ERK1/2 activation, and that MEKK1-deficient cells display reduced motility (Yujiri *et al.*, 1998, 2000). In this paper, our findings demonstrate that MEKK1<sup>-/-</sup> fibroblasts have an increased adherence but display normal extension of the leading edge during migration. Thus, the loss of migration in MEKK1<sup>-/-</sup> fibroblasts is due to the increased adherence and a diminished ability to detach the trailing end of the cell, rather than decreased forward extension. We have demonstrated by co-immunoprecipitation that MEKK1 is associated with FAK-associated protein complexes, and that these complexes were localized in adhesion complexes. MEKK1 has also been proposed to co-localize with  $\alpha$ -actinin and actin stress

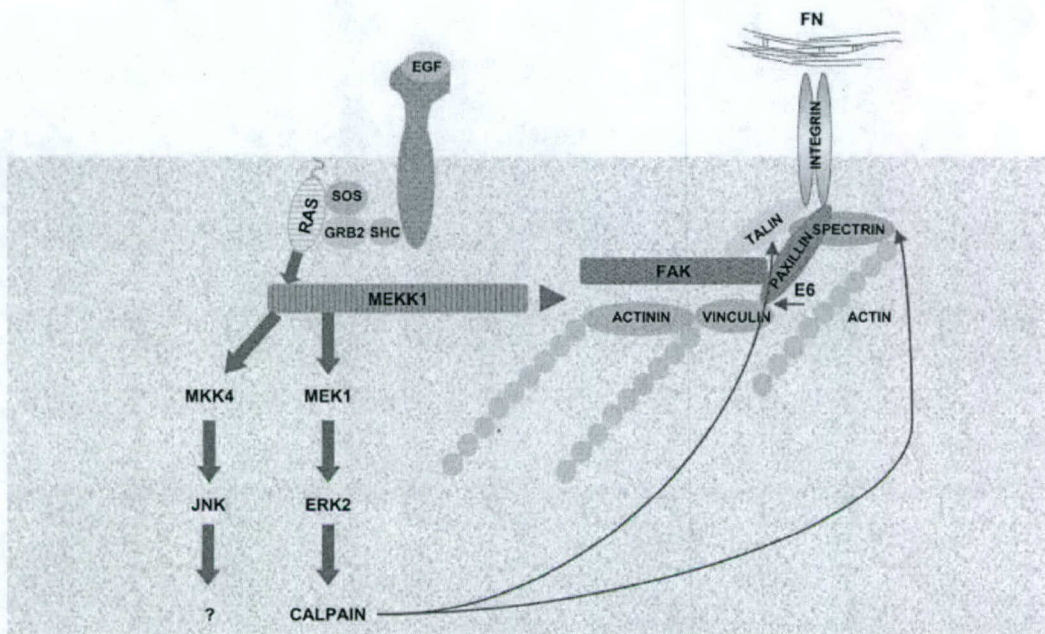


**Fig. 8.** Model depicting the FAK-MEKK1-MEK1/2-ERK2 pathway controlling calpain activation and the disruption of focal adhesion-actin cytoskeletal complexes. MEKK1<sup>-/-</sup> cells are defective in focal adhesion composition and regulation of the ERK2-calpain activation pathway (see text for details).

fibers (Christerson *et al.*, 1999), and our immunofluorescence studies support that contention. Thus, our findings reveal that the cellular location of MEKK1 is well suited to regulate signal transduction in response to cell adhesion or cytoskeletal changes. Indeed, we have previously shown MEKK1 to regulate signaling in response to cytoskeletal alteration (Yujiri *et al.*, 1999, 2000). Activation of the MEK-ERK1/2 pathway initiated by changes in integrin interactions with focal adhesion proteins is well characterized (Howe *et al.*, 2002), and our findings with MEKK1 knockout fibroblasts demonstrate this response is, in part, dependent on the expression of MEKK1.

The protease calpain has recently been implicated in the control of cell migration through regulation of de-adhesion from matrix substratum. We have demonstrated that MEKK1 expression is critical for calpain activity regulation. Glading *et al.* (2001) have recently shown that membrane-proximal ERK1/2 activity is required for EGF-induced m-calpain activity, and we demonstrate that MEKK1 is required for regulation of calpain activation. While our studies did not rule out that MEKK1-dependent MEK activity might phosphorylate proteins other than ERK1/2 that are required for calpain activity, recent studies (Glading *et al.*, 2001) indicate that appropriate localization of ERK activity is the key MEK-dependent factor in calpain activation. It is possible that MEKK1 might also influence calpain cellular location, but we were unable to detect any MEKK1-dependent calpain localization (data not shown). Importantly, reconstitution of the wild-type phenotype by expression of MEKK1 confirms that the defects we have measured in MEKK1<sup>-/-</sup> fibroblasts are a direct consequence of MEKK1 deficiency and not an epigenetic difference between cell lines.

Calpain has been shown to be associated with focal adhesions, and two primary substrates for calpain in

fibroblasts are the structural proteins spectrin and talin (Glading *et al.*, 2002). Through vinculin, both spectrin and talin are linked to  $\alpha$ -actinin and the actin cytoskeleton (Petit and Thiery, 2000). Calpain-dependent cleavage of these two proteins thus alters the tethering of the cytoskeleton to focal adhesion complexes and the plasma membrane. Regulation of limited calpain cleavage of these proteins requires MEKK1 regulation of the ERK1/2 pathway. The requirement of MEKK1 expression for the control of adhesion probably explains, at least in part, the defective eyelid closure of MEKK1-deficient mice due to impaired epithelial cell migration. Furthermore, other MEKK1<sup>-/-</sup> cell types including neutrophils and macrophages appear to have compromised migration (our unpublished observations), indicating that MEKK1 contributes to the regulation of migration of multiple cell types.

The significance of our work is that a focal adhesion-regulated pathway controlling cell adherence and migration has now been genetically defined. Targeted disruption of FAK (Ilic *et al.*, 1995), MEKK1 (Yujiri *et al.*, 2000), MEK1 (Giroux *et al.*, 1999), ERK2 (Saba El-Leil, 2002) and calpain (Dourdin *et al.*, 2001) demonstrates defects in cell migration (Figure 8). Pharmacological inhibitors of MEK1 and calpain mimic the loss of expression of component members of this pathway by blocking migration and influencing adherence. Interestingly, only the loss of MEKK1 expression yields viable animals, the other knockouts are embryonic lethal. This result is most likely related to the requirement of FAK to initiate multiple signals from focal adhesions, and the involvement of MEK1 and ERK2 in many diverse functions regulated by members of the Raf family (A-Raf, B-Raf and c-Raf), Mos, Tpl-2 and MEKK1, all MAPK kinase kinases defined genetically to regulate the ERK1/2 pathway (Schlesinger

*et al.*, 1998). At low growth factor levels, which are most likely physiologically relevant, it is apparent that MEKK1 is critical for normal ERK1/2 activation. At higher growth factor concentrations, the activation of Raf proteins probably rescues the MEKK1 deficiency by activating the ERK1/2 pathway. Thus, pharmacological inhibition of MAPK kinase kinases such as MEKK1 would predictably have greater specificity in selectively inhibiting migration in pathological states such as cancer metastasis than inhibition of MEK1, ERK1/2 or calpain.

## Materials and methods

### Antibodies and reagents

Anti-phospho ERK, ERK2 and FAK (C-terminal) antibodies used for immunoblotting were from Santa Cruz Biotechnology, Inc. (Santa Cruz, CA). Anti-phosphotyrosine and anti-FAK (N-terminal) antibodies were from Upstate Biotechnology (Lake Placid, NY). Fibronectin-coated tissue culture plates were from BD Biosciences (Bedford, MA). Anti-vinculin (V-4505) and FITC-conjugated donkey anti-mouse antibodies were from Sigma (St Louis, MO). HRP-sheep anti-mouse IgG was from Amersham (Piscataway, NJ). Protein A-HRP conjugate was from Zymed Laboratories (San Francisco, CA). PKH67 and PKH26 vital dyes were from Sigma. PD150606 and SP600125 were from Calbiochem (San Diego, CA). UO126 was from Promega (Madison, WI). SLLVY-AMC was from Peptides International (Louisville, KY). The MEKK1 sequence DTVD (amino acids 871–874) was substituted with alanines by a PCR strategy, and then subcloned into pEGFP-C1 (BD Biosciences Clontech, Palo Alto, CA).

### Fibroblasts

The development of MEKK1<sup>-/-</sup> mice has been described previously (Yujiri *et al.*, 2000). Mouse embryo fibroblasts were isolated from E14.5 embryos. Immortalized fibroblasts were isolated after continuous passage for 3 months or by expression of papilloma E6/E7 oncoproteins. All results comparing wild-type fibroblasts and MEKK1<sup>-/-</sup> fibroblasts were characterized with similar results in primary and immortalized fibroblasts. The MEKK1 add-back fibroblasts were made by stable transfection of immortalized MEKK1<sup>-/-</sup> fibroblasts using a full-length mouse MEKK1 cDNA in pHCHX. MEKK1 expression as determined by immunoblotting was ~20% of the MEKK1 expression of wild-type fibroblasts. The FAK<sup>-/-</sup> fibroblasts were a generous gift from Dr Dusko Ilic, University of California at San Francisco.

### Cell culture

Fibroblasts were cultured in IMDM medium (Gibco, Grand Island, NY) containing penicillin/streptomycin (1%; Gibco), L-glutamine (2 mM; Gibco), monothioglycerol (0.0012%; Sigma) and 10% (v/v) fetal calf serum (Gemini Bioproducts, Woodland, CA) at 37°C in a humidified atmosphere. Human FGF-2 was purchased from Upstate Biotechnology (Lake Placid, NY) and murine EGF from Sigma.

### Immunoprecipitation

After stimulation, fibroblasts were washed twice with cold PBS and lysed in 20 mM Tris-HCl pH 7.6, 0.5% NP-40, 250 mM NaCl, 3 mM EDTA, 3 mM EGTA, 1 mM PMSF, 2 mM sodium orthovanadate, 20 µg/ml aprotinin, 1 mM DTT and 5 µg/ml leupeptin. Lysates were cleared by centrifugation at 14 000 g for 10 min at 4°C, incubated with the appropriate antibody for 16 h at 4°C, and then with protein G-Sepharose for 1 h. The beads were washed three times, then resuspended in sample buffer (125 mM Tris-HCl pH 6.8, 20% glycerol, 4.6% SDS, 0.1% bromophenol blue and 10% 2-mercaptoethanol) for SDS-PAGE.

### Immunoblotting

After stimulation, cells were lysed in 0.5 ml of sample buffer and incubated at room temperature for 20 min. After centrifugation at 14 000 g for 5 min, post-nuclear detergent cell lysates were collected. Proteins were separated by SDS-PAGE and transferred to nitrocellulose (Sleicher & Schuell, Keene, NH). Membranes were blocked in 5% milk (diluted in Tris-buffered saline and 0.1% Tween-20) and incubated with the appropriate antibody at 4°C overnight. HRP-protein A or HRP-sheep anti-mouse IgG was used as secondary reagent. After extensive washing, the targeted proteins were detected by enhanced chemiluminescence

(ECL). Where indicated, blots were stripped by treatment with 2% SDS and 100 mM 2-mercaptoethanol in TBS, and then reprobed with desired antibodies and detected by ECL.

### In vitro wound healing assessment

Fibroblasts were grown on coverslips (10<sup>6</sup> cells) until confluent. The culture was 'wounded' with a razor blade by swiping the coverslip to generate an open area with no cells. The coverslips were rinsed and cells allowed to migrate into the wound site in complete media with or without inhibitors for 5 h unless noted otherwise. Fibroblast migration was assessed by live cell microscopy. For the mixed cell experiments, the fibroblasts were stained with either PKH26 or PKH67 fluorescent vital dyes (Sigma), mixed and allowed to grow together overnight before wounding and assessment by fluorescence microscopy. To measure healing time, cells were grown in tissue culture dishes until confluent, wounded with an 18g needle and then periodically examined until the wound was completely sealed. The data were analyzed by Student's *t*-test.

### Transwell chemotaxis assay

Fibroblasts were typsinized, washed and suspended in IMDM with 5% BSA. A total of 10<sup>5</sup> cells were then loaded into the upper chamber of a Transwell (Corning, Corning, NY) migration plate (8 µm pore) and allowed to migrate toward IMDM ± 5% fetal bovine serum for 5 h at 37°C. After migration, the upper surface of the membrane was thoroughly cleaned with a cotton swab, stained with Wright stain (Sigma) and the cells that migrated to the lower surface counted (five random 20× fields/well).

### Calpain fluorescence assay

Fibroblasts were seeded into 96-well plates (10<sup>4</sup> cells/well) and allowed to attach overnight. The cells were then serum starved for 8 h before treatment with 10% FBS in IMDM for 30 min. The medium was removed and 200 µl of 62.5 mM SLLVY-AMC, a cell-permeable calpain substrate, in reaction buffer (115 mM NaCl, 1 mM KH<sub>2</sub>PO<sub>4</sub>, 5 mM KCl, 2 mM CaCl<sub>2</sub>, 1.2 mM MgSO<sub>4</sub> and 25 mM HEPES pH 7.25) were added and fluorescence assessed using a Perkin Elmer 7000 BioAssay Reader (360/465 nm). When inhibitors were used, the cells were incubated with the inhibitor for 1 h prior to addition of the substrate, and the assay conducted in the presence of the inhibitor.

### Centrifugation adherence assay

Cells were seeded into a 96-well plate (2000 cells/well) and allowed to attach overnight. Cells were serum starved for 8 h before treatment with or without 10% FBS in IMDM for 30 min. The plate was then sealed, inverted and centrifuged at 2300 g for 5 min at 37°C. After rinsing, the remaining attached cells were stained with Wright stain (Sigma) and counted. Cell adherence is represented as the percent of the total remaining serum-treated cells compared with the non-treated cells.

### Fibroblast attachment rate

MEKK1<sup>+/+</sup> (wild-type) or MEKK1-deficient fibroblasts were resuspended in complete media and allowed to attach in either untreated or fibronectin-coated tissue culture plates (Becton Dickinson, Bedford, MA). The number of attached cells was determined over the course of 2 h by phase microscopy of a defined plate area.

### Immunofluorescence

Cells were transfected with lipofectamine and grown on glass coverslips. Two days after transfection, the cells were treated with 50 ng/ml EGF or serum-free medium alone for 30 min, then the medium was removed and the cells fixed in 3% paraformaldehyde/3% sucrose in phosphate-buffered saline (PBS) for 10 min. Following three PBS washes, the cells were permeabilized for 10 min with 0.1% Triton X-100 in PBS. After washing, the cells were blocked in 10% donkey serum in PBS for 1 h at room temperature. The coverslips were then incubated with anti-FAK (BD Transduction Laboratories) in 3% BSA/PBS for 1 h. After three washes, the coverslips were incubated with Cy5-conjugated anti-mouse antibodies (Jackson Immunoresearch) and rhodamine-phalloidin (Molecular Probes) in 3% BSA/PBS for 1 h. Following washing, cells were mounted in 75% glycerol/25% PBS/Tris pH 7.5.

### Quantitation of vinculin in focal adhesions

Cells migrating into the wound area resulting from the razor swipe of a confluent monolayer of fibroblasts were paraformaldehyde fixed at 12 h post-wounding. Cells were stained with the mouse anti-vinculin antibody followed by FITC-conjugated donkey anti-mouse antibody. Images were taken every 0.4 µm along the Z-axis and deconvolved using the nearest-

neighbors algorithm Slidebook program from Intelligent Imaging, Inc. (Denver, CO). The section at the substratum interface with the best in-focus vinculin staining was selected for measurement of the integrated fluorescence intensity in focal adhesions. The cell area for the section was also determined using Slidebook. The fluorescence intensity of vinculin per cell area was calculated for MEKK1<sup>+/+</sup>, MEKK1<sup>-/-</sup> and add-back clones from three independent experiments. The data were pooled and analyzed statistically using Student's *t*-test.

#### Supplementary data

Supplementary data are available at *The EMBO Journal* Online.

#### References

- Arthur,J.S., Elce,J.S., Hegadorn,C., Williams,K. and Greer,P.A. (2000) Disruption of the murine calpain small subunit gene, *Capn4*: calpain is essential for embryonic development but not for cell growth and division. *Mol. Cell. Biol.*, **20**, 4474–4481.
- Beckerle,M.C., Burridge,K., DeMartino,G.N. and Croall,D.E. (1987) Colocalization of calcium-dependent protease II and one of its substrates at sites of cell adhesion. *Cell*, **51**, 569–577.
- Bialkowska,K., Kulkarni,S., Du,X., Goll,D.E., Saido,T.C. and Fox,J.E. (2000) Evidence that  $\beta$ 3 integrin-induced Rac activation involves the calpain-dependent formation of integrin clusters that are distinct from the focal complexes and focal adhesions that form as Rac and RhoA become active. *J. Cell Biol.*, **151**, 685–696.
- Cary,L.A., Klinghoffer,R.A., Sachsenmaier,C. and Cooper,J.A. (2002) SRC catalytic but not scaffolding function is needed for integrin-regulated tyrosine phosphorylation, cell migration and cell spreading. *Mol. Cell. Biol.*, **22**, 2427–2440.
- Christerson,L.B., Vanderbilt,C.A. and Cobb,M.H. (1999) MEKK1 interacts with  $\alpha$ -actinin and localizes to stress fibers and focal adhesions. *Cell Motil. Cytoskeleton*, **43**, 186–198.
- Cooray,P., Yuan,Y., Schoenwaelder,S.M., Mitchell,C.A., Salem,H.H. and Jackson,S.P. (1996) Focal adhesion kinase (pp125FAK) cleavage and regulation by calpain. *Biochem. J.*, **318**, 41–47.
- Dourdin,N., Bhatt,A.K., Dutt,P., Greer,P.A., Arthur,J.S., Elce,J.S. and Huttenlocher,A. (2001) Reduced cell migration and disruption of the actin cytoskeleton in calpain-deficient embryonic fibroblasts. *J. Biol. Chem.*, **276**, 48382–48388.
- Fanger,G.R., Johnson,N.L. and Johnson,G.L. (1997) MEK kinases are regulated by EGF and selectively interact with Rac/Cdc42. *EMBO J.*, **16**, 4961–4972.
- Fincham,V.J., James,M., Frame,M.C. and Winder,S.J. (2000) Active ERK/MAP kinase is targeted to newly forming cell-matrix adhesions by integrin engagement and v-Src. *EMBO J.*, **19**, 2911–2923.
- Frame,M.C., Fincham,V.J., Carragher,N.O. and Wyke,J.A. (2002) v-Src's hold over actin and cell adhesions. *Nat. Rev. Mol. Cell Biol.*, **3**, 233–245.
- Giroux,S. et al. (1999) Embryonic death of Mek1-deficient mice reveals a role for this kinase in angiogenesis in the labyrinthine region of the placenta. *Curr. Biol.*, **9**, 369–372.
- Glading,A., Chang,P., Lauffenburger,D.A. and Wells,A. (2000) Epidermal growth factor receptor activation of calpain is required for fibroblast motility and occurs via an ERK/MAP kinase signaling pathway. *J. Biol. Chem.*, **275**, 2390–2398.
- Glading,A., Überall,F., Keyse,S.M., Lauffenburger,D.A. and Wells,A. (2001) Membrane proximal ERK signaling is required for M-calpain activation downstream of epidermal growth factor receptor signaling. *J. Biol. Chem.*, **276**, 23341–23348.
- Glading,A., Lauffenburger,D.A. and Wells,A. (2002) Cutting to the chase: calpain proteases in cell motility. *Trends Cell Biol.*, **12**, 46–54.
- Howe,A.K., Aplin,A.E. and Juliano,R.L. (2002) Anchorage-dependent ERK signaling—mechanisms and consequences. *Curr. Opin. Genet. Dev.*, **12**, 30–35.
- Huang,Y. and Wang,K.K. (2001) The calpain family and human disease. *Trends Mol. Med.*, **7**, 355–362.
- Huttenlocher,A., Palecek,S.P., Lu,Q., Zhang,W., Mellgren,R.L., Lauffenburger,D.A., Ginsberg,M.H. and Horwitz,A.F. (1997) Regulation of cell migration by the calcium-dependent protease calpain. *J. Biol. Chem.*, **272**, 32719–32722.
- Ilic,D. et al. (1995) Reduced cell motility and enhanced focal adhesion contact formation in cells from FAK-deficient mice. *Nature*, **377**, 539–544.
- Lotz,M.M., Burdsal,C.A., Erickson,H.P. and McClay,D.R. (1989) Cell adhesion to fibronectin and tenascin: quantitative measurements of initial binding and subsequent strengthening response. *J. Cell Biol.*, **109**, 1795–1805.
- Maheshwari,G., Wells,A., Griffith,L.G. and Lauffenburger,D.A. (1999) Biophysical integration of effects of epidermal growth factor and fibronectin on fibroblast migration. *Biophys. J.*, **76**, 2814–2823.
- Palecek,S.P., Huttenlocher,A., Horwitz,A.F. and Lauffenburger,D.A. (1998) Physical and biochemical regulation of integrin release during rear detachment of migrating cells. *J. Cell Sci.*, **111**, 929–940.
- Pereira,D.B., Carvalho,A.P. and Duarte,C.B. (2002) Non-specific effects of the MEK inhibitors PD098,059 and U0126 on glutamate release from hippocampal synaptosomes. *Neuropharmacology*, **42**, 9–19.
- Petit,V. and Thiery,J.P. (2000) Focal adhesions: structure and dynamics. *Biol. Cell*, **92**, 477–494.
- Pfaff,M., Du,X. and Ginsberg,M.H. (1999) Calpain cleavage of integrin  $\beta$  cytoplasmic domains. *FEBS Lett.*, **460**, 17–22.
- Potter,D.A., Tirnauer,J.S., Janssen,R., Croall,D.E., Hughes,C.N., Fiacco,K.A., Mier,J.W., Maki,M. and Herman,I.M. (1998) Calpain regulates actin remodeling during cell spreading. *J. Cell Biol.*, **141**, 647–662.
- Saba-El-Leil,M.K. (2002) Targeted inactivation of the Erk2 MAP kinase gene in the mouse. In *Abstracts of the Meeting on Protein Phosphorylation and Mechanisms of Cellular Regulation*, March 5–10, 2002, Taos, NM. Keystone Symposia.
- Schlesinger,T.K., Fanger,G.R., Yujiri,T. and Johnson,G.L. (1998) The TAO of MEKK. *Front. Biosci.*, **3**, D1181–D1186.
- Tong,X., Salgia,R., Li,J.L., Griffin,J.D. and Howley,P.M. (1997) The bovine papillomavirus E6 protein binds to the LD motif repeats of paxillin and blocks its interaction with vinculin and the focal adhesion kinase. *J. Biol. Chem.*, **272**, 33373–33376.
- Turner,C.E. (2000) Paxillin and focal adhesion signalling. *Nat. Cell Biol.*, **2**, E231–E236.
- Wang,K.K. (2000) Calpain and caspase: can you tell the difference? *Trends Neurosci.*, **23**, 20–26.
- Wang,K.K.W. and Yuen,P.-w. (1999) *Calpain: Pharmacology and Toxicology of a Cellular Protease*. Taylor & Francis, London, UK.
- Wang,K.K. et al. (1996) An  $\alpha$ -mercaptoacrylic acid derivative is a selective nonpeptide cell-permeable calpain inhibitor and is neuroprotective. *Proc. Natl Acad. Sci. USA*, **93**, 6687–6692.
- Widmann,C., Gerwins,P., Johnson,N.L., Jarpe,M.B. and Johnson,G.L. (1998) MEK kinase 1, a substrate for DEVD-directed caspases, is involved in genotoxin-induced apoptosis. *Mol. Cell. Biol.*, **18**, 2416–2429.
- Yamada,K.M. and Miyamoto,S. (1995) Integrin transmembrane signaling and cytoskeletal control. *Curr. Opin. Cell Biol.*, **7**, 681–689.
- Yujiri,T., Sather,S., Fanger,G.R. and Johnson,G.L. (1998) Role of MEKK1 in cell survival and activation of JNK and ERK pathways defined by targeted gene disruption. *Science*, **282**, 1911–1914.
- Yujiri,T., Fanger,G.R., Garrington,T.P., Schlesinger,T.K., Gibson,S. and Johnson,G.L. (1999) MEK kinase 1 (MEKK1) transduces c-Jun NH<sub>2</sub>-terminal kinase activation in response to changes in the microtubule cytoskeleton. *J. Biol. Chem.*, **274**, 12605–12610.
- Yujiri,T. et al. (2000) MEK kinase 1 gene disruption alters cell migration and c-Jun NH<sub>2</sub>-terminal kinase regulation but does not cause a measurable defect in NF- $\kappa$ B activation. *Proc. Natl Acad. Sci. USA*, **97**, 7272–7277.
- Yujiri,T., Nawata,R., Takahashi,T., Sato,Y., Tanizawa,Y., Kitamura,T. and Oka,Y. (2003) MEK kinase 1 interacts with focal adhesion kinase and regulates insulin receptor substrate-1 expression. *J. Biol. Chem.*, **278**, 3846–3851.

Received September 19, 2002; revised May 12, 2003;  
accepted May 13, 2003

## Reovirus-Induced Alteration in Expression of Apoptosis and DNA Repair Genes with Potential Roles in Viral Pathogenesis

Roberta L. DeBiasi,<sup>1,2,3</sup> Penny Clarke,<sup>2</sup> Suzanne Meintzer,<sup>2</sup> Robert Jotte,<sup>4,5</sup>  
B. K. Kleinschmidt-Demasters,<sup>2,6</sup> Gary L. Johnson,<sup>5,7</sup>  
and Kenneth L. Tyler<sup>2,3,8,9,10\*</sup>

Departments of Pediatrics,<sup>1</sup> Neurology,<sup>2</sup> Hematology and Oncology,<sup>4</sup> Pharmacology,<sup>5</sup> Pathology,<sup>6</sup> Medicine,<sup>8</sup> Microbiology,<sup>9</sup> and Immunology<sup>10</sup> and Program in Molecular Signal Transduction,<sup>7</sup> University of Colorado Health Sciences Center, and Denver Veterans Affairs Medical Center,<sup>3</sup> Denver, Colorado 80220

Received 14 January 2003/Accepted 19 May 2003

Reoviruses are a leading model for understanding cellular mechanisms of virus-induced apoptosis. Reoviruses induce apoptosis in multiple cell lines in vitro, and apoptosis plays a key role in virus-induced tissue injury of the heart and brain in vivo. The activation of transcription factors NF- $\kappa$ B and c-Jun are key events in reovirus-induced apoptosis, indicating that new gene expression is critical to this process. We used high-density oligonucleotide microarrays to analyze cellular transcriptional alterations in HEK293 cells after infection with reovirus strain T3A (i.e., apoptosis inducing) compared to infection with reovirus strain T1L (i.e., minimally apoptosis inducing) and uninfected cells. These strains also differ dramatically in their potential to induce apoptotic injury in hearts of infected mice in vivo—T3A is myocarditic, whereas T1L is not. Using high-throughput microarray analysis of over 12,000 genes, we identified differential expression of a defined subset of genes involved in apoptosis and DNA repair after reovirus infection. This provides the first comparative analysis of altered gene expression after infection with viruses of differing apoptotic phenotypes and provides insight into pathogenic mechanisms of virus-induced disease.

The mechanisms by which viruses cause cytopathic effects in infected host cells are complex and only partially defined. Apoptosis is a direct mechanism of cellular injury and death, which can occur in the course of normal tissue development or as a pathological response to a variety of noxious stimuli. Mammalian reoviruses have served as useful models for studies of the viral and cellular mechanisms that are operative in host cell damage and death (14, 57, 80, 81). Reoviruses induce apoptosis in a multiple cell lines in vitro and in murine models of encephalitis and myocarditis in vivo (18, 58, 68). Prototype strains serotype 3 Abney (T3A) and serotype 3 Dearing (T3D) induce apoptosis more efficiently than strain serotype 1 Lang (T1L). Differences in the capacity of reoviruses to induce apoptosis map to the viral S1 gene, which encodes the viral attachment protein  $\sigma$ 1 (15, 69, 82).

The signaling pathways by which reoviruses induce apoptosis in target cells are complex. Involvement of death receptor- and mitochondrion-mediated pathways of apoptosis as well as cysteine protease activation have been demonstrated (11, 43). Binding of tumor necrosis factor (TNF)-related apoptosis-inducing ligand (TRAIL) to its cell surface death receptors—DR4 and DR5—plays a central role in reovirus-induced apoptosis in HEK293 cells and in several cancer cell lines (11, 12), and other death-inducing ligands such as FasL are equally important in neurons (68). Activation of death receptor-related apoptotic pathways results in a coordinated pattern of caspase activation (43, 44, 68). Mitochondrial apoptotic path-

ways act to augment death receptor-initiated apoptosis, and apoptosis can be inhibited by stable overexpression of Bcl-2 (43, 44, 69). Blockade of cysteine protease activity using selective caspase inhibitors in vitro (11, 43) and calpain inhibitors in vivo (18) results in decreased apoptosis in target cells and tissues.

Reovirus infection results in activation of cellular transcription factors, including NF- $\kappa$ B (16) and c-Jun (13), and this activation plays a critical role in apoptosis. In the case of c-Jun, there is an excellent correlation between the capacity of viral strains to activate the JNK/c-Jun pathway and their ability to induce apoptosis (13). Inhibition of the activation of NF- $\kappa$ B by stable expression of the NF- $\kappa$ B inhibitor I $\kappa$ B, whether by the use of proteosome inhibitors or by targeted disruption of the genes encoding the p65 or p55 subunits of NF- $\kappa$ B, results in inhibition of reovirus-induced apoptosis (16). The close correlation between transcription factor activation and reovirus-induced apoptosis strongly suggests that new gene expression is critical for this process; therefore, we investigated the cellular response to reovirus infection at the transcriptional level. This was achieved by comparing transcriptional alterations after infection with a reovirus strain that efficiently induces apoptosis (i.e., T3A) with alterations after infection with a strain that induces minimal apoptosis (i.e., T1L). These strains also differ in their potential for inducing apoptotic myocardial injury in a murine model of viral myocarditis; T3A infection causes myocarditis and apoptotic myocardial injury, whereas T1L does not.

Using high-throughput screening of over 12,000 genes by using high-density oligonucleotide microarrays, we have identified transcriptional alterations in a defined subset of genes. When grouped into functional categories, a significant propor-

\* Corresponding author. Mailing address: Department of Neurology (B-182), University of Colorado Health Sciences Center, 4200 East 9th Ave., Denver, CO 80262. Phone: (303) 393-4684. Fax: (303) 393-4686. E-mail: Ken.Tyler@uchsc.edu.

tion of altered transcripts include genes involved in apoptosis and DNA repair, and it is this subset that forms the focus of this paper. The findings described herein are the first large-scale description of virus-induced alterations in apoptotic signaling at the transcriptional level, including kinetics of these changes after infection with strains that differ in apoptosis-inducing phenotype. These findings lend important insight into specific mechanisms of viral pathogenesis, since apoptosis has previously been demonstrated to be a critical mechanism for reovirus-induced damage *in vitro* and *in vivo*.

#### MATERIALS AND METHODS

**Cells, virus, and infection.** Human embryonic kidney 293 (HEK293) cells (ATCC CRL 1573) were plated in T75 flasks at a density of  $5 \times 10^6$  cells per flask in a volume of 12 ml of Dulbecco's modified Eagle's medium supplemented with 10% heat-inactivated fetal bovine serum, 2 mM L-glutamine (Gibco-BRL), 1 mM sodium pyruvate (Gibco-BRL), and 100 U of streptomycin (Gibco-BRL) per ml. Monolayers were infected 24 h after plating, when cells were 60 to 70% confluent. Reovirus strains T3Abney (T3A) and T1Lang (T1L) (P2 stock) were used to infect monolayers at a multiplicity of infection (MOI) of 100 PFU per cell. A high MOI was used to ensure that all susceptible cells were infected and because pilot studies in our laboratory indicated that high-multiplicity infection enhanced the reproducibility of gene expression studies. Virus was adsorbed for 1 h at 37°C in a volume of 2 ml, during which time flasks were rocked every 15 min. Following adsorption, flasks were incubated at 37°C after the addition of 10 ml of fresh medium. T3A-infected cells were harvested at 6, 12, and 24 h after viral infection. T1L-infected cells were harvested at 24 h postinfection. For control infections, HEK293 monolayers were inoculated with a cell lysate suspension, which was prepared identically to viral stocks but which lacked infectious virus.

**Cell harvests and RNA extraction.** Cells were harvested by gently pipetting adherent and nonadherent cells from the flasks into 50-ml centrifuge tubes. After centrifugation (DuPont Sorvall 6000) at 1,200 rpm for 5 min, cell pellets were resuspended in phosphate-buffered saline (PBS) and transferred to Eppendorf tubes for total RNA extraction (RNeasy Mini Total RNA isolation kit; QIA-GEN). Total RNA was extracted from each flask independently, resulting in duplicate RNA samples for each infection condition at 6, 12 (mock, T3A), and 24 (mock, T3A and T1L) h postinfection. A total of 16 RNA samples were prepared, and the yield and purity of extracted RNA were determined by spectrophotometry.

**Target preparation.** Biotinylated cRNA targets were prepared from a 10- $\mu$ g aliquot of each total RNA sample by following Affymetrix instructions and protocols. Briefly, total RNA was reverse transcribed to double-stranded cDNA (Superscript Choice; Gibco-BRL) by using high-pressure liquid chromatography-purified T7-(dT)<sub>24</sub> oligomer for first-strand cDNA synthesis. Second-strand synthesis was performed by using T4 DNA polymerase, and double-stranded cDNA was isolated by using phenol-chloroform extraction with phase-lock gels. Isolated cDNA was *in vitro* transcribed and labeled (by using biotin-UTP and biotin-CTP) to produce biotin-labeled cRNA (BioArray High-Yield RNA transcript labeling kit; ENZO). Labeled cRNA was isolated by using RNeasy Mini Kit spin columns (QIAGEN). Yield and purity were quantified by using spectrophotometry. Labeled cRNAs were fragmented in 100 mM potassium acetate, 30 mM magnesium acetate, and 30 mM Tris-acetate (pH 8.1) for 35 min at 94°C to produce labeled cRNA fragments of 60- to 300-bp length. For hybridization, cRNA target integrity was analyzed with Affymetrix control (Test 2) arrays to assess degradation and hybridization performance prior to hybridization to Affymetrix Human U95A high-density oligonucleotide microarrays. The U95A microarray contains cDNA oligomer that is complementary to 12,000 human genes with known function (no expressed sequence tags), which currently represents the most comprehensive coverage of the human genome represented on a single microarray. Each of the 16 prepared target cRNAs was independently hybridized to a U95A array. Eukaryotic hybridization controls bioB, bioC, bioD, and cre were also included in the hybridization cocktail. Hybridization was carried out for 16 h at 45°C with rotation at 60 rpm. Microarrays were washed and stained with streptavidin-phycocerythrin conjugate by using the Affymetrix GeneChip Fluidics Station 400, following standard Affymetrix protocols. Staining intensity was antibody amplified by using a biotinylated antistreptavidin antibody at a concentration of 3  $\mu$ g per ml which was followed by a second streptavidin-phycocerythrin conjugate stain, and hybridization intensity was analyzed by scanning at 570 nM. All hybridization and scanning steps were performed at the

University of Colorado Health Sciences Center Cancer Center Microarray Core Facility.

**Data analysis.** Each gene on the U95A array was represented by a group of 20 different 25-base cDNA oligomers that were complementary to a cRNA target transcript (i.e., perfect-match probes). As a hybridization specificity control, each perfect match oligomer was accompanied by an oligomer differing from the perfect match sequence by a single base pair substitution (i.e., mismatch probes). The combination of perfect-match and -mismatch cDNA oligomers for each gene is termed a probe set. Affymetrix-defined mathematical analyses (metrics) were performed to assess specific versus nonspecific hybridization of experimental cRNA targets to each probe set. Data files were analyzed by using GeneChip Microarray Suite software (version 4.0).

Initially, hybridization of cRNA targets derived from each of the 16 experimental samples was analyzed independently. By using Affymetrix-defined absolute mathematical algorithms describing perfect-match and -mismatch hybridization, each gene was defined as absent or present and was assigned a raw numerical value. Next, comparisons were made between virus-infected and mock-infected chips at each of the three time points postinfection. Raw numerical values were scaled to allow comparison between arrays. Genes considered absent (excess of mismatch hybridization or no hybridization) were not excluded from analysis, since genes changing from present to absent, absent to present, or present to present (but which increased in magnitude) were all important subsets of transcriptional alteration following viral infection compared to mock infection. By using Affymetrix-defined comparison mathematical algorithms, differential hybridization (between chips) to each cDNA probe was analyzed and designated as not changed, increased, marginally increased, decreased, or marginally decreased, and a change in expression (*n*-fold) was calculated. Finally, a four-way comparison of both virus-infected replicates to both mock-infected replicates at a given time point was assessed, and the mean change (*n*-fold) was calculated and reported along with standard error of the mean.

A gene was considered upregulated following virus infection if it was present in both virus-infected samples and if its expression increased by greater than or equal to twofold in each virus-infected sample compared to both mock-infected samples. Conversely, a gene was considered downregulated if it was present in both mock-infected samples and if its expression was decreased by greater than or equal to twofold in each virus-infected sample compared to both mock-infected samples. Genes whose expression changed by less than twofold were not considered up- or downregulated. Similarly, in order to ensure the reproducibility of the data presented, genes whose expression differed from mock-infected samples in only one of the two paired viral chips were not considered up- or downregulated.

To assess the reproducibility of hybridization results, the degree of variability in transcriptional expression among mock- and virus-infected replicate conditions was analyzed. For 99.6% of represented genes, expression was unchanged between mock-mock or virus-virus replicates. Transcriptional differences were noted in an average of  $0.4\% \pm 0.1\%$  of the total pool of transcripts between replicate conditions, but the genes involved represent a distinct population from the genes found to be up- or downregulated compared to virus-infected to mock-infected cells. The degree of variability in transcriptional expression as a function of time was also assessed by comparing differences in gene expression between mock infections following 6, 12, and 24 h of culture. A small proportion of transcripts were altered in response to duration of cell culture alone ( $1.2\% \pm 0.2\%$  of the total pool). These genes were excluded from subsequent analysis.

**RT-PCR.** Reverse transcriptase PCR (RT-PCR) was utilized to confirm changes in expression of selected genes as identified by analysis of oligonucleotide microarrays. For RT-PCR, RNA was extracted from infected and control HEK293 cells by using infection and extraction procedures identical to those described above. RNA was converted to cDNA by using the SuperScript pre-amplification system (Gibco-BRL) with the supplied oligo d(T)<sub>12-18</sub> primer. Reverse transcription was performed at 42°C for 1 h. Semiquantitative PCR was performed by using primers generated for human DR4 (forward, 5'-CTG AGC AAC GCA GAC TCG CTG TCC AC-3'; reverse, 5'-TCC AAG GAC ACG GCA GAG CCT GTG CCA T-3'), human DR5 (forward, 5'-GCC TCA TGG ACA ATG AGA TAA AGG TGG CT-3'; reverse, 5'-CCA AAT CTC AAA GTA CGC ACA AAC GG-3'), human DCR1 (forward, 5'-GAA GAA TTT GGT GCC AAT GCC ACT G-3'; reverse, 5'-CTC TTG GAC TTG GCT GGG AGA TGT G-3'), GADD 34 (U83981) (forward, 5'-ACA CGG AGG AGG AGG AAG AT-3'; reverse, 5'-ACA GAG GAG GAA GGC AAG GT-3'), Bcl-10 (AJ006288) (forward, 5'-TCC ACA CTT CTC AGG TTG CTT-3'; reverse, 5'-AAT GGG GAA GAA GGA GAG GA-3'), caspase 3 (forward, 5'-GGT TCA TCC AGT CGC TTT GT-3'; reverse, 5'-AAC CAC CAA CCA ACC ATT C-3'; 207-bp product), Par-4 (forward, 5'-CTG AA CAT TTG CAT CCC TGT-3'; reverse, 5'-ATG AAG CAG GGC AGA AAG AG-3'; 239-bp

product), SMN (U80017) (forward, 5'-CCA GAG CGA TGA TGA CA-3'; reverse, 5'-TGG GTA AAT GCA ACC GTC TT-3'; 246-bp product), DNA polymerase  $\alpha$  (L24559) (forward, 5'-TGC TTG ACC TGA TTG CTG TC-3'; reverse, 5'-ATG ACG GGA CAA AGA CAA GG-3'; 197-bp product), ParpL (AF057160) (forward, 5'-CGC AAG GTC CAG AGA GAA AC-3'; reverse, 5'-TCC CAG GTT CAC TTC TTT GG-3'; 244-bp product), SRP40 (U30826) (forward, 5'-AGA CGA AAT GCT CCA CCT GT-3'; reverse, 5'-CGA GAC CTG CTT CTT GAC CT-3'; 281-bp product), XP-C p125 (D21089) (forward, 5'-AGA GCA GGC GAA GAC AAG AG-3'; reverse, 5'-GAT GGA CAG GCC AAT AGC AT-3'; 199-bp product), and  $\beta$ -actin (forward, 5'-GAA ACT ACC TTC AAC TTC AAC TCC ATC-3'; reverse, 5'-CGA GGC CAG GAT GGA GCC GCC-3' (24). PCRs were performed by using serial dilutions of each cDNA (1:5, 1:10, and 1:20) to estimate the linear range for each primer pair by interpretation of band intensity. To avoid saturation of the PCR and maximize the ability to detect relative quantitative differences between experimental samples, the highest-input cDNA dilution that produced visible PCR products was utilized for comparisons of transcript abundance, and PCR cycles were limited to 25. RT-PCR for actin was performed in parallel with each PCR of interest for each experimental sample (as a control to ensure equal input load of cDNA in each reaction). PCR cycle conditions were 94°C for 30 seconds, 55°C for 30 seconds, and 72°C for 1 min for 25 cycles. PCR products were resolved on a 2% agarose-ethidium bromide gel run at 100 V for 1 h. Products were visualized by UV illumination with Fluor-S (Bio-Rad) software imaging. Each reaction was performed at least twice in independent experiments to confirm reproducibility.

**Animal infections and immunohistochemistry.** Reovirus strain 8B is an efficiently myocarditic reovirus that has been previously characterized (74) and has been shown to induce apoptotic myocardial injury in neonatal mice (18). Two-day-old Swiss-Webster (Taconic) mice were intramuscularly inoculated with 1,000 PFU of 8B reovirus (20- $\mu$ l volume) in the left hind limb. Mock-infected mice received gel saline vehicle inoculation (20- $\mu$ l volume; 137 mM NaCl, 0.2 mM CaCl<sub>2</sub>, 0.8 mM MgCl<sub>2</sub>, 19 mM H<sub>3</sub>BO<sub>3</sub>, 0.1 mM Na<sub>2</sub>B<sub>4</sub>O<sub>7</sub>, 0.3% gelatin). At 1 to 7 days postinfection, mice were sacrificed and hearts were immediately immersed in 10% buffered formalin solution. After mounting as transverse sections, hearts were embedded in paraffin and sectioned to 6- $\mu$ m thickness. For quantification of the degree of myocardial injury, hematoxylin- and eosin-stained midcardiac sections (at least two per heart) were examined at  $\times 125$  magnification by light microscopy and evaluated for histologic evidence of myocarditis.

Immunohistochemical analysis of survivin (SMN) expression was carried out on identical sections to assess expression over the 7 days following reovirus infection. SMN antiserum was produced in New Zealand White rabbits by immunization with the amino terminus of the surviving amino peptide sequence (PTLPPAWQPFLKDHR) linked to keyhole limpet hemocyanin by the method of Ambrosini. Immunoglobulins from the rabbit before immunization were purified by affinity chromatography with protein A (Pierce, Rockford, Ill.). Western blot analysis against total protein extract from HeLa cells showed reactivity with a single band of protein of approximately 16.5 kDa—consistent with the expected molecular mass. Western blotting with preimmune serum showed no immunoreactivity. Slides were deparaffinized through xylene and rehydrated through a graded alcohol series. Endogenous peroxidase was blocked with 3% hydrogen peroxide for 15 min. Antigen retrieval was performed with a 0.1 M citrate buffer for 10 min at 120°C. Primary antibody was diluted to 1.8 ng/ $\mu$ l in PBS (pH 7.4) with 1% bovine serum albumin applied to sections and incubated in a humidity chamber overnight at 4°C. Following three washes in PBS for 5 min each, incubation in secondary antibody labeled with polymer-linked horseradish peroxidase (Envision +; Dako, Carpinteria, Calif.) was carried out for 30 min at room temperature in a humidity chamber. Following three washes in PBS, sections were developed with 3'-diaminobenzidine (Dako) and counterstained with hematoxylin. Negative controls were performed by substitution with the preimmune immunoglobulin from the same rabbit. Positive control consisted of a colon carcinoma section that has been extensively studied in our laboratory and which shows strong staining that is consistently reproducible in this tissue.

## RESULTS

**Global analysis of gene expression following reovirus infection.** At 6, 12, and 24 h postinfection, transcriptional expression of each of 12,000 genes present on the HU95A microarray was compared for each pair of T3A (strongly apoptosis inducing [APO+]) virus-infected and mock-infected arrays. Similar analysis was carried out at 24 h postinfection for each pair of T1L (weakly apoptosis-inducing [APO-]) virus-infected and

mock-infected arrays. The subset of genes that were transcriptionally altered following T3A (APO+) infection compared to mock infection was determined. This subset of genes was also compared to those genes that were differentially expressed following T1L (APO-) infection compared to mock infection. At 6 h post-T3A (APO+) infection, expression of 18 genes (0.2% of the total genes present on the array) was altered (all with increased expression) by twofold or greater in T3A (APO+)-infected cells compared to mock-infected cells. By 12 h post-T3A (APO+) infection, expression of 86 genes (0.7%) was altered (29 genes with increased expression and 57 genes with decreased expression) in virus-infected compared to mock-infected cells. By 24 h post-T3A (APO+) infection, expression of 309 genes (2.6%) was altered (215 with increased expression and 94 with decreased expression) in virus-infected compared to mock-infected cells. In contrast, at 24 h post-T1L (APO-) infection, expression of only 59 genes (0.4%) was altered (45 with increased expression and 14 with decreased expression) in virus-infected compared to mock-infected cells. A complete listing of all genes with twofold or greater changes in expression following T3A and T1L infection is available online at <http://www.uchsc.edu/sm/neuro/tylerlab/personnel/completelist.pdf>. When categorized into functionally related families, a large number of differentially expressed genes following T3A (APO+) infection were noted to encode proteins involved in apoptosis (Table 1) and DNA repair (Table 2). These genes were not differentially expressed following T1L (APO-) infection [with the exception of five genes in common between T3A (APO+) and T1L (APO-)], indicating that these changes in gene expression likely correlate with differences in virus-induced pathogenicity rather than resulting from nonspecific cellular responses to viral infection.

**Reovirus-induced alteration in expression of genes involved in apoptosis.** Expression of 24 genes related to the regulation of apoptosis was altered in T3A (APO+) reovirus-infected cells. These genes encode proteins that participate in apoptotic signaling involving death receptors, endoplasmic reticulum (ER) stress, mitochondrial signaling, and cysteine proteases (Table 1). For 22 of these 24 genes, significant alteration (>2-fold) in expression was not apparent until 24 h postinfection. Only five of these genes were also differentially expressed following T1L (APO-) infection.

**Altered expression of genes involved in death receptor signaling pathways.** We have previously shown that members of the TNF receptor superfamily of cell surface death receptors, including DR4, DR5, and their apoptosis-inducing ligand, TRAIL, play a critical role in reovirus-induced apoptosis (11, 12). We wished to determine whether alterations in expression levels of genes encoding these proteins were altered following reoviral infection. Using oligonucleotide microarrays, we did not detect significant changes in gene expression of TRAIL or the death receptors DR5, decoy receptor 1 (DcR-1), or DcR-2 at 6, 12, and 24 h postinfection in reovirus-infected cells compared to mock-infected controls (Table 3). DR4 was not represented on the U95A microarray. Expression of genes encoding other important members of the TNF receptor superfamily and their ligands was also unchanged in reovirus-infected cells including Fas, Fas ligand, TNF- $\alpha$ , TNF- $\beta$ , and TNF receptor and TNF receptor-related protein (Table 3).

We performed additional analysis of death receptor-related

TABLE 1. Reovirus-induced alteration in expression of genes encoding proteins known to regulate apoptotic signaling

Gene	GenBank accession no. <sup>a</sup>	Change in expression ( <i>n</i> -fold) <sup>b</sup> at the indicated time (h) after infection with:			
		T3A			T1L
		6	12	24	
<b>Mitochondrial signaling</b>					
Pim-2 proto-oncogene homologue	U77735			$-2.2 \pm 0.1$	
MCL1	L08246			$2.0 \pm 0.0$	$2.2 \pm 0.0$
BAC 15E1-cytochrome C oxidase polypeptide	AL021546			$2.1 \pm 0.0$	
Par-4	U63809			$2.1 \pm 0.0$	
HSP-70 (heat shock protein 70 testis variant)	D85730			$2.2 \pm 0.1$	
BNIP-1 (BCL-2 interacting protein)	U15172			$2.3 \pm 0.2$	
SMN/Btfp44/NAIP (survival motor neuron/neuronal apoptosis inhibitor protein)	U80017			$2.5 \pm 0.1$	
DRAK-2	AB011421			$2.8 \pm 0.2$	
SIP-1	AF027150			$3.0 \pm 0.2$	
DP5	D83699			$5.5 \pm 1.1$	
<b>ER stress-induced signaling</b>					
ORP150	U65785			$-2.4 \pm 0.2$	
GADD 34	U83981	$6.8 \pm 0.2$		$3.7 \pm 0.2$	$2.9 \pm 0.2$
GADD 45	M60974		$3.3 \pm 0.2$	$4.9 \pm 0.1$	$4.4 \pm 0.1$
<b>Death receptor signaling</b>					
Bcl-10	AJ006288			$5.6 \pm 1.1$	
PML-2	M79463			$3.4 \pm 0.3$	
Ceramide glucosyltransferase	D50840			$4.0 \pm 1.2$	
Sp100	M60618			$6.5 \pm 0.3$	
				$5.8 \pm 0.6$	
<b>Proteases</b>					
Calpain (calcium-activated neutral protease)	X04366			$-2.6 \pm 0.1$	
Beta-4 adducin	U43959			$-2.1 \pm 0.1$	
Caspase 7 (lice-2 beta cysteine protease)	U67319			$2.6 \pm 0.2$	
Caspase 3 (CPP32)	U13737			$3.2 \pm 0.2$	$2.8 \pm 0.1$
<b>Undefined</b>					
Frizzled related protein	AF056087			$-2.5 \pm 0.1$	$-3.3 \pm 0.5$
TCBP (T cluster binding protein)	D64015			$3.3 \pm 0.2$	
Cug-BP/hNAb50 RNA binding protein	U63289			$6.6 \pm 1.1$	

<sup>a</sup> GenBank accession number corresponds to sequence from which the Affymetrix U95A probe set was designed.<sup>b</sup> Data are means  $\pm$  standard errors of the means.

gene expression, including DR4, DR5, DcR-1, and DcR-2 following T3A (APO+) infection by RT-PCR (Fig. 1). DR4 expression was increased at 12 and 24 h post-T3A infection compared to mock infection. In contrast, expression of DR5 was unchanged following T3A infection, thus confirming results obtained from microarray analysis. DcR-1 transcripts were not detectable in either mock- or T3A-infected cells. DcR-2 expression appeared to be decreased at 24 h post-T3A infection compared to mock-infected cells in this RT-PCR analysis. However, consistent with the microarray results, this decrease was not seen in RNase protection assays (data not shown).

Microarray analysis also revealed differential expression of four genes that encode proteins that may be involved in modulation of death receptor-associated signaling cascades in T3A (APO+)-infected cells at 24 h postinfection: PML-2, ceramide glucosyltransferase, Bcl-10, and Sp100 were increased  $3.4 \pm 0.3$ ,  $4.0 \pm 1.2$ ,  $5.6 \pm 1.1$ , and  $6.1 \pm 0.5$ -fold, respectively. We used RT-PCR to confirm the upregulated expression of BCL-10 at 24 h post-T3A (APO+) infection (Fig. 1). Taken together, these results suggest that, with the exception of DR4

TABLE 2. Reovirus-induced alteration in expression of genes encoding proteins known to be involved in DNA repair

Gene	GenBank accession no. <sup>a</sup>	Change in expression ( <i>n</i> -fold) <sup>b</sup> at the indicated time (h) after infection with:			
		T3A			T1L
		6	12	24	
<b>DNA ligase 1</b>					
DNA ligase 1	M36067			$-8.2 \pm 1.1$	
PARPL	AF057160			$-6.3 \pm 0.7$	
XP-C repair complementing protein (p125)	D21089			$-3.4 \pm 0.1$	
DNA polymerase gamma	U60325	$-1.9 \pm 0.1$	$-2.9 \pm 0.1$		
ERCC5	L20046	$-2.7 \pm 0.1$			
DNA polymerase alpha	L24559			$-2.5 \pm 0.2$	
HLP (helicase-like protein)	U09877	$-2.4 \pm 0.1$			
GTBP	U28946	$-2.0 \pm 0.1$	$-2.1 \pm 0.0$		
DDB2 (p48 subunit)	U18300			$-2.0 \pm 0.0$	
RAD 54 homologue	X97795			$-2.0 \pm 0.1$	
Mi2 autoantigen	X86691	$-1.3 \pm 0.1$	$-2.0 \pm 0.1$		
MMS2	AF049140			$2.1 \pm 0.0$	
Rad-51-interacting protein	AF006259			$2.6 \pm 0.2$	
Rec-1	AF084513			$2.4 \pm 0.4$	

<sup>a</sup> GenBank accession number corresponds to sequence from which the Affymetrix U95A probe set was designed.<sup>b</sup> Data are means  $\pm$  standard errors of the means.

TABLE 3. Genes encoding proteins known to be involved in apoptotic signaling which were not differentially expressed following reovirus T3A or T1L infection

Gene	GenBank accession no. <sup>a</sup>
Death receptor signaling	
TRAIL	U37518
DR5 (TRAIL-R2)	AF014794
Decoy receptor 1 (TRAIL-R3)	AF014794
Decoy receptor 2	AF029761
TNF	M16441
TNF- $\alpha$	X02910
TNF- $\beta$	D12614
TNF receptor	M58286
TNF receptor 2-related protein	L04270
Fas (Apo-1/CD95)	X83490, X83492, Z70519, X82279, X63717
Fas ligand (FasL)	U11821, D38122
Mitochondrial signaling	
Bcl-2	M13994, M14745 <sup>b</sup> , M13995 <sup>b</sup>
BAX alpha	L22473
BAX beta	L22474
BAX gamma	L22475 <sup>b</sup>
BAX delta	U19599
Proteases	
Caspase 2 (Ich-1)	U13021 <sup>b</sup> U13022 <sup>b</sup>
Caspase 9 (Mch-6)	U60521 <sup>b</sup>
Caspase 4 (ICErel-II)	U28014
Caspase 5 (ICErel-III)	U28015
Caspase 6 (Mch2)-isoform alpha	U20536
Caspase 8 (MACH-alpha 1, MACH-beta 1, MACH-beta 2)	X98172, X98176, X98175
Caspase 10 (Mch4)	U60519

<sup>a</sup> GenBank accession number corresponds to sequence from which the Affymetrix U95A probe set was designed. Multiple accession numbers are noted for multiple representations of a particular gene (unique probe sets) on the U95A microarray.

<sup>b</sup> Indicates multiple representations of a particular gene derived from the same GenBank sequence.

and DcR-2, changes in death receptor and ligand gene expression are unlikely to play a critical role in reovirus-induced apoptosis. However, transcriptional alterations in genes encoding proteins that modulate death receptor signaling may play a role in reovirus-induced apoptosis.

**Altered expression of genes involved in mitochondrial signaling pathways.** Mitochondrial pathways play an important role in reovirus-induced apoptosis in HEK293 cells (43, 44). Following reovirus infection, both cytochrome *c* and Smac/DIABLO are released from mitochondria and trigger the activation of caspase 9 as well as the degradation of inhibitors of apoptosis (43, 44). Reovirus-induced apoptosis in MDCK and HEK293 cells is inhibited by stable overexpression of Bcl-2 (43, 44, 69), which is consistent with a significant role for the mitochondrial apoptosis pathway during reovirus infection.

Among genes whose expression was altered in T3A (APO+) infected cells were 10 genes encoding proteins involved in mitochondrial signaling. This group included genes encoding a number of proteins known to interact with Bcl-2, including SMN, whose expression was increased  $2.5 \pm 0.1$ -fold, and SMN-interacting protein 1 (SIP-1), whose expression was increased  $3.0 \pm 0.2$ -fold. Expression of genes encoding several other Bcl-2-interacting proteins included the Bcl-2 family member MCL-1, prostate apoptosis response 4 (Par-4), DAP kinase-related apoptosis-inducing protein kinase 2 (DRAK-2), neuronal death protein 5 (DP-5), and Bcl-2-interacting protein 1 (BNIP-1), each of which were upregulated two- to sixfold following T3A (APO+) infec-

tion (Table 1). With the exception of MCL-1, expression of these genes was unaltered following T1L (APO-) infection. Bcl-2 itself was not differentially expressed in virus-infected cells, nor was the proapoptotic Bcl-2 family member BAX (Table 3).

We used RT-PCR to confirm changes in the expression of selected genes involved in mitochondrial signaling and interaction with Bcl-2 (Fig. 2). We found that the expression of SMN was increased at 24 h post-T3A (APO+) infection but not at earlier time points. Expression of Par-4 was increased at 12 and 24 h post-T3A (APO+) infection, thus confirming results obtained with oligonucleotide arrays.

These results add to previous data demonstrating that Bcl-2 plays an important regulatory role in reovirus-induced apoptosis by revealing a complex interplay of Bcl-2 regulatory factors at the transcriptional level in T3A (APO+)-infected cells.

#### Altered expression of genes involved in ER stress pathways.

In addition to death receptor and mitochondrial pathways of apoptosis, stress signals originating in the Golgi apparatus and ER can also trigger apoptosis (79, 86). Viral proteins are potent inducers of ER stress responses (7, 22, 64). Three genes

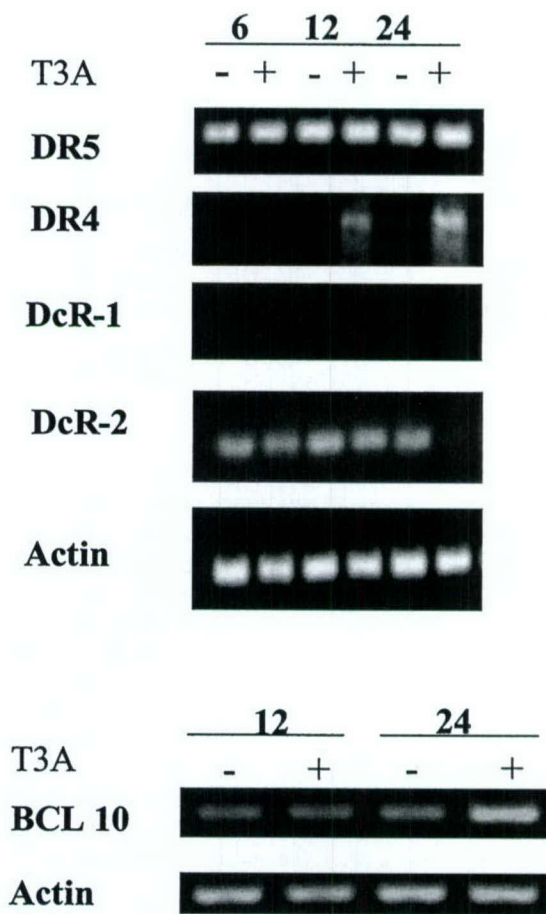


FIG. 1. Expression of genes related to death receptor-mediated apoptotic signaling is altered following reovirus T3A infection. HEK293 cells were either mock (-) or T3A (+) infected at an MOI of 100 PFU per cell. mRNA was collected at 6, 12, and 24 h postinfection and analyzed by semiquantitative RT-PCR for expression of selected transcripts encoding proteins involved in death receptor-mediated apoptotic signaling.

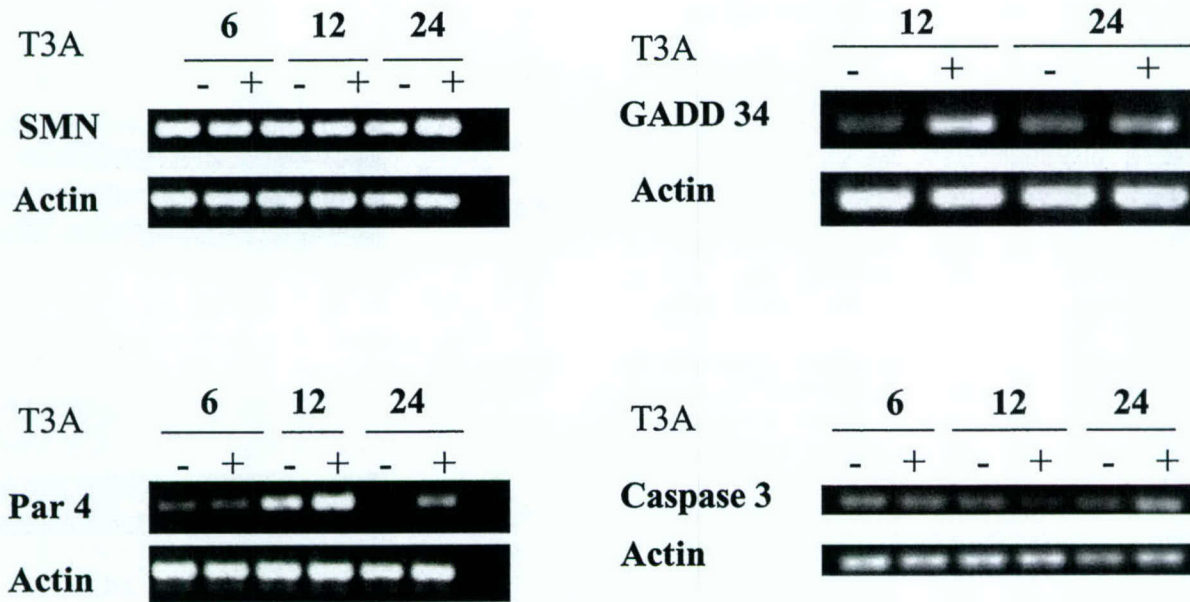


FIG. 2. Expression of genes related to mitochondrial-, ER stress-, and protease-mediated apoptotic signaling is altered following reovirus T3A infection. HEK293 cells were either mock (−) or T3A (+) infected at an MOI of 100 PFU per cell. mRNA was collected at 6, 12, and 24 h postinfection and analyzed by semiquantitative RT-PCR for expression of selected transcripts encoding proteins involved in mitochondrial (SMN and Par-4) and ER stress (GADD 34)-mediated apoptotic signaling as well as for caspase 3, a cysteine protease involved in apoptosis.

encoding proteins that are potentially involved in ER stress-related responses were differentially expressed following both T3A (APO+) and T1L (APO-) infection (Table 1). Two of these genes encode growth arrest and DNA damage (GADD)-inducible proteins GADD 34 and GADD 45. Alterations in the expression of these genes were among the earliest changes in gene expression detected in T3A (APO+)-infected cells. The increased expression of GADD 45 following reovirus infection has been discussed previously in terms of its role in reovirus-induced cell cycle regulation (65). Expression of GADD 34 was increased  $6.8 \pm 0.2$ -fold as early as 6 h post-T3A (APO+) infection. This was the largest increase in expression found for any apoptosis-related gene at any time following infection. Expression remained increased at 24 h postinfection, although the magnitude of the increase declined ( $3.7 \pm 0.2$ -fold). Expression of GADD 34 and GADD 45 was also upregulated at 24 h post-T1L (APO-) infection—by  $2.9 \pm 0.2$ -fold and  $4.4 \pm 0.1$ -fold, respectively. In order to confirm the increased expression of GADD 34 detected by using oligonucleotide arrays, we performed RT-PCR on reovirus-infected HEK293 cells by using GADD 34-specific primers. GADD 34 transcripts were increased at 12 and 24 h post-T3A (APO+) infection compared to mock infection (Fig. 2), thus confirming microarray results. In addition to transcriptional upregulation of genes encoding GADD proteins, transcripts for ORP150—an ER resident protein involved in the misfolded protein rescue response—were downregulated by  $2.4 \pm 0.2$ -fold following T3A (APO+)—not T1L (APO-)—infection.

These results suggest that ER stress-induced apoptotic signaling may play a role in reovirus infection. However, the fact that altered expression in GADD genes occurred following both T1L (APO-) and T3A (APO+) infection (although at lower levels in T1L [APO-] infection) suggests that these pathways may play a less-critical role in determining virus-

induced apoptotic injury and rather are activated as a nonspecific cellular response to reoviral infection.

**Altered expression of genes encoding cysteine proteases.** Initiation of apoptosis through death receptor, mitochondrial, or ER and Golgi pathways results in the activation of specific initiator caspases. These caspases in turn activate additional caspases, culminating in the activation of effector caspases. Effector caspases, exemplified by caspases 3 and 7, act on substrates, including laminins and the caspase-activated DNase responsible for inducing the morphological features of apoptosis in target cells (28). Caspases 3, 8, and 9 are activated in reovirus-infected cells, and inhibition of caspase activation inhibits apoptosis (43).

Expression of genes encoding the effector caspases 3 and 7 were increased at 24 h following T3A (APO+) reovirus infection but not at earlier time points, consistent with their role as downstream effector caspases that are activated at the terminus of caspase cascades. Caspase 7 expression was increased  $2.6 \pm 0.2$ -fold, and that of caspase 3 was increased  $3.2 \pm 0.2$ -fold (Table 1). Caspase 3 expression was also increased at 24 h post-T1L (APO-) infection at lower levels ( $2.8 \pm 0.1$ -fold). Expression of genes encoding other caspases was not significantly altered following reovirus infection, including that of caspases 2, 4, 5, 6, 8, 9, and 10 (Table 3). Caspases 11, 12, 13, and 14 were not represented on the U95A microarray.

Because of the importance and central role of caspase 3 as a common effector in death receptor, mitochondrial, and ER and Golgi apoptotic signaling pathways, we wished to confirm the increased expression of this gene by using RT-PCR. Caspase 3 expression was increased over expression levels in mock-infected cells at 24 h post-T3A (APO+) infection (Fig. 2), thus confirming results obtained via oligonucleotide microarrays. Although not detected by microarray analysis, caspase 3 expression was noted to be decreased at 12 h post-T3A

(APO+) infection, preceding the increase seen at 24 h postinfection.

These results suggest that although caspase activity is clearly modulated at the protein level following reovirus infection, transcriptional upregulation of genes encoding effector caspases may also play a role in effecting reovirus-induced apoptotic injury. The fact that caspase 3 transcripts were noted to initially decrease at 12 h postinfection and then increase at 24 h postinfection indicates that transcriptional regulation is likely a complex and dynamic process that is tightly linked to rapid changes in caspase protein levels and states within infected cells.

**Reovirus-induced alteration in expression of genes related to DNA repair.** DNA damage is one of the basic stimuli that induces apoptosis. Cells have evolved complex mechanisms for sensing both single-strand and double-strand DNA breaks and initiating their repair (67). Expression of 14 genes encoding multiple classes of DNA repair enzymes was altered in T3A (APO+)-infected cells (Table 2). For 9 of these 14 genes, significant alteration (>2-fold) in expression was not apparent until 24 h postinfection, and 11 of these 14 alterations represented downregulation of expression. Transcription of DNA repair genes was not altered following T1L (APO-) infection. This global transcriptional downregulation of multiple classes of DNA repair enzymes following T3A (APO+) infection, which ranged from two- to eightfold, has not previously been appreciated.

Among downregulated DNA repair enzymes, expression of poly(ADP-ribosyl)-transferase (PARP) was decreased  $6.3 \pm 0.7$ -fold, XP-C repair complementing protein 125 was decreased  $3.4 \pm 0.1$ -fold, and DNA polymerase  $\alpha$  was decreased  $2.5 \pm 0.2$ -fold compared to expression levels in mock- or T1L-infected cells. We used RT-PCR to confirm transcriptional alterations following T3A (APO+) infection compared to mock and T1L (APO-) infection in these three DNA-repair enzymes (Fig. 3). Transcripts for XP-C and DNA polymerase  $\alpha$  were decreased at 12 and 24 h post-T3A (APO+) infection, and PARP was downregulated at 24 h post-T3A (APO+) infection, thus confirming the decreases in expression detected by microarray analysis. In contrast, in T1L (APO-)infected cells, transcripts for PARP were unchanged, transcripts for XPC were only minimally decreased (much less so than the dramatic reductions seen in T3A [APO+]-infected cells), and transcripts for DNA polymerase  $\alpha$  were increased.

These results suggest that, as well as directly stimulating proapoptotic signaling pathways, T3A (APO+) reovirus infection may also facilitate apoptosis by downregulating the host cell's transcription of genes encoding proteins that have the capacity to repair DNA damage.

**Translation of microarray data into the *in vivo* model of reovirus-induced myocarditis.** Although changes in mRNA levels do not necessarily represent changes in protein expression, we next investigated whether previously unrecognized changes in gene expression identified by microarray analysis of reovirus-infected cells *in vitro* could be directly translated into delineation of pathogenic mechanisms of reovirus-induced apoptosis *in vivo*. Specifically, we wished to determine if an observed alteration in gene expression would be predictive of changes in expression of the relevant protein in a model of reovirus-induced tissue injury characterized by apoptosis. To

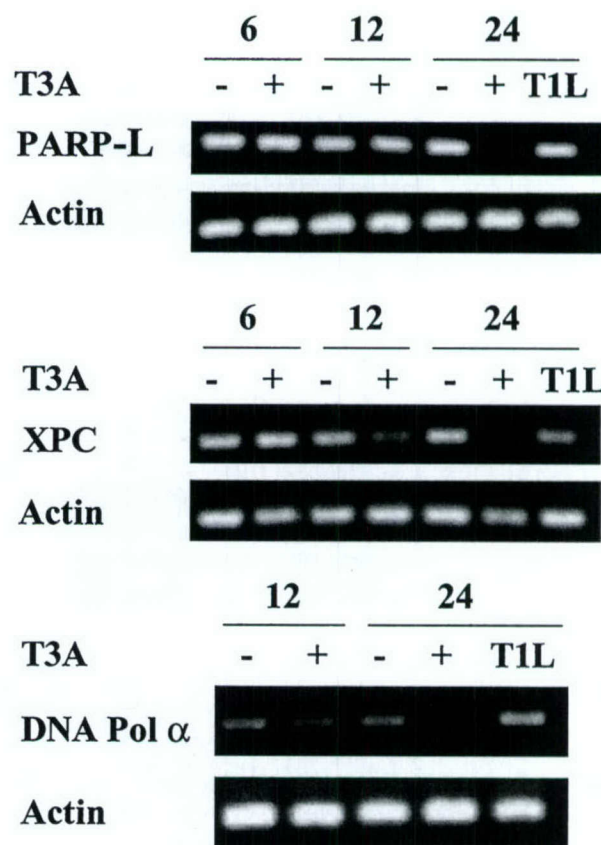
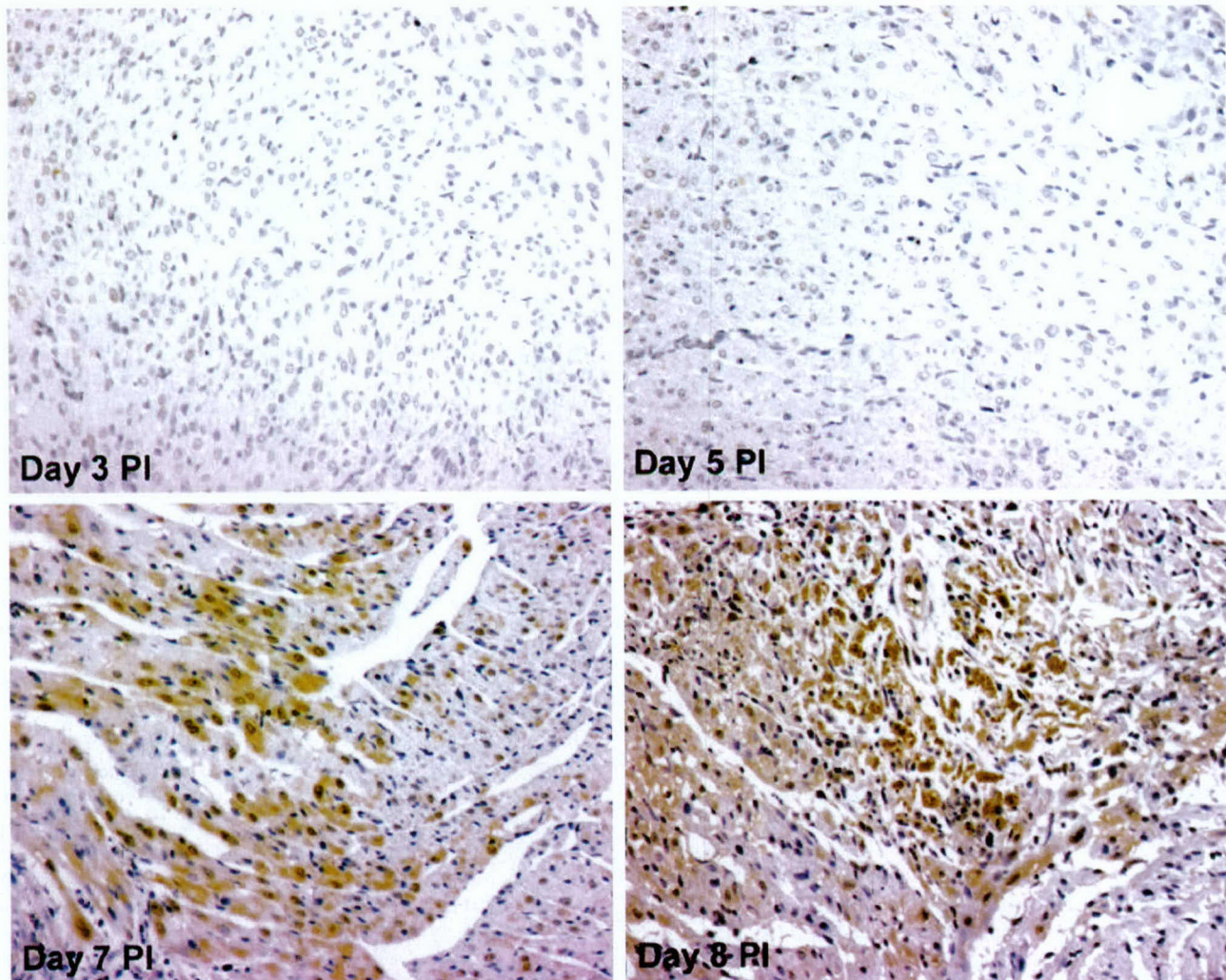


FIG. 3. Genes encoding DNA repair proteins are differentially expressed following reovirus infection. HEK293 cells were either mock (-) or T3A (+) infected at an MOI of 100 PFU per cell, and mRNA was collected at 6, 12, and 24 h postinfection. HEK293 cells were also infected with T1L at an MOI of 100 PFU per cell, with mRNA collected at 24 h postinfection. Samples were analyzed by semiquantitative RT-PCR for expression of selected transcripts encoding proteins important for DNA repair.

this end, we analyzed murine myocardial tissue following reovirus strain 8B infection, since 8B is efficiently myocarditic in neonatal mice (74), and we have previously shown that apoptosis is an important component of myocardial tissue injury following 8B infection (18).

Altered expression of genes encoding Bcl-2 regulatory proteins (which have an impact on mitochondrial apoptotic signaling) were among the most abundant changes detected by microarray analysis. We selected one of these Bcl-2 regulatory proteins, SMN, for analysis *in vivo*, since transcripts for SMN were noted to be selectively increased at 24 h following infection with the apoptosis-inducing strain in the microarray experiment, and this result was confirmed by RT-PCR. We therefore analyzed myocardial tissues from reovirus 8B-infected mice by immunohistochemistry on days 1 to 7 postinfection for expression of SMN in relation to histologic evidence of virus-induced apoptotic tissue damage. SMN was maximally expressed within myocardial lesions in temporal and spatial concordance with histologically detectable apoptotic myocardial injury on days 7 and 8 postinfection (Fig. 4). SMN was not detected in myocardial tissue without evidence of apoptotic myocardial injury on days 1, 3, and 5 postinfection, nor was



**FIG. 4.** SMN expression is increased in reovirus 8B-infected myocardial tissues, coincident with myocardial apoptotic injury. Neonatal Swiss-Webster mice were intramuscularly infected with 1,000 PFU of 8B virus. Myocardial tissues were analyzed on days 1 to 7 postinfection for histologic evidence of myocarditis as well as for expression of SMN by immunohistochemistry, since we have previously shown that apoptotic myocardial injury is detected at 7 days postinfection in this model. SMN protein was detected (brown stain) in infected myocardial tissue beginning on day 7 postinfection (at the time that histologic evidence of myocarditis was detected, within discrete myocardial lesions). Neither SMN nor evidence of myocardial injury was detected at earlier time points postinfection, as demonstrated on days 3 and 5 postinfection. Original magnification,  $\times 40$ .

it detected in tissues from mock-infected animals. The significance of SMN upregulation within injured myocardial tissue is being investigated further. However, these results illustrate that microarray analysis of transcriptional changes following reovirus infection may provide a useful springboard toward the delineation of critical virus-induced pathogenic signaling pathways that are operative at the protein level.

## DISCUSSION

**Transcriptional changes related to apoptosis.** Using high-throughput microarray analysis, we now demonstrate that reovirus infection is associated with differential expression of genes encoding proteins that participate in apoptotic signaling, including death receptor-, mitochondrion-, and ER stress-mediated pathways as well as DNA repair. These results represent

the first large-scale description of virus-induced alterations in apoptotic signaling at the transcriptional level, including the kinetics of these changes following infection with viral strains that differ in apoptosis-inducing phenotype. The fact that the majority of these alterations occurred preferentially in T3A (APO $+$ )- and not T1L (APO $-$ )-infected cells suggests that interpretation of these alterations may provide important insight into critical mechanisms of reovirus-induced pathogenesis.

Microarray analysis has been increasingly utilized to investigate global transcriptional alterations following viral infection of many types, including human immunodeficiency virus (20, 83), herpesviruses (i.e., herpes simplex virus, varicella-zoster virus, Epstein-Barr virus, cytomegalovirus, and Kaposi's sarcoma-associated herpesvirus) (10, 29, 36, 39, 90, 93), rotavirus (17), Sindbis virus (38), hepatitis B (32) and C (5) viruses,

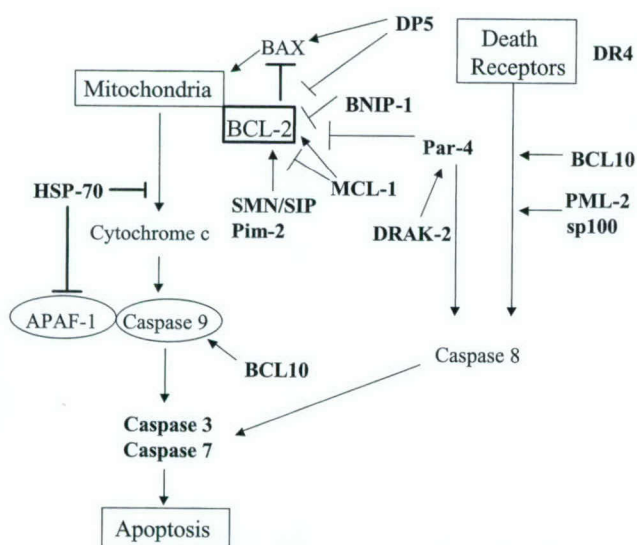


FIG. 5. Schematic of mitochondrion- and death receptor-related transcriptional alterations detected by microarray analysis following reovirus infection. Transcripts that were differentially expressed in HEK293 cells following reovirus infection compared to mock infection are indicated in boldface type. Please see Discussion for details of each indicated transcript.

measles virus (8), influenza virus (23), enterovirus (63), and papillomavirus (55). Although several groups have reported isolated alterations in transcription of genes related to apoptotic signaling following viral infection, none of these studies was specifically designed to understand the specific pathogenic mechanisms by which apoptosis-inducing viruses inflict damage on infected cells. In a comparison of two strains of Sindbis virus that differed in neurovirulence, differential transcriptional alteration of several genes related to mitochondrial apoptotic signaling was noted, including Bcl-2 family members *mcl-1*, *bfl-1*, and PBR (38). Transcriptional alteration of genes related to mitochondrial apoptotic signaling, including cytochrome *c* and inhibitors of apoptosis was also reported following rotavirus infection of Caco-2 cells (17). Altered transcripts for several members of death receptor-mediated signaling pathways were reported following hepatitis C infection of hepatocytes (5), including TRAIL, TNF-R, and Fas. Likewise, TRAIL and Fas transcripts were altered in a study of papillomavirus infection of cervical keratinocytes (55). Altered transcripts for caspase 8 and TRAF4, known to be involved in death receptor signaling, have also been reported following varicella-zoster virus infection of skin fibroblasts (39). In addition to these alterations, several groups have noted transcriptional alteration in genes encoding serpins, which are known to inhibit caspases (17, 39). Transcripts for NF- $\kappa$ B and c-Jun—which have been linked to apoptotic signaling pathways—have also been altered following several types of viral infection.

Our study is the first that was specifically designed to dissect virus-induced alteration in apoptosis-related transcription and the first to report alteration in coordinated groups of genes with relevance to several major apoptotic signaling pathways, as well as being the first to mention global (or even isolated) downregulation of DNA repair gene transcripts following viral infection. The potential implications of identified transcrip-

tional alterations are discussed in further detail below. Schematics that summarize the apoptosis-related transcriptional changes identified following reovirus infection are depicted in Fig. 5 (mitochondrial and death receptor signaling) and Fig. 6 (ER stress and death receptor signaling) for reference in this discussion.

**Death receptor pathways.** Members of the TNF receptor superfamily of cell surface death receptors—specifically DR4, DR5 and their apoptosis-inducing ligand, TRAIL—play a critical role in reovirus-induced apoptosis in HEK293 cells (11). We did not detect significant alteration in the expression of any TNF receptor superfamily members or their ligands by microarray analysis, but we did detect upregulation of transcripts for DR4 and downregulation of the decoy receptor DcR-2 by RT-PCR. This suggests, with the possible exception of DR4 and DcR-2, that reovirus activation of death receptor pathways does not involve changes in gene expression but rather occurs predominantly at the protein level. However, microarray analysis did detect alteration in the expression of genes encoding BCL-10, PML-2, and ceramide glucosyltransferase. The proteins encoded by these genes can modulate death receptor signaling, suggesting that reovirus-induced alterations in expression of these genes might influence death receptor signaling cascades.

Bcl-10 (derived from B-cell lymphomas) binds to TRAF2, a key accessory mediator of TNF-R signaling (78, 91). This binding can perturb TRAF-related activation of mitogen-activated protein kinases (MAPK), including JNK, and can induce the activation of the transcription factor NF- $\kappa$ B (25, 76, 78, 87, 91, 92). Bcl-10 contains a caspase activation and recruitment domain and can bind to pro-caspase-9, thereby promoting its autoproteolytic activation (45, 76, 92). Overexpression of Bcl-10 induces apoptosis in a variety of cells, including HEK293 cells (92), and it may provide a potential link between the capacity of reoviruses to activate JNK cascades, activate the transcription factor NF- $\kappa$ B, and induce apoptosis. PML-2 (encoded by the acute promyelocytic leukemia gene) has been

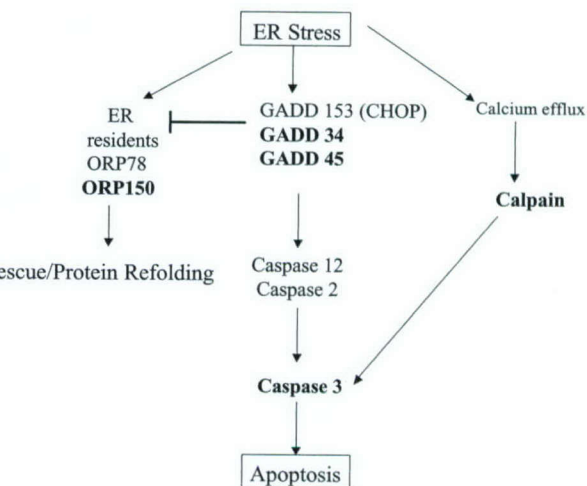


FIG. 6. Schematic of ER stress-related transcriptional alterations detected by microarray analysis following reovirus infection. Transcripts that were differentially expressed in HEK293 cells following reovirus infection compared to mock infection are indicated in boldface type. Please see Discussion for details of each indicated transcript.

shown to enhance activation of death receptor-mediated pathways involving Fas-Fas ligand and TNF and TNF-R (84, 85), suggesting the possibility that it could also potentiate signaling through DR4 and DR5. The mechanism of action of PML is unclear but appears to involve the activation of effector caspases, including caspase 3 (85). Ceramide has been implicated as an important signaling intermediary involved in both Fas-Fas ligand-mediated apoptosis and activation of MAPK cascades (27, 56, 62). Although expression of genes encoding ceramide synthesis were not altered in infected cells, the gene encoding ceramide glucosyltransferase was upregulated. This enzyme catalyzes the initial glycosylation step in glycosphingolipid synthesis to produce glucosylceramide, and its upregulation could potentially enhance ceramide signaling.

**Bcl-2 and mitochondrial signaling pathways.** Pro- and antiapoptotic members of the Bcl-2 family interact at the surface of the mitochondria, where complex homo- and heterodimeric interactions regulate release of proapoptotic molecules including cytochrome *c*, Smac/DIABLO, and apoptosis-inducing factor (28). Reovirus infection is associated with release of cytochrome *c* from the mitochondria into the cytoplasm and with activation of caspase 9 (43). Stable overexpression of the antiapoptotic molecule Bcl-2 inhibits reovirus-induced apoptosis in both MDCK (69) and HEK293 cells (43, 44). These results suggest that, in order to induce apoptosis, reovirus must overcome the antiapoptotic effects of Bcl-2 and related family members in order to activate mitochondrial apoptotic pathways.

Genes encoding several proteins that inhibit the activity of Bcl-2 and therefore facilitate apoptosis were found to be upregulated in reovirus-infected cells. These included Par-4, DRAK-2, DP5, and BNIP-1. Par-4 was initially identified in prostate tumor cells undergoing apoptosis but is widely expressed in human tissues (50). Although the exact mechanism of action of Par-4 is not known, it can facilitate apoptosis by suppression of Bcl-2 expression, inhibition of NF- $\kappa$ B activation, and activation of caspase 8 (2, 9, 21). DRAK-2 is a member of a novel family of nuclear serine-threonine kinases that can induce apoptosis (72). These kinases are known to associate with Par-4, and coexpression of Par-4 and the Zip kinase (42) (related to DRAK-2) enhances apoptosis (60). DP-5 (a death-promoting gene) contains a BH3 domain that allows it to interact with Bcl-2 family proteins. Overexpression of DP5 induces apoptosis in a variety of cells (33, 34). DP5 activation is linked with calcium release from ER stores, suggesting that DP-5 may play a role as a link between ER stress-induced and mitochondrial apoptotic pathways (33). BNIP-1 is a member of a novel BH3 domain-containing protein family that interacts with both Bcl-2 and Bcl-xL to inhibit their antiapoptotic actions, thereby enhancing apoptosis induction (49).

In addition to the upregulation of transcripts encoding Bcl-2-inhibitory proteins, downregulation of transcripts encoding proteins that promote Bcl-2 activity could contribute to promotion of apoptosis following reovirus infection. Pim 2 proto-oncogene homologue is a serine-threonine kinase that is highly expressed in a variety of tissues that may play an antiapoptotic role by enhancing Bcl-2 expression (3, 75). It is one of the few apoptosis regulatory genes that was downregulated following reovirus infection. Since the Pim 2 gene product enhances

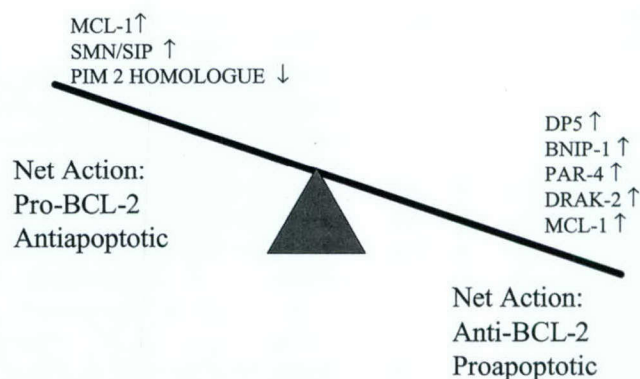


FIG. 7. Transcriptional regulation of Bcl-2 modulatory proteins is a central theme in reovirus-induced apoptosis. Expression of eight transcripts encoding proteins known to influence Bcl-2 activity was altered following reovirus infection. The predicted result of the observed transcriptional alterations would be net inhibition of Bcl-2, and thus promotion of apoptosis, in reovirus-infected cells. Please see Discussion for details of each indicated transcript.

Bcl-2 expression, its downregulation might reduce levels of Bcl-2 in infected cells and thereby enhance apoptosis.

In parallel with these transcriptional alterations with expected anti-Bcl-2 implications, alterations were also noted in expression of transcripts encoding proteins expected to promote the action of Bcl-2 and block apoptosis. Genes encoding two proteins that may act as positive modulators of Bcl-2—SMN and SIP—were found to be upregulated following reovirus infection. SMN interacts with Bcl-2 to enhance its antiapoptotic activity (35). SIP-1 interacts with SMN to form a heterodimeric complex (22a). Coexpression of SMN and Bcl-2 provides a synergistic protective effect against Bax-induced or Fas-mediated apoptosis (35, 73). Expression of the gene encoding the Bcl-2 family member MCL-1 was also upregulated following reovirus infection. MCL-1 may exert either pro- or antiapoptotic activity by modulation of the activity of Bcl-2 or by acting independently (6).

Taken together, these results suggest a model in which reovirus infection is associated with the altered expression of multiple modulators of Bcl-2 in infected host cells, with the balance tipped toward genes encoding proteins that would be predicted to inhibit Bcl-2 activity and thereby promote apoptosis (Fig. 7). Although changes in mRNA levels do not necessarily predict changes in protein expression, we demonstrated that at least one of these proteins, SMN, is altered *in vivo* in a biologically relevant model of reovirus infection, in close temporal and spatial association with evidence of virus-induced apoptotic myocardial tissue injury.

In addition to the modulatory struggle at the Bcl-2 level, alteration of a transcript encoding a protein with a separate role in mitochondrial apoptotic signaling was detected. HSP-70 homologue expression was increased following reovirus infection. HSP-70 is an antiapoptotic chaperone protein (52) that inhibits mitochondrial release of cytochrome *c* and blocks the recruitment of procaspase 9 to the apoptosome complex (4, 47, 71). Although the cellular actions of HSP-70 are predominantly antiapoptotic, the protein also plays a role during reovirus replication in facilitating the trimerization of the reovirus  $\sigma$ 1 protein (46). Since this protein is a critical determinant of

reovirus apoptosis and reovirus-induced activation of specific MAPK signaling cascades (13), HSP-70 homologue may also facilitate apoptosis through its actions during virion assembly.

**ER stress pathways.** The accumulation of abnormal quantities of protein or of malfolded proteins in the Golgi apparatus or ER may trigger kinase cascades that result in the activation of caspase 12 (7, 53, 54). This initiator caspase triggers activation of effector caspases, such as caspase 3. One of the cellular markers of Golgi and ER stress is an increase in the quantities of specific GADD proteins such as GADD 135/CHOP (41, 94). Expression of genes encoding two of the five currently described members of the GADD family, GADD 34 and GADD 45, were increased following reoviral infection. These genes were the earliest ones found to be significantly upregulated following reovirus infection. The upregulation of ER stress apoptosis-inducing transcripts was complemented by downregulated expression of the gene for ORP 150, which encodes a protein involved in refolding malfolded protein transcripts within the ER (32a). In addition to a potential role for GADD 34 for ER stress-mediated pathways, GADD 34 induction parallels that of BAX in other models of apoptosis (30), thus suggesting a possible link to mitochondrion-regulated apoptosis signaling pathways, which are known to play an important role in reoviral infection. These results suggest that ER stress pathways may be activated as an early event following reoviral infection and that ER stress-induced apoptotic signaling may contribute to reovirus-induced apoptosis. However, the fact that altered gene expression occurred following both T1L (APO-) and T3A (APO+) infection [although at lower levels in T1L (APO-) infection] suggests the possibility that this pathway may play a less-critical role in determining virus-induced apoptotic injury and rather is activated as a nonspecific cellular response to reoviral infection.

**Cysteine proteases.** Death receptor, mitochondrial, and Golgi and ER pathways of apoptosis all initiate the activation of specific initiator caspases, which in turn trigger the activation of a limited set of downstream effector caspases, including caspase 3. Caspases 3, 8, and 9 are all activated during reovirus infection (43), and inhibition of this activation inhibits reovirus-induced apoptosis. Expression of the genes encoding caspases 3 and 7 were increased following reovirus infection. This suggests that, as well as inducing the activation of specific caspases at the posttranslational level, reovirus infection also results in upregulation of caspase gene expression that would be predicted to increase the levels of key effector caspases in infected cells.

We have previously shown that the cysteine protease calpain is also activated in reovirus-infected fibroblasts and myocardial cells in vitro (19) and in the heart in vivo (18). This activation appears to be an extremely early event that can be detected as early as 30 min following infection of cells with purified virus. Inhibition of calpain activation inhibits apoptosis and reduces reovirus-induced cytopathic effects in vitro and prevents reovirus-induced apoptotic myocardial injury in vivo (18). The mechanism for the proapoptotic actions of calpains is not fully understood but may involve activation of and activation by several caspases (40, 51, 53, 66, 70, 88). Calpain can also facilitate activation of NF- $\kappa$ B by degrading its cytoplasmic inhibitor, I $\kappa$ B (1).

Surprisingly, rather than being upregulated, the expression

of the gene encoding calpain was downregulated in reovirus-infected cells. This downregulation was apparent only at 24 h postinfection and could potentially represent a negative feedback response to calpain activation at the protein level: initial increases in calpain activity in infected cells could potentially be countered by downregulation of calpain expression at the transcriptional level at later time points.

**Transcriptional changes related to DNA repair.** Expression of transcripts encoding multiple classes of DNA repair enzymes was decreased following T3A (APO+)—but not T1L (APO-)—reovirus infection. Most DNA repair mechanisms involve a recognition step in which single- or double-stranded DNA breaks are identified, followed by the sequential action of helices that unwind damaged segments, nucleases that incise the damaged region, polymerase that resynthesizes DNA, and ligases that repair DNA strand breaks. Failure of any of these steps can result in accumulation of DNA damage and the subsequent induction of apoptosis (67).

DNA nucleotide mismatches or mutations are recognized by a mismatch-binding factor that consists of two distinct proteins—hMSH2 and G/T mismatch binding protein (GTBP)—both of which are required for mismatch-specific binding (61). The gene encoding GTBP was downregulated >2-fold at both 12 and 24 h post-T3A (APO+) infection. Downregulation of GTBP would be expected to impede recognition of single-strand DNA breaks or mutations that distort the structure of the DNA helix.

Once damage has been sensed, helicases unwind damaged DNA as a precursor to excision of the damaged segments. RAD54 homologue, Mi2 autoantigen, and helicase-like protein are three helicases (26) whose transcripts were downregulated following reovirus infection. Genes encoding two nucleotide excision repair enzymes, ERCC5 and XP-C repair-complementing protein p125, were both downregulated following T3A (APO+) reovirus infection. These enzymes are involved in repairing single-strand DNA breaks or in repairing nucleotide mutations that distort the structure of the DNA helix (67). Damaged DNA binding protein 2 (DDB2) may also play a role in nucleotide excision repair (95)—and like ERCC5 and XP-C repair-complementing protein p125, expression of genes encoding DDB2 was also downregulated in T3A (APO+)-infected cells.

Once damage is recognized, the helix is unwound, the damaged area is excised, and new DNA synthesis is required to replace the damaged nucleotides. At least nine DNA polymerases involved in various aspects of DNA replication and repair have been identified in eukaryotes (31). DNA polymerase  $\alpha$  and DNA polymerase  $\gamma$  transcripts were both downregulated following T3A (APO+) reovirus infection. DNA polymerase  $\alpha$  is primarily required for DNA replication but also interacts with and coordinates other DNA polymerases and cellular factors required for DNA repair. DNA polymerase  $\gamma$  is the sole polymerase required for mitochondrial replication and plays an important role in the efficient repair of mismatched DNA in vitro as well as in the repair of damaged DNA (31, 89).

Following DNA synthesis, the repaired segment must be religated with the rest of the helix. DNA ligases promote the rejoicing of both double- and single-stranded DNA breaks (37, 77). Expression of the gene encoding DNA ligase 1 showed the most change in expression of any DNA repair-related gene

analyzed (downregulated  $8.2 \pm 1.1$ -fold at 24 h post-T3A infection). The second-largest change in gene expression following T3A reovirus infection was that of PARP1. PARP1 attaches poly(ADP-ribose) chains to damaged DNA, a process termed ribosylation. Ribosylation is a key step during DNA repair and transcription that prevents binding of transcription factors to regions of damaged DNA (48). Thus, PARP1 may serve as a molecular switch between transcription and repair of DNA to avoid expression of damaged genes (59).

The downregulation of genes encoding DNA damage and repair has not previously been appreciated as a consequence of reoviral infection. The fact this global downregulation occurred following T3A (APO+) and not T1L (APO-) reovirus infection suggests that, as well as directly stimulating proapoptotic signaling pathways, T3A reovirus infection may result in signaling pathways that facilitate apoptosis by hampering the capacity of the host cell to repair DNA damage.

Regulatory mechanisms involved in apoptosis, DNA repair, and cell cycle regulation are highly integrated and involve a number of overlapping and intersecting signaling pathways and proteins. Expression analysis performed by using high-density oligonucleotide arrays provides a unique opportunity to investigate the complex mechanisms responsible for pathogenic effects in reovirus-infected cells and tissues. Transcriptional analysis may not only be directly translatable into *in vivo* models of myocarditis and encephalitis, but more importantly, it may provide testable hypotheses that may not have been explored in the absence of a large-scale analysis of multiple concurrent signaling networks. Work is in progress to further investigate the models suggested in this report by manipulating genes with potentially central themes and observing effects on apoptosis and cell cycle arrest as well as effects on signaling cascades known to be operative in the reovirus model.

#### ACKNOWLEDGMENTS

We thank Samuel Pan for his contribution to RT-PCR validation of microarray data and Vicki VanPutten for technical assistance in analysis of microarray data.

#### REFERENCES

- Baghdiguian, S., M. Martin, I. Richard, F. Pons, C. Astier, N. Bourg, R. T. Hay, R. Chemaly, G. Halaby, J. Loiselet, L. V. Anderson, D. M. Lopez, M. Fardeau, P. Mangeat, J. S. Beckmann, and G. Lefranc. 1999. Calpain 3 deficiency is associated with myonuclear apoptosis and profound perturbation of the IκB α/NF-κB pathway in limb-girdle muscular dystrophy type 2A. *Nat. Med.* **5**:503–511.
- Barradas, M., A. Monjas, M. T. Diaz-Meco, M. Serrano, and J. Moscat. 1999. The downregulation of the pro-apoptotic protein Par-4 is critical for Ras-induced survival and tumor progression. *EMBO J.* **18**:6362–6369.
- Baytel, D., S. Shalom, I. Madgar, R. Weissenberg, and J. Don. 1998. The human Pim-2 proto-oncogene and its testicular expression. *Biochim. Biophys. Acta* **1442**:274–285. (Erratum, **1444**:312–313, 1999.)
- Beere, H. M., B. B. Wolf, K. Cain, D. D. Mosser, A. Mahboubi, T. Kuwana, P. Tailor, R. I. Morimoto, G. M. Cohen, and D. R. Green. 2000. Heat-shock protein 70 inhibits apoptosis by preventing recruitment of pro-caspase-9 to the Apaf-1 apoptosome. *Nat. Cell Biol.* **2**:469–475.
- Bigger, C. B., K. M. Brasky, and R. E. Lanford. 2001. DNA microarray analysis of chimpanzee liver during acute resolving hepatitis C virus infection. *J. Virol.* **75**:7059–7066.
- Bingle, C. D., R. W. Craig, B. M. Swales, V. Singleton, P. Zhou, and M. K. Whyte. 2000. Exon skipping in Mcl-1 results in a bcl-2 homology domain 3 only gene product that promotes cell death. *J. Biol. Chem.* **275**:22136–22146.
- Bitko, V., and S. Barik. 2001. An endoplasmic reticulum-specific stress-activated caspase (caspase-12) is implicated in the apoptosis of A549 epithelial cells by respiratory syncytial virus. *J. Cell Biochem.* **80**:441–454.
- Bolt, G., K. Berg, and M. Blixenkrone-Møller. 2002. Measles virus-induced modulation of host-cell gene expression. *J. Gen. Virol.* **83**:1157–1165.
- Camandola, S., and M. P. Mattson. 2000. Pro-apoptotic action of PAR-4 involves inhibition of NF-κB activity and suppression of BCL-2 expression. *J. Neurosci. Res.* **61**:134–139.
- Carter, K. L., E. Cahir-McFarland, and E. Kieff. 2002. Epstein-Barr virus-induced changes in B-lymphocyte gene expression. *J. Virol.* **76**:10427–10436.
- Clarke, P., S. M. Meintzer, S. Gibson, C. Widmann, T. P. Garrington, G. L. Johnson, and K. L. Tyler. 2000. Reovirus-induced apoptosis is mediated by TRAIL. *J. Virol.* **74**:8135–8139.
- Clarke, P., S. M. Meintzer, A. C. Spalding, G. L. Johnson, and K. L. Tyler. 2001. Caspase 8-dependent sensitization of cancer cells to TRAIL-induced apoptosis following reovirus-infection. *Oncogene* **20**:6910–6919.
- Clarke, P., S. M. Meintzer, C. Widmann, G. L. Johnson, and K. L. Tyler. 2001. Reovirus infection activates JNK and the JNK-dependent transcription factor c-Jun. *J. Virol.* **75**:11275–11283.
- Clarke, P., and K. L. Tyler. 2003. Reovirus-induced apoptosis: a minireview. *Apoptosis* **8**:141–150.
- Connolly, J. L., E. S. Barton, and T. S. Dermody. 2001. Reovirus binding to cell surface sialic acid potentiates virus-induced apoptosis. *J. Virol.* **75**:4029–4039.
- Connolly, J. L., S. E. Rodgers, P. Clarke, D. W. Ballard, L. D. Kerr, K. L. Tyler, and T. S. Dermody. 2000. Reovirus-induced apoptosis requires activation of transcription factor NF-κB. *J. Virol.* **74**:2981–2989.
- Cuadras, M. A., D. A. Feigelstock, S. An, and H. B. Greenberg. 2002. Gene expression pattern in Caco-2 cells following rotavirus infection. *J. Virol.* **76**:4467–4482.
- DeBiasi, R. L., C. L. Edelstein, B. Sherry, and K. L. Tyler. 2001. Calpain inhibition protects against virus-induced apoptotic myocardial injury. *J. Virol.* **75**:351–361.
- DeBiasi, R. L., M. K. Squier, B. Pike, M. Wynne, T. S. Dermody, J. J. Cohen, and K. L. Tyler. 1999. Reovirus-induced apoptosis is preceded by increased cellular calpain activity and is blocked by calpain inhibitors. *J. Virol.* **73**:695–701.
- de la Fuente, C., F. Santiago, L. Deng, C. Eadie, I. Zilberman, K. Kehn, A. Maddukuri, S. Baylor, K. Wu, C. G. Lee, A. Pumfrey, and F. Kashanchi. 2002. Gene expression profile of HIV-1 Tat expressing cells: a close interplay between proliferative and differentiation signals. *BMC Biochem.* **3**:14.
- Diaz-Meco, M. T., M. J. Lallena, A. Monjas, S. Frutos, and J. Moscat. 1999. Inactivation of the inhibitory κB protein kinase/nuclear factor κB pathway by Par-4 expression potentiates tumor necrosis factor α-induced apoptosis. *J. Biol. Chem.* **274**:19606–19612.
- Everett, H., and G. McFadden. 1999. Apoptosis: an innate immune response to virus infection. *Trends Microbiol.* **7**:160–165.
- Fischer, U., Q. Liu, and G. Dreyfuss. 1997. The SMN-SIP1 complex has an essential role in spliceosomal snRNP biogenesis. *Cell* **90**:1023–1029.
- Geiss, G. K., M. C. An, R. E. Bumgarner, E. Hammersmark, D. Cunningham, and M. G. Katze. 2001. Global impact of influenza virus on cellular pathways is mediated by both replication-dependent and -independent events. *J. Virol.* **75**:4321–4331.
- Griffith, T. S., S. R. Wiley, M. Z. Kubin, L. M. Sedger, C. R. Maliszewski, and N. A. Fanger. 1999. Monocyte-mediated tumoricidal activity via the tumor necrosis factor-related cytokine, TRAIL. *J. Exp. Med.* **189**:1343–1354.
- Guillet, C., and P. Vito. 2000. Caspase recruitment domain (CARD)-dependent cytoplasmic filaments mediate bcl10-induced NF-κB activation. *J. Cell Biol.* **148**:1131–1140.
- Hammermann, R., U. Warskulat, and D. Haussinger. 1998. Anisoosmotic regulation of the Mi-2 autoantigen mRNA in H4IIIE rat hepatoma cells and primary hepatocytes. *FEBS Lett.* **435**:21–24.
- Hannun, Y. A. 1996. Functions of ceramide in coordinating cellular responses to stress. *Science* **274**:1855–1859.
- Hengartner, M. O. 2000. The biochemistry of apoptosis. *Nature* **407**:770–776.
- Hobbs, W. E., and N. A. DeLuca. 1999. Perturbation of cell cycle progression and cellular gene expression as a function of herpes simplex virus ICP0. *J. Virol.* **73**:8245–8255.
- Hollander, M. C., Q. Zhan, I. Bae, and A. J. Fornace, Jr. 1997. Mammalian GADD34, an apoptosis- and DNA damage-inducible gene. *J. Biol. Chem.* **272**:13731–13737.
- Hubscher, U., H. P. Nasheuer, and J. E. Syvaoga. 2000. Eukaryotic DNA polymerases, a growing family. *Trends Biochem. Sci.* **25**:143–147.
- Iizuka, N., M. Oka, H. Yamada-Okabe, N. Mori, T. Tamesa, T. Okada, N. Takemoto, A. Tangoku, K. Hamada, H. Nakayama, T. Miyamoto, S. Uchimura, and Y. Hamamoto. 2002. Comparison of gene expression profiles between hepatitis B virus- and hepatitis C virus-infected hepatocellular carcinoma by oligonucleotide microarray data on the basis of a supervised learning method. *Cancer Res.* **62**:3939–3944.
- Ikeda, J., S. Kaneda, K. Kuwabara, S. Ogawa, T. Kobayashi, M. Matsumoto, T. Yura, and H. Yunagi. 1997. Cloning and expression of cDNA encoding the human 150 kDa oxygen-regulated protein, ORP150. *Biochem. Biophys. Res. Commun.* **230**:94–99.
- Imaiizumi, K., T. Moribara, Y. Mori, T. Katayama, M. Tsuda, T. Furuyama, A. Wanaka, M. Takeda, and M. Tohyama. 1999. The cell death-promoting gene DP5, which interacts with the BCL2 family, is induced during neuronal

- apoptosis following exposure to amyloid beta protein. *J. Biol. Chem.* **274**: 7975–7981.
34. Imaizumi, K., M. Tsuda, Y. Imai, A. Wanaka, T. Takagi, and M. Tohyama. 1997. Molecular cloning of novel polypeptide, DP5, induced during programmed neuronal death. *J. Biol. Chem.* **272**:18842–18848.
  35. Iwahashi, H., Y. Eguchi, N. Yasuhara, T. Hanafusa, Y. Matsuzawa, and Y. Tsujimoto. 1997. Synergistic anti-apoptotic activity between Bcl-2 and SMN implicated in spinal muscular atrophy. *Nature* **390**:413–417.
  36. Jenner, R. G., M. M. Alba, C. Boshoff, and P. Kellam. 2001. Kaposi's sarcoma-associated herpesvirus latent and lytic gene expression as revealed by DNA arrays. *J. Virol.* **75**:891–902.
  37. Johnson, A. P., and M. P. Fairman. 1997. The identification and purification of a novel mammalian DNA ligase. *Mutat. Res.* **383**:205–212.
  38. Johnston, C., W. Jiang, T. Chu, and B. Levine. 2001. Identification of genes involved in the host response to neurovirulent alphavirus infection. *J. Virol.* **75**:10431–10445.
  39. Jones, J. O., and A. M. Arvin. 2003. Microarray analysis of host cell gene transcription in response to varicella-zoster virus infection of human T cells and fibroblasts in vitro and SCIDhu skin xenografts *in vivo*. *J. Virol.* **77**: 1268–1280.
  40. Kato, M., T. Nonaka, M. Maki, H. Kikuchi, and S. Imajoh-Ohmi. 2000. Caspases cleave the amino-terminal calpain inhibitory unit of calpastatin during apoptosis in human Jurkat T cells. *J. Biochem. (Tokyo)* **127**:297–305.
  41. Kaufman, R. J. 1999. Stress signaling from the lumen of the endoplasmic reticulum: coordination of gene transcriptional and translational controls. *Genes Dev.* **13**:1211–1233.
  42. Kogel, D., H. Bierbaum, U. Preuss, and K. H. Scheidtmann. 1999. C-terminal truncation of Dlk/ZIP kinase leads to abrogation of nuclear transport and high apoptotic activity. *Oncogene* **18**:7212–7218.
  43. Kominsky, D. J., R. J. Bickel, and K. L. Tyler. 2002. Reovirus-induced apoptosis requires both death receptor- and mitochondrial-mediated caspase-dependent pathways of cell death. *Cell Death Differ.* **9**:926–933.
  44. Kominsky, D. J., R. J. Bickel, and K. L. Tyler. 2002. Reovirus-induced apoptosis requires mitochondrial release of Smac/DIABLO and involves reduction of cellular inhibitor of apoptosis protein levels. *J. Virol.* **76**:11414–11424.
  45. Koseki, T., N. Inohara, S. Chen, R. Carrio, J. Merino, M. O. Hottiger, G. J. Nabel, and G. Nunez. 1999. CIPER, a novel NF- $\kappa$ B-activating protein containing a caspase recruitment domain with homology to herpesvirus-2 protein E10. *J. Biol. Chem.* **274**:9955–9961.
  46. Leone, G., M. C. Coffey, R. Gilmore, R. Duncan, L. Maybaum, and P. W. Lee. 1996. C-terminal trimerization, but not N-terminal trimerization, of the reovirus cell attachment protein is a posttranslational and Hsp70/ATP-dependent process. *J. Biol. Chem.* **271**:8466–8471.
  47. Li, C. Y., J. S. Lee, Y. G. Ko, J. I. Kim, and J. S. Seo. 2000. Heat shock protein 70 inhibits apoptosis downstream of cytochrome c release and upstream of caspase 3 activation. *J. Biol. Chem.* **275**:25665–25671.
  48. Lindahl, T., and R. D. Wood. 1999. Quality control by DNA repair. *Science* **286**:1897–1905.
  49. Low, B. C., Y. P. Lim, J. Lim, E. S. Wong, and G. R. Guy. 1999. Tyrosine phosphorylation of the Bcl-2-associated protein BNIP-2 by fibroblast growth factor receptor-1 prevents its binding to Cdc42GAP and Cdc42. *J. Biol. Chem.* **274**:33123–33130.
  50. Mattson, M. P., W. Duan, S. L. Chan, and S. Camandola. 1999. Par-4: an emerging pivotal player in neuronal apoptosis and neurodegenerative disorders. *J. Mol. Neurosci.* **13**:17–30.
  51. McGinnis, K. M., M. E. Gney, Y. H. Park, N. Mukerjee, and K. K. Wang. 1999. Pro-caspase-3 and poly(ADP)ribose polymerase (PARP) are calpain substrates. *Biochem. Biophys. Res. Commun.* **263**:94–99.
  52. Mosser, D. D., A. W. Caron, L. Bourget, A. B. Merin, M. Y. Sherman, R. I. Morimoto, and B. Massie. 2000. The chaperone function of hsp70 is required for protection against stress-induced apoptosis. *Mol. Cell. Biol.* **20**:7146–7159.
  53. Nakagawa, T., and J. Yuan. 2000. Cross-talk between two cysteine protease families—activation of caspase-12 by calpain in apoptosis. *J. Cell Biol.* **150**: 887–894.
  54. Nakagawa, T., H. Zhu, N. Morishima, E. Li, J. Xu, B. A. Yankner, and J. Yuan. 2000. Caspase-12 mediates endoplasmic-reticulum-specific apoptosis and cytotoxicity by amyloid- $\beta$ . *Nature* **403**:98–103.
  55. Nees, M., J. M. Geoghegan, T. Hyman, S. Frank, L. Miller, and C. D. Woodworth. 2001. Papillomavirus type 16 oncogenes downregulate expression of interferon-responsive genes and upregulate proliferation-associated and NF- $\kappa$ B-responsive genes in cervical keratinocytes. *J. Virol.* **75**:4283–4296.
  56. Obeid, L. M., C. M. Linardic, L. A. Karolak, and Y. A. Hannun. 1993. Programmed cell death induced by ceramide. *Science* **259**:1769–1771.
  57. Oberhaus, S. M., T. S. Dermody, and K. L. Tyler. 1998. Apoptosis and the cytopathic effects of reovirus. *Curr. Top. Microbiol. Immunol.* **233**(Reovir.ii):23–49.
  58. Oberhaus, S. M., R. L. Smith, G. H. Clayton, T. S. Dermody, and K. L. Tyler. 1997. Reovirus infection and tissue injury in the mouse central nervous system are associated with apoptosis. *J. Virol.* **71**:2100–2106.
  59. Oei, S. L., J. Griesenbeck, M. Schweiger, and M. Ziegler. 1998. Regulation of RNA polymerase II-dependent transcription by poly(ADP-ribosylation) of transcription factors. *J. Biol. Chem.* **273**:31644–31647.
  60. Page, G., D. Kogel, V. Rangnekar, and K. H. Scheidtmann. 1999. Interaction partners of Dlk/ZIP kinase: co-expression of Dlk/ZIP kinase and Par-4 results in cytoplasmic retention and apoptosis. *Oncogene* **18**:7265–7273.
  61. Palombo, F., P. Gallinari, I. Iaccarino, T. Lettieri, M. Hughes, A. D'Arrigo, O. Truong, J. J. Hsuan, and J. Jiricny. 1995. GTBP, a 160-kilodalton protein essential for mismatch-binding activity in human cells. *Science* **268**:1912–1914.
  62. Perry, D. K. 1999. Ceramide and apoptosis. *Biochem. Soc. Trans.* **27**:399–404.
  63. Pietiainen, V., P. Huttunen, and T. Hyppia. 2000. Effects of echovirus 1 infection on cellular gene expression. *Virology* **276**:243–250.
  64. Ploegh, H. L. 1998. Viral strategies of immune evasion. *Science* **280**:248–253.
  65. Poggioli, G. J., R. L. DeBiasi, R. Bickel, R. Jotte, A. Spalding, G. L. Johnson, and K. L. Tyler. 2002. Reovirus-induced alterations in gene expression related to cell cycle regulation. *J. Virol.* **76**:2585–2594.
  66. Rami, A., R. Agarwal, G. Botez, and J. Winckler. 2000.  $\mu$ -Calpain activation, DNA fragmentation, and synergistic effects of caspase and calpain inhibitors in protecting hippocampal neurons from ischemic damage. *Brain Res.* **866**: 299–312.
  67. Rich, T., R. L. Allen, and A. H. Wyllie. 2000. Defying death after DNA damage. *Nature* **407**:777–783.
  68. Richardson-Burns, S. M., D. J. Kominsky, and K. L. Tyler. 2002. Reovirus-induced neuronal apoptosis is mediated by caspase 3 and is associated with the activation of death receptors. *J. Neurovirol.* **8**:365–380.
  69. Rodgers, S. E., E. S. Barton, S. M. Oberhaus, B. Pike, C. A. Gibson, K. L. Tyler, and T. S. Dermody. 1997. Reovirus-induced apoptosis of MDCK cells is not linked to viral yield and is blocked by Bcl-2. *J. Virol.* **71**:2540–2546.
  70. Ruiz-Vela, A., D. B. Gonzalez, and A. Martinez. 1999. Implication of calpain in caspase activation during B cell clonal deletion. *EMBO J.* **18**:4988–4998.
  71. Saleh, A., S. M. Srinivasula, L. Balkir, P. D. Robbins, and E. S. Alnemri. 2000. Negative regulation of the Apaf-1 apoptosome by Hsp70. *Nat. Cell Biol.* **2**:476–483.
  72. Sanjo, H., T. Kawai, and S. Akira. 1998. DRAKs, novel serine/threonine kinases related to death-associated protein kinase that trigger apoptosis. *J. Biol. Chem.* **273**:29066–29071.
  73. Sato, K., Y. Eguchi, T. S. Kodama, and Y. Tsujimoto. 2000. Regions essential for the interaction between Bcl-2 and SMN, the spinal muscular atrophy disease gene product. *Cell Death Differ.* **7**:374–383.
  74. Sherry, B., F. J. Schoen, E. Wenske, and B. N. Fields. 1989. Derivation and characterization of an efficiently myocarditic reovirus variant. *J. Virol.* **63**: 4840–4849.
  75. Shirogane, T., T. Fukada, J. M. Muller, D. T. Shima, M. Hibi, and T. Hirano. 1999. Synergistic roles for Pim-1 and c-Myc in STAT3-mediated cell cycle progression and antiapoptosis. *Immunity* **11**:709–719.
  76. Srinivasula, S. M., M. Ahmad, J. H. Lin, J. L. Poyet, T. Fernandes-Alnemri, P. N. Tsichlis, and E. S. Alnemri. 1999. CLAP, a novel caspase recruitment domain-containing protein in the tumor necrosis factor receptor pathway, regulates NF- $\kappa$ B activation and apoptosis. *J. Biol. Chem.* **274**:17946–17954.
  77. Teo, S. H., and S. P. Jackson. 1997. Identification of *Saccharomyces cerevisiae* DNA ligase IV: involvement in DNA double-strand break repair. *EMBO J.* **16**:4788–4795.
  78. Thome, M., F. Martinon, K. Hofmann, V. Rubio, V. Steiner, P. Schneider, C. Mattmann, and J. Tschopp. 1999. Equine herpesvirus-2 E10 gene product, but not its cellular homologue, activates NF- $\kappa$ B transcription factor and c-Jun N-terminal kinase. *J. Biol. Chem.* **274**:9962–9968.
  79. Tirasophon, W., K. Lee, B. Callaghan, A. Welihinda, and R. J. Kaufman. 2000. The endoribonuclease activity of mammalian IRE1 autoregulates its mRNA and is required for the unfolded protein response. *Genes Dev.* **14**:2725–2736.
  80. Tyler, K. L. 1998. Pathogenesis of reovirus infections of the central nervous system. *Curr. Top. Microbiol. Immunol.* **233** (Reovir.ii):93–124.
  81. Tyler, K. L., P. Clarke, R. L. DeBiasi, D. Kominsky, and G. J. Poggioli. 2001. Reoviruses and the host cell. *Trends Microbiol.* **9**:560–564.
  82. Tyler, K. L., M. K. Squier, S. E. Rodgers, B. E. Schneider, S. M. Oberhaus, T. A. Grdina, J. J. Cohen, and T. S. Dermody. 1995. Differences in the capacity of reovirus strains to induce apoptosis are determined by the viral attachment protein  $\sigma$ 1. *J. Virol.* **69**:6972–6979.
  83. van't Wout, A. B., G. K. Lehrman, S. A. Mikheeva, G. C. O'Keeffe, M. G. Katze, R. E. Bumgarner, G. K. Geiss, and J. I. Mullins. 2003. Cellular gene expression upon human immunodeficiency virus type 1 infection of CD4 $^{+}$  T-cell lines. *J. Virol.* **77**:1392–1402.
  84. Wang, Z. G., L. Delva, M. Gaboli, R. Rivi, M. Giorgio, C. Cordon-Cardo, F. Grosfeld, and P. P. Pandolfi. 1998. Role of PML in cell growth and the retinoic acid pathway. *Science* **279**:1547–1551.
  85. Wang, Z. G., D. Ruggero, S. Ronchetti, S. Zhong, M. Gaboli, R. Rivi, and P. P. Pandolfi. 1998. PML is essential for multiple apoptotic pathways. *Nat. Genet.* **20**:266–272.
  86. Welihinda, A. A., W. Tirasophon, and R. J. Kaufman. 1999. The cellular

- response to protein misfolding in the endoplasmic reticulum. *Gene Expr.* **7**:293–300.
87. Willis, T. G., D. M. Jadayel, M. Q. Du, H. Peng, A. R. Perry, M. Abdul-Rauf, H. Price, L. Karran, O. Majekodunmi, I. Wlodarska, L. Pan, T. Crook, R. Hamoudi, P. G. Isaacson, and M. J. Dyer. 1999. Bcl10 is involved in t(1;14) (p22;q32) of MALT B cell lymphoma and mutated in multiple tumor types. *Cell* **96**:35–45.
  88. Wood, D. E., and E. W. Newcomb. 1999. Caspase-dependent activation of calpain during drug-induced apoptosis. *J. Biol. Chem.* **274**:8309–8315.
  89. Wood, R. D., and M. K. Shivji. 1997. Which DNA polymerases are used for DNA repair in eukaryotes? *Carcinogenesis* **18**:605–610.
  90. Yang, W. C., G. V. Devi-Rao, P. Ghazal, E. K. Wagner, and S. J. Triezenberg. 2002. General and specific alterations in programming of global viral gene expression during infection by VP16 activation-deficient mutants of herpes simplex virus type 1. *J. Virol.* **76**:12758–12774.
  91. Yoneda, T., K. Imaizumi, M. Maeda, D. Yui, T. Manabe, T. Katayama, N. Sato, F. Gomi, T. Morihara, Y. Mori, K. Miyoshi, J. Hitomi, S. Ugawa, S. Yamada, M. Okabe, and M. Tohyama. 2000. Regulatory mechanisms of TRAF2-mediated signal transduction by Bcl10, a MALT lymphoma-associated protein. *J. Biol. Chem.* **275**:11114–11120.
  92. Zhang, Q., R. Siebert, M. Yan, B. Hinzmamn, X. Cui, L. Xue, K. M. Rakestraw, C. W. Naeve, G. Beckmann, D. D. Weisenburger, W. G. Sanger, H. Nowotny, M. Vesely, E. Callet-Bauchu, G. Salles, V. M. Dixit, A. Rosenthal, B. Schlegelberger, and S. W. Morris. 1999. Inactivating mutations and overexpression of BCL10, a caspase recruitment domain-containing gene, in MALT lymphoma with t(1;14)(p22;q32). *Nat. Genet.* **22**:63–68.
  93. Zhu, H., J. P. Cong, G. Mamtoro, T. Gingeras, and T. Shenk. 1998. Cellular gene expression altered by human cytomegalovirus: global monitoring with oligonucleotide arrays. *Proc. Natl. Acad. Sci. USA* **95**:14470–14475.
  94. Zinszner, H., M. Kuroda, X. Wang, N. Batchvarova, R. T. Lightfoot, H. Remotti, J. L. Stevens, and D. Ron. 1998. CHOP is implicated in programmed cell death in response to impaired function of the endoplasmic reticulum. *Genes Dev.* **12**:982–995.
  95. Zolezzi, F., and S. Linn. 2000. Studies of the murine DDB1 and DDB2 genes. *Gene* **245**:151–159.

# Human Herpesvirus 6 and Multiple Sclerosis: The Continuing Conundrum

Human herpesvirus 6 (HHV-6) is one of the latest in a long list of infectious agents postulated to play a role in the etiopathogenesis of multiple sclerosis (MS). It is essential in critically evaluating the still exceedingly controversial association between MS and HHV-6 to understand the basic biology of the virus. HHV-6 was first isolated in 1986 from human peripheral blood mononuclear cells (PBMCs) of patients with lymphoproliferative disorders [1]. Two "variants," HHV-6A and HHV-6B, that differ enough in their epidemiology, pathogenesis, and genomic sequence to essentially be considered separate viral species have been identified, although not yet taxonomically recognized as such. In 1988, HHV-6B was etiologically associated with a human disease, exanthema subitum (ES) [2]. HHV-6A is still essentially an orphan virus, although it is likely to induce disease similar to HHV-6B [3]. HHV-6A and HHV-6B, along with HHV-7, are members of the *Roseolovirus* genus of the  $\beta$ -herpesvirus subfamily. These viruses share the common properties of ubiquitous prevalence in human populations, a propensity to cause illnesses characterized by fever and rash, and the capacity to grow in lymphoid cells.

The basic structure of HHV-6 is similar

to that of other herpesviruses and includes a double-stranded DNA genome enclosed in an icosahedral protein capsid surrounded by a tegument. This entire structure is in turn contained within a host-cell-derived lipid envelope into which viral proteins are inserted. Infection is initiated when virus binds to CD46 [4], a 57–67-kDa type I transmembrane glycoprotein expressed on the surface of all nucleated human cells. CD46 is 1 of at least 6 glycoproteins belonging to the regulator of complement activation (RCA) protein family, several of which can serve as viral receptors. Interestingly, both HHV-6 and measles can use CD46 as a receptor, although they bind to distinct domains [5]. Increased levels of soluble CD46 can be detected in serum and cerebrospinal fluid (CSF) of patients with MS and other inflammatory diseases, compared with that in control subjects, although the pathogenetic significance of this remains uncertain [6].

The cell attachment protein of HHV-6 has not been definitely identified, although mapping of neutralization epitopes by monoclonal antibodies indicate that multiple envelope glycoproteins, including gp82-gp105 and the gH-gL complex, are likely candidates. Entry occurs through receptor-mediated endocytosis after which the virus envelope is removed, and the nucleocapsid is transported to the nucleus. The subsequent stages of viral replication are likely to be substantially similar to those of human cytomegalovirus (CMV), another  $\beta$ -herpesvirus [7, 8].

The HHV-6 genome has been completely sequenced [9]. It is between 159

and 170 kb long. Eighteen open-reading frames are unique to either HHV-6A or HHV-6B. The genome encodes a number of potential immunomodulatory molecules, including a CCR2 chemokine agonist (pU83), 2 functional  $\beta$ -chemokine receptors (pU12 and pU51), and a homologue of OX-2/CD100 (pU85) [10, 11]. HHV-6 also contains a gene encoding a protein (pU24) with a sequence of 7 aa ("PRTPPPS<sup>10</sup>") that are identical to aa 96–102 of human myelin basic protein (MBP), and recent studies suggest that T cells recognizing this peptide sequence occur with significantly higher frequency in patients with MS than among healthy control subjects [12]. T cells that react with this peptide after priming with MBP also were more frequent in patients with MS than among healthy control subjects, but the difference was not significant [12]. The molecular mimicry between pU24 and MBP raises the intriguing possibility that HHV-6 infection could contribute to the pathogenesis of MS by altering host immune responses to MBP. However, these results need to be interpreted with caution, because another study of T cell lines derived from patients with MS and control subjects did not show any significant differences in the ability of HHV-6 to activate MBP-reactive T cells [13].

In addition to the ability to cause lytic infections, HHV-6 shares with other herpesviruses the ability to become latent [7, 8]. Latency is generally inferred from the ability to detect viral genome, but not viral antigens or infectious virus, in cells or tissues at times remote from the initial primary infection. It is important to recog-

Financial support: US Army Medical Research and Materiel Command, Department of Veterans Affairs, National Institute on Aging, and Reuler-Lewin Family Professorship of Neurology.

Reprints or correspondence: Dr. Kenneth L. Tyler, Neurology B-182, Univ. of Colorado Health Sciences Center, 4200 E. 9th Ave., Denver, CO 80262 (Ken.Tyler@uchsc.edu).

**The Journal of Infectious Diseases** 2003;187:1360–4

© 2003 by the Infectious Diseases Society of America. All rights reserved.  
0022-1899/2003/18709-0002\$15.00

nize that not all cells harboring "latent" HHV-6 DNA may be able to support reactivation of infectious virus. Potential sites of HHV-6 latency include lymphoid cells, bone marrow, salivary glands, kidney, lung, and the central nervous system (CNS). During pregnancy, immunosuppression, hypersensitivity syndromes, and acute infection with some other viruses (e.g., dengue, measles, and possibly influenza), HHV-6 can reactivate, an event that can also occur even in critically ill immunocompetent patients [14].

Understanding of the pathogenesis of HHV-6 infection has been hampered by the lack of a suitable animal model, although the virus does infect primates other than humans. Seroepidemiological studies indicate that primary infection is acquired during the first 6 months of life, with <10% of infants seropositive at age 1 month, >66% by age 1 year, and ~95% by adult life [15, 16]. Primary HHV-6 infection occurs predominantly postnatally, with the likely source of infection virus shed in saliva and, possibly, in the female genital tract.

Primary HHV-6 infection most commonly produces an acute nonspecific febrile illness and may account for up to 20% of emergency department visits for febrile illness in children aged 6–8 months [16]. Primary HHV-6 infection also frequently presents as ES (roseola infantum), an illness characterized by several days of high fever followed by the appearance of a maculopapular rash starting on the trunk and spreading centrifugally to the face and limbs. Primary HHV-6 infection in adult life is unusual and, when documented, has typically presented as a mononucleosis-like syndrome rather than as ES [17]. CNS infection appears to be an integral feature of primary HHV-6 infection, with virus likely reaching the CNS through the bloodstream in association with infected lymphocytes and monocytes. The consequences of HHV-6 CNS infection are extremely variable, ranging from asymptomatic infection through febrile convulsions to rarer cases of severe menin-

goencephalitis [16, 18–20]. Asymptomatic CNS infection is probably the most common scenario, and HHV-6 DNA can be detected by polymerase chain reaction (PCR) in the CSF of ~25% of patients with ES, even in the absence of seizures or associated neurological manifestations. The next most common presentation is with febrile seizures, which occur in up to one-third of children with primary HHV-6 infection. HHV-6 infection probably accounts for one-third of all cases of febrile convulsions. In rare instances, primary infection is associated with more-severe CNS manifestations, including focal or diffuse meningoencephalitis with or without associated demyelination.

Both HHV-6A and HHV-6B are found more often in CSF specimens than in blood specimens, but the difference in frequency is much greater for HHV-6A, which has led to the suggestion that HHV-6A is more neurotropic and more likely than HHV-6B to persist in the CNS [21]. HHV-6A is also the variant most commonly isolated from brain tissues of patients with MS [22]. However, HHV-6B has been linked to encephalitis in adult bone marrow transplant recipients [23], indicating that both HHV-6 variants are extremely neurotropic. Not only does CNS involvement occur during primary infection but several cases of fatal encephalitis have been reported in immunocompromised individuals, predominantly bone marrow transplant recipients, although the source of viral reactivation (i.e., CNS or peripheral sites) has not been definitely established [23].

Interest in the association between HHV-6 infection and MS was triggered in 1995, when Challoner et al. [24] reported that they had detected a nucleotide fragment that was >99% identical to the major DNA-binding protein gene (MDBP) of HHV-6B (*U41*) by using representational difference analysis to search for potential pathogens in brain specimens from patients with MS. HHV-6 MDBP gene DNA was detected in 25 (78%) of 32 brain specimens from patients with MS and 40 (74%) of 54 brain specimens from control

subjects by nested PCR, with all amplicons typed as HHV-6B. Although the prevalence of amplifiable DNA was similar between brain specimens from patients with MS and control subjects, staining for HHV-6 antigen was found in oligodendrocyte nuclei of 12 (80%) of 15 brain specimens from patients with MS, predominantly in cells associated with MS plaques rather than normal white matter, and in none of 45 brain specimens from control subjects, suggesting that virus was actively replicating and not merely latent in brain specimens from patients with MS. A variety of other cell types, including neurons, astrocytes, macrophages, ependymal cells, choroid plexus epithelial cells, and endothelial cells, also showed positive staining, although this was essentially similar in brain specimens from both patients with MS and control subjects. Staining also was particularly striking in cases with inflammatory CNS disease, with antigen-positive cells usually being macrophages rather than lymphocytes. This finding and the known affinity with which HHV-6 replicates in many immune cells indicate the importance of considering the possibility that any association between HHV-6 and MS might simply reflect the presence of infiltrating inflammatory cells harboring HHV-6.

Subsequent attempts to confirm the association between MS and HHV-6 have taken several forms. Many of the available studies have recently been subjected to a systematic review [25]. One strategy has been to examine the relative prevalence or intensity of HHV-6-specific antibody responses in serum and CSF from patients with MS compared with control subjects. Not surprisingly, this approach has been of rather limited utility, given the almost universal prevalence of HHV-6 antibodies. The best-designed studies have not provided convincing evidence of differences between patients with MS and control subjects [25]. A second strategy, searching for differences in the prevalence of amplifiable HHV-6 DNA in serum or purified PBMCs from patients with MS and con-

trol subjects, has produced variable results but no conclusive evidence of significant differences in most carefully designed studies. One intriguing study suggested that PCR-amplifiable HHV-6 DNA was detected more frequently in the urine of patients with MS than in that of control subjects, but this has not yet been independently confirmed [22]. Attempts to compare differences in HHV-6 DNA detectability in patients with MS during remissions and relapses also have yielded conflicting results [26, 27]. PCR also has been used to search for HHV-6 DNA in CSF. In one well-designed study, no DNA was found in CSF from 32 patients with MS [28], and, in another study, the prevalence was reported to be 0% in control subjects with other neurological disease (OND), 7% in human immunodeficiency virus (HIV)-infected patients with neurological disease, and 11% in patients with MS [29]. Interestingly, when cellular, as opposed to cell-free, CSF was analyzed, the frequencies increased substantially, to 29% in control subjects with OND, 41% in HIV-infected patients, and 39% in patients with MS [29], which suggests that inflammatory cells present in CSF are the ones harboring the HHV-6 genome.

Because MS is a disease of brain tissue, solving the conundrum of the association between HHV-6 and MS is likely to depend on direct analysis of brain material. The simplest approach has been to attempt to amplify HHV-6 DNA from brain tissue by PCR. The design of several studies of this type has been suboptimal [25], but the general results have supported the original findings of Challoner et al. [24] in indicating that HHV-6 DNA can be amplified with high frequency from brain specimens from both patients with MS and control subjects.

PCR amplification of brain samples has two significant disadvantages. First, it is not possible to identify individual cells containing the viral genome, and, second, precise sampling of specific brain micro-regions (e.g., plaque-containing vs. normal-appearing white matter) is essentially

impossible. Two articles in this issue of *The Journal of Infectious Diseases* address both of these problems. The first article [30] uses a refinement of PCR technique, *in situ*-PCR (ISPCR), which can be performed directly on formalin-fixed tissue sections and therefore allows individual cells containing the HHV-6 genome to be identified. This group previously used this technique on autopsy brain tissue specimens from patients with established MS and found ISPCR-positive cells in 11 of 13 sections from 8 brain specimens, predominantly in oligodendrocytes [31]. By contrast, HHV-6 antigen was not detectable in oligodendrocytes, despite the use of antisera recognizing 3 different HHV-6 proteins (p41, p101, and gp116). Their current article [30] is essentially a repeat of the original study but now performed on surgical biopsy specimens from a subset of patients with MS presenting with new onset acute disease and therefore free from the potential confounding issues of drug therapy and the effects of chronic disease. Both studies [30, 31] suffer from the same potential methodological issues, including the lack of blinding, the use of historical controls with no definition of how they were selected, and the dependence on morphological criteria (rather than immunostaining for specific markers) to identify oligodendrocytes as the predominant cell infected. In this new study [30], 9 of 9 sections from the 5 brain specimens from patients with MS examined showed cells positive for the HHV-6 genome by ISPCR. As noted, the majority of positive cells were considered to be oligodendrocytes on the basis of their appearance and lack of staining for an immune cell marker (CD45). Some microglial (CD68<sup>+</sup>) cells also were positive. In contrast to the ISPCR result, no evidence of the HHV-6 antigen was found in any of the MS tissue specimens. The failure to detect *both* genome and antigen is unfortunate, because their concomitant presence would have provided strong support for the validity of both detection assays (immunocytochemistry and ISPCR), as

well as independent corroboration of the presence of HHV-6 infection. The presence of both genome and viral proteins is characteristic of lytic viral infection; however, during the latent state, in which virus is not replicating, only the genome and not the antigen would be detectable, and the results reported are certainly consistent with this interpretation.

In the second study in this issue [32], laser microdissection was used to specifically isolate tissue from plaque-containing and normal-appearing white matter from 13 patients with MS. The isolated material was then subjected to nested PCR to amplify the HHV-6 major capsid protein gene. The number of samples in which the HHV genome was detected (16%–27%) did not differ among healthy brain specimens, normal-appearing white matter in brain specimens from patients with MS, and brain tissue samples from patients with non-MS neurological disease. However, the HHV-6 genome was detected in 57% of samples from plaque-associated white matter in brain samples from patients with MS, a difference that was highly significant when compared with the other groups. The assays were done in a blinded fashion, although the mechanism for selection of "control" cases was not defined. There also was a striking and unexplained amount of variation between the results obtained from different plaques from the same brain and from different samples of the same plaque. If this sample variation is excluded by simply counting any patient with a positive sample as positive, the differences between groups are less impressive; 12 (92%) of 13 MS plaques had at least 1 positive sample, compared to 9 (75%) of 12 healthy brain specimens, 8 (62%) of 13 brain specimens from patients with non-MS disease, and 5 (50%) of 10 normal-appearing white matter brain samples from patients with MS. These differences are not statistically significant.

Where do these new studies leave us? They provide evidence that the HHV-6 genome is present in cells, including ol-

igodendrocytes, from brain specimens from patients with MS and may be more frequently detectable in areas with MS plaques than in normal-appearing white matter. The failure to detect viral antigen, especially in oligodendrocytes, in contrast to findings in some previous studies [24, 33], suggests that brains of patients with MS, like those of their unaffected counterparts, harbor latent, rather than actively replicating, virus and argues strongly against a model in which direct virus-induced oligodendrocyte injury contributes to the pathogenesis of MS. The high frequency with which the HHV-6 genome is detected in brain tissue specimens from patients with non-MS neurological disease suggests that the virus should be considered part of "normal brain flora," and the current studies do not explain how this ubiquitous virus might be involved in the etiopathogenesis of MS in some individuals while seemingly having no effect in others. The diverse immunomodulatory effects of HHV-6, including the potential for molecular mimicry, raise the possibility that it is not viral infection itself but rather unique aspects of the host response to this infection that may be key.

If HHV-6 does play a role in MS, the potential to alter the course of disease with antiviral therapy for HHV-6 would be of great interest. Most HHV-6 infections are benign self-limited illnesses and do not require specific antiviral therapy. Unfortunately, there are no controlled clinical trials of the use of antiviral agents in HHV-6 infection. In vitro, HHV-6A and HHV-6B have a similar pattern of antimicrobial sensitivity that closely resembles that of CMV, with isolates being resistant to acyclovir, famciclovir, and valacyclovir, and sensitive to foscarnet, ganciclovir, and valganciclovir. It should be noted that HHV-6 is less sensitive to ganciclovir than CMV, which is probably related to a lessened capacity of the HHV-6-encoded pU69 kinase to phosphorylate ganciclovir [34]. As a result of this pattern of susceptibility, the failure or limited efficacy of valacyclovir

in MS [35] would not be unexpected, even if HHV-6 had a role in the etiopathogenesis of MS.

Uncontrolled trials of treatment of HHV-6 CNS infection in hematopoietic stem cell recipients indicate that both ganciclovir and foscarnet therapy are associated with reduction in virus load in CSF and plasma, although the response was not universal and not always statistically significant [23, 36]. Ganciclovir also has been reported to be of benefit in prophylaxis against HHV-6 reactivation in patients receiving stem cell transplantation [36], which suggests that this drug would be a far better choice than acyclovir derivatives to target active HHV-6 infection. Interestingly, interferon (IFN)- $\beta$ , which is frequently used for the treatment of MS, significantly reduces HHV-6 replication in T cell lines in vitro. Patients with MS being treated with IFN- $\beta$  also have decreased levels of serum HHV-6 DNA, compared with that in untreated control subjects, or their own pretreatment serum, which suggests a possible antiviral effect in vivo [37]. It is important to recognize that any antiviral treatment strategy would only be useful if reactivation and active replication of HHV-6 were key events in the pathogenesis of MS. If virus is only present in a latent state, as suggested by the failure of some [30, 31], but not all [24, 33], studies to detect viral antigen, then no currently available antiviral agent would be expected to be of benefit in MS treatment.

### Kenneth L. Tyler

Departments of Neurology, Medicine, Microbiology, and Immunology, University of Colorado Health Sciences Center, Denver

### References

1. Salahuddin SZ, Ablashi DV, Markham PD, et al. Isolation of a new virus, HBLV, in patients with lymphoproliferative disorders. *Science* 1986; 234:596-600.
2. Yamanishi K, Okuno T, Shiraki K, et al. Identification of human herpesvirus-6 as a causal agent for exanthema subitum. *Lancet* 1988; i: 1065-7.
3. Hidaka Y, Kushuhara K, Takabayashi A, et al. Symptomatic primary infection with human herpesvirus 6 variant A. *Clin Infect Dis* 1997; 24:1022-3.
4. Santoro F, Kennedy PE, Locatelli G, et al. CD46 is a cellular receptor for human herpesvirus 6. *Cell* 1999; 99:817-22.
5. Greenstone HL, Santoro F, Lusso P, Berger EA. Human herpesvirus 6 and measles virus employ distinct CD46 domains for receptor function. *J Biol Chem* 2002; 277:39112-8.
6. Soldan SS, Fogdell-Hahn A, Brennan MB, et al. Elevated serum and cerebrospinal fluid levels of soluble human herpesvirus type 6 cellular receptor, membrane cofactor protein, in patients with multiple sclerosis. *Ann Neurol* 2001; 50:486-93.
7. Clark DA. Human herpesvirus 6. *Rev Med Virol* 2000; 10:155-73.
8. Pellett PE, Dominguez G. Human herpesviruses 6A, 6B, and 7 and their replication. In: Knipe DM, Howley PM, eds. *Fields virology*. 4th ed. Philadelphia: Lippincott William & Wilkins, 2001:2769-84.
9. Dominguez G, Damaugh TR, Stamey FR, et al. Human herpesvirus 6B genome sequence: coding content and comparison with human herpesvirus 6A. *J Virol* 1999; 73:8040-52.
10. Hoek RM, Ruuls SR, Murphy CA, et al. Down-regulation of the macrophage lineage through interaction with OX2 (CD100). *Science* 2000; 290:1768-71.
11. Luttmach HR, Lewis IC, Jensen PO, Moser C, Gerstoft J, Schwartz TW. A highly selective CCR2 chemokine agonist encoded by human herpesvirus 6. *J Biol Chem* 2003; 278:10928-33.
12. Tejada-Simon MV, Zang YC, Hong J, Rivera VM, Zhang JZ. Cross-reactivity with myelin basic protein and human herpesvirus-6 in multiple sclerosis. *Ann Neurol* 2003; 53:189-97.
13. Cirone M, Cuomo L, Zompetta C, et al. Human herpesvirus 6 and multiple sclerosis: a study of T cell cross-reactivity to viral and myelin basic protein antigens. *J Med Virol* 2002; 68:268-72.
14. Razonable RR, Fanning C, Brown RA, et al. Selective reactivation of human herpesvirus 6 variant A occurs in critically ill immunocompetent hosts. *J Infect Dis* 2002; 185:110-3.
15. Caserta MT, Mock DJ, Dewhurst S. Human herpesvirus 6. *Clin Infect Dis* 2001; 33:829-33.
16. Hall CB, Long CE, Schnabel KC, et al. Human herpesvirus-6 infection in children: a prospective study of complications and reactivation. *N Engl J Med* 1994; 331:432-8.
17. Akashi K, Eizuru Y, Sumiyoshi Y, et al. Brief report: severe infectious mononucleosis-like syndrome and primary human herpesvirus 6 infection in an adult. *N Engl J Med* 1993; 329: 168.
18. Suga S, Yoshikawa T, Asano Y, et al. Clinical and virological analyses of 21 infants with exanthema subitum (roseola infantum) and central nervous system complications. *Ann Neurol* 1993; 33:597-603.
19. Caserta MT, Hall CB, Schnabel K, et al. Neuroinvasion and persistence of human herpesvirus 6 in children. *J Infect Dis* 1994; 170: 1586-9.

20. McCullers JA, Lakeman FD, Whitley RJ. Human herpesvirus 6 is associated with focal encephalitis. *Clin Infect Dis* 1995; 21:571–6.
21. Hall CB, Caserta MT, Schnabel KC, et al. Persistence of human herpesvirus 6 according to site and variant: possible greater neurotropism of variant A. *Clin Infect Dis* 1998; 26:132.
22. Akhyani N, Berti R, Brennan MB, Soldan SS, Eaton JM, McFarland HF, Jacobson S. Tissue distribution and variant characterization of human herpesvirus (HHV)-6: increased prevalence of HHV-6A in patients with multiple sclerosis. *J Infect Dis* 2000; 182:1321–5.
23. Zerr DM, Gupta D, Huang M-L, Carter R, Corey L. Effect of antivirals on human herpesvirus 6 replication in hematopoietic stem cell transplant recipients. *Clin Infect Dis* 2002; 34: 309–17.
24. Challoner PB, Smith KT, Parker JD, et al. Plaque-associated expression of human Herpesvirus 6 in multiple sclerosis. *Proc Natl Acad Sci USA* 1995; 92:7440–4.
25. Moore FG, Wolfson C. Human herpes virus 6 and multiple sclerosis. *Acta Neurol Scand* 2002; 106:63–83.
26. Berti R, Brennan MB, Soldan SS, Ohayon JM, Casareto L, McFarland HF, Jacobson S. Increased detection of serum HHV-6 DNA sequences during multiple sclerosis (MS) exacerbations and correlation with parameters of MS disease progression. *J Neurovirol* 2002; 8: 250–6.
27. Alvarez-Lafuente R, Martin-Estefania C, de las Heras V, et al. Active human herpesvirus 6 infection in patients with multiple sclerosis. *Arch Neurol* 2002; 59:929–33.
28. Mirandola P, Stefan A, Brambilla E, et al. Absence of human herpes virus 6 and 7 from spinal fluid and serum of multiple sclerosis patients. *Neurology* 1999; 53:1367–8.
29. Liedtke W, Malessa R, Faustmann PM, Eis-Hubinger A-M. Human herpesvirus 6 polymerase chain reaction findings in human immunodeficiency virus associated neurological disease and multiple sclerosis. *J Neurovirol* 1995; 1:253–8.
30. Goodman AD, Mock DJ, Powers JM, Baker JV, Blumberg BM. Human herpesvirus 6 genome and antigen in acute multiple sclerosis lesions. *J Infect Dis* 2003; 187:1365–76 (in this issue).
31. Blumberg BM, Mock DJ, Powers JM, et al. The HHV6 paradox: ubiquitous commensal or insidious pathogen? A two-step *in situ* PCR approach. *J Clin Virol* 2000; 16:159–78.
32. Cermelli C, Bert R, Soldan SS, et al. High frequency of human herpesvirus 6 DNA in multiple sclerosis plaques isolated by laser microdissection. *J Infect Dis* 2003; 187:1377–87 (in this issue).
33. Knox KK, Brewer JH, Henry JM, Harrington DJ, Carrigan DR. Human herpesvirus 6 and multiple sclerosis: systemic active infection in patients with early disease. *Clin Infect Dis* 2000; 31:894–903.
34. De Bolle L, Michel D, Mertens T, et al. Role of the human herpesvirus 6 u69-encoded kinase in the phosphorylation of ganciclovir. *Mol Pharmacol* 2002; 62:714–21.
35. Bech E, Lyke J, Gadeberg P, et al. A randomized double-blind placebo-controlled MRI study of anti-herpes virus therapy in MS. *Neurology* 2002; 58:31–6.
36. Tokimasa S, Hara J, Osugi Y, et al. Ganciclovir is effective for prophylaxis and treatment of human herpesvirus-6 in allogeneic stem cell transplantation. *Bone Marrow Transplant* 2002; 29: 595–8.
37. Hong J, Tejada-Simon MV, Rivera VM, Zang YC, Zhang JZ. Anti-viral properties of interferon beta treatment in patients with multiple sclerosis. *Mult Scler* 2002; 8:237–42.

# Two Distinct Phases of Virus-induced Nuclear Factor $\kappa$ B Regulation Enhance Tumor Necrosis Factor-related Apoptosis-inducing Ligand-mediated Apoptosis in Virus-infected Cells\*

Received for publication, January 9, 2003, and in revised form, February 25, 2003  
Published, JBC Papers in Press, March 13, 2003, DOI 10.1074/jbc.M300265200

Penny Clarke‡, Suzanne M. Meintzer, Lisa A. Moffitt, and Kenneth L. Tyler§¶

From the Departments of Neurology, §Medicine, Microbiology, and Immunology, University of Colorado Health Science Center, Denver, Colorado 80262 and Denver Veterans Affairs Medical Center, Denver, Colorado 80220

**C**ellular transcription factors are often utilized by infecting viruses to promote viral growth and influence cell fate. We have previously shown that nuclear factor  $\kappa$ B (NF- $\kappa$ B) is activated after reovirus infection and that this activation is required for virus-induced apoptosis. In this report we identify a second phase of reovirus-induced NF- $\kappa$ B regulation. We show that at later times post-infection NF- $\kappa$ B activation is blocked in reovirus-infected cells. This results in the termination of virus-induced NF- $\kappa$ B activity and the inhibition of tumor necrosis factor  $\alpha$  and etoposide-induced NF- $\kappa$ B activation in infected cells. Reovirus-induced inhibition of NF- $\kappa$ B activation occurs by a mechanism that prevents I $\kappa$ B $\alpha$  degradation and that is blocked in the presence of the viral RNA synthesis inhibitor, ribavirin. Reovirus-induced apoptosis is mediated by tumor necrosis factor-related apoptosis inducing ligand (TRAIL) in a variety of epithelial cell lines. Herein we show that ribavirin inhibits reovirus-induced apoptosis in TRAIL-resistant HEK293 cells and prevents the ability of reovirus infection to sensitize TRAIL-resistant cells to TRAIL-induced apoptosis. Furthermore, TRAIL-induced apoptosis is enhanced in HEK293 cells expressing I $\kappa$ B $\Delta$ N2, which blocks NF- $\kappa$ B activation. These results indicate that the ability of reovirus to inhibit NF- $\kappa$ B activation sensitizes HEK293 cells to TRAIL and facilitates virus-induced apoptosis in TRAIL-resistant cells. Our findings demonstrate that two distinct phases of virus-induced NF- $\kappa$ B regulation are required to efficiently activate host cell apoptotic responses to reovirus infection.

Experimental infection with mammalian reoviruses has provided a classic model of viral pathogenesis (for review, see Ref. 1). Reovirus induces apoptosis both in cultured cells and in target tissues (for review, see Ref. 2). In the central nervous system and heart, virus-induced apoptosis correlates with pathology and is a critical mechanism by which disease is triggered in the host (3–5). Reovirus induces apoptosis by a p53-

independent mechanism that involves cellular proteases, including calpains (3, 6) and caspases (5, 7, 8).

We have previously shown that in a variety of human epithelial cell lines (7, 9) reovirus-induced apoptosis is mediated by tumor necrosis factor (TNF)<sup>1</sup>-related apoptosis-inducing ligand (TRAIL) (for review, see Ref. 10). However, reovirus infection triggers apoptosis in both TRAIL-sensitive (7, 9) and TRAIL-resistant cells (7). The question as to how reovirus induces apoptosis in TRAIL-resistant lines has been answered in part by the observation that reovirus can sensitize previously resistant cells to killing by TRAIL (7, 9). Reovirus-induced sensitization of cells to TRAIL requires caspase 8 activity and is associated with an increase in the cleavage of pro-caspase 8 in cells treated with TRAIL and reovirus compared with cells treated with TRAIL alone (9). The mechanism by which reovirus induces increased caspase 8 activation in TRAIL-treated cells is, however, unknown.

The NF- $\kappa$ B family of cellular transcription factors promotes the expression of a variety of cellular genes, including genes that have either pro- or anti-apoptotic effects, and it is thought that the balance of expression of NF- $\kappa$ B-regulated genes may determine cell fate (12). The prototypical form of NF- $\kappa$ B exists as a heterodimer of proteins p50 and p65 (RelA) (13, 14). NF- $\kappa$ B is normally sequestered in the cytoplasm by its binding to a family of inhibitor proteins, collectively known as I $\kappa$ B (15, 16). In response to a variety of stimuli, I $\kappa$ B is phosphorylated, resulting in its ubiquitination and subsequent degradation (17–20). This allows the release of NF- $\kappa$ B, which translocates to the nucleus (21), where it stimulates cellular gene transcription (for review, see Refs. 22 and 23). In a variety of cell types, the binding of reovirus to the cell surface receptors junctional adhesion molecule and sialic acid induces the activation of NF- $\kappa$ B (24, 25). In TRAIL-sensitive HeLa cells this activation is detected 2–12 h post-infection (pi), involves both the p65 and p50 subunits of NF- $\kappa$ B, and is required for reovirus-induced apoptosis (26). In HeLa cells reovirus-induced NF- $\kappa$ B activation and apoptosis require viral disassembly but not subsequent events of reovirus replication and are not inhibited by the viral RNA synthesis inhibitor ribavirin or by replication incompetent viruses (27).

The experiments described below investigate the role of NF- $\kappa$ B in reovirus-induced apoptosis in TRAIL-resistant HEK293 cells. These studies show that reovirus infection of HEK293 cells results in an initial, transient phase of NF- $\kappa$ B activation that is required for reovirus-induced apoptosis in

\* This work was supported by National Institute of Health Public Health Service Grant 1R01AG14071, Merit and Research Enhancement Award Program (REAP) grants from the Department of Veterans Affairs, U. S. Army Medical Research and Material Command Grant DAMD17-98-1-8614, and by the Reuler-Lewin Family Professorship of Neurology. The costs of publication of this article were defrayed in part by the payment of page charges. This article must therefore be hereby marked "advertisement" in accordance with 18 U.S.C. Section 1734 solely to indicate this fact.

‡ Supported by the Ovarian Cancer Research Fund.

¶ To whom correspondence should be addressed: Dept. of Neurology (B182), University of Colorado Health Sciences Center, 4200 East 9th Ave., Denver CO 80262. Tel.: 303-393-2874; Fax: 303-393-4686; E-mail: Ken.Tyler@uchsc.edu.

<sup>1</sup> The abbreviations used are: TNF, tumor necrosis factor; TRAIL, TNF-related apoptosis-inducing ligand; NF- $\kappa$ B, nuclear factor  $\kappa$ B; I $\kappa$ B, inhibitor  $\kappa$ B; pi, post-infection; EMSA, electrophoretic mobility shift assay; m.o.i., multiplicity of infection; HIV-1, human immunodeficiency virus type.

these cells. This is followed by a later phase of virus-induced NF- $\kappa$ B inhibition. Reovirus-induced inhibition of NF- $\kappa$ B activation is associated with impaired degradation of I $\kappa$ B and is inhibited by the viral RNA synthesis inhibitor, ribavirin. In contrast to findings in TRAIL-sensitive HeLa cells, in which ribavirin blocks reovirus replication but not apoptosis, both these events are blocked by ribavirin in TRAIL-resistant HEK293 cells. Ribavirin also inhibits reovirus-induced sensitization of HEK293 cells to TRAIL-induced apoptosis. We further show that HEK293 cells are sensitized to TRAIL-induced apoptosis by the expression of I $\kappa$ B $\Delta$ N2, which blocks the activation of NF- $\kappa$ B. This suggests that the ability of reovirus to block NF- $\kappa$ B activation at later times post-infection sensitizes HEK293 cells to TRAIL-induced apoptosis and is critical for apoptosis in TRAIL-resistant cells. The demonstration that multiple levels of virus-induced NF- $\kappa$ B regulation are required to efficiently activate host cell apoptotic responses to reovirus infection represents a novel mechanism of viral-induced apoptosis.

#### EXPERIMENTAL PROCEDURES

**Cells, Viruses, and Reagents**—HEK293 (ATCC CRL1573) were grown in Dulbecco's modified Eagle's medium supplemented with 100 units/ml each penicillin and streptomycin and containing 10% fetal bovine serum. HeLa cells (ATCC CCL2) were grown in Eagle's minimal essential medium supplemented with 2.4 mM L-glutamine, nonessential amino acids, 60 units/ml each penicillin and streptomycin and containing 10% fetal bovine serum (Invitrogen). HEK293 cells expressing I $\kappa$ B $\Delta$ N2, a strong dominant negative I $\kappa$ B mutant lacking the NH<sub>2</sub>-terminal phosphorylation sites that regulate I $\kappa$ B degradation and the consequent activation of NF- $\kappa$ B, were a kind gift from Dr. G. Johnson. Reovirus strain Type 3 Abney (T3A) was used for all experiments. T3A is a laboratory stock that has been plaque-purified and passaged (twice) in L929 (ATCC CCL1) cells to generate working stocks (28). TRAIL was obtained from Upstate Biotechnology and Sigma, TNF $\alpha$  was obtained from Invitrogen, and etoposide and ribavirin were obtained from Sigma. Ribavirin was used at a concentration of 200  $\mu$ M.

**Apoptosis Assays**—Cells were assayed for apoptosis by staining with acridine orange for determination of nuclear morphology and ethidium bromide to distinguish cell viability at a final concentration of 1  $\mu$ g/ml each (29). After staining, cells were examined by epifluorescence microscopy (Nikon Labophot-2, B-2A filter; excitation, 450–490 nm; barrier, 520 nm; dichroic mirror, 505 nm). The percentage of cells containing condensed nuclei and/or marginated chromatin in a population of 100 cells was recorded. The specificity of this assay has been previously established in reovirus-infected cells using DNA laddering techniques and electron microscopy (9, 30).

**Caspase 3 Activity Assays**—Caspase 3 activation assays were performed using a kit obtained from Clontech. Cells ( $1 \times 10^6$ ) were centrifuged at 200  $\times g$  for 10 min, supernatants were removed, and cell pellets were frozen at -70 °C until all time points were collected. Assays were performed in 96-well plates and analyzed using a fluorescent plate reader (CytoFluor 4000, PerSeptive Biosystems). Cleavage of DEVD-aminofluoromethylcoumarin, a synthetic caspase-3 substrate, was used to measure caspase 3 activation in reovirus-infected cells. Cleavage after the second Asp residue produces free aminofluoromethylcoumarin that can be detected using a fluorescent plate reader. The amount of fluorescence detected is directly proportional to the amount of caspase 3 activity.

**Electrophoretic Mobility Shift Assay (EMSA)**—Nuclear extracts were prepared from treated cells ( $5 \times 10^6$ ) by washing cells in phosphate-buffered saline followed by incubation in hypotonic lysis buffer (10 mM HEPES (pH 7.9), 10 mM KCl, 1.5 mM MgCl<sub>2</sub>, 0.5 mM dithiothreitol, 0.5 mM phenylmethylsulfonyl fluoride, and a protease inhibitor mixture (Roche Applied Science)) at 4 °C for 15 min. One-twentieth volume 10% Nonidet P-40 was added to the cell lysate, and the sample was vortexed for 10 s and centrifuged at 10,000  $\times g$  for 5 min. The nuclear pellet was washed once in hypotonic buffer, resuspended in high salt buffer (25% glycerol, 20 mM HEPES (pH 7.9), 0.42 M NaCl, 1.5 mM MgCl<sub>2</sub>, 0.2 mM EDTA, 0.5 mM dithiothreitol, 0.5 mM phenylmethylsulfonyl fluoride, and protease inhibitor mixture), and incubated at 4 °C for 2–3 h. Samples were centrifuged at 10,000  $\times g$  for 10 min, and the supernatant was used as the nuclear extract.

Nuclear extracts were assayed for NF- $\kappa$ B activation by EMSA using a <sup>32</sup>P-labeled oligonucleotide consisting of the NF- $\kappa$ B consensus binding

sequence (Santa Cruz Biotechnology). Nuclear extracts (5–10  $\mu$ g of total protein) were incubated with a binding reaction buffer containing 2  $\mu$ g of poly(dI:dC) (Sigma) in the presence of 20 mM HEPES (pH 7.9), 60 mM KCl, 1 mM EDTA, 1 mM dithiothreitol, and 5% glycerol at 4 °C for 20 min. Radiolabeled NF- $\kappa$ B consensus oligonucleotide (0.1–1.0 ng) was added, and the mixture was incubated at room temperature for 20 min. For competition experiments, a 10-fold excess of unlabeled consensus oligonucleotide or an oligonucleotide containing the SP-1 consensus site (Santa Cruz Biotechnology) were added to reaction mixtures. Nucleoprotein complexes were subjected to electrophoresis on native 5% polyacrylamide gels at 180 V, dried under vacuum, and exposed to Biomax MR film (Eastman Kodak Co.).

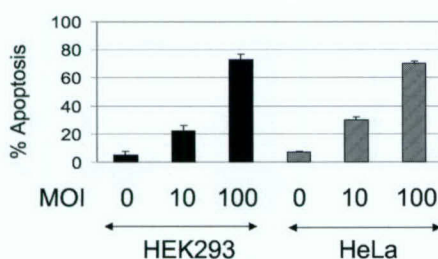
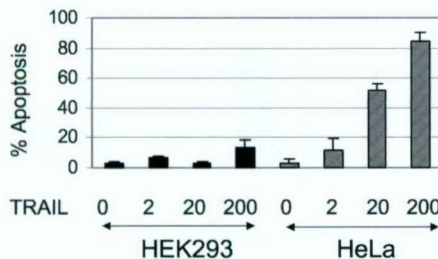
**Luciferase Gene Reporter Assays**—The NF- $\kappa$ B-dependent luciferase reporter construct was a gift from Dr. B. Sugden. The construct contains four NF- $\kappa$ B binding sites upstream of the luciferase gene. HEK293 cells ( $1.5 \times 10^5$ ) in 6-well tissue culture plates (Costar) were incubated for 24 h before being transfected with 1  $\mu$ g of the luciferase reporter construct and 1  $\mu$ g of a cytomegalovirus- $\beta$ -galactosidase reporter construct (Clontech) using LipofectAMINE (Invitrogen). After an additional 24-h incubation, cells were either mock-infected or infected with T3A at an m.o.i. of 100 plaque-forming units per cell and incubated at 37 °C for various intervals. Cells were then harvested and resuspended in 1 ml of sonication buffer (91 mM dithiothreitol, 0.91 M K<sub>2</sub>HPO<sub>4</sub> (pH 7.8), centrifuged at 2000  $\times g$  for 10 min, and resuspended in 100  $\mu$ l of sonication buffer. Cells were vortexed, frozen (-20 °C) and thawed three times, and centrifuged at 14,000  $\times g$  for 10 min. Samples (10  $\mu$ l) were assessed for luciferase activity after the addition of 350  $\mu$ l of luciferase assay buffer (85 mM dithiothreitol, 0.85 M K<sub>2</sub>HPO<sub>4</sub> (pH 7.8), 50 mM ATP, 15 mM MgSO<sub>4</sub>) by determining optical density in a luminometer (Monolight 2010, Analytical Luminescence Laboratory). Samples were assayed for  $\beta$ -galactosidase activity using standard procedures (32) to normalize for transfection efficiency.

**Western Blot Analysis**—After infection with reovirus, cells were pelleted by centrifugation, washed twice with ice-cold phosphate-buffered saline, and lysed by sonication in 200  $\mu$ l of a buffer containing 15 mM Tris, pH 7.5, 2 mM EDTA, 10 mM EGTA, 20% glycerol, 0.1% Nonidet P-40, 50 mM  $\beta$ -mercaptoethanol, 100  $\mu$ g/ml leupeptin, 2  $\mu$ g/ml aprotinin, 40  $\mu$ M Z-Asp-2,6-dichlorobenzoyloxime, and 1 mM phenylmethylsulfonyl fluoride. The lysates were then cleared by centrifugation at 16,000  $\times g$  for 5 min, normalized for the protein amount, mixed 1:1 with SDS sample buffer (100 mM Tris, pH 6.8, 2% SDS, 300 mM  $\beta$ -mercaptoethanol, 30% glycerol, and 5% pyronine Y), boiled for 5 min, and stored at -70 °C. Proteins were electrophoresed by SDS-PAGE (10% gels) and probed with antibodies directed against I $\kappa$ B $\alpha$  (Santa Cruz No. 203). All lysates were standardized for protein concentration with antibodies directed against actin (Oncogene No. CP01). Autoradiographs were quantitated by densitometric analysis using a Fluor-S MultiImager (Bio-Rad).

#### RESULTS

**Reovirus Induces the Activation of NF- $\kappa$ B in TRAIL-resistant HEK293 Cells**—Reovirus-induced apoptosis in a variety of epithelial cell lines, including HEK293 cells and HeLa cells, is mediated by TRAIL (7, 9). However, whereas reovirus induces similar levels of apoptosis 48 h pi in HeLa and HEK293 cells (Fig. 1A), these cell types differ substantially in their sensitivity to TRAIL-induced apoptosis (Fig. 1B).

We have previously shown that reovirus activates NF- $\kappa$ B in TRAIL-sensitive (HeLa) cells and that this activation is required for reovirus-induced apoptosis in these cells (15). To determine the role of NF- $\kappa$ B in reovirus-induced apoptosis in TRAIL-resistant cells we first investigated whether NF- $\kappa$ B is activated after reovirus infection of these cells. HEK293 cells were infected with reovirus (m.o.i. 100), and at various times pi nuclear extracts were prepared and incubated with a <sup>32</sup>P-labeled oligonucleotide probe comprising NF- $\kappa$ B binding sequences. After incubation with nuclear extracts from reovirus-infected cells the mobility of the oligonucleotide probe during electrophoresis was retarded, indicating the binding of activated NF- $\kappa$ B to the probe sequences (Fig. 2A). Activated NF- $\kappa$ B-probe complexes in reovirus-infected cells were present 2–4 h pi and were undetectable at later times pi. Binding specificity was demonstrated by the fact that an excess of cold NF- $\kappa$ B, but not SP-1, sequences prevented the appearance of

**A****B**

**FIG. 1. Reovirus and TRAIL-induced apoptosis in HeLa and HEK293 cells.** HEK293 and HeLa cells were treated with reovirus (m.o.i. 0, 10, 100) for 48 h (A) or TRAIL (0–200 ng/ml) for 24 h (B). The graph shows the mean percentage apoptosis obtained from three independent experiments. Error bars represent S.E.

both the reovirus-induced (Fig. 2, upper band) and non-stimulus-induced (Fig. 2, lower band) NF- $\kappa$ B-probe complexes (Fig. 2B).

Luciferase reporter gene assays were also used to show that NF- $\kappa$ B is activated after infection of HEK293 cells with reovirus infection. Cells were transfected with a construct containing the luciferase gene under the control of NF- $\kappa$ B binding sequences. After transfection, cells were infected with reovirus (m.o.i. 100), and at various times post-infection were harvested and assayed for luciferase activity. Fig. 2C shows that luciferase gene expression is increased after infection with reovirus. A 3-fold increase in reporter gene activity was detected as early as 6 h pi, peaked at 12 h pi (5-fold increase), and then declined (Fig. 2C). Luciferase reporter gene activity was not detected 12 h after reovirus infection of cells expressing a dominant negative form of I $\kappa$ B $\Delta$ N2, which lacks the sites necessary for I $\kappa$ B phosphorylation. The subsequent ubiquitination and degradation of I $\kappa$ B, which is necessary for NF- $\kappa$ B activation, is thus blocked in these cells. These results indicate that NF- $\kappa$ B is activated in a transient manner after reovirus-infection of HEK293 cells.

**NF- $\kappa$ B Activation Is Required for Reovirus-induced Apoptosis**—After having shown that NF- $\kappa$ B is activated after reovirus infection of TRAIL-resistant cells we next wished to determine whether NF- $\kappa$ B is required for reovirus-induced apoptosis in these cells. HEK293 were infected with reovirus, and at various times post-infection were harvested and assayed for apoptosis. Compared with mock-infected cells, reovirus infection resulted in a significant increase in the number of apoptotic cells at both 24 and 48 h pi. However, reovirus-induced apoptosis was blocked in cells expressing I $\kappa$ B $\Delta$ N2 (Fig. 3A). Reovirus-induced apoptosis was also assayed by measuring caspase 3-activity using a fluorogenic substrate assay. Increased caspase 3 activity, compared with mock-infected cells, was detected at 18 h (3-fold) and 24 h (7.5-fold) pi. Again, reovirus-induced caspase 3-activity was blocked in cells expressing I $\kappa$ B $\Delta$ N2 (Fig. 3B). These results indicate that NF- $\kappa$ B

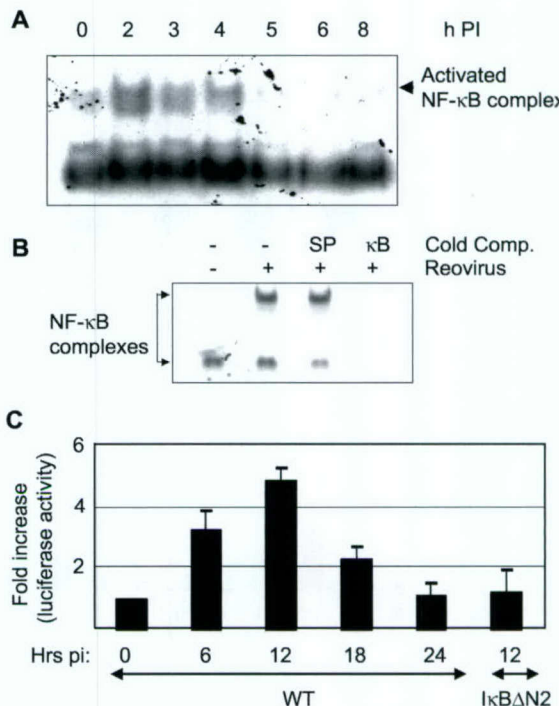


**FIG. 2. Activation of NF- $\kappa$ B after reovirus infection of HEK293 cells.** A, EMSA of reovirus-infected HEK293 cells. Nuclear extracts were prepared at various times after infection with reovirus (m.o.i. 100) and were incubated with a  $^{32}$ P-labeled oligonucleotide consisting of the NF- $\kappa$ B consensus binding sequence. Incubation mixtures were resolved by acrylamide gel electrophoresis, dried, and exposed to film. Reovirus-induced NF- $\kappa$ B-DNA complexes are indicated. B, specificity of reovirus-induced NF- $\kappa$ B-DNA complexes. HEK293 cells were infected with reovirus or were mock-infected. Nuclear extracts were prepared 4 h after infection, and EMSA analysis was performed using a  $^{32}$ P-labeled oligonucleotide consisting of the NF- $\kappa$ B consensus binding sequence. The gel shows NF- $\kappa$ B-DNA complexes present in nuclear extracts prepared from mock (lane 1) and reovirus (lane 2)-infected cells. Also shown are reactions from reovirus-infected cells incubated with an excess of cold oligonucleotide sequences comprising SP1 (lane 3) and NF- $\kappa$ B (lane 4) consensus binding sequences. C, NF- $\kappa$ B-dependent luciferase expression in reovirus-infected HEK293 cells. HEK293 cells ( $1.5 \times 10^5$ ) expressing wild type (WT) I $\kappa$ B or I $\kappa$ B $\Delta$ N2 were transfected with 1  $\mu$ g of a luciferase reporter construct containing NF- $\kappa$ B binding sites. After 24 h, cells were infected with T3A (m.o.i. 100) and incubated at 37 °C for the times shown. Cell extracts were then prepared, and luciferase activity was determined. The results are expressed as the mean luciferase units for three independent experiments. Error bars indicate S.E.

activation is required for reovirus-induced activation of caspase 3 and apoptosis.

**Reovirus Prevents the Activation of NF- $\kappa$ B by TNF $\alpha$  and Etoposide**—Although reovirus induces NF- $\kappa$ B after infection of HEK293 cells, this activation is transient in nature. We next investigated whether the transient nature of reovirus-induced NF- $\kappa$ B activation resulted from a block in NF- $\kappa$ B activation at later times pi. Both TNF $\alpha$  (100 ng/ml) and etoposide (100  $\mu$ M) are classic inducers of NF- $\kappa$ B and cause a rapid and robust activation of NF- $\kappa$ B in HEK293 cells as determined by the appearance of a shifted probe band after EMSA in treated, but not untreated cells (Fig. 4A). NF- $\kappa$ B binding was seen as early as 1 h after treatment with TNF $\alpha$  and etoposide and was persistent. Prior infection of cells with reovirus blocked the appearance of the TNF $\alpha$  and etoposide-induced-shifted probe band compared with that seen in mock-infected cells (Fig. 4B). In contrast, there was no difference in the intensity of the lower NF- $\kappa$ B-probe complex after etoposide or TNF $\alpha$  treatment in either mock or reovirus-infected cells. These results indicate that reovirus infection blocks the activation of NF- $\kappa$ B after treatment of HEK293 cells with TNF $\alpha$  or etoposide, indicating

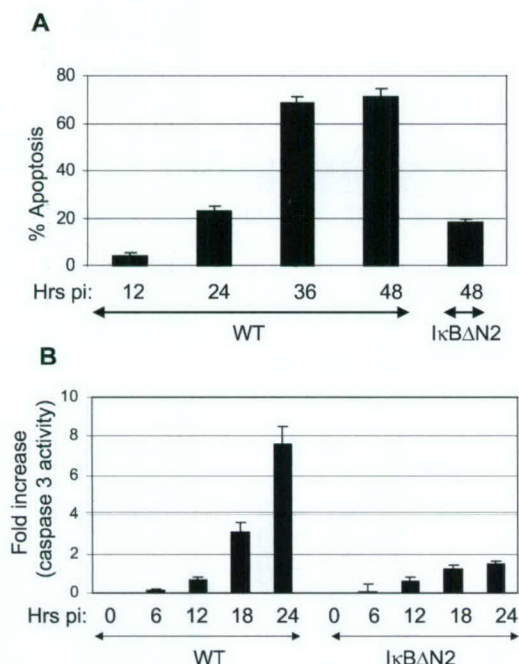


**FIG. 3. NF- $\kappa$ B activation is required for reovirus-induced apoptosis and caspase 3 activity.** HEK293 cells expressing wild type (WT) I $\kappa$ B or I $\kappa$ B $\Delta$ N2 were infected with reovirus (m.o.i. 100) and assayed for apoptosis (*A*) and caspase 3 activity (*B*) at various times p.i. The results are expressed as the mean percentage apoptosis or fold-activation obtained from three independent experiments. Error bars indicate S.E.

that reovirus infection both induces and then inhibits the activation of NF- $\kappa$ B.

**Reovirus Blocks the Degradation of I $\kappa$ B after Treatment of Cells with Etoposide and TNF**—Activation of NF- $\kappa$ B results from the stimulus-induced degradation of the inhibitor family of proteins, collectively known as I $\kappa$ B. Treatment of HEK293 cells with the NF- $\kappa$ B-inducing stimuli etoposide (100  $\mu$ M) and TNF (100 ng/ml) thus causes the degradation of I $\kappa$ B as detected by Western blot analysis using an antibody directed against I $\kappa$ B $\alpha$  (Fig. 5A). Degradation of I $\kappa$ B $\alpha$  is detectable around 1 h after treatment with both TNF and etoposide, and levels gradually decline over a 24-h period. In contrast, no changes in levels of I $\kappa$ B $\alpha$  were detected after reovirus infection (Fig. 5B). We next determined whether reovirus blocked etoposide- and TNF-induced activation of NF- $\kappa$ B by inhibiting I $\kappa$ B $\alpha$  degradation. Cells were infected with reovirus (m.o.i. 100). Then, at various times pi cells were treated with etoposide (100  $\mu$ M) or TNF (100 ng/ml). After a further 3 h, to allow etoposide and TNF-induced I $\kappa$ B $\alpha$  degradation, cells were harvested and assayed for the presence of I $\kappa$ B $\alpha$  by Western blot analysis. When etoposide was added 2 h after reovirus infection etoposide induced the degradation of I $\kappa$ B $\alpha$  as expected. However, by 4 h pi the ability of etoposide to induce the degradation of I $\kappa$ B $\alpha$  was inhibited, and at 12 h pi there was no degradation of I $\kappa$ B $\alpha$  after etoposide treatment (Fig. 5B). Similar results were obtained after TNF treatment of reovirus-infected cells (Fig. 5B). These results indicate that the mechanism by which reovirus inhibits NF- $\kappa$ B activation at later times pi involves inhibition of I $\kappa$ B degradation in reovirus-infected cells.

*Reovirus-induced Inhibition of Stimulus-induced IκBα Degradation Requires Viral RNA Synthesis*—The ability of reovirus to inhibit stimulus-induced IκBα degradation and subsequent NF-κB activation occurs somewhat later than would be expected for the initial events of viral infection, including re-

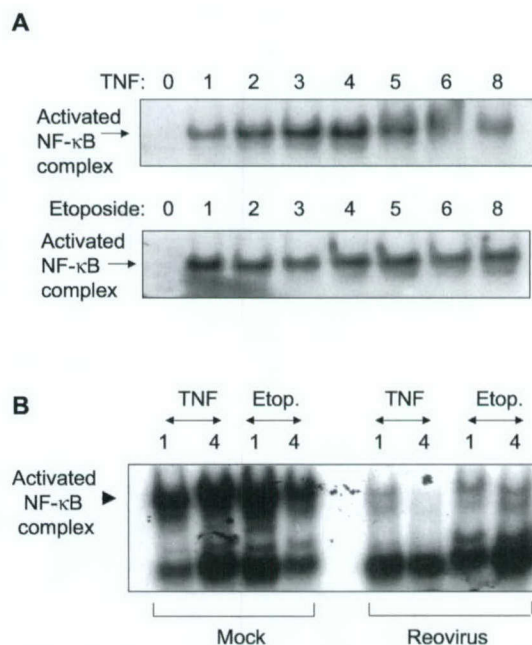


**FIG. 4. Reovirus prevents TNF $\alpha$  and etoposide-induced activation of NF- $\kappa$ B.** A, time course of NF- $\kappa$ B activation after treatment with TNF $\alpha$  and etoposide. HEK293 cells were treated with TNF $\alpha$  (100 ng/ml) or etoposide (100  $\mu$ M) for the indicated times. Nuclear extracts were then prepared, and EMSA analysis was performed using an oligonucleotide probe comprising NF- $\kappa$ B binding sequences. Shifted bands, corresponding to activated NF- $\kappa$ B-DNA complexes, are indicated. B, prior infection with reovirus prevents TNF $\alpha$ - and etoposide-induced NF- $\kappa$ B activation. HEK293 cells were infected with reovirus or were mock-infected. 12 h pi cells were treated with TNF $\alpha$  (100 ng/ml) or etoposide (100  $\mu$ M) (*Etop.*). Nuclear extracts were prepared after treatment at the times indicated, and EMSA was performed using an oligonucleotide probe comprising NF- $\kappa$ B binding sequences. Stimulus-induced NF- $\kappa$ B-DNA complexes are indicated.

ceptor binding, viral entry, and disassembly, and is more concurrent with the time at which viral proteins are produced in reovirus-infected HEK293 cells (not shown). Therefore we next investigated whether viral replication was required for reovirus-induced inhibition of I $\kappa$ B degradation. Ribavirin is a viral RNA synthesis inhibitor that inhibits reovirus replication (27). Cells were infected with reovirus (m.o.i. 100) in the presence or absence of ribavirin. 12 h after infection cells were treated with etoposide (100  $\mu$ M) for 3 h. They were then harvested and analyzed by Western blot analysis using an I $\kappa$ B antibody. Fig. 6A shows that etoposide treatment of mock-infected cells in the presence or absence of ribavirin, results in the degradation of I $\kappa$ B. As expected, in reovirus-infected cells the ability of etoposide to induce the degradation of I $\kappa$ B is blocked. However, etoposide does induce I $\kappa$ B degradation in cells treated with both reovirus and ribavirin, indicating that viral RNA synthesis is required for reovirus-induced inhibition of stimulus-induced I $\kappa$ B degradation.

**Reovirus-induced Apoptosis in HEK293 Cells Requires Viral RNA Synthesis**—Having shown that reovirus-induced inhibition of I $\kappa$ B degradation requires viral replication and is blocked in the presence of ribavirin, we investigated the effect of ribavirin on reovirus-induced apoptosis. HEK293 cells were infected with reovirus in the presence or absence of ribavirin. After 48 h cells were harvested and assayed for apoptosis. Ribavirin significantly inhibited reovirus (m.o.i. 100)-induced apoptosis in HEK293 cells (Fig. 6B), indicating that reovirus-induced inhibition of apoptosis of HEK293 cells requires viral RNA replication. In contrast, ribavirin did not inhibit reovirus-induced apoptosis in TRAIL-sensitive HeLa cells, as has previously been shown (27).

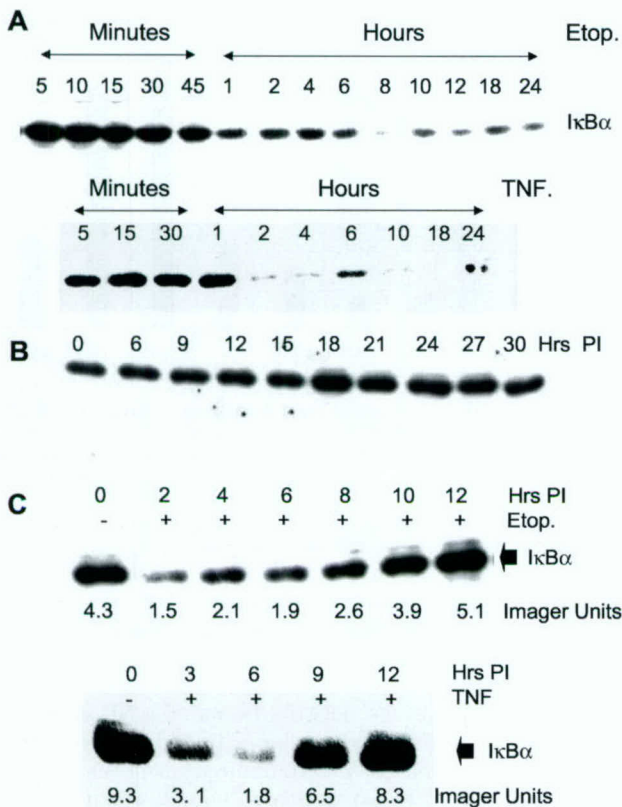


**FIG. 5. Reovirus prevents etoposide-induced degradation of IκB $\alpha$ .** *A*, time course of etoposide- and TNF-induced IκB $\alpha$  degradation. HEK293 cells were treated with etoposide (*Etop.*, 100  $\mu$ M) or TNF (100 ng/ml). After the indicated times cells were harvested for Western blot analysis. After SDS-PAGE, blots were probed with an anti-IκB $\alpha$  antibody. *B*, time course of levels of IκB $\alpha$  in reovirus-infected cells. HEK293 cells were infected with reovirus (m.o.i. 100). After the indicated times cells were harvested for Western blot analysis. After SDS-PAGE, blots were probed with an anti-IκB $\alpha$  antibody. *C*, reovirus prevents etoposide- and TNF-induced degradation of IκB $\alpha$ . HEK293 cells were infected with reovirus (m.o.i. 100). At the times indicated pi cells were treated with etoposide (100  $\mu$ M) or TNF (100 ng/ml). After a further 3 h, to allow these reagents to induce IκB $\alpha$  degradation, cells were harvested for Western blot analysis. After SDS-PAGE, blots were probed with an anti-IκB $\alpha$  antibody. Also shown are the results from densitometric analysis.

**Viral RNA Synthesis Is Required for Reovirus-induced Sensitization of Cells to TRAIL**—We have previously shown that reovirus sensitizes cells to TRAIL-induced apoptosis (7, 9). The fact that ribavirin blocks reovirus-induced apoptosis in TRAIL-resistant but not TRAIL-sensitive cells suggests the mechanism by which reovirus sensitizes cells to TRAIL requires viral RNA synthesis. HEK293 cells were thus infected with reovirus with or without ribavirin. 24 h post-infection cells were then treated with TRAIL, and apoptosis was assayed after a further 24 h. Fig. 6C shows that reovirus-induced sensitization of cells to TRAIL is inhibited in the presence of ribavirin, indicating that reovirus-induced sensitization of cells to TRAIL is dependent on viral RNA synthesis.

**Inhibition of NF- $\kappa$ B Activation Sensitizes Cells to Apoptosis Induced by TRAIL and TNF $\alpha$** —Our results indicate that ribavirin blocks both reovirus-induced apoptosis in TRAIL-resistant cells and reovirus-induced sensitization of TRAIL-resistant cells to TRAIL-induced apoptosis. Because ribavirin also blocks the ability of reovirus to inhibit NF- $\kappa$ B activation in infected cells at later times pi we wished to determine whether inhibition of NF- $\kappa$ B activation was the mechanism by which reovirus sensitizes TRAIL-resistant cells to TRAIL-induced apoptosis. HEK293 cells expressing IκB $\Delta$ N2 were treated with

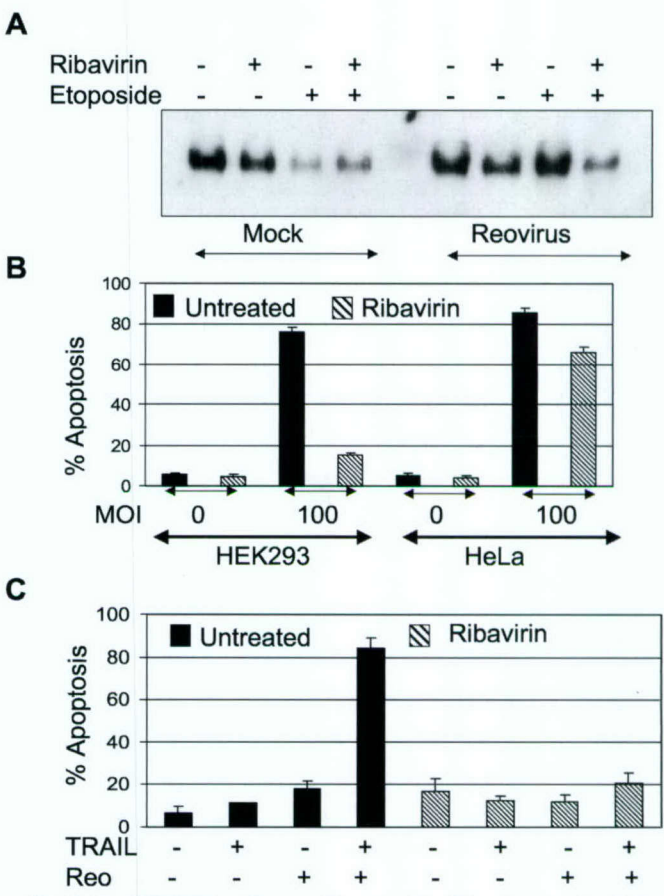


**FIG. 6. In HEK293 cells reovirus replication is required for reovirus-induced inhibition of NF- $\kappa$ B activation by etoposide, reovirus-induced apoptosis, and reovirus-induced sensitization of cells to TRAIL.** *A*, ribavirin blocks the ability of reovirus to inhibit etoposide-induced IκB $\alpha$  degradation. Cells were infected with reovirus or were mock-infected in the presence or absence of ribavirin. 12 h after infection, cells were treated with etoposide or were left untreated for 3 h before cells were harvested for Western blot analysis using an anti-IκB $\alpha$  antibody. *B*, ribavirin blocks reovirus-induced apoptosis in HEK293 cells. HEK293 cells and HeLa cells were infected with reovirus (m.o.i. 100) or were mock-infected (m.o.i. 0) in the absence (black bars) or presence (shaded bars) of ribavirin. After 48 h cells were harvested and assayed for apoptosis. The graph shows the mean percentage apoptosis obtained from three independent experiments. Error bars represent S.E. *C*, ribavirin blocks reovirus-induced sensitization of cells to TRAIL. HEK293 cells were infected with reovirus (m.o.i. 10) or were mock-infected in the absence (black bars) or presence (shaded bars) of ribavirin. 24 h after infection, cells were treated with TRAIL (20 ng/ml). After a further 24 h cells were harvested and assayed for apoptosis. The graph shows the mean percentage apoptosis obtained from three independent experiments. REO, reovirus. Error bars represent S.E.

various concentrations of TRAIL. At 24 h after treatment cells were harvested and assayed for apoptosis. High concentrations of TRAIL (200 ng/ml) did not induce significant levels of apoptosis in HEK293 cells expressing vector alone compared with untreated cells. In contrast, both 20 and 200 ng/ml TRAIL induced significant apoptosis in HEK293 cells expressing IκB $\Delta$ N2 (Fig. 7A). Apoptosis was also determined using caspase 3 activity assays. Cells were treated with similar concentrations of TRAIL and were harvested 4 h after treatment for caspase 3 activity assays. At 4 h pi TRAIL (20 and 200 ng/ml) induced caspase 3 activity in HEK293 cells expressing IκB $\Delta$ N2 but not in cells expressing vector alone (Fig. 7A). An 8-fold increase in caspase 3 activity was seen in TRAIL (20 ng/ml)-treated cells expressing IκB $\Delta$ N2 compared with cells expressing vector alone, and at 200 ng/ml TRAIL induced a 20-fold increase. The expression of IκB $\Delta$ N2, thus, sensitizes HEK293 cells to TRAIL-induced apoptosis, sug-

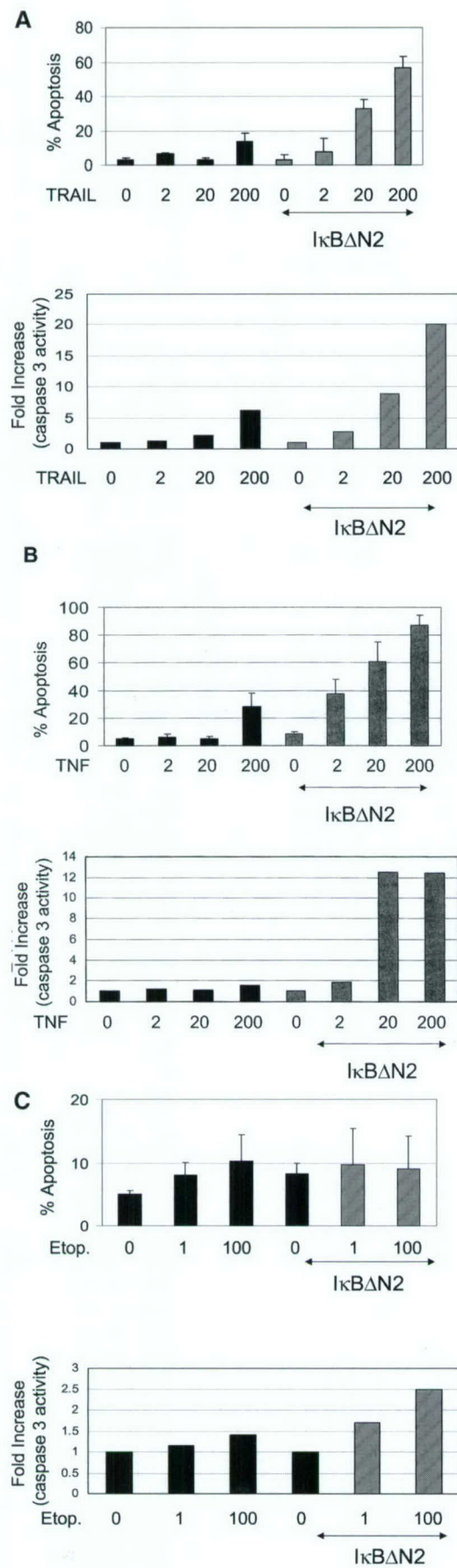


**FIG. 7. Expression of IκBΔN2 sensitizes cells to TRAIL and TNF $\alpha$ -induced apoptosis.** HEK293 cells expressing WT IκB or IκBΔN2 were treated with the indicated concentrations of TRAIL (A), TNF $\alpha$  (B), and etoposide (Etop., C). After treatment cells were harvested and assayed for apoptosis or caspase 3 activity. The graph shows the mean percentage apoptosis and fold-increase in caspase 3 activity obtained from three independent experiments. Error bars represent S.E.

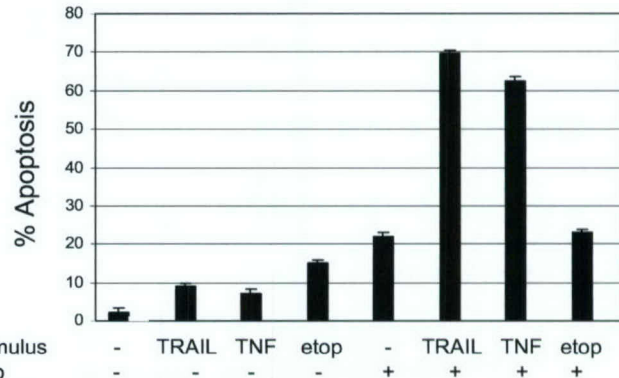


**FIG. 8. Reovirus sensitizes HEK293 cells to TRAIL and TNF $\alpha$ -induced apoptosis.** HEK293 cells were infected with reovirus (m.o.i. 10) or were mock-infected. 24 h after infection, cells were treated with TRAIL, TNF $\alpha$ , or etoposide (etop) or were left untreated. After a further 24 h, cells were harvested and assayed for apoptosis. The graph shows the mean percentage apoptosis obtained from three independent experiments. Error bars represent S.E. Reo, reovirus.

gesting that reovirus-induced inhibition of NF- $\kappa$ B activation is the mechanism by which reovirus sensitizes cells to TRAIL.

Fig. 4 shows that TNF $\alpha$  and etoposide induce the activation of NF- $\kappa$ B in HEK293 cells. TRAIL also induces NF- $\kappa$ B activation in these cells (31). Having shown that the expression of IκBΔN2 sensitizes cells to TRAIL-induced apoptosis, we next determined whether the expression of IκBΔN2 would also sensitize HEK293 cells to TNF and etoposide-induced apoptosis. Neither TNF $\alpha$  (200 ng/ml) nor etoposide (100  $\mu$ M) induced apoptosis in HEK293 cells. However, whereas levels of TNF $\alpha$  as low as 2 ng/ml induced significant apoptosis in cells expressing IκBΔN2 (Fig. 7B), the expression of IκBΔN2 did not sensitize cells to etoposide (100  $\mu$ M)-induced apoptosis (Fig. 7C). Similarly a 12-fold increase in caspase 3 activation was seen 24 h after TNF $\alpha$  (20 and 200 ng/ml) treatment of cells expressing IκBΔN2 but not after TNF $\alpha$  treatment of cells expressing vector alone (Fig. 7B). Again, caspase-3 activation was not enhanced in etoposide-treated cells expressing IκBΔN2 compared with cells expressing vector alone (Fig. 7C). These results indicate that the expression of IκBΔN2 sensitizes HEK293 cells to TRAIL and TNF $\alpha$  but not etoposide-induced apoptosis.

**Virus Infection Sensitizes HEK293 Cells to Apoptosis Induced by TNF $\alpha$  and TRAIL**—We have previously shown that reovirus infection sensitizes HEK293 cells to TRAIL-induced apoptosis. Results described above show that blocking NF- $\kappa$ B activation sensitizes cells to both TRAIL- and TNF $\alpha$ -induced apoptosis. Because reovirus-induced inhibition of NF- $\kappa$ B activation is the mechanism by which reovirus sensitizes cells to TRAIL-induced apoptosis, we wanted to determine whether the inhibition of NF- $\kappa$ B activation after reovirus infection would also sensitize these cells to TNF $\alpha$ -induced apoptosis. Cells were incubated with reovirus (m.o.i. 10). 24 h post-infection cells were then treated with TRAIL (20 ng/ml) or TNF $\alpha$  (20 ng/ml). Apoptosis was then determined after a further 24 h. Fig. 8 shows that TRAIL and TNF $\alpha$  alone do not induce apoptosis in HEK293 cells, as previously shown (Fig. 7). Infection of HEK293 cells with reovirus (m.o.i. 10) also induces only low levels (22%) of apoptosis in HEK293 cells (see Fig. 1). However, treatment of cells with TRAIL or TNF $\alpha$  in the presence of

TNF $\alpha$  (B), and etoposide (Etop., C). After treatment cells were harvested and assayed for apoptosis or caspase 3 activity. The graph shows the mean percentage apoptosis and fold-increase in caspase 3 activity obtained from three independent experiments. Error bars represent S.E.

reovirus produces high levels (70 and 63%) of apoptosis in HEK293 cells. These values are significantly greater than the sum of apoptosis induced by TRAIL and reovirus or TNF $\alpha$  and reovirus when these agents are used alone, indicating that reovirus infection acts synergistically with TRAIL and TNF $\alpha$  to induce apoptosis. In contrast, reovirus did not sensitize cells to etoposide-induced apoptosis, in agreement with the observation that the expression of I $\kappa$ B $\Delta$ N2 also does not sensitize these cells to etoposide.

#### DISCUSSION

Reovirus-induced apoptosis in human epithelial HEK293 cells and in several human cancer cell lines is mediated by TRAIL and is blocked by the presence of soluble TRAIL receptors and by anti-TRAIL antibodies (7, 9). However, reovirus can induce apoptosis in both TRAIL-sensitive and TRAIL-resistant cells. Reovirus, therefore, has the ability to sensitize TRAIL-resistant cells to TRAIL-induced apoptosis (7, 9). We have previously shown that in TRAIL-sensitive HeLa cells reovirus infection results in the activation of NF- $\kappa$ B and that this activation is required for reovirus-induced apoptosis (26). The results presented in this report describe the role of NF- $\kappa$ B in reovirus-induced apoptosis in TRAIL-resistant (HEK293) cells. We show that reovirus-induced NF- $\kappa$ B activation is highly regulated in these cells. At early times pi (2–4 h) reovirus activates NF- $\kappa$ B, as demonstrated by the presence of NF- $\kappa$ B in the nucleus of reovirus-infected cells and by the ability of this NF- $\kappa$ B to bind to radiolabeled oligonucleotide probe sequences comprising NF- $\kappa$ B binding sites. Activation of NF- $\kappa$ B-responsive genes after reovirus infection of HEK293 cells is also demonstrated by luciferase reporter gene assays. NF- $\kappa$ B activation is required for reovirus-induced apoptosis since reovirus-infection does not result in caspase 3 activity or apoptosis-associated changes in nuclear morphology in HEK293 cells expressing I $\kappa$ B $\Delta$ N2. These results are similar to those observed for TRAIL-sensitive HeLa cells and suggest that reovirus-induced apoptosis in TRAIL resistant cells also requires the expression of pro-apoptotic NF- $\kappa$ B-regulated genes.

Although required for virus-induced apoptosis, NF- $\kappa$ B activation is transient in both reovirus-infected TRAIL-sensitive and TRAIL-resistant cells. The transient nature of NF- $\kappa$ B activation in HEK293 cells results from the inhibition of NF- $\kappa$ B activation at later times pi since reovirus can block the ability of both etoposide and TNF $\alpha$  to induce NF- $\kappa$ B activation. This inhibition of NF- $\kappa$ B activation results from the inhibition of stimulus-induced I $\kappa$ B degradation and is time-dependent. Thus, at early times post-infection (2, 4 h) etoposide or TNF are still able to induce the degradation of I $\kappa$ B $\alpha$ . However, at later times post-infection (8–12 h) neither reagent induces I $\kappa$ B $\alpha$  degradation. These results are consistent with the fact that reovirus only activates NF- $\kappa$ B at early times pi.

Although the inhibition of NF- $\kappa$ B activation in reovirus-infected cells might be expected to induce a concordant increase in levels of I $\kappa$ B $\alpha$  at later times pi, we were unable to detect such a change. We predict that this is because of the low levels of NF- $\kappa$ B that are activated in reovirus-infected cells and the relative insensitivity of Western blotting compared with EMSA.

Reovirus-induced activation of NF- $\kappa$ B is not dependent on viral replication and occurs in the presence of ribavirin in both HeLa (27) and HEK293 cells.<sup>2</sup> Because the ability of reovirus to inhibit stimulus-induced NF- $\kappa$ B activation occurs somewhat later than the initial infection events (receptor binding, viral entry, and disassembly) and occurs around the time that viral

proteins are produced in reovirus-infected HEK293 cells (not shown), we next investigated whether viral RNA synthesis was required. In the presence of the viral RNA synthesis inhibitor ribavirin the ability of etoposide to induce the degradation of I $\kappa$ B was completely blocked, indicating that viral RNA synthesis is required for this process.

NF- $\kappa$ B regulates genes with both pro- and anti-apoptotic effects. The ability of reovirus to block NF- $\kappa$ B activation at later times post-infection enhances virus-induced apoptosis in TRAIL-resistant cells, as demonstrated by three lines of investigation. First, TRAIL-induced apoptosis is enhanced in HEK293 cells expressing I $\kappa$ B $\Delta$ N2. This indicates that blocking NF- $\kappa$ B activation sensitizes cells to TRAIL-induced apoptosis. Second, ribavirin, which blocks the ability of reovirus to inhibit stimulus-induced I $\kappa$ B degradation, blocks reovirus-induced apoptosis in TRAIL-resistant, but not TRAIL-sensitive cells. Finally, ribavirin also blocks the ability of reovirus to sensitize cells to TRAIL-induced apoptosis.

In neurons TNF $\alpha$  may be more important in mediating reovirus-induced apoptosis than TRAIL (5). The results presented here indicate that reovirus can also sensitize cells to TNF $\alpha$ -induced apoptosis by inhibiting NF- $\kappa$ B activation at later times pi, which may have important consequences for the ability of reovirus to induce apoptosis in these cells and to cause disease of the central nervous system in infected animals. The expression of I $\kappa$ B $\Delta$ N2 was not found to sensitize cells to etoposide-induced apoptosis. This suggests that etoposide induces apoptosis by a mechanism that is different from that induced by TRAIL and TNF $\alpha$ . Previous studies show that NF- $\kappa$ B activation is required for etoposide-induced apoptosis (32), supporting our observation that the expression of I $\kappa$ B $\Delta$ N2 does not sensitize HEK293 cells to etoposide-induced apoptosis.

Reovirus-induced apoptosis is mediated by TRAIL and involves the release of TRAIL from infected cells (7). Thus, the supernatant from reovirus-infected cells contains TRAIL and can induce apoptosis in TRAIL-sensitive cells (7). This apoptosis is blocked in the presence of soluble TRAIL receptors, indicating that it is specific to TRAIL and is not blocked in the presence of a neutralizing reovirus antibody, indicating that it is not due to residual virus in the supernatant. TRAIL released from reovirus-infected cells, thus, induces apoptosis by inducing receptor-mediated activation of caspase 8 (10). These results show that reovirus regulation of NF- $\kappa$ B is also critical for virus-induced apoptosis. NF- $\kappa$ B is first activated at early times after reovirus infection, an event that is required for apoptosis in both TRAIL-sensitive and TRAIL-resistant cells and which presumably acts to up-regulate the expression of pro-apoptotic NF- $\kappa$ B-regulated genes. Both TRAIL and its receptors are regulated by NF- $\kappa$ B (32–34). It is, thus, likely that the pro-apoptotic effects of NF- $\kappa$ B activation that are required for reovirus-induced apoptosis include the up-regulation of these genes.

TRAIL, DR4, and DR5 are up-regulated after reovirus-infection (7), although the involvement of NF- $\kappa$ B in this process has yet to be established. At later times pi, reovirus inhibits the activation of NF- $\kappa$ B in infected cells. This has the effect of blocking stimulus-induced NF- $\kappa$ B activation. In uninfected HEK293 cells TRAIL induces the activation of NF- $\kappa$ B (31). Our results suggest that TRAIL-induced NF- $\kappa$ B activation has an inhibitory effect on TRAIL-induced apoptosis in these cells. Thus, the ability of reovirus to block TRAIL-induced NF- $\kappa$ B activation will sensitize cells to TRAIL-induced apoptosis, therefore allowing both TRAIL and reovirus-induced apoptosis in TRAIL-resistant cells. The timing of reovirus-induced inhibition of stimulus-induced NF- $\kappa$ B activation is in accordance with TRAIL release from reovirus-infected cells, which occurs

<sup>2</sup> P. Clarke, S. M. Meintzer, L. Moffitt, and K. L. Tyler, unpublished data.

at later times pi (7). Thus, it appears that NF- $\kappa$ B activation is turned off in reovirus-infected cells before TRAIL is released to facilitate reovirus-induced apoptosis in TRAIL-resistant cells.

The ability of TRAIL to induce apoptosis in a variety of human cancer cells but not in normal cells has triggered the investigation of this reagent as a potential therapeutic agent for human cancers. However, many cancer cells are resistant to TRAIL-induced apoptosis. We have previously shown that reovirus can sensitize TRAIL-resistant human cancer cell lines to TRAIL-induced apoptosis. The results presented here suggest that the mechanism for this sensitization results from the ability of reovirus to block NF- $\kappa$ B activation. Other studies also indicate that blocking NF- $\kappa$ B activation can sensitize human cancer cells to TRAIL-induced apoptosis (35–37). Together these findings could have an important impact on the use of TRAIL as a potential cancer therapeutic in combination with other agents that inhibit NF- $\kappa$ B.

The NF- $\kappa$ B pathway provides an attractive target to viral pathogens for modulating host cell events. NF- $\kappa$ B promotes the expression of more than 100 genes that participate in the host immune response, oncogenesis, and regulation of apoptosis. In addition, activation of NF- $\kappa$ B is a rapid immediate early response that occurs within minutes after exposure to a relevant inducer, does not require *de novo* protein synthesis, and results in a strong transcriptional stimulation of several early viral as well as cellular genes. NF- $\kappa$ B is, thus, activated by multiple families of viruses, including human immunodeficiency virus type 1 (HIV-1) (38), human T-cell lymphotropic virus- (39), hepatitis B virus (40), hepatitis C virus (41, 42), Epstein-Barr virus (43), rotavirus (44), and influenza virus (45) to promote viral replication, prevent virus-induced apoptosis, and mediate the immune response to the invading pathogen (for review, see Ref. 46). In contrast, activation of NF- $\kappa$ B by Sindbis (47, 48) and Dengue virus (49) is associated with the induction of apoptosis, which may increase viral spread. In still other cases, proteins encoded by adenovirus (50), hepatitis C virus (51), and African swine fever virus (52) inhibit NF- $\kappa$ B activity to enhance replication or contribute to viral pathogenicity.

The results demonstrated here indicate that reovirus both activates and then inhibits NF- $\kappa$ B activity to efficiently induce apoptosis in infected cells. This is the first time that two phases of NF- $\kappa$ B regulation have been shown to be required to modulate viral-host interactions within a specific cell type. We propose that the complex regulation of NF- $\kappa$ B by reovirus is critical for TRAIL- and TNF $\alpha$ -induced apoptosis in reovirus-infected cells. Death receptor ligands are commonly used by viruses to induce apoptosis. For example, HIV infection increases the expression of TRAIL and sensitizes T-cells to TRAIL-mediated apoptosis (53). In addition, alteration of the cell surface expression of Fas may be involved in virus-induced or viral regulation of apoptosis in cells infected with influenza virus (54, 55), herpes simplex virus type 2 (56), bovine herpesvirus 4 (57), adenovirus (58) and HIV 1 (59, 60). Similarly, apoptosis induced by hepatitis B (61), HIV-1 (62), bovine herpesvirus 4 (57), and parvovirus H-1 (63) may involve the TNF receptor signaling pathway. NF- $\kappa$ B regulation is, thus, likely to have implications for apoptosis and disease resulting from a variety of viral infections.

## REFERENCES

- Tyler, K. L., Clarke, P., DeBiasi, R. L., Kominsky, D. J., and Poggioli, G. J. (2001) *Trends Microbiol.* **9**, 560–564
- Clarke, P., and Tyler, K. L. (2003) *Apoptosis* **8**, 141–150
- DeBiasi, R. L., Edelstein, C. L., Sherry, B., and Tyler, K. L. (2001) *J. Virol.* **75**, 351–361
- Oberhaus, S. M., Smith, R. L., Clayton, G. H., Dermody, T. S., and Tyler, K. L. (1997) *J. Virol.* **71**, 2100–2106
- Richardson-Burns, S. M., Kominsky, D. J., and Tyler, K. L. (2002) *J. Neurovirol.* **8**, 365–380
- DeBiasi, R. L., Squier, M. K. T., Pike, B., Wynes, W. M., Dermody, T. S., Cohen, J. J., and Tyler, K. L. (1999) *J. Virol.* **73**, 695–701
- Clarke, P., Meintzer, S. M., Gibson, S. B., Widmann, C., Garrington, T. P., Johnson, G. L., and Tyler, K. L. (2000) *J. Virol.* **74**, 8135–8139
- Kominsky, D. J., Bickel, R. J., and Tyler, K. L. (2002) *Cell Death Differ.* **9**, 926–933
- Clarke, P., Meintzer, S. M., Spalding, A. C., Johnson, G. L., and Tyler, K. L. (2001) *Oncogene* **20**, 6910–6919
- Ashkenazi, A., and Dixit, V. M. (1998) *Science* **281**, 1305–1308
- Deleted in proof
- Karin, M., and Lin, A. (2002) *Nat. Immunol.* **3**, 221–227
- Baeuerle, P., and Baltimore, D. (1989) *Genes Dev.* **3**, 1689–1698
- Ghosh, S., Gifford, A., Riviere, L., Tempst, P., Nolan, G., and Baltimore, D. (1990) *Cell* **62**, 1019–1029
- Baeuerle, P., and Baltimore, D. (1988) *Science* **242**, 540–546
- Verma, I. M., Stevenson, J. K., Schwarz, E. M., van Antwerp, D., and Miyamoto, S. (1995) *Genes Dev.* **9**, 2723–2735
- Brockman, J. A., Scherer, D. C., McKinsey, T. A., Hall, S. M., Qi, X., Lee, W. Y., and Ballard, D. W. (1995) *Mol. Cell. Biol.* **15**, 2809–2818
- Brown, K., Gersterberger, S., Carlson, L., Franzoso, G., and Siebenlist, U. (1995) *Science* **267**, 1485–1488
- Chen, Z., Hagler, J., Palombella, V. J., Melandri, F., Scherer, D., Ballard, D., and Maniatis, T. (1995) *Genes Dev.* **9**, 1585–1597
- Traenker, E. B., Pahl, H. L., Henkel, T., Schmidt, K. N., Wilk, S., and Baeuerle, P. A. (1995) *EMBO J.* **14**, 2876–2883
- Beg, A. A., Ruben, S. M., Scheimann, R. I., Haskill, S., Rosen, C. A., and Baldwin, A. J. (1992) *Genes Dev.* **6**, 1899–1913
- May, M. J., and Ghosh, S. (1997) *Semin. Cancer Biol.* **8**, 63–73
- Teodoro, J. G., and Branton, P. E. (1997) *J. Virol.* **71**, 1739–1746
- Connolly, J. L., Barton, E. S., and Dermody, T. S. (2001) *J. Virol.* **75**, 4029–4039
- Barton, E. S., Forrest, J. C., Connolly, J. L., Chappell, J. D., Liu, Y., Schnell, F. J., Nusrat, A., Parkos, C. A., and Dermody, T. S. (2001) *Cell* **104**, 441–451
- Connolly, J. L., Rodgers, S. E., Clarke, P., Ballard, D. W., Kerr, L. D., Tyler, K. L., and Dermody, T. S. (2000) *J. Virol.* **74**, 2981–2989
- Connolly, J. L., and Dermody, T. S. (2002) *J. Virol.* **76**, 1632–1641
- Tyler, K. L., Squier, M. K. T., Brown, A. L., Pike, B., Willis, D., Oberhaus, S. M., Dermody, T. S., and Cohen, J. J. (1996) *J. Virol.* **70**, 7984–7991
- Duke, R. C., and J. J. Cohen. (1992). *Current Protocols in Immunology*, pp. 3.17.1–3.17.16, John Wiley & Sons, Inc., New York
- Tyler, K. L., Squier, M. K. T., Rodgers, S. E., Schneider, B. E., Oberhaus, S. M., Grdina, T. A., Cohen, J. J., and Dermody, T. S. (1995) *J. Virol.* **69**, 6972–6979
- Shetty, S., Gladden, J. B., Henson, E. S., Hu, X., Villanueva, J., Haney, N., and Gibson, S. B. (2002) *Apoptosis* **7**, 413–420
- Gibson, S. B., Oyer, R., Spalding, A. C., Anderson, S. M., and Johnson, G. L. (2000) *Mol. Cell. Biol.* **20**, 205–212
- Ravi, R., Bedi, G. C., Engstrom, W., Zeng, Q., Mookerjee, B., Gelinas, C., Fuchs, E. J., and Bedi, A. (2001) *Nat. Cell Biol.* **3**, 409–416
- Spalding, A. C., Jotte, R. M., Scheinman, R. I., Geraci, M. W., Clarke, P., Tyler, K. L., and Johnson, G. L. (2002) *Oncogene* **21**, 260–271
- Thomas, R. P., Farrow, B. J., Kim, S., May, M. J., Hellmich, M. R., and Evers, B. M. (2002) *Surgery* **132**, 127–134
- Keane, M. M., Rubinstein, Y., Cuello, M., Ettenberg, S. A., Banerjee, P., Nau, M. M., and Lipkowitz, S. (2000) *Breast Cancer Res. Treat.* **64**, 211–219
- Oya, M., Ohtsubo, M., Takayanagi, A., Tachibana, M., Shimizu, N., and Murai, M. (2001) *Oncogene* **20**, 3888–3896
- Roulston, A., Lin, R., Beauparlant, P., and Wainberg, J. (1995) *Microbiol. Rev.* **59**, 481–505
- Sun, S. C., and Ballard, D. W. (1999) *Oncogene* **18**, 6948–6958
- Weil, R., Sirma, H., Giannini, C., Kremsdorff, D., Bessia, C., Dargemont, C., Brechet, C., and Israel, A. (1999) *Mol. Cell. Biol.* **19**, 6345–6354
- You, L. R., Chen, C. M., and Lee, Y. H. W. (1999) *J. Virol.* **73**, 1672–1681
- Tai, D. I., Tsai, S. L., Chen, Y. M., Chuang, Y. L., Peng, C. Y., Sheen, I. S., Yeh, C. T., Chang, K. S., Huang, S. N., Kuo, G. C., and Liaw, Y. F. (2000) *Hepatology* **31**, 656–664
- Sylla, B. S., Hung, S. C., Davidson, D. M., Hatzivassiliou, E., Malinin, N. L., Wallach, D., Gilmore, T. D., Kieff, E., and Mosialos, G. (1998) *Proc. Natl. Acad. Sci. U. S. A.* **95**, 10106–10111
- Casola, A., Garofalo, R. P., Crawford, S. E., Estes, M. K., Mercurio, F., Crowe, S. E., and Brasier, A. R. (2002) *Virology* **298**, 8–19
- Pahl, H. L., and Baeuerle, P. A. (1997) *Trends Biochem. Sci.* **22**, 63–67
- Hiscott, J., Kwon, H., and Genin, P. (2001) *J. Biol. Chem.* **107**, 143–151
- Lin, K. I., Lee, S. H., Narayanan, R., Baraban, J. M., Hardwick, J. M., and Ratan, R. R. (1995) *J. Cell Biol.* **131**, 1149–1161
- Lin, K. I., DiDonato, J. A., Hoffmann, A., Hardwick, J. M., and Ratan, R. R. (1998) *J. Cell Biol.* **141**, 1479–1487
- Jan, J. T., Chen, B. H., Ma, S. H., Liu, C. I., Tsai, H. P., Wu, H. C., Jiang, S. Y., Yang, K. D., and Shiao, M. F. (2000) *J. Virol.* **74**, 8680–8691
- Shao, R., Hu, M. C. T., Zhou, B. P., Lin, S. Y., Chiao, P. J., von Lindern, R. H., Spohn, B., and Hung, M. C. (1999) *J. Biol. Chem.* **274**, 21495–21498
- Shrivastava, A., Manna, S. K., Ray, R., and Aggarwal, B. B. (1998) *J. Virol.* **72**, 9722–9728
- Powell, P. P., Dixon, L. K., and Parkhouse, M. E. (1996) *J. Virol.* **70**, 8527–8533
- Jeremias, I., Herr, I., Boehler, T., and Debatin, K.-M. (1998) *Eur. J. Immunol.* **28**, 143–152
- Takizawa, T., Matsukawa, S., Higuchi, Y., Nakamura, S., Nakanishi, Y., and Fukuda, R. (1993) *J. Gen. Virol.* **74**, 2347–2355
- Takizawa, T., Fukuda, R., Miyawaki, T., Ohashi, K., and Nakanishi, Y. (1995) *Virology* **209**, 288–296
- Sieg, S., Yildirim, Z., Smith, D., Kayagaki, N., Yagita, H., Huang, Y., and

- Kaplan, D. (1996) *J. Virol.* **70**, 8747–8751
57. Wang, G. H., Bertin, J., Wang, Y., Martin, D. A., Wang, J., Tomaselli, K. J., Armstrong, R. C., and Cohen, J. I. (1997) *J. Virol.* **71**, 8928–8932
58. Tollefson, A. E., Hermiston, T. W., Lichtenstein, D. L., Colle, C. F., Tripp, R. A., Dimitrov, T., Toth, K., Wells, C. E., Doherty, P. C., and Wold, W. S. (1998) *Nature* **392**, 726–730
59. Conaldi, P. G., Biancone, L., Bottelli, A., Wade-Evans, A., Racusen, L. C., Boccellino, M., Orlandi, V., Serra, C., Camussi, G., and Toniolo, A. (1998) *J. Clin. Invest.* **102**, 2041–2049
60. Kaplan, D., and Sieg, S. (1998) *J. Virol.* **72**, 6279–6282
61. Su, F., and Schneider, R. J. (1997) *Proc. Natl. Acad. Sci. U. S. A.* **94**, 8744–8749
62. Herbein, G., Mahlknecht, U., Batiwalla, F., Gregerson, P., Pappas, T., Butler, J., O'Brian, W. A., and Verdin, E. (1999) *Nature* **395**, 189–194
63. Rayet, B., Lopez-Guerrero, J.-A., Rommelaere, J., and Dinsart, C. (1998) *J. Virol.* **72**, 8893–8903



## Reovirus-induced apoptosis: A minireview\*

P. Clarke and K. L. Tyler

Departments of Neurology (P. Clarke, K. L. Tyler), Medicine, Microbiology and Immunology (K. L. Tyler), University of Colorado Health Sciences, Denver, CO 80262 and Denver Veteran's Affairs Medical Center (K. L. Tyler), Denver, CO 80220, USA

**Reoviruses infect a variety of mammalian hosts and serve as an important experimental system for studying the mechanisms of virus-induced injury.** Reovirus infection induces apoptosis in cultured cells *in vitro* and in target tissues *in vivo*, including the heart and central nervous system (CNS). In epithelial cells, reovirus-induced apoptosis involves the release of tumor necrosis factor (TNF)-related apoptosis-inducing ligand (TRAIL) from infected cells and the activation of TRAIL-associated death receptors (DRs) DR4 and DR5. DR activation is followed by activation of caspase 8, cleavage of Bid, and the subsequent release of pro-apoptotic mitochondrial factors. By contrast, in neurons, reovirus-induced apoptosis involves a wider array of DRs, including TNFR and Fas, and the mitochondria appear to play a less critical role. These results show that reoviruses induce apoptotic pathways in a cell and tissue specific manner. *In vivo* there is an excellent correlation between the location of viral infection, the presence of tissue injury and apoptosis, indicating that apoptosis is a critical mechanism by which disease is triggered in the host. These studies suggest that inhibition of apoptosis may provide a novel strategy for limiting virus-induced tissue damage following infection.

**Keywords:** apoptosis; caspases; death receptors; mitochondria; reovirus.

### Introduction: Mammalian reoviruses

Reoviruses are non-enveloped, cytoplasmically replicating viruses comprised of two concentric protein capsids surrounding a genome consisting of 10 segments of double-stranded (ds) RNA.<sup>1</sup> Each dsRNA segment encodes a single protein, except for the S1 gene segment,

which is bicistronic. Reoviruses are ubiquitous viruses that have been isolated from a wide variety of mammalian species including humans. In humans, the viruses are still considered 'orphan viruses' as they have not been definitively linked to disease, although they have been associated with diarrheal illnesses, upper respiratory infections, hepatobiliary diseases, including biliary atresia, and rare cases of central nervous system (CNS) infection.<sup>2</sup> By contrast, natural and experimental infection of animals produces a wide variety of diseases. The most extensively studied experimental system involves infection of neonatal mice, where, depending on the viral strain and route of inoculation, reovirus infection in mice can produce disease in a variety of organs including the CNS and heart.<sup>2</sup>

### Reovirus-induced apoptosis is determined by the reovirus S1 and M2 gene segments

One of the most useful properties of reoviruses is the capacity to generate reassortant viruses when cells or animals are simultaneously coinfecte with two different strains of virus. Reassortants are progeny viruses that contain different combinations of gene segments derived from two infecting parental strains. By comparing the phenotype of these reassortant viruses to that of the parental viruses the role of specific virus genes in the determination of viral-induced phenotypes can be determined. This strategy has been employed to identify viral determinants of apoptosis in a variety of cultured cells. For example, the prototype reovirus strains, Type 1 Lang (T1L), Type 3 Dearing (T3D) and Type 3 Abney (T3A) differ in their ability to induce apoptosis in infected L929 fibroblasts, with T3D and T3A being significantly more apoptogenic than T1L. Analysis of two independent sets of reassortant viruses generated from T1L × T3D and T1L × T3A both identified a significant association between the capacity of viral reassortants to induce apoptosis and the presence of the T3 S1 and M2 gene segments.<sup>3,4</sup> These same two gene segments were also identified as important determinants

\*This work was supported by Public Health Service grant 1R01AG14071 from the National Institute of Health (KLT), Merit and REAP grants from the Department of Veterans Affairs (KLT), a U.S. Army Medical Research and Material Command grant #DAMD17-98-1-8614 (KLT), the Reuler-Lewin Family Professorship of Neurology (KLT) and the Ovarian Cancer Research Fund (PC).

Correspondence to: Dr. K. L. Tyler, Department of Neurology (B 182), University of Colorado, Health Sciences Center, 4200 East 9th Ave., Denver, CO 80262, USA. Tel: (+1) 303 393 2874; Fax: (+1) 303 393 4686; e-mail: Ken.Tyler@uchsc.edu

of apoptosis in Madin-Darby canine kidney (MDCK) cells and the S1 gene segment alone as a determinant of apoptosis in HeLa cells.<sup>5,6</sup>

In addition to determining the ability of reoviruses to induce apoptosis in infected cells the S1 gene segment is also a key determinant of reovirus-induced G<sub>2</sub>/M cell cycle arrest, an effect that results from inhibition of the G<sub>2</sub>/M regulatory kinase p34<sup>cdc2</sup> and the resulting inhibition of cellular DNA synthesis.<sup>4,7,8</sup> G<sub>2</sub>/M cell cycle arrest has recently been shown to be the result of the activity of the non-structural S1-encoded protein σ1s.<sup>7</sup> Infection of cells with a reovirus σ1s null-mutant virus (clone 84 MA) results in apoptosis without associated cell cycle arrest indicating that apoptosis and cell cycle dysregulation can be dissociated.<sup>7,9</sup> In addition, treatment of infected cells with caspase inhibitors, calpain inhibitors, or inhibition of NF-κB activation, all of which prevent apoptosis (see below), have no effect on reovirus-induced cell cycle arrest.<sup>7</sup>

In distinction to the key role played by the σ1s protein in reovirus-induced cell cycle arrest, several lines of evidence suggest that it is the S1-encoded σ1 protein that is the major determinant of reovirus-induced apoptosis. First, apoptosis can be induced by UV-inactivated replication-incompetent virions, which lack σ1s.<sup>3</sup> Second, apoptosis can also be induced at non-permissive temperatures by a variety of reovirus temperature-sensitive (ts)-mutants, which are arrested at defined steps in viral replication and fail to synthesize σ1s in infected cells.<sup>10</sup> Finally, the reovirus σ1s-null mutant clone 84MA fails to induce G<sub>2</sub>/M arrest in infected cells, but retains the capacity to induce apoptosis, indicating that σ1s is not required for this process.<sup>7,9</sup>

In both L929 cells and MDCK cells, but not HeLa cells, the reovirus M2 gene is associated with the S1 gene as a determinant of apoptosis. The M2 gene encodes the major viral outer capsid protein μ1/μ1c.<sup>3–6</sup> Linear regression analysis indicates that both the S1 and M2 genes contribute to the apoptotic phenotype and that the M2 effects are not simply the result of S1 and M2 being linked or co-segregating in the reassortant pools.<sup>3–5</sup> Incubation of infected cells with monoclonal antibodies (MAbs) directed against either the σ1 (viral attachment), σ3 or μ1 proteins (outer capsid) can inhibit apoptosis.<sup>3</sup> In the case of the σ1 MAbs this almost certainly reflects their capacity to inhibit viral cell attachment. However, both anti-μ1 and anti-σ3 MAbs, which do not inhibit viral cell attachment, but which do prevent virion-uncoating, can inhibit apoptosis.<sup>11</sup> These MAb studies and the determination of the M2 gene as a determinant of apoptosis, suggest that early events during viral entry, but subsequent to virus engagement of cellular receptors, are required for apoptosis. This interpretation has subsequently been supported by experiments using temperature sensitive (ts)-mutants blocked at different stages in the reovirus

replication cycle and pharmacological inhibitors of reovirus uncoating.<sup>10</sup>

## The reovirus attachment protein σ1

In virions, the reovirus σ1 protein is a homotrimer comprised of an elongated fibrous tail, which inserts into the virion, and an externally facing globular head.<sup>12</sup> The head of both the T1L and T3D σ1 proteins contain an independent receptor-binding domain that binds junction adhesion molecule (JAM).<sup>13</sup> The fibrous tail of the reovirus σ1 protein also contains receptor-binding domains.<sup>14</sup> In T3σ1 this additional region binds α-linked sialic acid, whereas a separate region of the T1 σ1 mediates the binding of T1L to an as yet unidentified cell surface carbohydrate.<sup>13–15</sup>

To investigate the contribution of the JAM and sialic acid binding domains during T3 reovirus infection mono-reassortant viruses were constructed containing the S1 gene from either the non-sialic-acid-binding strain T3C44 (strain T3SA–) or from the sialic-acid-binding strain T3C44-MA (strain T3SA+) on a T1L background.<sup>16–18</sup> As expected, experiments using these reassortant viruses show that T3SA– binds JAM while T3SA+ binds both JAM and sialic acid.<sup>13</sup> In addition, it was found that MAbs directed against hJAM (J10.4) completely block the ability of T3SA– to bind to human neuronal precursor (NT2) cells, indicating the requirement of JAM for T3 reovirus binding in the absence of sialic acid.<sup>13</sup> Antibodies directed against hJAM also significantly block the ability of T3SA+ to bind to NT2 cells and HeLa cells, although residual binding activity above background remained.<sup>13,18</sup> The fact that growth of T3SA+ in HeLa cells in the presence of mAb J10.4 is only minimally reduced (less than 2-fold at 48 hr) suggests that this residual binding activity is sufficient to act as a functional receptor when hJAM is absent or inaccessible.<sup>13</sup> T3SA– and T3SA+ grow equally well in L929 cells, however in HeLa cells T3SA– growth is reduced compared to that of T3SA+.<sup>6</sup> The binding of sialic acid in addition to JAM at early times post attachment is thus proposed to enhance both reovirus-attachment and growth in some cell types.<sup>6,18</sup>

Whereas there seems to be some flexibility on the binding of sialic acid and JAM for reovirus growth both of these receptors are required for the ability of reovirus to induce apoptosis in infected cells. Thus, T3SA+ induces high levels of apoptosis in both HeLa and L929 cells, whereas T3SA– induces little or no apoptosis in these cell types.<sup>6</sup> In addition, the removal of cell surface sialic acid with neuraminidase or the incubation of virus with sialyllectose, a trisaccharide comprised of lactose and sialic acid abolishes the capacity of T3SA+ to induce apoptosis.<sup>6</sup>

## Reovirus-induced apoptosis requires viral disassembly but not viral replication

Although the induction of apoptosis in reovirus-infected cells is dependent on viral binding to both the JAM receptor and sialic acid co-receptors, engagement of these receptors alone is not sufficient to elicit apoptosis and early steps in the viral replication cycle are also required. Following viral cell attachment and subsequent receptor-mediated endocytosis, reovirions are proteolytically disassembled to form infectious sub-virion particles (ISVPs); a process characterized by the removal of the outer capsid protein  $\sigma 3$ , proteolytic cleavage of  $\mu 1/\mu 1C$  and conformational changes in  $\sigma 1$ . Blocking proteolysis of reovirus virions with ammonium chloride, which inhibits endosomal acidification, or E64, which inhibits cysteine-containing endocytic proteases, blocks reovirus-induced apoptosis, indicating that viral disassembly is required for apoptosis in infected cells.<sup>10</sup> *In vitro* generated ISVPs are capable of inducing apoptosis, however like virions their ability to induce apoptosis is blocked by ammonium chloride suggesting that endosomal events are critical in inducing apoptosis and that this is not simply a result of the role endosomes play in mediating conversion of virions to ISVPs.<sup>10</sup>

Treatment of infected cells with the viral RNA synthesis inhibitor ribavirin does not prevent apoptosis.<sup>10</sup> In addition, particles lacking genomic dsRNA are capable of inducing apoptosis, indicating that the key apoptosis-initiating event precedes and does not require viral RNA synthesis.<sup>10</sup> Further, ts reovirus mutants with mutations resulting in defects in outer capsid assembly (tsB352/L2 gene), and in dsRNA synthesis (tsD357/L1 gene, tsE320/S3 gene) are capable of inducing similar levels of apoptosis at both non-permissive (39°C) and permissive (32°C) temperatures. Temperature sensitive mutants with defects in viral core (tsC447/S2 gene) and outer capsid assembly (tsG453/S4 gene) also still induce apoptosis at 39°C, but only about half as efficiently as they do at 32°C.<sup>10</sup> Since all these ts mutants undergo endosomal processing, their ability to induce apoptosis is consistent with a key role for endosomal vesicle-related events in apoptosis induction. However, the fact that assembly defects can influence the efficiency of this process suggests that non-endosomal factors also modulate this process.

The observation that UV-inactivated reovirions can induce apoptosis also indicates that replication is not absolutely required for induction of apoptosis, provided the inoculum size is sufficient.<sup>3</sup> Further support for the lack of a requirement for replication comes from studies in L929 and MDCK cells, which indicate that there is little correlation between the efficiency with which reovirus strains replicate in particular cells, and their capacity to induce apoptosis.<sup>3,5</sup> Consistent with these results, inhibition of

apoptosis in reovirus-infected cells, typically has either no effect on viral titer or results in modest titer reduction on the order of 0.5 log.<sup>19–21</sup>

## Reovirus induced apoptosis requires activation of the transcription factor NF- $\kappa$ B

Nuclear factor kappa B (NF- $\kappa$ B) is a transcription factor that is normally prevented from migrating to the nucleus and binding to DNA by its association in the cytoplasm with members of the I $\kappa$ B family of inhibitory proteins. Site specific phosphorylation, followed by ubiquitination and proteosomal degradation of I $\kappa$ B, allow for NF- $\kappa$ B activation. Reovirus-infection transiently activates NF- $\kappa$ B in a variety of cell types, including L929, MDCK and HeLa cells.<sup>20</sup> This activation can be detected by electrophoretic mobility shift assays (EMSA) as early as 4 h post infection (pi) and peaks at 10 h pi.<sup>20</sup> Similarly, expression of an NF- $\kappa$ B-dependent luciferase reporter gene is transient in reovirus-infected cells where expression is detectable at 12 h pi and peaks at 18 h pi.<sup>20</sup> Inhibition of NF- $\kappa$ B by stable over-expression of an I $\kappa$ B super-repressor or treatment of cells with a proteasome inhibitor that blocks I $\kappa$ B degradation (Z-L<sub>s</sub>VS) inhibits reovirus-induced apoptosis.<sup>20</sup> Apoptosis is also inhibited in immortalized mouse embryo fibroblasts (MEFs) with targeted disruptions in the genes encoding the p50 or p65 subunits of NF- $\kappa$ B.<sup>20</sup> These results suggest, in contradistinction to many other models of apoptosis, that at early times following reovirus infection NF- $\kappa$ B exerts a pro rather than anti-apoptotic influence.

Similar to reovirus-induced apoptosis, NF- $\kappa$ B activation in reovirus-infected cells requires the engagement of both the sialic acid and JAM receptors by the reovirus viral attachment protein,  $\sigma 1$ .<sup>6,13</sup> This observation, suggests that only sialic acid-binding reovirus strains, including most T3 strains, but no T1 strains, would activate NF- $\kappa$ B, a prediction that has not yet been tested. Again, similarly to reovirus-induced apoptosis, NF- $\kappa$ B activation in reovirus-infected cells requires viral disassembly but not viral replication.<sup>10</sup> The exact mechanism by which receptor engagement and viral disassembly activate NF- $\kappa$ B remains unknown although numerous potential mechanisms have been discussed.<sup>10,13,23</sup> It has been suggested that the conformational change in  $\sigma 1$  that occurs during disassembly may enhance the affinity of  $\sigma 1$  for sialic acid, JAM, or both receptors, leading to receptor aggregation and stimulation of intracellular signaling. Proteolytic processing of  $\mu 1/\mu 1C$  during virion disassembly may also influence virus-receptor interactions and would provide a mechanistic explanation for the contribution of the M2 gene to the efficiency of apoptosis.<sup>3–5</sup> Finally, JAM exists in a complex of tight junction proteins that includes the

ras-interacting protein AF-6. Since ras-mediated pathways have been implicated in the activation of NF- $\kappa$ B this may also constitute a mechanism whereby NF- $\kappa$ B is activated in reovirus-infected cells.

### **Reovirus-induced apoptosis is associated with the activation of JNK and the JNK-dependent transcription factor c-Jun**

Reovirus infection results in viral strain-specific patterns of selective activation of the c-Jun N-terminal kinase (JNK), extracellular-related kinase (ERK), and p38 mitogen-activated protein kinase (MAPK) signaling pathways in infected cells.<sup>23</sup> Activation of JNK can be detected within 10 h of T3-, but not T1L-, reovirus infection in L929 cells and increases steadily for the first 24 h. ERK shows a bimodal pattern of activation with an early phase resolving within 30 min of infection followed by a second activation phase detectable at 2 h pi. In distinction to JNK activation, the late phase of ERK activation appears equally robust in cells infected with T1L, T3A, and T3D.<sup>23</sup> In contrast to their activation of ERK and JNK, reovirus strains do not appear to activate p38 MAPKs.<sup>23</sup>

Pharmacologic inhibition of ERK activation does not either augment or inhibit reovirus-induced apoptosis indicating that the activation of this kinase is not required for reovirus-induced apoptosis.<sup>23</sup> By contrast, the capacity of reovirus strains to activate JNK correlates closely with their capacity to induce apoptosis.<sup>23</sup> In addition, experiments using T1L  $\times$  T3D reassortants indicate that the same viral gene segments that determine apoptosis induction (S1 and M2) are also key determinants of JNK activation.<sup>23</sup> Preliminary studies also suggest that inhibition of JNK activation with pharmacologic inhibitors inhibits reovirus-induced apoptosis (unpublished).

Reovirus-induced JNK activation is associated with the subsequent activation-related phosphorylation of the JNK-dependent transcription factor c-Jun.<sup>23</sup> Increased activation of c-Jun is detectable by 12 h pi, peaks at 12–24 h pi and then gradually declines to baseline by 48 hrs pi.<sup>23</sup> Although the specific receptor requirement for JNK and c-Jun activation has not been identified, the results described above suggest that, like apoptosis, engagement of both JAM and sialic acid will be necessary for JNK activation.

The requirement for and association of transcription factor activation with reovirus-induced apoptosis suggests that *de novo* expression of cellular genes and/or the consequences of activation of cellular MAPK signaling pathways mediate this process. Oligonucleotide micro-arrays have been utilized to analyze reovirus-induced changes in gene expression in infected cells and applica-

tion of this technology to identify changes in expression of apoptosis-related-genes and their transcription factor dependence is underway.<sup>24</sup>

### **Reovirus-induced apoptosis is initiated by activation of death receptors**

Many types of apoptosis triggered by extrinsic stimuli are initiated by activation of members of the tumor necrosis factor receptor (TNFR) superfamily of cell surface death receptors. In a wide variety of non-neuronal cells including L929 cells, human embryonic kidney (HEK293) cells and several human cervical (HeLa), breast, and lung cancer derived cell lines, TNF-related apoptosis-inducing ligand (TRAIL) and its receptors play a key role in reovirus-induced apoptosis.<sup>21,25</sup> TRAIL is a widely expressed type-2 membrane protein that was identified by its homology to Fas ligand (FasL) and TNF $\alpha$ . Following its release from cells TRAIL can induce apoptosis by binding to specific cell surface death receptors (DRs), DR4 (also called TRAIL-R1) and DR5 (also called Apo2, TRAIL-R2, TRACK2 or KILLER). TRAIL can also bind to the receptors DcR-1 (for Decoy Receptor 1) and DcR-2. These decoy receptors do not transduce apoptotic signals and can prevent the induction of apoptosis in TRAIL-treated cells. TRAIL-mediated activation of DR4 and DR5 triggers the onset of DR induced apoptosis, which involves DR oligomerization and the close association of their cytoplasmic death domains (DDs). This is followed by a DD-associated interaction with the cytosolic adapter molecule FADD (for Fas associated death domain), and the recruitment of pro-caspase 8 to form a death inducing signaling complex (DISC), where the cleavage of pro-caspase 8 results in the generation of the active initiator caspase, caspase 8. Caspase 8 then activates the effector caspases (caspases 3, 6 and 7), which are the proteolytic engines of cell death.<sup>26</sup>

In HEK293 cells, L929 cells and a variety of different cell lines derived from human cancers, reovirus-induced apoptosis is inhibited by the presence of anti-TRAIL antibodies or soluble TRAIL receptors (Fc:DR4 and Fc:DR5) and by the over-expression of the non-apoptosis-inducing TRAIL receptor DcR-1.<sup>21,25</sup> In contrast, antibodies directed against Fas and soluble TNF receptors appeared to have no effect on reovirus-induced apoptosis in these cells. Events downstream of TRAIL-receptor binding are also activated following reovirus infection. For example, pro-caspase 8 is cleaved to form the active initiator caspase, caspase 8.<sup>25,27</sup> In HEK293 cells the activation of caspase 8 occurs in two phases. An initial phase occurs between 8 and 14 h pi and a later phase occurs between 24 and 34 h pi, by which time all pro-caspase 8 has been cleaved.<sup>27</sup> Caspase-8-activity is required for reovirus-induced apoptosis in

HEK293 cells. Hence the expression of DN-FADD, and a peptide inhibitor of caspase 8-activity (IETD-FMK) block reovirus-induced apoptosis.<sup>21,27</sup> Caspase-8 activation following reovirus-infection is required for the activation of caspase 3, as demonstrated by the inhibition of reovirus-induced activation of caspase 3, in cells expressing FADD-DN.<sup>27</sup> Again reovirus-induced activation of caspase 3 is biphasic, with the first phase beginning around 8 hours pi and a second activation beginning at 24 h pi.<sup>27</sup> The kinetics of caspase 8 and caspase 3 activation suggest that these two events occur in rapid succession in reovirus-infected cells. Reovirus-induced caspase 3-activity corresponds closely to the cleavage of the cellular substrate PARP, indicating that caspase 3 has biological activity in infected cells and can participate in the cleavage of cellular substrates to induce the morphological hallmarks of apoptosis.<sup>10,25,27</sup>

Reovirus-infected cells release soluble TRAIL into the supernate, providing a potential mechanism for initiating both autocrine and exocrine (bystander) apoptosis. TRAIL release from infected cells can be detected using supernatant transfer experiments.<sup>21,25</sup> In these experiments cells are infected with reovirus and then, at various times following infection, the culture supernatant is removed and used to inoculate a TRAIL-sensitive indicator cell line (HeLa cells). Apoptosis is then determined 24 h following media-transfer. Apoptosis is induced in TRAIL-sensitive indicator cells following treatment with media taken from virus-infected HEK293 cells at 24, 38 and 48 h post-infection (18, 30 and 68% respectively).<sup>21</sup> This apoptosis is inhibited by soluble TRAIL receptors (Fc:DR5 or Fc:DR4) indicating it is TRAIL-specific. In contrast, apoptosis in the indicator cells is not blocked with a neutralizing polyclonal antireovirus antiserum that neutralizes both reovirus infection and apoptosis, indicating that apoptosis in the indicator line is not mediated by virus present in the transferred supernatant.

It has recently been shown that regulation of TRAIL and DR-expression is mediated by NF- $\kappa$ B in a variety of systems and that NF- $\kappa$ B activation is required for the up-regulation of TRAIL and DR-expression in cells undergoing apoptosis induced by HTLV-1 Tax and the chemotherapeutic agents etoposide and doxorubicin.<sup>28-31</sup> Studies are now underway to determine the role of NF- $\kappa$ B in mediating TRAIL and DR-expression during reovirus-induced apoptosis.

Binding of TRAIL to DR4/DR5 can induce activation of JNK and c-Jun through a TRAF 1/2-dependent process, providing a potential link between reovirus-induced death receptor activation and MAPK induction.<sup>32</sup> However, inhibition of TRAIL binding, using soluble Fc:DR5, inhibited reovirus-induced apoptosis but had no effect on reovirus-induced c-Jun activation.<sup>23</sup> In addition JNK activity in reovirus-infected cells precedes detectable TRAIL release.<sup>21,23,25</sup> These results indicate that JNK activation

in reovirus-infected cells is not merely a consequence of TRAIL/receptor binding and that other mechanisms of activation must be present.

## Reovirus-induced activation of mitochondrial apoptosis pathway

In addition to activating the effector caspases, caspase 8 can also cleave the pro-apoptotic Bcl-2 family member, Bid.<sup>33,34</sup> Cleaved Bid translocates to the mitochondria where, in conjunction with other pro-apoptotic Bcl-2 family proteins (e.g. Bak and Bax), it contributes to the opening, or modification, of channels in the mitochondrial membrane, allowing the release of pro-apoptotic factors, including cytochrome *c* and a second mitochondrial activator of apoptosis (Smac, also called DIABLO). Cytochrome *c* assists with the formation of a macromolecular complex (the apoptosome), which utilizes the apoptotic protease activating factor (APAF)-1 to mediate activation of the initiator caspase, caspase 9.<sup>35</sup> Smac/DIABLO binds to cellular inhibitor of apoptosis proteins (IAPs), preventing their inhibitory actions on caspase activity.<sup>36</sup> In addition to activating the effector caspases, caspase 9 can also cleave pro-caspase 8, through the activation of caspase 3, which may act to amplify the apoptotic response.<sup>37</sup> It is thought that in addition to releasing cytochrome *c* and Smac/DIABLO the mitochondria may also contribute to apoptosis by releasing stores of pro-caspase 8, which then become available for activation.<sup>38</sup> In some cell types activation of the mitochondrial pathway, through the caspase 8-dependent cleavage of Bid may be required for ligand-induced apoptosis, whereas other cells undergo ligand-mediated apoptosis without the involvement of the mitochondria. At the molecular level these cell types differ principally in the amount of caspase 8 recruited to the ligand-activated receptor.

The first indication that mitochondrial events were involved in reovirus-induced apoptosis came from the observation that reovirus-induced apoptosis is inhibited in MDCK cells that over-express Bcl-2, which inhibits the formation of pores in the mitochondrial membrane by binding to pro-apoptotic "pore-forming" Bcl-2 family members.<sup>5</sup> It was subsequently found that Bid is cleaved in HEK293 cells following infection with reovirus.<sup>27</sup> Similar to the activation of caspase 8, Bid cleavage is biphasic. The release of cytochrome *c* from the mitochondria of reovirus-infected cells at 10 hours pi and the associated activation of caspase 9 at approximately the same time, suggest that cleaved Bid is able to induce the activation of mitochondrial apoptotic pathways in reovirus-infected cells.<sup>27</sup> Both Bid cleavage and the release of cytochrome *c* are blocked in cells expressing DN-FADD, indicating that caspase 8 activity is required for activation of the mitochondrial apoptotic pathway in reovirus-infected cells.<sup>27</sup>

Smac/DIABLO is also released from the mitochondria of reovirus-infected cells with similar kinetics to the release of cytochrome *c* and, like cytochrome *c*, Smac/DIABLO release is blocked by the over-expression of Bcl-2.<sup>27</sup> Although reovirus-infection results in both cytochrome *c*-mediated caspase 9 activation and Smac/DIABLO release, recent studies suggest that it is likely that Smac/DIABLO release, rather than caspase 9 activation, plays a critical role in the mitochondrial-related augmentation of death-receptor initiated apoptotic pathways.<sup>39</sup> Thus, stable transfection of HEK293 cells with DN-caspase 9 (caspase 9b) only inhibits caspase 9-activation, unlike Bcl-2 over-expression, which blocks all mitochondrially-mediated events.<sup>39</sup> Similarly, caspase 9b expression prevents the activation of caspase 9 in reovirus-infected cells but does not affect reovirus-induced activation of caspase 3 or reovirus-induced PARP cleavage, suggesting that although caspase 9 is activated in reovirus-infected cells, other pathways are necessary for effector caspase activation.<sup>39</sup>

As noted, Smac/DIABLO acts as a pro-apoptotic factor by inhibiting IAP-mediated caspase inhibition.<sup>36</sup> This may be mediated through direct binding of Smac/DIABLO with target IAPs.<sup>36,40–42</sup> Alternatively, IAP degradation has also been shown to represent an important apoptotic event in both mammalian cells and in drosophila where proteins with regions homologous to Smac/DIABLO (Grim and REAPER) promote ubiquitin-mediated DIAP1 degradation.<sup>43–46</sup> The fact that in reovirus-infected cells some cellular IAPs (survivin, cIAP1 and XIAP) undergo proteolytic cleavage and degradation following reovirus-infection, and that this can be prevented in cells over-expressing Bcl-2, is consistent with a key role for Smac/DIABLO in mediating mitochondrial-related reovirus-induced apoptotic pathways.<sup>39</sup>

In addition to cytochrome *c* and Smac/DIABLO, a variety of other mitochondrial apoptotic factors have been identified, including apoptosis inducing factor (AIF). Reovirus infection is not associated with release of AIF in HEK293 cells.<sup>39</sup> Neither does it result in disruption of mitochondrial transmembrane potential, indicating that the release of pro-apoptotic factors from the mitochondria following reovirus infection is selective.<sup>39</sup> This is consistent with ultrastructural studies in reovirus-infected cells that suggest that disruption of mitochondrial architecture is not a typical feature of reovirus infection.

As previously described, activation of both caspase-8 and Bid show a biphasic pattern with an early-activation phase at 8–10 h pi followed by a later activation phase.<sup>27</sup> In contrast, reovirus-induced release of Smac/DIABLO is not biphasic and occurs just after the early phase and before the late phase of caspase 8-activation and Bid cleavage.<sup>27</sup> Over-expression of Bcl-2 inhibits the late phase of caspase 8 activation without affecting the early phase, suggesting that the late phase is mitochondrial-dependent. Taken to-

gether these results are consistent with a model in which death-receptor activation initiates reovirus apoptosis, and results in early low level activation of effector caspases. Mitochondrial-events, likely initiated by Bid translocation and involving release of Smac/DIABLO, then amplify the initial death receptor-initiated signal and dramatically augment effector caspase activation.

In addition to caspase 3, the effector caspase, caspase 7 is also activated following reovirus infection.<sup>27</sup> This activation occurs later than the first phase of caspase 3-activity and is less robust suggesting that caspase 7 activation may play a less critical role in reovirus-induced apoptosis than caspase 3. In addition, the observations that caspase 7 activation parallels that of caspase 9 and is not biphasic suggest that it may result from the activation of caspase 9.

## Reovirus sensitizes cells to TRAIL—Induced apoptosis

In addition to inducing the release of TRAIL from infected cells, reovirus-infection also sensitizes cells to TRAIL-induced apoptosis.<sup>21,25</sup> This sensitization is detectable around 12 h pi and increases until 48 h pi when the majority of cells are apoptotic.<sup>21</sup> Reovirus infection and TRAIL treatment have synergistic rather than merely additive effects on apoptosis, and infection can confer TRAIL sensitivity to previously TRAIL-resistant cells as well as increasing the TRAIL sensitivity of partially resistant lines.<sup>21,25</sup> For example, reovirus infection increases apoptosis in TRAIL-treated HEK293 cells from 30% to 90%, in a TRAIL-treated human breast cancer cell line (ZR75-1) from <10% to 80%, in a TRAIL-treated human lung cancer cell line (H157) from 10% to 70% and in a TRAIL-treated human ovarian cancer cell line (OVCAR-3) from 10% to 80% (unpublished).<sup>21,25</sup> This finding may increase the potential utility of TRAIL as an agent for cancer therapy, which is currently limited by the fact that cancer cells of all types differ in sensitivity to TRAIL-induced apoptosis. Although TRAIL receptor expression may be up-regulated in HEK293 cells the ability of reovirus to sensitize cells to TRAIL does not appear to reflect an increase in the expression of TRAIL receptors in several human cancer cell lines.<sup>21</sup> In the human lung cancer cell line, H157, reovirus-induced sensitization of cells to TRAIL is associated with an increase in the activation of caspase 8 and caspase 3 and is blocked by the caspase 8 inhibitor IETD-FMK.<sup>25</sup>

## Reovirus-induced apoptosis requires calpain

Although the caspase family of cellular proteases are central to reovirus-induced apoptosis, the calcium dependent

papain-like neutral cysteine protease, calpain, also plays a role in this process. Calpain is distributed widely throughout the cytosol of many cell types and exists as an inactive pro-enzyme in steady state with its endogenous inhibitor calpastatin. Calpains have been demonstrated to mediate differentiation and necrosis and to participate in caspase-dependent and caspase-independent apoptosis.

Reovirus-induced apoptosis in L929 cells and in myocardiocytes is associated with an increase in cellular calpain activity.<sup>19,47</sup> Increased calpain activity is seen in reovirus-infected cells, compared to mock-infected cells, as early as 2 h pi and this activation is suppressed by the addition of the calpain active-site inhibitor, N-acetyl-leucyl-leucyl-norleucinal (aLLN, calpain inhibitor 1) and by a second calpain inhibitor, PD150606, an  $\alpha$ -mercaptopropionic acid derivative that selectively blocks calpain's calcium-binding site inhibitor.<sup>19</sup> Calpain inhibitors also block apoptosis induced by T3A, T1L and UV-inactivated reovirus indicating the role of calpain in this process. Calpain activation has also been shown to occur in reovirus-infected primary cardiac myocytes and again treatment of these cells with a calpain inhibitor (Z-leu-aminobutyric acid-CONH(CH<sub>2</sub>)<sub>3</sub>-morpholine, CX295) protects them from reovirus-induced apoptosis. Further, CX295 also dramatically reduces the extent of apoptotic myocardial injury in reovirus-infected mice (see below).<sup>47</sup> The precise step in reovirus-induced apoptosis at which calpains act is unclear. In most models of apoptosis calpains act upstream of caspases and the early onset of calpain activity in reovirus-infected cells suggests that this may also be true for reovirus-induced apoptosis. Experiments showing the effect of calpain inhibitors on caspase-activation would be useful to confirm this possibility. Calpain has also been implicated in the regulation of a variety of cellular transcription factors, including NF- $\kappa$ B and c-Jun activation, which may both play a role in reovirus-induced apoptosis.<sup>48–50</sup>

## Reovirus-induced apoptosis in the mouse CNS

It has long been known that T3 reovirus strains infect neurons within specific regions of neonatal mouse brain producing a lethal meningoencephalitis. Viral replication and pathology co-localize in the brain and have a predilection for the cortex hippocampus and thalamus. It has now been shown that reovirus induces apoptosis in the brain following intracerebral inoculation of newborn mice with T3D and fragmentation of DNA into oligonucleosomal length ladders can be detected in tissue samples prepared from T3D— but not mock-infected brain (8–9 days pi), coinciding with maximal viral growth.

In an effort to determine the relationship between pathology, apoptosis, and viral infection, brain sections

have been stained with TUNEL and antibodies specific for activated caspase 3 to detect apoptosis, and with polyclonal anti-reovirus antisera to detect viral antigen. At a macroscopic level there is an excellent correlation between areas of tissue injury, the presence of apoptotic cells, and the localization of viral infection.<sup>51,52</sup> At a microscopic level, individual cells can also be analyzed for the presence of viral antigen and apoptosis. In brain, most cells in infected regions are both TUNEL-positive and reovirus antigen-positive, however there are cells in these regions that are apoptotic but antigen negative.<sup>51,52</sup> This suggests that apoptosis occurs both as a result of direct viral infection, and in uninfected 'bystander' cells adjacent to productively infected cells.

Studies of reovirus-infection in a mouse neuroblastoma-derived cell line (NB41a3) and in primary mouse cortical cultures (MCC) derived from embryonic (E20) mice indicate that reovirus-induced apoptosis of neurons is similar to reovirus-induced apoptosis of non-neuronal cells in that it is associated with increased levels of caspase 3-activity and is blocked with the caspase 3-inhibitor DEVD-FMK.<sup>52</sup>

Again, similar to the mechanism of reovirus-induced apoptosis in epithelial cells reovirus infection induces increased caspase 8 activation in infected neurons, indicating that neuronal apoptosis, like that in its epithelial cell counterparts, involves death-receptor activation.<sup>52</sup> However, the ligand-receptor trigger for this activation appears to be less specific than that observed in epithelial cells. Thus, whereas reovirus-induced apoptosis in HEK293 cells is selectively inhibited by blocking TRAIL ligand/receptor interaction, reovirus-induced apoptosis in NB4 cells is inhibited by treating cells with both soluble TRAIL receptors (Fc:DR5) and soluble TNFR (FcTNFR-1), and reovirus-induced apoptosis in MCCs is inhibited by Fc:TNFR-1 and Fc:Fas.<sup>52</sup>

Another distinction between reovirus-induced apoptosis in neuronal and epithelial cells may be the extent of involvement of the mitochondrial pathway. In contrast to HEK cells, in which reovirus infection is associated with robust release of cytochrome *c* and the subsequent activation of caspase 9, in neuronal cultures cytochrome *c* release appears to occur only at low levels and at later times following infection.<sup>52</sup> As would be predicted from this result, there is only low level activation of caspase 9 in these cells.<sup>52</sup> Consistent with these findings, the caspase 9 inhibitor Z-LEHD-FMK has little effect on reovirus-induced neuronal apoptosis, which is significantly inhibited by either caspase 8 (Z-IETD-FMK), caspase 3 (Z-DEVD-FMK) or pan-caspase inhibitors.<sup>52</sup> Studies are currently underway to determine if Smac/DIABLO or other pro-apoptotic factors are released during reovirus-induced neuronal apoptosis.

Studies of reovirus-infection in neuronal cultures also provide further evidence of bystander apoptosis seen

following reovirus infection and in both MCC and NB4 cells dual labeling with immunocytochemistry and TUNEL showed that although a great majority of infected cells were undergoing apoptosis there was also a subset of apoptotic cells that were uninfected but located in proximity to virus-infected cells.<sup>52</sup> Bystander apoptosis could result from the release of TRAIL, or other death ligands, from reovirus-infected cells. If this is the case the amount of bystander apoptosis would reflect the sensitivity of the surrounding cells to the released ligand.

## Reovirus-induced apoptosis is responsible for tissue injury

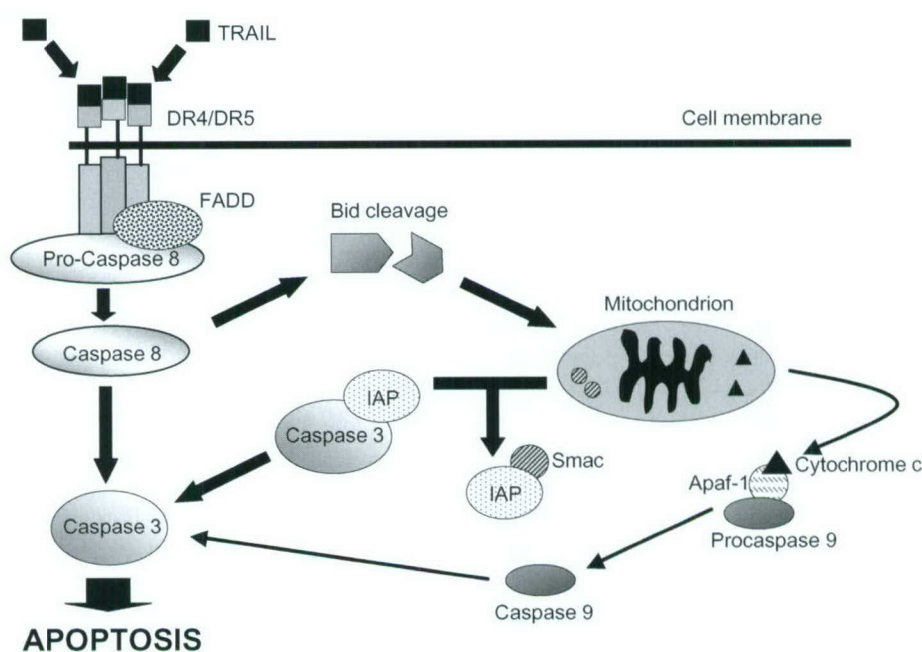
Although studies in the mouse CNS show that apoptotic cells are restricted to the same regions of the brain in which infected cells and tissue damage occur, the actual demonstration that reovirus-induced disease results from apoptosis came from studies using reovirus strain 8B, a virus that efficiently produces myocarditis in infected neonatal mice.<sup>43</sup> In this model, reovirus infection results in apoptosis in the heart. Similar to results seen in the mouse brain, DNA extracted from the hearts of reovirus-infected mice is fragmented into oligonucleosomal-length ladders, indicative of apoptosis.<sup>47</sup> Also similar to results seen in

reovirus-infected brain tissue, areas of TUNEL positive cells in 8B infected hearts correlate with areas of histologic damage and reovirus antigen.<sup>47</sup> Injury to the heart following reovirus-infection occurred in the absence of an inflammatory response, also suggesting that it results from apoptotic cell death.<sup>47</sup>

Treatment of mice with the calpain inhibitor CX295 (dipeptide alpha-ketoamide calapin inhibitor z-Leu-aminobutyric acid-CONH(CH<sub>2</sub>)<sub>3</sub>-morpholine) is protective against reovirus induced-myocarditis and produces a dramatic reduction in histopathologic evidence of myocardial injury, a reduction in serum creatine phosphokinase (an intracellular enzyme whose release into the serum is a quantitative marker of skeletal and cardiac muscle damage) and improved weight gain.<sup>47</sup> Prevention of myocardial injury is accompanied by a virtually complete inhibition of apoptotic myocardial cell death, strongly suggesting that virus-induced apoptosis is a key mechanism of cell death, tissue injury and mortality in reovirus-infected mice.

Although treatment of reovirus-infected animals results in a marked decrease in apoptosis in infected tissues, the impact on viral titer is less dramatic, and only a 0.5 log<sub>10</sub> PFU/ml reduction is observed at the site of primary replication primary (hind limb) and only a 0.7 log<sub>10</sub> PFU/ml reduction is observed in the heart.<sup>47</sup> These

**Figure 1.** TRAIL mediated apoptosis in reovirus-infected epithelial cells. Reovirus induces the release of TRAIL from infected cells. TRAIL binds to DR4 and DR5 initiating their association with FADD and pro-caspase 8. Cleavage of pro-caspase 8 results in the activation of caspase 8, which then activates caspase 3 to induce apoptosis. Caspase 8 also cleaves Bid to activate the mitochondrial apoptotic pathway resulting in the release of cytochrome c and Smac/DIABLO into the cytosol. Cytochrome c assists with the formation of the apoptosome, which utilizes APAF-1 to mediate activation of caspase 9. The release of Smac/DIABLO from the mitochondria results in the release of IAP inhibition of caspase 3-activity and leads to the onset of apoptosis. The broad arrows indicate events that are thought to be critical for reovirus-induced apoptosis in HEK cells, whereas the thin arrows represent events that may be less important.



results are similar to those obtained *in vitro* and indicate that inhibiting apoptosis has only a modest effect on virus growth.

## Conclusions and future directions

Over the past few years considerable advances have been made in our knowledge of reovirus-induced apoptosis, both *in vitro* and *in vivo*. Reovirus triggers apoptosis during its attachment and disassembly in infected cells. In epithelial cells, these events stimulate a variety of cellular pathways, including the activation of the cellular transcription factors NF- $\kappa$ B and c-Jun, the release of TRAIL from infected cells and the subsequent activation of TRAIL-apoptotic pathway. TRAIL-induced apoptosis in reovirus-infected cells is associated with the activation of the death-receptor associated caspases, caspase 8 and 3 (Figure 1). The subsequent activation of the mitochondrial apoptotic pathway in reovirus-infected cells, which requires caspase 8 activity, releases both cytochrome *c* and Smac/DIABLO into the cytoplasm. The action of Smac/DIABLO appears to be a key mitochondrial event in augmenting reovirus induced apoptosis, presumably through its action on cellular IAPs. In neurons, the pathways of virus-induced apoptosis are also initiated through death receptors, although both TNFR and Fas may play a role in addition to DR4/DR5. In addition, the mitochondrial pathway may be less important in augmenting DR-initiated apoptosis in neurons, as compared to epithelial cells, although the precise role of Smac/DIABLO remains to be established in these cells. The differences between neurons and non-neuronal cells clearly indicate that the same virus may differentially activate cellular apoptotic pathways in a cell and tissue specific manner.

Although the mechanisms of reovirus-induced apoptosis are becoming increasingly understood, a number of important questions remain. For example: (1) What are the specific links between the requirement for cellular transcription factors such as NF- $\kappa$ B and c-Jun and the initiation of cellular apoptotic pathways? (2) What role does the selective activation of MAPK cascades play in reovirus-induced apoptosis and how is this mediated? (3) What role does calpain play in reovirus-induced apoptosis, and how is this linked to caspase cascades, transcription factor activation, and MAPK cascades? (4) Can organ specific differences in apoptotic pathways be identified, and will this influence the response of these organs to specific anti-apoptotic therapies?

## References

- Nibert ML, Schiff, LA. Reoviruses and their replication. In: Fields BN, Knipe DM, Howley PM, eds. *Fields Virology*. Philadelphia: Lippincott-Raven Publisher, 2001: 1679–1728.
- Tyler KL. Mammalian reoviruses. In: Fields BN, Knipe DM, Howley PM, eds. *Fields Virology*. Philadelphia: Lippincott-Raven Publisher, 2001: 1729–1747.
- Tyler KL, Squier MKT, Rodgers SE, et al. Differences in the capacity of reovirus strains to induce apoptosis are determined by the viral attachment protein sigma 1. *J Virol* 1995; 69: 6972–6979.
- Tyler KL, Squier MKT, Brown AL, et al. Linkage between reovirus-induced apoptosis and inhibition of cellular DNA synthesis: Role of the S1 and M2 genes. *J Virol* 1996; 70: 7984–7991.
- Rodgers SE, Barton ES, Oberhaus SM, et al. Reovirus-induced apoptosis of MDCK cells is not linked to viral yield and is blocked by Bcl-2. *J Virol* 1997; 71: 2540–2546.
- Connolly JL, Barton ES, Dermody TS. Reovirus binding to cell surface sialic acid potentiates virus-induced apoptosis. *J Virol* 2001; 75: 4029–4039.
- Poggio GJ, Keefer C, Connolly JL, Dermody TS, Tyler KL. Reovirus-induced G<sub>2</sub>/M cell cycle arrest requires σ1s and occurs in the absence of apoptosis. *J Virol* 2000; 74: 9562–9570.
- Poggio GJ, Dermody TS, Tyler KL. Reovirus-induced G<sub>2</sub>/M cell cycle arrest is associated with inhibition of p34<sup>cdc2</sup>. *J Virol* 2001; 74: 9562–9570.
- Rodgers SE, Connolly JL, Chappell JD, Dermody TS. Reovirus growth in cell culture does not require a full complement of viral proteins: Identification of a σ1s-null mutant. *J Virol* 1998; 72: 8597–8604.
- Connolly JL, Dermody TS. Virion disassembly is required for apoptosis induced by reovirus. *J Virol* 2002; 76: 1632–1641.
- Virgin HW 4th, Mann MA, Tyler KL. Protective antibodies inhibit reovirus internalization and uncoating by intracellular proteases. *J Virol* 1994; 68: 6719–6729.
- Chappell JD, Prota AE, Dermody TS, Stehle T. Crystal structure of reovirus attachment protein sigma 1 reveals evolutionary relationship to adenovirus fiber. *EMBO J* 2002; 15: 1–11.
- Barton ES, Forrest JC, Connolly JL, et al. Junction adhesion molecule is a receptor for reovirus. *Cell* 2001; 104: 441–451.
- Chappell JD, Duong JL, Wright BW, Dermody TS. Identification of carbohydrate-binding domains in the attachment proteins of Type 1 and Type 3 reoviruses. *J Virol* 2000; 74: 8472–8479.
- Lerner AM, Cherry JD, Finland M. Haemagglutination with reoviruses. *Virology* 1963; 19: 58–65.
- Dermody TS, Nibert ML, Bassel-Duby R, Fields BN. A σ1 region important for haemagglutination by serotype 3 reovirus strains. *J Virol* 1990; 64: 5173–5176.
- Chappell JD, Gunn VL, Wetzel JD, Baer GS, Dermody TS. Mutations in type 3 reovirus that determine binding to sialic acid are contained in the fibrous tail domain of viral attachment protein σ1. *J Virol* 1997; 71: 1834–1841.
- Barton ES, Connolly JL, Forrest JC, Chappell JD, Dermody TS. Utilization of sialic acid as a coreceptor enhances reovirus attachment by multistep adhesion strengthening. *J Biol Chem* 2001; 276: 2200–2211.
- DeBiasi RL, Squier MKT, Pike B, et al. Reovirus-induced apoptosis is preceded by increased cellular calpain activity and is blocked by calpain inhibitors. *J Virol* 1999; 73: 695–701.
- Connolly JL, Rodgers SE, Clarke P, et al. Reovirus-induced apoptosis requires activation of transcription factor NF-κB. *J Virol* 2000; 74: 2981–2989.
- Clarke P, Meintzer SM, Gibson S, et al. Reovirus-induced apoptosis is mediated by TRAIL. *J Virol* 2000; 74: 8135–8139.

22. Tyler KL, Clarke P, DeBiasi RL, Kominsky D, Poggioli GJ. Reoviruses and the host cell. *TRENDS in Microbiology* 2001; 9: 560–564.
23. Clarke P, Meintzer SM, Widmann C, Johnson GL, Tyler KL. Reovirus infection activates JNK and the JNK-dependent transcription factor c-Jun. *J Virol* 2001; 75: 11275–11283.
24. Poggioli GJ, DeBiasi RL, Bickel RB, et al. Reovirus-induced alterations in gene expression related to cell cycle regulation. *J Virol* 2002; 76: 2582–2594.
25. Clarke P, Meintzer SM, Spalding AC, Johnson GL, Tyler KL. Caspase 8-dependent sensitization of cancer cells to TRAIL-induced apoptosis following reovirus-infection. *Oncogene* 2001; 20: 6910–6919.
26. Ashkenazi A, Dixit VM. Death receptors: Signaling and modulation. *Science* 1998; 281: 1305–1308.
27. Kominsky DJ, Bickel RJ, Tyler KL. Reovirus-induced apoptosis requires both death receptor- and mitochondrial-mediated caspase-dependent pathways of cell death. *Cell Death and Differentiation* 2002; 9: 926–933.
28. Ravi R, Bedi GC, Engstrom LW, et al. Regulation of death receptor expression and TRAIL/Apo2L-induced apoptosis by NF- $\kappa$ B. *Nature Cell Biol* 2001; 3: 409–415.
29. Gibson SB, Oyer R, Spalding AC, Anderson SM, Johnson GL. Increased expression of death receptors 4 and 5 synergizes the apoptosis response to combined treatment with etoposide and TRAIL. *Mol Cell Biol* 2000; 20: 205–212.
30. Spalding AC, Jotte RM, Scheinman RI, et al. TRAIL and inhibitors of apoptosis are opposing determinants for NF- $\kappa$ B-dependent, genotoxin-induced apoptosis of cancer cells. *Oncogene* 2002; 21: 260–271.
31. Rivera-Walsh I, Waterfield M, Xiao G, Fong A, Sun S-C. NF- $\kappa$ B signaling pathway governs TRAIL gene expression and HTLV-1 Tax-induced T-cell death. *J Biol Chem* 2001.
32. Hu WH, Johnson H, Shu HB. Tumor necrosis factor related apoptosis inducing ligand signals NF- $\kappa$ B and JNK activation and apoptosis through distinct pathways. *J Biol Chem* 1999; 274: 30603–30610.
33. Li H, Zhu H, Xu CJ, Yuan J. Cleavage of Bid by caspase 8 mediates the mitochondrial damage in the Fas pathway of apoptosis. *Cell* 1998; 91: 479–489.
34. Luo X, Budihardjo I, Zou H, Slaughter C, Wang X. Bid, a Bcl-2 interacting protein, mediates cytochrome *c* release from mitochondria in response to activation of cell surface death receptors. *Cell* 1998; 94: 481–490.
35. Zou H, Li Y, Liu X, Wang X. An APAF-1 cytochrome *c* multimeric complex is a functional apoptosome that activates pro-caspase 9. *J Biol Chem* 1999; 274: 11549–11556.
36. Verhagen AM, Ekert PG, Pakusch M, et al. Identification of DIABLO, a mammalian protein that promotes apoptosis by binding to and antagonizing IAP proteins. *Cell* 2000; 102: 43–53.
37. Slee EA, Harte MT, Kluck RM, et al. Ordering the cytochrome *c*-initiated caspase cascade: Hierarchical activation of caspases -2, -3, -6, -7, -8, and -10 in a caspase-9-dependent manner. *J Cell Biol* 1999; 144: 281–292.
38. Qin Z-H, Wang Y, Kikly KK, et al. Pro-caspase 8 is predominantly localized in mitochondria and released into cytoplasm upon apoptotic stimulation. *J Biol Chem* 2001; 276: 8079–8086.
39. Kominsky DJ, Bickel RJ, Tyler KL. Reovirus-induced apoptosis requires mitochondrial release of Smac-DIABLO and involves reduction of cellular inhibitor of apoptosis protein levels. *J Virol* 2002; 76: in press.
40. Chai J, Shiozaki E, Srinivasula SM, et al. Structural basis of caspase 7-inhibition by XIAP. *Cell* 2001; 104: 769–780.
41. Huang Y, Park YC, Rich RL, Segal D, Myszka DG, Wu H. Structural basis of caspase inhibition by XIAP: Differential roles of the linker versus the BIR domain. *Cell* 2001; 104: 781–790.
42. Riedl SJ, Renatus M, Schwartzenbacher R, et al. Structural basis for the inhibition of caspase-3 by XIAP. *Cell* 2001; 104: 791–800.
43. Johnson DE, Gastman BR, Wieckowski E, et al. Inhibitor of apoptosis protein hILP undergoes caspase-mediated cleavage during T lymphocyte apoptosis. *Cancer Res* 2000; 60: 1818–1823.
44. Deveraux QL, Leo E, Stennicke HR, Welsh K, Salvesen GS, Reed JC. Cleavage of human inhibitor of apoptosis protein XIAP results in fragments with distinct specificities for caspases. *EMBO J* 1999; 18: 5242–5251.
45. Yang Y, Fang S, Jensen JP, Weissman AM, Ashwell JD. Ubiquitin protein ligase activity of IAPs and their degradation in proteasomes in response to apoptotic stimuli. *Science* 2000; 288: 874–877.
46. Palaga T, Osborne B. The 3Ds of apoptosis: Death degradation and DIAPs. *Nature Cell Biol* 2002; 4: E149–151.
47. DeBiasi RL, Edelstein CL, Sherry B, Tyler KL. Calpain inhibition protects against virus-induced apoptotic myocardial injury. *J Virol* 2001; 75: 351–361.
48. Baghdiguian S, Martin M, Richard I, et al. Calpain 3 deficiency is associated with myonuclear apoptosis and profound perturbation of the I $\kappa$ B/NF- $\kappa$ B pathway in limb-girdle muscular dystrophy type 2A. *Nature Med* 1999; 5: 503–511.
49. Chen F, Lu Y, Kuhn DC, Maki M, Shi X, Demers LM. Calpain contributes to silica-induced I $\kappa$ B degradation and nuclear factor  $\kappa$ B activation. *Arch Biochem Biophys* 1997; 34: 383–388.
50. Watt F, Molloy PL. Specific cleavage of transcription factors by the thiol protease m-calpain. *Nucleic Acids Res* 1993; 21: 5092–5100.
51. Oberhaus SM, Smith RL, Clayton GH, Dermody TS, Tyler KL. Reovirus infection and tissue injury in mouse central nervous system are associated with apoptosis. *J Virol* 1997; 71: 2100–2106.
52. Richardson-Burns SM, Kominsky DJ, Tyler KL. Reovirus-induced neuronal apoptosis is mediated by caspase 3 and is associated with the activation of death receptors. *J NeuroVirol* 2002; 8: 1–16.